On-line Non-Destructive Ultrasonic Rheology Measurement of Solder Pastes

the UNIVERSITY *of* GREENWICH

A thesis submitted to the University of Greenwich in partial fulfilment of the requirements for the degree of Doctor of Philosophy

By

Anton Seman

Electronic Manufacturing Engineering Research Group (EMERG)

University of Greenwich, School of Engineering, Medway Campus,

Chatham, Kent, ME4 4TB, UK

2010

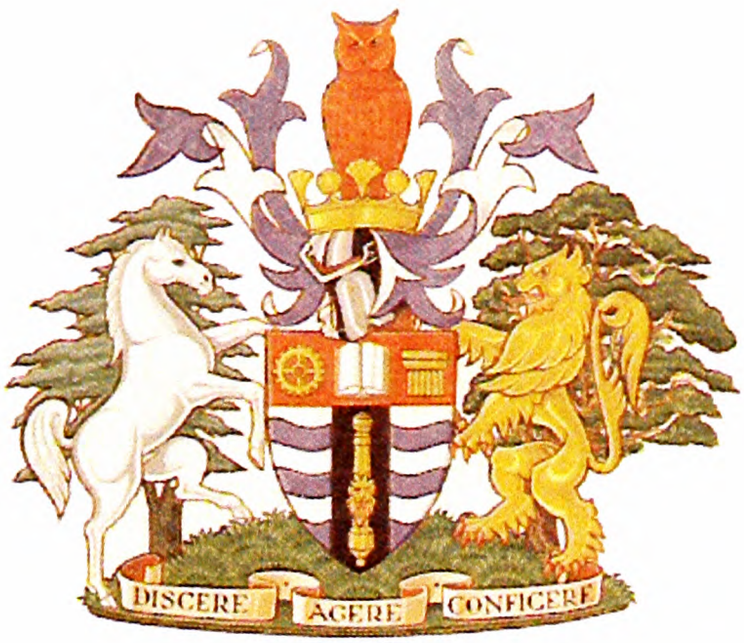

'Learn, practise, accomplish'

Dedicated to the memory of my late beloved father:

"Even when I walk through the valley of death, I shall not be afraid, for you are so close beside me."

Table of Contents

List of Figures

List of Tables

Abstract

In surface mount technology (SMT) electronics assembly, the solder paste is printed onto the PCB's surface through a stencil and the components are later placed over the solder paste deposits. Since 2007, the use of extremely small SMT components for assembly of SMT devices has been widespread, and achieving consistent print deposits for fine pitch (the distance between the leads of the components) components has become a real challenge. The majority of the defects at the printing stage, such as skipping and bridging, were found to be related to the quality of the solder paste. These defects are usually carried over to the reflow process, causing defective final products. Hence, it is important to monitor the quality of the solder paste.

Conventional techniques for monitoring the quality of solder pastes during the production and packaging stage are usually based on the viscosity measurements of the solder pastes from the viscometer and rheometer. One of the potential limitations of viscometer- and rheometer-based measurements is that the collection and preparation of the solder paste samples can irreversibly alter the structure and flow behaviour of the sample. Due to the sample preparation process (removal, pre-shear/pre-mixing), repeatability issues were often encountered when taking measurements using a viscometer or rheometer. Secondly, rheological measurements and the interpretation of rheological data comprise a very technical and time-consuming process, which requires professionally trained research and development (R&D) personnel. Finally, the monitoring/inspection process usually employs random sampling technique from the production batch. Hence, measurement may not represent the actual quality of the whole production batch. This would mean that the conventional solder paste quality control that has been employed in the industry as a benchmark for printability (i.e. checking the viscosity of the paste before being despatched to the customers), would need to be re-evaluated for its feasibility and other possible methods of solder paste quality control would need to be considered. This has brought the ultrasound technique into context as it can offer a non-destructive evaluation of the quality of the solder paste in terms of viscosity. Also, it can be used at different stages of paste production and processing. It is for these

reasons that materials suppliers that formulate and produce solder pastes, as well as solder paste consumers (especially contract electronics manufacturers), are keen to see the development of simple, easy-to-use and accurate techniques for the rheological characterisation of solder pastes.

This thesis concerns the study of a non-destructive ultrasonic technique for characterising the rheological properties of solder pastes and, specifically, the use of through-mode microsecond ultrasonic pulses for evaluation of viscoelastic properties of solder paste materials. In this study, a wide range of flux systems and solder alloy particle distributions used in the industry are investigated to determine the correlation of the ultrasound attenuation and velocity to the viscosity of the solder paste and their correlation to paste printing performance. The work is part of a bigger study aimed at the development of an on-line quality control technique for paste manufacture based on both conventional rheological tests and ultrasound measurements.

Results from the work on the comparative study of standard fluids and both commercial and newly formulated solder pastes and flux vehicle systems have been used to demonstrate the utilisation of the ultrasound technique for on-line, non-destructive measurement of the viscosity of non-Newtonian materials such as solder pastes. The study also found that the viscosity of the solder paste is governed by the intermolecular forces between the solder particles and the flux. The strength of these intermolecular forces depends on the probability of these particles rubbing up against one another while the paste is being sheared. Provided that the right correction factor for a particular shear rate is used, the ultrasound viscosity results obtained were found to be comparable to the rheometer viscosity results or to the viscosity provided by the solder paste manufacturer. The ultrasound technique produced consistent results and was also proven to work at low temperatures. The ultrasound technique may be used to help solder paste manufacturers to add the correct amount of flux or solder particles to their paste in order to reach a desired viscosity. Otherwise, it can be used as a quick go/no-go monitoring tool in the production line for predicting printing quality. Based on the foregoing, it can be concluded that the ultrasound technique is a viable alternative to using a rheometer.

Acknowledgements

I would like to express my sincere thanks to my supervisor, Prof Ndy Ekere. I have been very fortunate in having such an enthusiastic supervisor. I would like to thank him for all his unrivalled guidance and input for my PhD work. In addition, I would like to take this opportunity to thank Dr Stuart Ashenden, my second supervisor, who has been very supportive and helpful in many ways throughout this research work.

I would also like to thank all my colleagues from Electronics Manufacturing Engineering Research Group (EMERG), especially Dr R. Durairaj, Sabuj Mallik, Christopher Hughes and Anthony Marks, for their moral support, and also to all workshop technicians, especially David Weeden, John Jenkins and Terry Wightwick, for their assistance in producing the experimental rigs used. I would further like to thank Mr Ian Cakebread, the Support Services Manager, for providing access to the workshop and necessary materials. I would particularly like to thank Dr Tim Lawrence, material scientist with Multicore Solders (now Henkel Technologies) of Hemel Hempstead, for providing the solder paste samples used in the experiments.

I would like to thank my examiners, Prof Andrew Holmes and Dr Dele Owodunni, for their pertinent questions and suggestions which have added quality to the thesis.

Last but not the least, I would like to thank my family for their love, continuous support, encouragement and undying trust in me.

Nomenclature

ABS	acrylonitrile butadiene styrene
ADC	analogue-to-digital converter
Ag	silver (*argentum*)
ANSI	American National Standards Institute
ASTM	American Society for Testing and Materials
Au	gold (*aurum*)
°C	degree Celsius
CNC	computer numerically controlled
CT	computerised tomography
CTE	coefficient of thermal expansion
Cu	copper (*cuprum*)
dB	decibel
DIN	Deutches Institut für Normung, German Institute for Standards
EIA	Electronics Industries Alliance
EMAT	electromagnetic transducer
HDPE	high-density polyethylene
IC	integrated circuit
IPC	Institute for Printed Circuits (*also known as* the Institute of Interconnecting and Packaging Electronic Circuits)
JEDEC	Joint Electron Devices Engineering Council
JIS	Japanese Industrial Standard
J-STD	Joint Industry Standard
η	viscosity
ln	natural logarithm
MIL	American military standard
Neper	dimensionless logarithmic unit of ratio (~8.68 dB)
Ø	diameter
PAA	polyacrylic acid
Pb	lead (*plumbum*)
PBB	polybrominated biphenyls
PBDE	polybrominated diphenyl ethers

PCB	printed circuit board
PCM	photochemical machining
PDMS	polydimethylsiloxanes
PE	pulse echo
PSD	particle size distribution
R&D	research and development
RMS	root mean square
SEM	scanning electron microscope
SMD	surface mount device
SMT	surface mount technology
Sn	tin (*stannum*)
TT	through transmission
TÜV	Technischer Überwachungs-Verein (Technical Inspection Association)
VOC	volatile organic compound
WEEE	Waste Electrical and Electronic Equipment
XRD	x-ray diffraction
XRF	x-ray fluorescence
ω	angular velocity

CHAPTER 1

INTRODUCTION

1.1. Context

This thesis concerns the use of ultrasound techniques to study the quality of solder paste, which is normally characterised through the measurement of viscosity. The viscosity of solder paste has been empirically used as a key indicator to the quality of the solder paste as it can be used as a rough guide to predict the resulting solder paste printing process. Although there are various techniques (using viscometers and rheometers) available to obtain the viscosity of the solder paste, these techniques usually require removal of the sample or tampering with the sample, hence altering/destroying the sample's structure. Consequently, the results obtained may be invalidated as they may not reflect the true properties of the solder paste. In addition, these techniques usually require skilled personnel to operate the relevant equipment.

These techniques have been extensively exploited and researched to generate a map to link the rheological properties (viscosity, yield stress, storage modulus, loss modulus, complex modulus, creep compliance, recovery compliance, phase angle, frequency, and angular velocity) of solder paste directly to good and bad print deposits. However, in practice it is very difficult to apply this knowledge as there is no clear-cut answer to the question, 'What is the optimum value of the rheological properties that gives good print deposits?' The myriad combinations of these properties that produce good print deposits actually generate more questions than answers. The ultrasound studies in many other materials have provided an indication that there might be a much simpler solution in relation to determining the printing quality of solder paste.

1.2. SMT electronics manufacturing process and defects in assembly

The assembly of surface mount technology (SMT) electronic products usually comprises several processes (see Figure 1.1), such as solder paste printing (screen printing), surface mount device (SMD) components placement, reflow, visual inspection and in-circuit testing. Although manufacturing assembly error can happen at any stage of the process, an error as early as the solder paste printing stage should be prevented. As a result of failing to detect the cause of the problem as early as possible, it could lead to a very costly loss of production: there would be wasted time and resources, such as electricity, components and consumables, and the disposal cost for faulty products generated. Troubleshooting this kind of problem has been a great challenge for the people working in the industry.

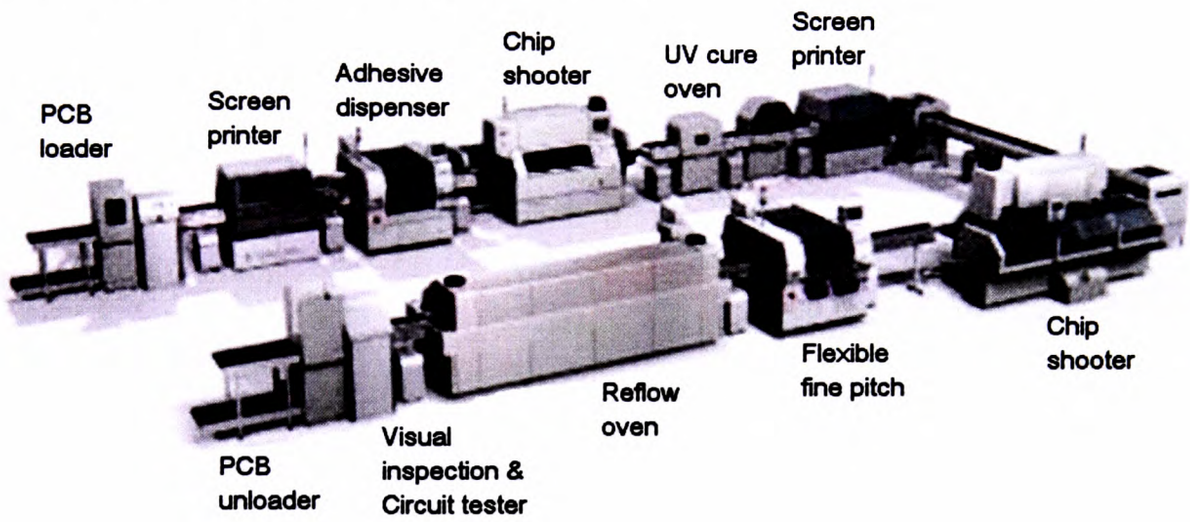

Figure 1.1: Typical manufacturing line for assembly of SMD components onto PCB. (Fisher *et al*, 2000)

Moreover, the lead-free solder paste introduced as a replacement for lead-based solder paste for SMT assembly requires a higher reflow temperature (see Figure 1.2) – a change from 180°C to 230°C, and some solder pastes would even require 250°C. A temperature above 230°C is proven to be too high for some components and can cause a 'popcorn effect' (Tenya and Adams, 2000) in which the components, especially large packages, can burst open due to the rapid change of moisture content in the moulding/encapsulant compound of the components. Since 2007, the use of extremely small SMT components (for example, those labelled as '0201' and '01005' in Figure 1.3) has been widespread and the additional problem arising from a thermal expansion

mismatch between the printed circuit board (PCB) and its components is becoming an issue. This is because the PCB is expanding significantly more than the size of the component itself; hence, during the cooling down of the reflow process, many of these small components can encounter the 'tombstone effect' (see Figure 1.4).

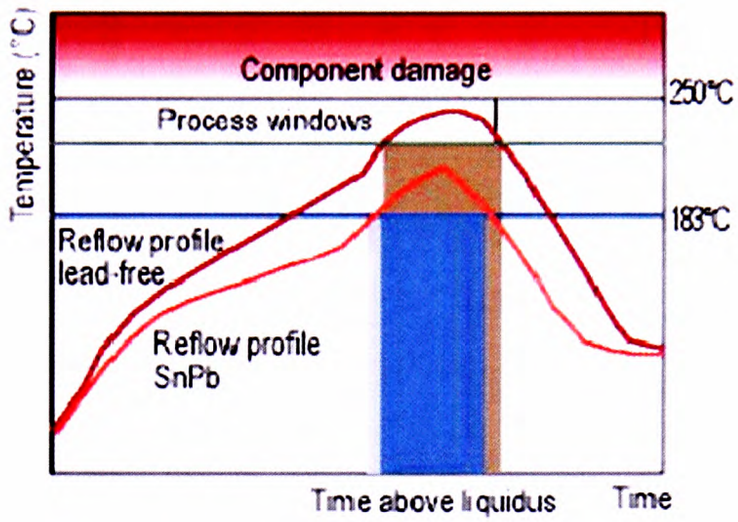

Figure 1.2: Typical reflow profile of lead-based and lead-free solder paste. (Diepstraten, 2004)

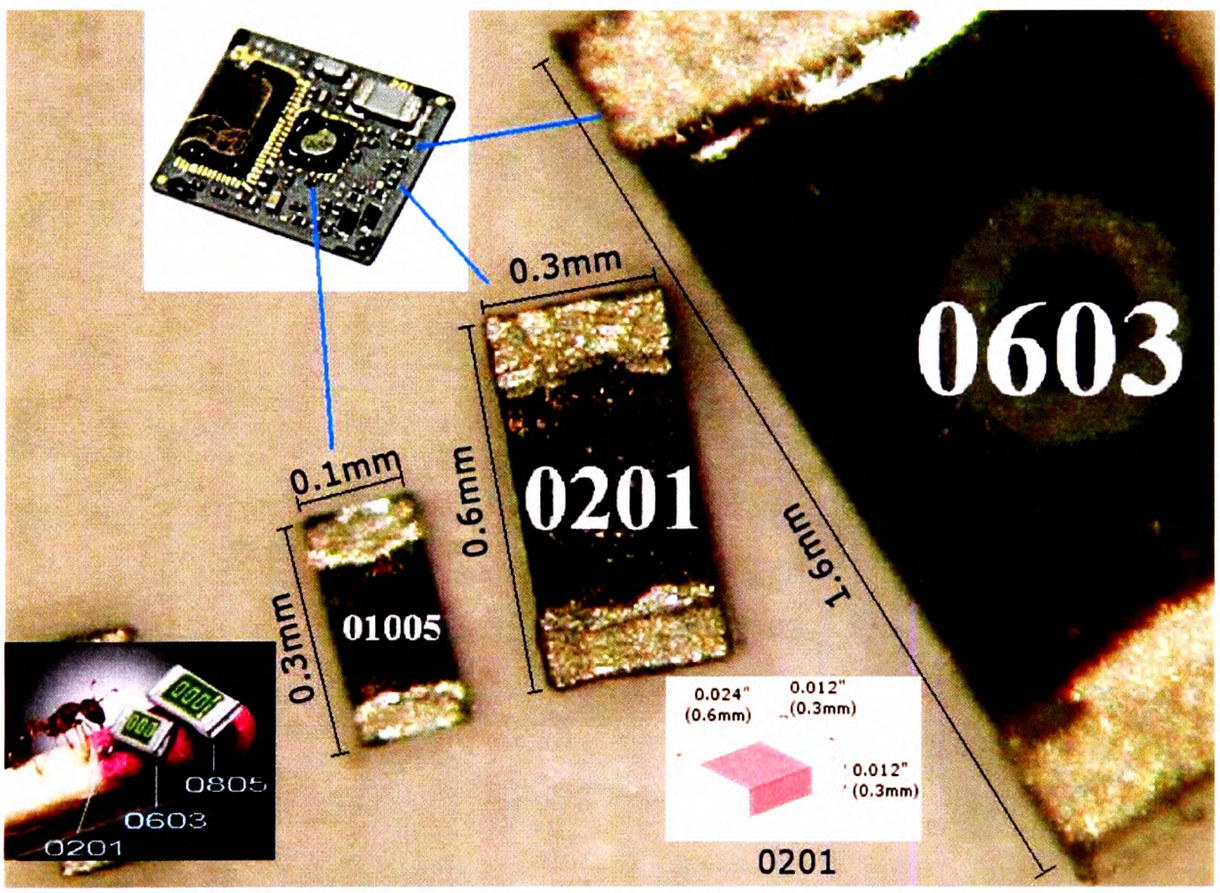

Figure 1.3: Illustration of the size of SMD components used in today's electronic products. (Source: various)

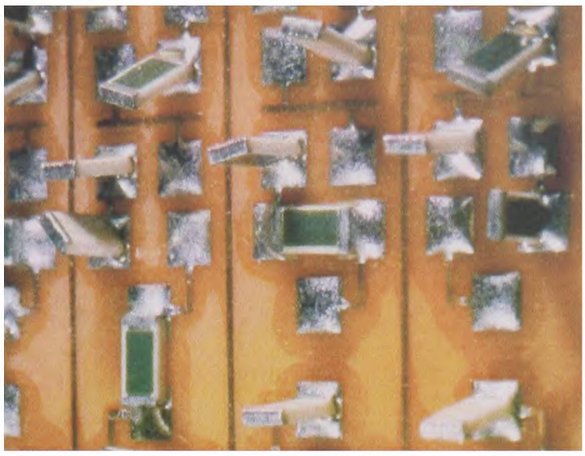

Figure 1.4: Tombstone effect on small SMD component. (Source: ITRI)

Other defects that are often encountered during the manufacturing process include:

- imprecision in placing the extremely tiny components;
- wrong component used;
- defective component used; and
- electrostatic discharge damage.

1.2.1. Defects originating at stencil printing of solder paste

In SMT electronics assembly, the solder paste is printed onto the PCB's surface through a stencil. A stencil is a thin metal foil with a pattern of holes matching the pattern on the PCB. The stencil can be produced by electroforming, by laser cut or through a photochemical machining (PCM) process. Figure 1.5 illustrates the stencil printing process of solder paste, showing the paste rolling over the stencil surface, flowing into the holes of the stencil and being deposited onto the surface of the PCB. The stencil printing process is then completed by removing the PCB in a vertical direction, leaving the solder paste deposits on the surface of the PCB. The components are later placed over the solder paste deposits.

The majority of the defects at the printing stage were found to be related to the quality of the solder paste (Mannan *et al* 1993, Hillman *et al* 2005). The most common defects during the stencil printing process, such as skipping and bridging, are shown in Figure 1.6. These defects are usually carried over to the reflow process, causing defective final products.

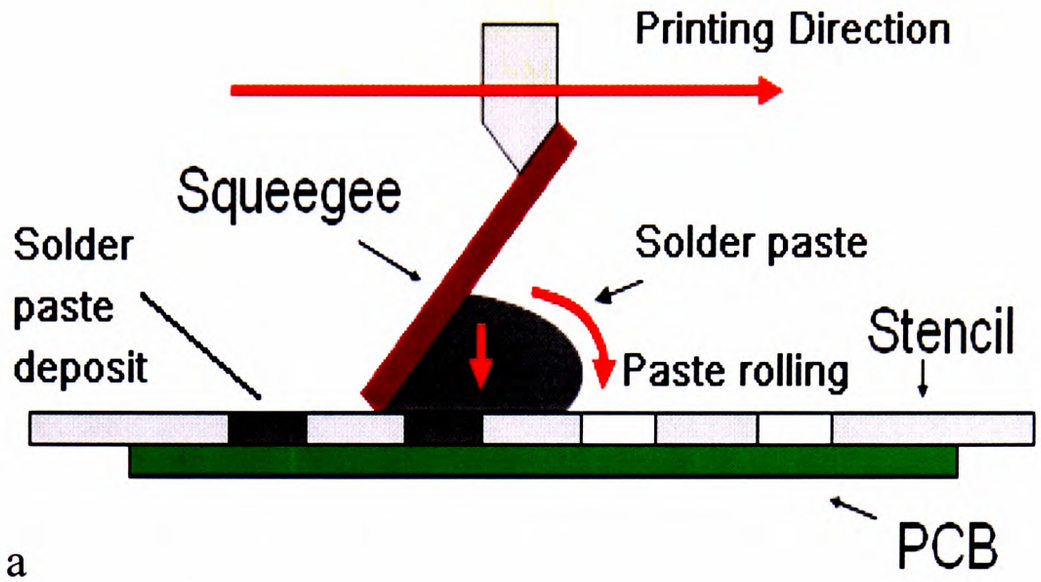

a

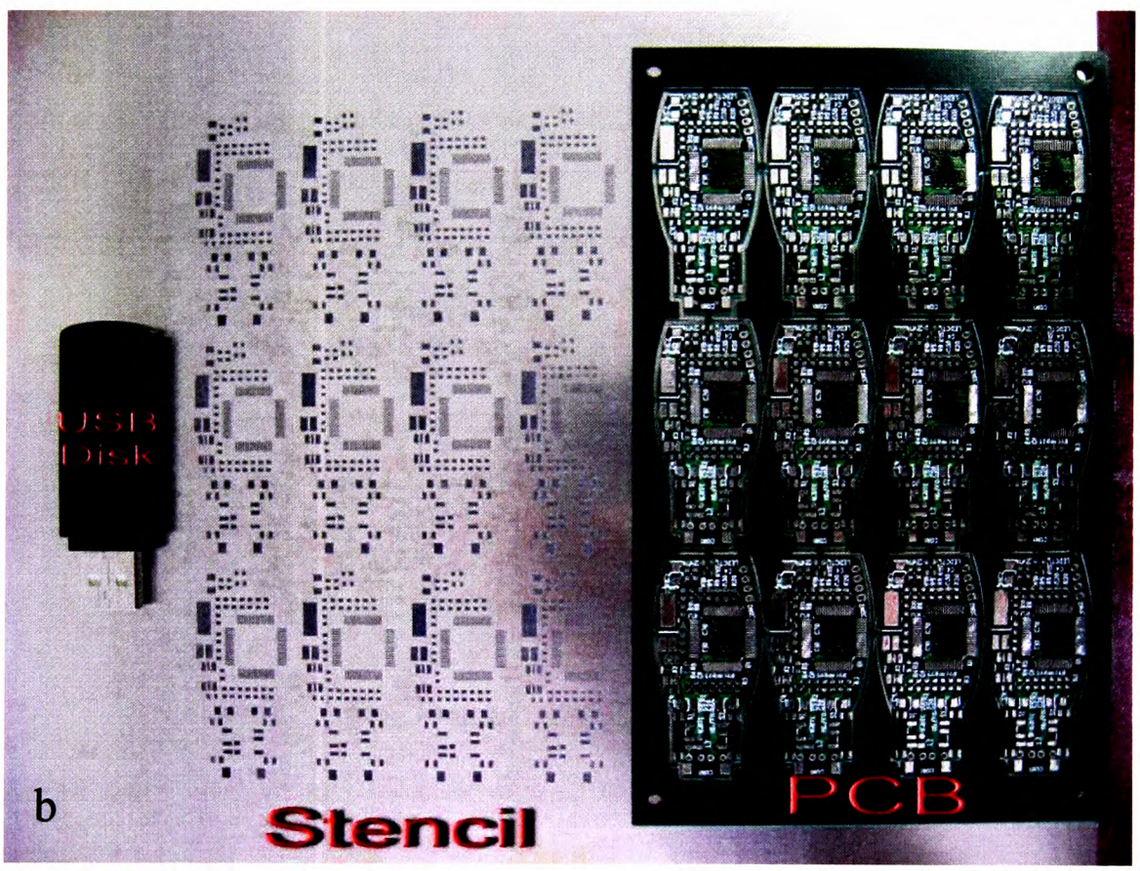

b

Figure 1.5: (a) Stencil printing process, representing how solder paste is deposited onto the PCB through the use of a stencil with matching pattern of mesh to the pads on the PCB; (b) Example of stencil for USB disk and the corresponding PCB.

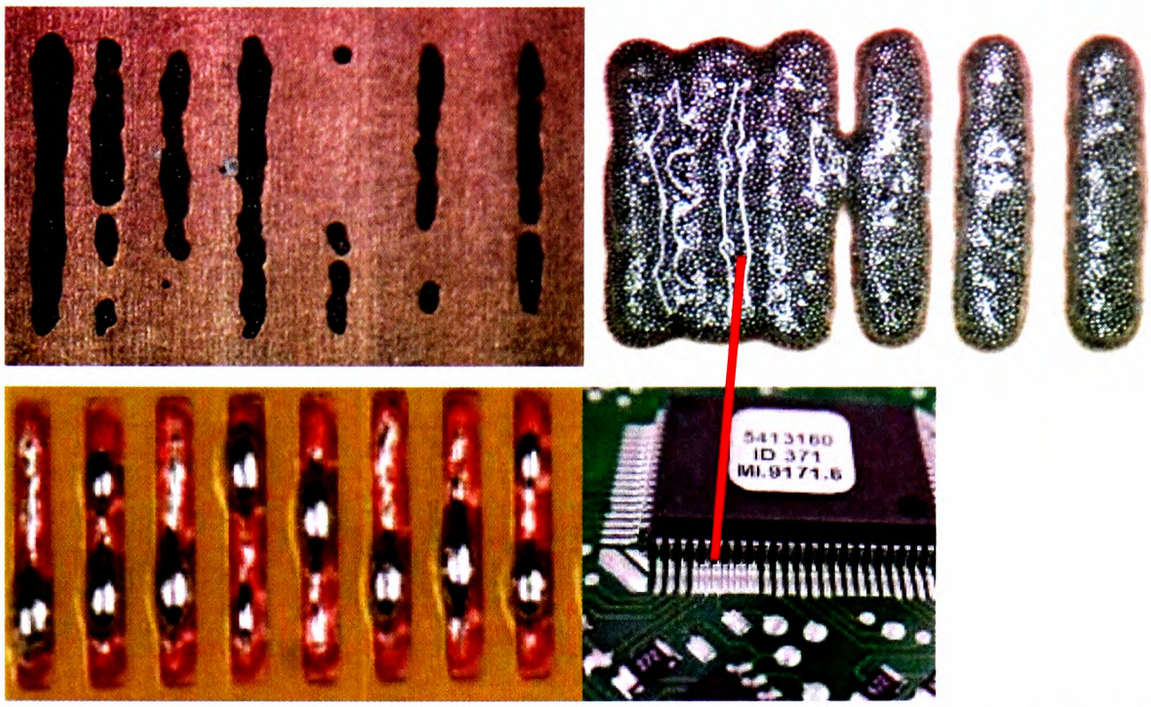

Figure 1.6: Skipping and bridging of solder paste are the most common defects originating at the stencil printing stage. Top: after stencil printing process; bottom: after reflow process.

A rework to repair these kinds of defects is usually too costly – if not impossible – to be performed, due to the tiny size, time and overhead cost required. Usually most of the defective products will be disposed of. With this insight, it is obvious that any error at the printing stage is very detrimental to the end stage of the assembly process. However, this kind of error can be significantly reduced by a better understanding of the rheology of the solder paste and improved quality control within the solder paste manufacturing process.

1.3. Conventional solder paste quality control process

Conventional quality control of solder paste is usually performed by conducting a viscosity test using either a Brookfield or a Malcom viscometer (see Section 4.5, Appendix L and Appendix M for details) but the process heavily relies on print trials results (Burr, 1997). The print trials and viscosity tests are usually carried out regardless of whether the solder paste concerned is an experimental or working (commercial) formulation. During the stencil-printing print trials, the following properties of the solder paste are checked: wetting, solder balling, slump, tack

performance and flux residue. The print trials are crucial for solder paste of an experimental (new) formulation, where the wetting, solder balling, slump, tack performance and flux residue behaviour are unknown. For working formulations of solder paste, however, these tests are not intended to be carried out any more as the print behaviour of the paste can be taken as already known. Furthermore, these kinds of quality control technique do not represent the quality of every jar of solder paste manufactured. This is because the sampling is usually done randomly out of, say, 50 jars, or through choice of only the first and the last jars in a manufacturing run, because of the time required to complete all the tests mentioned previously.

1.4. Problem statement and research objectives

The conventional technique to verify the quality of solder paste is usually carried out using a viscometer or rheometer (see Section 4.5, Appendix L and Appendix M for details). These conventional techniques of rheological characterisation are supposed to provide a forecast for the printing performance of the paste. However, repeatability issues (see Figure 1.7) are often encountered when taking measurements using a viscometer or rheometer, mainly due to the sample preparation process (removal, pre-shear/pre-mixing). This has caused the use of these techniques and the analysis of results based on these techniques to be taken back to the drawing board. From the data set provided in Figure 1.7, it is very difficult to justify or set the optimum viscosity values (maximum and minimum) for solder paste that produces good print deposits since even a very short pre-mixing during sample preparation can adversely affect the viscosity measurements. Moreover, the following settings can also affect the measurement results:

- measuring geometries of the same diameter, e.g. cone plate, parallel plate, cup-and-bob, and other spindle types (RV, T, LV, vane);
- gap height; and
- surface roughness.

The severity of these problems was reported by Durairaj (2006) and Mallik (2008), as shown in Figures 1.8–1.11.

This would mean that the conventional solder paste quality control used in the industry, which has been used as a benchmark for printability (i.e. checking the viscosity of the paste before being despatched to the customers), would need to be re-evaluated for its feasibility and other possible methods of solder paste quality control would need to be considered. This has brought the ultrasound technique into context as it can offer a non-destructive evaluation of the quality of the solder paste in terms of viscosity. Also, it can be used at different stages of the paste production and processing stages.

The aim of this study is to apply the ultrasonic technique so as to provide a means of non-destructive method for measuring the viscosity of solder pastes. In order to achieve that, the following objectives were set out:

- to develop a methodology to characterise the viscosity of solder pastes using an ultrasound technique; and
- to demonstrate how the technique can be used for evaluating the batch-to-batch quality variation of the solder pastes (based on viscosity measurements).

The work completed in this study can be summarised into seven main parts:

a) verification of previous work on the use of ultrasound for evaluation of the sand content in cement pastes;
b) verification and validation of an ultrasound test rig (sensor and data acquisition and analysis equipment) using standard viscosity fluids;
c) design, development and implementation of an experimental testing rig for ultrasound measurement of solder paste viscosity;
d) providing a theoretical correlation between ultrasound results and viscosity;
e) characterisation of the rheology of flux vehicle systems and solder pastes using the Bohlin rheometer;
f) on-line non-destructive measurement of the viscosity of non-Newtonian fluids using the ultrasound test rig; and

g) comparative study of solder paste viscosity using the Bohlin rheometer and the ultrasonic technique, and developing a methodology for on-line solder paste quality control.

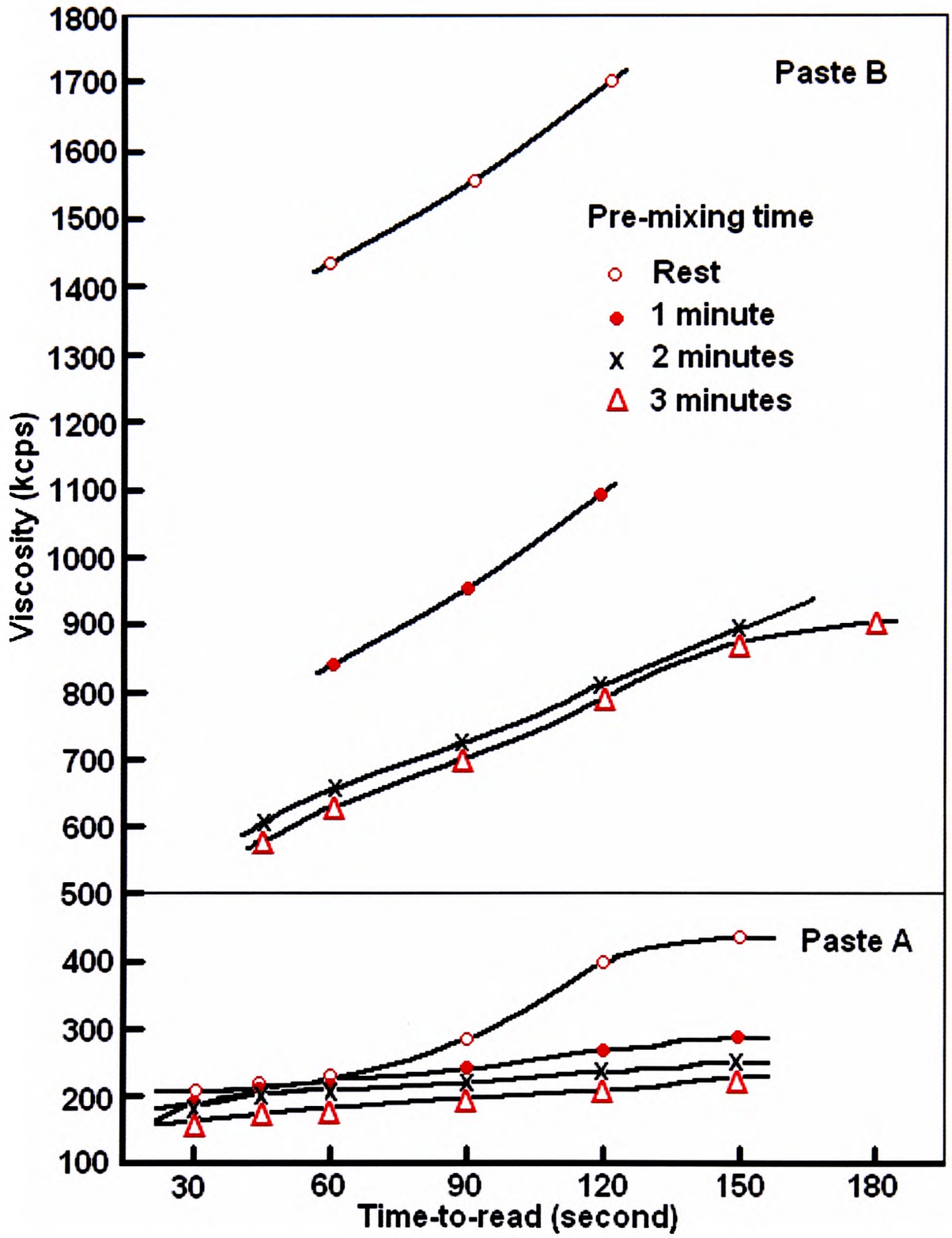

Figure 1.7: Viscosity versus time-to-read at four pre-mixing time. (Hwang, 1996)

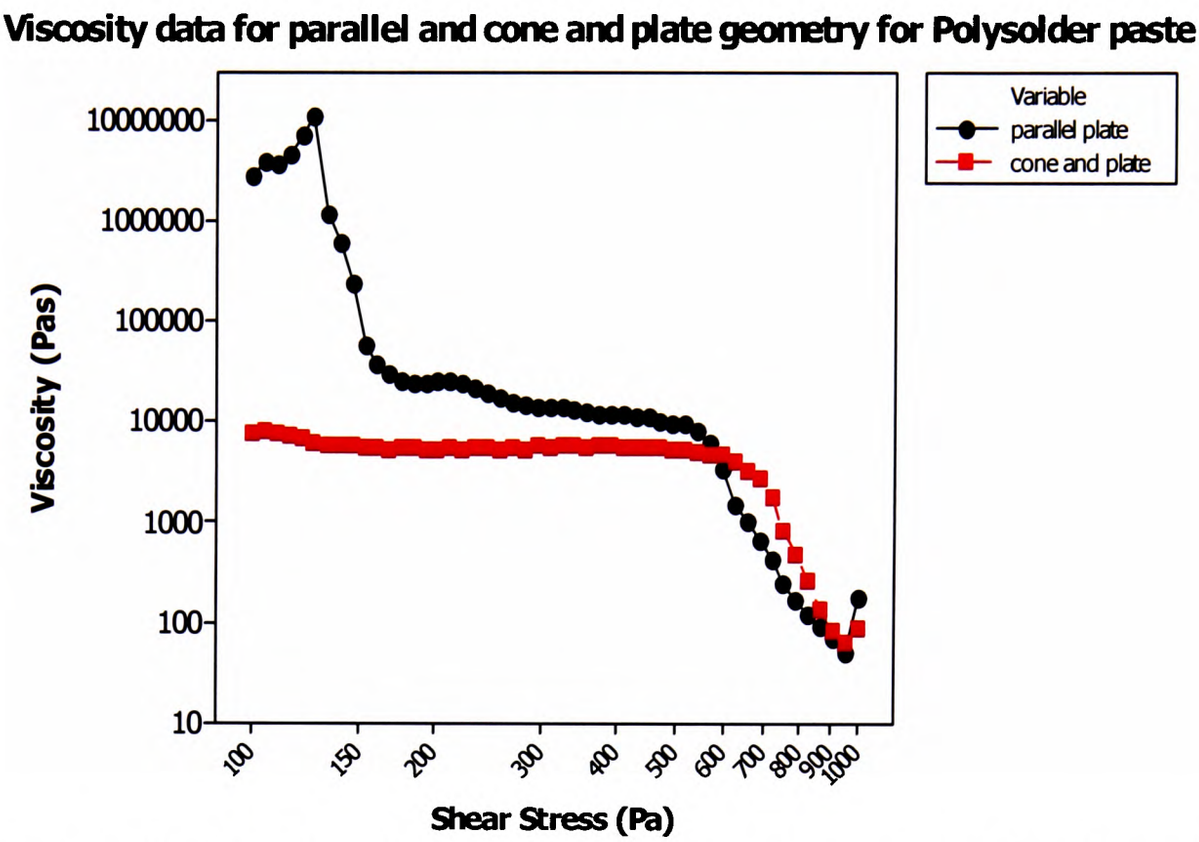

Figure 1.8: Viscosity of Polysolder solder paste using parallel plate and cone and plate. (Durairaj, 2006)

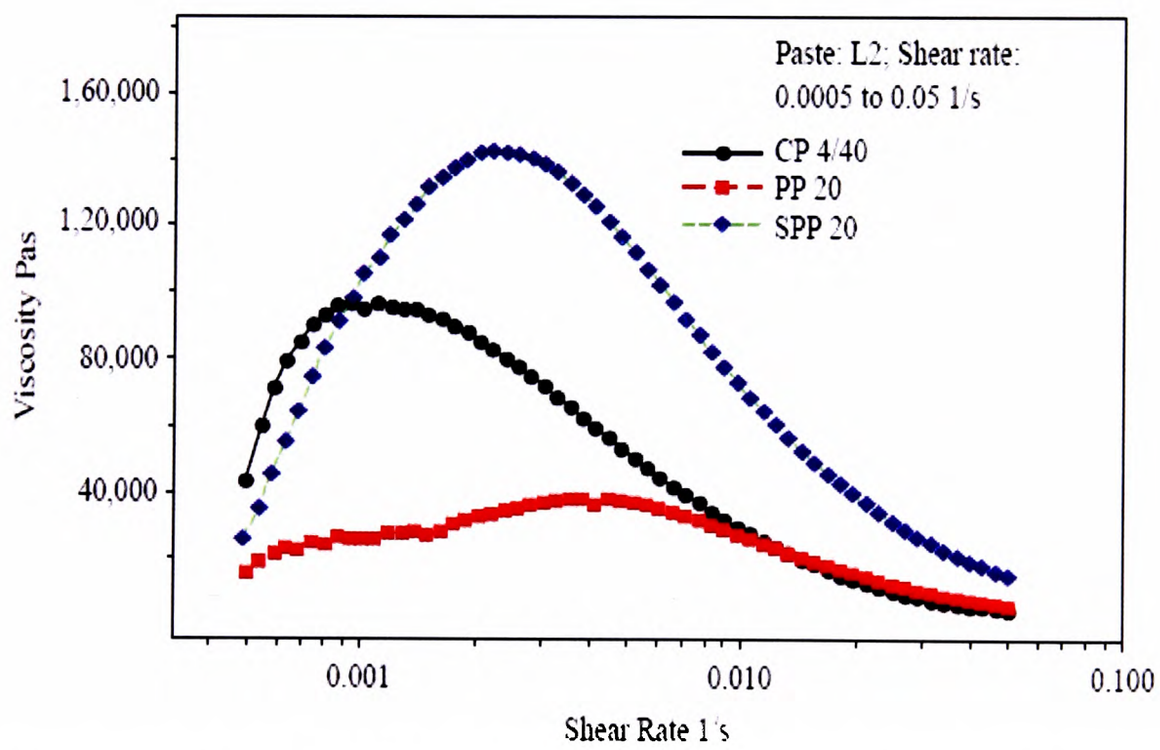

Figure 1.9: Viscosity of L2 solder paste using cone and plate, parallel plate and serrated parallel plate. (Mallik, 2008)

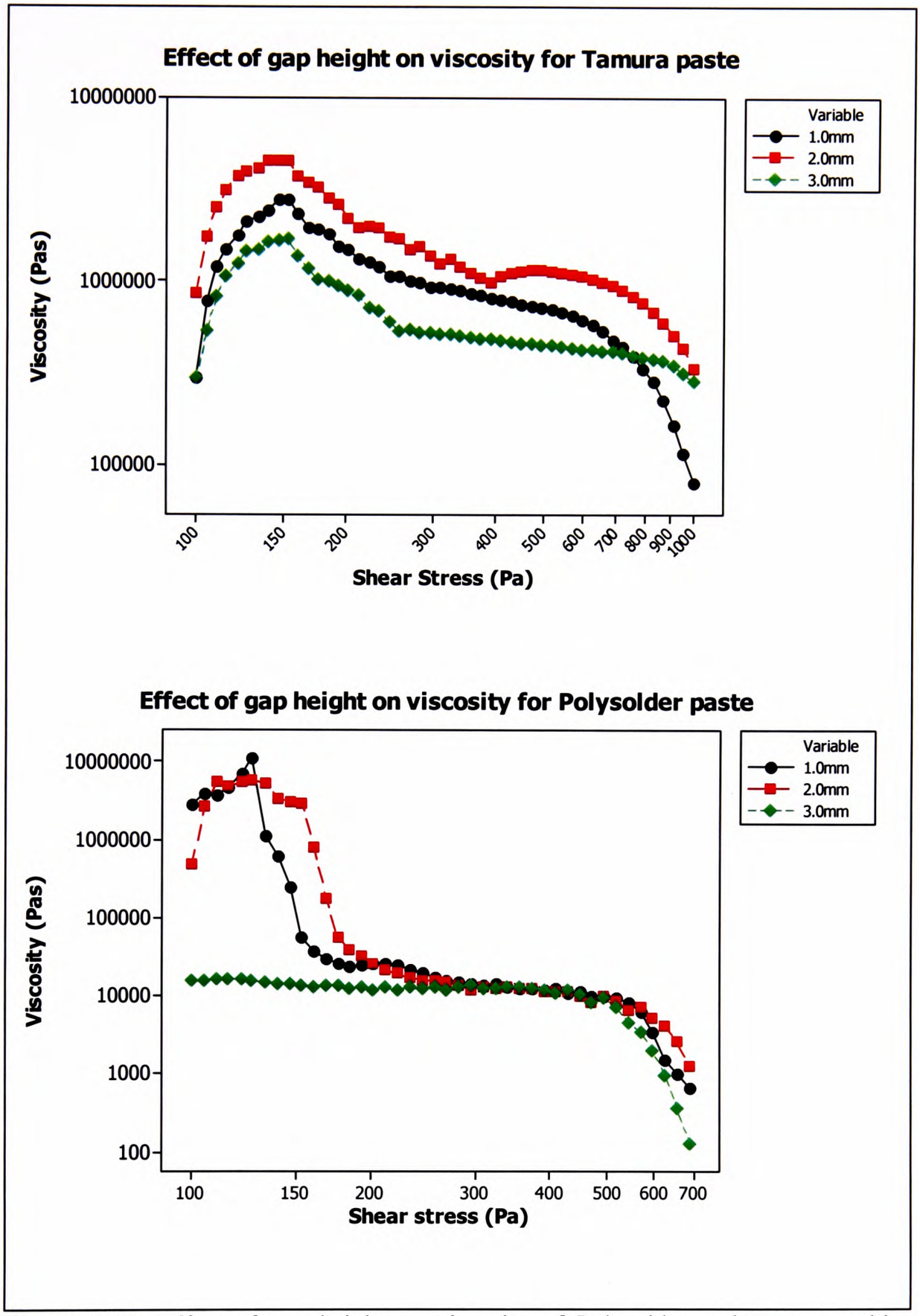

Figure 1.10: Effect of gap height on viscosity of Polysolder and Tamura solder pastes. (Durairaj, 2006)

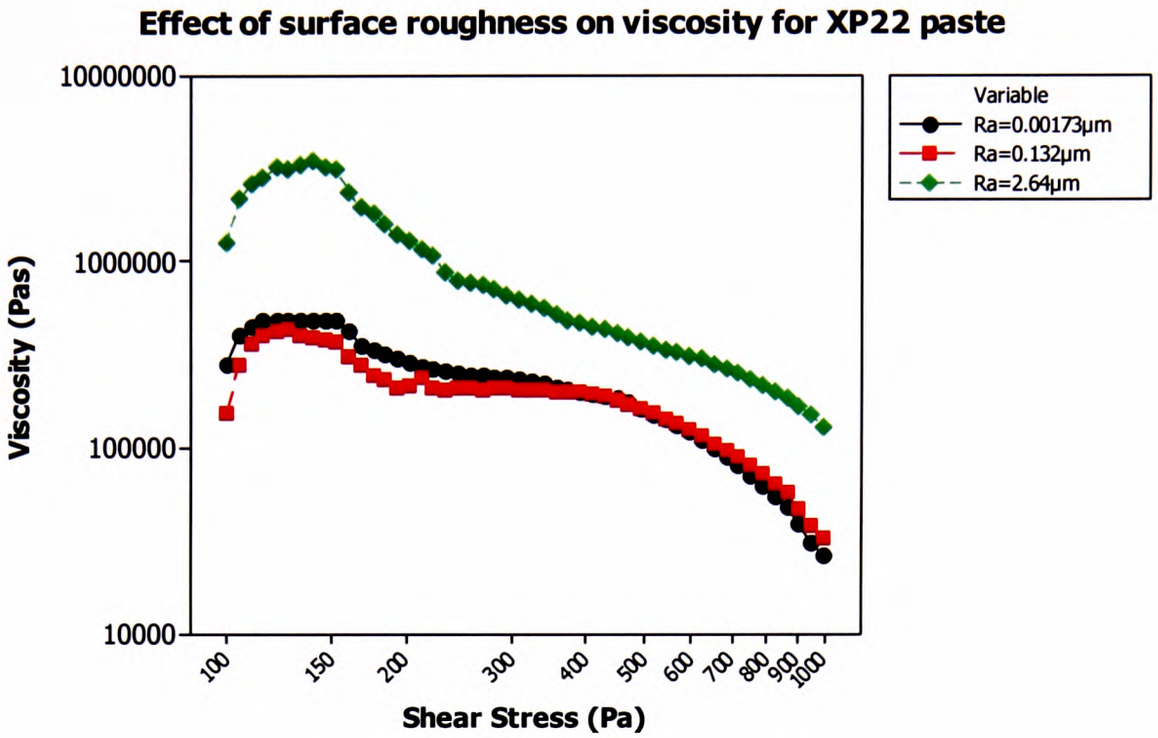

Figure 1.11: Effect of surface roughness on viscosity of XP22 solder paste. (Durairaj, 2006)

Measuring viscosity of materials flowing in a pipe (flowing system) using ultrasonics has been reported by Tabidze *et al* (1981) and Köseli *et al* (2006). The first patent for such a technique was probably by Sheen *et al* in 1994. The majority of the earlier patents utilising ultrasound for materials characterisation were filed for detecting flaws in materials. Most of the techniques reported in the patents utilise a short pulse echo ultrasonic wave (Firestone, 1942; Renaut and Dory, 1965) for monitoring the viscosity of the material. Other patents regarding the use of ultrasound were also found for monitoring high-temperature resin curing (Hinrichs and Thuen, 1985), composite material (Cohen-Tenoudji *et al*, 1988) and high-temperature viscosity measurement of molten material using laser-induced ultrasound (Singh *et al*, 1997). One of the latest patents for a similar purpose was filed by Farone *et al* (2002), claiming the use of ultrasound for measuring viscosity of food products. To date, the author is not aware of any publication or patent filed for measuring viscosity for 'non-flowing systems'. In this study, the author presents a novel technique for monitoring the viscosity of paste materials in a non-flowing system, based on ultrasonic techniques.

1.5. Overview of the thesis

Chapter 1 presents an introduction to electronics assembly processes and the assembly defects during stencil printing processes. This chapter also highlights the importance of rheological characterisation for reducing printing defects, outlines the challenges with conventional techniques, and argues the case for the use of a non-destructive technique such as the ultrasound.

Chapter 2 presents information on the solder paste manufacturing process, classifications, and the chemical and physical requirements standards for SMT assembly.

Chapter 3 presents the concept of ultrasound propagation in different mediums, historical development in ultrasound technology and literature review of material characterisation using ultrasound techniques. This chapter also presents the basic principles of ultrasound testing and the application of ultrasound testing in various fields.

Chapter 4 presents the basics and principles of rheology, as well as the measurement techniques used in conventional equipment, highlighting the limitations of such equipment.

Chapter 5 presents the details of selected case studies, focussing on the aspects that may affect the measurement of ultrasound techniques and the properties that can be measured using ultrasound techniques.

Chapter 6 presents a description of the experimental test rigs built according to the specifications found in the literature review and the modified rigs customised for used with solder paste inspection.

Chapter 7 presents the preliminary results of the work using the experimental rig on cement paste, i.e. an initial attempt to correlate the viscosity of non-Newtonian material to ultrasound measurements.

Chapter 8 presents a study aiming to provide a theoretical model to describe the viscosity of non-Newtonian materials using ultrasound techniques.

Chapter 9 presents the comparative study of the solder paste and flux mediums using the ultrasound technique and a rheometer. This chapter also illustrates how ultrasound measurements can be used as a guide to predict the printing results.

Chapter 10 presents overall conclusions of the work described in this thesis, and contributions made from this study. The chapter concludes with recommendations for future work.

CHAPTER 2

SOLDER PASTE TECHNOLOGY

2.1. Introduction

This chapter presents basic information concerning the material being studied in this thesis. Although the information provided in this chapter is not extensive, it should provide the reader with necessary knowledge of the world of solder paste production and processing. This chapter should provide the reader with an appreciation of the critical nature of the composition of the solder paste mix and the importance of this work in electronics manufacturing.

2.2. Solder paste materials and origin of resin

Solder paste is a material used as a medium to bond electronics components to the printed circuit board (PCB).

Figure 2.1: Solder paste in a 500g jar, Semco tube, and small syringe.

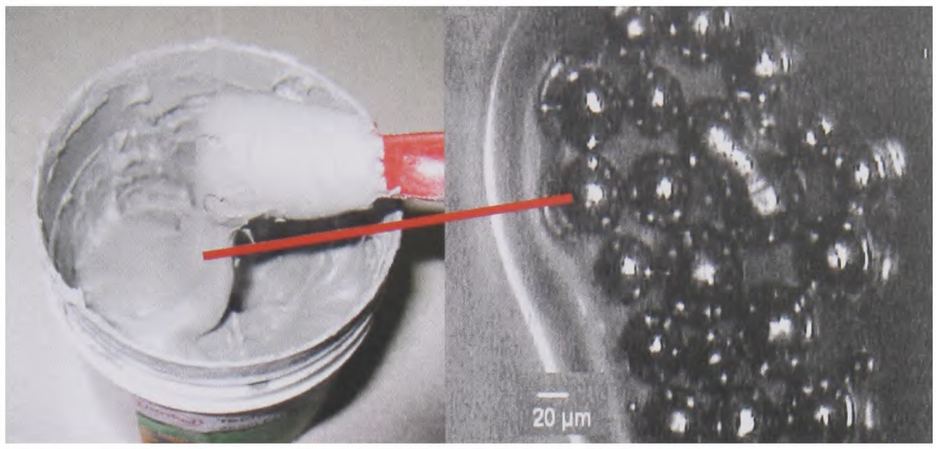

Figure 2.2: Solder paste in a 500g jar, and view of the solder metal particles (without flux medium) under a microscope.

Solder paste is a highly dense suspension composed of flux and alloy of various types of metals such as tin (Sn), silver (Ag), copper (Cu), indium (In), antimony (Sb) and bismuth (Bi), as disclosed by Currie *et al* (2001), Wicker and Han (2005) and Ueshima (2006) in the latest patents regarding lead-free solder paste. Solder paste usually contains 85–90% metal content by weight (about 50% by volume). Lead-based solder paste has been banned since the introduction of the WEEE (Waste Electrical and Electronic Equipment) Directive 2002/95/EC by the European Parliament; however, military products were exempt from this. This regulation has been introduced to combat toxic and hazardous substances leaching from waste electrical and electronics equipment that has been disposed of inappropriately. The leaching of toxic materials such as lead, mercury, cadmium, hexavalent chromium, polybrominated biphenyls (PBB) and polybrominated diphenyl ethers (PBDE) can result in these materials entering the human food-chain through water systems, or through animals reared or crops grown on contaminated soil.

Solder pastes are normally available in different particle size distribution (PSD) of solder metals set out by IPC (Institute for Printed Circuits) in J-STD 005: Requirements for soldering pastes. Currently, the electronics manufacturing industry is using IPC PSD Type 3 (25–45µm) and Type 4 (20–38µm) solder pastes. In the near future, the use of Type 5 (15–25µm) and Type 6 (5–15µm) solder paste might become very common as the size of electronics components and their footprints are reduced, hence requiring solder paste that can form smaller

interconnections. Possible issues with using Type 5, Type 6 or even Type 7 solder paste for the ultra-fine pitch stencil-printing process include aperture filling and emptying issues, which can lead to clogging of the stencil and paste slump as reported by Jackson *et al* (2005). However, the results reported by Jackson confirmed that it would still be possible to achieve desired printing deposits provided that state-of-the-art stencils were used.

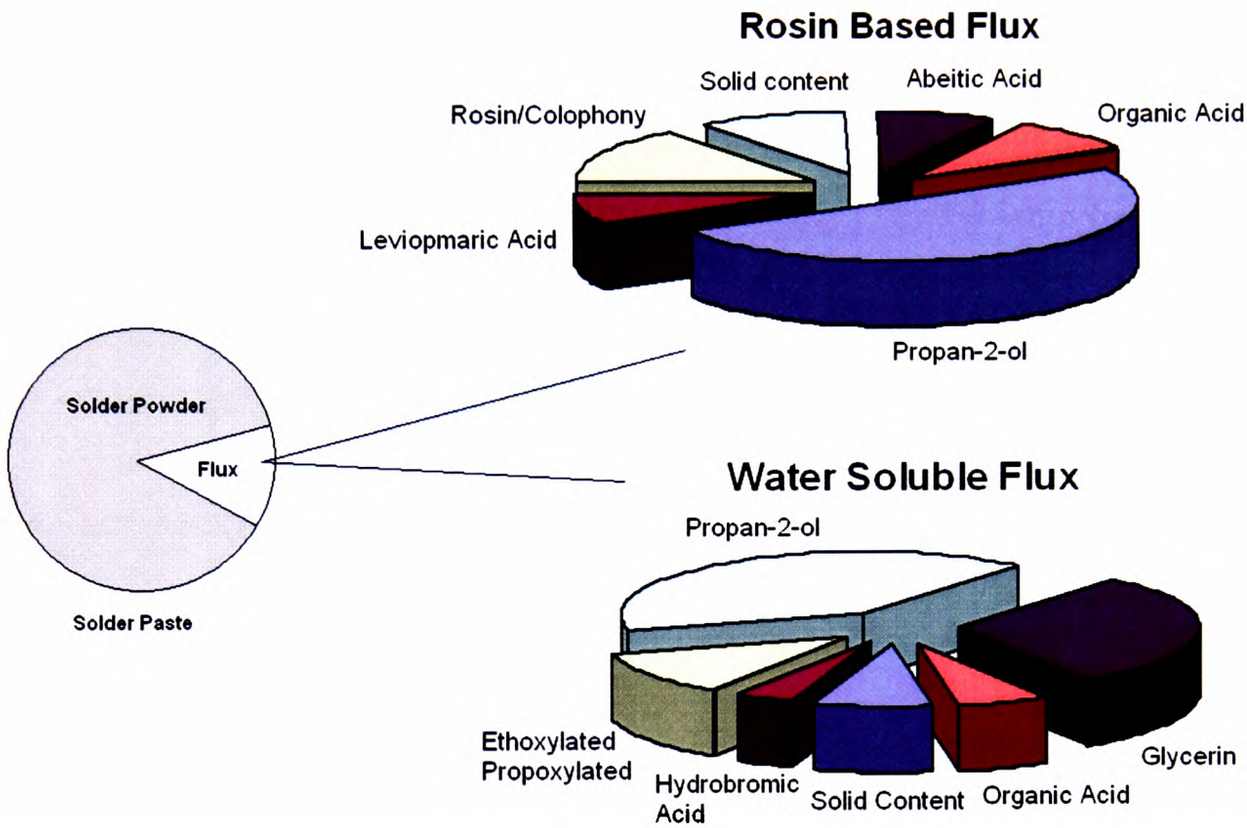

Figure 2.3: General composition of solder paste and flux (for illustration only, not scaled to exact fraction of the actual constituents).

To achieve good printing and good reflow results, solder paste usually contains a certain amount of flux, usually not exceeding 20% total weight as represented in Figure 2.3. An excessive amount of flux can significantly reduce the volume of solder deposits after the reflow process because the flux content usually evaporates; furthermore, it can cause excessive corrosion of solder joints as the flux contains high amount of acids. The amount of the metal content in the paste can significantly affect the height of the print deposit after reflow such that a change from 90% to 80% weight in metal content can halve the height of the reflowed print deposit (Peterson, 1987). The exact amount of the constituents in the flux is proprietary to the solder

paste manufacturer. Some of the manufacturers may choose not to use a certain constituent in their water-soluble flux or rosin-based flux; but the general constituents, consisting of alcohol-based chemicals, acid and solid content, would usually be found in the flux. The classification of flux shown in Figure 2.3 divides the rosin-based flux into four further categories: non-activated rosin (R), mildly activated rosin (RMA), activated rosin (RA) and super-activated rosin (RSA). Meanwhile, the water-soluble flux is subdivided into two further categories: organic and inorganic. This method of classification is commonly known as the 'traditional' method.

Apart from the method of classification mentioned above, there is also an industry-accepted classification of flux, as set out in IPC Joint Industry Standard 004, see Table 2.1. Flux is classified into four categories with their respective symbols:

- rosin (RO);
- resin (RE);
- organic (OR); and
- inorganic (IN).

These fluxes are subdivided into further groups according to the residue activity for copper mirror testing (flux-induced corrosion), surface insulation resistance and halide content.

In J-STD 004, it is clearly defined that rosin is a solid form of resin, see Figure 2.4, obtained from the sap of various pine species from the conifer genus. It is also known as colophony or Greek pitch (*pix græca*), produced by heating the fresh sap to vaporise the volatile liquid-terpene components. Rosin is brittle at room temperature, but melts at around 100°C. Chemically, rosin constitutes a combination of at least seven acids: 34% abeitic acid, 24% dehydroabeitic acid, 9% palustric acid, 6% isopimaric acid, 5% dihydroabeitic acid, 5% pimaric acid, 3% neoabetic acid and a small amount of other acids totalling 14%. Commercial-grade rosin is usually found in a semi-transparent to opaque state, which varies in colour from yellow or brown to pitch-black according to the species of the tree, its age, and the degree of heat applied during distillation. This variation highly affects batch-to-batch quality for solder paste production.

Resin-based flux is a synthetically produced replacement for natural rosin, and the resin has low molecular weight and amorphous properties.

Organic flux usually contains carboxylic acid, such as 1-napthylacetic acid, blended with rosin and isopropanol. Some organic fluxes may also use water as one of their main ingredients instead of using alcohol.

Inorganic flux usually contains synthetic compounds having an aromatic ring with the hydroxyl (–OH), Amine (–NHR) or thiol (–SH) functional group blended with rosin and isopropanol.

Figure 2.4: Natural rosin from various species of pine tree. (Photo courtesy of Ecclestacy Arts).

The flux activity level describes the flux ability to remove oxides and tarnish from solderable surface. Flux activity level test is normally tested according to IPC-TM-650: 2.3.32, see Appendix P1 for detailed testing method. High flux activity level represents >50% breakthrough of the targeted cleaning area.

Flux Materials of Composition	Flux Activity Levels, (% Halide), Flux Type	Flux Designator
ROSIN (RO)	Low, (0%), L0	ROL0
	Low, (<0.5%), L1	ROL1
	Moderate, (0%), M0	ROM0
	Moderate, (0.5-2.0%), M1	ROM1
	High, (0%), H0	ROH0
	High, (>2.0%), H1	ROH1
RESIN (RE)	Low, (0%), L0	REL0
	Low, (<0.5%), L1	REL1
	Moderate, (0%), M0	REM0
	Moderate, (0.5-2.0%), M1	REM1
	High, (0%), H0	REH0
	High, (>2.0%), H1	REH1
ORGANIC (OR)	Low, (0%), L0	ORL0
	Low, (<0.5%), L1	ORL1
	Moderate, (0%), M0	ORM0
	Moderate, (0.5-2.0%), M1	ORM1
	High, (0%), H0	ORH0
	High, (>2.0%), H1	ORH1
INORGANIC (IN)	Low, (0%), L0	INL0
	Low, (<0.5%), L1	INL1
	Moderate, (0%), M0	INM0
	Moderate, (0.5-2.0%), M1	INM1
	High, (0%), H0	INH0
	High, (>2.0%), H1	INH1

Table 2.1: Classification of fluxes according to J-STD 004 and their designation code for commercial labelling.

Both methods of classification, the J-standards and the traditional method, are still in use today in Europe and the United States. Several other standards have also been introduced to classify solder paste and flux, such as DIN and TÜV, which are commonly used in Germany. Separately, MIL (American Military) standard is usually used for manufacturing militarily related electronics products. Japan also has its own standard called JIS (Japanese Industrial Standard) for solder paste related products.

Recently, there have been two new types of flux introduced onto the market: low-VOC (volatile organic compound) flux and no-clean flux. These types of flux have started to dominate the UK market because of the enforcement by the UK government for supporting ecologically sustainable manufacturing environments. The exact composition of these fluxes has never been disclosed but, from the materials safety data sheet provided, it is indicated that these new fluxes contain high amounts of alcohol-based chemicals such as isopropanol, propan-2-ol and methanol.

The flux plays a major role both in the printing and in the reflow process (see Figure 2.5); this includes binding the component to the board before reflow, remove oxides layer from the pads, and preventing any drying-up of the paste.

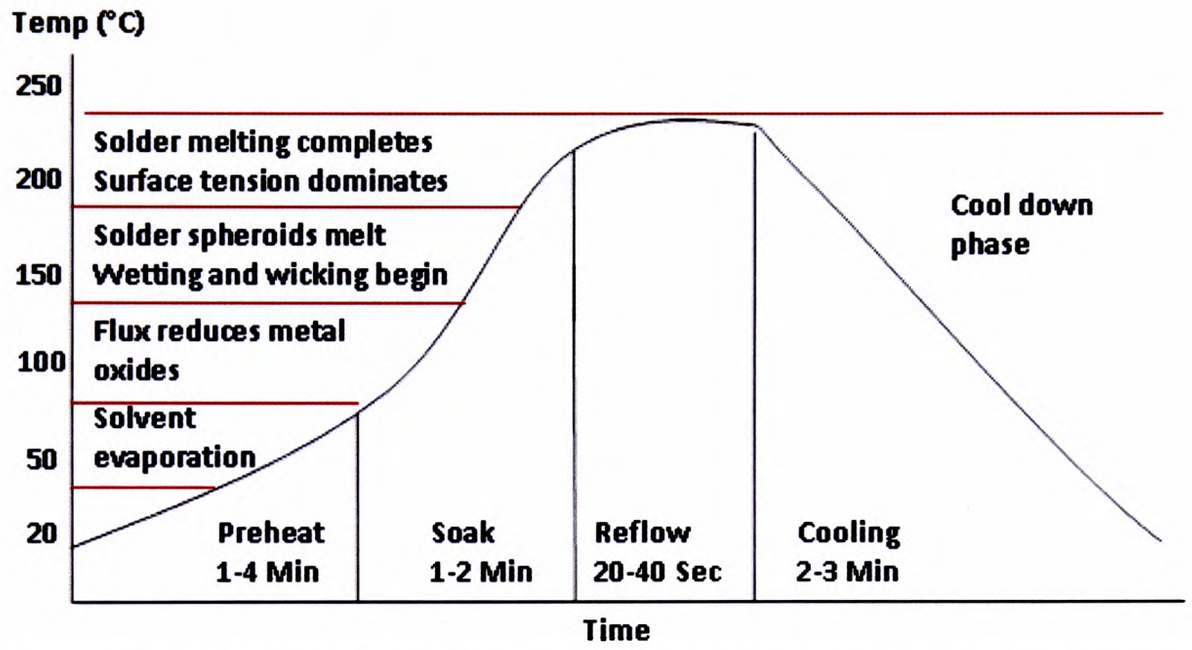

Figure 2.5: Typical lead-free reflow profile and the function of flux during the ramp-up stage of reflow, according to the IPC/JEDEC J-STD 020C standard.

2.3. Production of the metal powders/particles

Solder metal powders are usually produced by using an atomisation method (Fulwylwer and Hatcher, 1976) in order to achieve uniformly spherical particles that cannot be achieved using other production processes. Solder paste containing metal particles of irregular shape has the tendency to form particle clusters or agglomeration

in the paste, and this can lead to clogging of the stencils during the printing process (He *et al*, 2003). Although the powders do not need to be perfectly spherical (see Figure 2.6a), variations such as shown in Figure 2.6b are not acceptable. He *et al* also reported (2003) that in order to achieve good printing, the solder paste must consist of metal of various sizes with a range of particle distribution, as this will help to improve printing consistency.

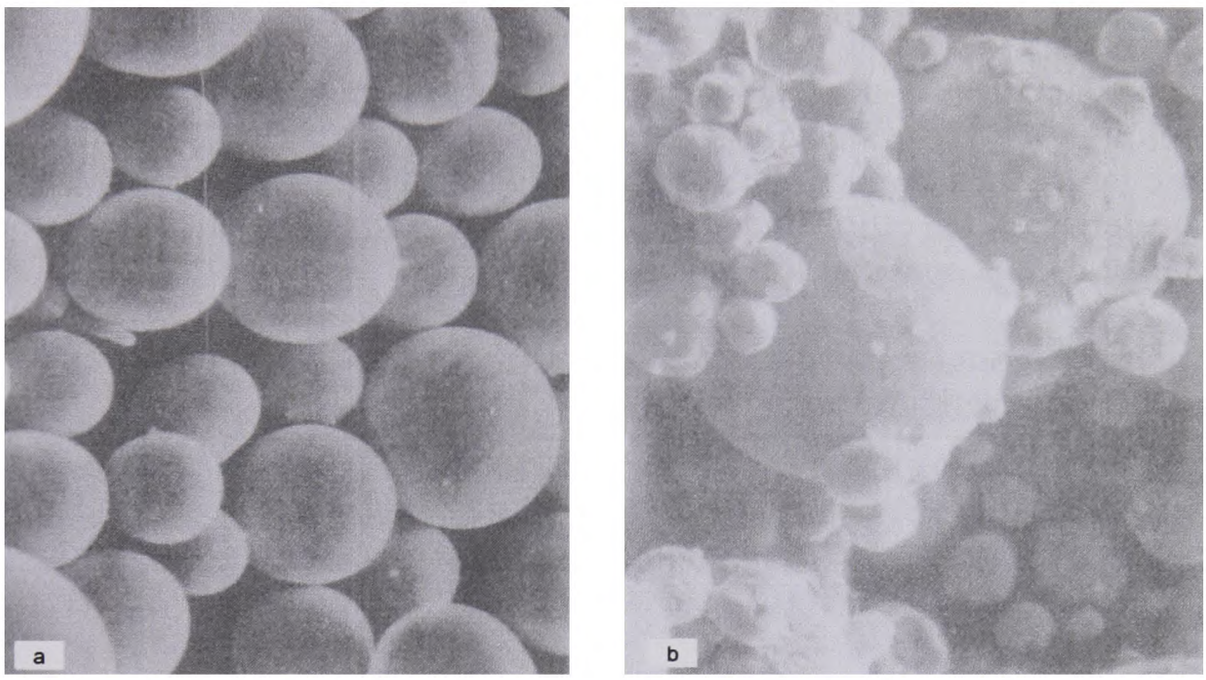

Figure 2.6: (a) Perfectly spherical and (b) Unacceptable solder particles in solder paste (Prasad, 1997, p.389).

2.4. Activators and additive solvents

Apart from rosin, solder flux also contains other chemical constituents (Currie *et al*, 2001; Wicker and Han, 2005; Ueshima 2006), including activators, thickeners or rheological modifiers, and solvents. Alcohol-based solvents such as ethanol, isopropanol or butanol are usually used to dissolve the rosins and activators.

The activators are added to the flux to help oxide removal from the surface of pads being soldered. The activators are usually made up of acids, salts or halides, such as glutaric acid, levulinic acid, stearic acid and aniline hydrochloride, and ethanolamine hydrochloride. The amount of such activators contained in the flux determines the

corrosive level of the flux residues after soldering. The amount of halide activator used in the solder paste is normally indicated as %halide (see Table 2.1). The test for flux activator residue is defined by IPC-TM-650: 2.3.33 (see Appendix P2) in which the flux will be designated with '0' for pass or '1' for fail.

A small amount of thickener or rheological modifier, such as glycerine, castor wax, plasticiser, or polyethylene glycol, is usually added to the flux to keep the flux to the desired viscosity given the addition of alcohol solvent to the flux. The thickener will also suspend the powder motion in the flux, preventing it from settling and separating to the bottom of the container.

CHAPTER 3

BASICS, PRINCIPLES OF NON-DESTRUCTIVE ULTRASONIC TESTING AND LITERATURE REVIEW

3.1. Introduction

This chapter provides a general overview of the history of ultrasonic testing of materials, the issues relevant to the related experimental techniques, and the development of ultrasonics since its discovery some 170 years ago. This chapter will thus provide the reader with background knowledge for understanding how ultrasound can be used for characterising solder paste materials, by looking into the basic principles of ultrasound and the application of ultrasound techniques for non-destructive testing of suspensions and other materials.

3.2. Nature of sound

Sound is the vibration of molecules in a medium in the form of a wave generated by moving bodies. Without a medium (gas, liquid or solid), sound cannot travel – for example, it cannot travel in a vacuum space. Music and other sounds are usually composed of a range of harmonic frequencies oscillating through the air. It is possible to transmit only a single frequency of sound wave using a tuning fork or signal generator. Generally, human hearing is limited to the frequency range of about 20Hz to 20kHz (Figure 3.1).

Sound waves with frequencies beyond the human hearing range are known collectively as 'ultrasound', or sometimes 'ultrasonics'. The application of sound waves in the ultrasonic range is increasingly becoming a common tool in industrial applications, such as locating defects/cracks in metal, 3D imaging of the foetus, particle sizing, sonar (sound navigation ranging), the establishing of material elasticity

and the concentration of materials. One of the unique features of ultrasound is its ability to travel through any material non-destructively and non-invasively without altering the physical or chemical properties of the material. To understand how ultrasound is used for different industrial applications, further understanding of the behaviour of sound through materials and the response by the materials is required, which will be explained in detail in the sections below.

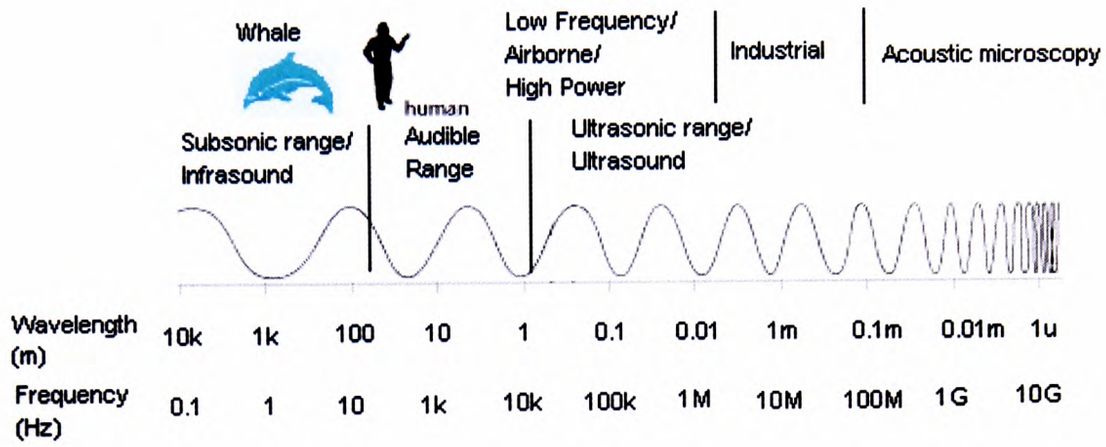

Figure 3.1: Acoustic spectrum.

3.3. Properties of sound waves

A sound wave is characterised by several properties, such as amplitude, frequency and wavelength. Very often, other properties related to the sound are also used, such as attenuation/absorption and velocity. The relationship between these properties is illustrated in Figure 3.2 below.

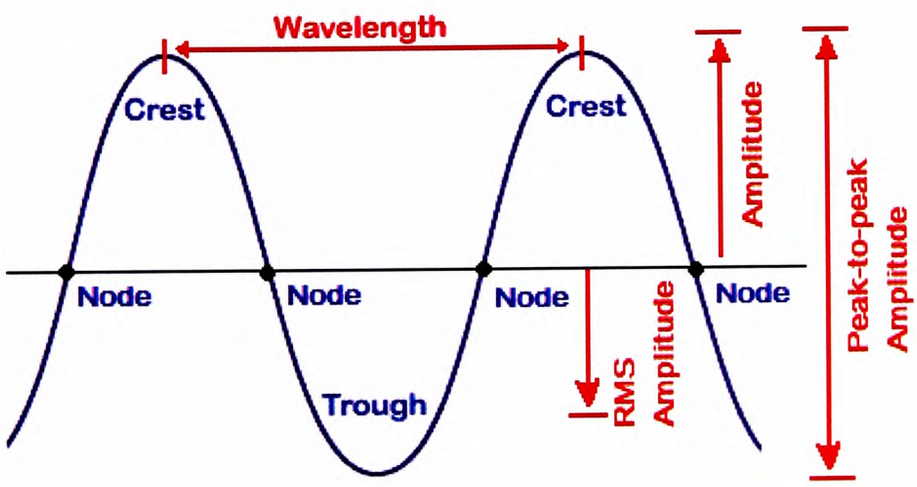

Figure 3.2: Amplitude and wavelength of a sinusoidal wave.

'Wavelength' is defined as the distance covered between the crests of the propagating sinusoidal wave, as indicated in Figure 3.2. Sometimes a wavelength is also defined as the distance covered between three consecutive nodes of the wave. The amount of time required to travel one wavelength is called the 'period', usually measured in seconds.

'Frequency' is defined as the number of repeating events per unit of time. As illustrated on Figure 3.1, frequency has an inverse relationship to wavelength. Hence, sound with higher frequency will have shorter wavelength.

By definition, frequency f is given by

$$f = \frac{1}{T} , \tag{3.1}$$

where

f = frequency (Hz)

T = period (s).

At low frequency range (50Hz to 5000Hz), the velocity of sound travelling through most materials is almost constant. Therefore, frequency can also be written as:

$$f = \frac{v}{\lambda} , \tag{3.2}$$

where

v = velocity (m/s)

λ = wavelength (m).

'Amplitude' is defined as the measure of magnitude of a wave's oscillation. Amplitude is usually measured in volt, using either one of the three most commonly used terms to measure amplitude of harmonic wave. The first measure is 'peak amplitude', measured from the baseline to the peak of a wave. The second measure is 'RMS (root mean square) amplitude', which is defined as 0.707 times the peak

amplitude ($A_{RMS} = 0.707 A_{Peak}$). The final measure is the 'peak-to-peak amplitude', which is measured as an absolute value of the sum of amplitude of the peaks.

3.4. Wave propagation

Sound waves can propagate either longitudinally or transversely (the latter being known as a 'shear wave'). Longitudinal waves are identified by the wave travelling parallel to the direction of particle displacement (see Figure 3.3).

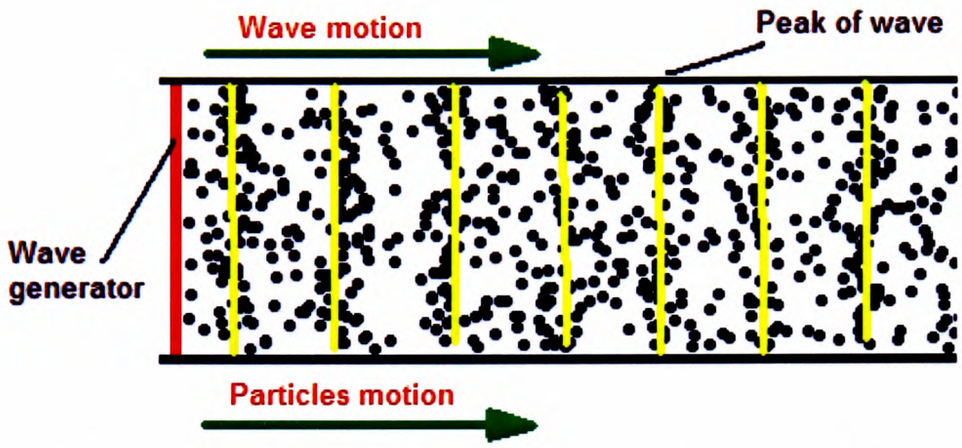

Figure 3.3: Illustration of longitudinal wave propagation.

For a transverse (or shear) wave, the direction of the wave propagation is perpendicular to particle displacement (see Figure 3.4).

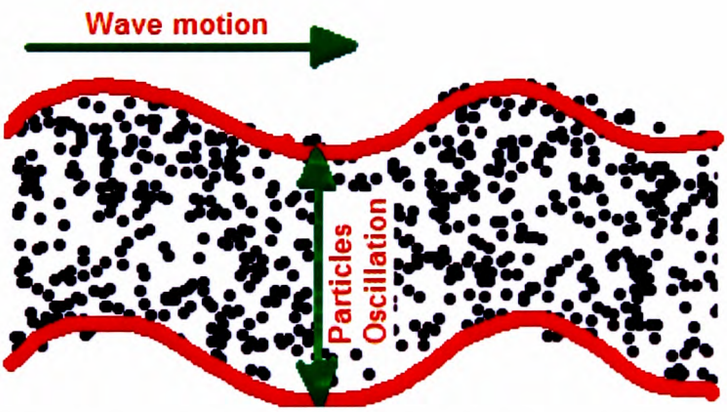

Figure 3.4: Illustration of transverse/shear wave propagation.

When ultrasound propagates through any material, the sound wave will be attenuated as a result of reflection, refraction, diffraction or scattering effects. The magnitude of attenuation will depend on the medium (gas, liquid or solid) and the chemical structure (H-bond, covalent bond, long chain polymer) of the material. When sound waves interact with the material (see Figure 3.5), the wave might encounter reflection or a combination of reflection and scattering, or all the effects mentioned previously.

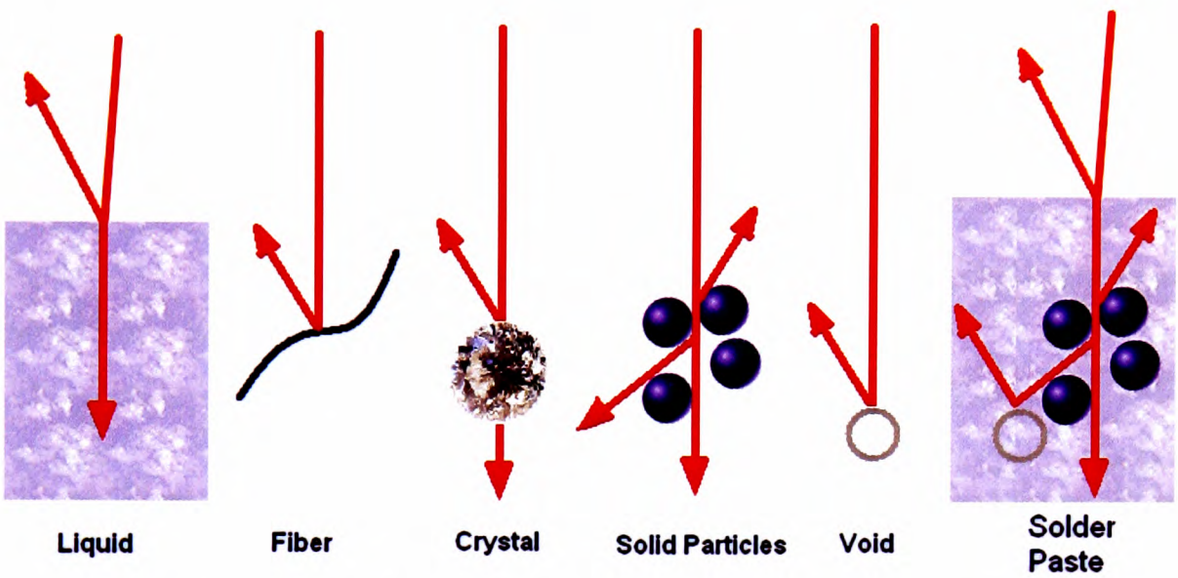

Figure 3.5: Illustration of ultrasound propagation through different materials.

When an ultrasound wave propagates through a medium/material, it transmits mechanical energy to the medium/material on impact, causing the medium's particles to vibrate. The vibrations are usually extended to the neighbouring particles or layer of particles, from end to end (see Figure 3.6). These vibrations can result in the loss of ultrasound energy and can be considered as an absorption mechanism by the medium. The ability of the medium to transmit mechanical energy is highly dependent on the packing ratio of the material (see Figures 3.7 and 3.8), the bond strength of the material and whether the material has a short or long molecular chain (see Figures 3.9 and 3.10).

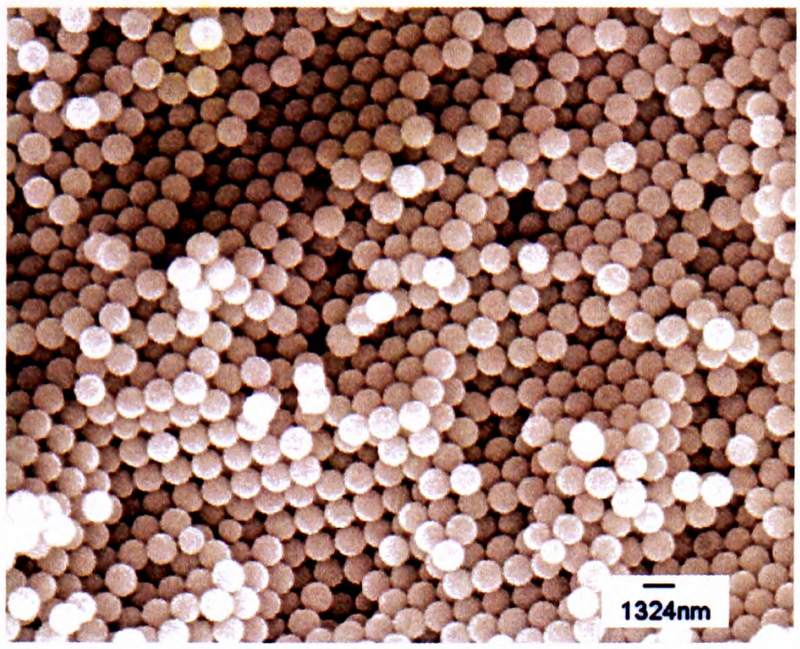

Figure 3.6: Scanning electron microscope (SEM) image of silica particles. Image shown is not at molecular size. (Zhou *et al*, 2003)

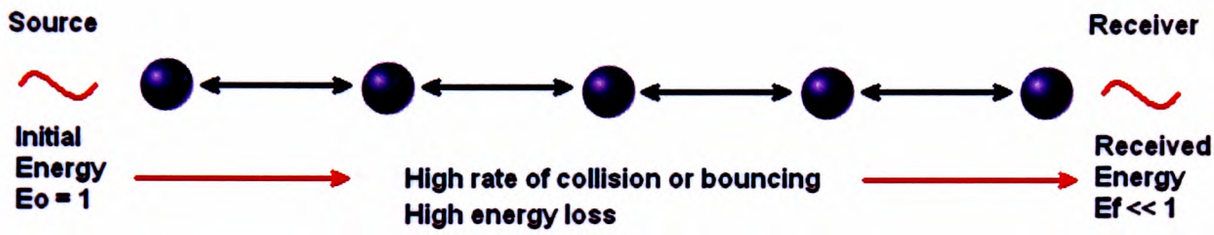

Figure 3.7: Ultrasound propagation through low-packing-ratio materials.

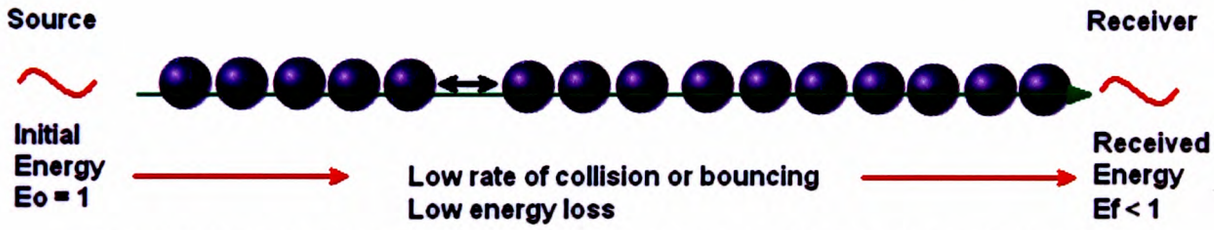

Figure 3.8: Ultrasound propagation through high-packing-ratio materials.

For long-chain molecules a huge amount of the mechanical energy will be lost when the ultrasound propagates through the material, as most of the energy will be lost to compress the molecular chain of the material (see Figures 3.9 and 3.10). Polymer materials usually have long molecular chains (see Figure 3.11) that can easily contract and expand as the ultrasound propagates through the material. Solids and liquids also behave in a similar manner when ultrasound propagates through them (Landau and Rumer, 1937; Kneser, 1938; Landau and Lifshitz 1986). For an isotropic solid or

liquid, the material's chemical bonds are similar in all directions throughout the volume. Therefore, in pure solids and liquids the attenuation can be assumed to be fully governed by the intrinsic loss mechanisms due to bidirectional vibrations and contractions of the bonds.

In terms of velocity, pure solid materials and polymers are usually formed from closely packed atoms (i.e. with a very low void count) or networks of molecules, where the ultrasound velocity through these materials is significantly higher due to shorter wave paths, as described by Ye *et al* (2004) and shown later in Figure 3.39. Hence, it is very likely that two materials of the same density can have significantly different ultrasound velocity.

Figure 3.9: Illustration of long-molecule-chain materials.

Figure 3.10: Illustration of short-molecule-chain materials.

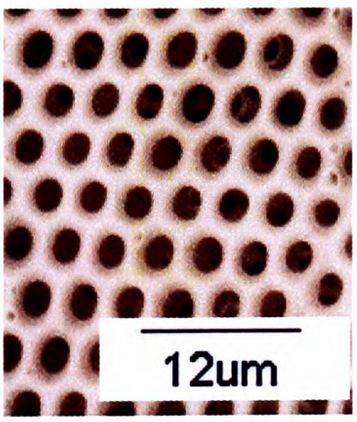

Figure 3.11: SEM image of a polyphenylene polymer. (Tian *et al*, 2006). The dark areas are hollow spaces. Image shown is not at molecular size.

3.4.1.Reflection and refraction

Ultrasound reflection (back scattering) and refraction mechanisms are similar to those for light reflection and refraction. If an ultrasound wave is propagated at an angle and arrives at the interface between two different mediums, then there will be a reflected wave and refracted wave (see Figure 3.12). A reflected wave always has the same angle to the incoming wave ($\theta_1 = \theta_1'$). If the second medium is denser than the first medium, then a small portion of the wave will be reflected with 180° phase difference, otherwise the reflected wave is in phase with the incoming wave ($\theta_1 = \theta_1'$). In the second medium, the wave will be bent (refracted) towards or away from the centreline depending on whether the second medium is denser or lighter than the first medium. The relationship between ultrasound velocity and refraction phenomena can be explained using Snell's law:

$$\frac{Sin\theta_1}{v_1} = \frac{Sin\theta_2}{v_2}, \tag{3.3}$$

where

θ_1 is the incident angle and θ_2 is the refraction angle

v_1 and v_2 respectively are the ultrasound velocity in the first medium and the second medium.

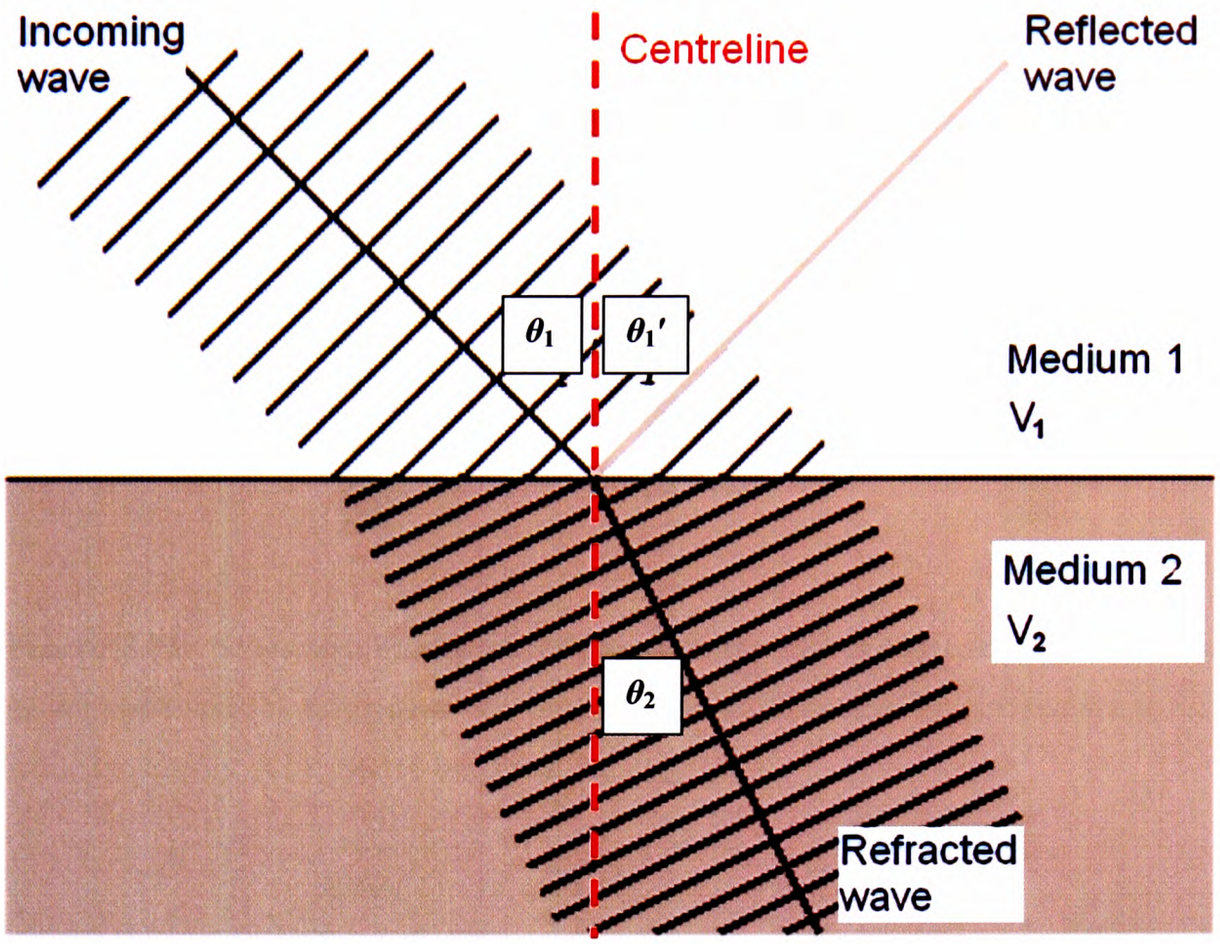

Figure 3.12: Illustration of wave reflection and refraction.

3.4.2. Diffraction and scattering

Ultrasonic waves can also exhibit diffraction phenomena, in which the incoming wave bends around a small object or spreads out when it passes through a narrow opening (see Figures 3.13–3.15). The diffraction mechanism can be used to explain how an ultrasonic wave propagates through colloids or suspension mediums with various packing ratios (Dukhin and Goetz 2002). Diffraction of waves can affect the amount of wave energy that can be transmitted through the medium.

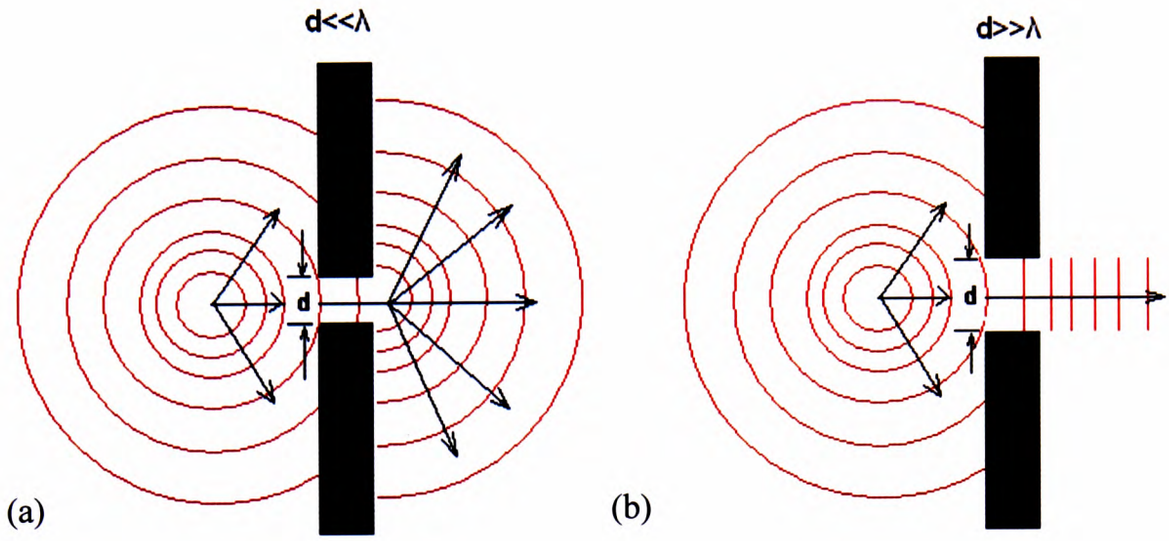

Figure 3.13: Schematic illustration of sound diffraction at high frequency for (a) solder paste and (b) suspension. The wave energy is dissipated in all direction in (a), while the energy is focused to one direction only in (b).

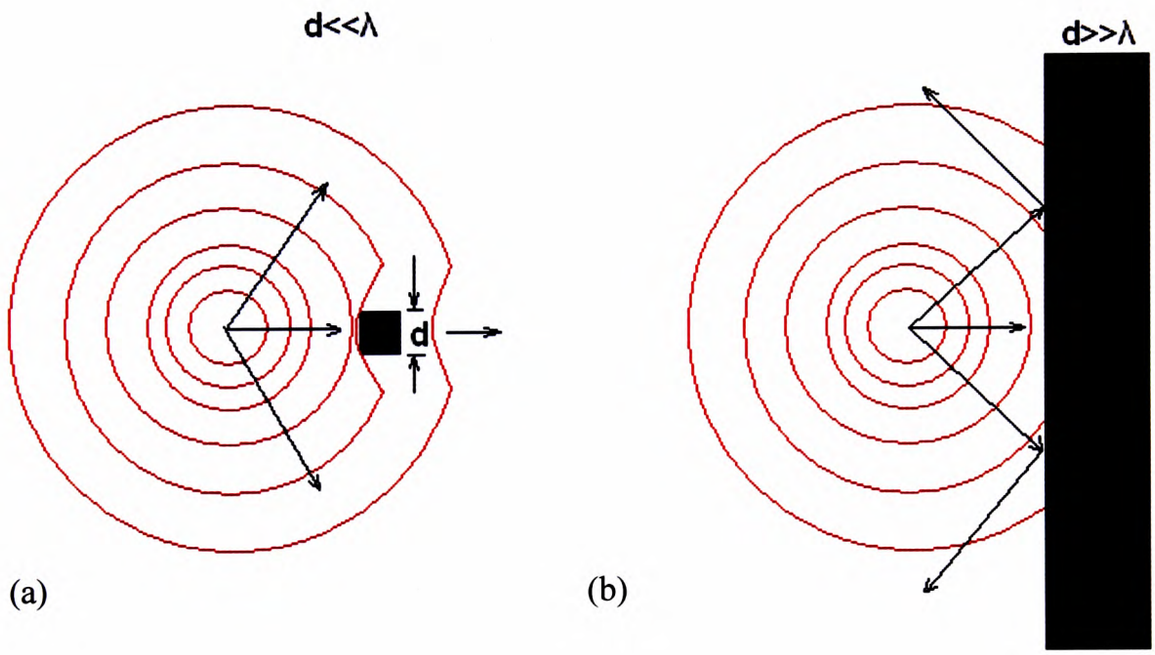

Figure 3.14: Schematic illustration of (a) sound diffraction around a small particle and (b) sound reflection on impact with a big particle.

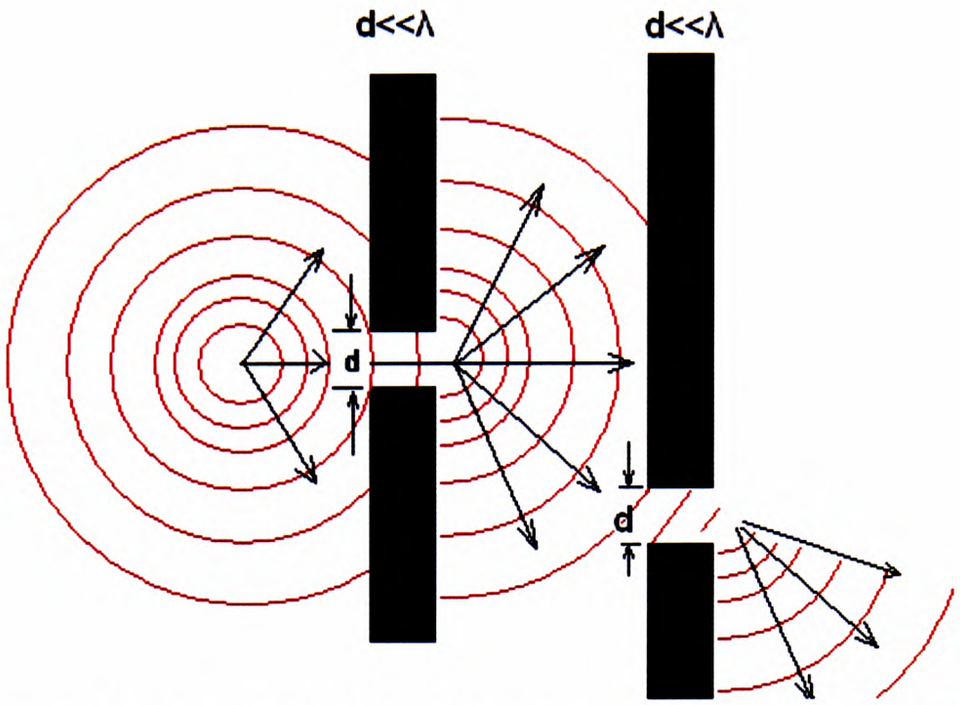

Figure 3.15: Schematic illustration of sound diffraction through multiple lattices of a high-volume fraction and small particle size medium (e.g. solder paste).

Apart from reflection, the scattering of ultrasonic waves is known to be one of the dominant factors responsible for wave attenuation. Scattering of waves is usually indicated by the returning of the incoming wave as if the object or particle were actually emitting the wave signal (see Figure 3.16). Scattering tends to return most of the incoming wave against the direction of the incoming wave. Scattering also reduces the amount of energy that can propagate through the medium, because the scattered wave will cancel out a significant proportion of the incoming wave energy. The difference between reflection of a wave and scattering of a wave is shown in Figure 3.17.

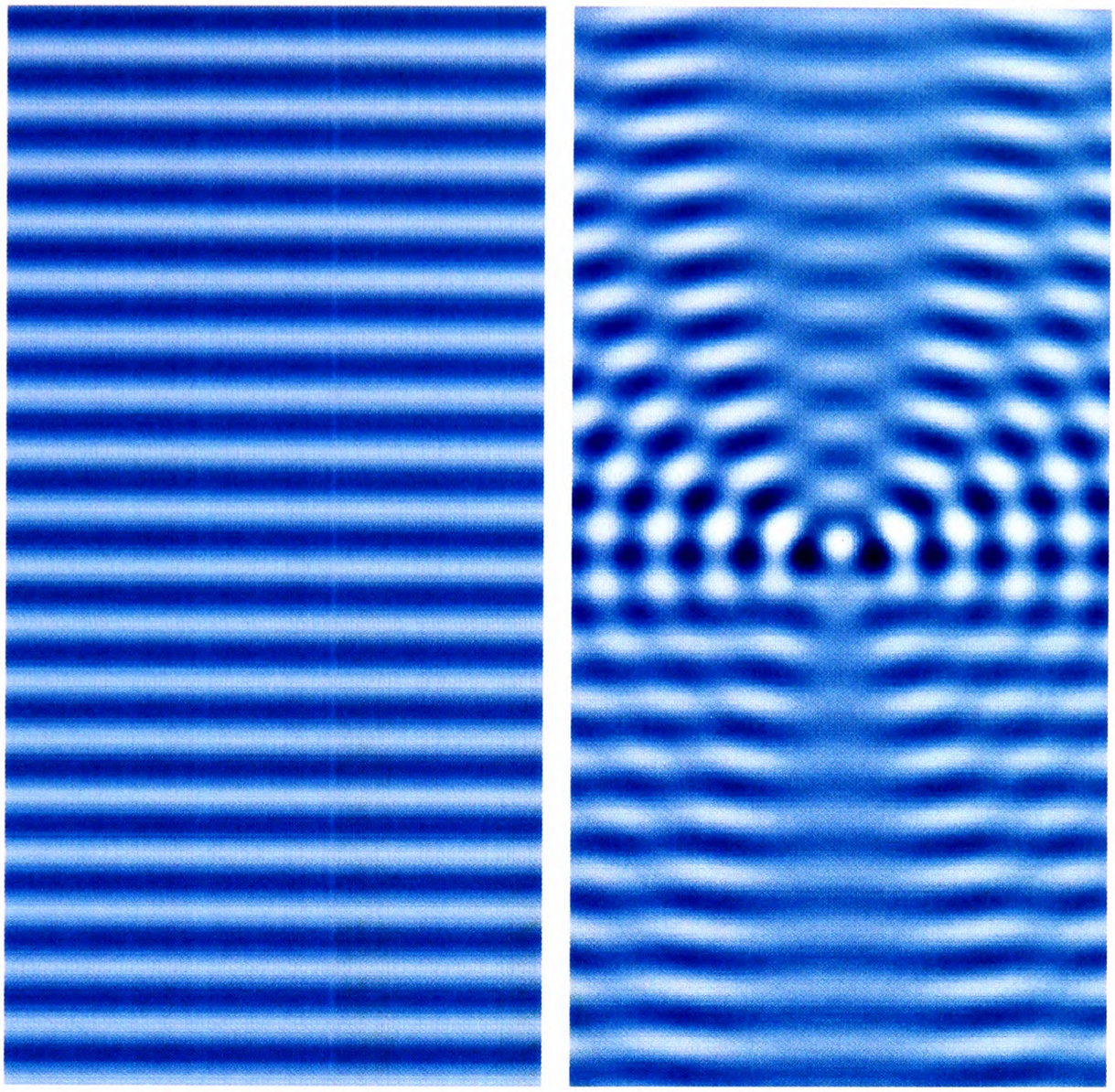

Figure 3.16: Longitudinal wave travelling downwards (left), and scattering of the longitudinal wave when the wave hits a very small object placed in its path (right). The scattering is indicated by the circular pattern developing against the incoming wave. (Source: Oleg Alexandrov, MATLAB)

Wave scattering phenomena have been well reviewed by many researchers, such as Kirchoff (1868), Rayleigh (1892), Epstein (1941), Biot (1956a, 1956b), Biot and Willis (1957) and Ogilvy (1987), using perturbation techniques for rough surfaces and irregularly shaped objects. The explanation of the scattering phenomena is usually based on the assumption that scattering on rough surfaces or with irregularly shaped objects can be derived from the scattering patterns of known shapes such as cylinders and spheres.

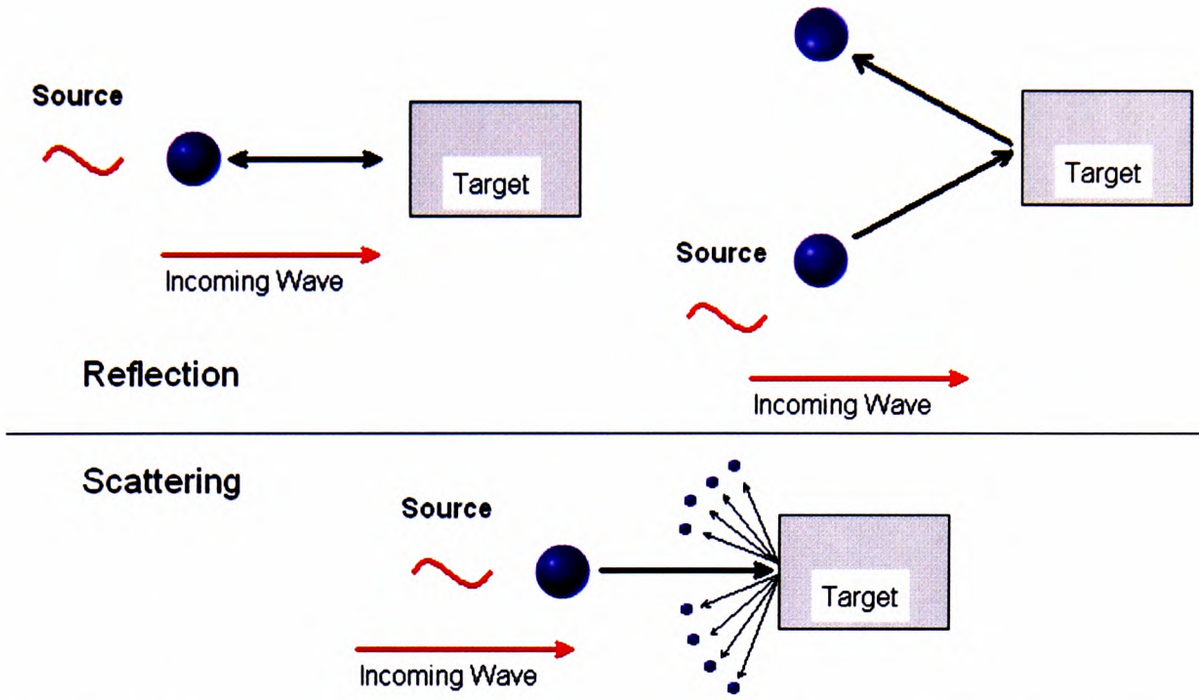

Figure 3.17: Illustration of reflection and scattering of wave, where a ball is used to represent the incoming wave.

Scattering theory is much more difficult to express in mathematical terms compared with reflection, because scattering theory of ultrasound waves is part of the study of quantum mechanics (i.e. particle–wave duality phenomena) – see Belkić (2003). In order to express the scattering theory in mathematical formulae, boundary conditions must be set (Trusler, 1991) and simplification of the scattering scenario will be needed (single scattering rather than multiple/successive scattering). Simplification is required because the use of a multiple-scattering scenario would normally require time-consuming repeated computer-simulated iterations in order to obtain a solution.

In general, most scattering theories have been derived from Hooke's elastic wave theory (Morse and Ingard, 1986).

To describe a simple model for scattering of ultrasound wave in an inhomogeneous medium by spherically shaped objects, we can consider that the medium has no absorption, with small changes in density (ρ) and compressibility (β). Thus, inside the sphere, at any radius (r):

$$\rho(r) = \rho_0 + \rho_1$$
$$\beta(r) = \beta_0 + \beta_1 \tag{3.4}$$

and outside the sphere:

$$\rho(r) = \rho_0$$
$$\beta(r) = \beta_0 \tag{3.5}$$

Hence, density and compressibility fraction can be expressed as:

$$\tilde{\rho}(r) = \frac{\rho_1(r)}{\rho_0}$$
$$\tilde{\beta}(r) = \frac{\beta_1(r)}{\beta_0} \tag{3.6}$$

The 'general wave equation' across the boundary (in one dimension, r, and time, t) is represented by:

$$\nabla^2\Phi(r,t) - \frac{1}{v^2}\frac{\partial^2\Phi(r,t)}{\partial t^2} = 0 \tag{3.7}$$

where ∇^2 is the Laplacian, v is the sound velocity in the medium and $v = \frac{1}{\sqrt{\rho_0\beta_0}}$.

But in the case of scattering, turbulence is usually present. Hence, Equation 3.7 is not equal to zero. Now, the equation has to include compressibility and density fraction in order to reach energy equilibrium (Morse and Ingard, 1986). Hence this would yield:

$$\nabla^2\Phi(r,t) - \frac{1}{v^2}\frac{\partial^2\Phi(r,t)}{\partial t^2} = \frac{1}{v^2}\frac{\partial^2\Phi(r,t)}{\partial t^2}\tilde{\beta}(r) + div\left[\tilde{\rho}(r)grad\Phi(r,t)\right] . \tag{3.8}$$

Applying Green's function method to Equation 3.8 by considering the right-hand side as the source term that behaves like a point source radiator (Morse and Feshbach, 1953; Morse and Ingard, 1986) would lead to the following solution:

$$\Phi(r,t) = \Phi_i(r,t) + \int_{-\infty}^{\infty} \partial t_0 \int_{volume} \left\{ \frac{1}{v^2} \frac{\partial^2 \Phi(r_0,t_0)}{\partial t^2} \tilde{\beta}(r_0) + div\left[\tilde{\rho}(r_0) grad\Phi(r_0,t_0)\right] G(r_0,r,t_0,t) \partial^3 r_0 \right\}, \quad (3.9)$$

where

$$G(r_0,r,t_0,t) = \frac{\delta\left(t - t_0 - \frac{|r-r_0|}{v}\right)}{4\pi|r-r_0|} . \quad (3.10)$$

δ is the additional density change.

For complex objects or a scattering problem in three dimensions, the Green's function in Equation 3.10 would have to include *x, y, z* and *t* terms. This leads to some difficulty in solving the integral equation in Equation 3.9 as all the variables (Φ, β, ρ) in Equation 3.9 would need to have *x, y, z* and *t* terms. Solving the integral equation in Equation 3.9 for simple objects can be done by using Born's approximation (Ballentine, 1998; Belkić, 2003; Scherrer, 2006) based on the assumption that scattering is weak and changes in density ($\tilde{\rho}$) and compressibility ($\tilde{\beta}$) are very small.

To achieve a realistic scattering solution for a material such as solder paste, it has to be assumed that multiple scattering is present and the change in density ($\tilde{\rho}$), compressibility ($\tilde{\beta}$) and viscosity (η) all have to be taken into consideration. A simple model for this, based on the experiment of various gases in Kundt's tube as proposed by Stokes (1845) will be described in Section 3.8.

3.5. Ultrasonic signal generation

Ultrasonic signals can be produced using a device called a signal generator (see Chapter 6, Figures 6.2 and 6.15). This device can usually generate a sine wave, a triangular wave or a square wave up to a few megahertz. There are two kinds of signal generator normally used for generating ultrasound signals: an analogue signal generator and a digital signal generator. The difference between the two wave generators is that the signal generated by an analogue signal generator is composed of random distortions (see Figure 3.18) in contrast with smooth waveform pattern of the digital signal generator (see Figure 3.19). The signal resolutions, i.e. the signal width in x and y axes, of a digital signal can be adjusted by creating a shorter 0 (zero) or 1 (one) pulse; however, this is usually limited by the hardware capability. A modern digital signal generator can usually be programmed to generate any wave form at a continuous, pulsed or random time interval. Unlike analogue signal generators, digital signal generators are capable of repeating a single cycle or several cycles of signal at any frequency intermittently for any duration or for as brief a period as a few nanoseconds. This intermittent short pulse is called a 'tone burst' (see Figure 3.20). This technique allows the signal generator to send only one cycle or a few cycles of, say, 500 cycles at 500kHz rather than the full 500 cycles at 500kHz, thus allowing the recording of high-frequency signals at reduced interference due to the echoes.

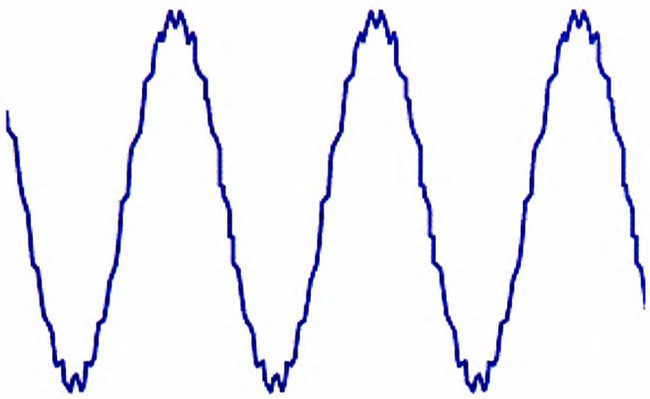

Figure 3.18: Illustration of analogue signal of sinusoidal wave.

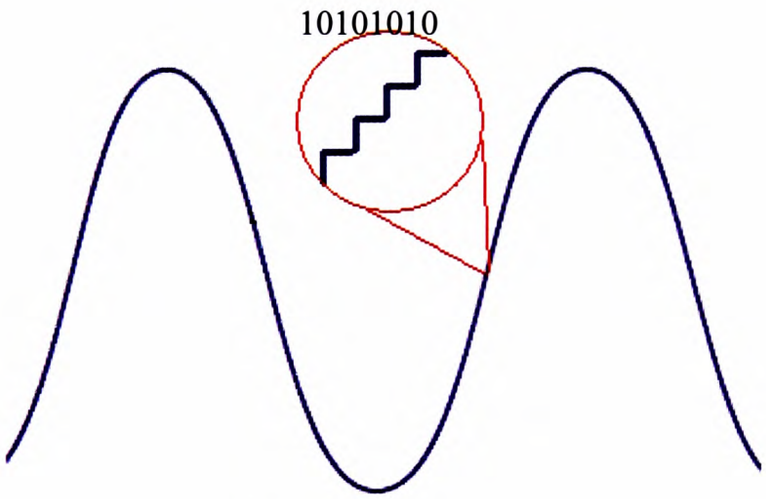

Figure 3.19: Illustration of digital signal of sinusoidal wave.

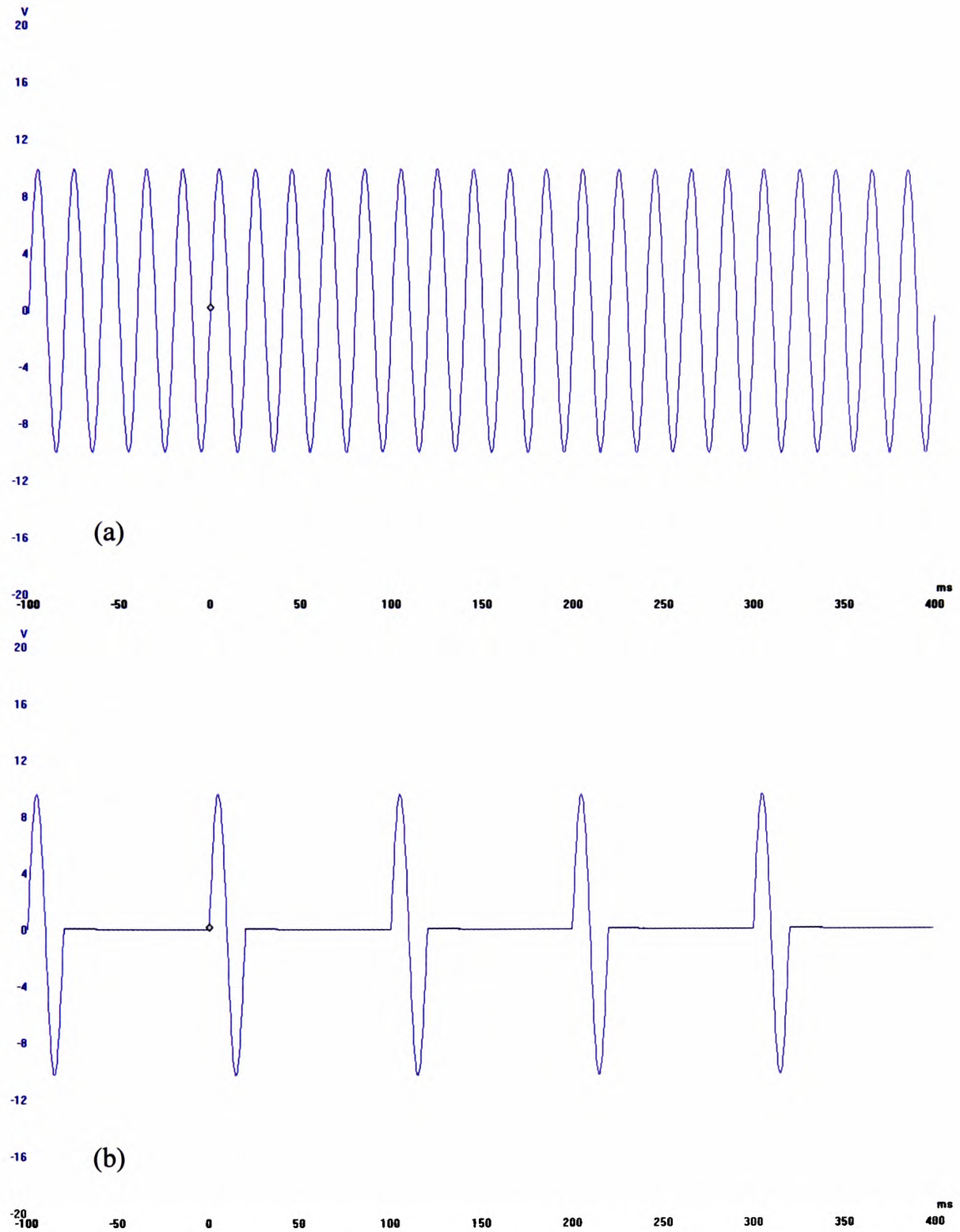

Figure 3.20: Illustration of (a) normal and (b) tone-burst signal of a 50Hz sinusoidal wave.

3.6. Ultrasonic transducers: materials and construction

There are two types of ultrasonic transducer commonly used for non-destructive testing, namely the 'transverse/shear wave' transducer and the 'longitudinal wave' transducer – see Figure 3.21. Most ultrasonic transducers can be used either as a receiver or a transmitter unit for receiving or transmitting ultrasonic sound waves. For very attenuating materials or for very thick objects, the longitudinal wave transducer is preferred to the shear wave transducer because the shear wave generated by the latter type of transducer can only penetrate a few millimetres into the surface of the object being tested. For this reason, shear wave transducers are often referred to as 'surface wave' transducers. Both shear wave and longitudinal wave transducers can be configured for use as 'normal beam' or 'angle beam' measurement configurations. The normal beam configuration is used when full-depth penetration of the test object is required, whereas an angle beam configuration is normally used for detecting flaws in thin objects. Although the angle beam configuration shown in Figure 3.22 has a reduced penetration depth, it has the advantage of being able to measure Young's modulus (Young 1807 and 1821), the Poisson ratio (Poisson 1833) and the shear modulus simultaneously. This is due to the presence of the longitudinal and refracted shear wave generated by the angle beam configuration.

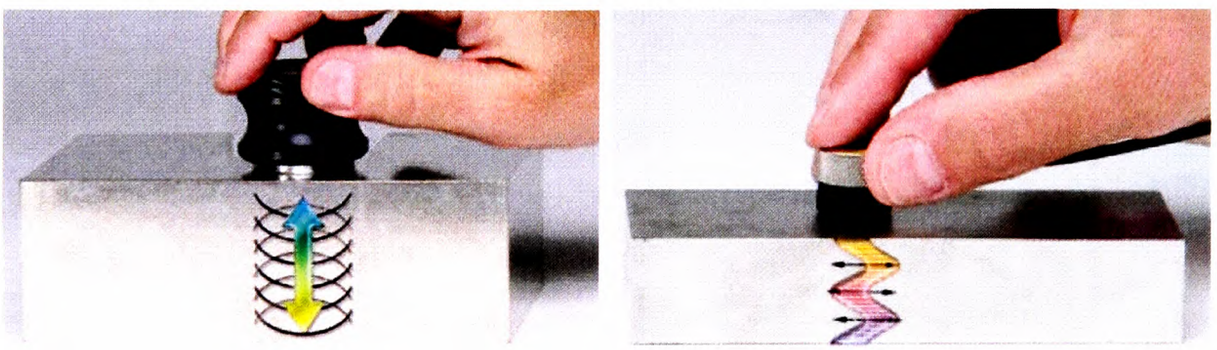

Figure 3.21: Illustration of wave propagation on a stainless steel block using a longitudinal wave transducer (left) and a shear wave transducer (right). (Photo courtesy of Olympus NDT)

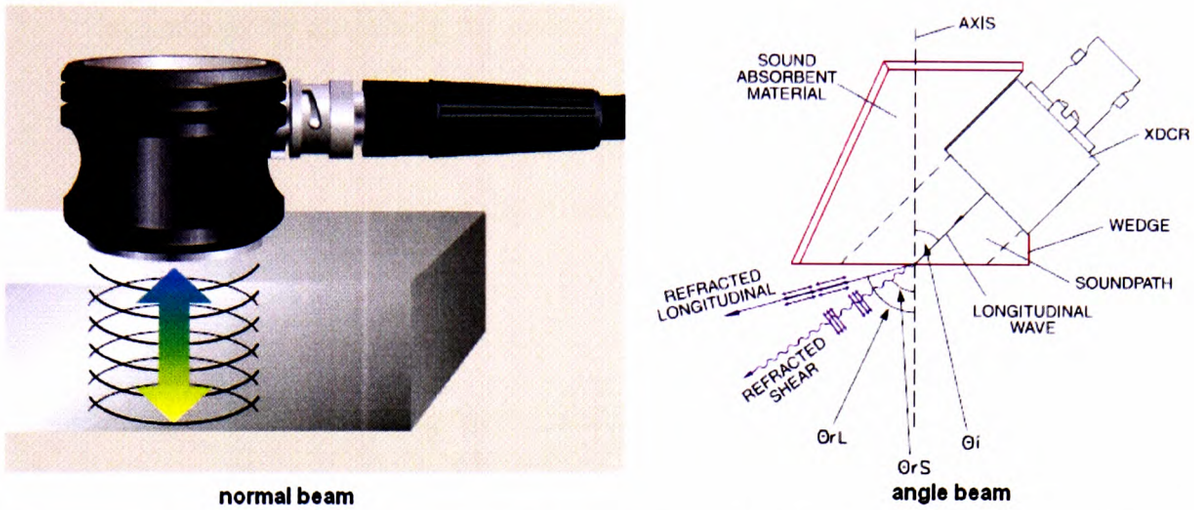

Figure 3.22: Normal beam and angle beam configuration ultrasonic techniques. (Photo courtesy of Olympus NDT)

An ultrasound transducer usually consists of several main parts, as shown on Figure 3.23 and as set out next:

- **Wear plate that directly contacts the surface of the object of investigation.** The wear plate is designed to provide a good acoustic impedance matching with many materials. However, a thin layer of coupling material such as silicone oil is usually needed to provide a good acoustic impedance at very high frequencies since high-frequency sound waves do not propagate very well in air. To protect the wear plate from damage, a replaceable wear plate attachment made out of nylon, epoxy or membrane can be fitted to protect the wear plate surface.
- **Electrodes.** The electrodes are used to provide electrical contact for generating potential difference between the top and the bottom part of the piezoelectric element.
- **Piezoelectric element.** The piezoelectric element (sometimes called the ferroelectric element) converts electrical energy from an excitation pulse to mechanical energy in the form of an ultrasound wave. The effect is usually reversible. A piezoelectric element is usually made from polarized ceramics such as lead zirconate titanate, barium titanate, potassium niobate, quartz or Rochelle salt.
- **Backing material.** The backing material is usually made from a highly attenuative high-density material used to control the vibration of the

transducer by absorbing the energy released from the piezoelectric element. A correctly matched acoustic impedance of the backing material and the piezoelectric element results in a heavily damped transducer that gives good resolution range but lower signal amplitude.

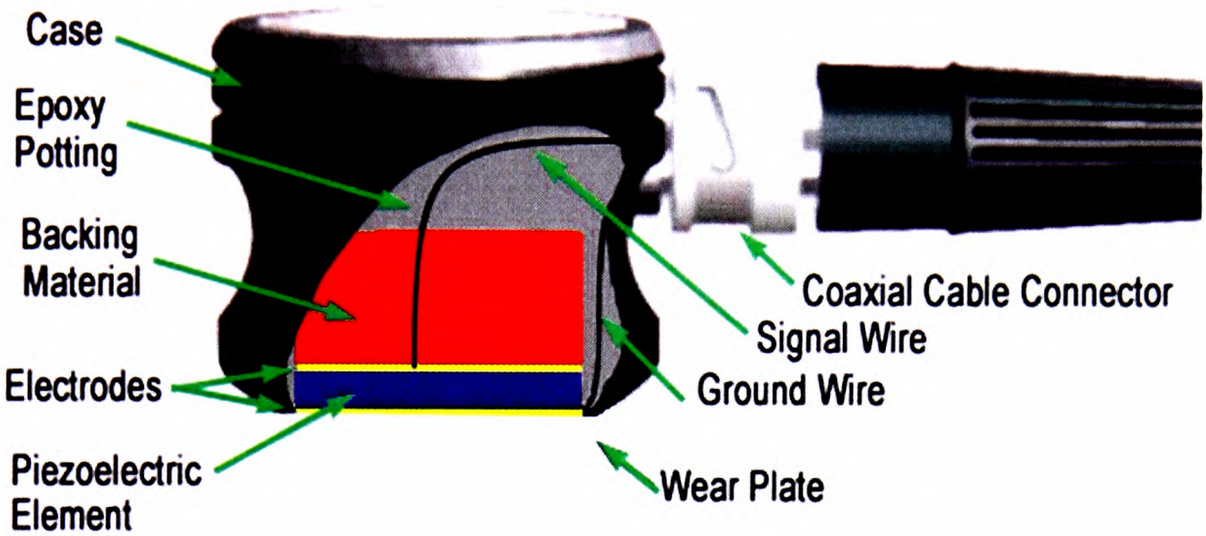

Figure 3.23: Internal construction of an ultrasound transducer.

Some manufacturers of ultrasonic sensors also provide specialist transducers, such as the:

- electromagnetic acoustic transducer (EMAT);
- dual-element transducer (in which one element is always used for transmitting the signal and the other element is always used for receiving) – see Figure 3.24; and
- immersion transducer – see Figure 3.25.

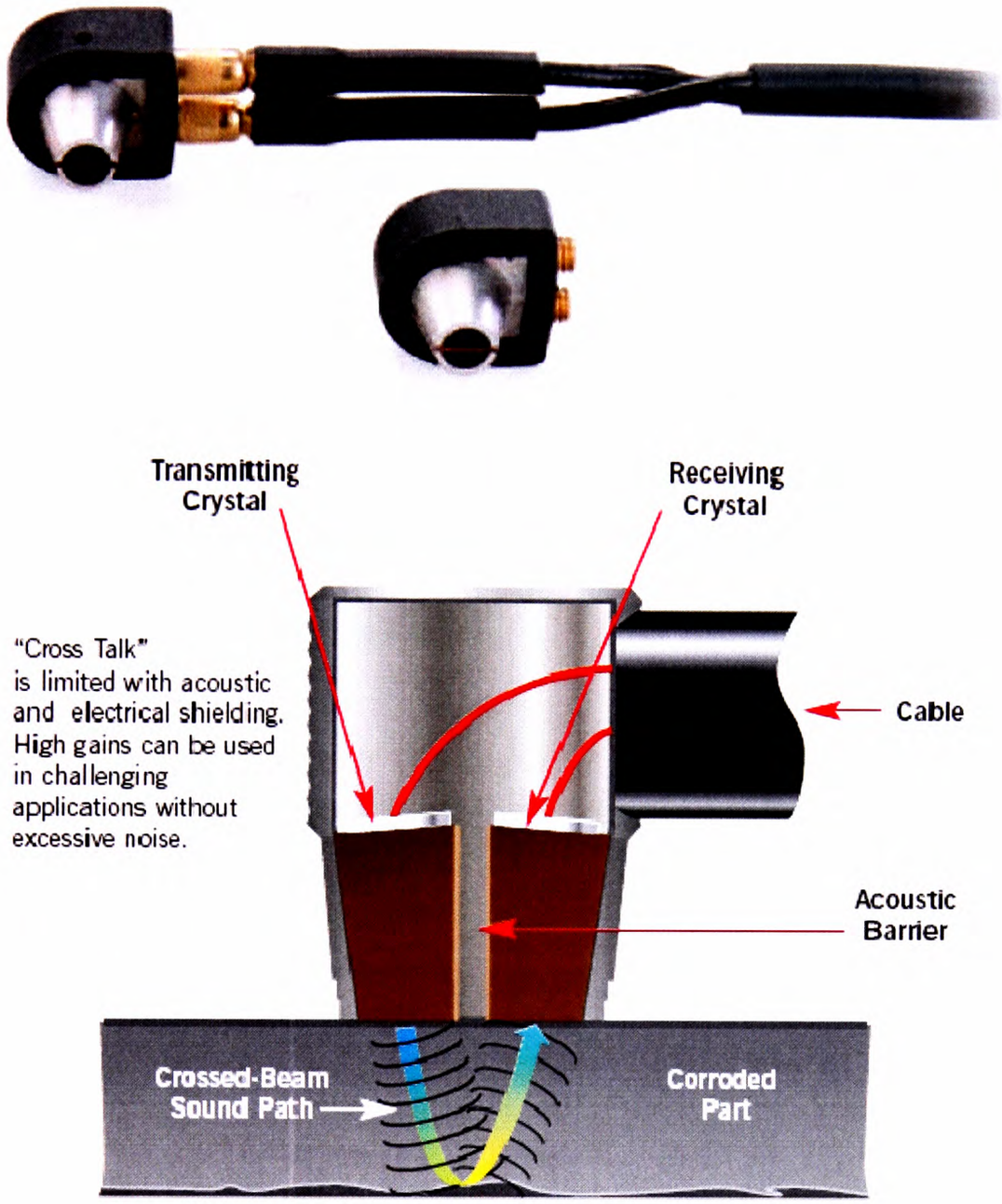

Figure 3.24: Dual-element ultrasonic transducer. (Photo courtesy of Olympus NDT)

Figure 3.25: Immersion ultrasonic transducers. (Photo courtesy of Olympus NDT)

3.7. Ultrasonic modes of detection

There are several modes of ultrasonic detection (see Figure 3.26). Some of these scanning modes would require more than two transducers (i.e. an array) in order to achieve the scanning results illustrated in Figure 3.26. However, they can generally be categorised into two main groups: pulse echo (PE) transmission and through transmission (TT).

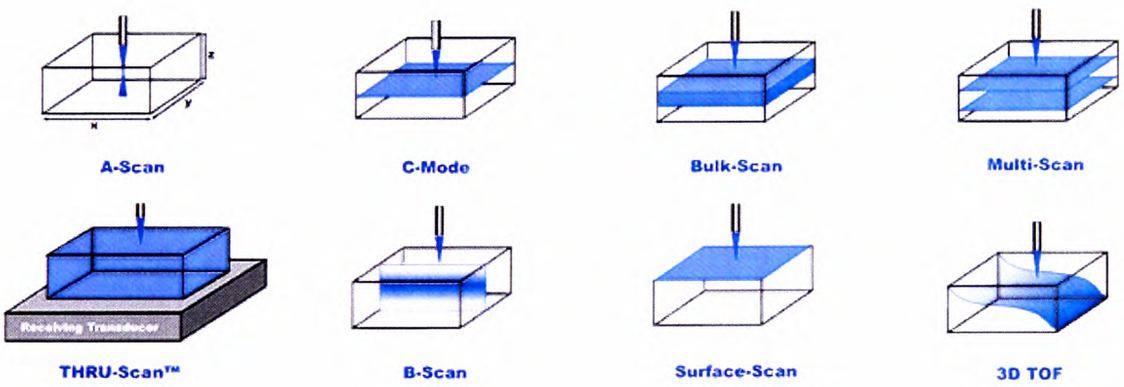

Figure 3.26: Ultrasonic modes of detection. (Diagram courtesy of Sonoscan.com)

3.7.1. Pulse echo (PE) transmission

In PE transmission mode, only 1 ultrasound transducer is needed to transmit the pulse and receive the echo signal. The set-up for typical pulse-echo mode transmission is shown in Figure 3.27. As the name suggests, the pulse echo mode set-up uses the same unit of equipment to generate a pulse and also to listen at the same time for the echo from a single ultrasound transducer; this equipment is usually called a 'pulser-receiver'. Even though many have argued that the pulse echo technique is more reliable than the through transmission, there are three main disadvantages to using the pulse echo technique:

- Delay-time correction or calibration. The pulser-receiver unit has to generate a sinusoidal wave and also receive the echo signal from the transducer in a fraction of a microsecond. In practice, the pulser-receiver has to send the signal to the transducer, stop sending the signal and quickly switch to receiving mode to listen for the echo. Because of this, any such system automatically inherits a flaw of a delay time of a few microseconds, which if uncorrected will cause unreliable readings, especially for ultrasound velocity measurement of material. Apart from that, the calibration process to correct the delay time is not straightforward, as it would require a calibration against several calibrated metal standards of different thickness or by calibrating it against water at several path lengths. The following formula can be used to calculate the delay time based on the knowledge that ultrasound velocity through the same medium remains constant with the change in the distance of the travelling path of the ultrasound wave:

$$\frac{S_2}{S_1} = \frac{t_2 - \Delta t}{t_1 - \Delta t}, \tag{3.11}$$

where

S_1, S_2 are the path lengths at position 1 and position 2,

t_1, t_2 are the times required to travel the distances S_1 and S_2 respectively, and

Δt is the delay time of the pulser-receiver unit.

- Missing data. As previously mentioned, the pulser-receiver has to continuously switch from pulser mode to receiver mode, and this also causes a significant loss of data if the receiver has not listened long enough to gather all the required data to regenerate the complete echo signal. Since the material to be investigated is usually of unknown ultrasound velocity, it is very difficult to programme the pulser-receiver to listen long enough to obtain a complete echo waveform even with a guessing method.
- Overlapping signals. In use of the pulse echo technique, the signal of consecutive echoes might interfere with an incoming pulse. This in effect will either cause a destructive or constructive interference of ultrasound signal, which can alter the amplitude of the signal.

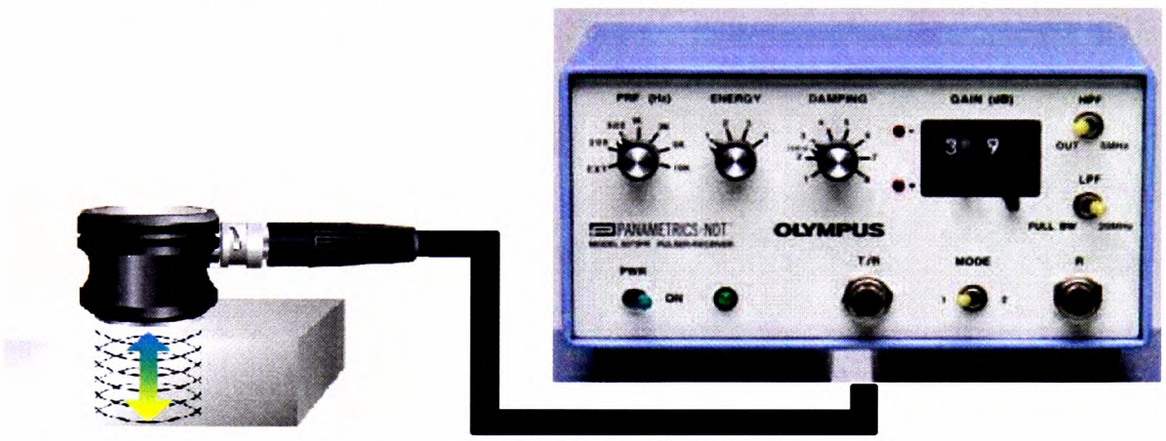

Figure 3.27: Pulse echo set-up with a combined pulser-receiver unit. (Photo courtesy of Olympus NDT)

The use of a dual-element transducer for pulse echo mode would improve the measurement as it could reduce the possibility of overlapping signals in the transducer since the incoming and returning signal would be delivered on separate cables, but this does not solve the problem of the overlapping signal in the material under investigation.

3.7.2. Through transmission (TT)

In through transmission (TT) mode (see Figure 3.28), a pair of ultrasound transducers is normally used – one as a transmitter and the other as a receiver. This is because the measurement is not taken by comparing the echo signals, but rather by comparison of

the original signal with the transmitted signal. Therefore, there is no problem of echo signal interference with the incoming signal, as the measurement is not based on the echo signal. Earlier TT mode techniques used a pulser-receiver unit to generate and receive signals, but the disadvantages of using a pulser-receiver far outweighs their merits, as mentioned in Section 3.7.1. Hence, most of the TT mode equipment now uses a dedicated signal generator to generate ultrasonic signals and a separate multichannel analogue-to-digital converter (ADC) to receive the reference signal from the signal generator and the output signal from the receiver-transducer. Because of the shorter wave path, the TT mode is ideal for measuring very attenuating material, as the wave only needs to travel once through the material.

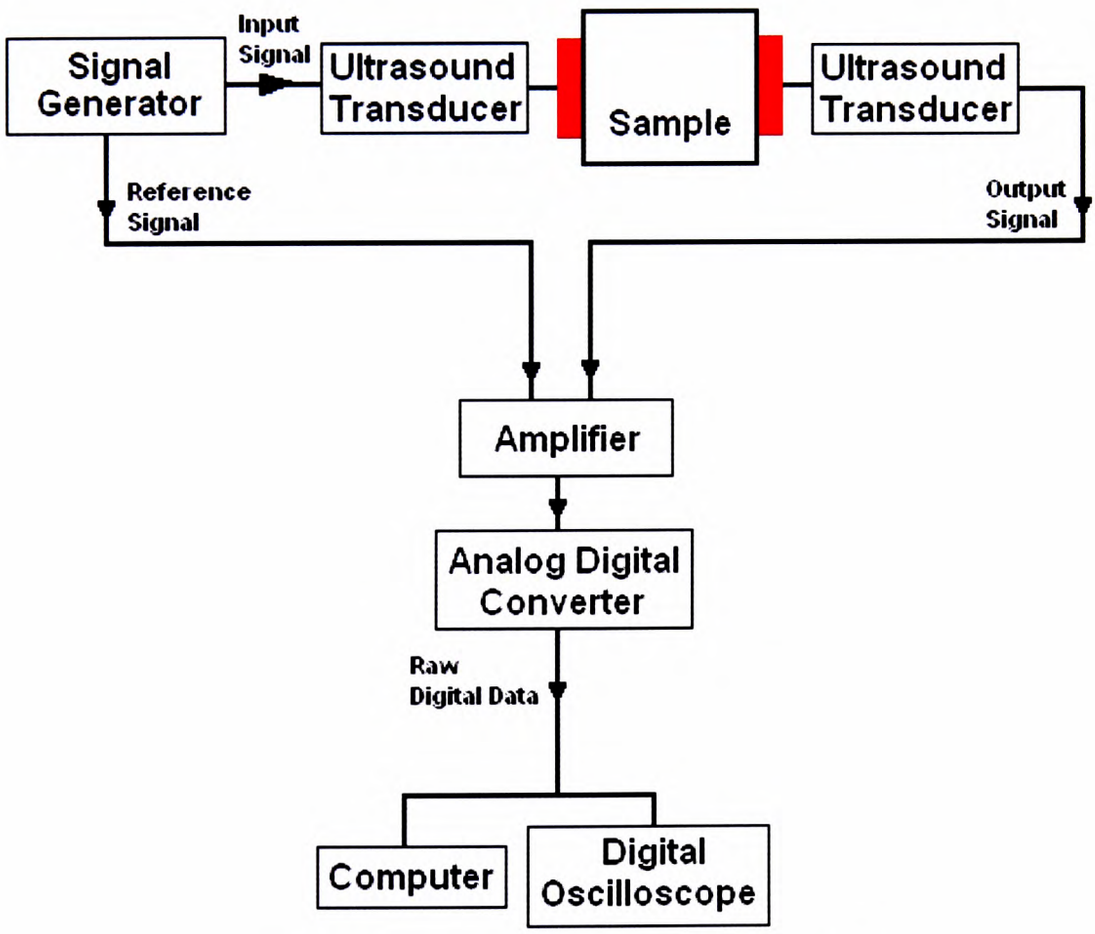

Figure 3.28: Through transmission mode set-up.

3.8. Measureable ultrasound parameters

There are several measurable ultrasound parameters typically used for non-destructive testing: attenuation, velocity, phase shift and acoustic impedance. These parameters are dependent on the specific material's properties, such as the material's physical and chemical structure, and can be correlated to the density, viscosity, Young's modulus and shear modulus of the material. Each parameter is described further next.

3.8.1. Attenuation

'Attenuation' is defined as the reduction of the amplitude of an ultrasound signal due to a scattering and absorption mechanism.

Attenuation of sound due to the effect of viscosity, density and compressibility can be described by the formula proposed by Stokes (1845, 1847). According to Stokes (1845), the friction force in one direction can be described by:

$$\frac{\partial^2 u}{\partial t^2} - a^2 \frac{\partial^2 u}{\partial x^2} - \frac{4\eta}{3\rho_0} \frac{\partial^3 u}{\partial x^2 \partial t} = 0 \tag{3.14}$$

where $a^2 = \frac{\partial P}{\partial \rho}$, a is the common velocity due to pressure (∂P) and density ($\partial \rho$).

Now suppose that a harmonic wave of wavelength λ maintained at the origin ($x = 0$) fades away as x increases. Assuming that the velocity u (in x direction) varies as a function of e^{int} then:

$$u = Ae^{-\alpha x}\cos(nt - \beta x), \tag{3.15}$$

where

$$\beta^2 - \alpha^2 = \frac{n^2 a^2}{a^4 + \frac{16\eta^2 n^2}{9\rho_0^2}}, \qquad 2\alpha\beta = \frac{\frac{4\eta n^3}{3\rho_0}}{a^4 + \frac{16\eta^2 n^2}{9\rho_0^2}} \tag{3.16}$$

In the application of these formulae to air at ordinary pressure, viscosity (η) may be considered to be a very small quantity; hence its square may be neglected. Therefore:

$$\beta = \frac{n}{a}, \qquad \alpha = \frac{2\eta n^2}{3\rho_0 a^3} . \tag{3.17}$$

If angular frequency, n, is replaced by $2\pi a\lambda^{-1}$, then the formula for attenuation α can be written as:

$$\alpha = \frac{8\pi^2\eta}{3\lambda^2\rho_0 a} . \tag{3.18}$$

Attenuation is normally expressed as an amplitude fraction $A(\omega)$ of the source signal $A_0(\omega)$ and returned signal $A_1(\omega)$. Most of the published works on non-destructive testing of ultrasound attenuation are usually reported in nepers per metre (Neper/m), although there are some that are reported in decibels per metre (dB/m). Amplitude fraction can then be expressed as:

$$A(\omega) = \frac{1}{L} 20\log_{10}\left|\frac{A_0(\omega)}{A_1(\omega)}\right| dB/m = \frac{1}{L}\ln\left|\frac{A_0(\omega)}{A_1(\omega)}\right| Neper/m . \tag{3.19}$$

A conversion table for certain values is given in Table 3.1 below.

Amplitude ratio	Decibel (dB)	Neper
1.41	3	0.345
2	6	0.691
3.16	10	1.151
10	20	2.302
31.6	30	3.454
10000	80	9.210

Table 3.1: Conversion table for amplitude ratio.

3.8.2. Velocity

Ultrasound velocities (shear and longitudinal) can be measured independently using an appropriate transducer. A shear wave transducer must be used to obtain shear

velocity; and as a shear wave cannot penetrate liquid materials, most of the non-destructive tests are done by utilising longitudinal waves.

Longitudinal velocity and shear velocity of homogenous isotropic materials can be derived from elasticity theory. An isotropic material usually has 36 elastic constants that form a six-by-six matrix. The elastic matrix can be described by:

$$\begin{bmatrix} T_1 \\ T_2 \\ T_3 \\ T_4 \\ T_5 \\ T_6 \end{bmatrix} = \begin{bmatrix} \lambda+2\mu & \lambda & \lambda & 0 & 0 & 0 \\ \lambda & \lambda+2\mu & \lambda & 0 & 0 & 0 \\ \lambda & \lambda & \lambda+2\mu & 0 & 0 & 0 \\ 0 & 0 & 0 & \mu & 0 & 0 \\ 0 & 0 & 0 & 0 & \mu & 0 \\ 0 & 0 & 0 & 0 & 0 & \mu \end{bmatrix} \begin{bmatrix} S_1 \\ S_2 \\ S_3 \\ S_4 \\ S_5 \\ S_6 \end{bmatrix} \tag{3.20}$$

where μ and λ are Lamé constants, and T and S respectively are stress and strain tensors.

Ignoring whole-body forces such as gravity, the equation of motion in vector form can be obtained by applying Newton's second law and conservation of mass to the elemental volume that gives (Auld, 1973):

$$\rho \frac{\partial^2 \boldsymbol{X}}{\partial t^2} = \nabla T \ . \tag{3.21}$$

where $\boldsymbol{X}$ is the displacement.

For small stresses in an isotropic elastic material, the displacement $\boldsymbol{X}$ is linearly related to the stress according to Hooke's law (1678) in the following relationship:

$$T = \lambda I \nabla \bullet \boldsymbol{X} + \mu(\nabla \boldsymbol{X} + \boldsymbol{X} \nabla) \ , \tag{3.22}$$

where I is the identity matrix.

Substituting Equation 3.22 into Equation 3.21 gives:

$$\rho \frac{\partial^2 \boldsymbol{X}}{\partial t^2} = (\lambda+2\mu)\nabla(\nabla \bullet \boldsymbol{X}) + \mu \nabla \times (\nabla \times \boldsymbol{X}) \ . \tag{3.23}$$

Using the Helmholtz decomposition, the vector $\boldsymbol{X}$ can be written in terms of a scalar potential, φ, and a vector potential, $\boldsymbol{A}$, as:

$$\boldsymbol{X} = \nabla\varphi + \nabla \times \boldsymbol{A} \tag{3.24}$$

Substituting Equation 3.24 into Equation 3.23 gives:

$$\nabla\left[\rho\frac{\partial^2\varphi}{\partial t^2} - (\lambda+2\mu)\nabla^2\varphi\right] + \nabla\times\left[\rho\frac{\partial^2 A}{\partial t^2} - \mu\nabla^2 A\right] = 0 \ , \tag{3.25}$$

where ∇^2 is the Laplacian. Hence, the scalar and vector potential parts can be separated to obtain longitudinal and shear velocities which can be written as:

$$\frac{\partial^2\varphi}{\partial t^2} = c_l{}^2\nabla^2\varphi \qquad \text{and} \qquad \frac{\partial^2 A}{\partial t^2} = c_s{}^2\nabla^2 A \ , \tag{3.26}$$

where c_l and c_s are respectively the longitudinal and shear velocities given by:

$$c_l = \sqrt{\frac{\lambda+2\mu}{\rho}} \qquad \text{and} \qquad c_s = \sqrt{\frac{\mu}{\rho}} \ . \tag{3.27}$$

The longitudinal velocity and the shear velocity have been found to be directly related to the Young's modulus of the material in question and its shear modulus based on the following correlation:

$$E = \frac{\mu(3\lambda+2\mu)}{\lambda+\mu} \qquad \text{and} \qquad \upsilon = \frac{\lambda}{2(\lambda+\mu)} \ . \tag{3.28}$$

where υ is the Poisson's ratio, and E is the Young's modulus of elasticity.

Hence, it is often found that longitudinal velocity and shear velocity are also written as:

$$c_l = \sqrt{\frac{\lambda+2\mu}{\rho}} = \sqrt{\frac{E}{\rho}\frac{1-\upsilon}{(1+\upsilon)(1-2\upsilon)}} \quad \text{and} \quad c_s = \sqrt{\frac{\mu}{\rho}} = \sqrt{\frac{E}{\rho}\frac{1}{2(1+\upsilon)}} = \sqrt{\frac{G}{\rho}} \ , \tag{3.29}$$

where υ is the Poisson's ratio, E is the Young's modulus of elasticity, and G is the shear modulus.

Note: Poisson's ratio for most solids and semi-solids are around 0.1 to 0.45. Hence, $\frac{1-\upsilon}{(1+\upsilon)(1-2\upsilon)}$ is close to 1. Therefore, $c_l \approx \sqrt{\frac{E}{\rho}}$

These formulas have been used to determine the longitudinal velocity and shear velocity of many solid and liquid materials. The longitudinal velocity, used in conjunction with the shear velocity, has been widely used in the industry to obtain the Young's modulus of solid materials e.g. metals. The use of shear wave is limited to solids only as shear wave cannot travel through liquids.

3.8.3. Phase shift

Ultrasonic phase shift occurs as a result of the effect of the attenuation process on the incoming signal. Because of the phase shift, even though the frequency remains the same, the return signal can either be out of phase slightly or sometimes 180° out of phase (see Figure 3.29). Phase shift is one of the least used parameters in non-destructive testing of materials.

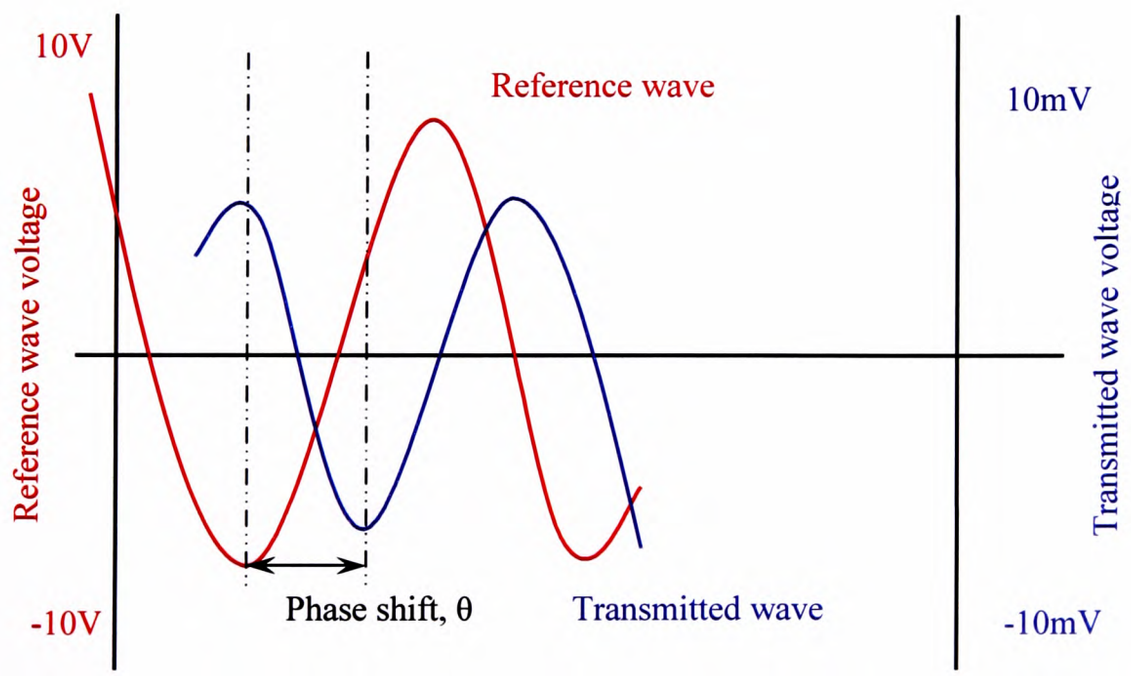

Figure 3.29: Illustration of phase shift.

3.8.4. Acoustic impedance

Acoustic impedance is usually measured using longitudinal waves, due to the limitation of a shear wave to propagate through liquid and gaseous materials. Acoustic impedance can be expressed as:

$$Z = \rho \cdot c_l \ , \tag{3.30}$$

where Z is the acoustic impedance (in units of [M L^{-2} T^{-1}]; Pa.s/m), ρ is the density (in [M L^{-3}]; kg/m^3), and c_l is the longitudinal velocity (in [L T^{-1}]; m/s).

Acoustic impedance is normally used to determine the amount of the signal that has been reflected and absorbed at the boundary of two different materials – see Figure 3.30. The power fraction of reflected (R) and transmitted (T) signal can be calculated using the following formulae (Auld, 1973):

$$R = \left[\frac{Z_2 - Z_1}{Z_2 + Z_1}\right]^2 \qquad \text{and} \qquad T = 1 - \left[\frac{Z_2 - Z_1}{Z_2 + Z_1}\right]^2 \tag{3.31}$$

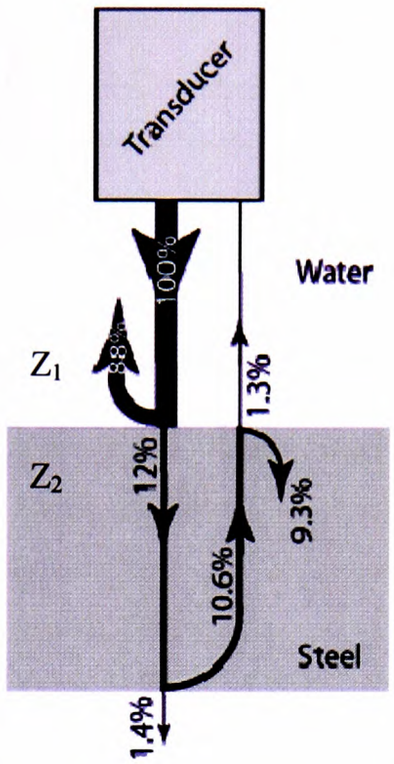

Figure 3.30: Representation of reflection and transmission of ultrasound wave at the boundary of two materials. (Auld, 1973)

3.9. Literature review of ultrasound applications

George Gabriel Stokes (1845), a Cambridge mathematician and physicist, is thought to be the first person to document his observations of sound absorption in relation to the viscosity of fluids. His work on dissipation of sound energy in viscous fluids (primarily gases) was later refined by Kirchoff (1868). Kirchoff postulated that the vibration of a sound wave momentarily creates heated regions in the fluid medium, which is responsible to the dissipation of sound energy. The combination of Stokes's and Kirchoff's theories (Stokes 1880-1905) of sound absorption due to viscosity is purely based on mathematical modelling from analytical deduction thinking. No experimental work to measure viscosity of fluids was carried out at that time due to limited techniques and equipment. However, it should be noted that most of the work done was accurate enough even though most of the experimental work was carried out in Kundt's tube (Kundt 1866,1868; Rayleigh 1876, 1884) using various kinds of gases and was as crude in form as striking a bell under water in Lake Geneva (Colladon and Sturm, 1872). Other significant findings prior to Stokes include the work of von Guericke (1672), in which he demonstrated that sound does not propagate in a

vacuum, a finding that was also reported by Boyle (1660). In the very same year (1660) Viviani and Boreli successfully measured the speed of sound in air (Boschiero, 2005). This finding led Euler (1757a; 1757b, 1761; 1765) and Poisson (1808, 1818) to model the appropriate equations and to provide an exact solution to describe the propagation of finite-amplitude waves. Soon after that, Laplace (1816) proposed a model to calculate the speed of sound in a gas at adiabatic conditions.

Later, Lord Rayleigh (1878) made a major breakthrough by introducing the concept of acoustic scattering in viscous fluids, using a sphere suspended in a non-viscous fluid. Lord Rayleigh laid the foundation for work in acoustics when he published *The Theory of Sound*, a two-volume book on various aspects of sound. Rayleigh's theories were later confirmed by Duff (1898), Altberg (1907) and Neklepajew (1911) through experimental observations that viscosity itself would not contribute to such a high loss of sound energy. Duff suggested that materials that exhibit a sound-attenuating nature, such as air, should be assigned a constant of radiation in order to know how attenuative the given material is compared with other materials.

Cady (1920) discovered that quartz crystals can be used as a stable electromechanical oscillators. The study of ultrasound achieved another milestone when Landau and Rumer (1937) were able to explain that the attenuation of ultrasonic waves in solids was due to the interaction with vibration of phonons in a rigid crystal lattice, such as the atomic lattice of a solid. A similar concept of ultrasound attenuation in liquids was then proposed by Kneser (1938). Biquard and Ahier (1943) developed the pulse echo technique for measuring ultrasound properties in liquids, which led to the finding that ultrasound can cause light diffraction. Pinkerton (1949) used the same technique and documented ultrasonic absorption in various liquids.

During the first decade of 1900, most of the work in the field of ultrasound was focussed on the study of absorption in suspensions or of scattering due to small spherical particles, aspects originating from Rayleigh's concept of acoustic scattering by small particles. Because of the limitation of the equipment capable of measuring high levels of attenuation in viscous fluids with suspended particles, Sewell (1910) continued the challenge by conducting similar experiments using heavy particles suspended in a gas, which produced lower levels of attenuation. The aim was to

demonstrate the scattering process of ultrasound due to small particles as proposed by Rayleigh. Later, Lamb (1945) simplified Sewell's acoustic scattering model by studying sound scattering using mobile particles. The theory was then refined by Epstein (1941) by considering a mobile rigid sphere, or an elastic solid or a viscous fluid, as the spherical object that was suspended in the viscous fluid.

Urick (1948) and Stakukis *et al* (1955) independently conducted experiments in aqueous suspensions and reported that the high level of ultrasonic absorption in aqueous suspensions was due to the viscous drag from the movement of particles with respect to the continuous phase. Isakovich (1948) pointed out that these movements may be the cause of a significant temperature gradient between the particles and the continuous phase even when the test was conducted in adiabatic conditions. In 1953, Epstein and Carhart refined scattering theory by introducing the concept that ultrasound dissipates the sound energy to thermal energy internally and externally to the suspended sphere. This concept is still widely used today to predict sound absorption in atmospheric fogs. However, the concept is not applicable to solid particulate suspensions. With regard to the latter, Biot (1956a, 1956b, 1957) postulated a theory for sound scattering in porous elastic solids saturated in a viscous fluid. The theory accounts for average motion of both solid and fluid parts through a macroscopic energy balance of which each part has a contribution towards the average bulk modulus. Because of the unique ultrasonic response of materials tested at various frequencies, Krautkramer (1959) suggested the use of wide-bandwidth ultrasonic frequency experiments to yield more information from a test sample.

From 1960 to 1970, most of the major developments of ultrasound techniques were focussed on the medical field, leading to the stable and reliable use of ultrasound for non-destructive imaging purpose in hospitals up to the present day. Hunter and Derdul (1967) attempted to correlate the dynamic viscosity of long-chain polymers to acoustic absorption as a function of temperature and molecular weight. Later, in 1972, Allegra and Hawley set out to refine the Epstein–Carhart model to include both solid and liquid particulates in suspension (see Figure 3.31). Their theory is verified by experimental works performed in both solid and liquid particulates in suspension.

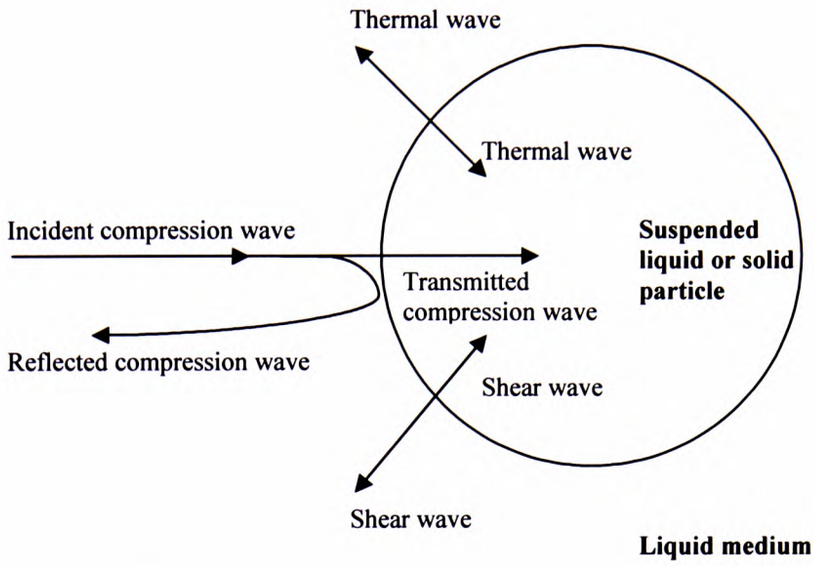

Figure 3.31: Representation of Allegra and Hawley model of ultrasonic wave scattering.

In 1978, Ince reported the temperature dependence of ultrasound on the velocity and attenuation of biological materials such as blood and fatty tissue. Ince found that ultrasound velocity increases according to the increase in temperature, based on the relationship that $V = V_0(1 + \alpha\Delta T)$, where V_0 is the ultrasound velocity at 0°C, α is the attenuation coefficient and ΔT is the change in temperature.

The first patent for a practical ultrasound application for cement paste was probably filed by Rao and Sutton (1981). In the patent, Rao describes the use of the through transmission technique to measure the compressive strength of cement paste in a controlled temperature and pressure environment (see Figures 3.32 and 3.33). It was reported that the transit time of the ultrasound through the cement paste is directly related to the compressive strength of the cured cement paste.

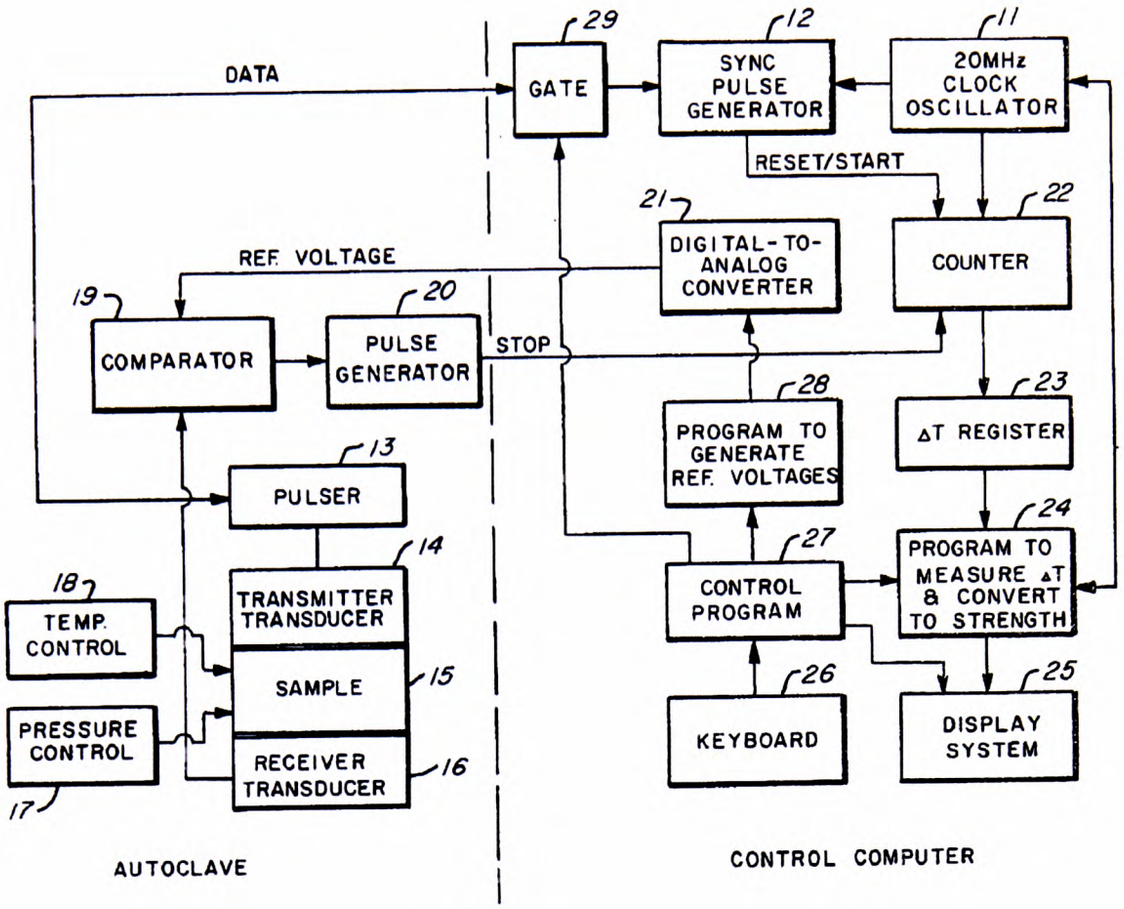

Figure 3.32: Ultrasonic set-up schematic diagram for measuring the compressive strength of cement paste. (Rao and Sutton, 1981)

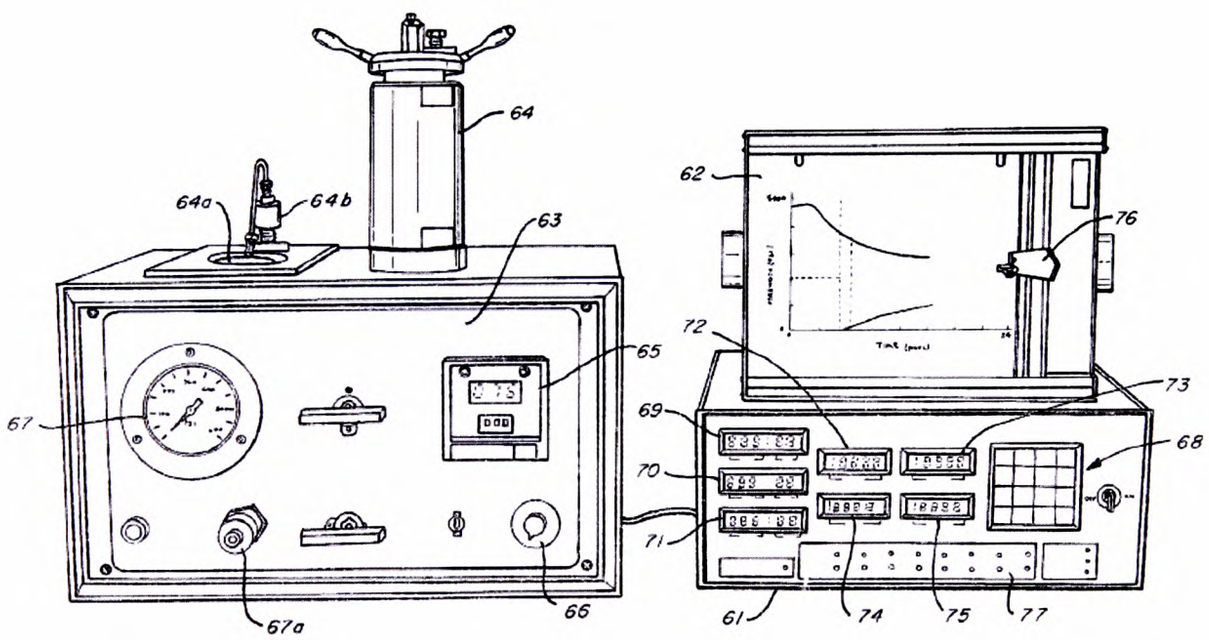

Figure 3.33: Ultrasonic system, showing controlled pressure and temperature autoclave chamber on the left. The pulse generator, digital-to-analogue converter, and graph plotter are shown on the right. (Rao and Sutton, 1981)

Later in 1982, Pereira investigated ultrasound attenuation and velocity in aqueous solutions and reported the temperature dependence of ultrasound attenuation. To monitor changes in the material, the adiabatic compressibility of the material derived from the ultrasonic velocity and density measurement were used. Sidkey and Abd El Aal (1986) conducted a study of the dynamic behaviour of macromolecules of polyisoprene rubber under the action of elastic strain and reported the results of ultrasonic absorption with regard to the flexibility of the polymer chain. Brown (1988) later continued the work done by Pereira and came to the conclusion that the ultrasonic attenuation is probably caused by the polymer network rather than a solvent–polymer network interaction.

The use of ultrasonic techniques in civil engineering for inspecting the structural integrity of concrete was then developed by Damaj (1990). The inspection technique uses transmitter and receiver transducers to detect corrosion of embedded metal and cracking flaws within a concrete structure of different sizes and surface conditions. Attenuation was found to be the precursor to indicating corrosion and cracking flaws within the concrete structure. Challis (1990, *et al* 2005) reported experiments using transmitter and receiver transducer pairs with the pulse echo technique, in which ultrasonic absorption of various liquids undergoing flocculation was investigated. Challis *et al* (1998a, 1998b) also attempted to formulate a mathematical equation to reduce error caused by the scattering of ultrasound when measuring using the pulse echo technique. Prosser and Green (1990) conducted an ultrasound study on graphite–epoxy composites by evaluating the elastic and non-linear stress/strain behaviour of the composites by theoretical and experimental methods. It was reported that the measured stress constant by ultrasound is more reliable than the results obtained from the theoretical calculation, which is based on assumptions and approximations related to the subject material's properties.

Tavakoli and Evans (1991) reported the use of ultrasound to detect changes of mineral content in bone. The work showed that both the ultrasound attenuation and velocity can be used to detect changes of mineral content in the bone. It was pointed out that samples with relatively similar density could have extremely large differences in attenuation and velocity. Although samples showed a similar trend with weight loss

after chemical treatment with nitric acid, there is no way anyone could determine that the sample has low mineral content just from the velocity or attenuation measurement value alone. The work was inconclusive since the change in mineral content was evaluated by using an assumption that the density of bone would reduce linearly with the loss of mineral content. No chemical assay has been performed to explain why different samples with relatively similar density sometimes have higher attenuation and sometimes has lower attenuation. No explanation has been provided to account for these discrepancies.

Ultrasonics have also been used by Fairley (1992) to study aerated foods such as beer, whipped cream and yogurt. Fairley utilised a pulse echo transmission technique to study the foods samples and found that the technique fails to obtain any measurement at high volume fractions of air. However, Fairley managed to correlate the bubble size in whipped yogurt with ultrasound velocity. The technique was reportedly able to discriminate between the conventional whipped cream and sprayed cream, but was not able to characterise a fermented dough.

The use of an ultrasonic transmitter-and-receiver transducer pair was again reported by Landis and Shah (1995), in which the attenuation of cement paste at various frequencies was measured. It was reported that the inhomogeneity in the material could have affected attenuation measurements. Scattering of ultrasound due to the existence of aggregates in the cement paste was considered to be a dominant factor affecting the attenuation measurement. The scattering effect was then verified experimentally and theoretically by Anugonda *et al* (2001).

Jaafar (1996) presented a study of various ultrasonic techniques and configurations to evaluate the composition of natural rubber latex suspensions. Jaafar reported that the technique was in good agreement with the conventional method used to measure the suspensions up to 40% of dry rubber content. Both attenuation and velocity of ultrasound were found to be able to characterise the rubber content of the suspensions at various temperatures. In contrast to the measurements taken at various temperatures, at constant temperature, the difference between various levels of rubber content is too small to notice in the ultrasound velocity. The ultrasound measurements

of the rubber suspensions were found to match the Allegra and Hawley (1972) wave scattering model very well. Round (1996) also employed various ultrasonic set-ups and transducers for studying the setting of cement-based ceramics using a frequency range of 50 kHz to 10 MHz. The setting process was monitored using the through transmission technique in which two transducers were used, with the test sample being placed in between the transducers. The elastic properties of the material were determined from the ultrasonic velocity measurements and were found to be dependent upon the filler volume fraction. The measured elastic modulus was found to increase exponentially as porosity decreased, and this effect might possibly be used to estimate porosity.

Tebbutt (1996) presented a detailed modelling and simulation of ultrasound propagation in a two-phase medium using the Allegra–Hawley model, by developing a versatile software package to simulate the ultrasonic phase velocity and attenuation in suspensions, emulsions and solids in solid dispersions. The simulation using Allegra–Hawley model in non-Newtonian fluids showed a reasonable degree of accuracy to predict the ultrasonic phase velocity and attenuation in real experimental measurements.

Supported by the availability of the commercial high-temperature ultrasonic transducer, Shepard and Smith (1997) conducted an experiment to investigate the resin curing process and its composites during the injection moulding period. Further work in this area was then reported by Döring (1998). Both Shepard/Smith and Döring used the through transmission technique with a pair of high-temperature transducers installed on the top and bottom mould. The work has enabled the operator to determine the exact time to remove the final product from the mould. Similar work to polymer injection moulding was also reported by Brown (1998), Michaeli and Stark (2005) and Schmachtenberg *et al* (2005). While Michaeli and Schmachtenberg and their colleagues concentrated on the study of the resin curing process, Brown studied polymer melt extrusion using ultrasonic velocity measurements to provide an indication of degradation or change in the material. It was found that ultrasonic velocity is very sensitive to fluctuations in the extrusion pressure. The extruded melt flow rate, which is empirically used to determine the quality of the extruded polymer,

was found to be related to the ultrasound velocity of the extrusion. Verdier *et al* (1998) and Longin *et al* (1998) reported the use of the pulse echo ultrasound technique to extend the range of shear rate for the loss and storage moduli of polymers, obtained by rheometer. The loss and storage moduli at high frequencies were studied to understand the behaviour of the polymer undergoing crystallisation at low temperatures.

Ultrasound has also been used by Chanamai *et al* (1998) to detect flocculation in oil-in-water emulsions. It was reported that ultrasound attenuation can provide an indication of emulsions creaming, and to determine which emulsions are likely to cream faster than others. Challis *et al* (1998a) demonstrated that there are three models available to describe the scattering of ultrasound: the first is the Epstein–Carhart model (for liquid particles in liquid media); the second is the Allegra–Hawley model (for solid or liquid particles in liquid media); and the third is the Ying–Truell (1956) model (for solid particles in solid media). The analysis was intended to provide a theoretical representation for experimental ultrasound attenuation measurements of homogenous particle distributions in homogeneous media. In another paper, Challis *et al* (1998b) reported inherent errors and uncertainties when conducting tests using the pulse echo technique, in which 21–78% of errors in impedance and 11–45% of standard errors in attenuation should be expected. Ultrasound has also been reported by Freemantle and Challis (1998) for monitoring the curing of adhesives, in which the through transmission technique was employed.

McIntyre (1999) developed an air-coupled ultrasonic transducer that enables ultrasound experiments to be conducted using air as the coupling material. Although this is another major breakthrough in ultrasound transducer technology, the finding has limited use as the transducers can only generate or record very weak signals, e.g. amplitudes up to 0.4V and frequency up to 100kHz. This limitation means that the transducer cannot be used for very attenuating materials because the signal amplitude is too weak to pass through the material and the use of a high voltage or an amplifier to trigger the ultrasound wave generation could potentially damage the transducer itself. Later, Harwood (2000) reported on studies using a very high voltage (1kV) low frequency (100kHz) ultrasonic transducer for detecting voids within bitumen samples.

At the same time, Long (2000) presented a study to improve ultrasonic testing on concrete by providing a comparative analysis of different coupling materials such as rubber, grease and a water-filled membrane. The work showed that the transducer attached via the water-filled membrane provided better repeatability than using other couplants. Meanwhile, Smith (2000) was investigating the effect of filler concentrations on HDPE (high-density polyethylene) polymer melt extrusion using real-time ultrasound measurement. The work showed that different grades of HDPE melts, identified by their viscosity, can be distinguished by monitoring the changes in the transit time (ultrasound velocity) of an ultrasound wave. Chapman (2001) used ultrasound to study the degradation of aqueous ferrofluids. The work showed that the degradation can be observed from the changes in ultrasound attenuation and ultrasound velocity of the ferrofluid. The degradation is indicated by the 'clumping' or agglomeration process, which increases the ultrasound attenuation.

Grosse (1999; 2000) and his team at the University of Stuttgart, Germany, were also very active in ultrasound technique R&D for evaluation of cement and concrete. They documented their work on monitoring the curing process of cement paste based on the velocity and energy measurement using the through transmission ultrasound technique. Their technique (see Figure 3.34) was later refined and patented by Reinhardt *et al* (2003). Reports in the literature (see Alig and Lellinger, 2000; Alig *et al*, 2005) show that another German research group, based at University of Technology of Darmstadt, was also working on the characterisation of polymeric materials. They reported on the use of ultrasonic shear waves (see Figure 3.35) for the measurement of the storage and loss moduli of polymeric materials (e.g. acrylic glue) in its aqueous and crystalline states. The validity of this technique is still in question as shear waves normally do not travel through any liquids or aqueous materials. It was also reported that the attenuation of ultrasonic longitudinal wave measurements provides equivalent results to the viscosity values obtained by using an in-line slot die rheometer. The work in polymer resin was then continued by Fengler *et al* (2004), whereby the flow and curing of thermoset polymer resin at various moulding temperatures were investigated using the through transmission technique (see Figure 3.36). It was reported that use of lead as a coupling material could improve the ultrasound measurements at elevated temperatures.

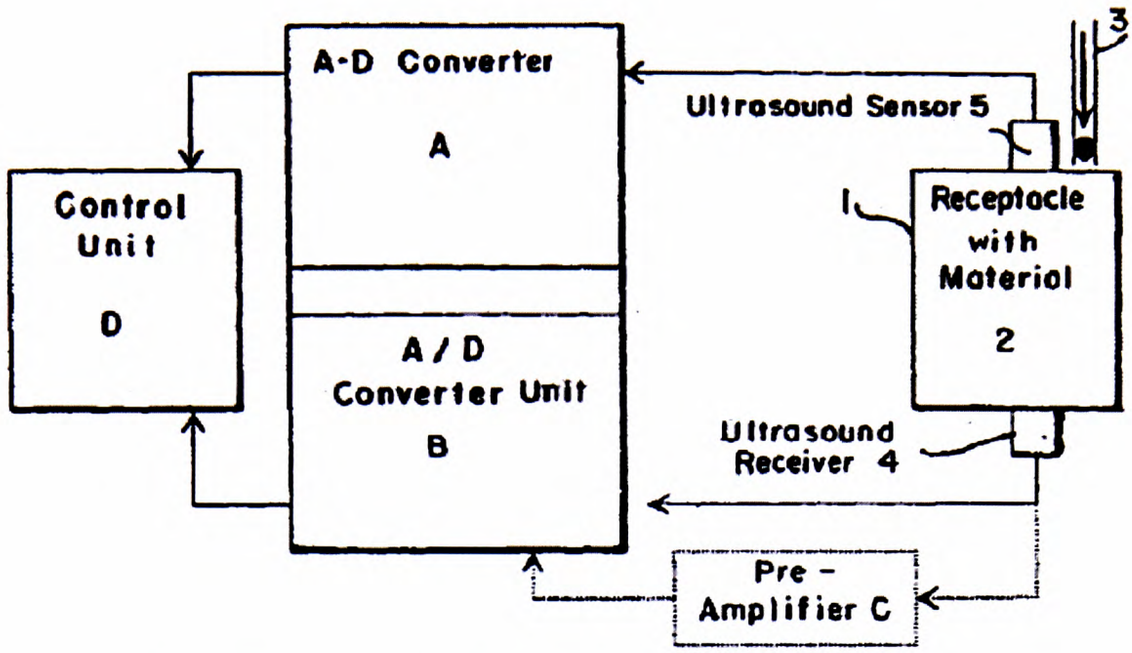

Figure 3.34: Ultrasonic set-up patented by Reinhardt *et al* for monitoring the curing rate of cement paste. (Reinhardt *et al*, 2003)

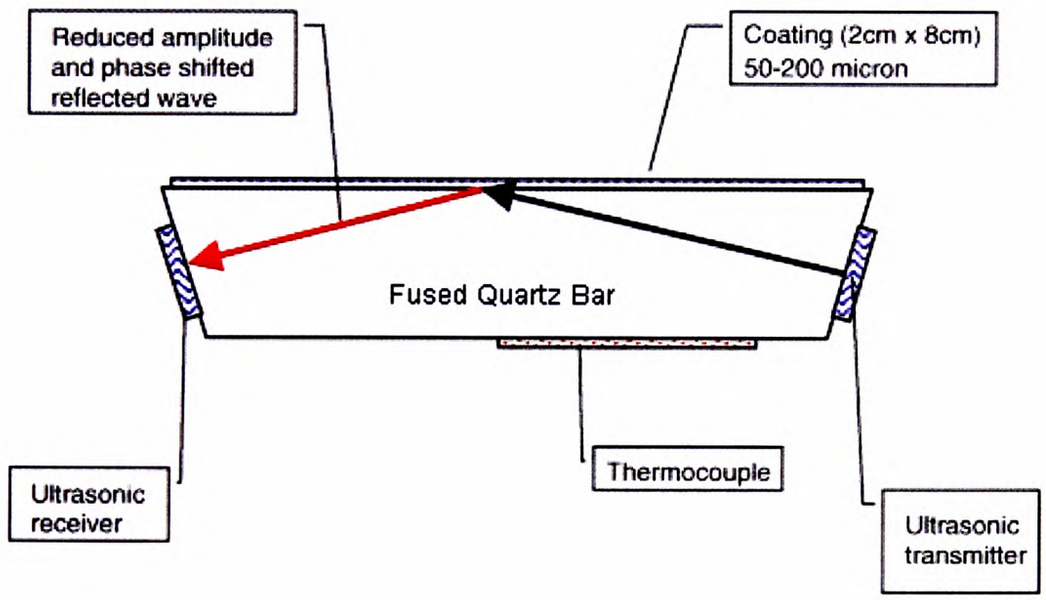

Figure 3.35: Ultrasonic set-up using shear wave transducers for measuring the loss and storage moduli of aqueous acrylic glue. (Alig and Lellinger, 2000; Alig *et al*, 2005)

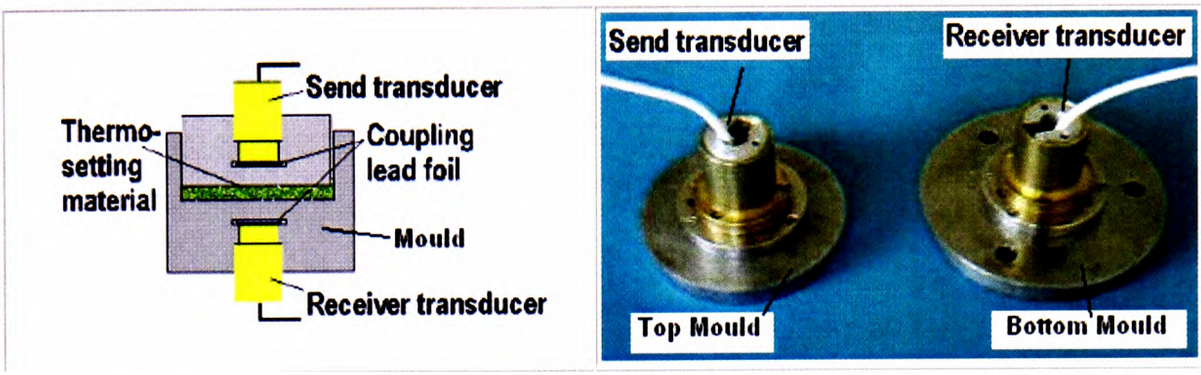

Figure 3.36: Ultrasonic set-up for studying the curing of thermoset resin in a mould. (Fengler *et al*, 2004)

Another interesting study on the use of shear wave ultrasound for characterising wheat–flour–water dough was reported about the same time by Létang *et al* (2001). Létang and colleagues reported that the results were congruent with the fact that shear waves do not travel in liquid. Létang described how 'The velocity is found to be zero for water to dough ratio above 1 (in proportion to the flour weight)'. Létang also added that the ultrasonic velocity for dough with a water-to-dough ratio between 0.6 and 1.0 is also quite slow (<10m/s). The technique was successfully used to determine the loss and storage moduli of dough with a water-to-dough ratio of less than 0.6.

The use of ultrasound for dairy products, specifically for detecting coagulation in milk, was reported by Smyth (2001). It was reported that chemical reactions during pre-gelation cause changes in ultrasonic velocity and attenuation response, and this can be used for detecting the onset of coagulation in milk.

Choi (2002) reported another experiment using an air-coupled transducer with various types of gas. The work was carried out to investigate the interaction of a high-pressure gas jet with the ultrasonic field, where the ultrasonic transducer is placed within the gas jet itself. It was reported that the direction and the spread of the gas jet can be influenced by ultrasound.

Temperature-dependent behaviour within the pulse echo ultrasound technique was reported by Llull *et al* (2002) while studying the texture of meat using ultrasound. It was reported that although the ultrasound velocity is relatively constant over a wide

range of frequencies, the ultrasound velocity measurement of the meat samples at increasing temperature has demonstrated a reduction in velocity. Although the change in velocity (<3m/s) is almost negligible for every 1°C difference in temperature, the change in velocity for every 10°C difference in temperature is greater than 50m/s and should not be ignored.

Apart from using a viscometer or rheometer, the viscosity of a flowing liquid in a pipe can also be measured accurately by applying the Doppler principle with an ultrasound technique (Ouriev and Windhab, 2002; Köselí *et al*, 2006). The Doppler principle, when applied to the flowing liquid, can easily be used to determine the viscosity of the liquid because a liquid with high viscosity will move away slowly from the transducer, reflecting the ultrasound back to the transducer slower than a liquid with lower viscosity. Ouriev and Windhab (2007) have patented this technique, which is very similar to that patented by Orj (1982). The key difference between the two is that Orj uses a pair of ultrasound transducers and the through transmission technique (see Figure 3.37) whereas Ouriev and Windhab use a single transducer and the pulse echo mode technique.

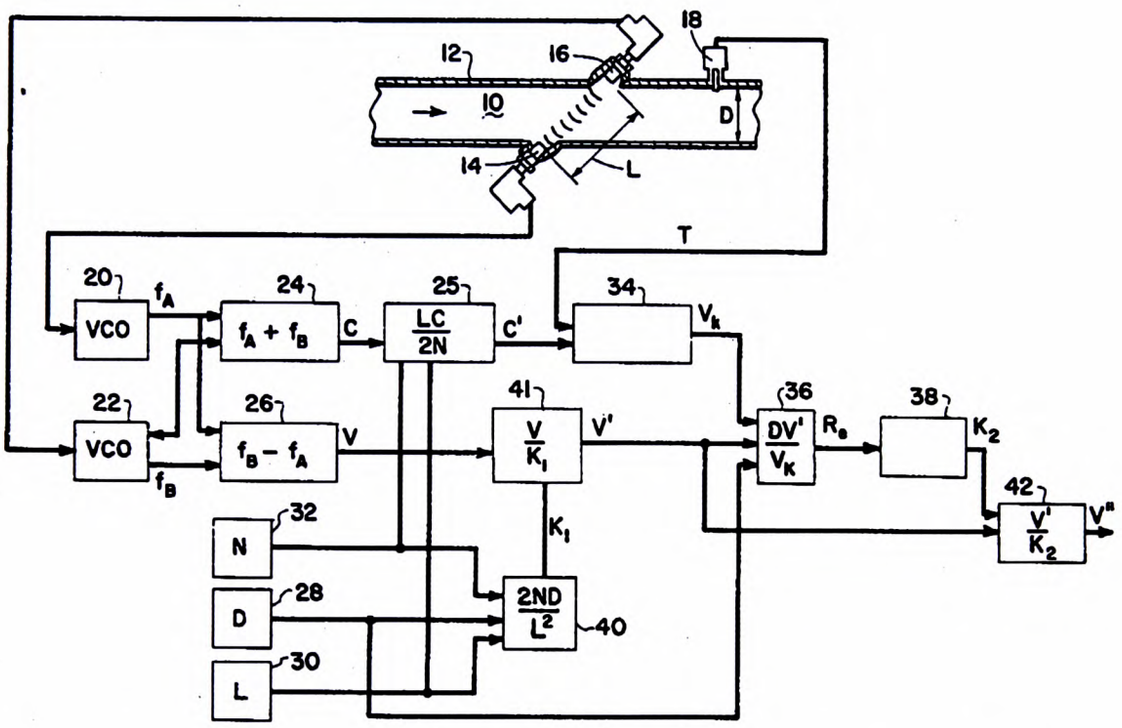

Figure 3.37: Schematic diagram of Orj's patent for measuring viscosity and flow rate of fluid. (Orj, 1982)

Daniels (2002) investigated using ultrasound techniques the shelf life of cosmetic products and found that shelf life is related to the ultrasound velocity response over time. Another significant work on product ageing was conducted by Dwyer (2004), who reported that the attenuation of ultrasound was related to post-mortem changes in meat and dairy colloids. The attenuation of ultrasound was also used to define the stages of internal changes in the ageing of dairy products; further work in this area was conducted by Lehmann (2005) to study the heat stability of milk and the gelatinisation process.

In 2003, Romoscanu and colleagues reported on another technique for measuring the viscosity of fluids in a flowing pipe. Although the technique is not based on the piezoelectric ultrasound transducer, it employs a pair of magnets and electrical coils around the pipe of flowing fluid to generate ultrasonic resonance in the fluid. It is claimed that the equipment shown in Figure 3.38 is able to measure the viscosity by measuring the frequency required to cause resonance to the flowing fluid. In the same year, Dogan (2003) reported the study of various in-line ultrasonic systems for measuring the viscosity of flowing fluids. The systems reported by Romoscanu *et al* (2003) and Dogan (2003) were based on 'ultrasound pulsed Doppler velocimetry', in which at any given pipe pressure a fluid with higher viscosity will have lower velocity than that of a low-viscosity fluid in the pipe. A good correlation to viscosity was found using both a through transmission mode and a pulse echo mode configuration. Later, Wang (2004 with colleagues; 2005) continued the work done by Dogan (2003) by investigating the effects of temperature gradients. It was found that not all materials experience a drastic change in ultrasound velocity at elevated temperature; some of the materials have almost constant ultrasound velocity from 0°C to 80°C.

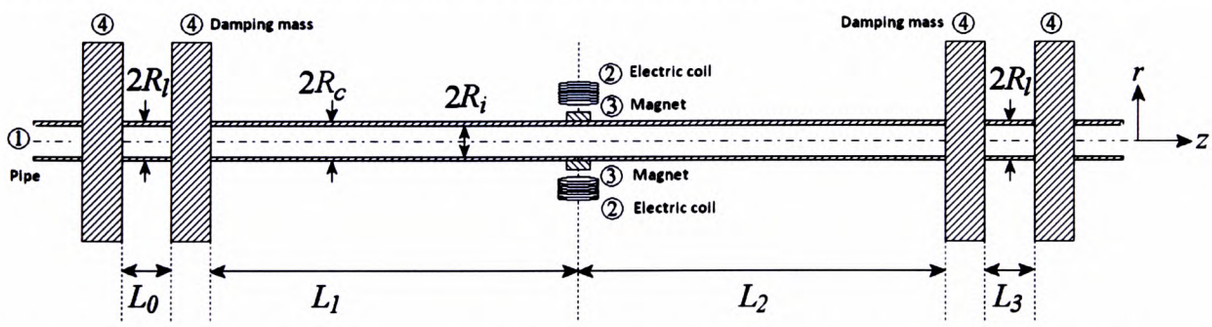

Figure 3.38: Diagram of Romoscanu's resonance pipe for measuring viscosity. (Romoscanu *et al*, 2003)

Ross (2004) investigated the effect of the mixing time of dough (a wheat-flour and water mixture) to rheology by comparing measurements using a rheometer and ultrasound. Ross found that excessive mixing time will reduce both the loss and storage moduli of the dough. This means that the dough would be found to be less viscous than the dough mixed at optimum mixing time. Although Ross did not explain the nature of the reduction in loss and storage moduli in great detail, it can be speculated that the reduction in viscosity due to excessive mixing time could be due to the increasing temperature of the dough mixture combined with the breaking of bigger particles into smaller ones. It is known that most fluids exhibit lower viscosity behaviour at higher temperatures, but the breaking of the particles could be the most dominant factor causing the change in viscosity since this change is usually obvious from visual observation that pastes mixed for a longer time will have a very fine texture.

The demand for non-contact, air-coupled ultrasound techniques for non-destructive investigation of concrete was also driven by the increasing concern for structural integrity of ageing concrete motorway structures in many countries. The idea was to put forward a mobile ultrasound scanning system that could be mounted on a vehicle to provide a real-time analysis of the structural defects of the concrete structure under the road surface. However, this idealised solution has not been realised to date due to the limitation of the low penetration depth of air-coupled ultrasound transducers. One of the interesting studies has been reported by Berriman (2004), on the use of an array of air-coupled ultrasound transducers based on the pulse echo technique. This work showed images of embedded metal bars in concrete and concluded that the defects can be observed using the air-coupled system. However, one of the main challenges of using the air-coupled system is the inherent noise in the received signal, and the thickness of the structure that can be investigated by this technique remains a big limitation.

Ye *et al* (2004) reported on the study of ultrasound propagation through materials of different levels of porosity, providing a detailed explanation of the propagation of ultrasound signals by simulating the evolution of the microstructure of cement paste

during the hydration period. This work showed that the hydration process increases the total volume of the connected particles in the solid, which provides a shorter path for the ultrasound to travel from the transmitter to the receiver end (see Figure 3.39). Ultrasound velocity increases linearly as the hydration process progresses, until it reaches maximum solid percolation; then the velocity remains almost constant (see Figure 3.40).

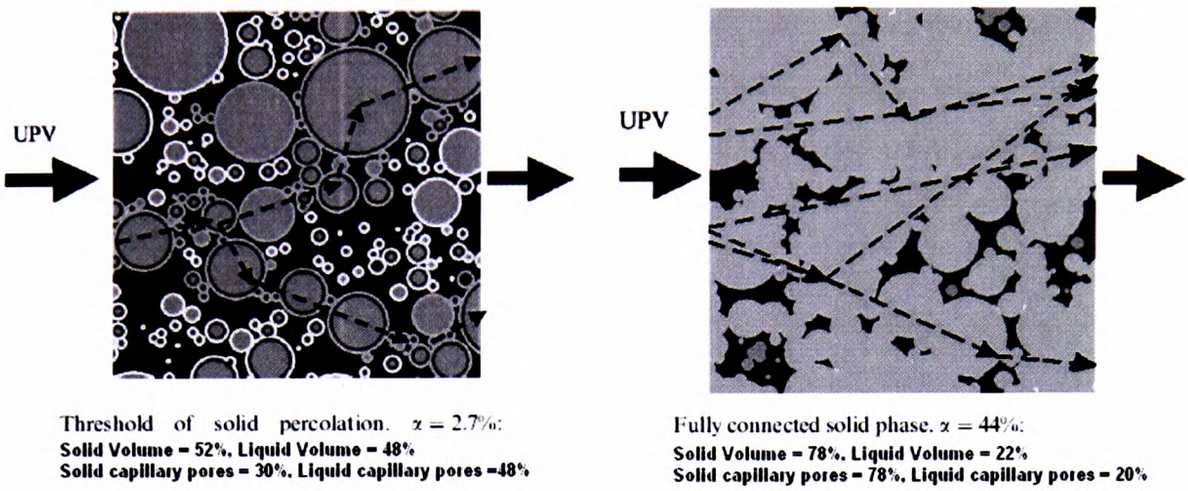

Figure 3.39: Ultrasound propagation at early and later stages of cement paste hydration. (Ye *et al*, 2004)

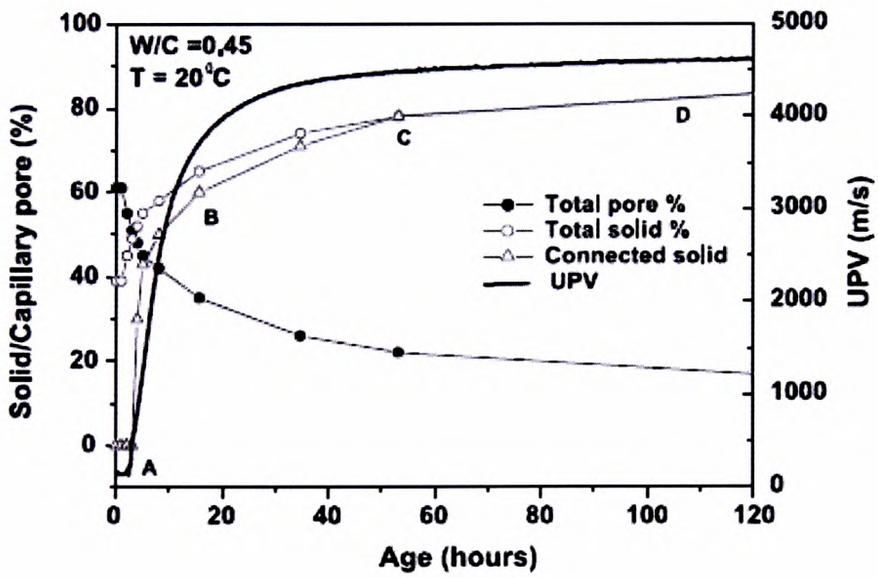

Figure 3.40: Correlation between ultrasonic pulse velocity and phase volume fraction of cement paste. (Ye *et al*, 2004)

A similar experiment reported by Aggelis and Philippidis (2004) provided results that agree with those of Ye *et al* in their 2004 work. Aggelis and Philippidis (2004) also

investigated the effect of different sand content in cement paste on ultrasonic velocity and amplitude signal response at various frequencies. Their study showed that the technique can be used to determine the water-to-cement ratio and the sand content of the cement paste. However, entrapped air voids in the cement paste have been reported in the same research to affect the accuracy of the measurements, in particular at low frequencies (below 10kHz). Bouhadjera and Bouzrira (2005) investigated the correlation of ultrasound with the elasticity and age of cement paste by applying longitudinal and shear waves to the sample. In a separate study, Öztürk *et al* (2006) used ultrasound to determine the final setting time of cement paste. Punurai *et al* (2006) and Chaix *et al* (2006) reported the study of void-induced micro-crack simulation, which is consistent with the results reported by Ye *et al* (2004) and Aggelis and Philippidis (2004). The results indicate that an increment in void fractions increases ultrasound attenuation significantly.

Use of ultrasound for measuring the properties of food, such as the firmness and sugar content of products, was reported by Mizrach (2004), while Wang *et al* (2004) and Gülseren and Coupland (2007) reported ultrasonic velocity measurement of a sucrose solution at various temperatures. Wang and colleagues paid particular interest in a study of the changes in viscosity of flowing sucrose due to temperature gradient. Kuo (2008) found that sugar content and viscosity in orange juice can be quantified effectively using ultrasound velocity. Another interesting study of ultrasound techniques for food was reported by Álava *et al* (2007), where the team used ultrasound to determine the consistency of dough by comparing the results to the rheological data obtained using an Alveograph. An Alveograph (also known as a 'Chopin Alveograph') is a tool used to indicate how elastic the dough is by measuring the pressure and time required to cause and burst a large air bubble in the dough. The results from the Alveograph are usually presented in the form of resistance against extensibility. To illustrate these in rheological terms, the extensibility of the dough would be representing the shear rate, while the resistance to stretch would be representing the viscosity. The work showed that ultrasound attenuation and velocity (see Figure 3.41) also have a correlation to the rheological properties of the dough.

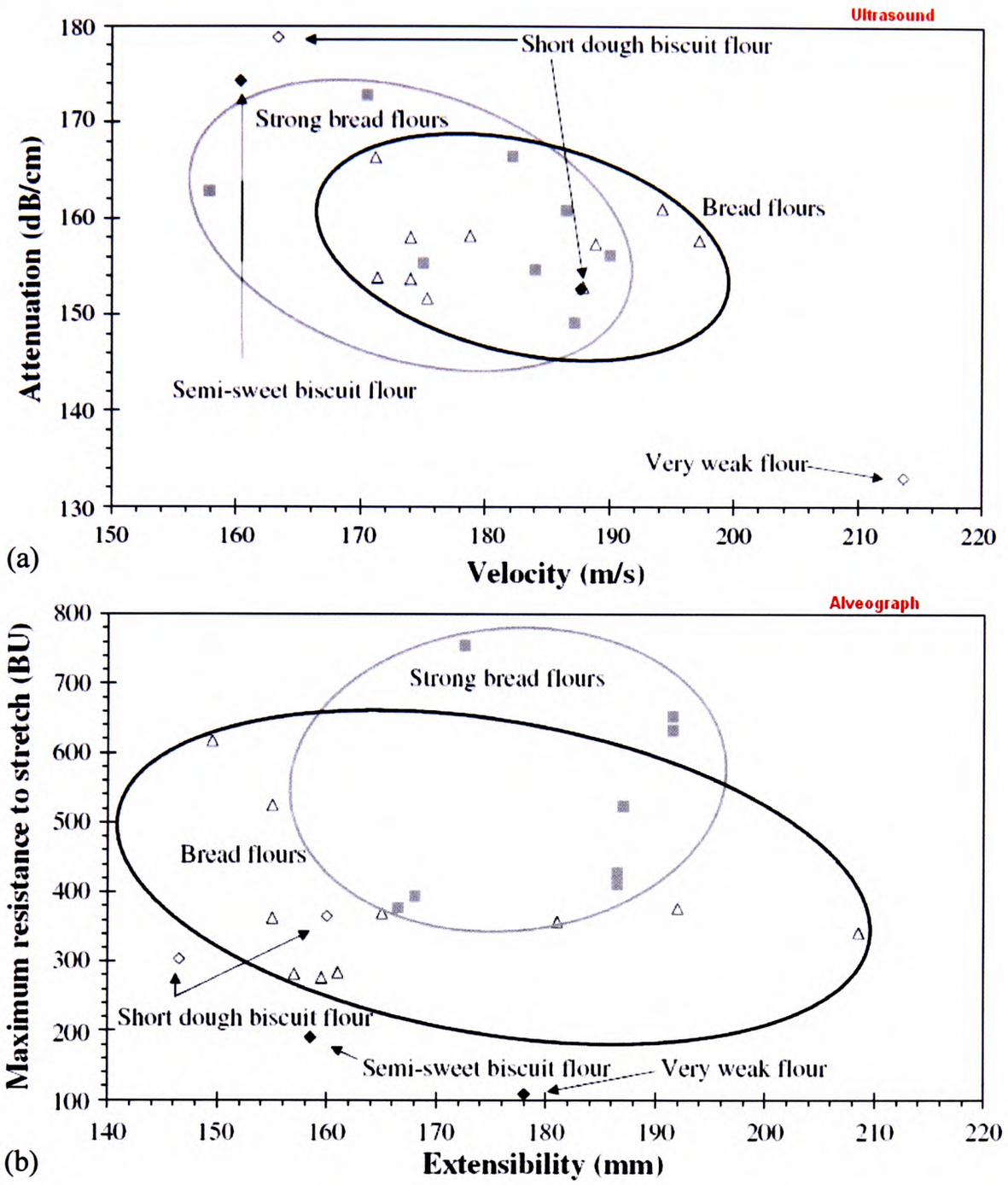

Figure 3.41: Comparison between (a) ultrasound and (b) Alveograph results for determining the rheological properties of dough. (Álava *et al*, 2007)

Because of the nature of induced cavitations (Matsumoto *et al*, 2005) that generate high heat and pressure, a continuous ultrasound wave has long been employed as an alternative method for disinfecting foods. Latest research of ultrasound for disinfection was reported by Duckhouse (2006), in which multiple frequencies were applied simultaneously with the use of hypochlorite. The method was reported to significantly reduce the formation of bacteria after water treatment.

Ultrasonics has also been reported for characterising the particle size of solid material suspended in liquid. Povey (2006) found that materials of different particle size, when dissolved in water, produce different attenuation profiles that are unique to each particular material. However, it was reported that the attenuation level of materials with similar particle size, suspended in water, was also dependent on the frequency of the ultrasound.

Guo *et al* (2007) presented a study on barium sulphate ($BaSO_4$) crystal nucleation caused by continuous ultrasound waves. The work studied the relationship between the input energy and activation energy of nucleation. It was reported that use of high input energy of ultrasound does not cause any chemical reaction in the material, but evidence of physical changes such as crystal nucleation (i.e. splitting into smaller pieces) is observed.

Over the years, the use of ultrasound techniques for investigating various materials remains almost unchanged, with most of the experiments usually conducted using the pulse echo technique to measure changes in attenuation or velocity. The sensitivity of the material to attenuation or velocity is entirely dependent on the material being tested. The pulse echo technique has been well developed to use for checking cracks in metals and can easily be adopted for use with many other materials. However, this technique also has its limitations as it requires, firstly, a compensation for time delay as it usually uses the same device (pulser-receiver) to send and receive ultrasonic pulses to the ultrasonic transducer; hence the system usually has a time delay that is dependent on how fast the pulser can switch to receiver mode to listen to the pulse and vice versa. The time delay can cause a significant amount of error in velocity measurement if it remains uncorrected. Secondly, the pulse echo technique inherits a problem of multiple echoes, caused by reflection between the reflector and the material. Thirdly, it is usually difficult to identify the pulse signal from the echo signal because both of the signals are usually merged as a single set of raw data, and they would be very difficult to separate into individual parts. Lastly, due to the length of the path that the sound wave needs to travel before it reaches the transducer, the technique is not suitable for use with highly attenuating materials because the sound

energy becomes completely absorbed by the material being tested before the echoes reach the transducer.

The reported use of ultrasound for measuring viscosity of materials is usually based on flowing systems, of which the flow rate and the pressure of the material in the systems are known. The viscosity in such a system can be easily calculated and referenced to the attenuation and velocity of the ultrasound waves themselves.

3.10. Concept of ultrasonic viscosity measurement

The hypothesis for the concept of ultrasonic viscosity measurement is based on the following postulation: 'If the viscosity of any material that flows can be measured, then it might be possible to measure the viscosity of the material by making the material flow for a very short period of time by generating a very short vibration using ultrasound.' The concept is supported by the fact that all Newtonian materials have constant viscosity regardless of the flow rate (shear rate). In contrast to that, non-Newtonian materials have variable viscosity dependent on the flow rate. In order to justify the use the ultrasound technique to measure the viscosity of non-Newtonian materials, the equipment will need to be calibrated against Newtonian fluids of known viscosity values. By doing so, the ultrasound measurement results may be used as a 'look-up table' so that the corresponding ultrasound measurement may represent a particular viscosity value.

Since viscosity is a measure of the resistance to flow or the relative movement between the particles in a material as described later in Section 4.3.3, passing ultrasound through a material to move the particles and measuring its feedback may ultimately provide an indication or a measure of the material's viscosity. There are two approaches which can be adopted to prevent or minimise the likelihood of cavitations. The first approach is by generating or using a low-power ultrasound wave. The second approach is by using a very short pulse of ultrasound wave. The ultrasound technique used in this study is based on the combination of both approaches i.e. low-power-microsecond-pulse ultrasonic wave.

3.11. Summary

Ultrasound is a high-frequency (above 20kHz) sound wave beyond the normal human hearing frequency range (20-20kHz). Ultrasound can propagate through any medium, but not through a vacuum. The scattering and reflection of ultrasound waves are the dominant factors for attenuation of the amplitude of ultrasound waves. Ultrasound shear and longitudinal velocity are respectively related to the shear modulus and Young's modulus of the material.

The following points describe the general findings from the literature review of the ultrasound applications:

- The transit time of ultrasound through a cement paste is directly related to the compressive strength of the cured cement paste.
- Scattering of ultrasound due to the existence of aggregates in the cement paste is considered to be a dominant factor affecting attenuation measurement.
- Ultrasound attenuation may be dependent on the temperature of the material, particle size, volume fraction and any inhomogeneity in the material. Ultrasound attenuation can be used to monitor the process of flocculation in various liquids. It can provide an indication of emulsions creaming and a determination of which emulsions are likely to cream faster than others. It can also be used to indicate corrosion levels and cracking flaws within a concrete structure.
- Both ultrasound attenuation and velocity can be used to detect changes of mineral content in bone, and to characterise the content of rubber suspensions at various temperatures.
- Ultrasound velocity has been used to correlate the bubble size in whipped yogurt.
- The elastic modulus of a material can be determined from the longitudinal velocity measurement of ultrasound waves.
- Excessive mixing time can reduce both the loss and storage moduli of wheat-flour–water mixtures of dough.

- Ultrasonic velocity measurements (longitudinal and shear) have been found to be dependent upon the material's volume fraction and the type of material.
- The pulse echo ultrasound technique has been used to obtain the loss and storage moduli of polymer.
- The through transmission ultrasound technique has been used to monitor the curing of adhesive and injection-moulding polymers. The end state of the curing process is indicated by a high value of ultrasound velocity and amplitude.
- Use of lead as a coupling material could improve ultrasound measurement at elevated temperatures.
- Possibility for application in dense suspensions such as solder pastes and fluxes.

CHAPTER 4

FUNDAMENTALS OF RHEOLOGY

4.1. Introduction

This chapter presents an introduction to the fundamental principles of rheology. Apart from the basic terms, definitions and mathematical equations used in this branch of science, the chapter will also present a view on the conventional equipment used to study the rheology of material and the type of fluids normally encountered in industry or daily life. In addition, this chapter will also provide a literature review on previous work done in the field on solder paste materials.

4.2. Rheology

Rheology is defined as the science of the deformation and flow of matter. The word 'rheology' was first used by Eugene C Bingham in 1928 when he described the term as *πανταρει* (transliterated 'panta rhei'), correlating it with the works of Heraclitus, a pre-Socratic Greek philosopher who lived around 500BC. 'Panta rhei' means 'everything flows'.

The field of rheology is very broad and has been regularly used to describe the relationship between applied stress and deformation over time for a wide range of materials, such as rubber, oils, molten plastics, inks, polymers, slurries and pastes, blood, clays and paints. Non-drip paint and bubble-jet printer ink are the result of technological breakthroughs using rheology to prevent smudging. Most of these materials show remarkably complex yet unique rheological properties that classical fluid mechanics and the theory of elasticity cannot fully describe. For most

commercial products, a good understanding of the rheological behaviour of the product can make a certain brand gain a better market share due to its superior performance to rival products, even though it might not reduce the production cost in order to achieve that superior rheological performance.

In this respect, rheology may also be defined as a science concerned with the behaviour of liquid or semi-liquid and even solid materials that exhibit more than one fundamental rheological property during deformation, such as shear thinning, dilatant, pseudo-plastic, thixotropic and rheopectic forms of deformation. Thus, rheology describes phenomena that occur in a very broad intermediate range between the solid and fluid states of matter (Ferguson and Kemblowski, 1991)

4.3. Rheology terms and types of fluid

4.3.1. Shear stress

To describe shear stress, consider the circumstance when a force (F) is applied parallel to the surface area (A) of a cubical solid body. Since most fluids or suspensions consist of smaller particles, the interactions between the suspended particles and the liquid can only be accounted for properly if the smallest elemental unit area (δA) of the material of the body and the smallest unit of force (δF) acting on that surface area are being considered. Hence, the relationship can be mathematically written as:

$\tau = \frac{\delta F}{\delta A}$, where τ is the shear stress with the unit of pascal (Pa). (4.1)

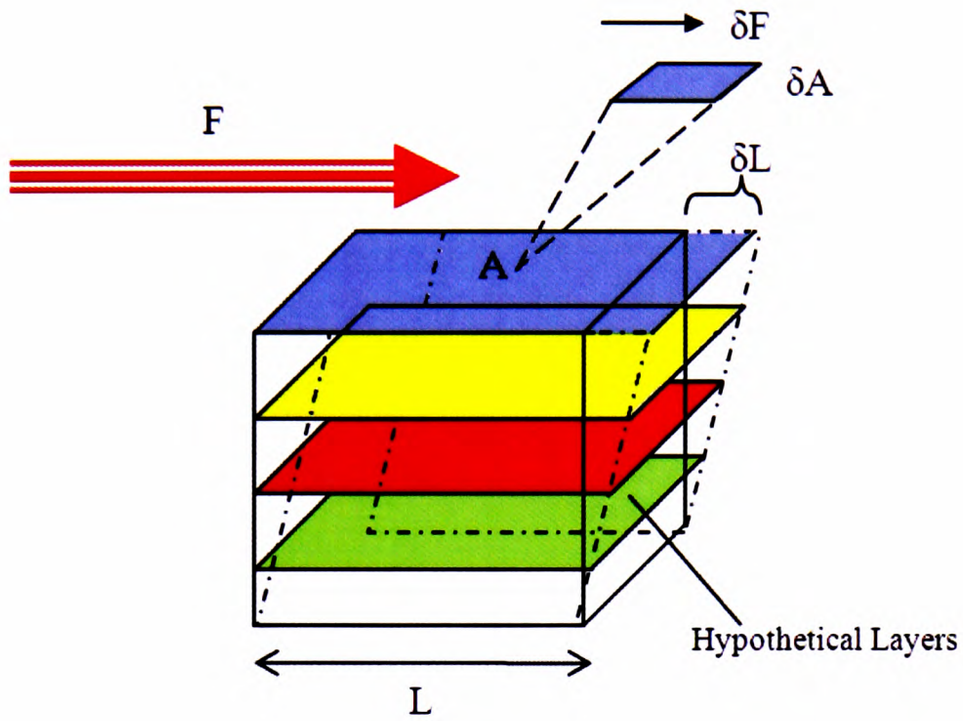

Figure 4.1: Representation of material deformation under shear stress.

4.3.2. Shear rate

Shear rate determines the rate of deformation of a material due to the applied shear stress.

Consider a cubical solid body subjected to simple shear stress as shown in Figure 4.1 being placed between two parallel plates each of area A. The top plate is subjected to a force F, moving with a velocity of v, resulting in a shear stress $\tau = F/A$. This stress is the same throughout the material once it reaches a steady-state flow. Now imagine that the material is composed of very thin (hypothetical) layers, δy, stacked on top of each other. As the top plate moves, these layers slide over each other, producing deformation as shown in Figures 4.2 and 4.3. This assumption has been found representative of the known effects, provided that there is no violent motion in the flow or turbulence. The fluid velocity will range from zero at the bottom of the plate to that of the velocity of the top plate. The shear rate is the rate of change of velocity (δv) with respect to the distance y (δy), the distance above bottom plate. Thus, the shear rate can be written as:

$$\dot{\gamma} = \frac{\delta v}{\delta y}, \tag{4.2}$$

where $\dot{\gamma}$ is the shear rate with the unit of s^{-1}.

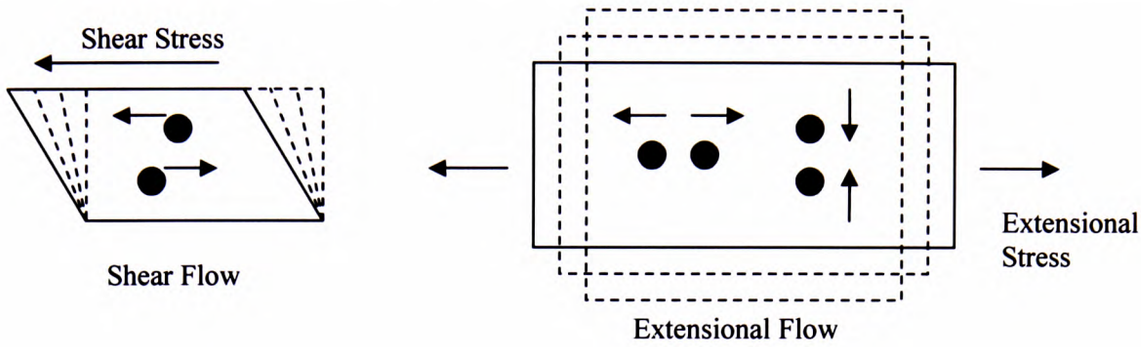

Figure 4.2: Particle movement in shear and extensional flows.

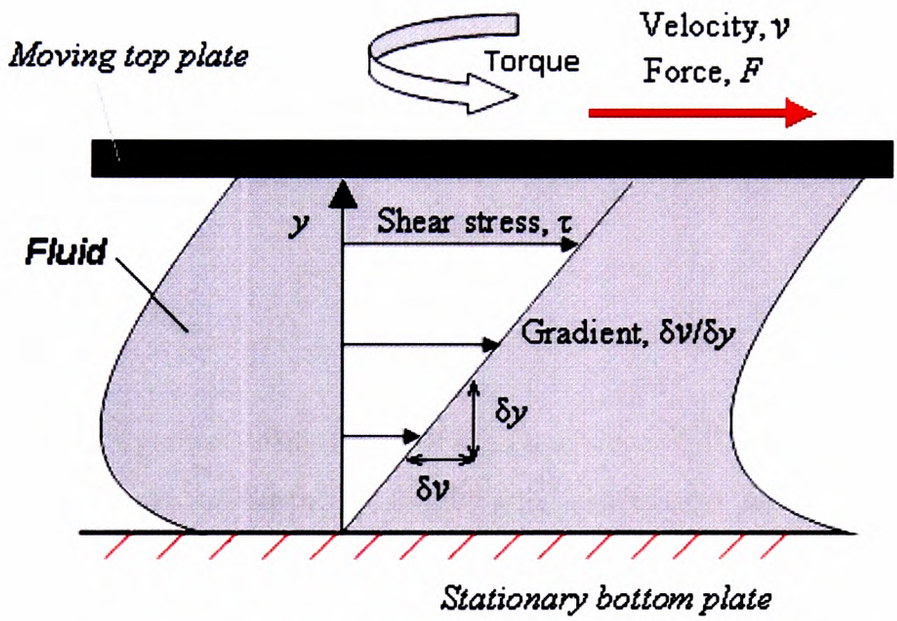

Figure 4.3: Illustration of material flow under parallel plates.

4.3.3. Viscosity

Viscosity is defined as a measure of the resistance of a fluid that is being deformed by either shear stress or extensional stress, which is commonly perceived as 'thickness' or resistance to pouring. Barnes (2000) described viscosity as internal resistance of a fluid's hypothetical layers to flow. Material with high viscosity has high friction between the internal hypothetical layers, thus requiring greater shear stress or force to

deform or cause the material to flow. Most of the viscosity values of materials are recorded using a viscometer or a rheometer at standard room temperature (25°C).

In general, in any flow, the liquid hypothetical layers as shown in Figure 4.3 will move at different velocities and the fluid's viscosity arises from the shear stress between these layers that ultimately oppose any applied force. Sir Isaac Newton postulated that, for straight, parallel and uniform flow, the applied shear stress, τ, between the liquid layers is proportional to the velocity gradient, $\delta v/\delta y$, as given thus (Barnes, 2000):

$$\tau = \eta \frac{\delta v}{\delta y} \tag{4.3}$$

The constant η is known as the 'coefficient of viscosity', 'dynamic viscosity' or even just 'viscosity'. From the definition of $\delta v/\delta y$ as shear rate $\dot{\gamma}$ in Equation 4.2, Equation 4.3 can be rewritten as:

$$\tau = \eta\dot{\gamma} \ . \tag{4.4}$$

The SI unit of dynamic viscosity is the pascal–second (Pa.s) which is identical to 1kg/(m.s) or 1N.s/m^2. Apart from the SI unit, viscosity is sometimes quoted in cgs units as poise, in recognition of Poiseuille a French physician who had been interested in blood flow. One centipoise (cP) is equivalent to one millipascalsecond (mPa.s).

Sometimes, the term 'kinematic viscosity' is used when the material concerned is subjected to an inertial force. However, it should be noted that kinematic viscosity is the ratio of the dynamic viscosity of a fluid to its density, which can be written as:

$$\upsilon = \frac{\eta}{\rho} \ , \tag{4.5}$$

where υ is the kinematic viscosity (m^2/s).

The cgs unit for kinematic viscosity is the stokes (st), named after George Gabriel Stokes. One centistokes (cSt) is equivalent to one square millimetre per second (mm^2/s).

In the study of rheology, fluids can be categorised into Newtonian and non-Newtonian fluids. Newtonian fluids usually have constant viscosity over a wide range of shear rates, while non-Newtonian fluids exhibit a variable viscosity dependent on the shear rates encountered. Newtonian fluids usually obey Hooke's Law, which states that an applied force is directly proportional to the deformation and independent of the rate of deformation, and they can be considered as elastic materials in nature. If F is the applied force and y is the resulting deformation, Hooke's Law can be expressed mathematically as:

$F = ky$, where k is the force constant or spring constant. (4.6)

Based on Young's (1807, 1821) theory of elasticity, Hooke's Law has been adapted so that the applied stress τ becomes directly proportional to the deformation y and independent of the rate of deformation $\delta v/\delta y$. Hence, according to Young's (1807, 1821) elasticity theory:

$\tau = Ey$, where E is the modulus of elasticity (or Young's modulus). (4.7)

Young's modulus has been regularly used to indicate how elastic a material is, and it has been considered a very useful parameter for determining the elasticity of solid materials.

4.3.4. Storage and loss moduli (G' and G")

An oscillatory shear test is normally conducted to study the storage and loss moduli (G' and G'') of materials. As the names imply, the storage and loss moduli are a measure of stress response, i.e. how elastic/solid a material is (storage modulus) or

how viscous/liquid a material is (loss modulus) when a small sinusoidal oscillating strain is being applied to the material. Oscillatory strain is defined as:

$$\gamma = \gamma_0 \sin(\omega t) \tag{4.8}$$

and the shear rate is given by:

$$\dot{\gamma} = \gamma_0 \omega \cos(\omega t), \tag{4.9}$$

where ω is the angular velocity, γ_0 is the shear strain amplitude, and $\gamma_0\omega$ can be defined as the amplitude of shear rate. The shear stress response of a material usually consists of both the storage and loss moduli terms; hence, the shear stress response as a function of time, t, can be written as:

$$\tau(t) = \gamma_0[G' \sin(\omega t) + G'' \cos(\omega t)] \ . \tag{4.10}$$

Since the complex modulus, G^*, is defined by

$$G^* = \frac{\tau}{\gamma}, \tag{4.11}$$

rearranging Equation 4.10 gives us:

$$G^* = G' + iG'' \ . \tag{4.12}$$

Hence, the phase angle of the complex modulus, ς, can be expressed as:

$$\tan\varsigma = \frac{G''}{G'} \ . \tag{4.13}$$

In relation to that equation, the complex viscosity, η^*, can be defined by:

$$\eta^* = \eta' - i\eta'' = \frac{G^*}{i\omega} = \frac{G' + iG''}{i\omega} = \frac{G'' - iG'}{\omega}, \tag{4.14}$$

where η' is the dynamic viscosity associated with the viscous response and η'' is the viscosity associated with the storage response. Therefore:

$$\tan \varsigma = \frac{G''}{G'} = \frac{\eta'}{\eta''} \tag{4.15}$$

The phase angle ς is a measure of the fluidity and solidity of a given viscoelastic material under a given oscillatory shear strain.

The storage and loss moduli (G' and G'') can also be used to give an indication of when a material is going to turn from solid to liquid form in terms of the oscillation frequency of the shear rate. In order to measure the storage and loss moduli, the rheometer will oscillate back and forth at a fix frequency of say 5Hz, shearing the material with a certain range of shear rate or angular velocity. The solder paste response to oscillation frequency sweep shown in Figure 4.4 indicates that the solder paste starts to turn from a solid state to a liquid state in the range of 5rad/s to 50rad/s: this is indicated by the irregular data-point plot during the state of transition. It can be seen that initially the storage modulus G' is dominant over the loss modulus G'', but at the end of the transition the loss modulus G'' is dominant over the storage modulus G'. The initial transition is point dependent on the shear stress applied, i.e. a higher shear stress would lower the initial angular velocity transition point.

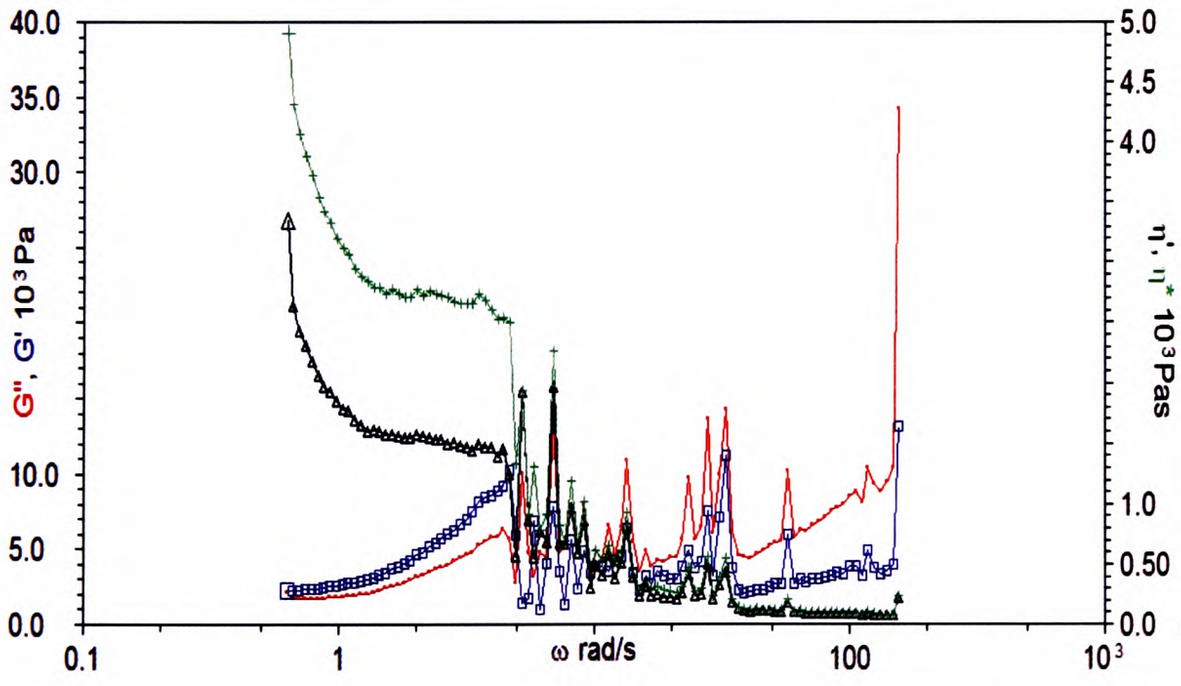

Figure 4.4: Solder paste response to oscillation sweep at 10Pa shear stress, 1Hz.

4.3.5. Newtonian fluids

Newtonian fluids can be easily identified if the fluids exhibit a linear relationship between shear stress τ and shear rate $\dot{\gamma}$. This implies that the viscosity curve for a Newtonian fluid in relation to shear stress and shear rate is a straight line going through the origin of the axes. A plot of τ versus $\dot{\gamma}$ is called a *flow curve*, and Figure 4.5 is showing an example of a flow curve of a Newtonian fluid. Fluids that do not exhibit this kind of behaviour ($\tau = f(\dot{\gamma})$) or that have a flow curve that is not linear and not going through the origin of the axes at a given temperature and pressure are regarded as non-Newtonian fluids.

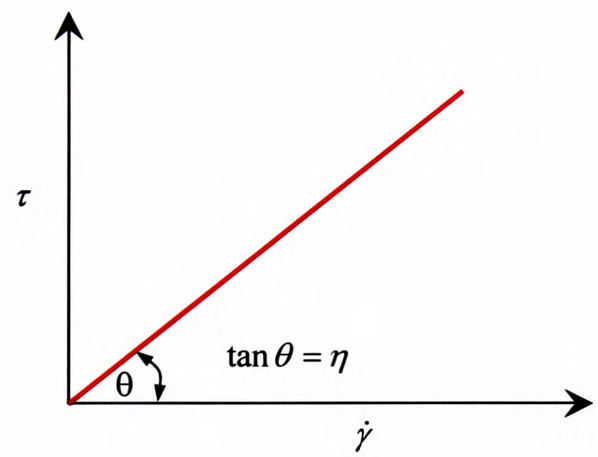

Figure 4.5: Flow curve of a Newtonian fluid.

Some of the fluids used in our daily life, such as water, air, petrol and honey, can be satisfactorily described as being Newtonian, but most of them are not. Common examples of non-Newtonian fluids include mayonnaise, yogurt, peanut butter, toothpaste, egg white, washing-up liquid and multigrade engine oil. Other examples, such as molten polymers, wet cement pastes, glues, rubber latex, blood, bread dough and slurries, are also considered as non-Newtonian fluids. A distinguishing feature of many non-Newtonian fluids is that they have microscopic- or molecular-level structures that can self-rearrange substantially during flow.

4.3.6. Non-Newtonian fluids

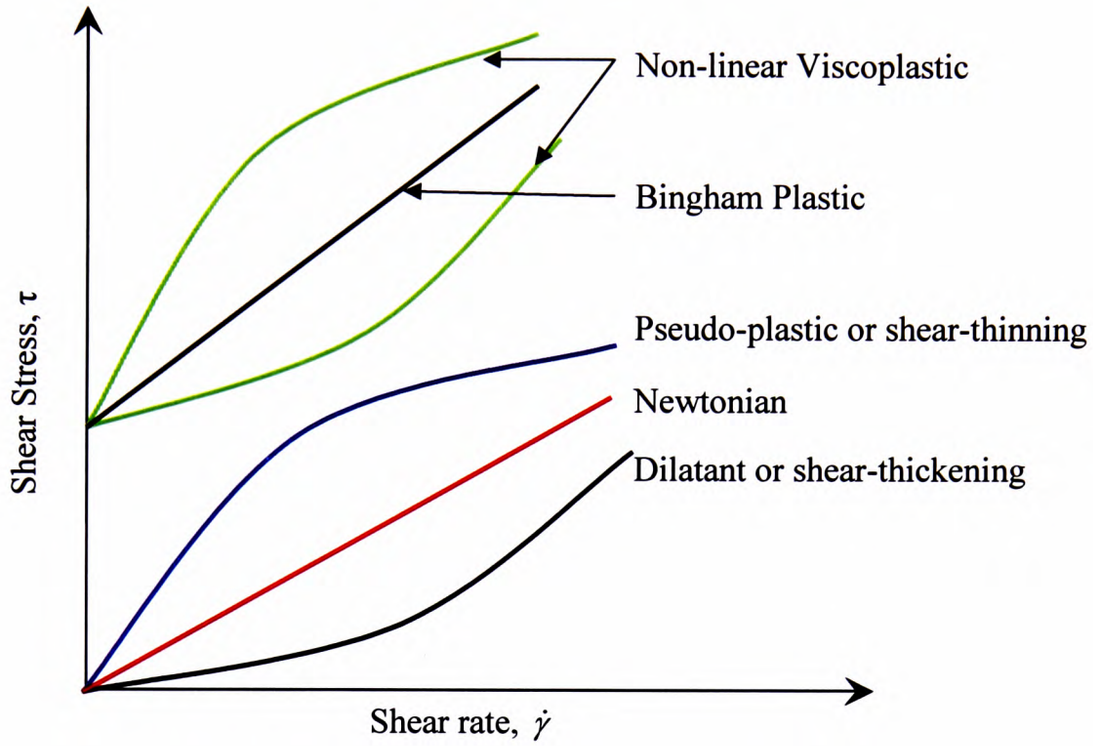

Figure 4.6: Flow curves of Newtonian and non-Newtonian fluids.

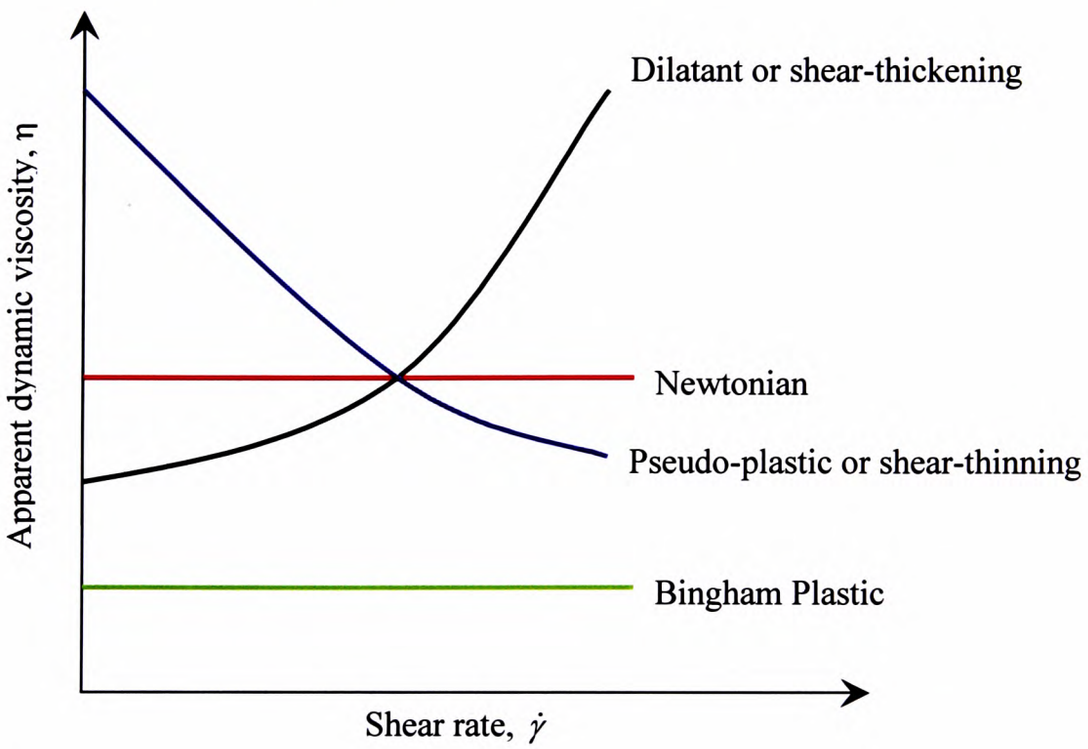

Figure 4.7: Rheogram of Newtonian and non-Newtonian fluids.

As explained above, non-Newtonian fluids generally exhibit a non-linear flow curve that does not pass through the origin of the axes (see Figures 4.6 and 4.7). These fluids are sometimes described as 'viscoelastic' fluids, as these fluids usually exhibit both elastic and viscous (non-elastic) properties at the same time. Moreover, non-Newtonian fluids can be classified further into six categories according to their viscosity response to increasing shear rate.

a. Pseudo-plastic fluids

Pseudo-plastic or shear-thinning fluids are usually composed of a suspension of solid particles or long-chain branched polymer molecules suspended in a liquid medium. When a pseudo-plastic fluid is subjected to increasing shear rate, the solid particles can usually move freely to rearrange the structure of the fluid so that it becomes more organised, leading to less resistance to fluid flow. As a result, a decrease in apparent viscosity or shear-thinning behaviour can be observed – see Figure 4.7. Pseudo-plastic behaviour is regarded as one of the most common material behaviours found in non-Newtonian fluids. Common examples of materials that have this property include molten polyethylene, ketchup, blood, paint and nail polish.

Ostwald (1925 and 1929) postulated a 'power law' model that can be used to model the rheological behaviour of pseudo-plastic fluids satisfactorily. The power law model can be mathematically expressed as:

$$\tau = k\dot{\gamma}^{b}, \tag{4.16}$$

where the parameter k is defined as the pre-exponential factor or consistency index and b as the exponential factor or the flow behaviour index. The value of constant k gives an indication of the viscous behaviour of the fluid, while the value of the index b describes the extent of the deviation of the fluid's behaviour from Newtonian behaviour. For pseudo-plastic fluids, b must be less than unity: if b is equal to unity, then Equation 4.16 reduces to the Newtonian model shown in Equation 4.4 and k becomes the Newtonian viscosity η. When b is greater than unity, the fluid is said to exhibit 'shear thickening' behaviour.

b. Thixotropic fluids

Thixotropic fluids have almost similar behaviour to pseudo-plastic fluids. However, a thixotropic fluid exhibits a decrease in viscosity at constant shear rate over time (see Figure 4.8) while a pseudo-plastic fluid exhibits a decrease in viscosity at increasing shear rate. Thixotropic fluids can also be created from suspensions, gels or colloids. Some of the fluids can exhibit both pseudo-plastic and thixotropic behaviour at very high shear rate, but at very low shear rate most of the high-viscosity fluids will not exhibit thixotropic behaviour – for example, pitch (bitumen), solder paste, clay, drilling mud, synovial fluid or gearbox transmission fluid. These fluids will exhibit constant apparent viscosity at very low shear rate as if they were Newtonian fluids (see Figure 4.9). Early pioneering work of problem solving on exact solutions for materials exhibiting thixotropic behaviour includes the work done by Rivlin (1948), Oldroyd (1950) and Lodge (1951). Rivlin suggests the use of stress tensors, velocity and acceleration elements in isotropic materials in order to calculate the viscosity of the fluid; however, the equation is very difficult to implement as there are too many unknown time-dependent derivatives.

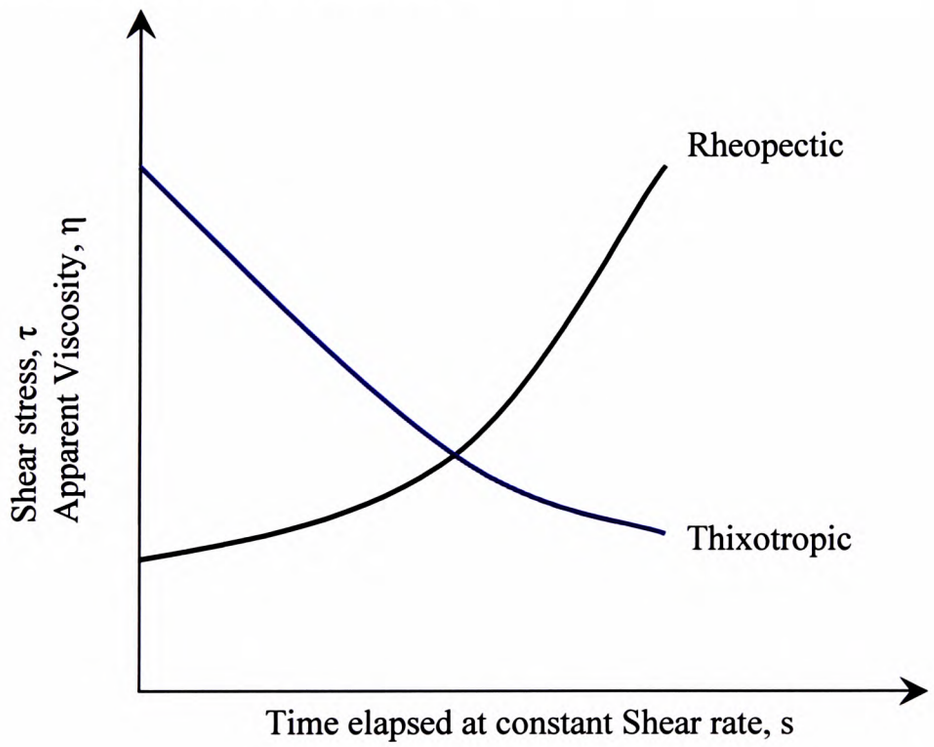

Figure 4.8: Illustration of flow curve of time-dependent fluids.

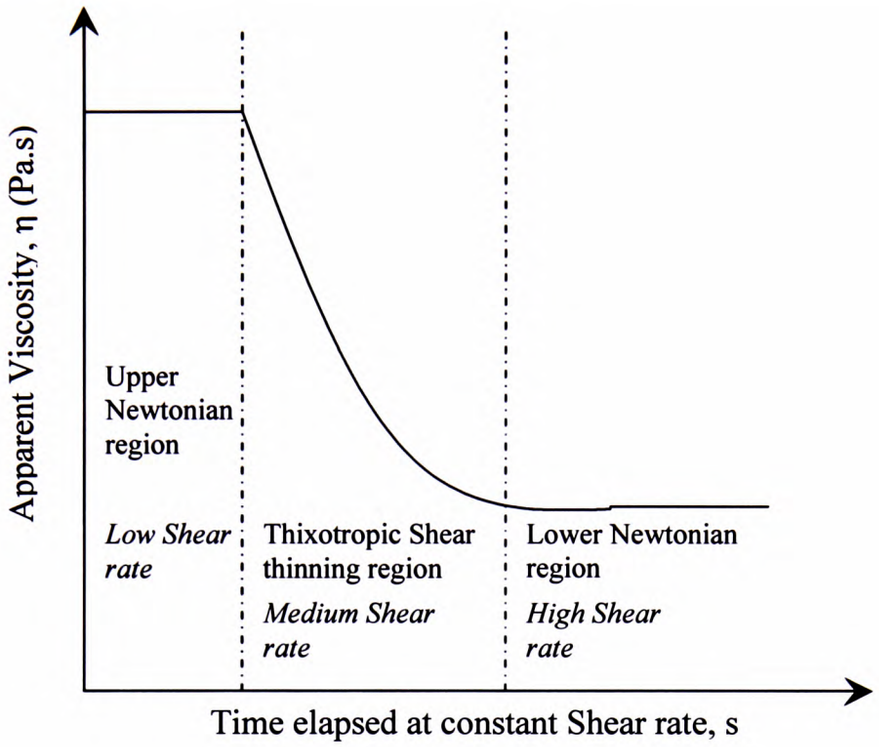

Figure 4.9: Illustration of flow curve of thixotropic fluids at various levels of constant shear rates.

Thixotropic fluids can be modelled using the Cross model (see Equation 4.17), which incorporates two terms η_0 and η_∞ that correspond respectively to the constant viscosity at very low and very high shear rates (Cross, 1965). The term K in Equation 4.17 has the dimension of time, while the index m is a dimensionless term indicating the degree of shear thinning. Values of m tending towards zero indicate a more Newtonian behaviour for a liquid, whilst liquids showing the most shear-thinning behaviour have a value of m tending towards unity.

$$\frac{\eta-\eta_\infty}{\eta_0-\eta_\infty}=\frac{1}{1+(K\dot{\gamma})^m} \quad . \tag{4.17}$$

c. Dilatant fluids

Dilatant or shear-thickening fluids usually exhibit an indication of increasing resistance to flow with increasing shear rate. As a result, the apparent viscosity of this type of fluid always increases with increasing shear rate. Dilatant fluids usually contain a high concentration of solid particles that are porous or fragile and can easily

disintegrate into smaller and smaller particles with the introduction of increasing shear rate. The reorganisation of bigger to smaller particles fills the voids in the fluid systems, therefore increasing the apparent viscosity as the increasing packing fraction reduces the freedom of movement of the particles in the system (Fletcher and Hill, 2008). A cornstarch-in-water mix is a typical example of a dilatant fluid. Dilatant fluids can also be modelled using the power-law model explained previously.

d. Rheopectic fluids

Non-Newtonian fluids that exhibit rheopectic behaviour will display an increase in viscosity with constant shear rate over time. A rheopectic fluid is probably one of the most uncommon liquid behaviours to be found in the study of rheology. Although there are not many examples of rheopectic fluids, this type of fluid can usually be engineered – printer's ink, electrorheological fluid, magnetorheological fluid and gypsum could be the only few examples of rheopectic fluid readily found today.

Rheopectic and thixotropic fluids are time-dependent fluids that have varying apparent viscosity with constant shear rate (see Figure 4.8). These types of fluid are very difficult to study because the apparent viscosity varies with time as well as with shear rate and temperature. Johnson and Kevra (1989) explained that shear-thickening or rheopectic behaviour could be due to insufficient liquid to fill the spaces between the solid particles, leading to increasing direct particle-to-particle contact.

e. Bingham fluids

A Bingham fluid is sometimes referred to as a 'plug-flow' fluid, as it requires the development of a significant level of shear stress, or the yield stress value being exceeded, before flow will begin, as illustrated in Figures 4.6 and 4.7. Once the flow starts, there is essentially a linear slope to the flow curve, indicating a constant apparent viscosity. Some examples of Bingham fluids include chocolate, ketchup, mustard, mayonnaise, toothpaste and grease. Bingham (1922) proposed a model, which is called the Bingham model, to explain the behaviour of this type of fluid using the following equation:

$$\tau = \tau_y + \eta\dot{\gamma}\,, \tag{4.18}$$

where τ_y is the yield stress (in Pa), η is the apparent viscosity (in Pa.s) and $\dot{\gamma}$ is the shear rate (in sec^{-1}).

f. Non-linear viscoplastic fluids

Fluids with a yield stress are sometimes referred to as viscoplastic fluids, which can be classified as 'Bingham plastic' and 'non-linear viscoplastic' (non-Bingham) fluids. As shown in Figure 4.6, there are two types of non-linear viscoplastic fluids: yield pseudoplastic and yield dilatant. Like Bingham plastic fluids, these fluids also possess a yield stress value; however, the flow curve of viscoplastic fluids is not linear like the Bingham fluids. A yield-pseudoplastic fluid behaves similarly to a pseudoplastic (or shear-thinning) fluid, but it requires a minimum amount of applied shear (yield stress) before it will flow like a fluid. On the other hand, a yield-dilatant fluid behaves similarly to a dilatant (or shear-thickening) fluid but with a yield stress value. The simplest rheological model for the flow curves of non-linear viscoplastic fluids is the Herschel–Bulkley model, which is given by the following equation:

$$\tau = \tau_y + k\dot{\gamma}^n. \tag{4.19}$$

Equation 4.19 is quite similar to the power law model (Equation 4.16) except that it has got an additional yield stress term, τ_y. Like a power law fluid, the value of the constant k gives an indication of the viscous behaviour of the fluid, while the value of the index n describes the extent of the deviation of the fluid's behaviour from Newtonian behaviour. For yield-pseudoplastic fluids, the value of n is less than unity. If n is equal to unity, then Equation 4.19 reduces to the Bingham model (Equation 4.18). When n is greater than unity, the fluid is regarded as yield-dilatant.

4.4. Rheology of paste and suspension fluids

Paste and suspension fluids usually consist of solid particles distributed in a liquid medium, although very often these fluids may also consist of more than one type of solid or liquid mixed together to form a product used in our daily life – for example, cosmetic cream, lipstick, hair colourant, nail polish, toothpaste, cough syrup, and antiseptic cream. Solder paste can be classified as a non-colloidal dense suspension as the particle size of the solder alloy particles is typically greater than 1μm and the volume fraction is approximately 50%. When a particulate material is added to a Newtonian fluid, the system can become a non-Newtonian fluid. As a result, the rheological behaviour of the system becomes unpredictable and a full understanding of the nature of the system can be known only if the system undergoes full rheological tests.

4.4.1. Factors influencing the rheology of paste and suspension fluids

Provided that the atmospheric pressure and temperature are held constant, the rheological behaviour of paste and suspension materials is usually influenced by the following factors (Mazzeo, 2002):

- volume fraction of the dispersed phase;
- viscosity of the medium phase;
- particle size of the dispersed phase;
- particle size distribution of the dispersed phase;
- particle shape of the dispersed phase; and
- electrochemical interaction between the particles and the medium phase.

Each of these factors is described next.

a) Volume fraction

Volume fraction of the dispersed phase represents the ratio of suspended phase to the medium phase. The viscosity of the suspension normally increases with increasing volume fraction of particles. Einstein (1906; 1911) proposed a solution relating the viscosity to the volume fraction of the suspended solid particles, as shown in Equation 4.20. However, the equation is based on the assumption that the volume fraction of the solid is less than 0.01. Although this equation may work well for very dilute suspensions, it will not work for a paste.

$$\eta = \eta_f(1+2.5\phi)\,, \tag{4.20}$$

where η_f is the viscosity of the medium fluid, ϕ is the volume fraction and η is the viscosity of the suspension.

Batchelor (1974; 1977) refined Einstein's formula for use with higher-volume fraction suspensions (ϕ <0.15) and suggested:

$$\eta = \eta_f(1+2.5\phi+k_2\phi^2+k_3\phi^3)\,, \tag{4.21}$$

where k_2 and k_3 are constant values, ranging from 5 to 15, that have to be determined experimentally.

For higher-volume fractions ($\phi \geq 0.15$), the Kreiger and Dougherty (1959) equation seems to describe the viscosity of the suspension better than Batchelor's or Einstein's. This equation is given by:

$$\frac{\eta}{\eta_f} = \left(1-\frac{\phi}{\phi_m}\right)^{-[\eta]\phi_m}\,, \tag{4.22}$$

where $\frac{\eta}{\eta_f}$ is usually referred to as relative viscosity, ϕ_m is the maximum packing fraction of the particles in the suspension and $[\eta]$ is the intrinsic viscosity of the system – which is 2.5 for suspensions with rigid-sphere particles.

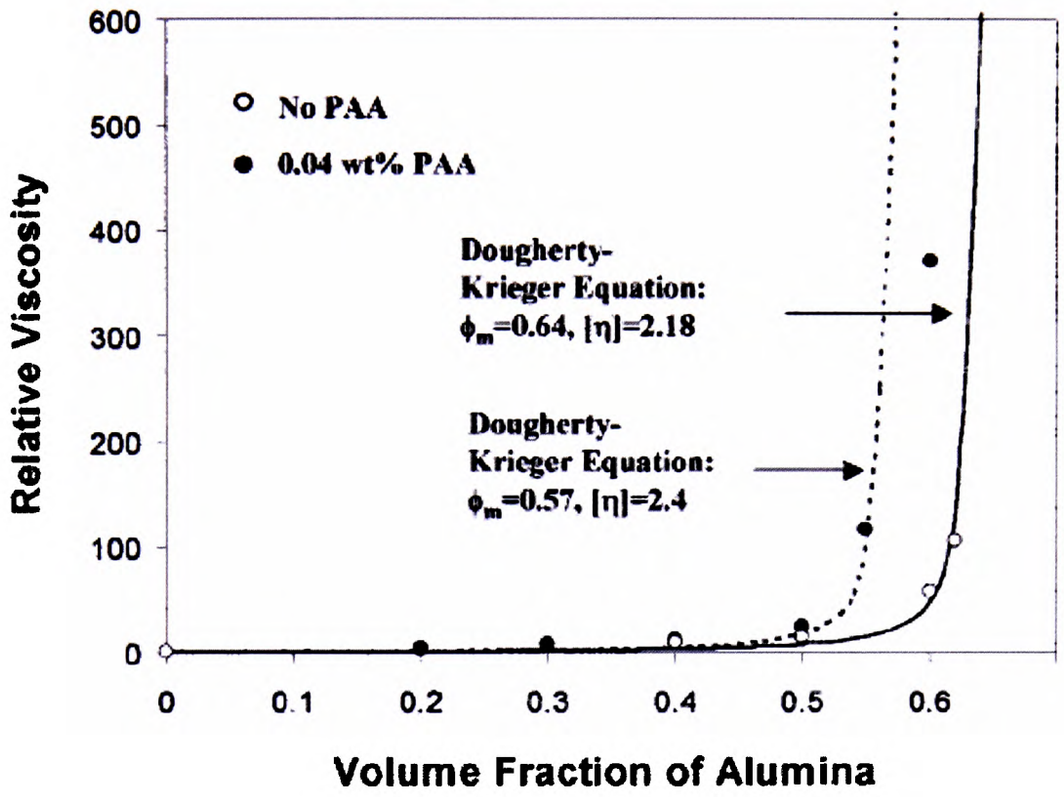

Figure 4.10: Relative viscosity dependence of Al_2O_3 suspension loading at a shear rate of 1030 s^{-1}. Al_2O_3 powder sphere diameter = 45 μm. (Yang and Sigmund, 2001).

The correlation of volume fraction to viscosity of a suspension is illustrated in Figure 4.10, in which alumina (Al_2O_3) powder spheres were suspended in deionised water. It is shown that the relative viscosity of the suspension increases rapidly as the volume fraction (ϕ) approaches the maximum packing fraction (ϕ_m) of particles that can be accommodated in the suspension before flow ceases. The increase in the relative viscosity with the addition of polyacrylic acid (PAA) to the alumina suspension is deemed to be due to the fact that the polyacrylic particles have similar particle size to the alumina powder, hence reducing the maximum packing fraction of the system. Additionally, the acid solution itself would also contribute an increase in the viscosity of the suspension.

As mentioned earlier, addition of a particulate material to a Newtonian fluid can cause the system (suspension) to become a non-Newtonian fluid. Suspensions with relatively low volume fraction tend to behave like Newtonian fluids, with viscosity independent of shear rate. Increasing the volume fraction leads to shear-thinning behaviour. The increasing shear thinning as volume fraction increases is illustrated in Figure 4.11 for a latex/pressure-sensitive adhesive system. In this particular example, it is shown that a suspension with 45% solid ($\phi = 0.45$) is showing almost Newtonian behaviour as the viscosity of the suspension remains almost constant over a range of shear rates.

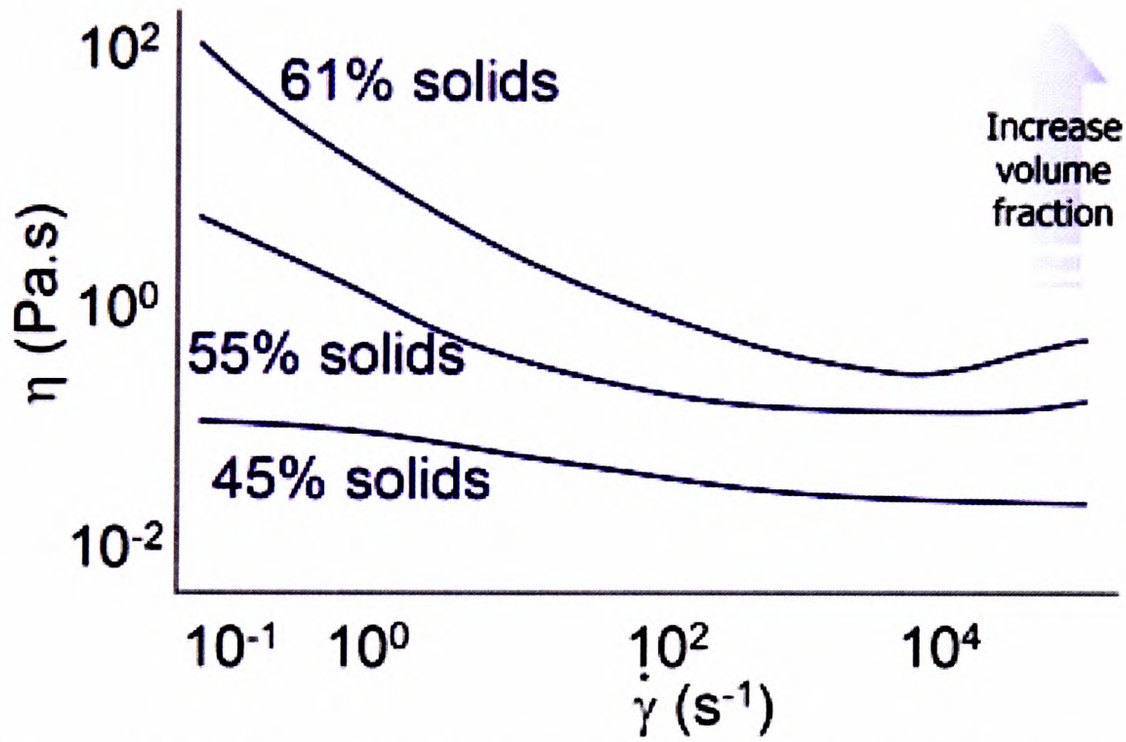

Figure 4.11: Viscosity as a function of shear rate for different volume fractions, for a latex/pressure-sensitive adhesive system (Fletcher and Hill, 2008).

b) Viscosity of medium phase

The viscosity of the medium-phase fluid will directly affect the change of the system's viscosity when a particulate material is added to it. A medium fluid with very high viscosity will show a very small reduction in viscosity when a small amount of particulate (less than 1% volume) are added to the system. However, for a very low viscosity medium fluid, a small addition of particulate usually increases the system's viscosity regardless of the particle size of the particulate added – see Figure 4.12.

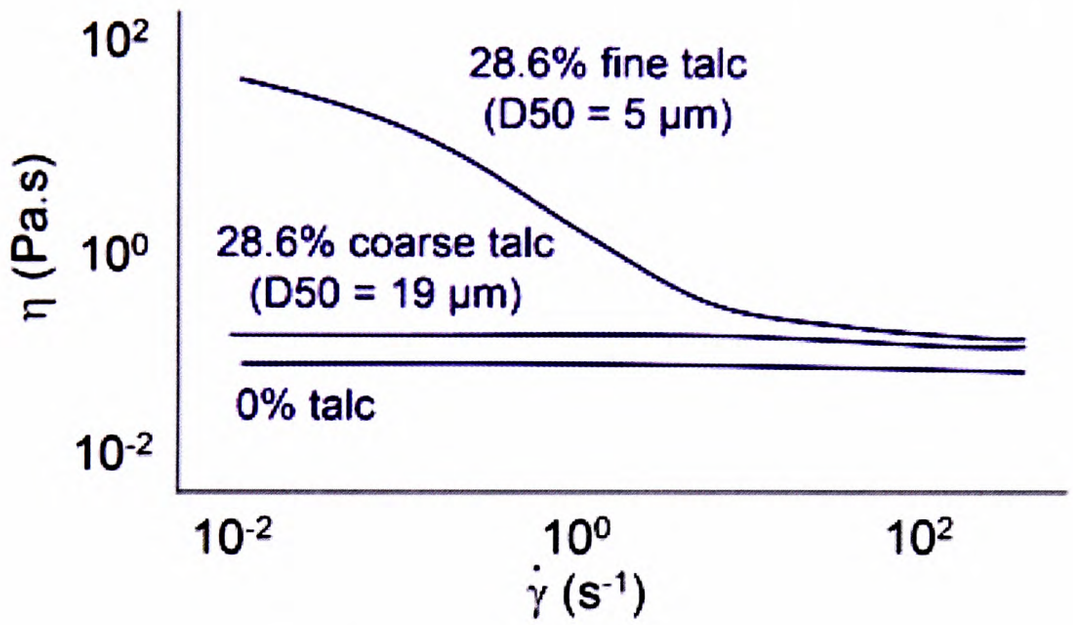

Figure 4.12: Effect of adding particulate on low-viscosity medium fluid. (Fletcher and Hill, 2008)

c) Particle size

Particle size can affect the maximum packing fraction of a suspension, with smaller particles having a higher maximum packing fraction for the same volume of suspension. A suspension with homogeneous (single-modal) particle size also tends to have a lower maximum packing fraction compared with a suspension with bimodal or multimodal particle size. This is because the same volume of space in the suspension can accommodate slightly more than twice the initial amount of the particles if the particle size is reduced by half. When these particles are suspended in a fluid, the

increase of total particle amount results in a higher probability of friction between the particles in the suspension, hence increasing suspension viscosity. The effect of a reduction in particle size on viscosity is illustrated in Figure 4.13.

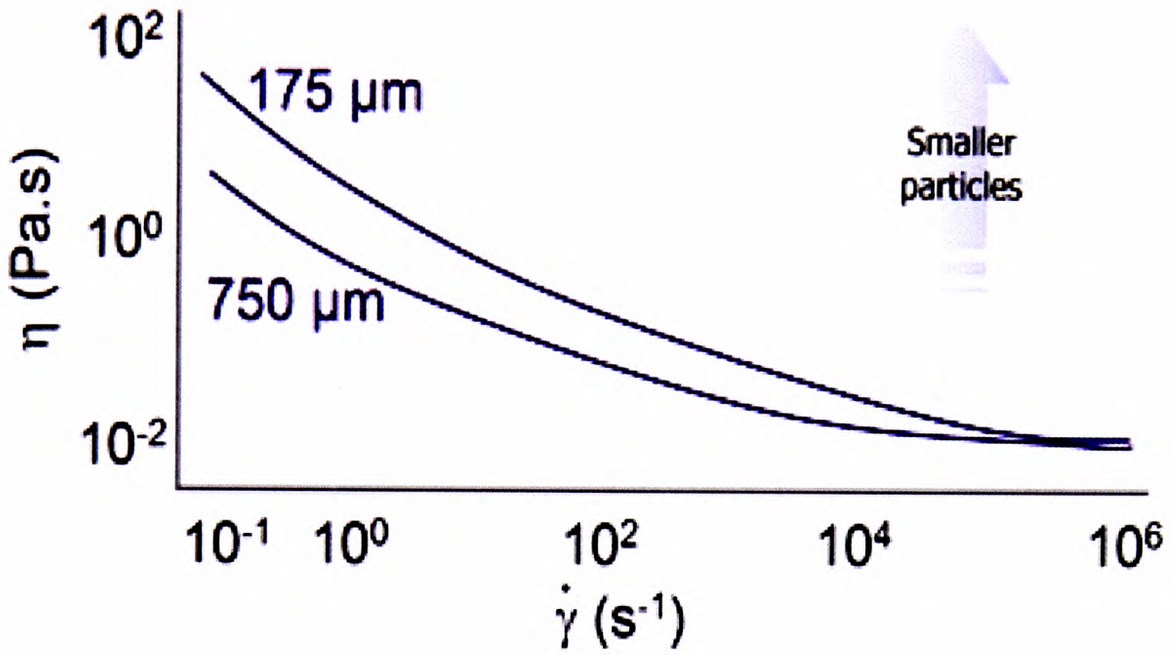

Figure 4.13: Effect of particle size reduction on viscosity in a latex suspension. (Fletcher and Hill, 2008)

d) Particle size distribution

The type of particle size distribution (PSD) can affect the viscosity of the suspension as it affects the maximum packing fraction of the suspension. To improve the packing fraction a normal (broad particle size range) PSD or log-normal (narrow particle size range) PSD may be used. The packing fraction can be improved significantly because the distribution usually consist of a continuous range of particle size with big (around 70%) and small (around 30%) particle size – see Figure 4.14. These smaller-sized particles can effectively fill the voids between the larger particles. To achieve an even higher packing fraction, a combination of two different PSDs (bimodal distribution) or a multimodal PSD arrangement is sometimes used (He and Ekere, 2004). A multimodal PSD can usually achieve a maximum packing fraction close to 75% – see Figure 4.15.

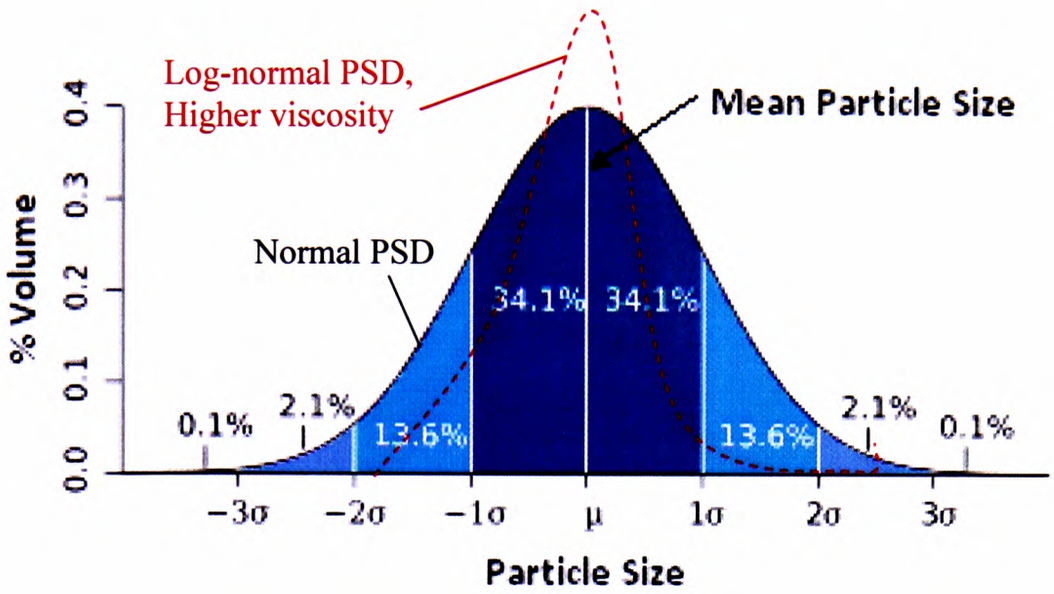

Figure 4.14: Normal and log-normal distribution particle-size curve.

Generally, the viscosity of a suspension can also be altered by changing the PSD for a given volume fraction of solid content. PSD can be effectively used to reduce the viscosity of a system that has a fixed volume fraction, whilst maintaining the same solid content (i.e. percentage by weight) (Barnes *et al*, 1989). Viscosity as a function of homogeneous particle size and particle size distribution is illustrated in Figure 4.16. It is shown there that, in order to achieve the lowest viscosity, a suspension containing a combination of two homogenous particle sizes (big and small) must be used. This also means that if a certain viscosity of suspension is desired, the desired viscosity can be easily achieved by introducing an additional amount of small or big sized particles. However, if the volume of solid content must remain constant, a broader PSD can be used to lower the viscosity; conversely, a narrower PSD (towards all big or all small particles only) can be used to increase the viscosity.

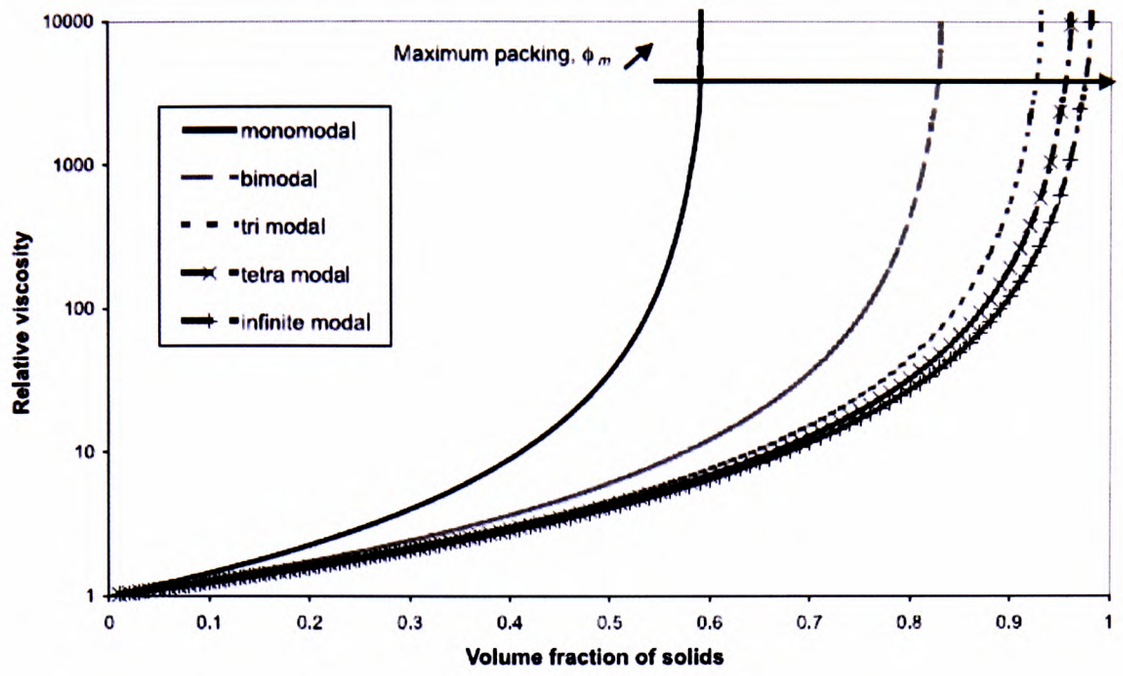

Figure 4.15: Viscosity as a function of multimodal solid-volume fraction. (Farris, 1968)

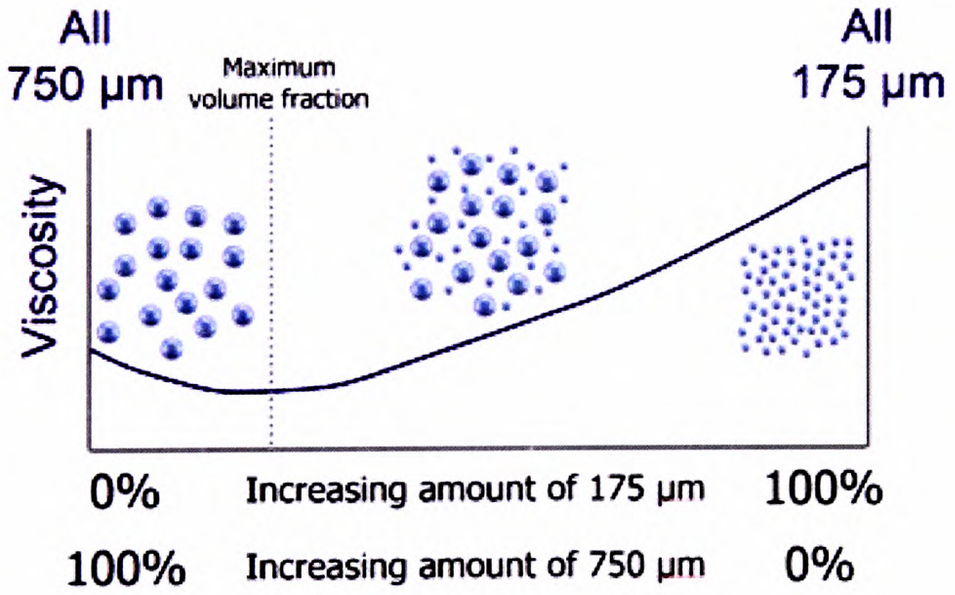

Figure 4.16: Viscosity as a function of polydispersity. (Fletcher and Hill, 2008)

e) Particle shape

Generally, the viscosity of a suspension with the same volume fraction would increase in ascending order of spheres, grains, plates and rods if the shape of the suspended particles is changed (Barnes *et al*, 1989) – see also Figure 4.17. The Maron-Pierce

equation can be used to describe the viscosity of various suspensions with different shapes of suspended particles (Ferguson and Kemblowski, 1991):

$$\eta_r = \frac{1}{\left(1 - \frac{\phi}{\phi_{max}}\right)^2}, \tag{4.23}$$

where η_r is relative viscosity (ratio of system viscosity to the medium fluid viscosity) and ϕ is a constant representing the solid volume fraction. The maximum packing fraction value, ϕ_{max}, varies between 0.74 and 0.63 for monodispersed spheres, reducing to 0.18 for fibres with an aspect ratio (ratio of major axis to minor axis) of 27 (Ferguson and Kemblowski, 1991). Thus, for a given solid-volume fraction ϕ, η_r will increase as particle aspect ratio increases.

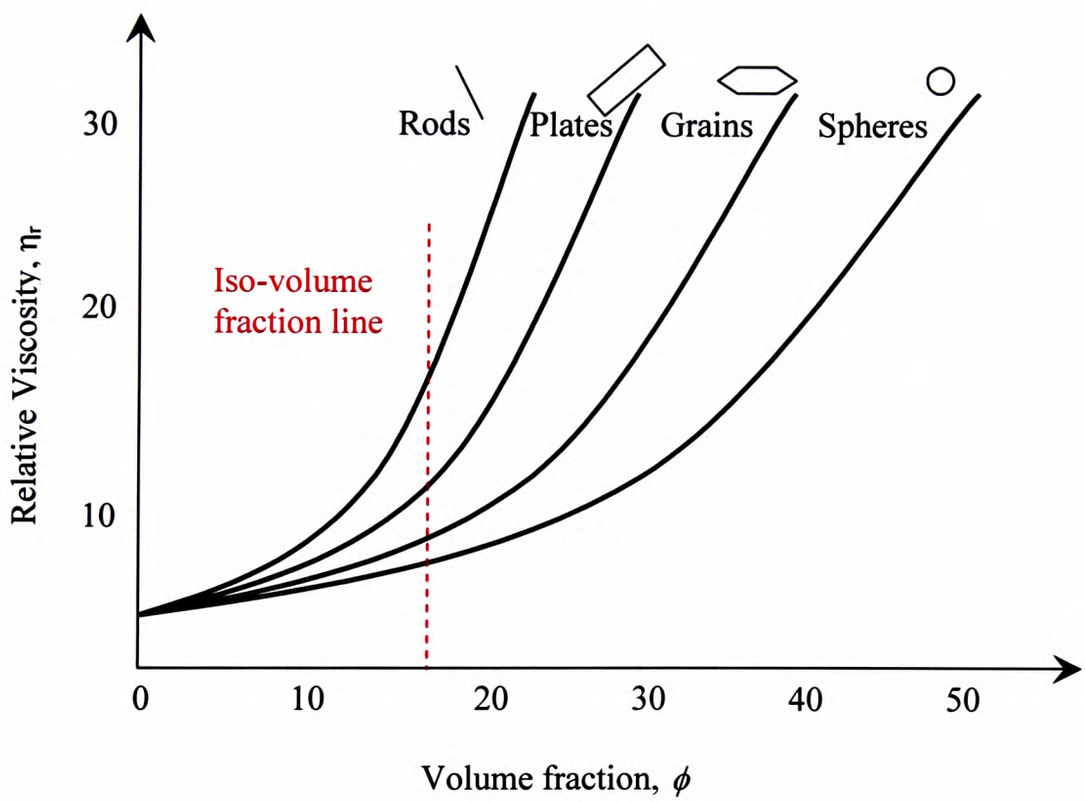

Figure 4.17: Viscosity as a function of volume fraction for various particle shapes. (Barnes *et al*, 1989)

f) Electrochemical particle interaction

Inter-particle interactions in a suspension can affect the viscosity of the suspension. These interactions usually increase significantly as the volume fraction of the solid content increases (Macosco and Mewis, 2004). However, the magnitude of the increase in viscosity varies from one suspension to another depending on the microstructure and the electrochemical reaction of the particles in the suspension. For a suspension with very small particle size, the electrochemical interactive forces cannot be ignored as the particles usually possess either a positive or negative charge, which can cause repulsion or attraction amongst the particles, in turn affecting the flow in the suspension. When a suspension has both positively and negatively charged particles, sedimentation of solid particles in the suspension can occur regardless of the solid-volume fraction. In contrast, if the suspension contains purely positively or negatively charged particles, sedimentation will never happen as the particles keep bouncing off each other at high speed, creating the effect of a 'cloudy' suspension even at low solid-volume fractions. These interactions can be further sub-categorised as set out next:

(i) Van-der-Waals forces

Van-der-Waals forces refer to the attractive or repulsive forces between molecules (or between parts of the same molecule) of the same substance. They are also known as intermolecular forces. Van-der-Waals forces are not the same as the forces that make up the molecule, i.e. intra-molecular forces (such as covalent and ionic bonds). Van-der-Waals forces arise due to fluctuating polarisation of neighbouring molecules. Essentially, the Van-der-Waals force is an overall force contributed to by dispersion forces and dipole–dipole forces, which can be explained next.

Dispersion forces are temporary attractive forces that result from electrons in two adjacent molecules occupying positions that make the molecules form temporary dipoles. They are also known as 'London dispersion forces', named after the German-American physicist Fritz London who first suggested how they might arise. Both the molecular size and shape significantly affect the strength of the dispersion forces.

Larger and heavier atoms or molecules exhibit stronger dispersion forces than smaller and lighter ones. Bigger molecules have more electrons and longer distances over which temporary dipoles can develop, leading to greater dispersion forces. The shape of the molecules also affects the magnitude of the dispersion forces: long-and-thin molecules can develop greater temporary dipole force due to electron movement than short-and-fat ones that contain the same number of electrons. Non-polar molecules usually exhibit a fluctuating dispersion force. Although polar molecules also exhibit a dispersion force, the magnitude of the dispersion force is less than the force attributed by the polar dipoles.

Dipole–dipole forces occur in polar molecules, i.e. molecules that have an unequal sharing of electrons. For instance, a hydrogen chloride (HCl) molecule has a permanent dipole because chlorine is more electronegative than hydrogen. These permanent in-built dipoles will cause the molecules to attract each other more than they otherwise would if they had to rely only on dispersion forces. It is important to note that all molecules experience dispersion forces. Dipole–dipole interactions are not an alternative to dispersion forces – they occur in addition.

(ii) Electrostatic forces

Electrostatic forces refer to the attractive or repulsive forces between the charged particles in a suspension. The relative charge between the two particles determines whether the force between the charged particles is attractive or repulsive. If the surfaces of the two particles are covered with opposite charges, they will attract each other, while if their charges are similar they will repel each other. In the case of a suspension, the electrostatic forces are most important where the continuous phase itself is polarised. The presence of charges on the particle surface often facilitates the formation of an 'electrical double layer' around the particle with charges of opposite sign from the continuous phase. The presence of this electrical double layer has a profound effect on the viscosity of the suspension. Ferguson and Kemblowski (1991) pointed out that, for a suspension with very small solid particles, an increase in the viscosity will be observed due to the additional work required during the flow to produce the distortion of the electrical double layer. It is also indicated that the increase in viscosity can be caused by electromotive (the movement of electron or

proton) repulsion between particles with similar surface charge. In order to overcome this repulsion, a greater force is required to shear the material; hence, the material exhibits higher viscosity. Another factor that could change the viscosity of a suspension is the coating of particle surfaces with polyelectrolytic stabilisers. Such action will disturb the pH balance and electrolyte concentration in the suspension, effectively changing the viscosity.

(iii) Steric forces

Steric force can arise as a result of a change in reactivity pattern of a molecule surface. Usually, the change is introduced by coating the particles in the suspension with a polymer layer, hence limiting the free surface area of the charged particles to react with other particles or the medium fluid. The existence of steric force can stop a chemical reaction from taking place, hence creating a stable suspension.

4.4.2. Interaction of physical and intrinsic forces in solder paste

In terms of physical forces, the friction force between the hypothetical layers caused by high packing fraction can affect the solder paste viscosity. The friction force in the vertical plane is normally strong enough to counteract the gravitational force, preventing sedimentation of the alloy particles in solder paste.

In terms of intrinsic forces, the sedimentation effect is also greatly reduced because of the polarity of the flux medium and the solder alloy particles. The acid and alcohol constituents (i.e. abeitic acid and propanol) in the solder paste are in fact chemicals of the second and third most polar organic compounds (Ophardt, 2003; Reusch, 2007; Carey and Sundberg, 2007). These acid and alcohol constituents contain a high density of positively and negatively charged ions in the flux medium. The solder alloy particles themselves are positively charged in nature (with relatively high electronegativity: Sn 1.96, Ag 1.93, Cu 1.9).

In the solder paste itself, because both the flux medium and the alloy particles are charged (see Figure 4.18), the difference in polarity or electronegativity allows the Van-der-Waals and electrostatic forces between pair of particles and between particles

and the flux to come into action as the distance between the particles is very small – usually the inter-particle distance is 1–2μm. These forces create attraction and repulsion between the particles and the flux, affecting fluency or viscosity in the paste. This is one of the reasons that a certain flux medium with less polar additive would have lower viscosity. Materials with high polarity/electronegativity would normally have strong intermolecular bonds; hence, they would need more energy to cause a flow to the paste since more energy would be required to break the intermolecular bonds in the material. The demand for higher energy levels to break these bonds is usually reflected in the viscosity of the paste itself. It is also worth noting that since the flux is highly polar, the flux–particle forces are usually significantly stronger than the inter-particle forces.

During a stencil printing process, these forces control and prevent the paste from slumping after the solder paste is printed on the PCB. The strong intermolecular bonds enable the flux medium to bind the solder alloy particles, keeping the shape of the deposited solder paste. However, if the bond is too strong, the paste would not be able to flow easily through small stencil apertures. Thus, it is important to understand that the viscosity or rheology of solder paste is governed not only by the physical shape or packing fraction of the solder alloy particles but also by the intrinsic chemical bonds/forces in the solder paste itself.

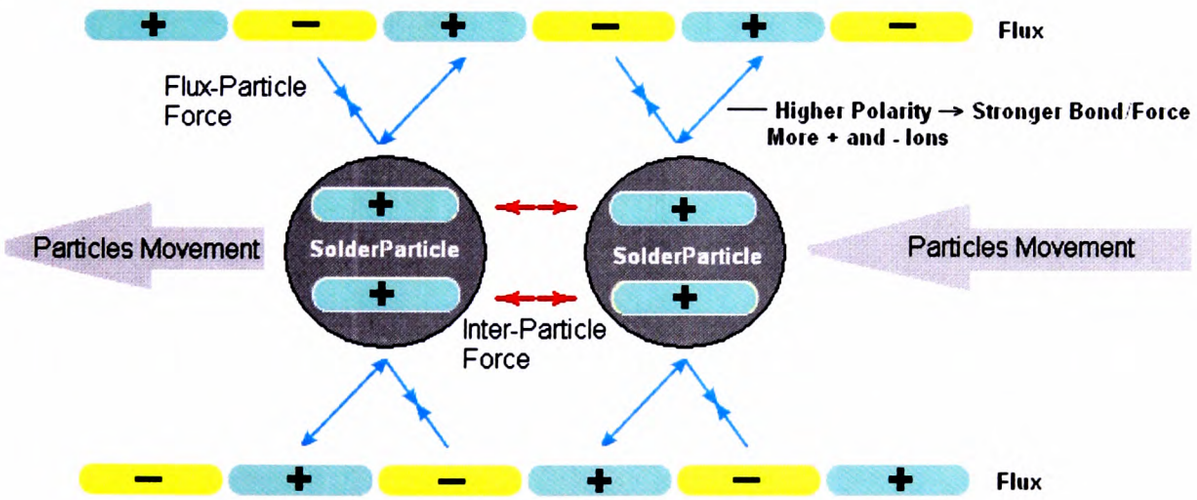

Figure 4.18: Illustration of interaction of forces in solder paste.

4.5. Equipment used for rheology characterisation

The most common method for measuring the viscosity of a fluid is by using U-shaped viscometer. This type of viscometer is usually made out of glass, very easy to use, accurate and suitable for Newtonian fluids. There are various names given to this type of viscometer because slightly varied designs exist, but generally they share a general U-shape characteristic, as shown in Figure 4.19. Some of the names for this type of viscometer include: Ubbelohde Viscometer, Ostwalt Viscometer, Cannon Fenske Viscometer, Zeitfuchs Cross Arm Viscometer, Suspended Level Viscometer, U-Tube Reverse Flow Viscometer, and Glass Capillary Viscometer. However, there is a limitation on the measurable viscosity range detected using any one of this type of viscometer and, as a result, a number of different viscometer sets are generally required in order to cover a broad range of viscosity values.

The general principle when measuring the viscosity of a fluid using this equipment is to draw the liquid into the upper bulb by suction, then release it to flow through the capillary into the lower bulb. The time taken for the level of the liquid to pass between two marked points on the upper bulb, multiplied by a factor unique to the viscometer, should give the value of the kinematic viscosity. All commercial units are provided with a conversion factor, or can be calibrated by a fluid of known properties. The viscometers are usually placed in a constant-temperature water bath because temperature affects the viscosity of a fluid.

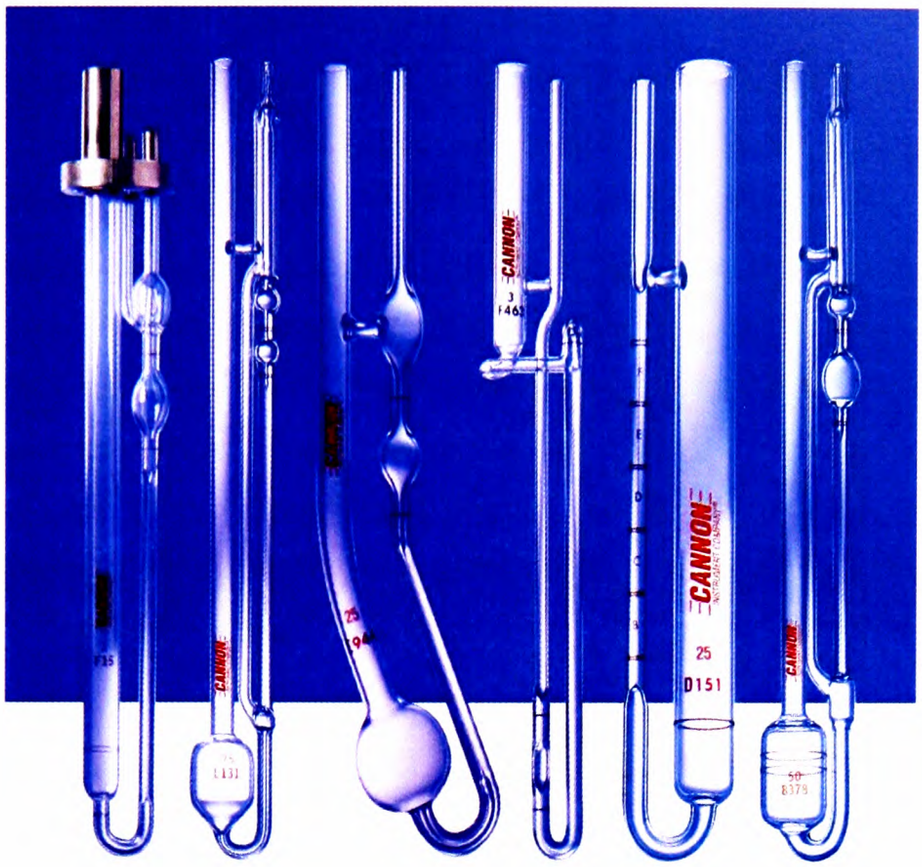

Figure 4.19: Various types of U-shape viscometer. (Photo courtesy of Cannon)

Another type of viscometer having an almost similar operating principle to the U-shaped version is also commonly used to measure viscosity of liquid. This viscometer is called the 'falling sphere' viscometer or 'falling needle' viscometer (see Figure 4.20). In this type of viscometer, a sphere of known size and density is allowed to drop through a liquid in a vertical glass tube. If the right mass of sphere is selected, it will reach a terminal velocity. Since the density, size of sphere and terminal velocity are known, the viscosity can be calculated using Stokes' Law.

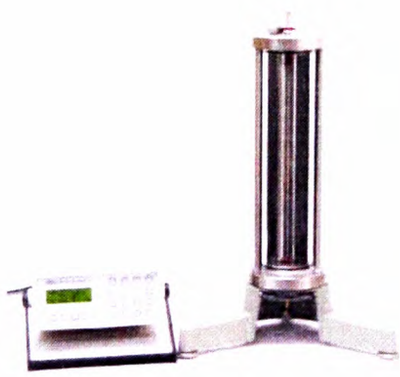

Figure 4.20: Falling needle viscometer (Photo courtesy of Betatek Inc.)

Brookfield and Malcom viscometers (see Figure 4.21) have long been used to measure the viscosity of viscous material, especially for formulations such as cough syrup and toothpaste, where high shear-rate resistance is required to prevent the material from dripping or squirting out from the container or bottle when dispensed. Another area of use for this type of viscometer is the automotive lubrication oil, as defined by the American Society for Testing and Materials (ASTM). The requirement set by ASTM (ASTM D4683) is that, in order to meet a certain grade of the standard, the oil needs to have a low enough viscosity at temperature of 150°C with the highest possible rotational speed of the spindle during test. This requirement exists because of engine oil exposure to the high temperatures and high shear rates of engine piston movement (a few thousand rpm).

Figure 4.21: Brookfield DVIII plus and Malcom PCU201 viscometers. (Photos courtesy of Brookfield Engineering and Malcomtech Inc, respectively)

The principal operating method of these machines is very similar to those of the household electric blender, but they are equipped with a microcontroller and a tachometer to monitor the rotational speed of the spindle on the machine. The microcontroller can compute how much electrical energy has been used to generate (say) a 10rpm spindle movement. Based on this information and the geometry of the spindle fitted to the machine, a viscosity value is generated and displayed on an LCD

screen. The Brookfield or Malcom viscometer is not equipped with temperature control equipment, so most experiments will be conducted at the expense of unregulated room temperature. For this reason, a stand-alone water bath needs to be used when conducting a test.

The relevant standard for rheological characterisation of solder paste is normally based on a viscosity test according to the IPC-TM-650 2.4.34 single-point viscosity measurement, using either a Brookfield or Malcom machine, which can be explained using the following procedures:

- Place the container (minimum volume requirements: 4cm diameter, 10cm depth) of solder paste in a water bath at 25°C ±0.5°C.
- When the paste has reached thermal equilibrium, place the container under the T-bar spindle (type F) so that it is at the centre of the surface of the sample.
- (Brookfield machine) Start the viscometer at 5rpm and bring the helipad stand to descent. The helipad stand is a motorised unit that climbs at a certain rate up and down the stand, which the viscometer is attached to. The Malcom machine does not have a helipad stand, but the unit is equipped with a mechanism to lower and raise the T-bar spindle during the test at programmable descent/climb rate.
- Two minutes after the T-spindle has cut into the top surface of the paste, the viscosity value should be recorded. The spindle should not touch the bottom of the container.
- Remove the T-spindle from the container.
- The viscosity is expressed as a value calculated from the average of the peak and valley of the last two cycles (A total of 5 cycles are normally recorded). If the average of the first two cycles is more than 10% higher than the last two cycles, the test is invalid and additional equilibrium time is required.

The rheometer can be considered one of the most advance viscosity measuring devices currently available. The rheometer is superior to a viscometer as it can measure multiple viscosity points, which is usually done by working in controlled stress mode or controlled shear mode. Another benefit of using a rheometer is its

ability to measure a wide range of viscosity values for non-Newtonian fluids and opaque fluids.

A rheometer is usually composed of several different components, such as air filter/regulator, power box, motor cooler, external Peltier plate temperature controller, and cooling unit with integrated water pump (see Figure 4.22). Most rheometers utilise a frictionless air bearing to perform perfect rotational measurements, operating at an air pressure of 3bar. Experiments at constant or variable temperature are controlled via the Peltier plate temperature controller. All rheometer functions, including data transfer, are controlled via a computer link.

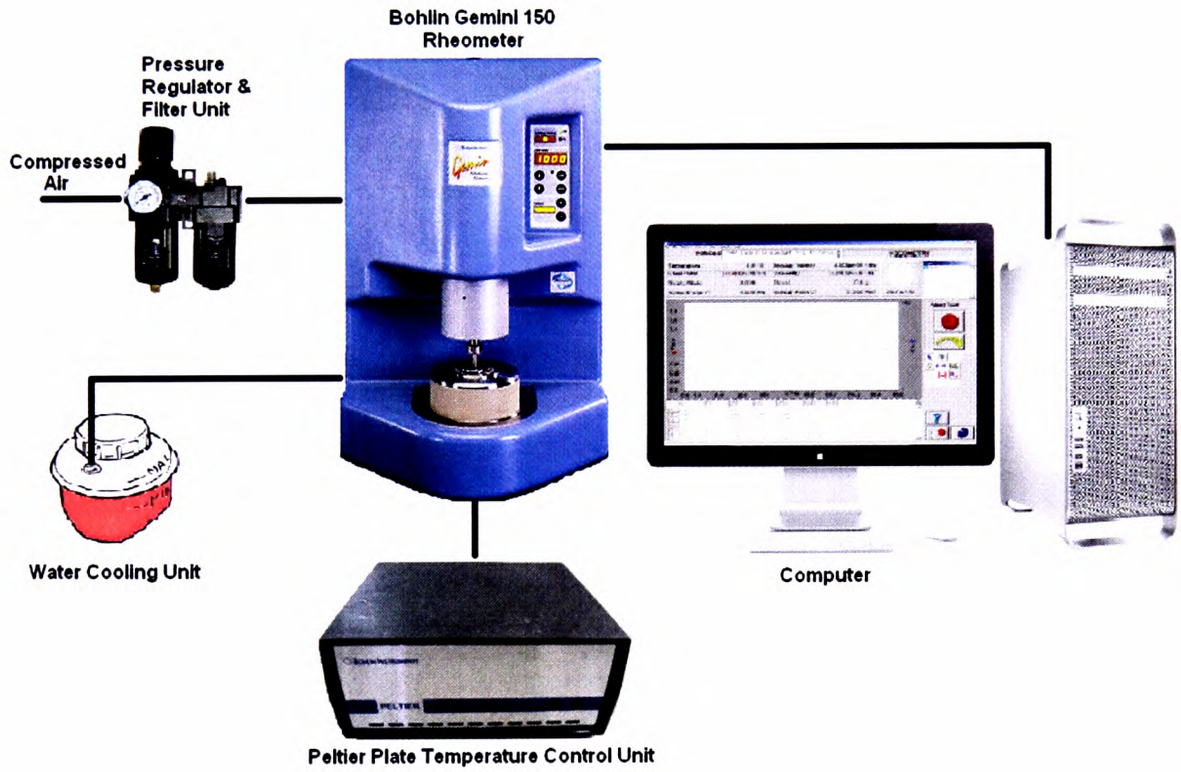

Figure 4.22: Bohlin Gemini 150 rheometer system. (Photo courtesy of Malvern Instrument)

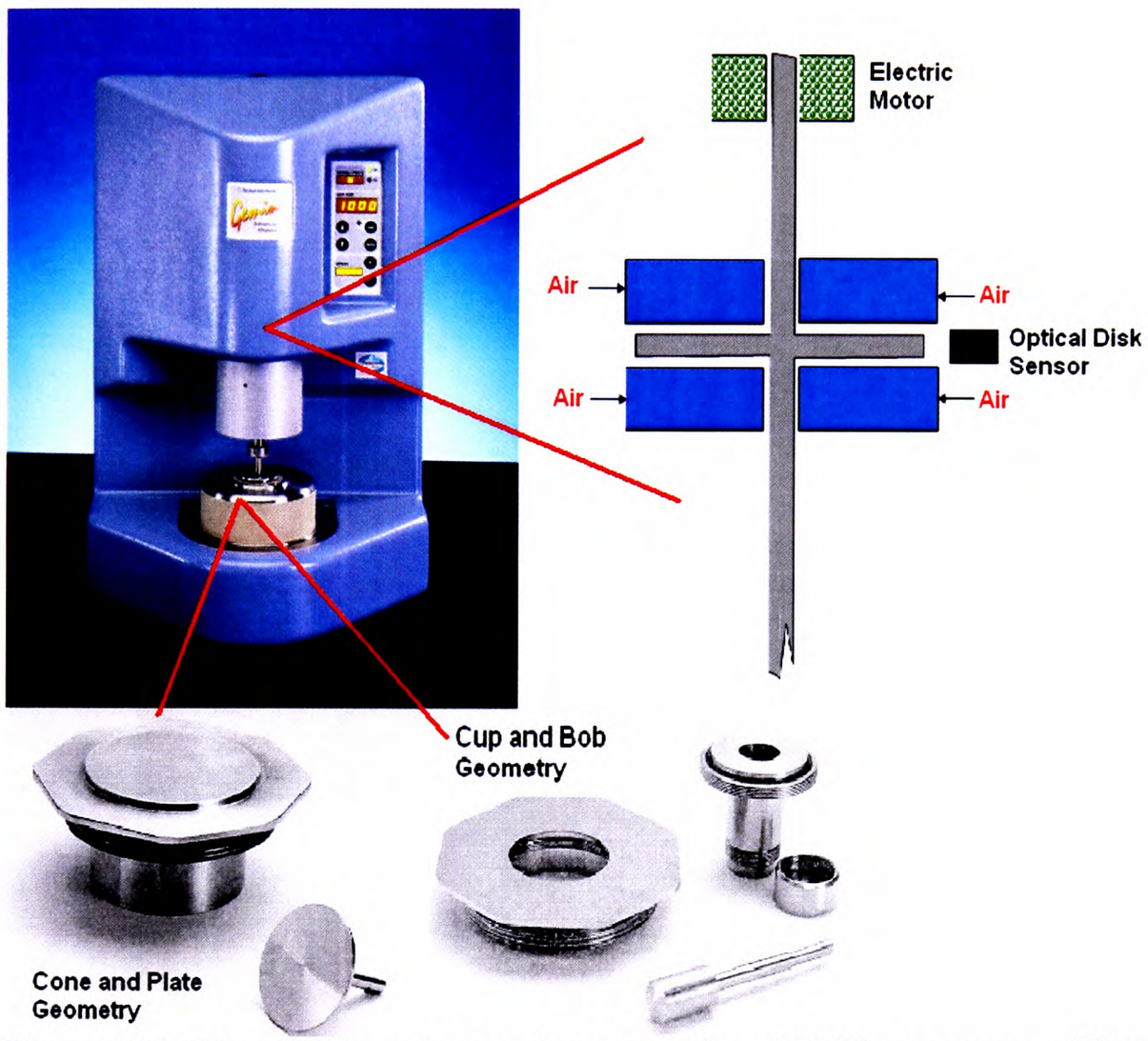

Figure 4.23: Internal parts and measuring geometries of Bohlin rheometer. (Photo courtesy of Malvern Instrument)

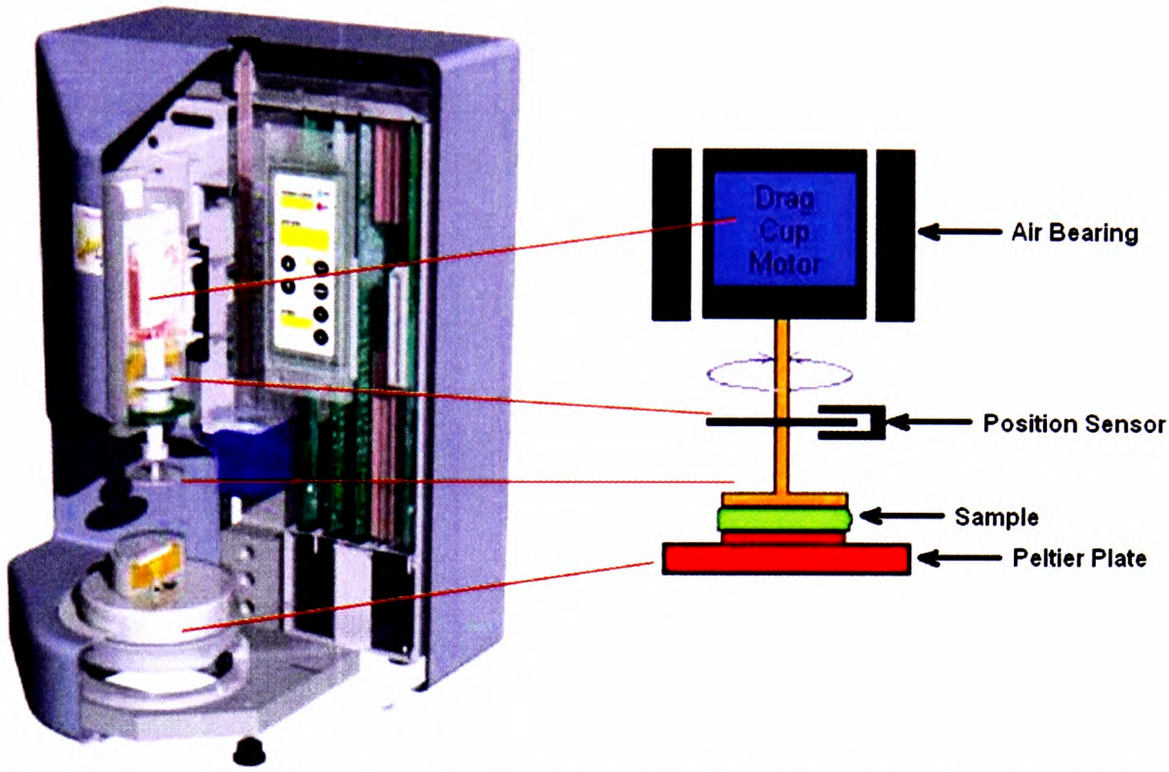

Figure 4.24: Cut-away view of Bohlin rheometer. (Photo courtesy of Malvern Instrument)

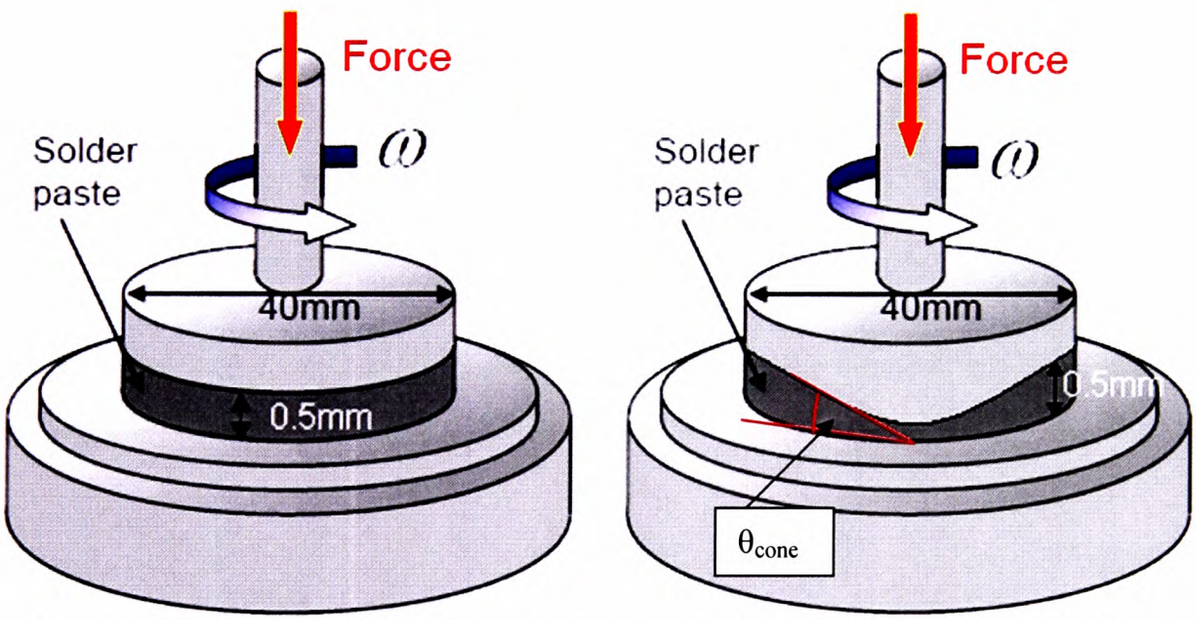

Figure 4.25: Representation of applied force and torque on parallel-plate and cone-and-plate measuring geometries.

The operating principle of the rheometer is based on the technology to control and measure the amount of voltage (V) and current (I) sent to the electric motor inside the rheometer (see Figures 4.23 and 4.24). The torque produced by the electric motor is

directly proportional to the voltage and the current sent to the motor. At the same time, by measuring the displacement on the disc using the optical disc method, the angular velocity of the disc movement, ω *(rad/s)*, can be calculated. Hence, the torque (T) can be calculated using the following relationship:

$$\begin{aligned} Power &= Torque \times \omega \\ V \times I &= T \times \omega \end{aligned} \tag{4.24}$$

Accordingly, the torque is correlated to the shear stress based on the following equation:

$$\tau = \frac{3T}{2\pi R^3} \tag{4.25}$$

where τ is the shear stress, T is the torque and R is radius of the plate.

The shear rate for parallel-plate and cone-plate are defined as:

$$\dot{\gamma} = \frac{R \cdot \omega}{h} \qquad \text{and,} \qquad \dot{\gamma} = \frac{\omega}{\theta_{cone}} \tag{4.26}$$

where $\dot{\gamma}$ is the shear rate, ω is the angular velocity, h is the gap height and θ_{cone} is the cone angle.

Hence, accordingly the viscosity using parallel-plate and cone-plate can be correlated using the following equation:

$$Viscosity = \frac{ShearStress}{ShearRate} \rightarrow \eta = \frac{3T \cdot h}{2\pi R^4 \cdot \omega} \qquad \text{and,} \qquad \eta = \frac{3T \cdot \theta_{cone}}{2\pi R^4 \cdot \omega} \tag{4.27}$$

As shown in Equation 4.26, the shear rate is dependent upon the radius and the gap between the plates. For parallel-plate geometry of any size, the magnitude of the shear rate is not constant across the plate: the shear rate is zero on the centre of the plate and maximum on the edge of the plate. Thus, in order to obtain the shear rate, the software in the Bohlin rheometer has been programmed to calculate the shear rate using the

median radius of the plate instead of the actual radius of the plate (i.e. for parallel plate with radius of 20mm, a 10mm radius was used in the calculation). As a result, the shear rate obtained using parallel-plate geometry is an average shear rate. For cone-and-plate geometry, since the cone angle (θ_{cone}) is constant from the centre of the plate to the edge of the plate, the result is a constant shear rate throughout the plate, from the centre to the edge. Regardless of whichever geometry is used, the operator is given the freedom to select the range of the shear rate to be applied to the sample. However, the minimum and maximum shear rate also has a limit due to limitation of the minimum value of the angle the stepper motor can move as well as the power of the motor. This means that, in order to apply a very high shear rate, a smaller size plate must be used.

The viscosity measured by Equation 4.27 is usually referred as the 'dynamic/ absolute viscosity', with the SI (International System of Units) physical units of the Pascal–second (Pa.s).

Due to extensive exposure to operating two different types of rheometer (controlled stress and controlled strain) in the University of Greenwich's EMERG laboratory, and various viscometers including the Brookfield and U-tube viscometers in the fluids laboratory, the author has been able to compile a chart based on the features available on the equipment. The chart is shown in Figure 4.26 and will help readers to decide which equipment should be used for specific application and what kind of test should be run.

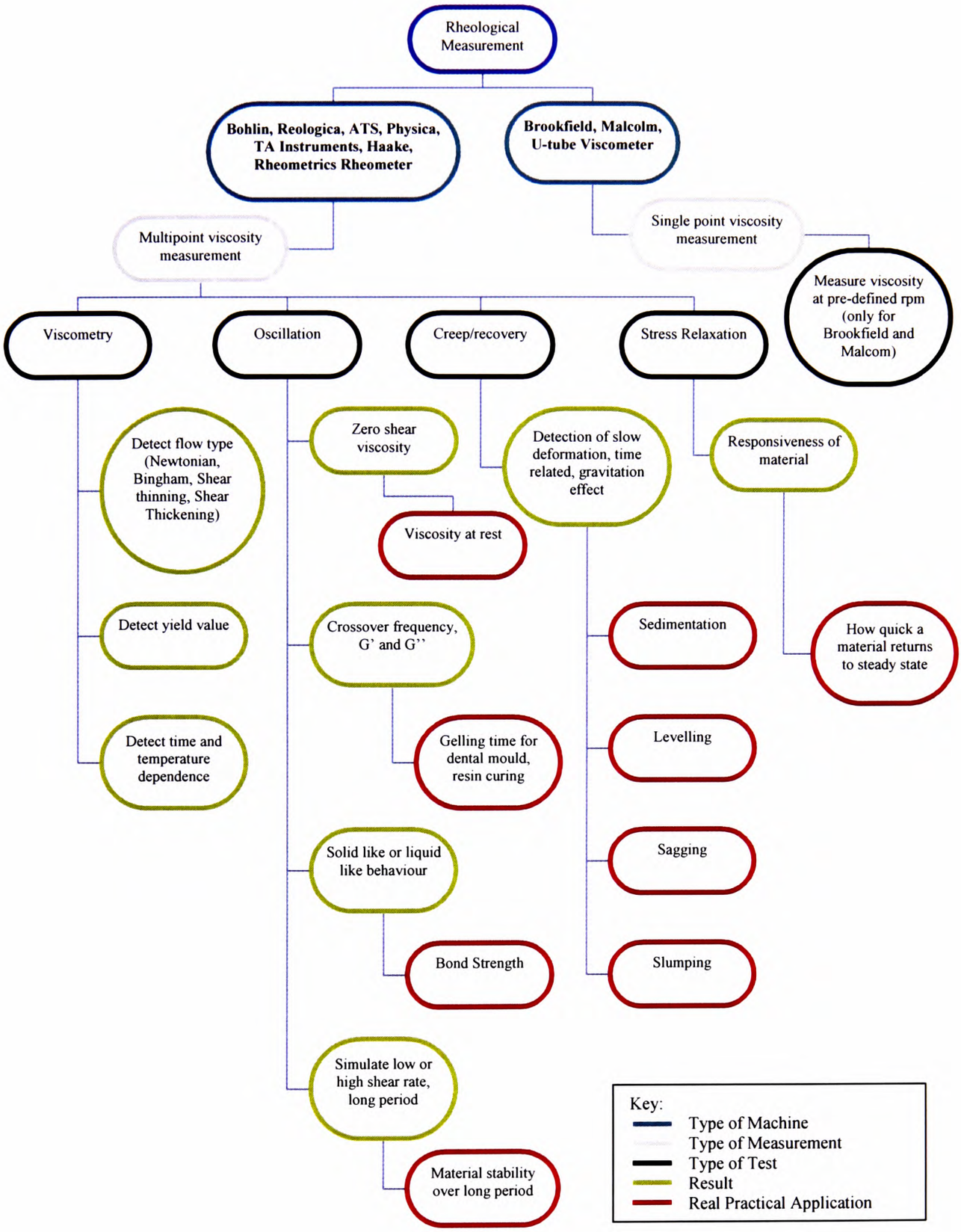

Figure 4.26: Rheology equipment selection chart, related to the practical application of viscosity in industry.

Although Figure 4.26 lists other capabilities of a rheometer, only viscometry tests can be used to simulate the tests performed on the Brookfield or Malcolm viscometers – i.e. those that the solder-paste manufacturing industry is currently using for its quality-control standard. Rheometers would be more appropriate to be used for non-Newtonian materials because of their ability to measure a very wide range of viscosity values. Other benefits of using rheometers include the ability to identify material behaviour through various shear rates, such as non-drip paint, which is otherwise not possible using single-point data obtained from the Malcom or Brookfield viscometers.

This clearly shows that the rheometer is in principle a superior piece of measuring equipment compared with a viscometer for the purpose of quality control. Nevertheless, the industry remains sceptical about using rheometers for quality control due to the following constraints:

- tests performed using a rheometer take longer to complete;
- rheometer price (currently around £16,000);
- the requirement that the user has to be trained to analyse a rheogram;
- the requirement for judgement by the user, possibly resulting in biased results; and
- the nature of time-dependent fluids.

One way to illustrate the problem of relying on information related to a single-point viscosity value is that two solder pastes with different types of flux could have similar single-point viscosity yet perform differently at the printing stage. But by using a rheometer, we can analyse the flow graph from a good paste and use it as a benchmark for new paste formulations because the effect of increasing or reducing the proportion of a certain flux constituent can easily be pinpointed from the flow graph. In other words, it would be possible to know which constituent to add or adjust in order to reach a desired result.

4.6. Summary

The rheological properties of solder paste are governed by physical and intrinsic forces. Volume fraction, particle size and the shape of the solder particles dissolved in the flux medium can each greatly affect the viscosity profile of the solder paste. These factors also determine the storage and loss moduli (G' and G'' respectively) of the solder paste, which are indicators of the stress response behaviour of the paste. The storage and loss moduli can be used to provide an indication of whether a solder paste can easily flow through a printing stencil's apertures and the paste's ability to hold its shape. Intrinsic forces such as electrochemical interactions between the solder particles and the flux medium are difficult to quantify, but they play a role in the rheology of the paste.

CHAPTER 5

CASE STUDIES

5.1. Introduction

This chapter presents a few examples of case studies on the use of ultrasound techniques to study the properties of materials – for example, the effect of air bubbles, temperature and cavitation related to the use of ultrasound.

Although there might be other case studies available for study, the case studies presented in this chapter have been carefully selected as these cases are the ones which are most relevant to a study of the behaviour and properties of solder paste. These case studies have provided the author with the opportunity to analyse and review why and how various ultrasound techniques have been used in the non-destructive testing and characterisation of materials. These case studies also present the challenge of using ultrasound techniques to solve problems where conventional techniques encounter reliability problems due to limitation of an operator's skills or natural changes to a material's properties.

5.2. Case study of fresh mortar

The use of non-destructive ultrasound techniques for concrete or fresh mortar arises because most often it is difficult – if not impossible – to cut a section of a concrete structure just to examine its quality without jeopardising the integrity of the structure itself. The use of ultrasound techniques for studying concrete or fresh mortar properties has been in existence almost from the time when ultrasound techniques were first used for studying cracks in metal or welding joints, i.e. at least 50 years to

date (Krautkramer, 1959). The use of ultrasound techniques for concrete, fresh mortar or cement is mainly targeted at investigating the following properties:

- porosity estimation;
- permeability estimation (the ability to absorb and hold water); and
- compressive strength.

The most significant example of work to study the porosity of cement paste using ultrasound was presented by Hernández *et al* (2000, 2006a, 2006b). Similar studies were also reported by Grosse *et al* (1999), Kamada *et al* (2005) and Punurai *et al* (2006). The conventional method for studying the porosity of cement paste is by measuring the changes in total volume before and after the cement and water were mixed. For concrete sample, a mercury or vacuum porosimeter is used. Other alternatives include using x-ray or computerised tomography (CT) imaging, but these techniques can be very time consuming as layer-by-layer scanning is required to produce a reliable estimate of the porosity in the cement paste or concrete sample.

Hernández, Grosse, Kamada and Punurai and their colleagues all used a similar equipment set-up for their studies on porosity estimation, which were all based on the through transmission mode of working. Only Hernandez used immersible ultrasound transducers, with the samples to be tested fully immersed in a water tank (see Figure 5.1). This is understandable because an air-coupled ultrasound system normally returns a very faint signal, especially with highly attenuating material such as cement paste or concrete. Hernández used the micromechanical model to correlate the porosity, density and ultrasound properties of the sample materials. The model was derived from stress/strain tensors acting on isotropic material (see Section 3.8.2 above), in which porosity can be correlated with the cement matrix according to the following elastic stiffness equations (Hernández *et al* 2000, 2002):

$$C_{11} = C_{11}^{m} + \frac{x\left[C_{11}^{m} - \frac{4}{3}\left(C_{44}^{m}\right)\right]\left(\langle T_{1111}\rangle + 2\langle T_{1122}\rangle\right)}{1 - x + x\left(\langle T_{1111}\rangle + 2\langle T_{1122}\rangle\right)} - \frac{\frac{8}{3}x\left(C_{44}^{m}\right)\langle T_{1212}\rangle}{1 - x + 2x\langle T_{1212}\rangle} \tag{5.1}$$

$$C_{44} = C_{44}^{m} - \frac{2x\left(C_{44}^{m}\right)\langle T_{1212}\rangle}{1 - x + 2x\langle T_{1212}\rangle} \tag{5.2}$$

where x is the volume fraction of pores, T is the stress/strain tensor, and C_{11} and C_{44} are elastic constants that are normally referred to as E (Young's modulus) and G (shear modulus) respectively.

Hence, the elastic constants can be correlated with ultrasonic velocity using the following relationship (Hernández *et al* 2000, 2002):

$$V_L = \sqrt{\frac{C_{11}}{\rho}} \qquad V_T = \sqrt{\frac{C_{44}}{\rho}} \tag{5.3}$$

where V_L and V_T respectively are the longitudinal and transverse ultrasonic velocities.

Hernández's study showed that using ultrasound techniques produced comparable results to those for the conventional destructive-test technique (see Tables 5.1 and 5.2). This is highlighted by almost similar deviations between the destructive method and the non-destructive ultrasonic technique. The results also hint that higher deviations normally occur in relation to a high water-to-cement ratio. This could be due to the assumption used in the micromechanical model that the voids in the test material will increase proportionally when more water is present in the cement paste (see Figures 5.2 and 5.3).

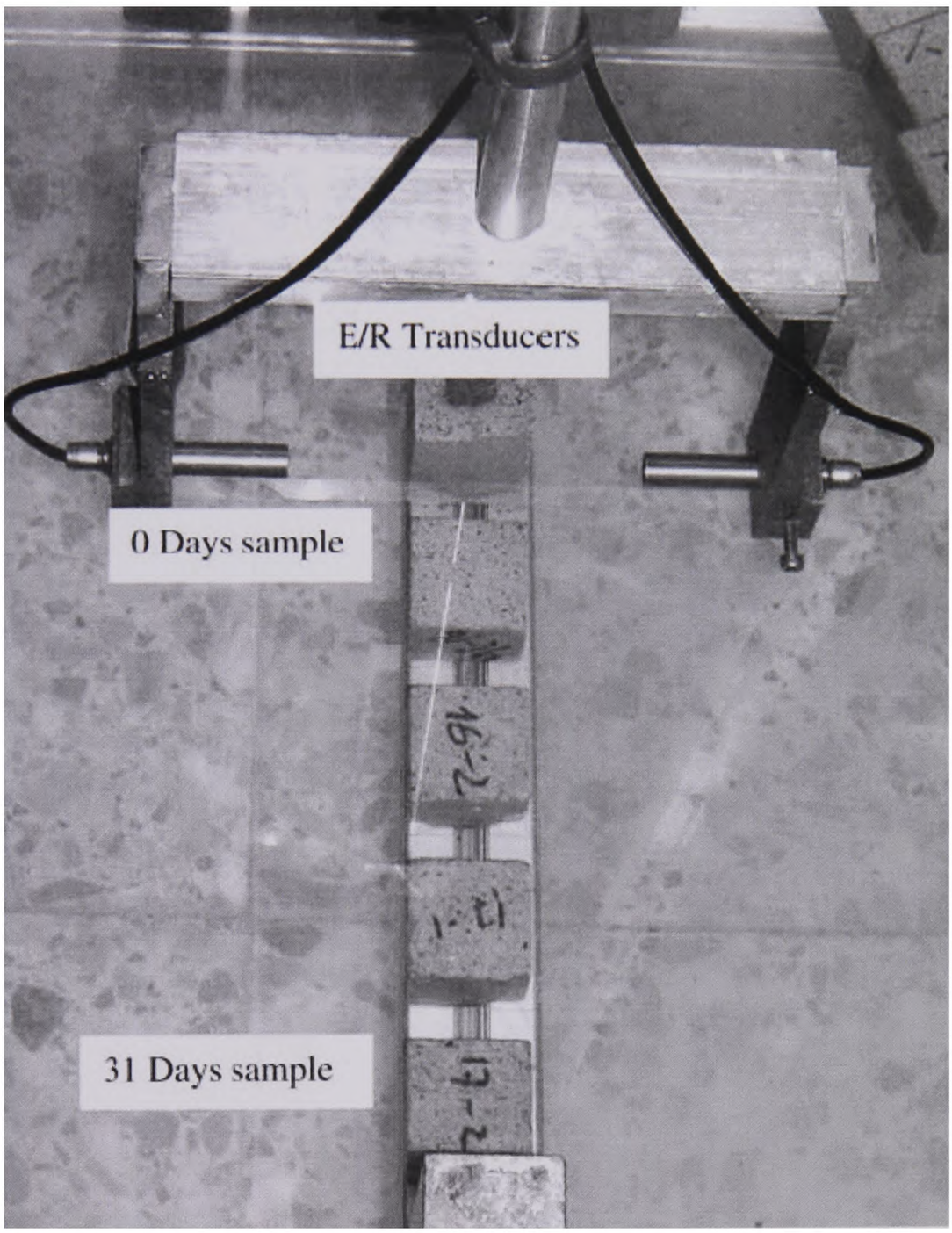

Figure 5.1: Water-submersible through-transmission ultrasound system for cement block, with samples immersed in a water tank. (Hernández *et al*, 2006a).

Destructive measurement

W/C ratio	Porosity (%)	Apparent density (g/cm^3)	Real density ($g\ cm^3$)	Standard deviation of porosity
0.45	15.95	2.45	2.91	0.18
0.50	18.04	2.45	2.98	0.14
0.55	19.94	2.49	3.11	0.12
0.60	20.81	2.52	3.18	0.25

Table 5.1: Correlation of porosity and density of concrete using a destructive technique (Hernández *et al*, 2000).

Nondestructive measurement

W/C ratio	Measured V_L (m s) (mean value)	Calculated Young's modulus (GPa)	Calculated porosity (%)	Standard deviation of porosity (%)
0.45	4098.2	38.96	15.93	0.12
0.50	3915.6	35.57	18.04	0.26
0.55	3815.0	34.30	19.94	0.25
0.60	3775.6	34.02	20.81	0.29

Table 5.2: Correlation of porosity and density of concrete using a non-destructive ultrasound technique (Hernández *et al*, 2000).

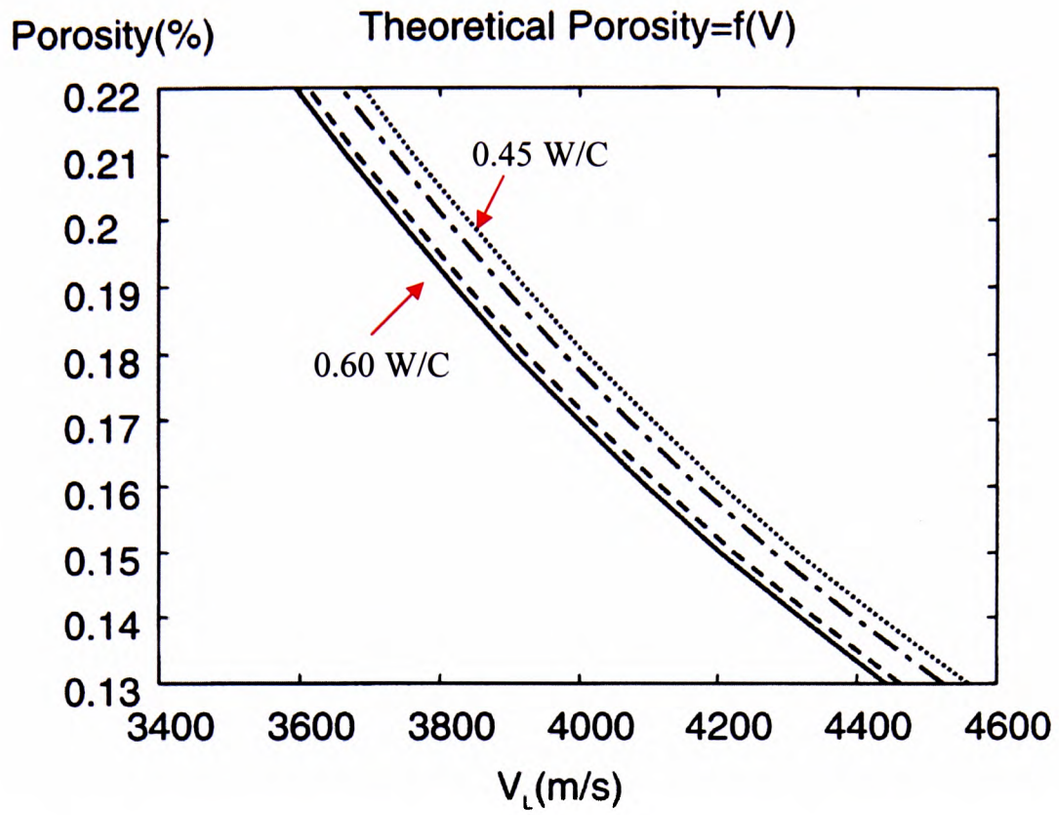

Figure 5.2: Correlation of porosity of concrete of various water-to-cement ratios (0.45, 0.50, 0.55, 0.60) to longitudinal ultrasonic velocity. (Hernández *et al*, 2000).

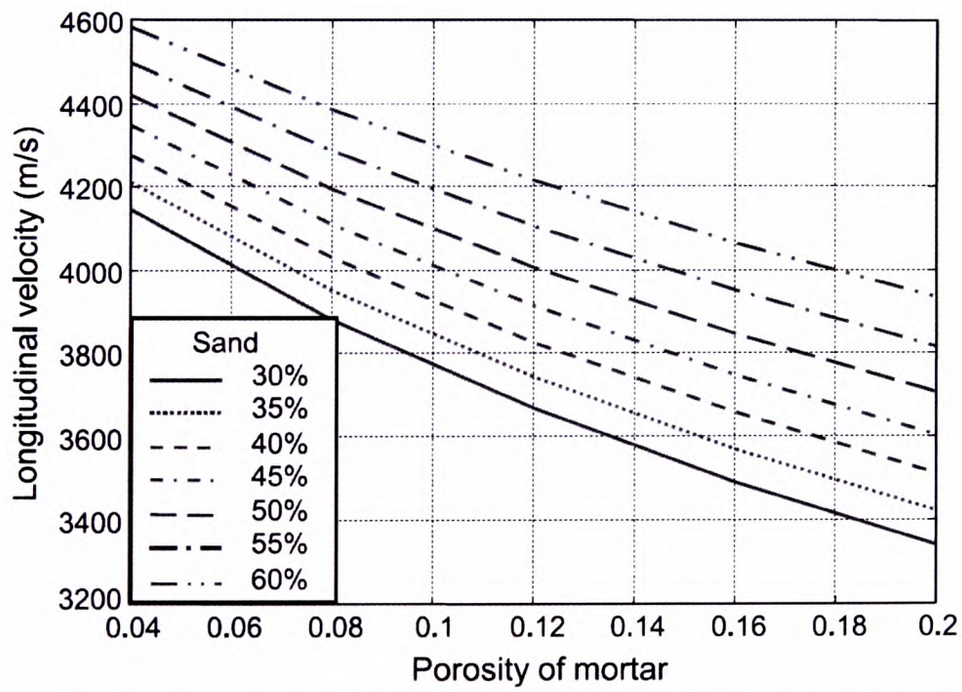

Figure 5.3: Influence of porosity and volume fraction of sand on longitudinal velocity in mortar. (Hernández *et al*, 2006b).

The inclusion of sand to a cement paste that had a fixed water-to-cement ratio resulted in higher ultrasound velocity because the sand particles replaced the pores in the cement paste matrix. This process resulted to higher ultrasound velocity as the sound waves then had shorter alternatives paths to reach the receiver-transducer (see Chapter 3 Figure 3.39 above).

Kamada *et al* (2005) also worked exclusively on cement paste and reported the correlation, during the cement curing process, of ultrasound parameters (velocity and amplitude) with the changes of viscosity. The viscosity was independently recorded using a rotational viscometer such as those shown in Figure 4.21 on half the sample, while the other half of the sample was being tested using ultrasound techniques. Although the properties of the cement can still be monitored using ultrasound after it is fully cured, it is not possible to keep recording the viscosity for more than 4 hours as the hardening paste can damage the electric motor of the viscometer and the spindle. Consequently, the work was more concentrated on Stage 1 (early curing) and Stage 2 (fully cured) rather than Stage 3 (matured concrete). Results given in Figures 5.4–5.6 also indicate that it is not necessary to monitor the cement at Stage 3 as the ultrasound velocity and amplitude are nearly constant.

The most interesting part of Kamada's (2005) work was the provision of the SEM pictures (see Figure 5.7). These helped to explain the morphological development of the microstructure of the cement paste during curing, which can be used to support the theory that when the paste is fully cured there are fewer bigger pores in the cement matrix due to branching, which leads to shorter wave paths and hence higher ultrasound velocity. The branching causes the big chunky particles to break into smaller and longer interconnecting rods.

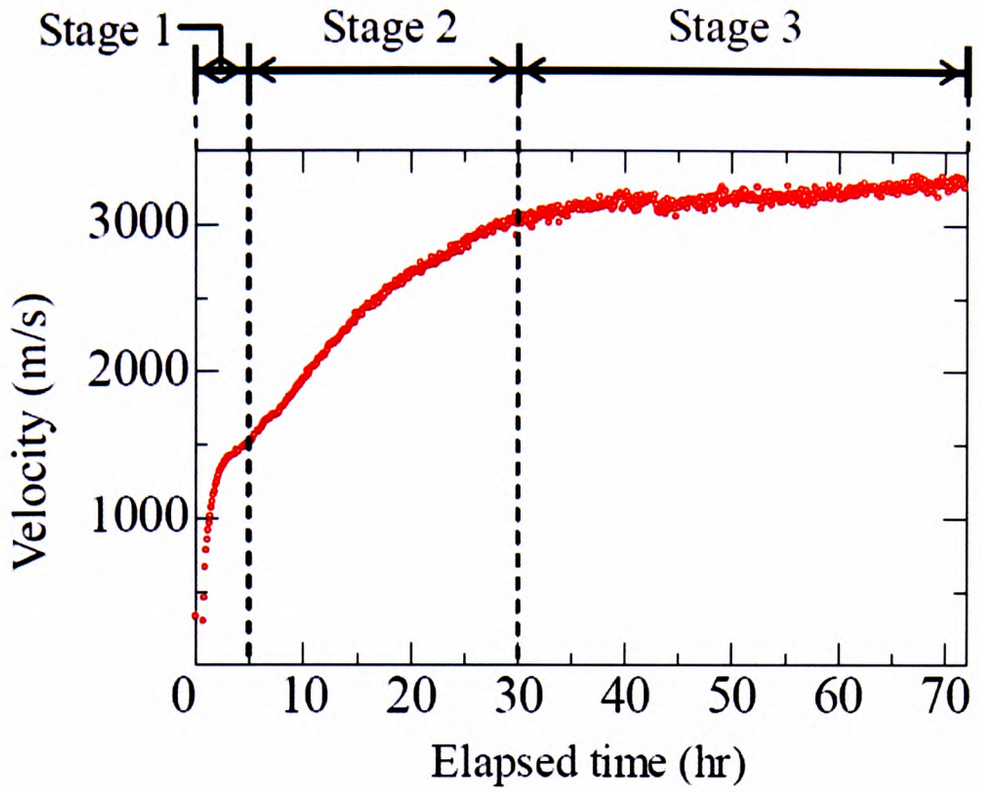

Figure 5.4: Ultrasonic velocity of cement with 0.3 water-to-cement ratio. (Kamada *et al*, 2005).

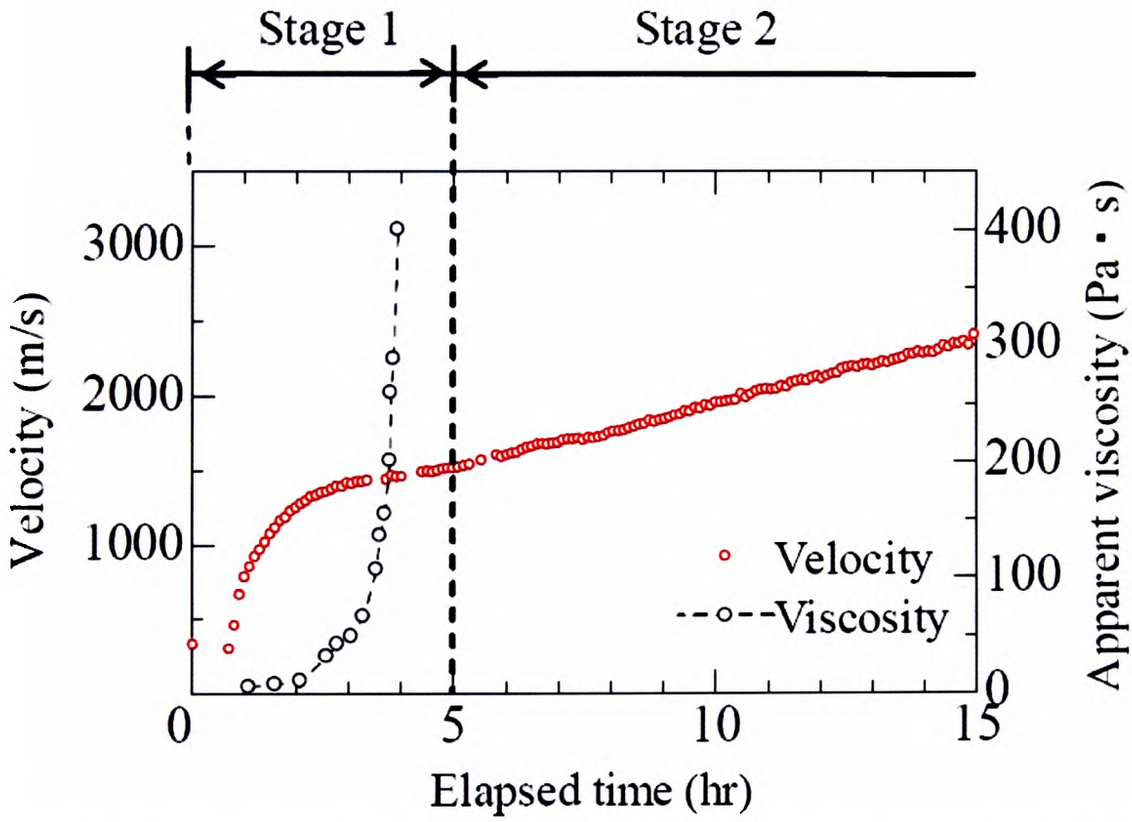

Figure 5.5: Ultrasonic velocity and viscosity of cement with 0.3 water-to-cement ratio. (Kamada *et al*, 2005).

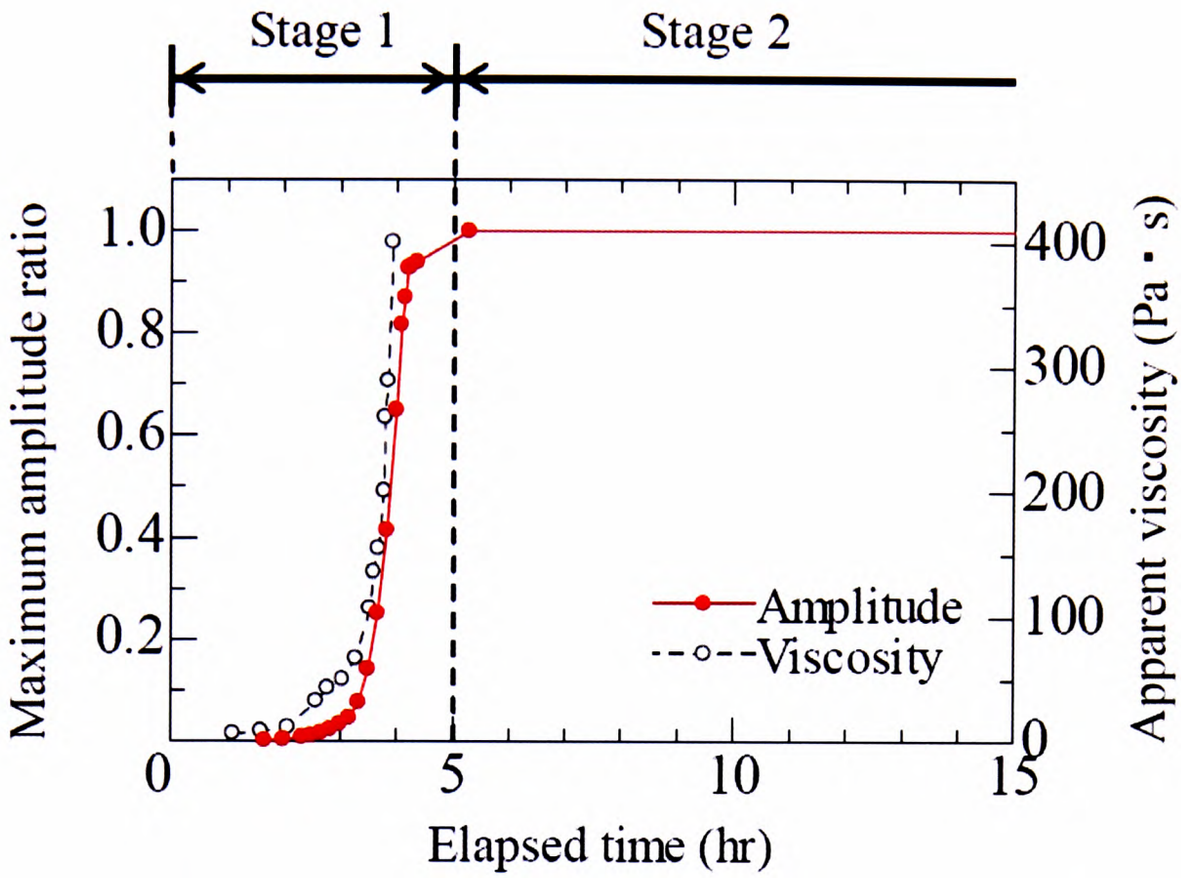

Figure 5.6: Ultrasonic amplitude and viscosity of cement with 0.3 water-to-cement ratio. (Kamada *et al*, 2005).

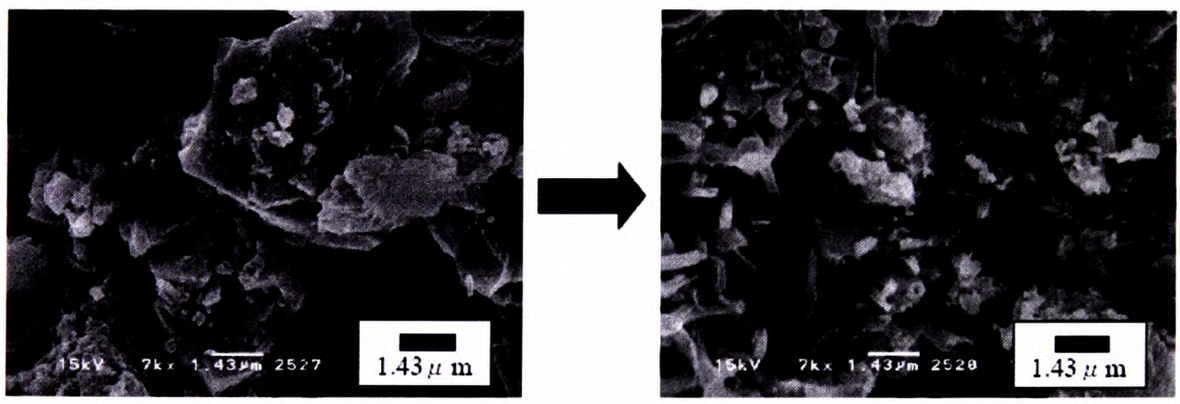

Elapsed time: 0 hour 04 minutes

Elapsed time: 12 hours 00 minutes

Figure 5.7: SEM images of cement-paste microstructure transformation during the curing process. (Kamada *et al*, 2005).

In a separate work, Grosse *et al* (1999) demonstrated that the addition of admixtures to a cement paste can affect ultrasound velocity. The increase or decrease in

ultrasound velocity can be assumed to be related to the particle size of the admixture itself – for example, the addition of accelerator admixture would increase the ultrasound velocity because the presence of an accelerator in the cement paste induces the rapid collapse of the bubbles or voids in the paste, and hence the cement cures faster. In contrast, the addition of retarder admixture would induce growth of large bubbles or voids in the paste (see Figure 5.8) and slow the ultrasound velocity. This example clearly demonstrates that ultrasound velocity may be sensitive to particle size, particle distribution and packing fraction of material. The effect of packing fraction and particle size to ultrasound parameters was later confirmed by Punurai *et al* (2006) – see Figures 5.9 and 5.10. However, Punurai's work showed that both the packing fraction and particle size were more sensitive to ultrasound attenuation.

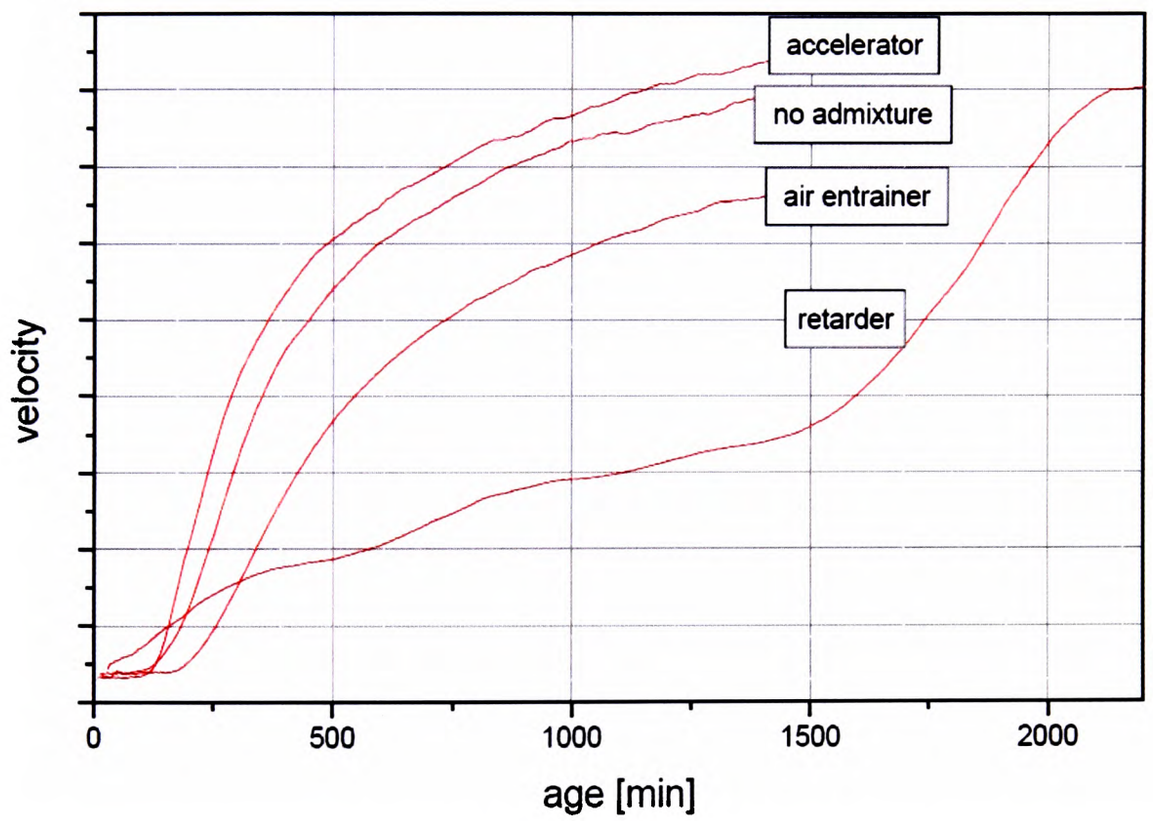

Figure 5.8: Effect on ultrasound velocity of adding cement paste admixture. (Grosse *et al*, 1999).

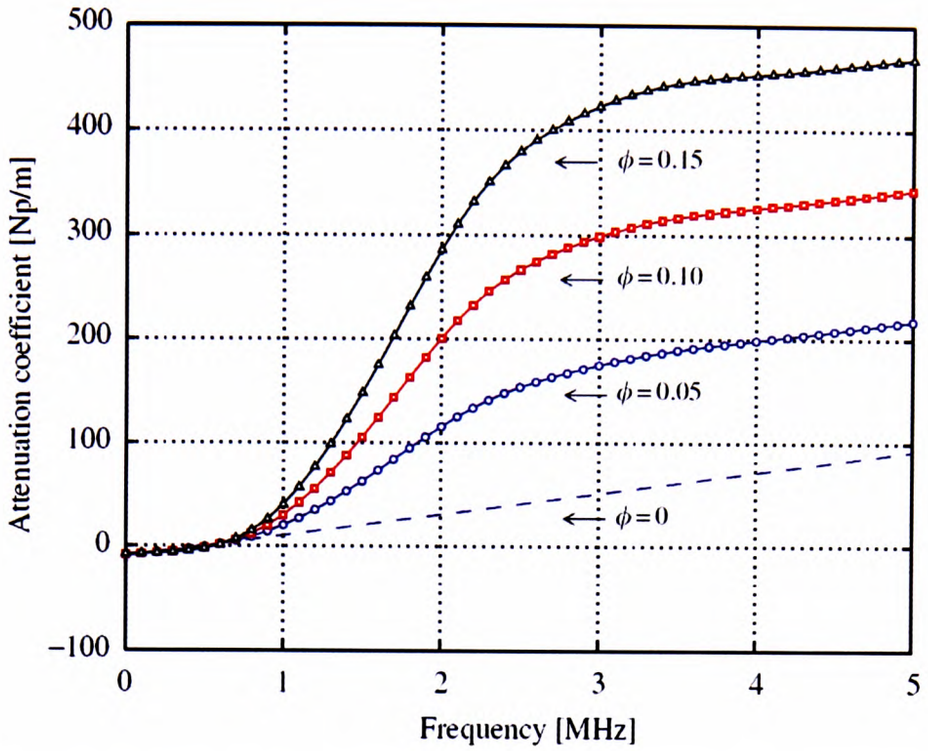

Figure 5.9: Attenuation of cement paste (water to cement = 0.4) for different void fraction, ϕ, where void radius is fixed (a=0.3mm). (Punurai *et al*, 2006)

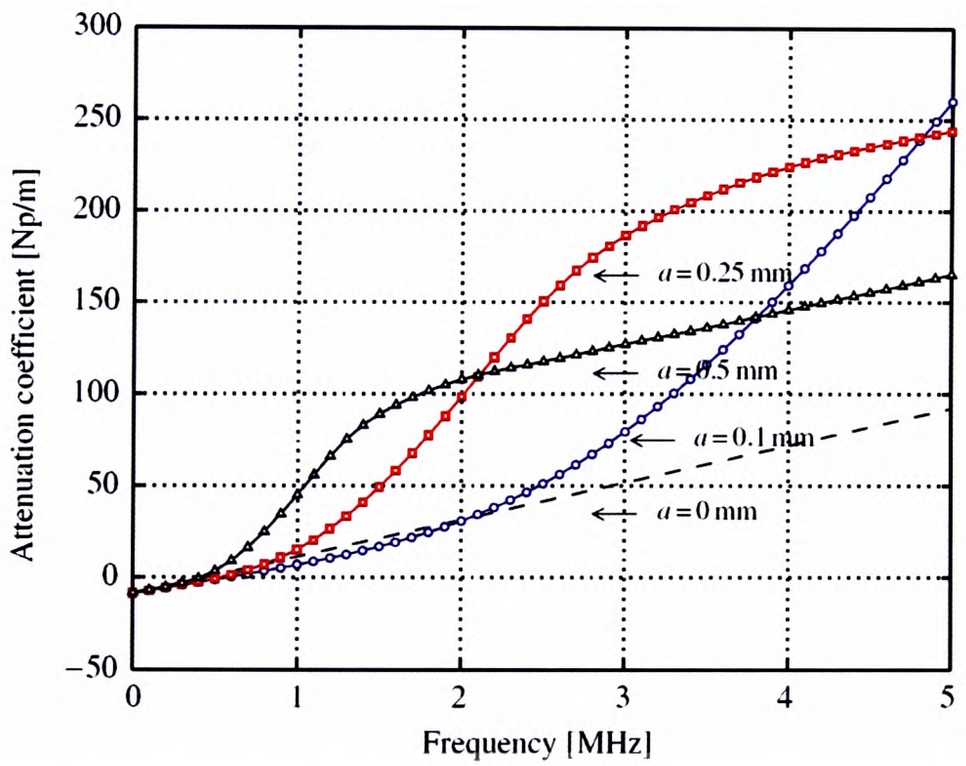

Figure 5.10: Attenuation of cement paste (water to cement = 0.4) for different void radii, a, and fixed void fraction ϕ = 5% . (Punurai *et al*, 2006)

5.3. Case study on the effect of temperature gradient in food suspensions

The most significant work on the effect of the temperature of materials on ultrasound can be illustrated by the work of Gülseren and Coupland (2007) and Wang (2004 with others; 2005). Those pieces of work demonstrate that not all materials will experience a drastic change in ultrasound velocity due to an increase in temperature. This can be explained by the fact that different materials have different melting, boiling or freezing points. Thus, when there are no structural changes in the material, there are little or no changes in ultrasound velocity – see Figures 5.11 and 5.12. Water and water-based suspensions normally encounter structural anomalies in which the volume increases as it reaches 0°C (impurities in water can lower freezing point), unlike most other materials where volume shrinkage occurs. This could be the reason why sunflower oil shows a decrease in ultrasound wave velocity when the temperature is increased – see Figure 5.13. It was found that when the temperature was increased, the sunflower oil encountered volume expansion due to the stretching of hydrocarbon chemical chains within it, and hence a decrease in ultrasound velocity. But since sucrose and tomato sauce contain water, the increasing temperature will cause the water to evaporate first (indicated by a sudden change of curve gradient at 35 °C); hence there is a reduction in the volume of such suspensions, which was found to lead to increasing ultrasound velocity for sucrose and tomato sauce.

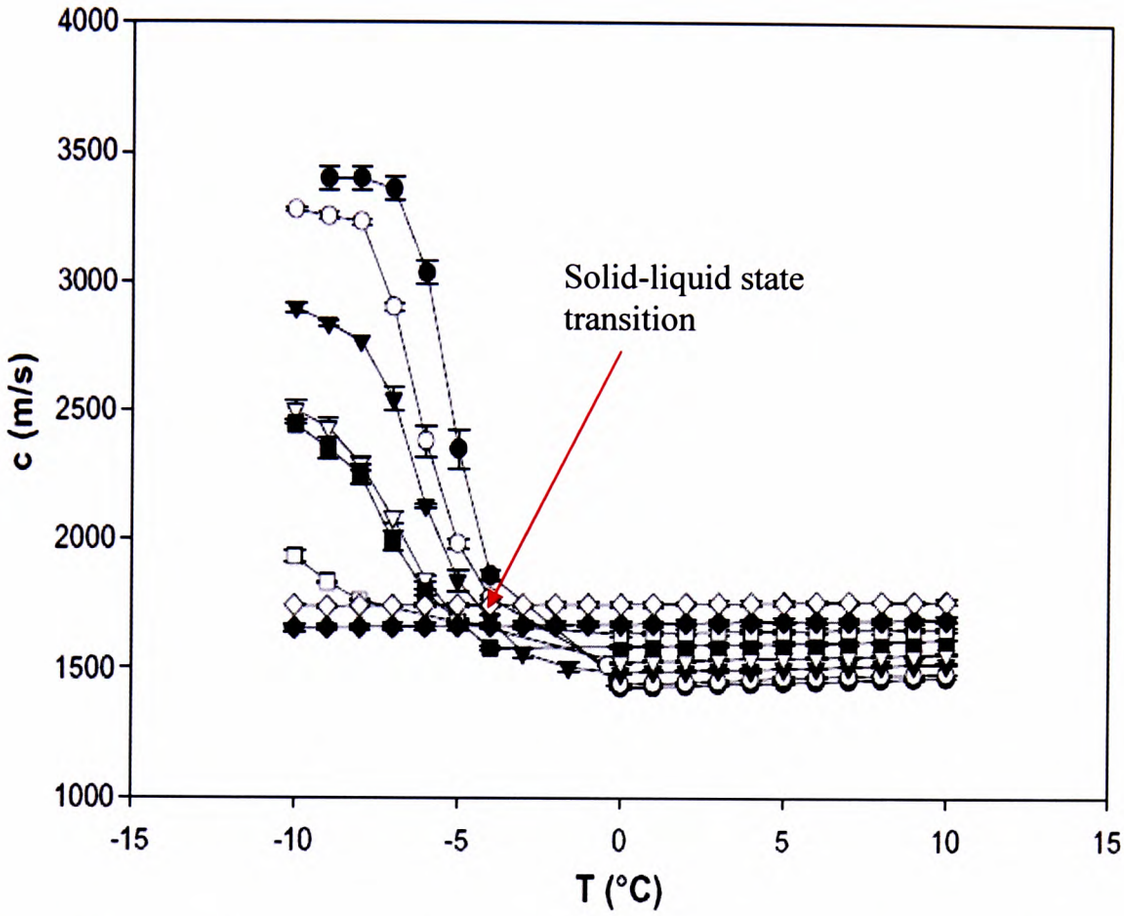

Speed of sound in sucrose solutions (●: 5%, ○: 10%, ▼: 20%, ▽: 30%, ■: 40%, □: 50%, ♦: 60%, ◇: 70%) as a function of temperature. The formation of ice corresponded to the discontinuity seen.

Figure 5.11: Ultrasound velocity for sucrose solutions as a function of temperature. (Gülseren and Coupland, 2007).

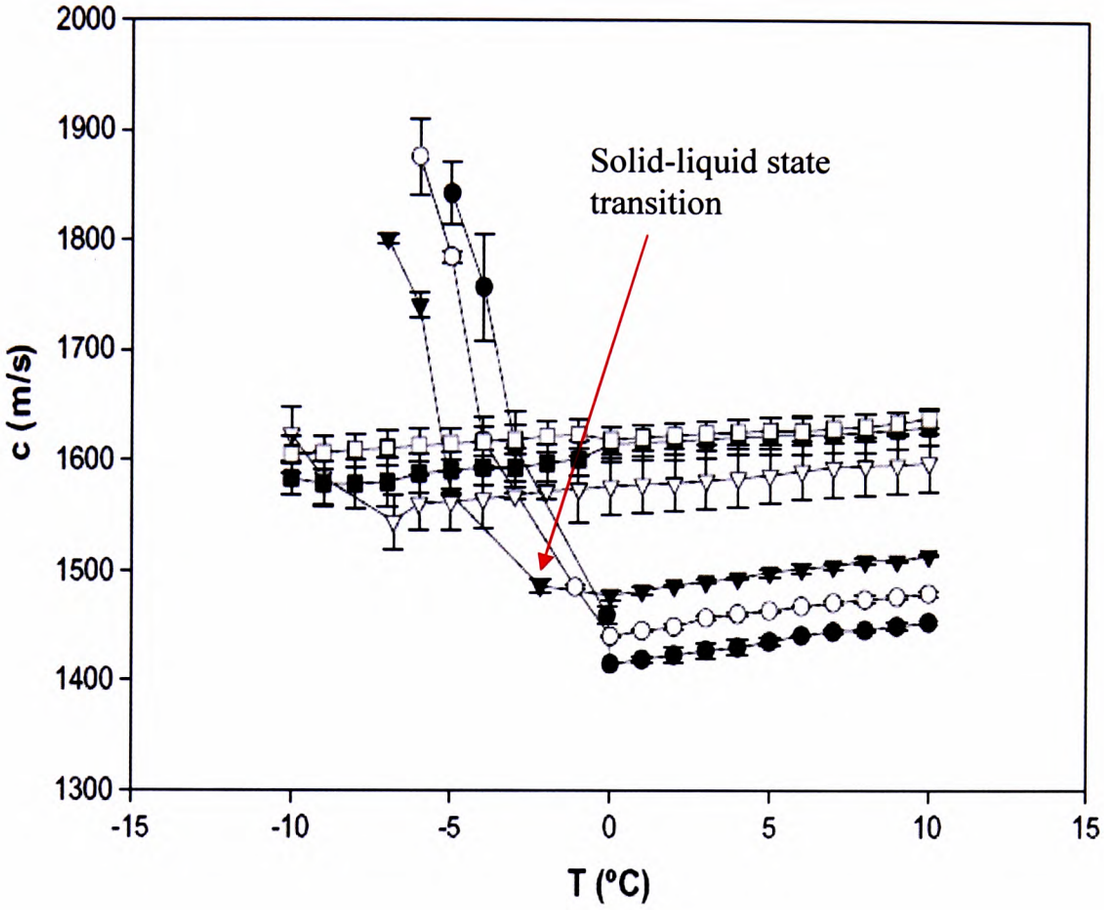

Speed of sound in glycerol solutions (●: 1%, ○: 5%, ▼: 10%, ▽: 20%, ■: 25%, □: 30%) as a function of temperature. The formation of ice corresponded to the discontinuity seen.

Figure 5.12: Ultrasound velocity for glycerol solutions as a function of temperature. (Gülseren and Coupland, 2007).

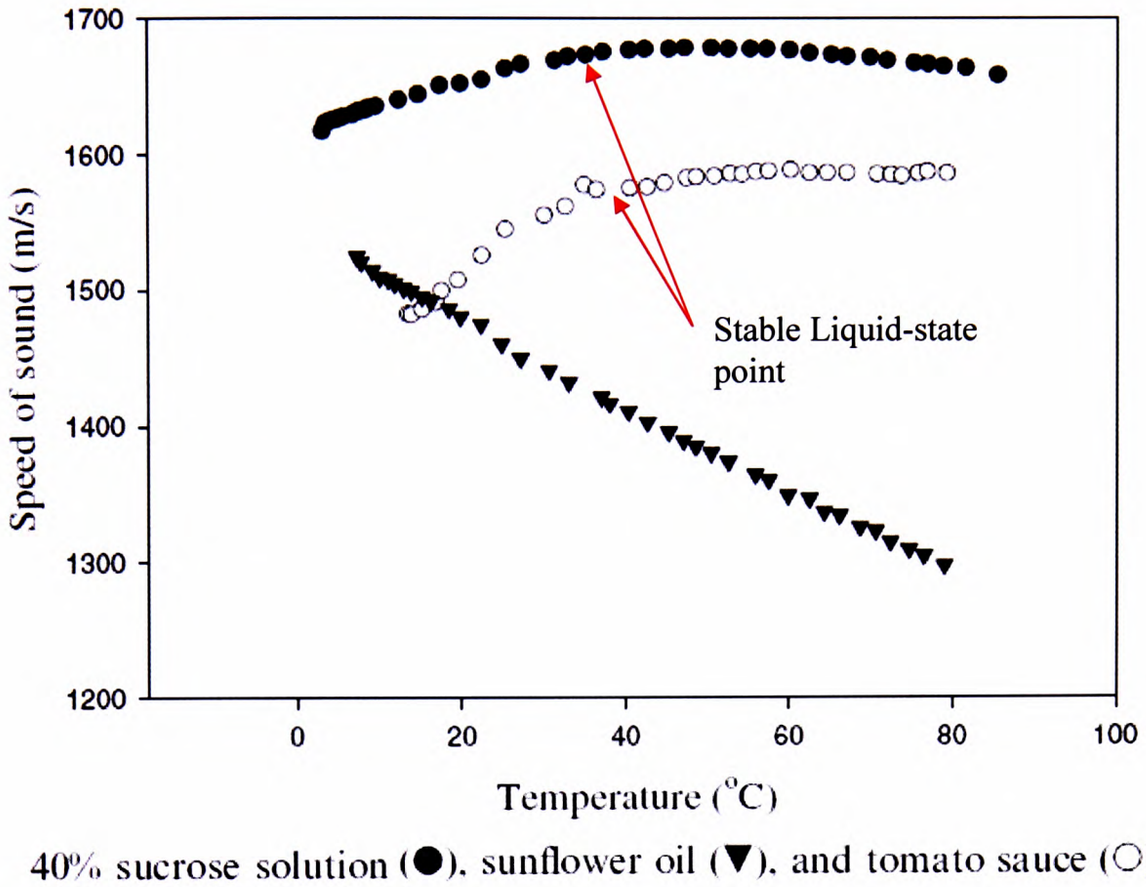

Figure 5.13: Ultrasound velocity for sucrose solution, sunflower oil and tomato sauce as a function of temperature. (Wang *et al*, 2004).

5.4. Case study of orange juice viscosity

The case study by Kuo (2008) relating to reconstituted orange juice provides an example of the use of ultrasound to measure sugar content and to give information on indirect correlation with juice viscosity. Conventional sugar-content measurement of orange juice is by using a Brix meter or Sacchari meter, which provides a measurement of the dissolved-sugar-to-water mass ratio from the refractive index of the liquid. The viscosity of the sugar was independently measured for Kuo's study using a Brookfield rotational viscometer similar to the one shown in Figure 4.21. The work indicated that sugar content and viscosity can be correlated to ultrasound velocity by pulse echo or through transmission mode. No results were reported for the relationship of sugar content to ultrasound attenuation. Unfortunately, although the sugar content showed an almost linear relationship of ultrasound velocity at a very

narrow range of viscosity (see Figure 5.14), the ultrasound velocity actually follows a logarithmic increase against viscosity at high Brix level (see Figure 5.15).

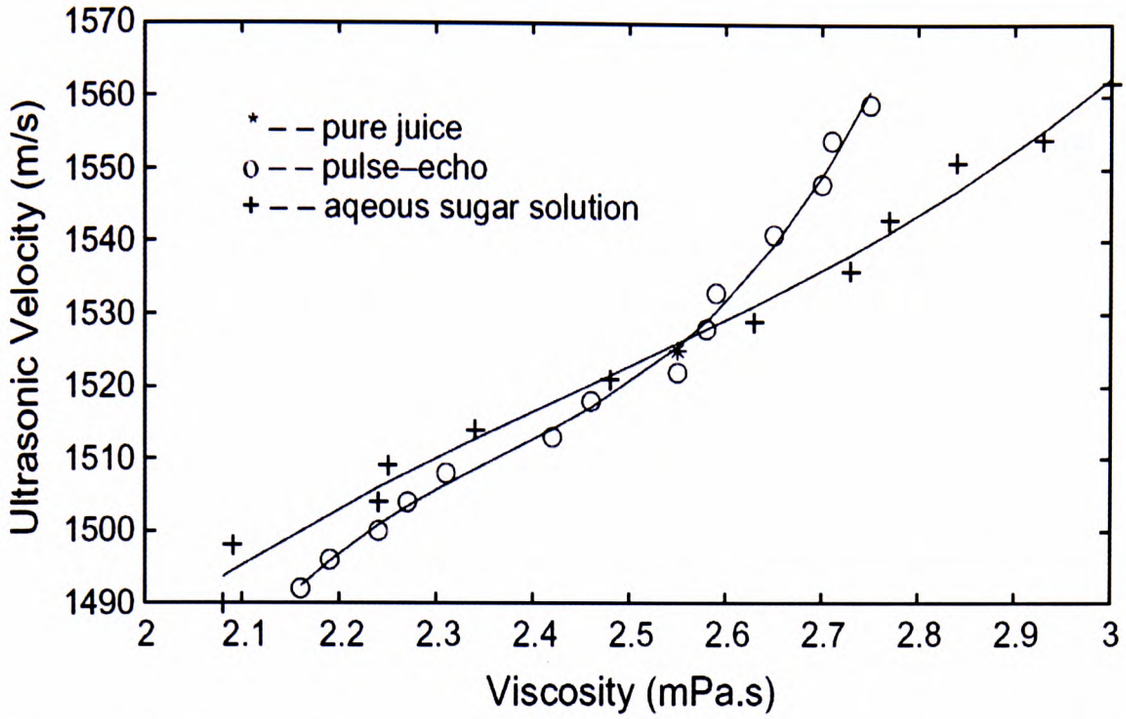

Figure 5.14: Ultrasound velocity for orange juice and sugar solutions as a function of viscosity. (Kuo, 2008).

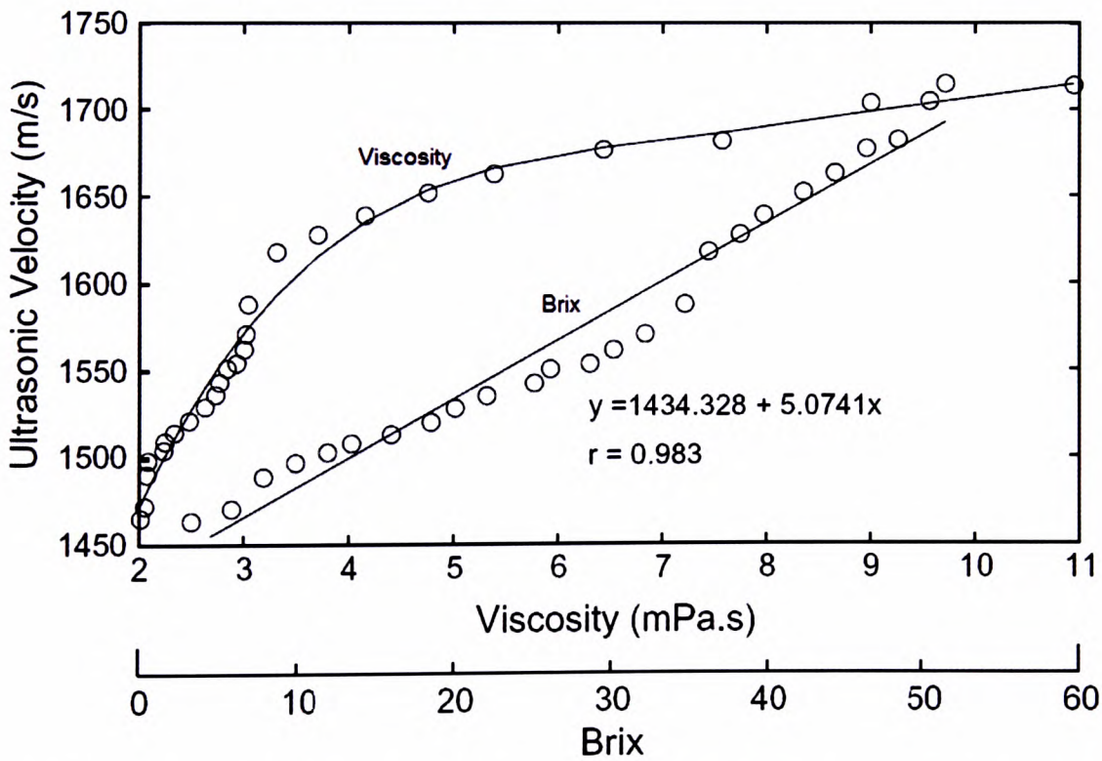

Figure 5.15: Ultrasound velocity for sugar content as a function of viscosity and Brix. (Kuo, 2008).

5.5. Case study of polydimethylsiloxanes (PDMS) samples

Verdier *et al* (1998) conducted experiments to compare PDMS samples using the through transmission mode at a frequency range of 1–25 MHz. However, the results were presented in radians per second (rad/s) format rather than the normally used pascal–second (Pa.s). It is clear from the results shown in Figure 5.16 that Verdier and his colleagues assumed that the angular shear velocity applied by their rheometer to the sample was similar to that of the velocity of actual mechanical vibrational waves that were produced by the ultrasound transducer. The work was mainly focussed on shear velocity values of the samples, which relate to the storage and loss moduli (G' and G''). Although it is normal to plot the storage and loss moduli curve against frequency (in Hz), there is no evidence that angular shear velocity (in rad/s) is exactly equivalent to frequency, i.e. 1Hz ≠ 1rad/s. Most researchers would avoid investigating the shear velocity of very high viscosity materials due to the knowingly low shear velocities obtained from these samples. Verdier *et al* (1998) reported that all the PDMS samples returned ultrasound shear velocities of about 100m/s, compared with 1000m/s for longitudinal velocities.

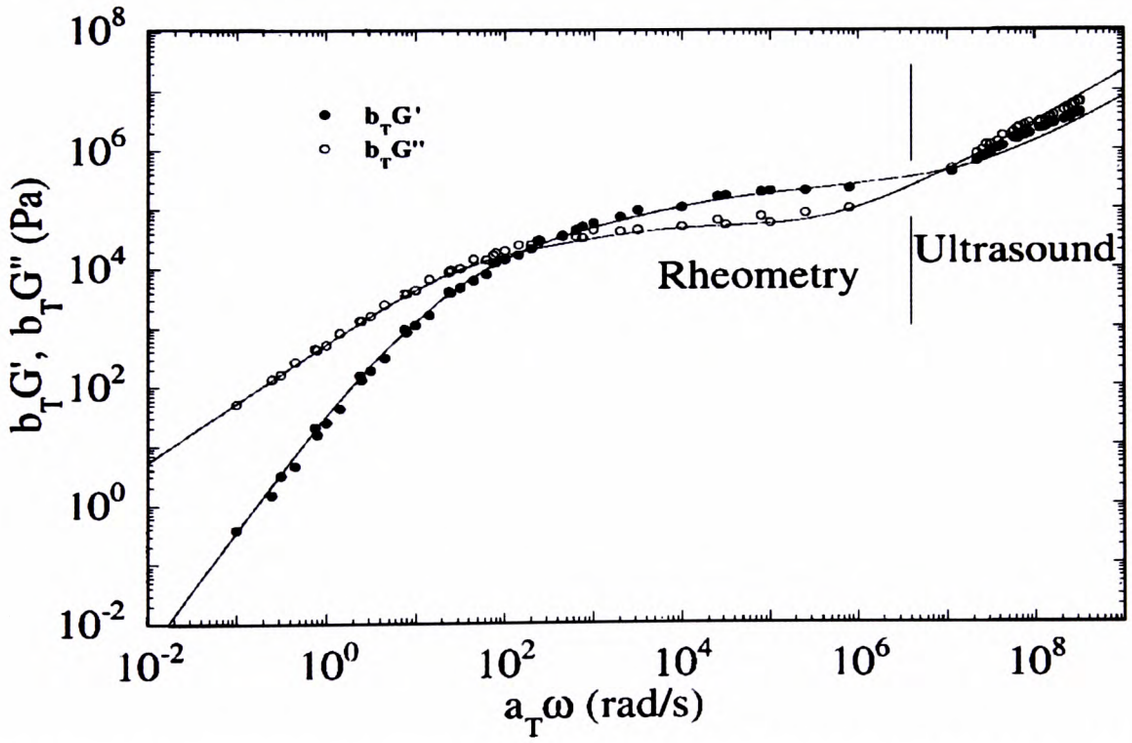

Figure 5.16: Storage (G') and loss (G'') moduli of 500 Pa.s PDMS at 20°C. (Verdier *et al*, 1998).

As a result of different ranges of frequency coverage pertaining between rheometry and the ultrasound technique, Verdier *et al* (1998) suggested using a lower-frequency transducer (1kHz to 100kHz) to investigate PDMS samples in order to obtain a comparable result in the same frequency range.

5.6. Case study of natural rubber latex suspensions

The case study conducted by Jaafar (1996) on natural rubber latex suspensions provides a good insight into investigating material properties using ultrasound techniques. There are two conventional techniques for analysing the properties of natural rubber latex suspensions. The first technique would normally require chemical assay and a standard rheometry test in the laboratory. The second technique only requires a hydrometer to measure the density of the suspensions, but this technique is highly unreliable because the density of the suspensions does not have any direct relationship to the qualities of the suspensions (the viscosity, total solid content, alkalinity and dry rubber content). Although the viscosity of natural rubber latex suspensions (800–1,600mPa.s at 25°C) is not as high as solder paste (400,000–750,000 mPa.s at 25°C), it is a good material to be compared with solder paste as both of these materials exhibit viscoelastic behaviour.

The technique used in Jaafar's study was reviewed to enhance the understanding of how suspensions response to ultrasound waves. Although natural rubber latex suspensions normally don't contain any metal particles, the suspensions themselves do have traces of particles for elements such as potassium, magnesium, copper, iron, sodium, calcium as well as certain phosphates (collectively not more than 0.5% by volume of the suspensions). The effect of ultrasound scattering due to the existence these particles or any other foreign particles introduced to the suspensions was also studied, although it should be borne in mind that the results may not necessarily represent exactly how ultrasound scattering would happen for solder pastes, as solder pastes have metal particles as the major constituent of the suspensions. This affects the interpretation of results, as a multiple-scattering scenario is more likely to occur in solder paste due to the very high volume content of metal particles.

5.6.1. Ultrasound techniques for determination of dry rubber content

There are several ultrasound techniques possible to be used for investigating the dry rubber content of natural rubber latex suspensions. These techniques were principally based on through transmission mode and pulse echo mode, with several possible sub-variations. The basics of the through transmission mode and pulse echo mode techniques have been previously explained in detailed in Chapter 3; hence only a brief description of the sub-variations will be presented here using diagrams.

Jaafar *et al* (1996) considered many techniques and attempted to build both a pulse-echo mode rig and a through-mode rig (see Figures 5.17–5.26). The performance and feasibility of both techniques have also been thoroughly reviewed. Due to the very thin layer of liquid sample used by Jaafar and colleagues, regardless of whichever technique was used the results are in good agreement with each other. The work has not provided any information regarding changes in viscosity in relation to the dry rubber content of the natural rubber latex suspensions; nevertheless, one can always safely presume that natural rubber latex suspensions are non-Newtonian and their viscosity will increase as a function of temperature or the dry rubber content. Thus, measurements reported by Jaafar *et al* with respect to the relationship between dry rubber content and its ultrasound properties may possibly hold true for viscosity as well.

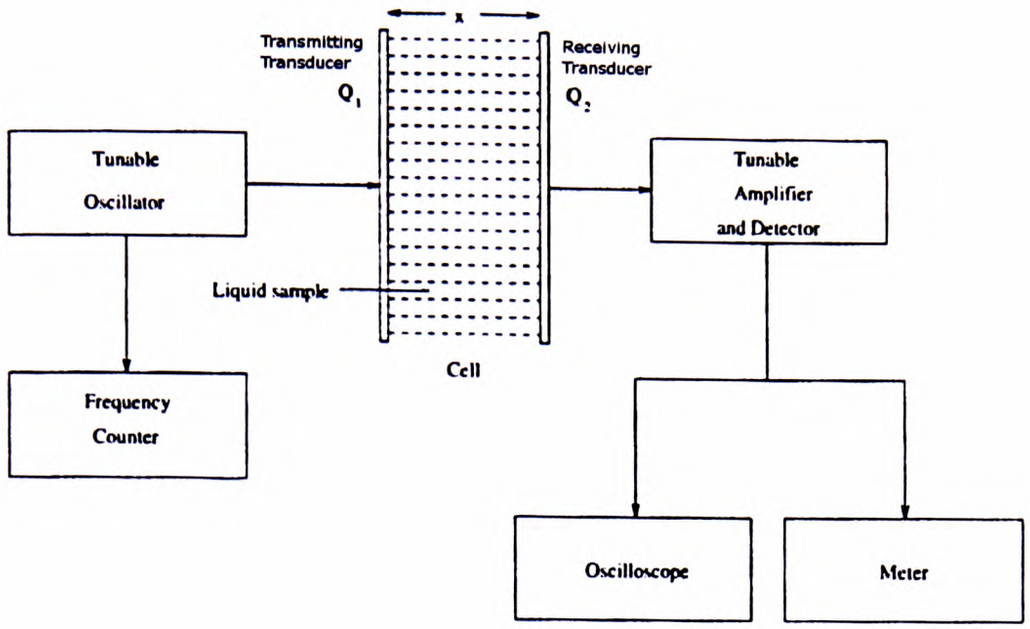

Figure 5.17: Continuous wave ultrasonic resonator system. (Jaafar *et al*, 1996).

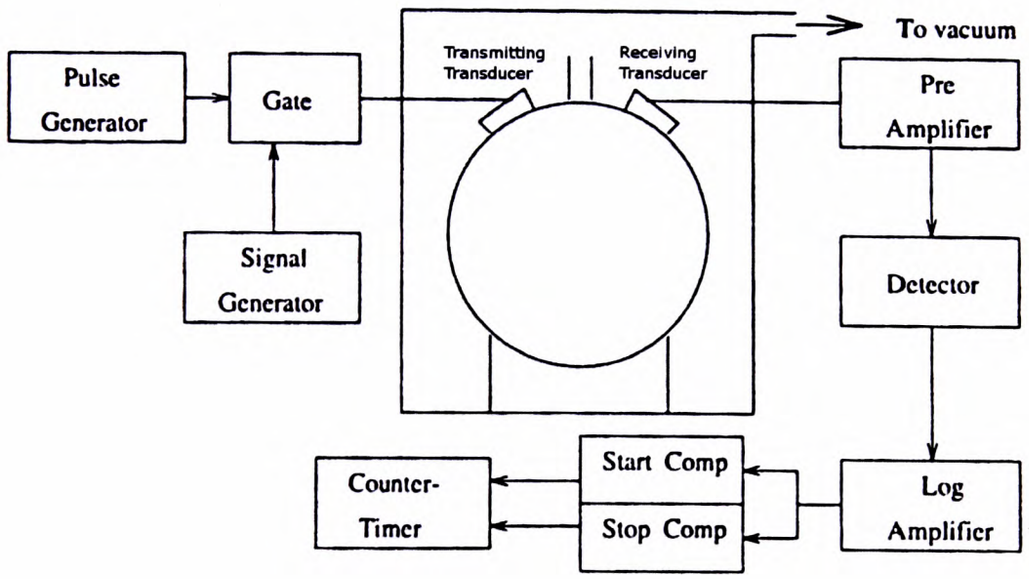

Figure 5.18: Acoustic reverberation ultrasonic system. (Jaafar *et al*, 1996).

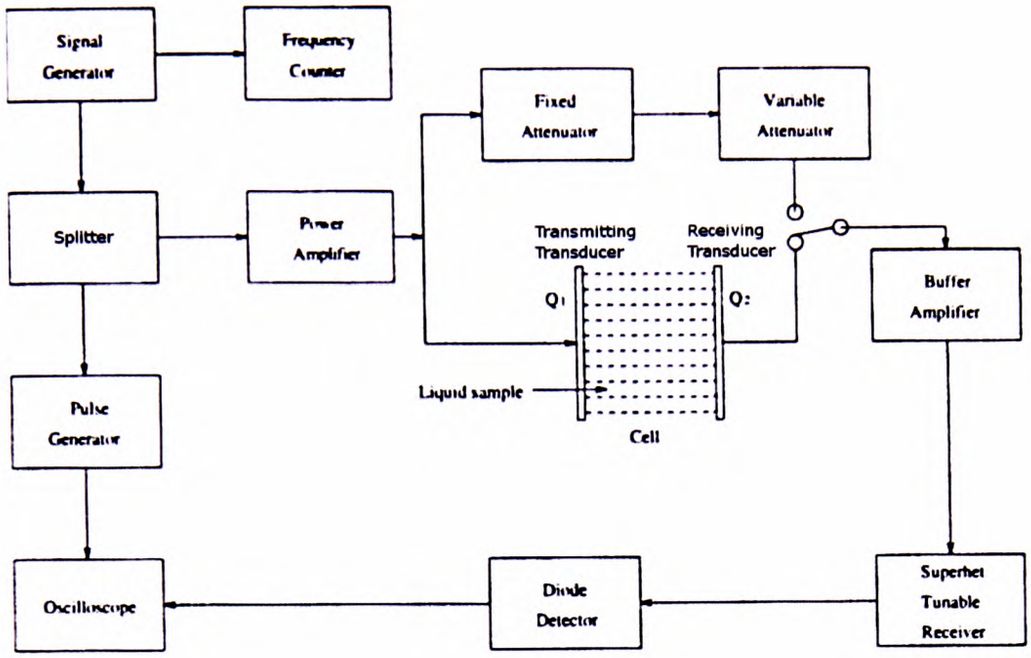

Figure 5.19: Fixed-path-length pulse ultrasonic system. (Jaafar *et al*, 1996).

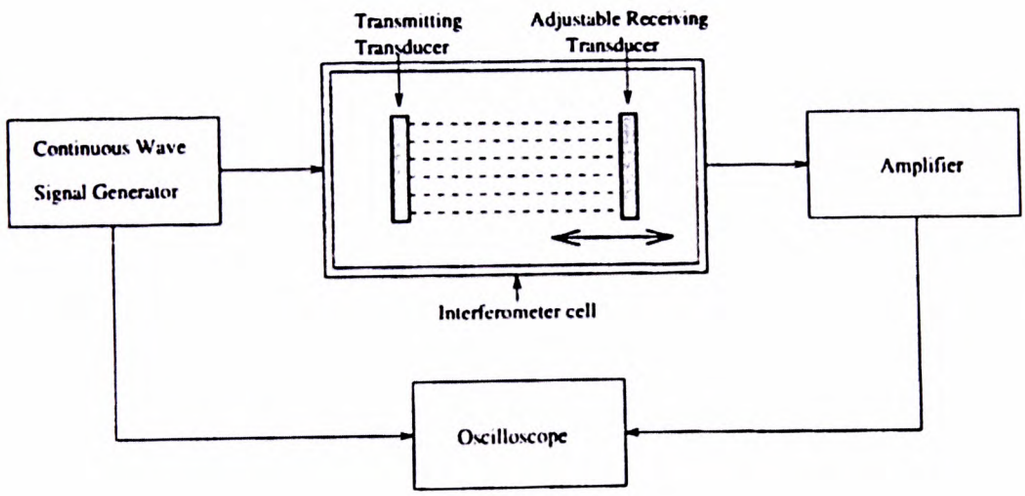

Figure 5.20: Variable-path-length continuous wave ultrasonic system. (Jaafar *et al*, 1996).

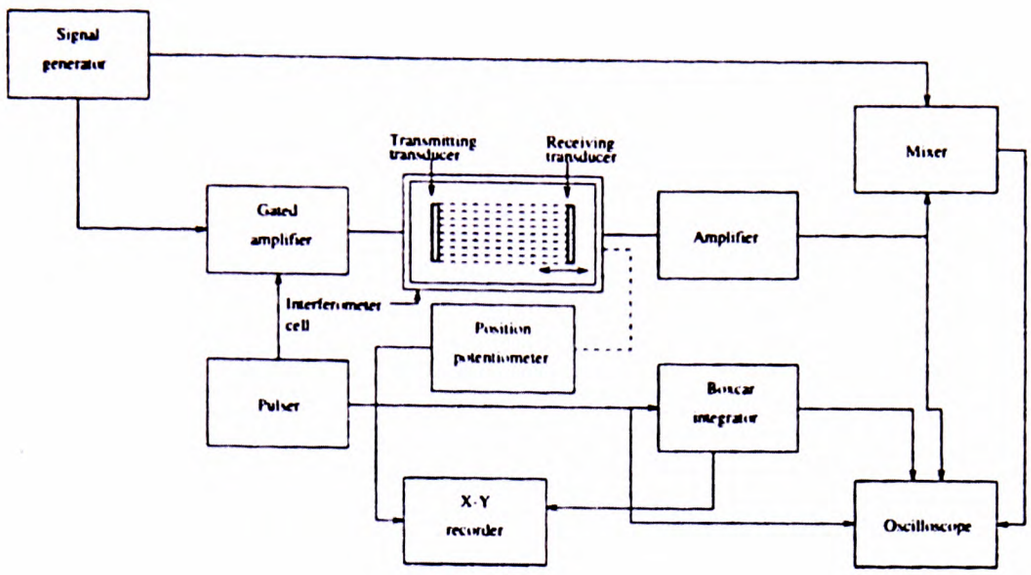

Figure 5.21: Variable-path-length pulse ultrasonic system. (Jaafar *et al*, 1996).

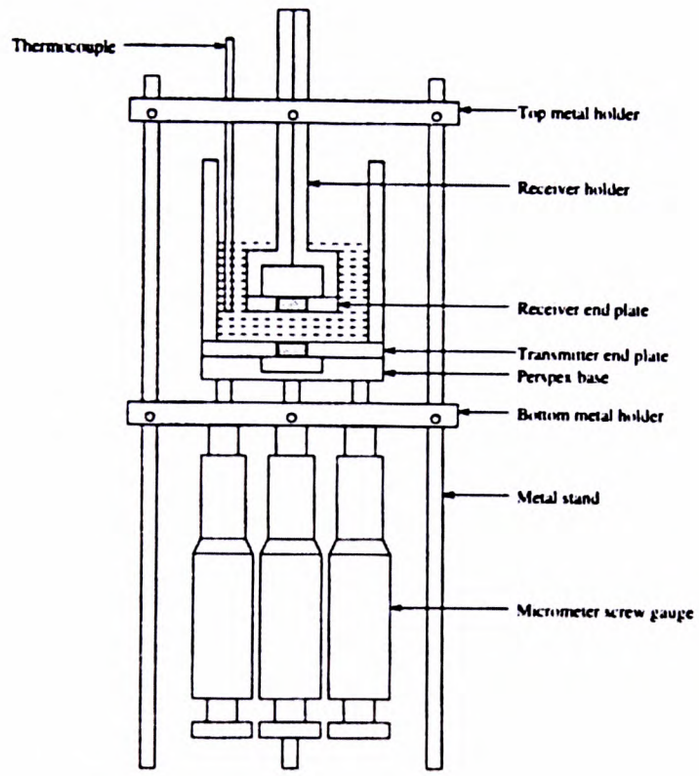

Figure 5.22: Variable–path-length pulse transmission ultrasonic system test rig. (Jaafar *et al*, 1996).

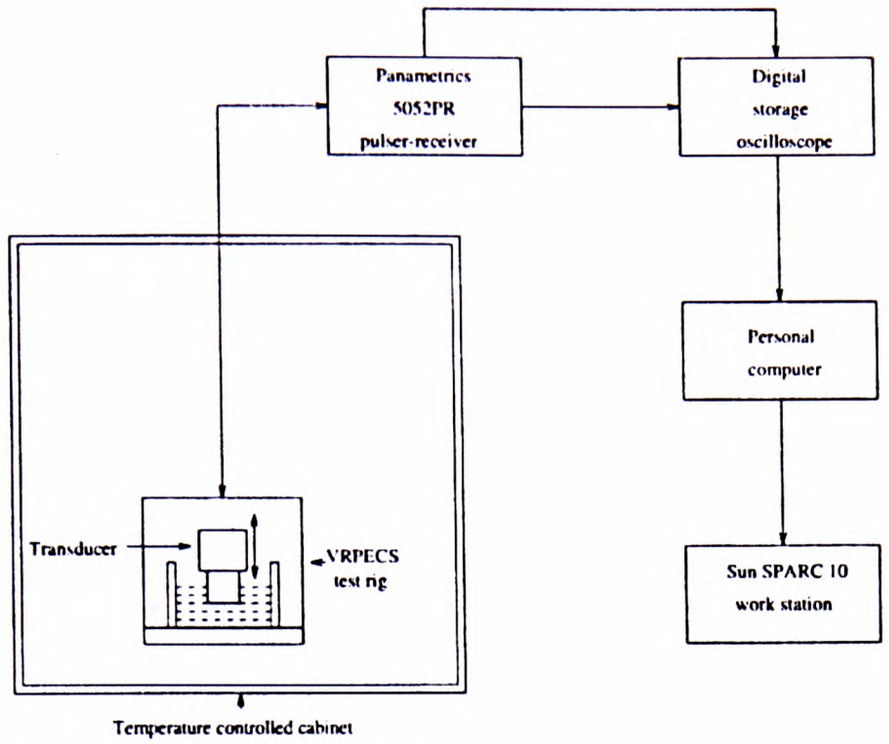

Figure 5.23: Variable reflected pulse-echo ultrasonic system. (Jaafar *et al*, 1996).

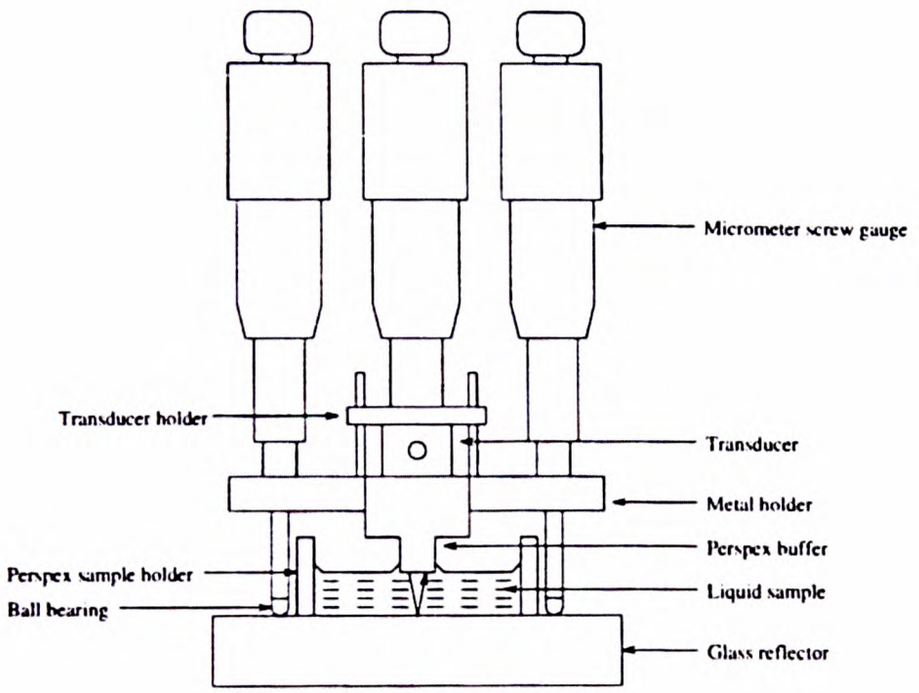

Figure 5.24: Variable reflected pulse-echo ultrasonic system test rig. (Jaafar *et al*, 1996).

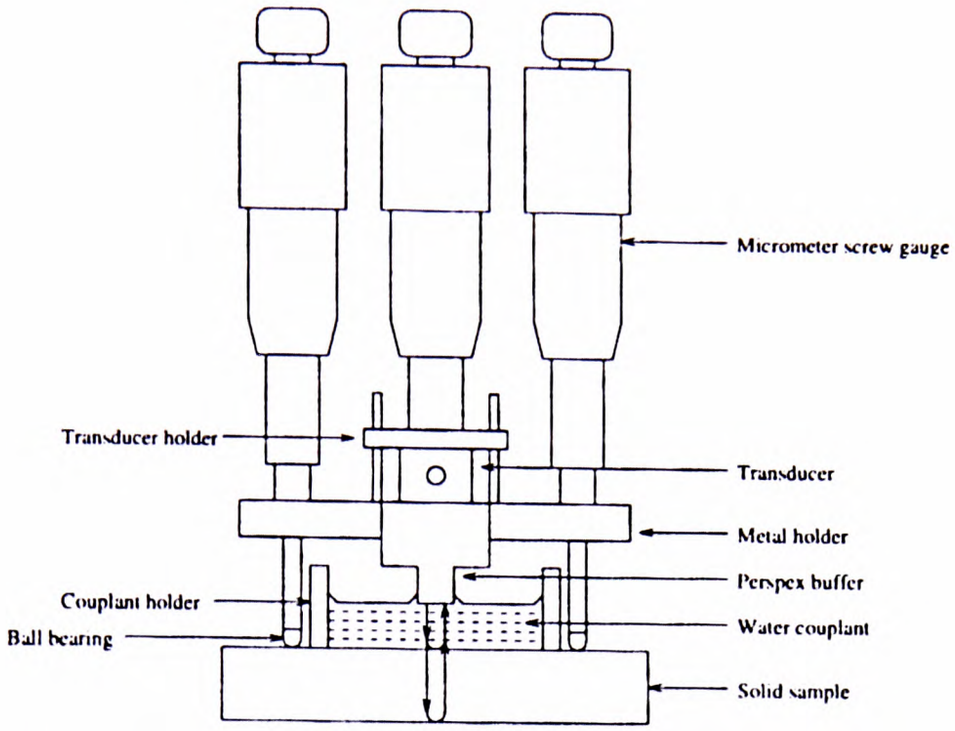

Figure 5.25: Variable reflected pulse-echo ultrasonic system test rig for solid samples. (Jaafar *et al*, 1996).

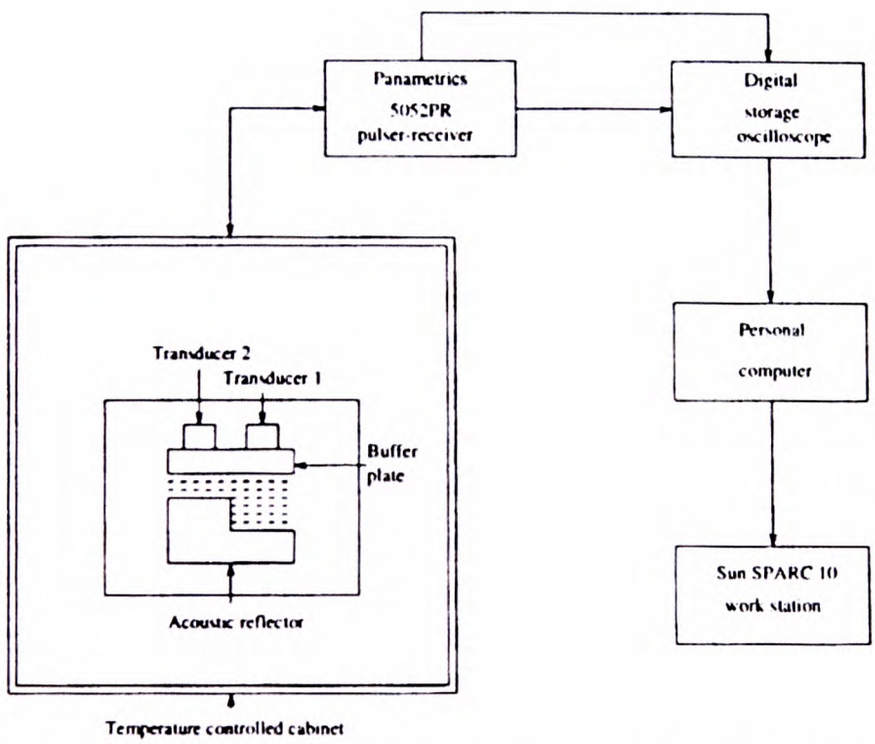

Figure 5.26: Dual-transducer pulse-echo ultrasonic system. (Jaafar *et al*, 1996).

a) Error correction technique

Jaafar *et al* (1996) avoided the use of the through transmission technique because of a misconception that sound waves travel in a linear pattern rather than in a 3D hemi-spheroid or 3D hemi-ellipsoid pattern. The poor understanding of how ultrasound propagates has led Jaafar to believe that a small angulation (as little as one degree) of the sensor on the test rig (see Figure 5.27) could have a very significant effect on ultrasound velocity (see Figure 5.28). Most of the ultrasonic transducers have normally got directivity sensitivity covering a 50° angle or more (see Appendix I1). Thus, the issue of a small angulation error in connection with ultrasound velocity or absorption may have been an overstatement. This is also supported by the fact that Figure 5.28 represents an illogical concept that a shorter-path-length test rig requires a longer time (thus lower velocity) for the ultrasound wave to travel the distance than with the longer-path-length test rig.

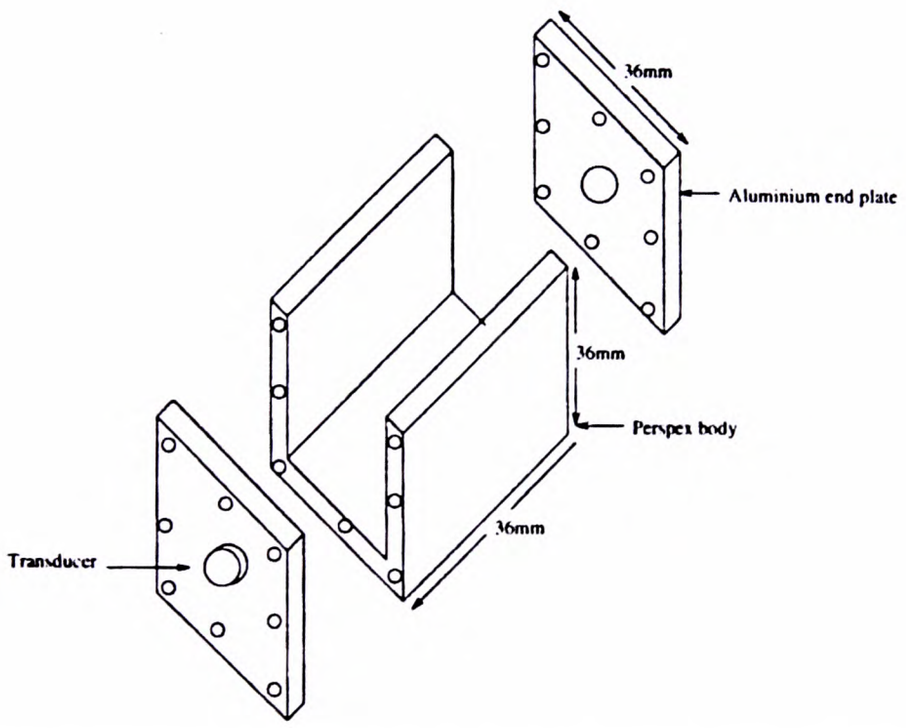

Figure 5.27: Through transmission ultrasonic system test rig. (Jaafar *et al*, 1996).

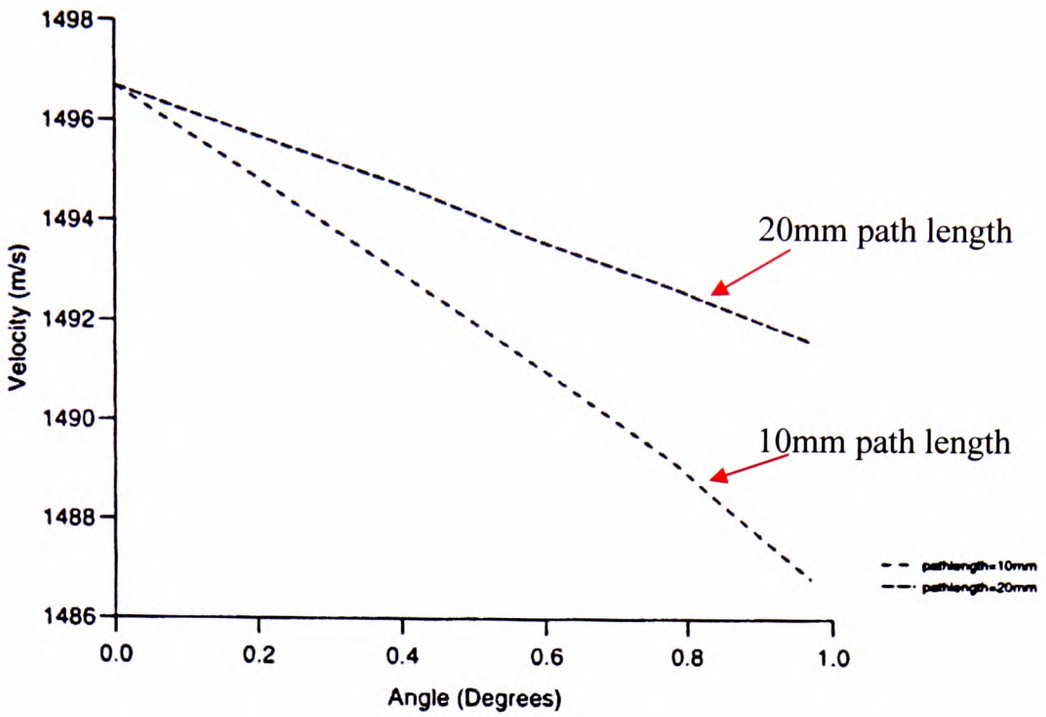

Figure 5.28: Effect of angulation on ultrasound velocity in water for 10mm and 20mm path lengths. (Jaafar *et al*, 1996).

Apart from that misconception, Jaafar (1996) also suggested a useful error-correction technique by using coherent averaging in which the input signal is repeated 1000 times and added synchronously to reduce random noise when acquiring the raw data.

Jaafar *et al* (1996) also commented that the test rigs shown in Figures 5.22–5.25 suffered sensor alignment problems using the micrometer screw. The error arises because measured ultrasonic velocity using these configurations was too high due to the very short path length (the thin layer of liquid sample was less than one millimetre in thickness).

One of the designs implemented by Jaafar *et al* (1996) was the dual-transducer pulse-echo ultrasonic system. In using this technique, Jaafar and his colleagues had to implement a transducer response correction program because the corresponding transducers used in this technique are usually not 100 per cent identical. Non-identical transducers normally return slightly different ultrasound absorption and velocity readings from the same sample. Theoretically, ultrasound velocity in a homogenous

material should be constant regardless of the material's thickness. When two non-identical transducers are used in pulse echo mode as shown in Figure 5.26, the ultrasound velocity measurement taken should be the average (mean) of the measurements from both transducers.

b) Correlation of ultrasonic measurements with dry rubber content

The work by Jaafar (1996) using the test rig shown in Figure 5.26 has provided the correlation of ultrasonic measurements of natural rubber latex suspensions at various temperatures with the dry rubber content. Jaafar *et al*, however, refer to these correlation curves as 'calibration curves'. Two of the most significant of these calibration curves from the study are presented in Figures 5.29 and 5.30.

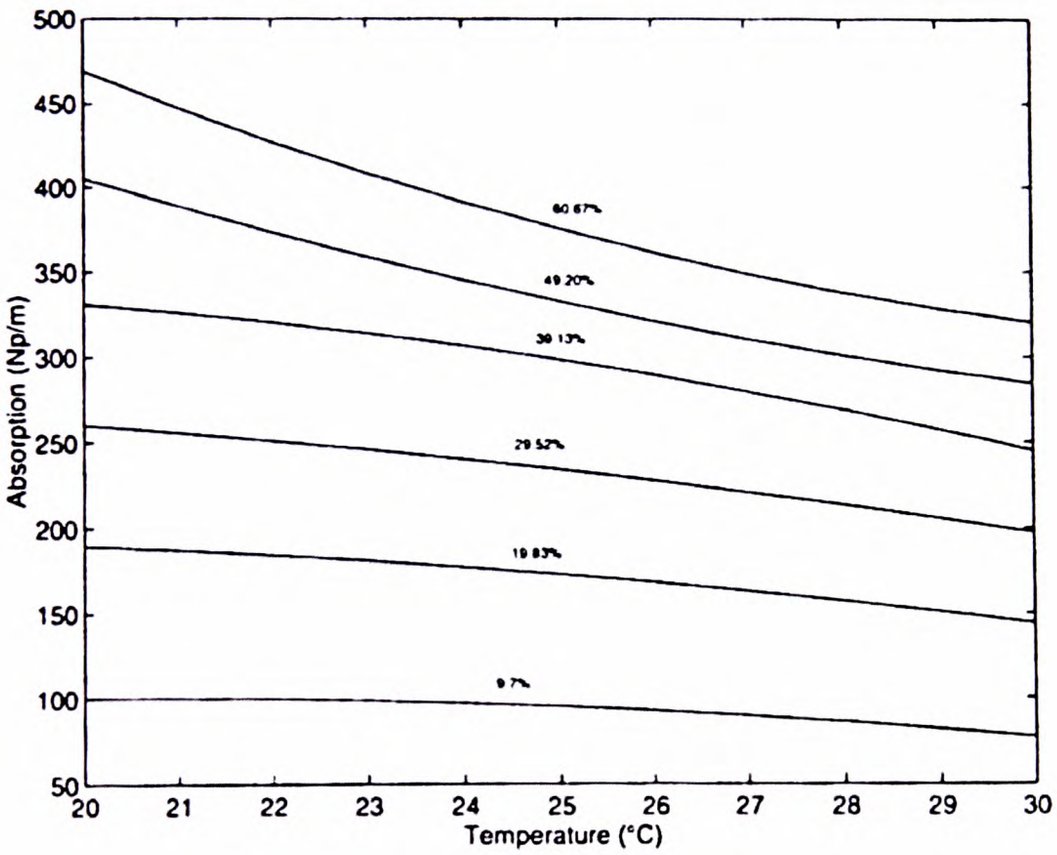

Figure 5.29: Ultrasonic absorption as a function of temperature of various dry rubber contents (9.7% to 60.67%) at 9.96MHz. (Jaafar *et al*, 1996).

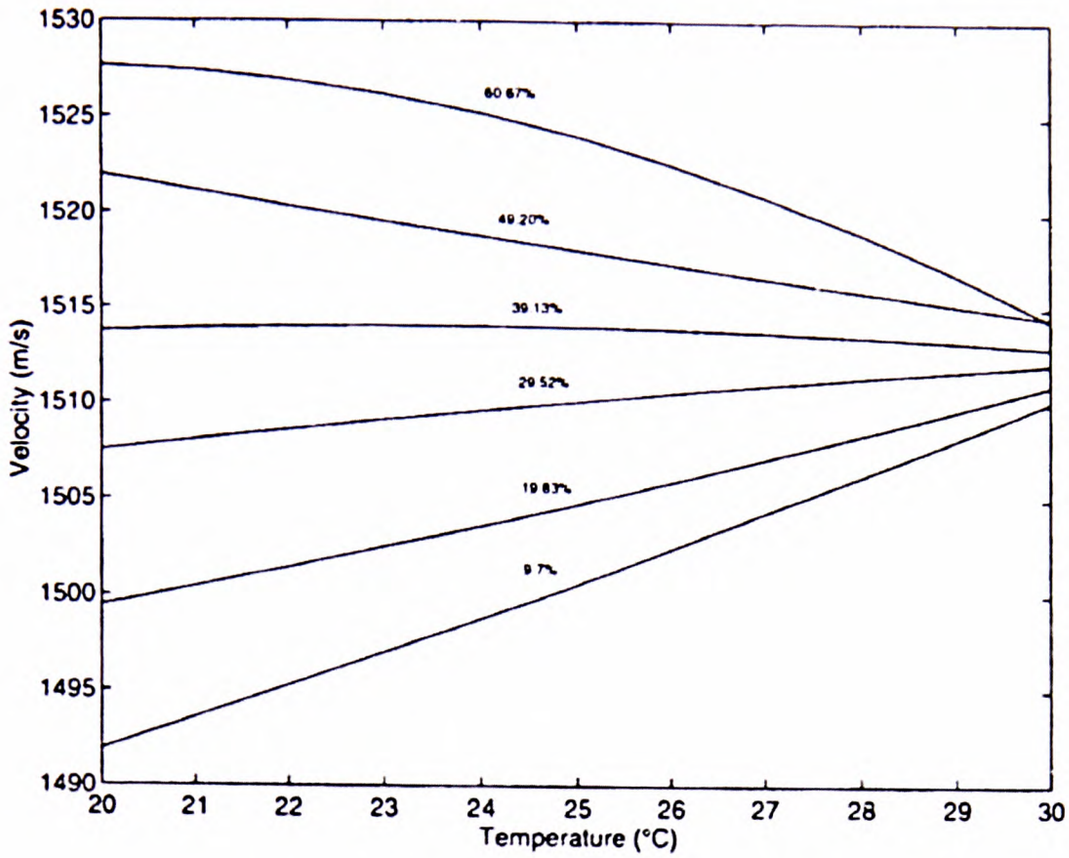

Figure 5.30: Ultrasonic velocity as a function of temperature of various dry rubber contents (9.7% to 60.67%) at 9.96MHz. (Jaafar *et al*, 1996).

c) Detection of adulterant materials in natural rubber latex

As every material returns a unique response to an ultrasonic wave passed through it, it is ideal to use ultrasonic techniques to identify different materials or contaminants in a medium of known ultrasonic 'signature'. This signature can be the ultrasonic velocity, ultrasonic attenuation or a combination of the two.

In this particular example, Jaafar *et al* (1996) used 30% and 40% dry rubber content within natural rubber latex suspensions as control samples. These samples were compared with the adulterant intentionally introduced to the respective control samples. The adulterants used were tapioca powder, coconut powder, rice powder and plain flour. The results of how these adulterants affected the ultrasound measurement of 30% dry rubber content of natural rubber latex suspensions are presented in Figures 5.31–5.34. It is understood that a reduction in ultrasound absorption is only noticeable

after 5 minutes because the powder granules need time to absorb the liquid. During this process, the powder granules dissolve and disperse (split) into smaller particles, and this event effectively blocks most of the ultrasonic wave and causes a high absorption level at the beginning. But the absorption level gradually reduces as sedimentation starts to take place. It is also clear that, since rice powder and coconut powder do not disperse so easily even after 20 minutes' time, the absorption level remains almost unchanged throughout.

The most important point to note from this study is that, at time zero, each and every contaminated sample exhibits a different level of absorption but each reaches a relatively similar absorption level after 20 minutes, which may be due to the completion of the sedimentation process.

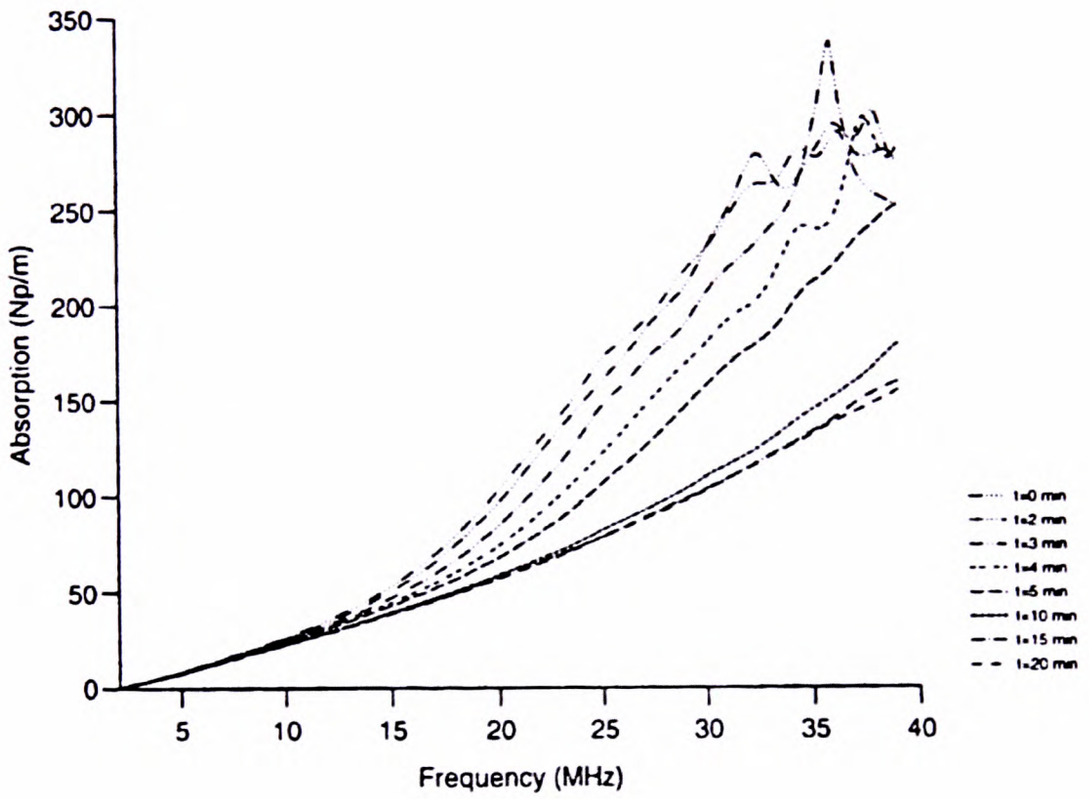

Figure 5.31: Ultrasonic absorption as a function of frequency of 30% dry rubber content in latex + 10% tapioca powder. (Jaafar *et al*, 1996).

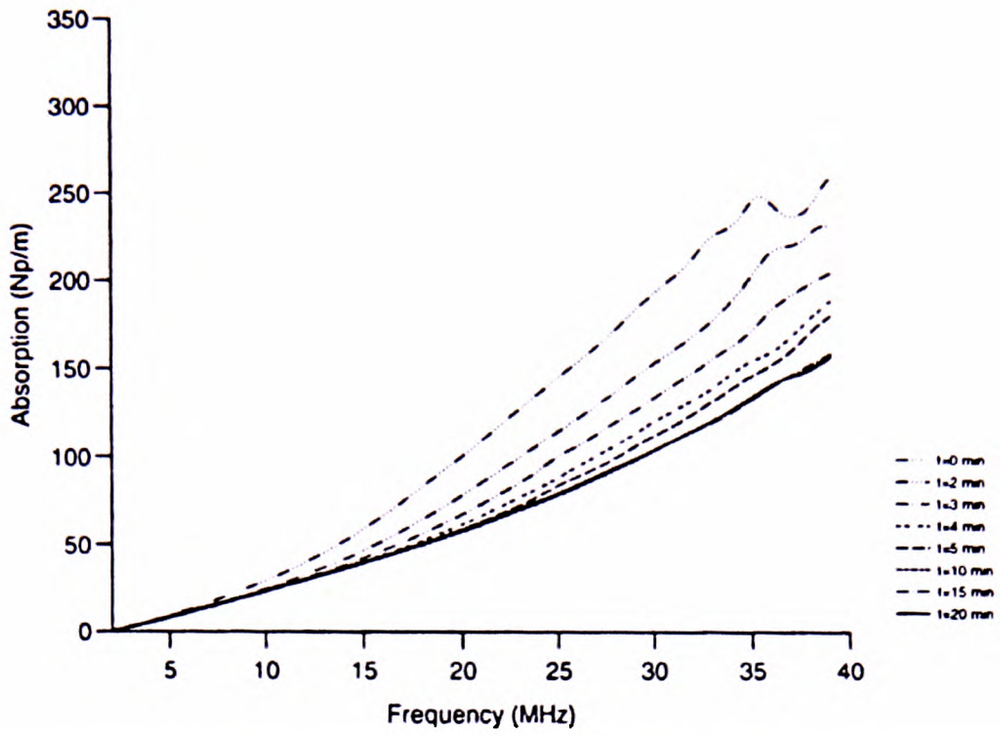

Figure 5.32: Ultrasonic absorption as a function of frequency of 30% dry rubber content in latex + 10% plain flour. (Jaafar *et al*, 1996).

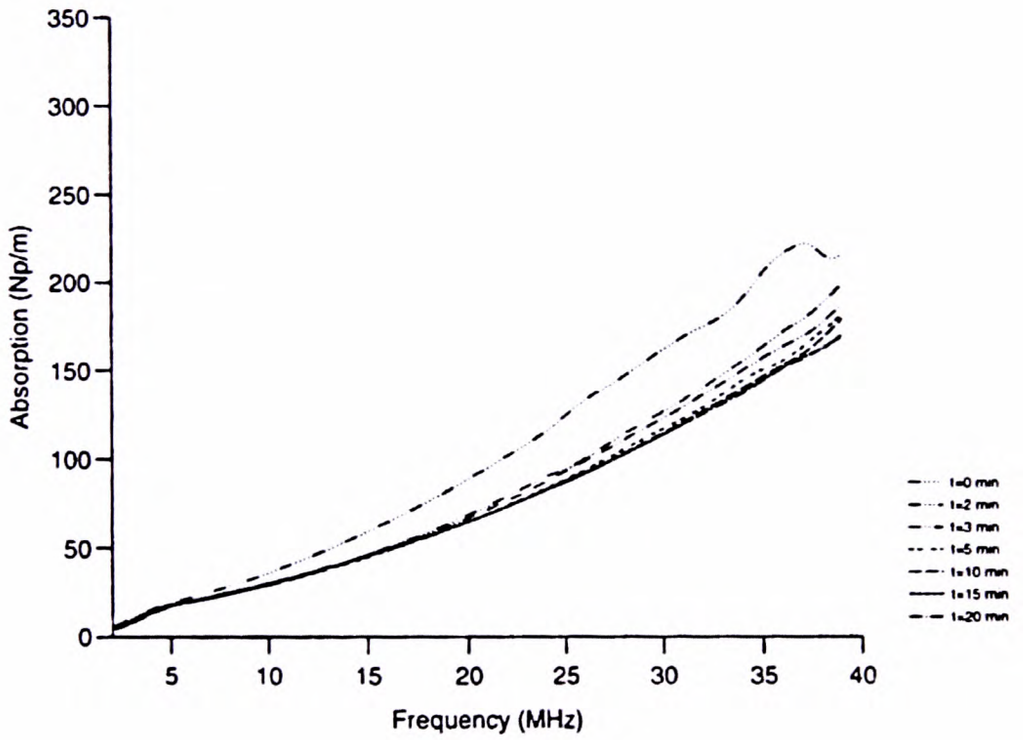

Figure 5.33: Ultrasonic absorption as a function of frequency of 30% dry rubber content in latex + 10% rice powder. (Jaafar *et al*, 1996).

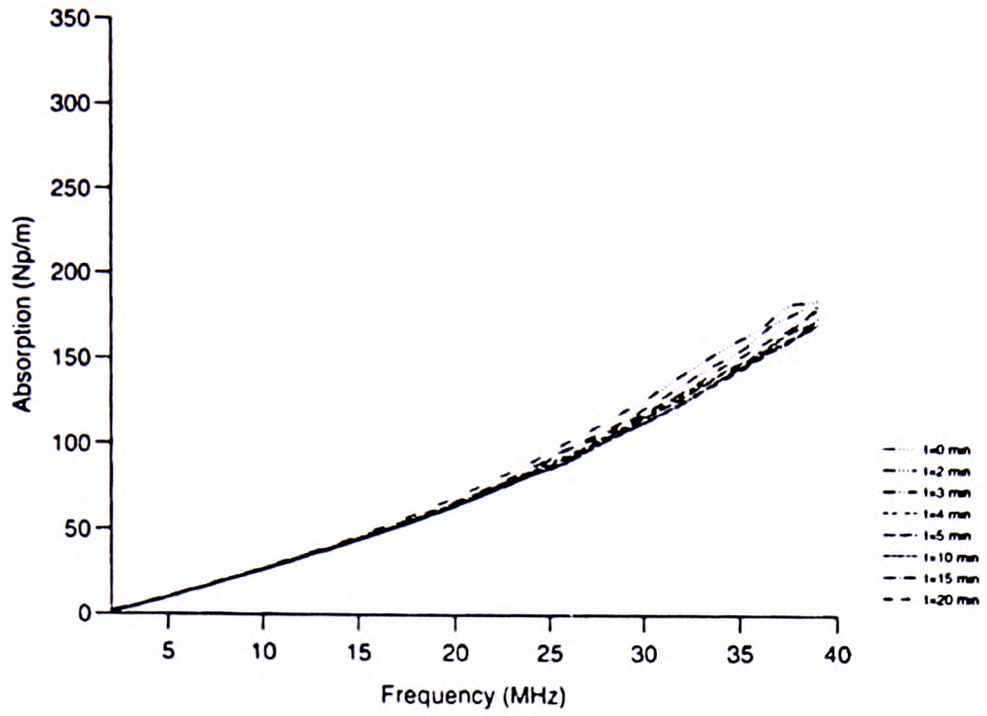

Figure 5.34: Ultrasonic absorption as a function of frequency of 30% dry rubber content in latex + 10% coconut powder. (Jaafar *et al*, 1996).

5.7. Summary

The case studies in this chapter indicate that there are no records of previous work on the use of ultrasound techniques for solder paste characterisation or for the measurement of the viscosity of non-flowing materials (static system).

The case studies show that ultrasound velocity and attenuation may be sensitive to particle size, particle distribution and packing fraction of the materials tested – generally, higher packing fraction increases both ultrasound velocity and attenuation. The case studies also indicate that the changes in ultrasound velocity with respect to the temperature of water-based materials is insignificant compared with oil-based materials. The studies demonstrate that not all materials may experience drastic change in ultrasound velocity due to an increase in temperature – for example, rubber suspension. The findings of the case studies in this chapter can be summarised in Table 5.3.

Although there was an example of indirect use of ultrasound to obtain the viscosity of Newtonian liquids, such as orange juice and sugar solution, getting the technique to work with solder paste materials is viewed as a challenge. This is because solder pastes have extremely high viscosity, contain metal particles and are non-Newtonian in nature. There are no known natural Newtonian materials with viscosity as high as that of solder paste. The case studies show that the ultrasound technique may provide good correlation with the properties of the materials non-destructively; however, the vibration could alter the fluid characteristics in the same way that it can assist the particles to flow.

Thus, further study will be needed to adopt an ultrasound technique for the measurement of viscosity for solder pastes using minimally invasive ultrasound technique. It is expected that ultrasound parameters such as attenuation and velocity may even be able to be directly used to predict stencil printing quality with or without the link to viscosity.

Case studies	Investigated Properties	Findings
Fresh mortar	Estimation of water-to-cement ratio (w/c), porosity, permeability, compressive strength, curing state/rate	Utilised longitudinal wave and attenuation. Shear wave was only used to obtain Young's modulus and shear modulus. Higher longitudinal velocity reflects lower w/c, higher Young's modulus and lower porosity. Higher density → higher w/c ratio → higher porosity (see Table 5.1). Ultrasound velocity may not reflect density of material. Voids/air bubbles reduce ultrasound velocity. Indirect measurement of viscosity through ultrasound amplitude and velocity (Kamada *et al*, 2005) Chemical reactions or admixtures can affect ultrasound velocity. Ultrasound attenuation is related to packing fraction.
Temperature gradient	Temperature	Not all materials experience a decrease in ultrasound velocity from an increase in temperature (-10°C to 80°C)
Orange juice viscosity	Sugar content	Indirect ultrasound velocity to viscosity correlation. Exponential correlation.
PDMS	Storage and loss moduli	Comparison of storage and loss moduli measurement using ultrasound and rheometer. Use of lower-frequency ultrasound sensors was suggested.
Rubber latex	Dry rubber content (drc), adulterant	Higher drc → higher ultrasound attenuation regardless of the temperature. Higher drc → higher ultrasound velocity but dependent on the temperature (see Figure 5.30). Detection of adulterant at an early stage.

Table 5.3: Summary of findings from case studies.

CHAPTER 6

DESIGN AND DEVELOPMENT OF EXPERIMENTAL RIG

6.1. Introduction

This chapter presents several experimental rig designs developed during the experimentation that forms the basis for this thesis. Each of the rigs was designed to test the performance of the ultrasound technique being considered, with the intention of producing a rig that would be capable of testing solder paste samples in bottles with good signal resolution (i.e. minimum noise or interference).

There were several challenges encountered during the construction of the experimental set-up for testing solder paste, such as the following:

- Solder paste is a very attenuating material, and therefore it was necessary to decide which and what type of sensors (broadband or narrowband frequency bandwidth, magnetic or capacitive or piezoelectric, longitudinal or shear wave), beam width and size of sensors should be used. Also, there was a need to investigate the best frequency to run the test at, in order to achieve a readable and reliable signal (i.e. minimum noise).
- Scanning methods (pulse echo or through mode) needed to be selected.
- The alignment of ultrasonic sensors was significant.
- The selection of appropriate signal generators (continuous or tone burst, minimum pulse duration, frequency range, maximum voltage output) needed to be made carefully.
- The selection of a signal amplifier and noise filter (low pass, band pass or high pass) needed to be made.

To address these challenges, three experimental rigs were built. The experimental rig A was built to solve the issue of the scanning method and to investigate the maximum penetration depth of the transducers in relation to the solder pastes. Experimental rig B was built with the intention of achieving better signal quality: separating noise from the true signal, identifying source and returned signals, and creating an ability to extract and save the experimental data to a computer. Finally, experimental rig C was constructed as an adaptation of experimental rig B. This rig used purpose-built sample holders that allowed solder paste samples to be tested without having to remove the samples from their airtight sealed bottles. Another improvement applied on experimental rig C was the use of broadband high-frequency industrial ultrasonic transducers.

6.2. Experimental rig design A

Based on the literature review from Section 3.9 and the case studies presented in Chapter 5, the through-transmission detection mode was considered for building experimental rig A. This decision is supported with the general knowledge that liquid-like materials such as water or suspensions tend to attenuate sound much better than metallic materials – although solder paste contains both metal and liquid content and this adds another dilemma to the choice of which system to use. However, this problem has been discussed earlier, in Section 3.7, highlighting the merit of through transmission mode over pulse echo mode, and hence the choice of the former.

Experimental rig A was built using equipment available from Greenwich University's electronics laboratory. The set-up of the equipment was crude, but this fulfilled the intention of the exercise, which was to gain an understanding of how the chosen systems work and to allow further equipment improvement. The schematic diagram of the set-up is shown in Figure 6.1.

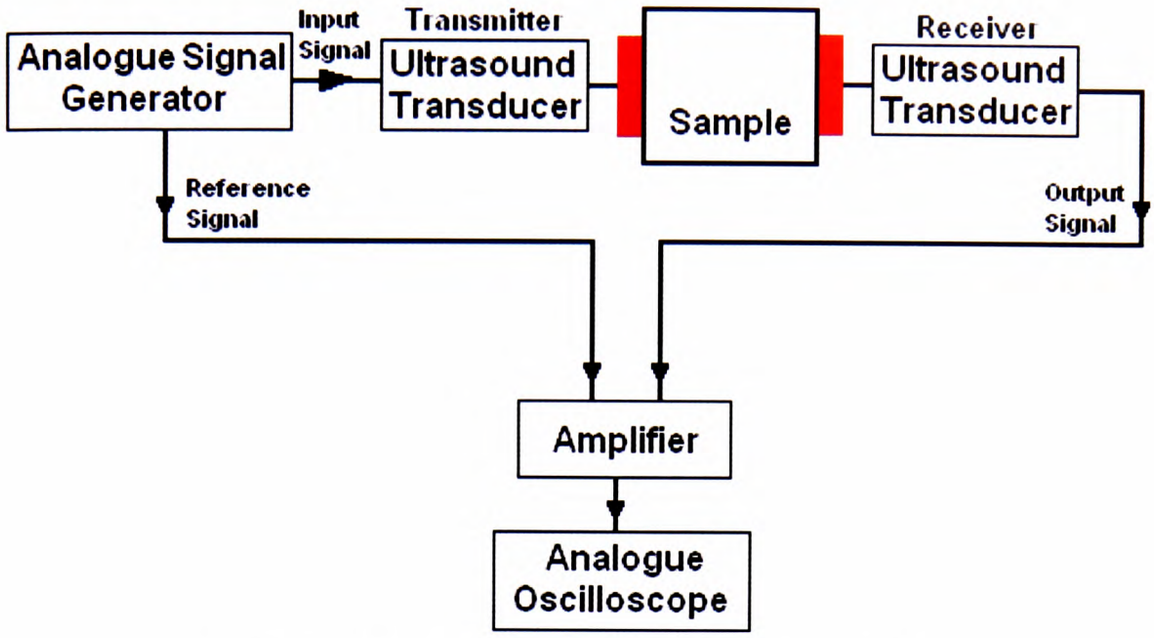

Figure 6.1: Schematic diagram of experimental rig A.

The set-up of experimental rig A consists of:

- Feedback FG601 analogue signal generator (see Figure 6.2);
- Hameg HM203-6 20MHz oscilloscope (see Figure 6.3);
- EG&G Brookdeal 9452 two-in-one amplifier filter unit (see Figure 6.4);
- a pair of Murata MA40E waterproof 40kHz ultrasonic transducers, a pair of Murata MA40S open-structure 40kHz ultrasonic transducers and a pair of Murata MA200A1 200kHz ultrasonic transducers (see Figure 6.5).

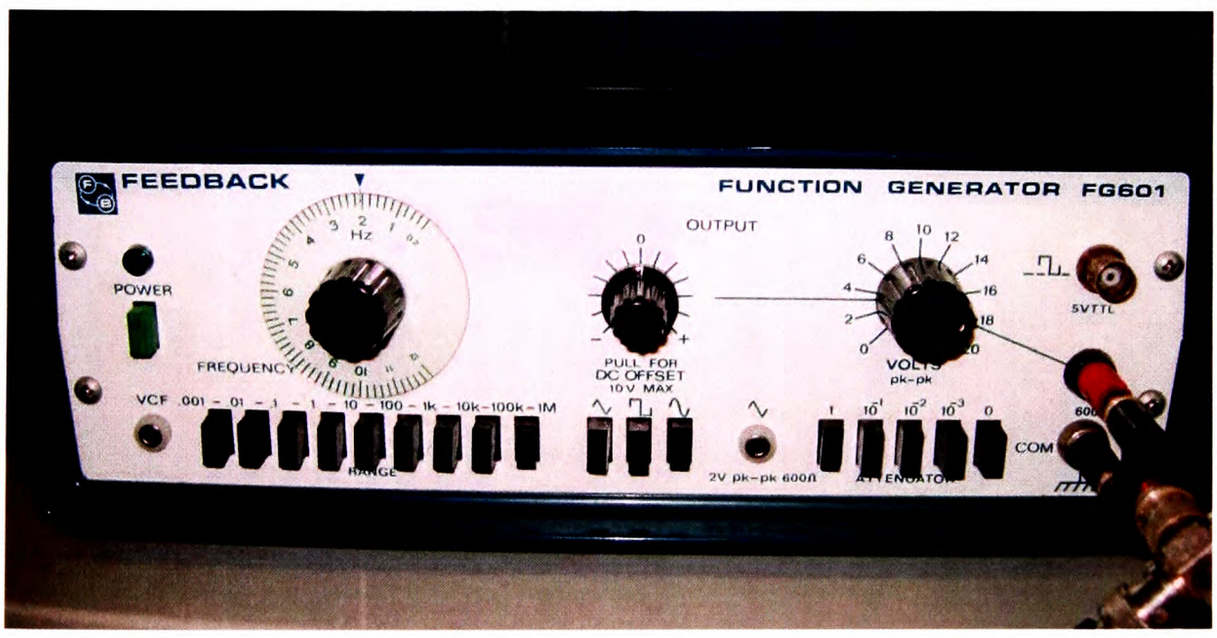

Figure 6.2: Feedback FG601 analogue signal generator.

Figure 6.3: Hameg HM203-6 20MHz oscilloscope.

Figure 6.4: EG&G Brookdeal 9452 two-in-one amplifier filter unit.

Figure 6.5: Murata ultrasonic sensors.

Full specifications of the transducers, including their beam spread and symmetry characteristics are provided in Appendix I1.

The samples were loaded onto a U-shaped sample holder (see Figure 6.6). Although the focal length of the ultrasonic sensors was known, because of the unknown penetration depth of the ultrasound wave in solder paste material, three different sizes of sample holder were produced to investigate the maximum penetration depth produced by the sensors. The sample holders have thicknesses of 20mm, 30mm and 40mm respectively and have a volume of 30.6 cm^3, 45.9 cm^3 and 61.2 cm^3 respectively. Exact dimensions of the U-shape sample holders can be found in Appendix H1, H2 and H3. The sample holders were made from ABS (acrylonitrile butadiene styrene) plastic, constructed using a rapid prototyping machine.

In order to prevent misalignment of the sensors, the sensor holders and the U-shaped sample holders were secured with four 3mm bolts. The sensor brackets were cut using a CNC (computer numerically controlled) machine to avoid eccentricity between the centre point of the receiver and transmitter sensors. By doing so, every time a measurement is taken, the sensors are aligned to each other at the same exact position.

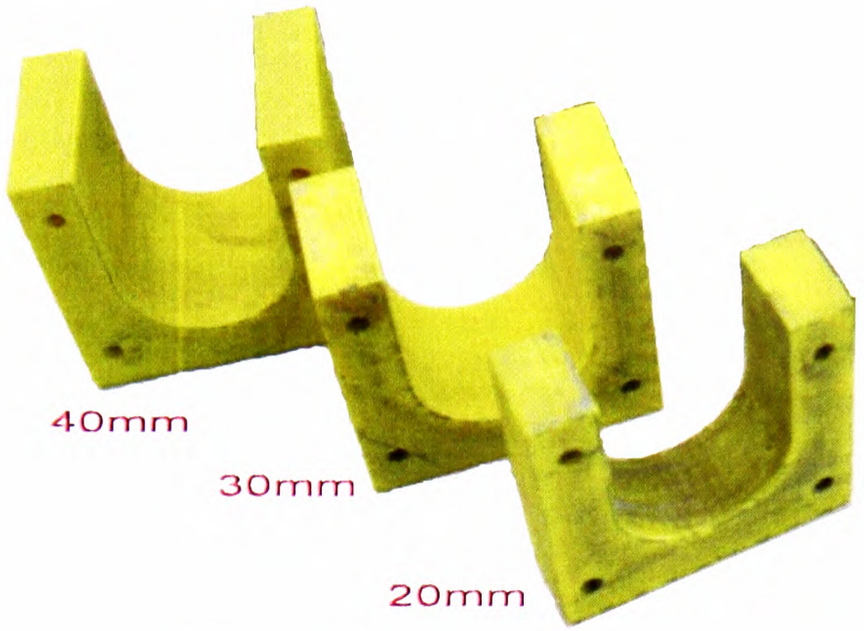

Figure 6.6: U-shaped sample holders.

Tests using rig A were constructed by mounting the U-shaped sample holder together with the sensor holder as shown in Figure 6.7.

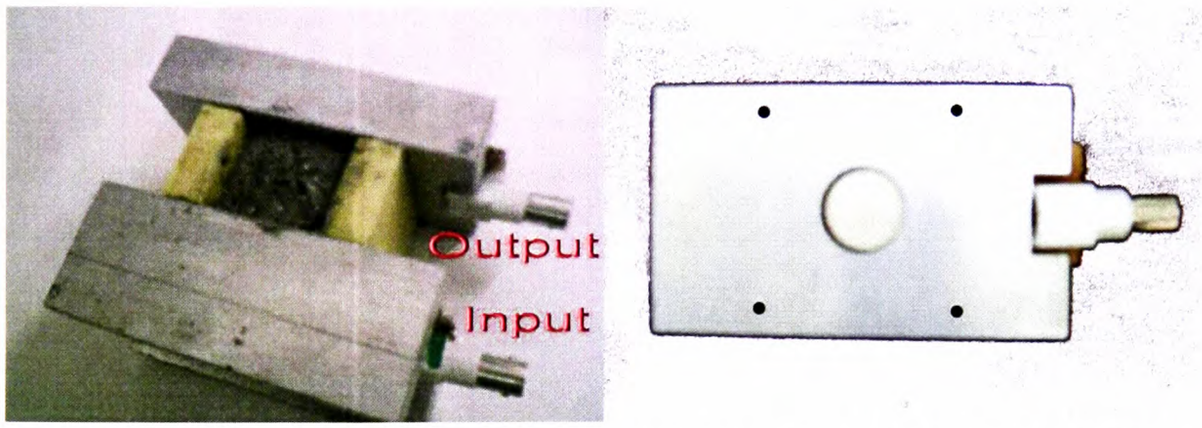

Figure 6.7: Experimental Rig A assembly, with solder paste in the sample holder.

6.2.1. System overview and limitations of experimental rig design A

The test results obtained from experimental rig A have some common problems:

- difficulty in differentiating source and return signals (see Figure 6.10);
- difficulty in locating the exact transmission time of the wave through the sample;

- due to using an analogue signal generator and an analogue oscilloscope, at high resolution, signals arriving at low voltage cannot be captured and will be ignored. It appears as if there is a huge time delay caused by the equipment, as reported in some papers, including the ones by Landis (1993), Landis and Shah (1995) and Povey (2006), in which they are suggesting a calibration using a known medium or testing the same medium at different path lengths. Some researchers mistakenly ignore the reading, which therefore contributes to erroneous ultrasound velocity results.
- an inability to locate first maxima or minima in captured data; and
- an inability to save data or results – findings must be observed and manually entered into a computer.

Initially, it was very difficult to read the signal from the measurement of the solder paste samples due to very high attenuation. At times, without the use of an amplifier filter, the signal was completely lost. However, when the EG&G Brookdeal 9452 combined amplifier-filter was used, not only was the returned signal amplified but also the surrounding noise from the laboratory. This led the author to build an in-house customised active band-pass amplifier-filter module (see Figure 6.8), and the schematic diagram of this module is provided in Appendix J. However, it did not exactly solve the problem as the module was unable to provide enough signal amplification.

In this part of the design of rig A, the open structure transducers were conceived for attempting to test the solder paste sample in the bottle without having to make physical contact with the sample or remove the sample from the bottle. However, it was found that, due to the highly attenuating nature of the solder paste material, it did not seem possible to transmit ultrasound through these materials using air as the coupling medium. So, at this stage, direct measurement of a sample in a bottle was another challenge to solve.

Possible solutions considered were to build a good amplifier-filter system or to use another type of transducer. Alternatively, applying a thin layer of soft coupling medium such as grease or oil as reported by Fengler *et al* (2004) to the surface of the

bottle had also been considered. The last option was to use a 'delay line transducer', which has a coupling material attached to it (see Figure 6.9). However, there are some concerns about using a delay line transducer as it is still unknown whether the flat surface of the coupling material could really provide better ultrasound propagation on a rounded contour bottle surface of highly attenuating materials such as solder pastes.

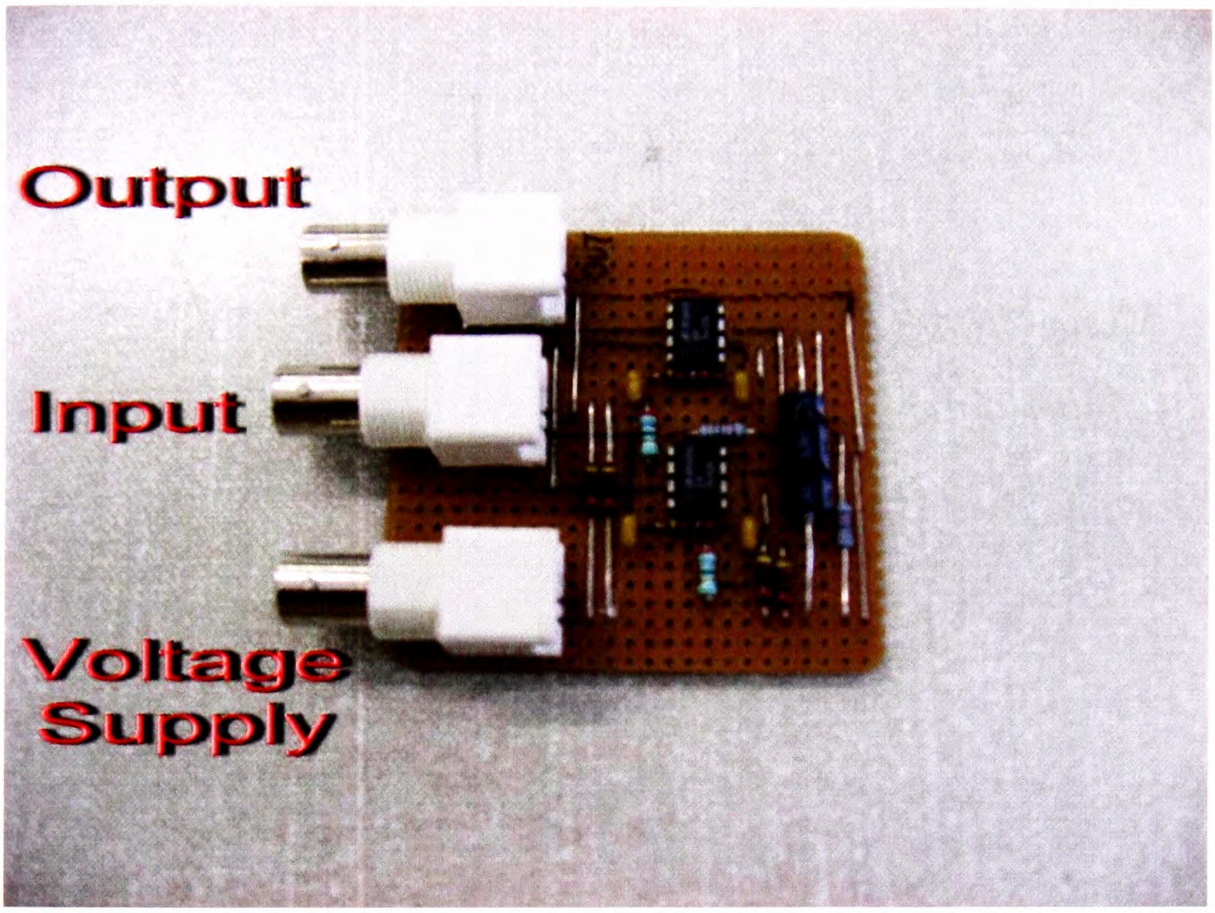

Figure 6.8: In-house customised band-pass amplifier filter module.

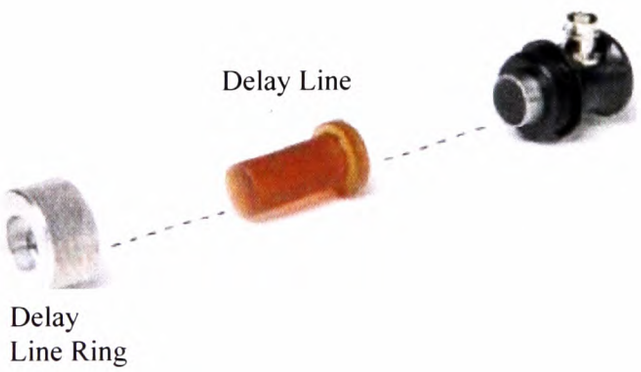

Figure 6.9: Delay line transducer. (Photo courtesy of Olympus NDT)

The result in Figure 6.10 shows that the oscilloscope captured both the source and transmitted signal simultaneously. However, this model of oscilloscope is not capable of capturing the very first few frames of the signals (the first few microseconds of the transmitted signal and source signal). Another problem encountered was the precision of the timescale: even though the timescale axis can be adjusted or magnified, it cannot provide precision to the nearest decimal point but can only give estimated readings to the nearest significant figure (Because the reading is analogue rather than digital). The precision of the timescale readings would directly affect the reliability of the ultrasound velocity values.

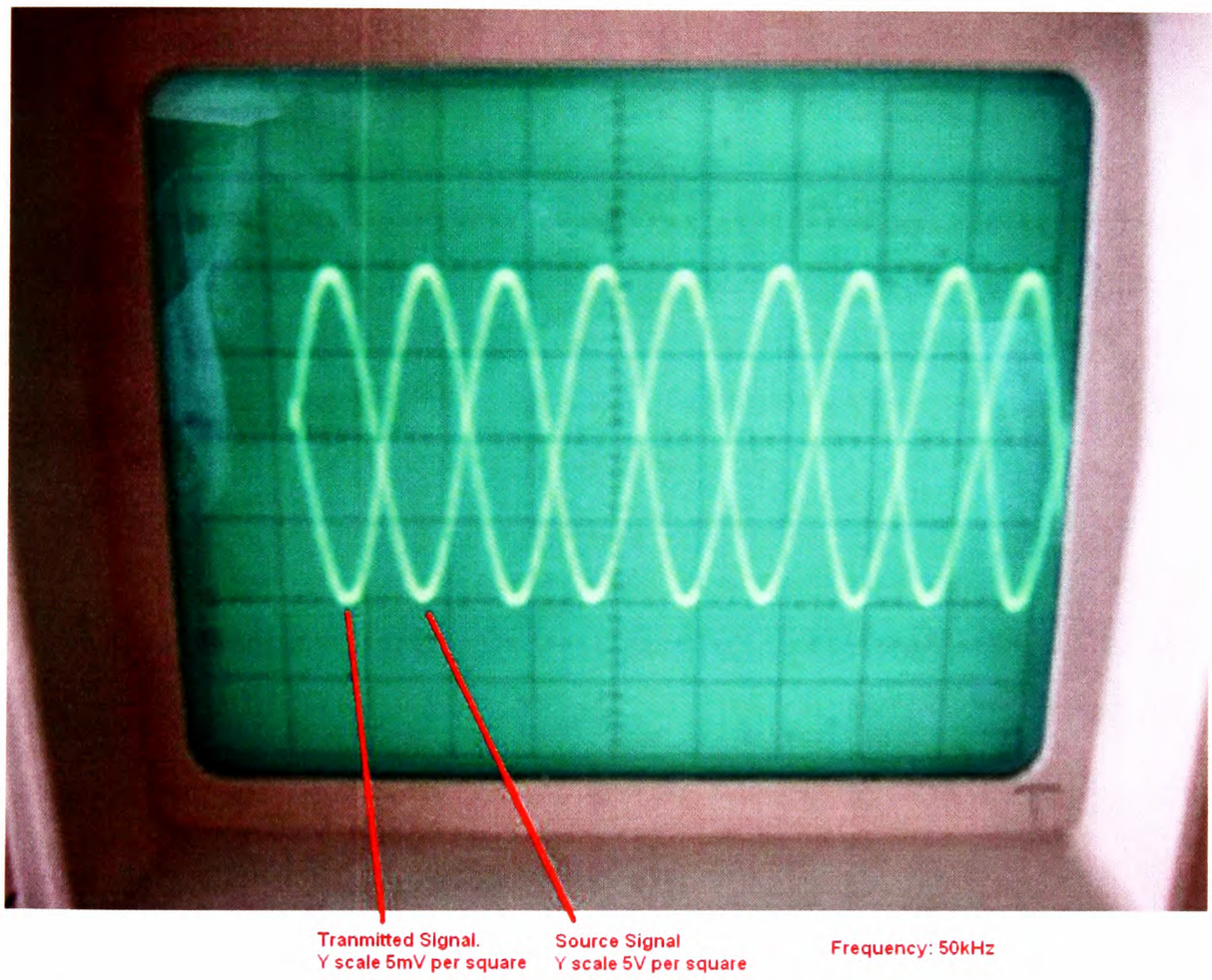

Figure 6.10: Example of measurement result from experimental rig A. The sample used is distilled water at 20°C.

6.3. Experimental rig design B

Experimental Rig B was built to solve the problem of recording data from the measurement. This was achieved by replacing the analogue oscilloscope with the Picotech ADC212 analogue-to-digital converter (see Figure 6.11), which can capture the measurement data directly and save it to a computer.

The analogue-to-digital converter (ADC) has two input channels that can record data independently. This means that the reference signal can be recorded simultaneously yet independently from the transmitted signal. The sampling rate of the ADC is 3 million samples per second, with a 12-bit resolution. The complete specification of the ADC is provided in Appendix K. The decision for selecting which type of ADC to use was based on the several factors, in the order of importance:

- **Resolution (8 bits, 12 bits, or 16 bits).** The resolution will determine the precision of the data – for example, 8-bit resolution over 10 volts measurement would be able to detect a change in voltage as small as 10/256 (~39mV), while comparable figures for 12-bit and 16-bit resolution would be 10/4096 (~2.4mV) and 10/65536 (~152μV) respectively.
- **Sampling rate (samples per second).** The sampling rate determines how many data points can be received per second. A very fast repeating signal of a very high frequency would require a very high sampling rate.
- **Bandwidth.** The bandwidth of the ADC can be defined as the maximum frequency that can be measured by the ADC. Normally, the ADC should have higher-frequency bandwidth than the signal to be measured.
- **Input and output channel number.** This would usually correspond to the number of the input signal that needs to be converted, or where the ADC needs to be synchronised with another device.
- **Integrated amplifier and filter.**

Figure 6.11: Picotech ADC212/3 analogue-to-digital converter.

Additionally, to examine the response of the solder paste to a broader ultrasound frequency range, a pair of 0.5Mhz Panametrics V413-SB broadband transducers (see Figure 6.12) were incorporated into the design of experimental rig B.

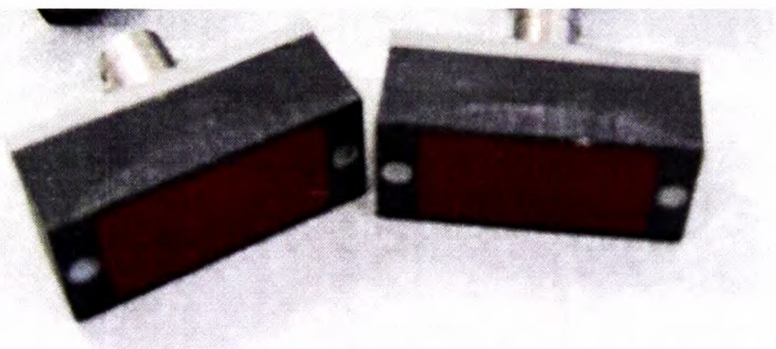

Figure 6.12: 0.5 Mhz Panametrics V413-SB broadband transducers.

The schematic of experimental rig B is shown in Figure 6.13. In this part of the design, an adjustable bracket (see Figure 6.14) has been implemented in order to attempt to test the samples in the bottle without having to remove a sample and place it in the U-shaped sample holder.

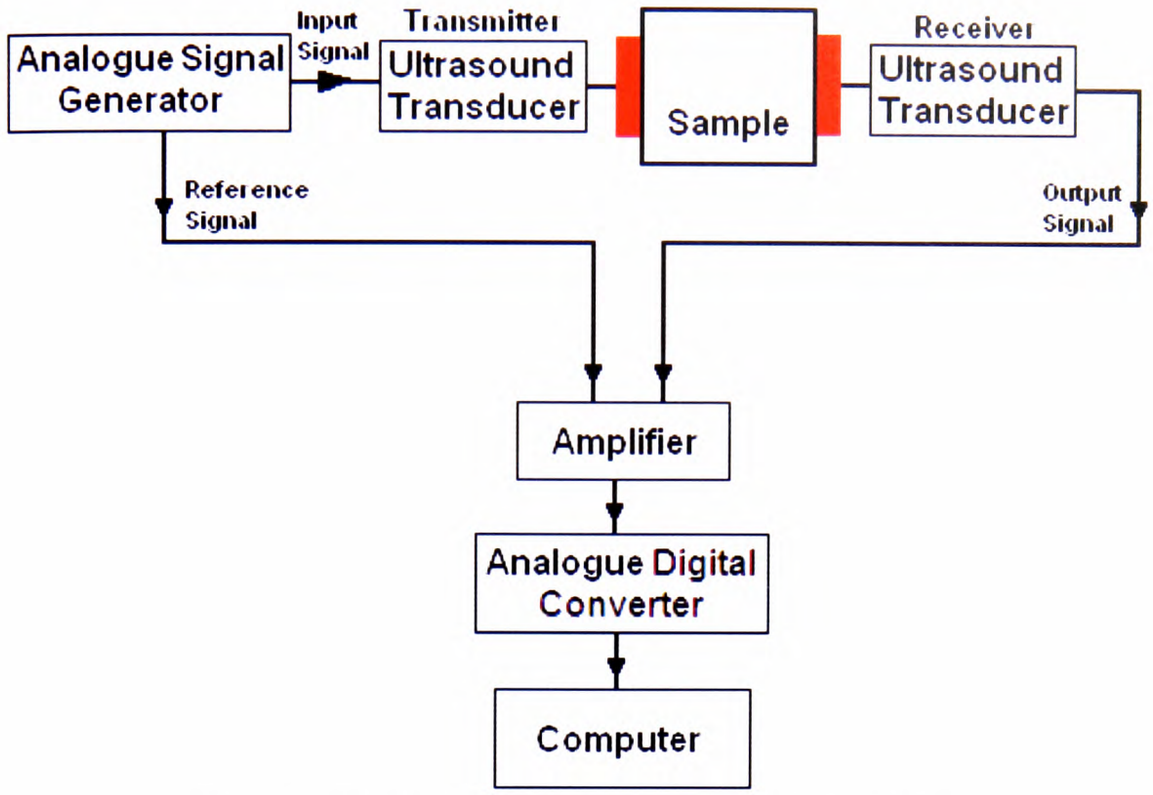

Figure 6.13: Schematic diagram of experimental rig B.

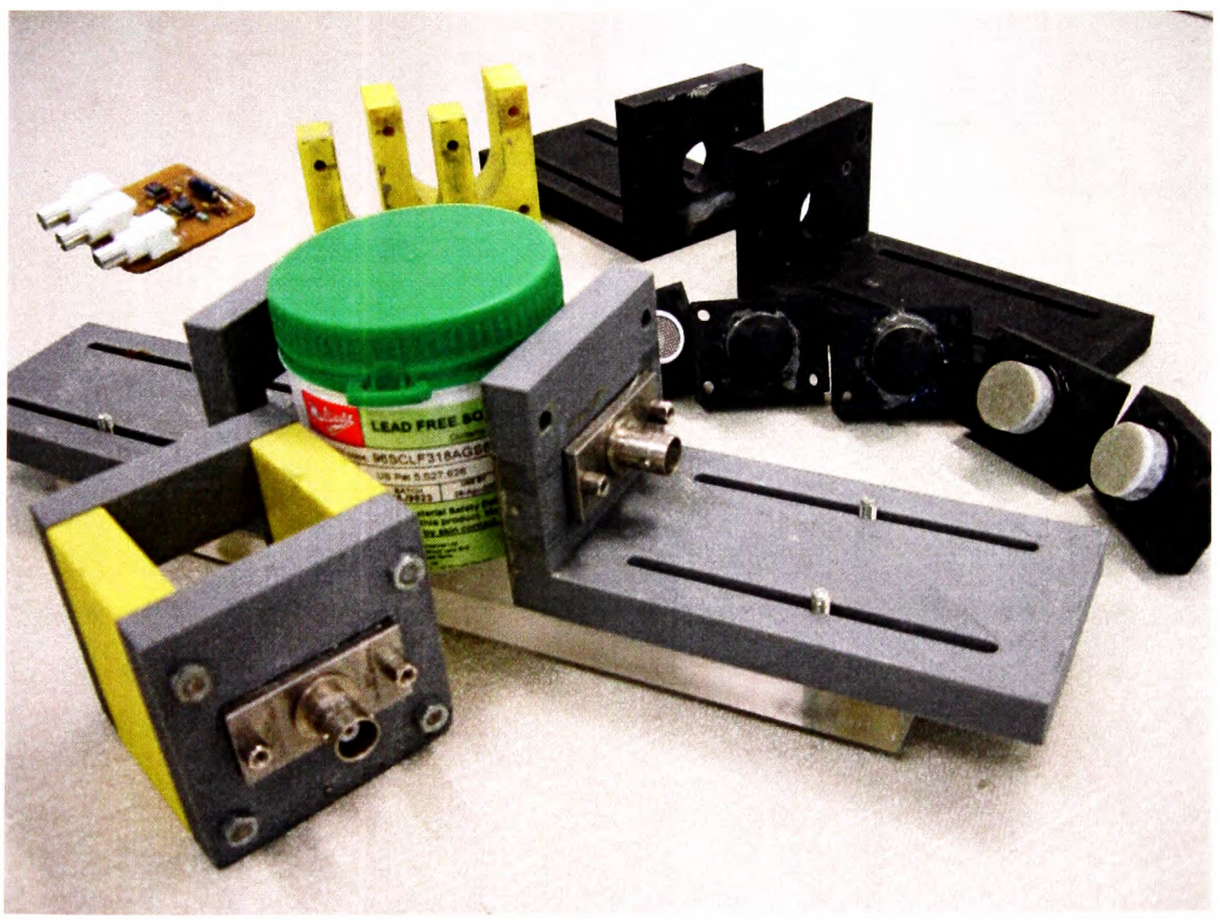

Figure 6.14: Sample holders and sensor brackets for experimental rig B.

6.3.1. System overview and limitations of experimental rig design B

Through preliminary tests using rig B, it can be concluded that the use of broadband Panametrics transducers did indeed – as expected – produce more reliable results than the Murata transducers, due to their larger element size. The Panametrics transducers have wider elements, hence wider beam directivity (see Appendix I1), which allow the transducers to have beam directivity of the width of the element (25mm) compared with only 18.7mm for those of Murata's.

It was also found that use of an ADC would allow further simplification of the system of experimental rig B. Because of the high resolution of the ADC unit, it was possible to eliminate the external amplifier-filter unit and read the raw data directly or to use the supplied ADC software for magnification purposes instead. Eliminating the external amplifier-filter unit also resolves the issue of noise amplification, as the amplifier-filter will usually not only amplify weak signals but also weak background noise.

Although experimental rig B allowed the user to see and compare the reference signal and the transmitted signal, it was not possible to use the result to calculate ultrasound velocity through the sample. This is because the signal generated by the analogue signal generator is a continuous sinusoidal wave, so there is no beginning or end point of the signal that can be used as a time-point marker to compare the reference signal and transmitted signal; to obtain the ultrasound velocity of the material being tested, an end point of the reference signal and the beginning point of the transmitted signal are required. Therefore, the system needs to be upgraded to allow recording of the ultrasound velocity, as accuracy of ultrasound velocity measurement plays a significant part in determining the viscosity of material through ultrasound techniques, as demonstrated later in Section 7.2.

6.4. Experimental rig design C

Experimental rig C employed an Agilent 33220A arbitrary waveform digital signal generator (see Figure 6.15) to solve the ultrasound velocity measurement problem. By using a digital signal generator, the ultrasound velocity can be measured because the digital signal generator can produce a pulse/tone burst (single frequency at one wavelength pulse) waveform repeated over a certain duration of time. Because tone burst waveform is not a continuous waveform but an intermittent waveform, it allows the operator to identify the start and end of time the transmitted signal, which can then be used to calculate the ultrasound velocity. The ability to transmit a signal digitally also allows better signal quality. Unlike an analogue signal, a digital signal doesn't contain uneven or instantaneous random fluctuations when viewed at high resolution or during a very narrow time span.

The schematic diagram of experimental rig C is represented by Figure 6.16. A detailed diagram of the signal processing route for this rig is included in Appendix C.

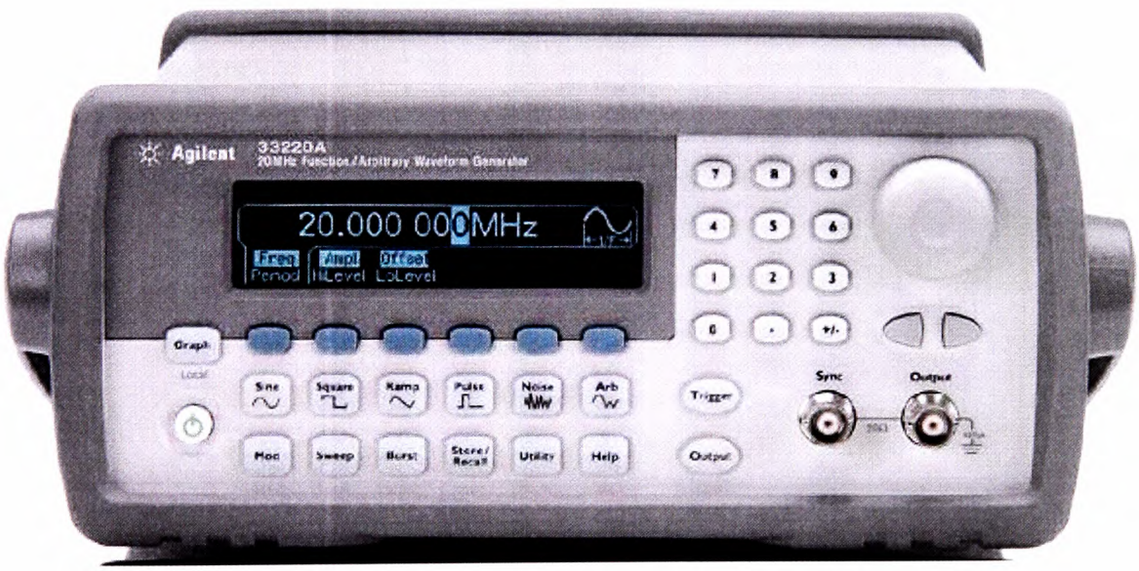

Figure 6.15: Agilent 33220A arbitrary digital signal generator.

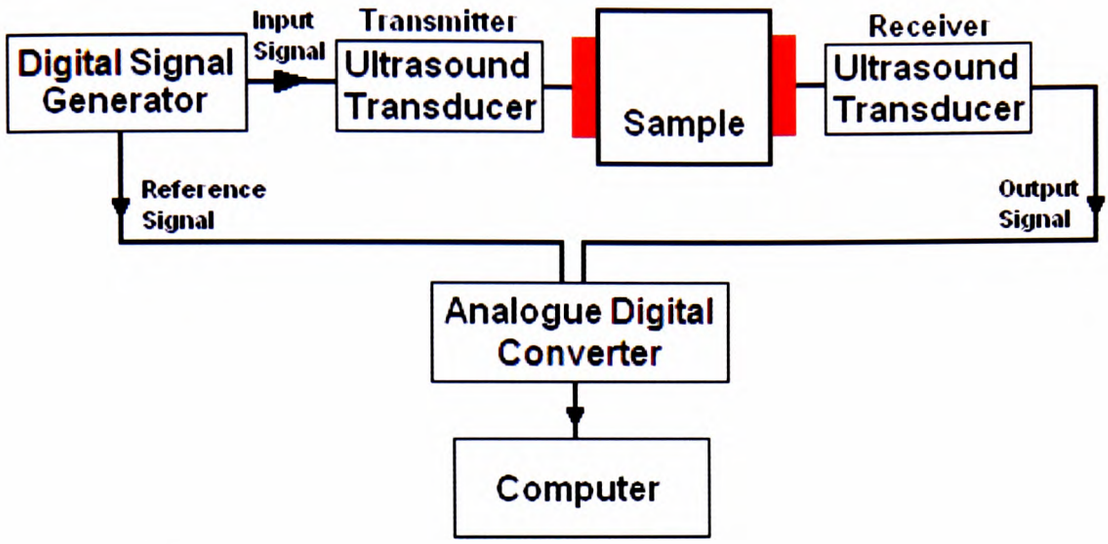

Figure 6.16: Schematic diagram for experimental rig C.

In this test, a single pulse of say 40kHz frequency was repeated at an interval of 20ms. So in this case the signal will last for 25μs (one wavelength of 40kHz) and repeated every 20ms interval. Because there is an interval of 20ms between the consecutive pulses, the start and end of signal is clear. Therefore, it is now possible to measure the velocity of the transmitted signal.

With the problem of ultrasound velocity measurement solved, the attention of the project now shifted to designing a rig that could test the sample without removing it from the bottle. Given that the ultrasound attenuation profile of solder pastes using the Murata and Panametrics transducers had been studied, it was decided to use the same transducers in the design of rig C and to use water as the coupling medium. This technique is more effective than coating the surface of the bottles with a thin layer of oil or water, hence avoiding the need to order custom-made delay line transducers that fit the contour of the bottle. Thus, two round-shaped sample holders, which also housed the transducers, were produced out of ABS plastic using a rapid prototyping machine (see Figures 6.17–6.20). The full dimensions of these sample holders are provided in Appendices G3 and G4. The sample holders each have a volume of 318cm^3 (318ml).

Figure 6.17: Testing of solder paste in plastic bottle using Panametrics transducers.

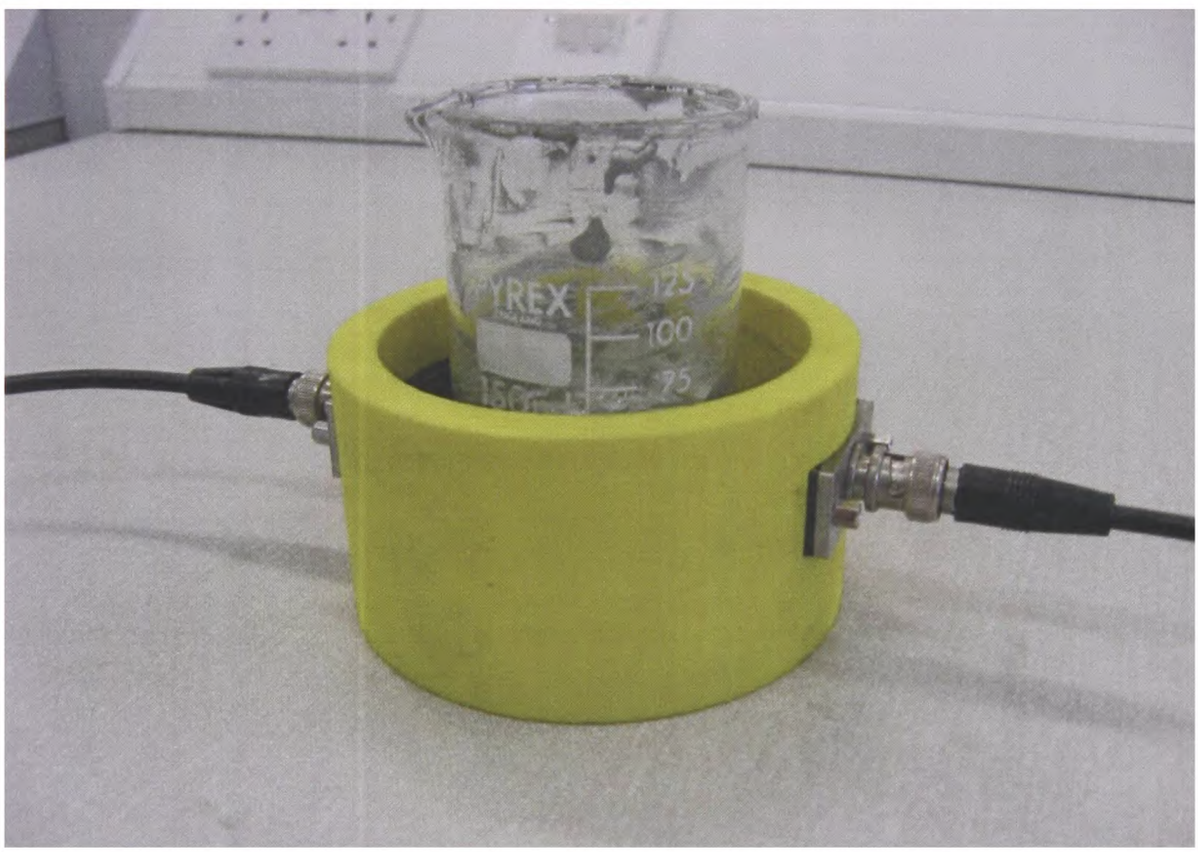

Figure 6.18: Testing of solder paste in glass container using Panametrics transducers.

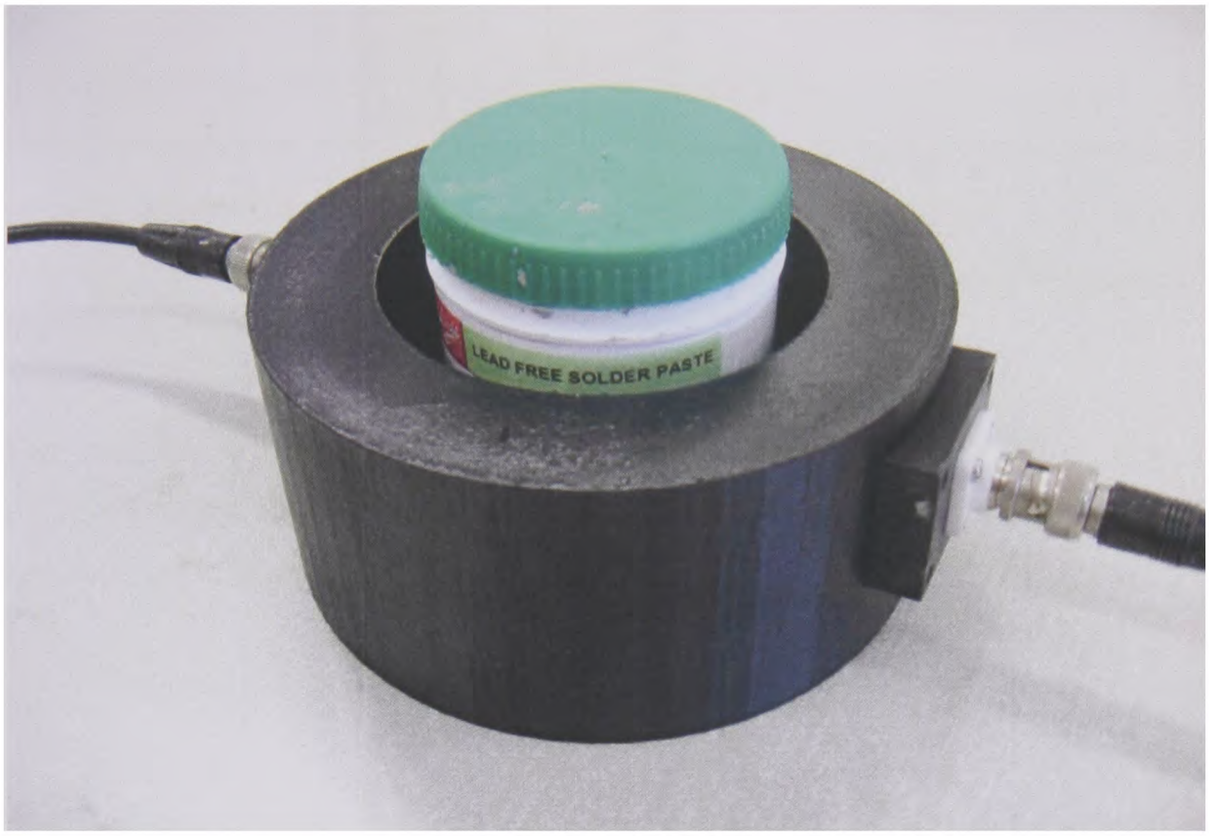

Figure 6.19: Testing of solder paste in plastic bottle using Murata transducers.

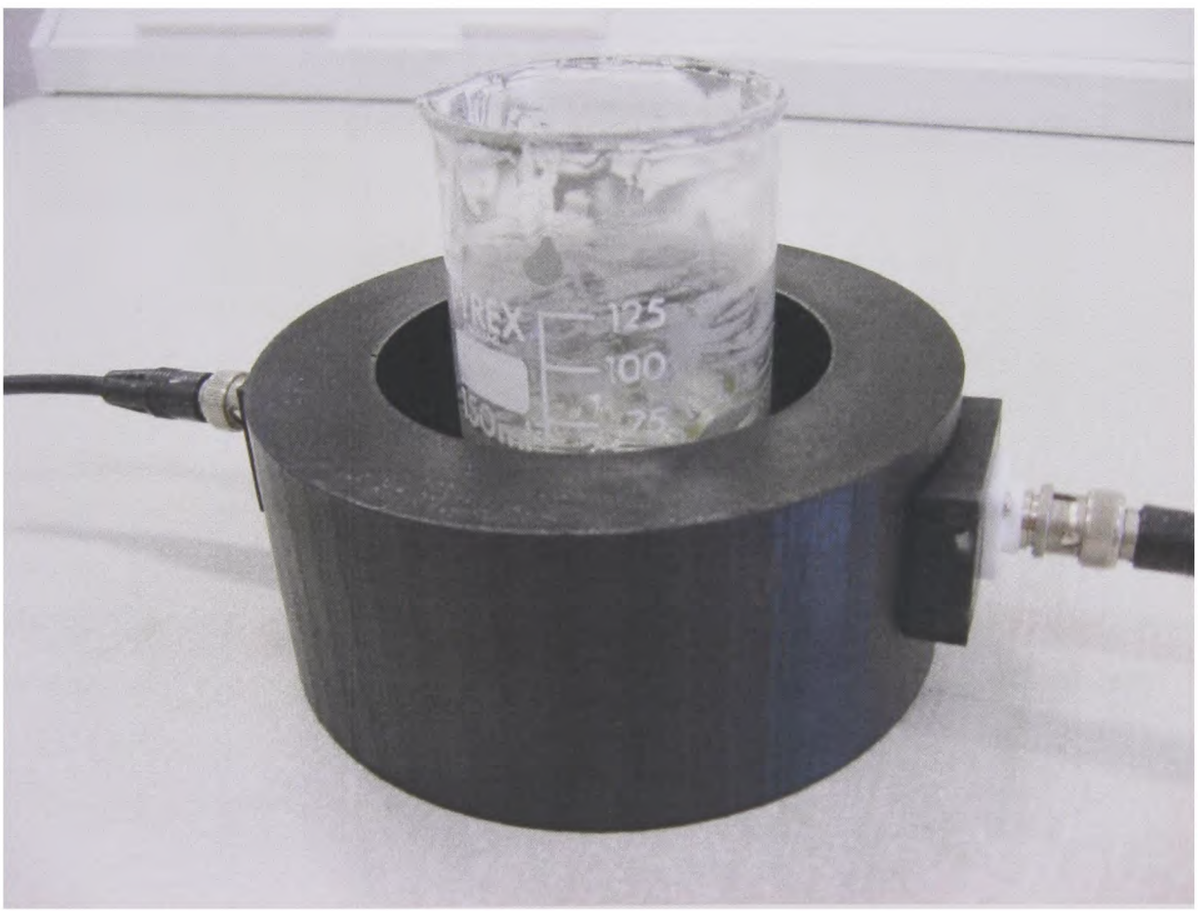

Figure 6.20: Testing of solder paste in glass container using Murata transducers.

A computer program using Microsoft Visual Basic software was used to extract the raw digital data from the ADC unit to obtain a measurement of the ultrasound velocity and attenuation. This program can be integrated into Microsoft Excel as a macro to help generate the graph of the measurements taken. Further detail of the program is provided in Appendix A.

Experimental rig C was the final rig developed for this study of *in situ* testing of solder paste samples. The rig was used throughout the research project to collect the data reported in Chapter 7 onwards.

6.4.1. Calibration of transducers

There are two common methods normally used to calibrate the ultrasound velocity of transducers, namely using a well characterised sample such as water or using a standard reference calibration block (see Figure 6.21).

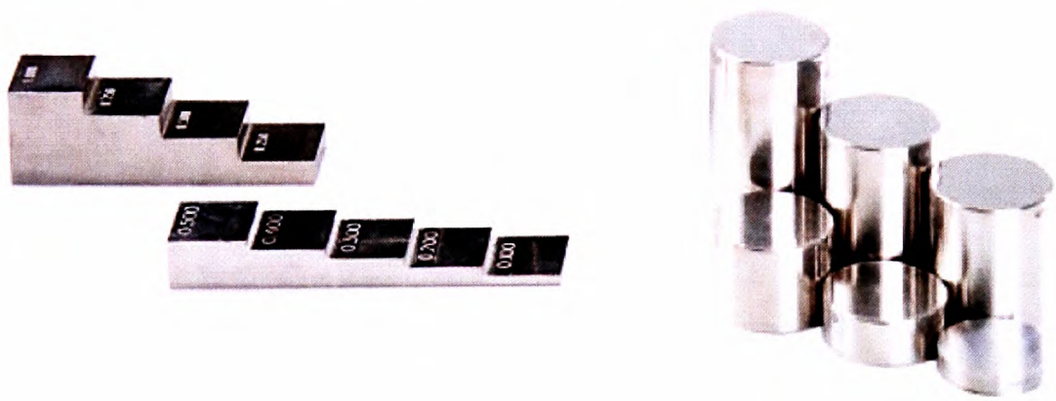

Figure 6.21: Standard reference calibration blocks for calibrating ultrasound velocity.

All the transducers used in this experiment were calibrated using distilled water because the ultrasound velocity of water at various temperatures at normal atmospheric pressure has been well documented and can be easily derived based on the following formula (Marczak, 1997):

$$c = 1.402385\times10^{3} + 5.038813T - 5.799136\times10^{-2}T^{2} + 3.287156\times10^{-4}T^{3} - 1.398845\times10^{-6}T^{4} + 2.787860\times10^{-9}T^{5} \quad (6.1)$$

where c is the ultrasound velocity of water and T is the temperature of water. The formula is valid for 0–95°C at normal atmospheric pressure. To the best of the author's knowledge, there is no limitation on a particular frequency range that Equation 6.1 is restricted to. Marczak (1997) compared the findings with other researchers who reported their work at 4, 5, and 16MHz and reported that the deviations are negligible.

Based on this equation, the ultrasound velocity of water at different temperatures is as shown in Table 6.1. In order to verify that the test rig is working as it supposed to be, the ultrasound velocity measurement of water obtained at 10, 20, 30 and 40°C were compared against the values shown in Table 6.1. It was found that the measured values were within the range shown in Table 6.1 with an average deviation of ±5m/s (see Figure 6.22).

Temperature (°C)	Ultrasound velocity (m/s)
0	1,403
5	1,427
10	1,447
20	1,481
30	1,507
40	1,526
50	1,541
60	1,552
70	1,555
80	1,555
90	1,550
100	1,543

Table 6.1: Ultrasound velocity of water at various temperatures.

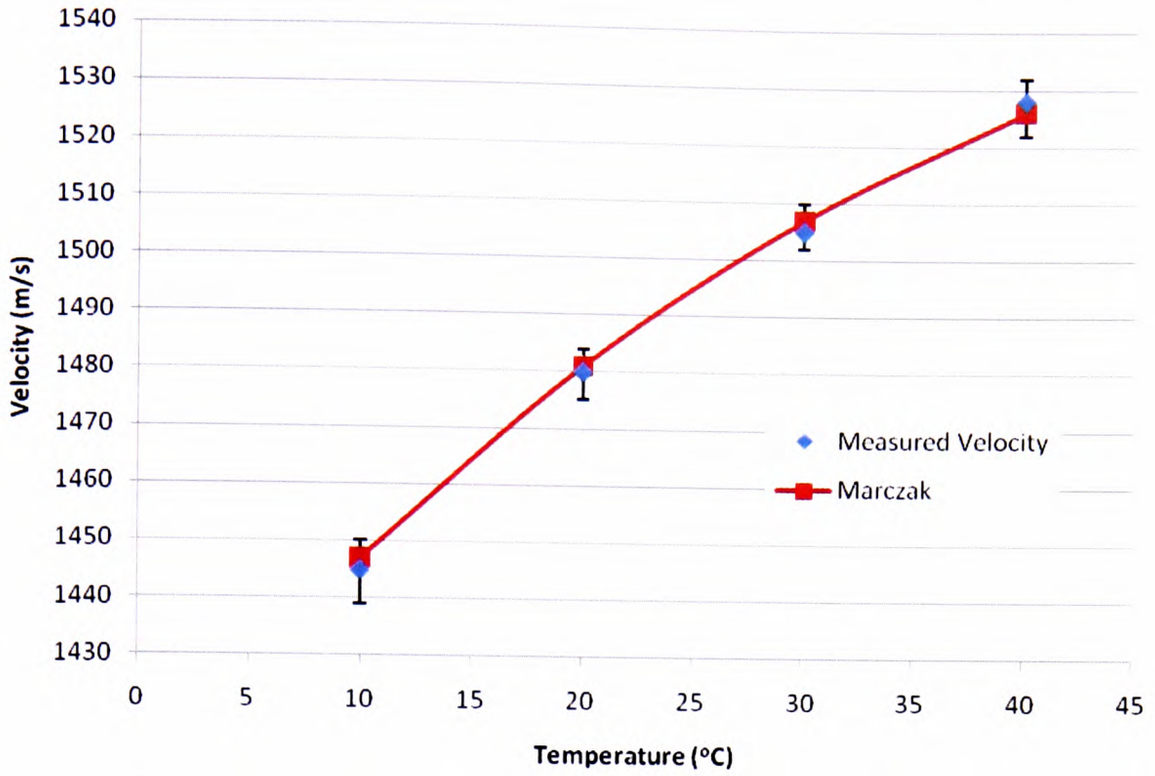

Figure 6.22: Verification of ultrasound velocity of water at various temperatures.

6.5. Summary

The design and development of the experimental rigs for testing solder paste consisted of three design stages. Technical challenges encountered during the initial development process (rig A) included difficulty in differentiating source and returned signals, difficulty in determining the transmission time through the sample, and the inability to save test data. During this process it was found that, due to the high attenuation nature of the solder paste materials, air cannot be used as the coupling medium. This problem has been well reported in the literature review especially for cured cement paste. Most of the reported works involving cured cement paste use a coupling gel or immersing the sample in water approach in order to resolve the high attenuation problem.

The issue of the inability to save test data was resolved in the second stage of the design (rig B). Continuous sinusoidal wave transmission was found to be hampering the effort to record ultrasound velocity accurately. At this particular stage, the phase

angle difference can be easily identified from the results, which can be used to determine the storage and loss moduli of the material being used.

The final stage of the development process (rig C) resolved the problem of recording the ultrasound velocity by employing tone-burst ultrasound waves produced using a digital signal generator. Water was found suitable to be used as the coupling medium for testing solder paste. The performances of four pairs of transducers were re-evaluated against the solder paste sample. The Panametrics transducers outperformed other transducers because of their broadband frequency coverage and larger size of element.

CHAPTER 7

PRELIMINARY TESTS ON CEMENT PASTE SAMPLES

7.1. Introduction

This chapter presents the preliminary experimental tests using experimental rig B previously described in Section 6.3 above. This preliminary study used cement paste and mixtures of various compositions of cement and sand as the samples under investigation. The study was conducted to validate the design of experimental rig B and to verify the use of the same transducers on experimental rig C. In this particular respect, the results of this study were compared with the results of Aggelis and Philippidis (2004).

7.2. Materials and test set-up

A test set-up similar to that of experimental rig B (see Figure 6.13) was used in this preliminary set of experiments, and the particular rig used for this study is shown in Figure 7.1. The cement used was Lafarge Portland cement (Portland PC CEM II 32.5), and distilled water was used to liquify the cement samples. Because of the small amounts of sample used, the cement was hand-mixed in a small plastic container. In all cases, the cement used was 300g (weighted to 0.1mg accuracy) of cement powder mixed with a known amount of distilled water to make up the required water-to-cement ratio (w/c) – for example, a 200g water and 300g cement mix would be identified as 0.6 w/c. When sand was added to the sample mixture, the amount of sand was measured as a percentage of the cement mass used in the mix. Hence a 0.6 w/c with 10% sand content should contain 30g of sand in the mixture. The sand used

comprised fine sand particles with particle size no greater than 1000μm, and 67% of the sand particles were in the range of 500–800μm (filtered using wire mesh sieves). The test was conducted at a room temperature of 25°C.

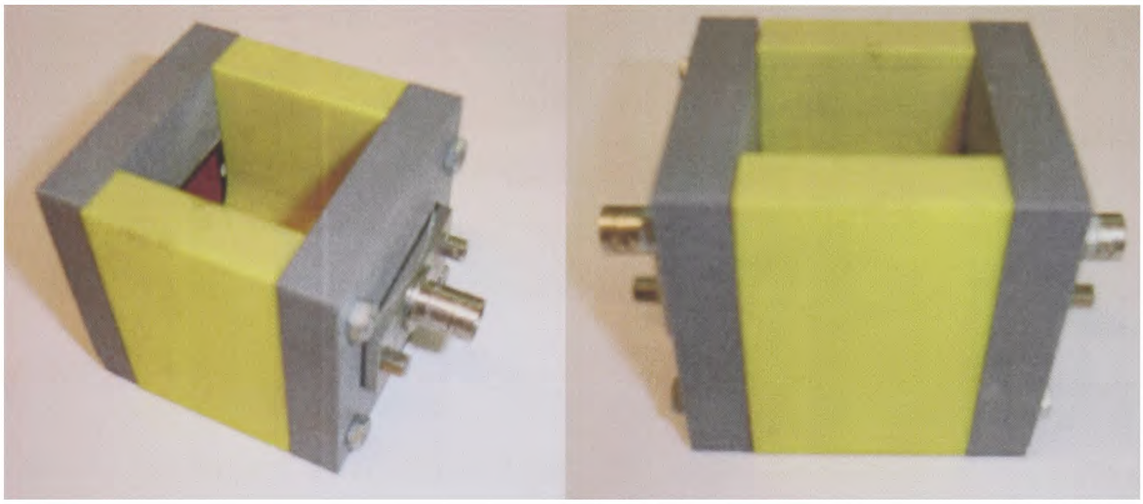

Figure 7.1: Ultrasonic test rig for cement paste using 500kHz ultrasonic transducers.

7.3. Objectives of preliminary study

The objectives of the study were to repeat the previous works (Landis and Shah, 1995; Aggelis and Philippidis, 2004; Ye *et al* 2004; Kamada *et al* 2005), in order to verify that the rig worked as it supposed to be and to validate the measurement results by comparing them to the previous works. Cement pastes were chosen for this study as their properties at early curing state were quite similar to solder paste i.e. high viscosity, containing solid and liquid phase.

The primary aim of this study was to validate that the test results obtained using the test rig is comparable to the previously reported works. In order to confirm what Aggelis and Philippidis (2004) had reported, a similar equipment set-up was used; this included the use of 500kHz Panametrics ultrasonic sensors. In that particular paper, Aggelis and Philippidis were trying to use ultrasound to characterise cement paste by investigating the effect from the water-to-cement ratio and sand content. Useful parameters that can be gathered during the tests using ultrasonic techniques included velocity and attenuation/absorption for the ultrasonic waves.

The secondary aim was to demonstrate that tests conducted using ultrasonic techniques are reproducible and reliable.

7.4. Experimental results and analysis

Because the measurement results presented in Section 7.4.1 and 7.4.2 were based on curing cement it would be difficult to make sense of the measurement results. However, the work was required to corroborate previous works.

Section 7.4.1 below presents the results and analysis for cement pastes using ultrasound techniques, in comparison with the technique reported by Aggelis and Philippidis (2004). Section 7.4.2 presents the rheology test results and analysis of the same cement pastes as described in the first section. Finally, Section 7.4.3 presents a comparison between the ultrasound and rheometer viscosity test results.

7.4.1. Ultrasound tests of Portland cement pastes

All the ultrasound measurements for the cement paste samples were conducted approximately 10 minutes after mixing, since it would require that time after mixing and compaction to reduce unwanted air bubbles trapped in the paste. The bubble formation can be observed during the mixing process, while the collapse of the bubbles is observable during the compaction process. Since cement powder undergoes physical change and chemical reaction when water is added to it, and will continuously do so for a few hours, the ultrasonic velocity of the paste is also changing continuously (Figure 7.2). The chemical reaction of the cement paste is indicated by heat generation to the mixing bowl. It should further be noted that once the cement paste is completely cured (Stage2), see Figure 5.4 and 5.5, the ultrasonic wave may not propagate through the cured cement any more (very weak signal amplitude) as a great deal of the water that acts as the coupling medium in the paste has evaporated causing many tiny voids in the cured cement. The volume of the

cement paste tested was 30.6 cm^3. Each data point only requires a few microseconds to collect the data from the sensor.

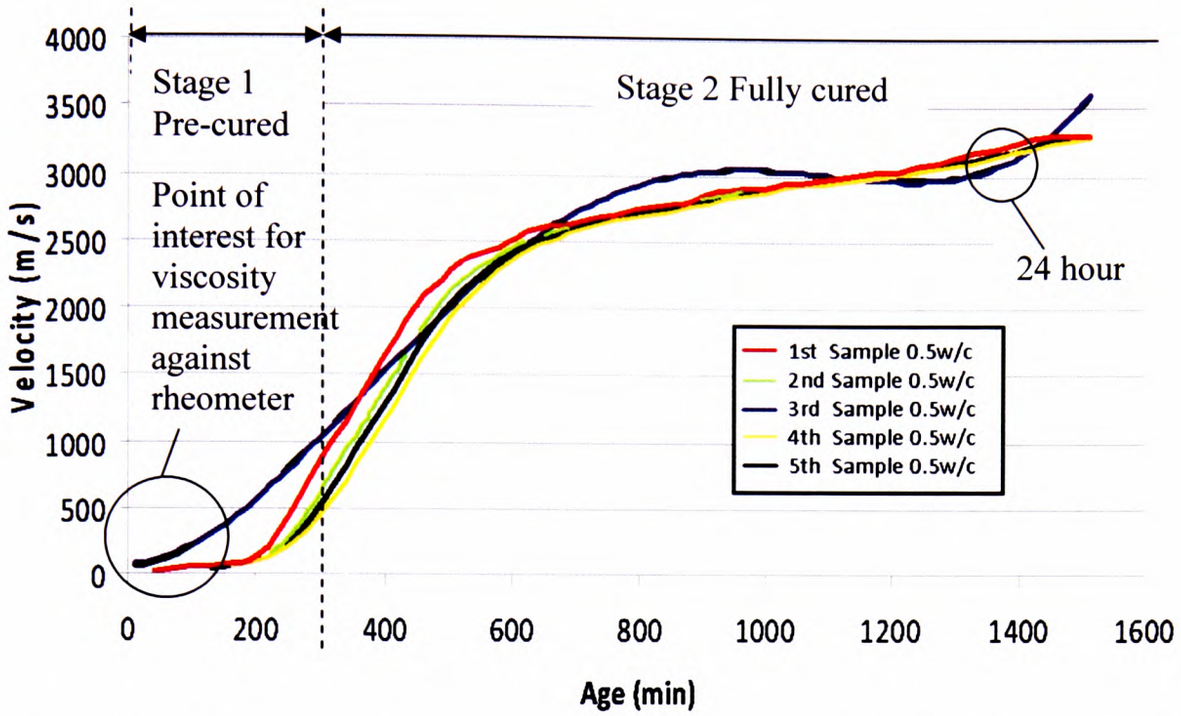

Figure 7.2: Ultrasonic velocity reproducibility test of 0.5 w/c cement paste at 500kHz.

As indicated in Figure 7.2, repeated tests of pure cement paste with a 0.5 water-to-cement ratio show a good reproducibility of ultrasonic velocity. The average deviation of the velocity at any time was found to be 37m/s. The deviations in the results might be due to reason that the samples were individually prepared for this test, and also due to the slight difference attributed to the starting time of the recording in relation to the sample preparation.

The ultrasonic velocity with different water content and sand content in Figure 7.5 to Figure 7.9 were recorded at 24hour(Stage2), such as indicated in Figure 7.2. As the data (0 to 820kHz) is collected within 1 second, the effect of time on curing is not significant. The increasing ultrasonic velocity measured against the frequency was as expected. Many materials reported in the literature review exhibit similar trend in which the ultrasound velocity increases significantly with frequency at lower frequency but remain almost constant at higher frequency, for example see Figure 7.3 and 7.4.

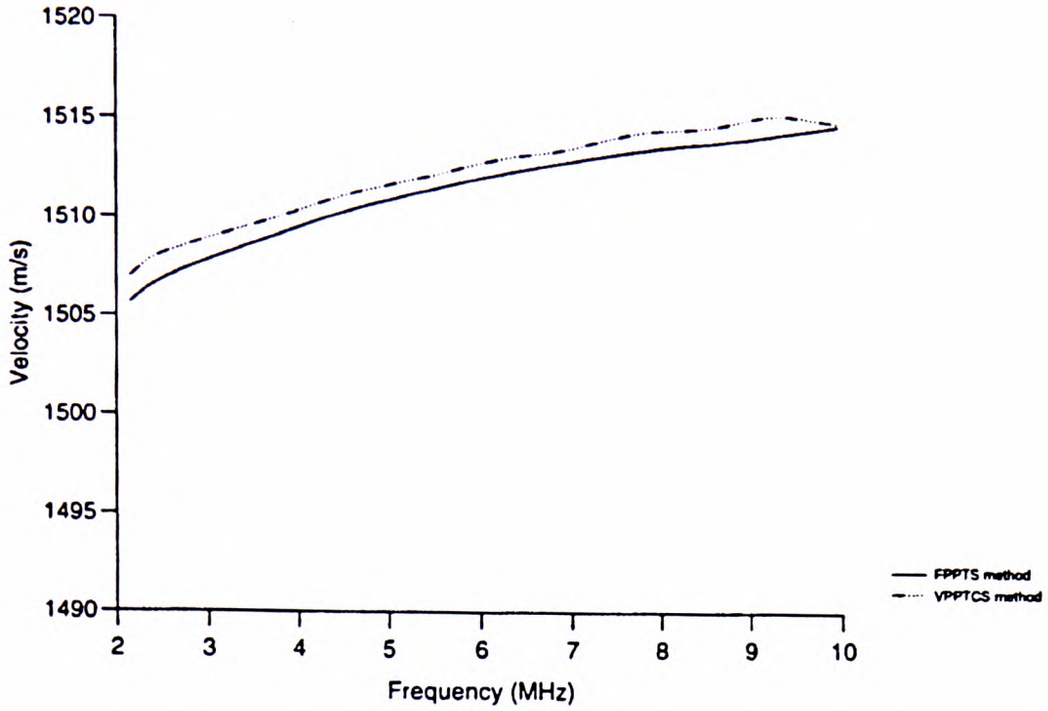

Figure 7.3: Ultrasonic velocity results of 50% d.r.c. of natural rubber latex. (Jaafar, 1996)

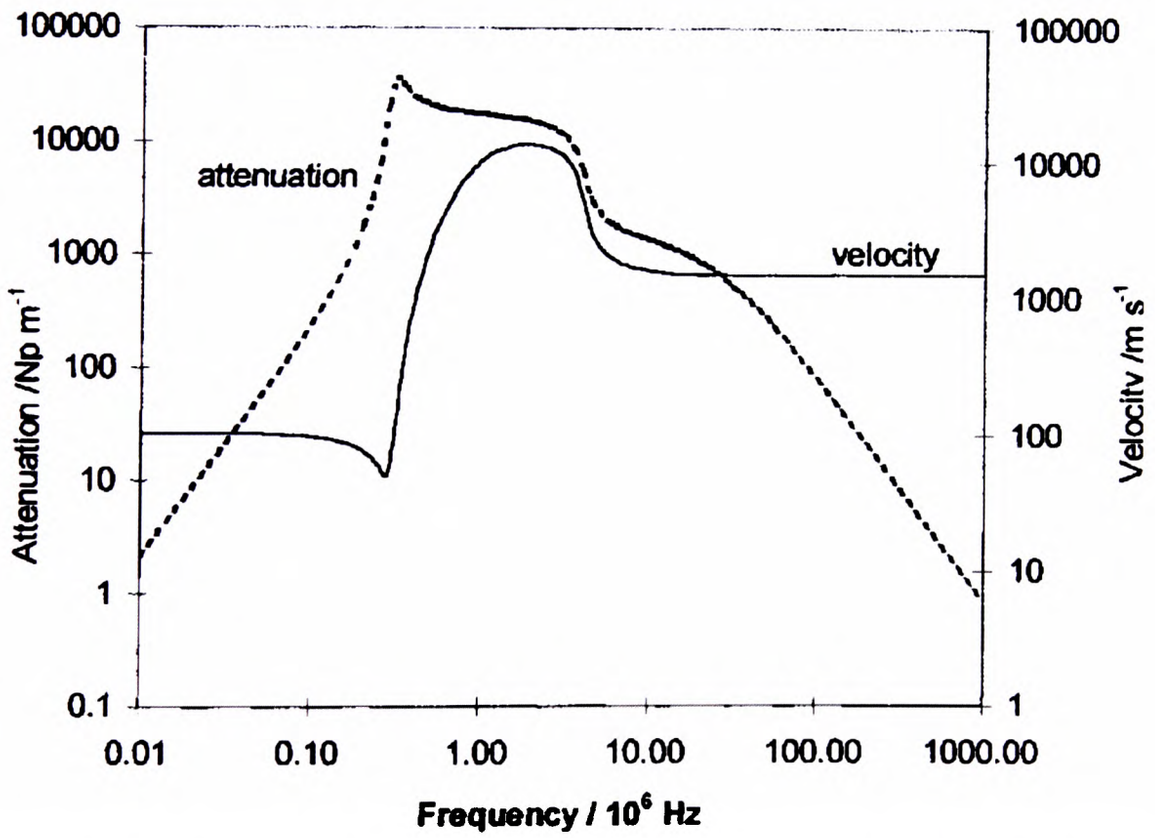

Figure 7.4: Ultrasonic velocity and attenuation as a function of frequency for a 2% volume fraction suspension of 10μm bubbles in water. (Povey, 1998)

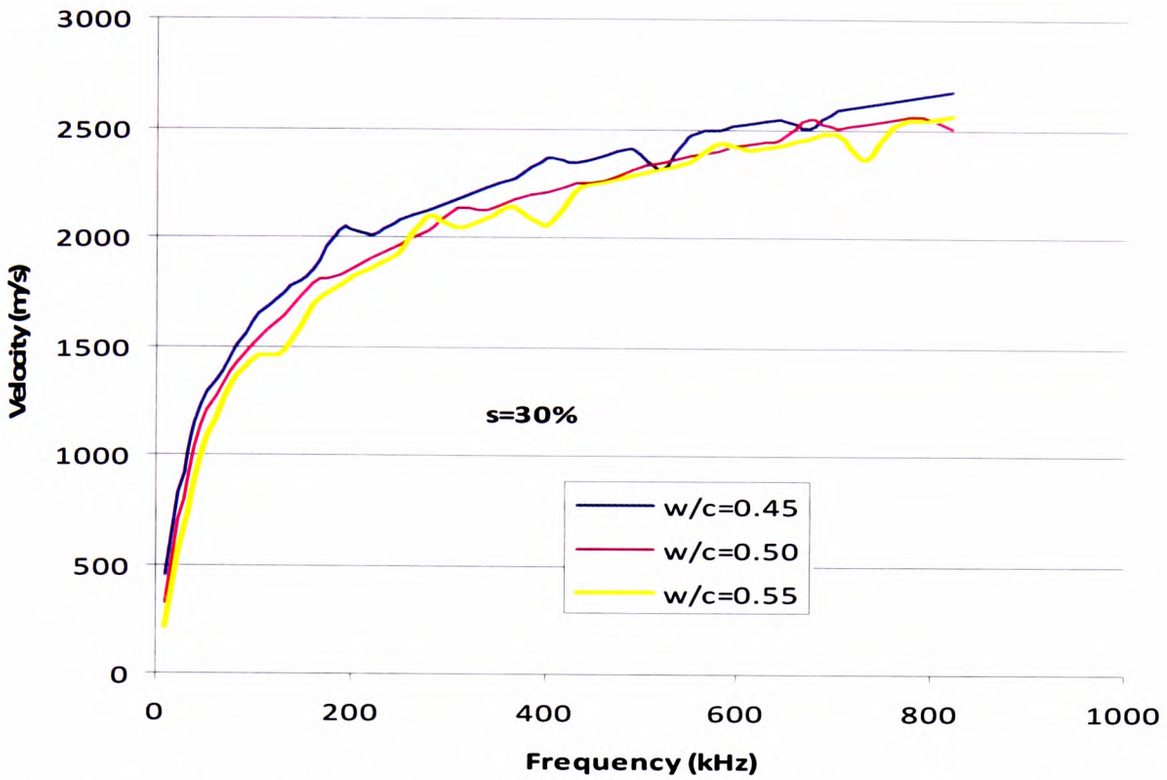

Figure 7.5: Ultrasonic velocity of cement pastes with 30% sand content with respect to various water-to-cement ratios.

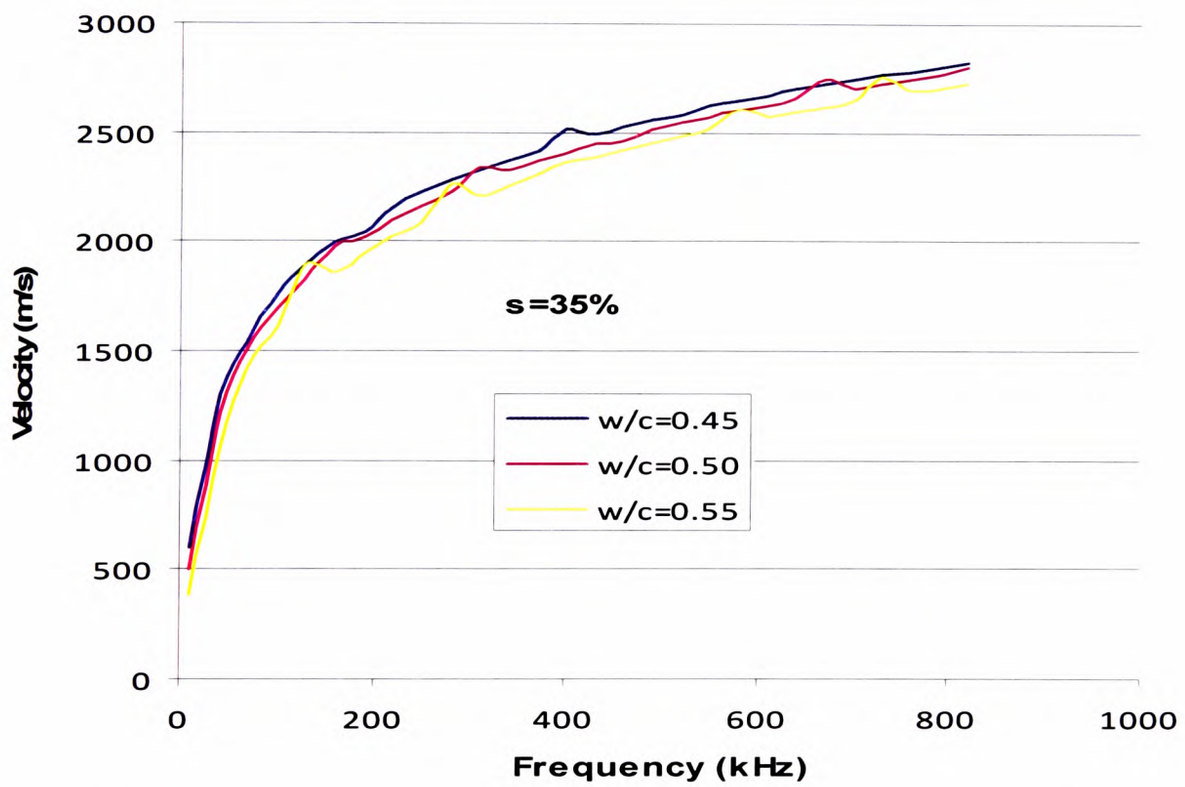

Figure 7.6: Ultrasonic velocity of cement pastes with 35% sand content with respect to various water-to-cement ratios.

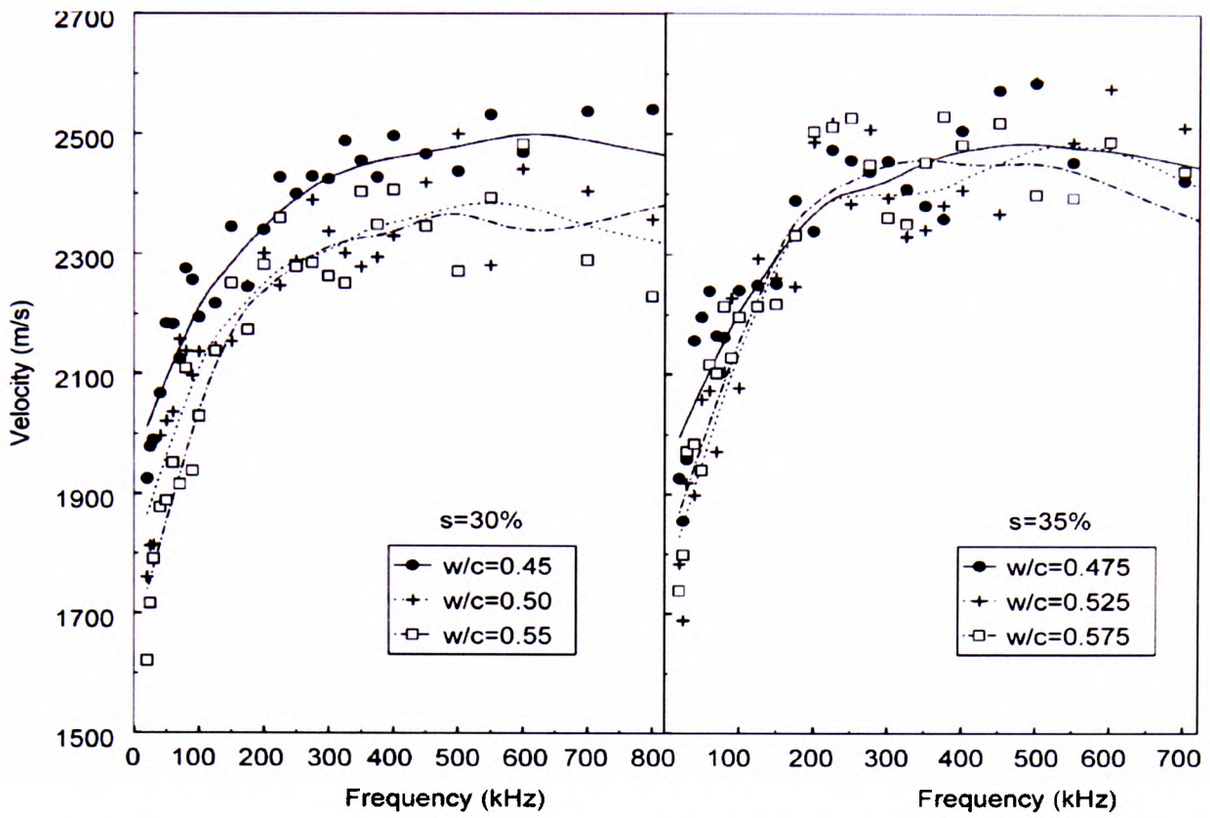

Figure 7.7: Aggelis's ultrasonic velocity results for cement pastes of 30% and 35% sand content with respect to various water-to-cement ratios. (Aggelis and Philippidis, 2004)

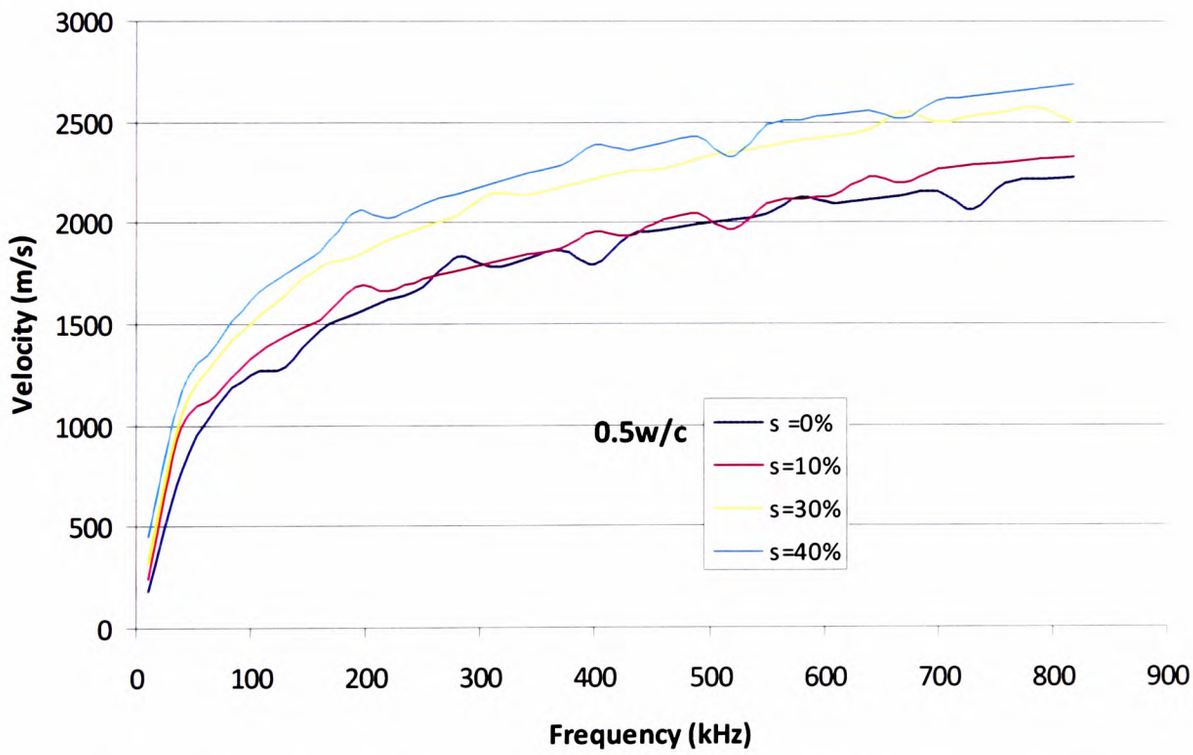

Figure 7.8: Ultrasonic velocity of 0.5 w/c cement pastes with respect to various sand contents.

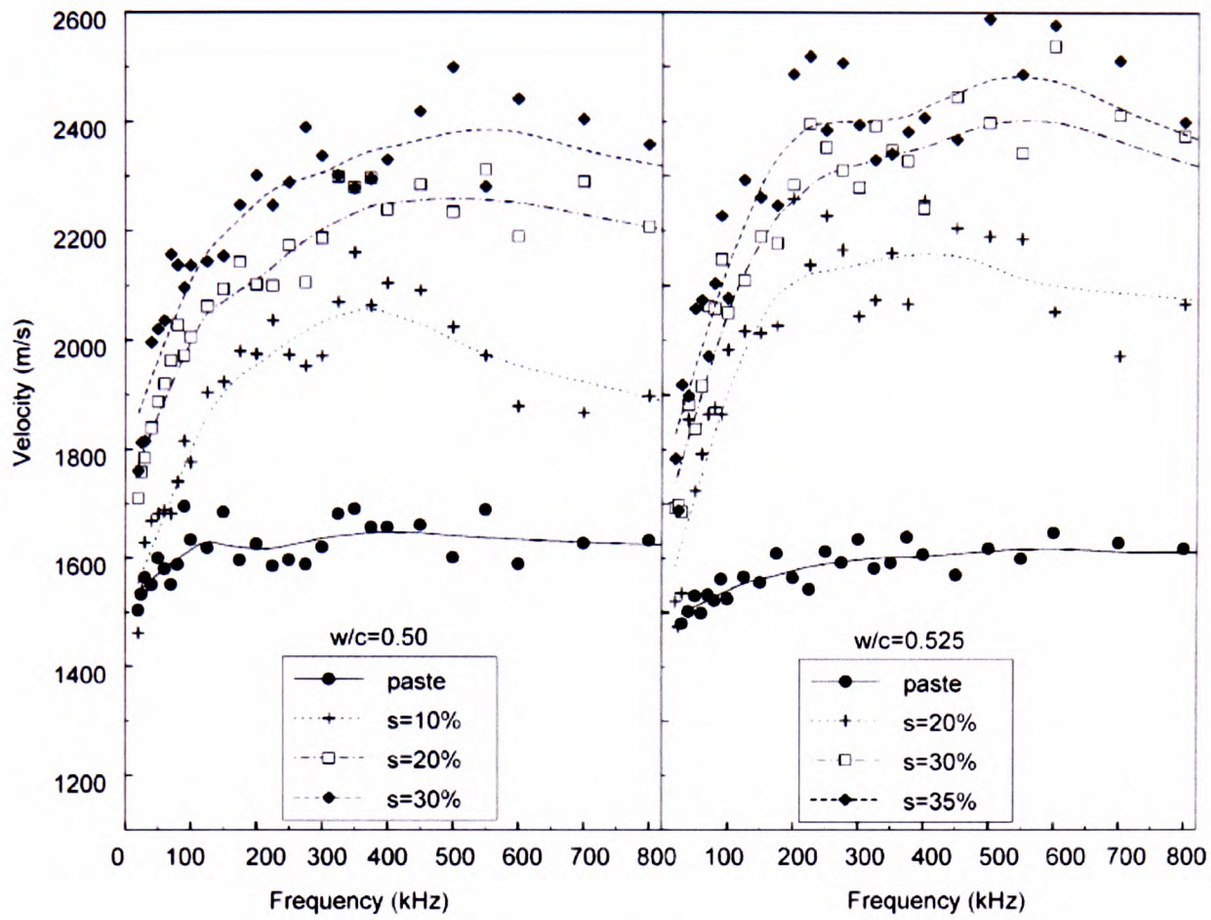

Figure 7.9: Aggelis's ultrasonic velocity results of 0.5 w/c and 0.525 w/c cement pastes with respect to various sand contents. (Aggelis and Philippidis, 2004)

In terms of ultrasound attenuation, increasing the sand content in the cement paste significantly increases the attenuation level of the ultrasonic wave, as shown in Figure 7.10. The attenuation in ultrasonic wave is supposed to be caused by the scattering of the waves by the sand particles. As this is the case, ultrasonic attenuation can be used as a measure of the sand content in the paste.

It was found that changing the water-to-cement ratio of the paste would not change the attenuation level of the ultrasonic wave significantly. But the addition of sand to the paste would significantly increase the attenuation level of the paste, of which this significant difference is more noticeable at higher frequency, as shown in Figure 7.10.

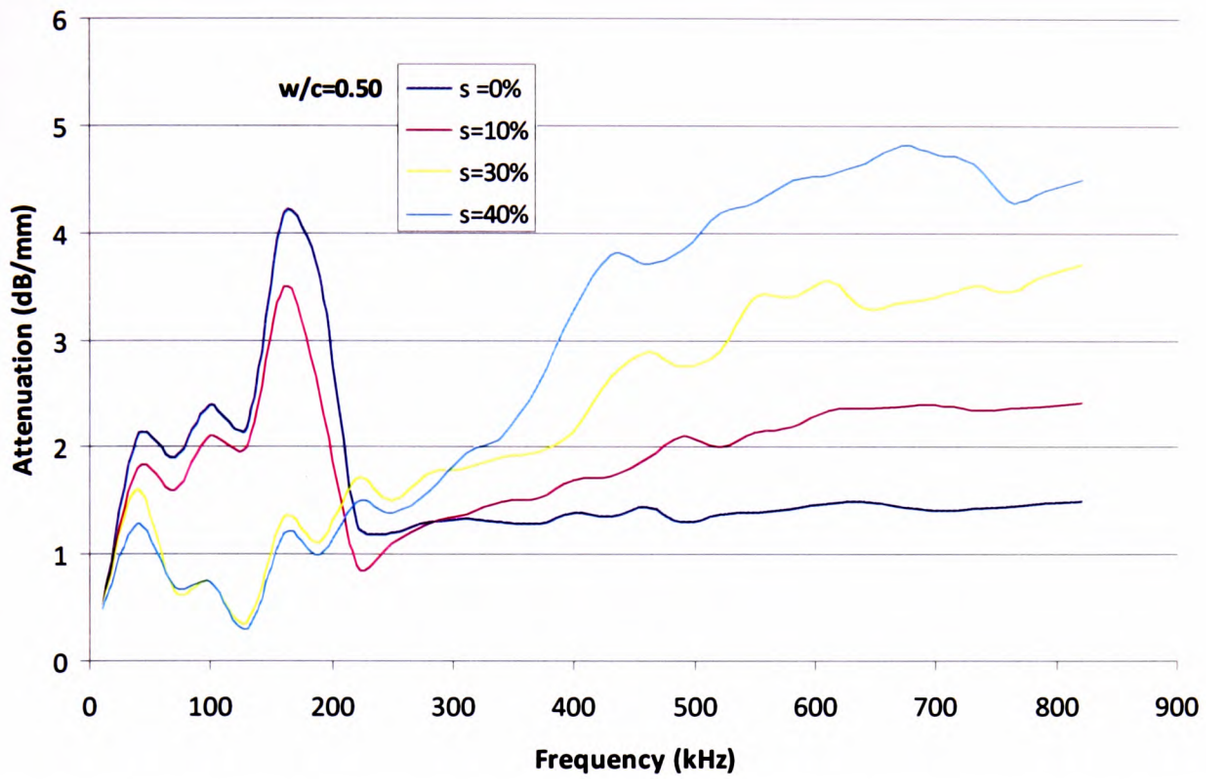

Figure 7.10: Ultrasonic attenuation of 0.5 w/c cement pastes with respect to various sand contents.

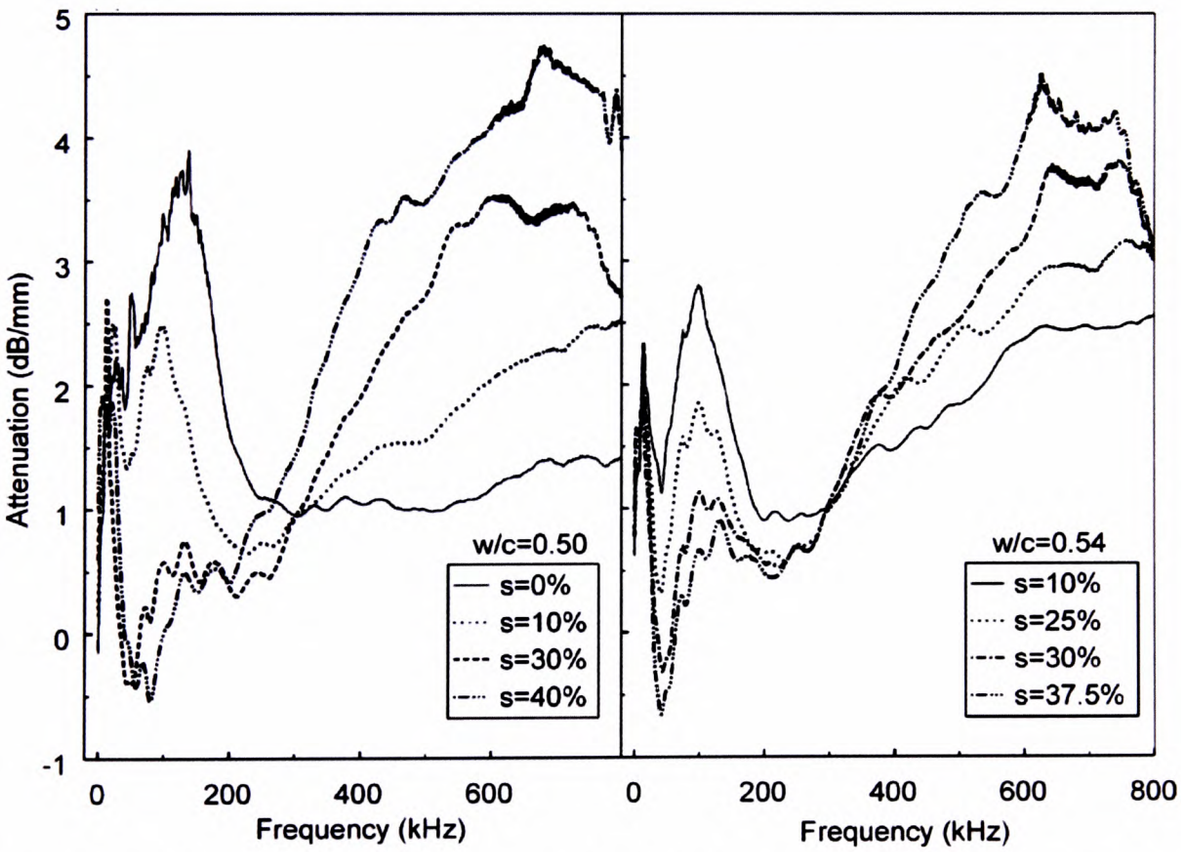

Figure 7.11: Aggelis's ultrasonic attenuation results of 0.5 w/c and 0.54 w/c cement pastes with respect to various sand contents. (Aggelis and Philippidis, 2004)

The attenuation of the cement paste with high sand content is considered to be due to the scattering and reflection of the ultrasonic waves. It can be deduced that this effect is only observed at high frequency because at high frequency the ultrasonic wavelength may be a lot smaller than the size of the sand particles; therefore, a greater portion of the ultrasonic wave is reflected and scattered.

From the analysis of all the graphs from Figure 7.5 to Figure 7.11, there are significant fluctuations along the individual curves. Although Aggelis and Philippidis (2004) did not comment on the fluctuations, one can understand that the ongoing chemical reactions and the collapse of the voids in the sample pastes might be the main cause. The curves on Figure 7.2 are relatively smooth as there are more data points collected at regular interval over a long period of time, hence producing smooth average curves. Attenuation of the ultrasonic wave is a more effective means of distinguishing pastes of different sand content.

The results from these experiments were found to agree with the findings reported by Aggelis and Philippidis (2004). Scattering of ultrasound is a dominant mechanism in cement paste containing sand particles.

Entrapped air bubbles in cement paste are also considered as one of the sources of inhomogeneity in cement paste, significantly affecting the attenuation of the ultrasound waves. Paste with very large numbers of air bubbles can cause a porous structure even after the cement is completely set. These bubbles reduce the overall concrete strength of the structure and can initiate a micro-crack in the concrete structure (Ye *et al* 2004, Punurai *et al* 2006, Grosse *et al* 2007).

7.4.2. Rheometer tests of Portland cement pastes

Previous rheometer tests have confirmed that cement pastes are non-Newtonian materials, as their viscosity is dependent on the shear rate. Thus, in order to determine the viscosity of paste samples, tests were set up to be conducted under a range of shear rates. In this particular set of experiments, a range of shear rate from 0.5–10s^{-1} was used. This range of relatively high shear rates is commonly used to test high-viscosity materials as this is the range of shear rates normally encountered in industrial applications e.g. spraying, brushing, and mixing. The tests were conducted immediately after mixing the cement powder with water (approximately 10 minutes preparation time) and the rheometer tests lasted 220 seconds. As a precaution to prevent damage to the rheometer there was no intention to run the tests longer than 220 seconds. This is because if the cement developed to a fully cured state (Stage 2), it can seize the motor of the rheometer. The test results in Figures 7.12 show that the viscosity of the pastes with higher cement content (smaller w/c value) tends to be higher too. These results are consistent with the Kreiger and Dougherty theoretical model described in Section 4.4.1.a above, at 5s^{-1} shear rate (see Table 7.1). Fletcher and Hill (2008) – see Figure 4.11 – also reported a similar trend with the latex/pressure-sensitive adhesive system. This test was conducted within the Stage1 curing state shown in Figure 7.2, also in line with the Stage1 of Figure 5.4 and 5.5. With respect to the curing state in Figure 5.4, this 220seconds of experiment is only 1.2% out of the 5hours window of Stage1.

Water-to-cement ratio of sample	Viscosity@5s^{-1} (Pa.s)	Relative viscosity based on Kreigher-Dougherty's model
0.3	83	–
0.36	75	77.7
0.4	30	29.0
0.42	22	20.9
0.5	3	9.2

Table 7.1: Relative viscosity of various cement pastes according to Kreiger-Dougherty's model. Note: $[\eta]=8.1$ and maximum packing fraction is at 0.3w/c hence $\phi_m=0.3$.

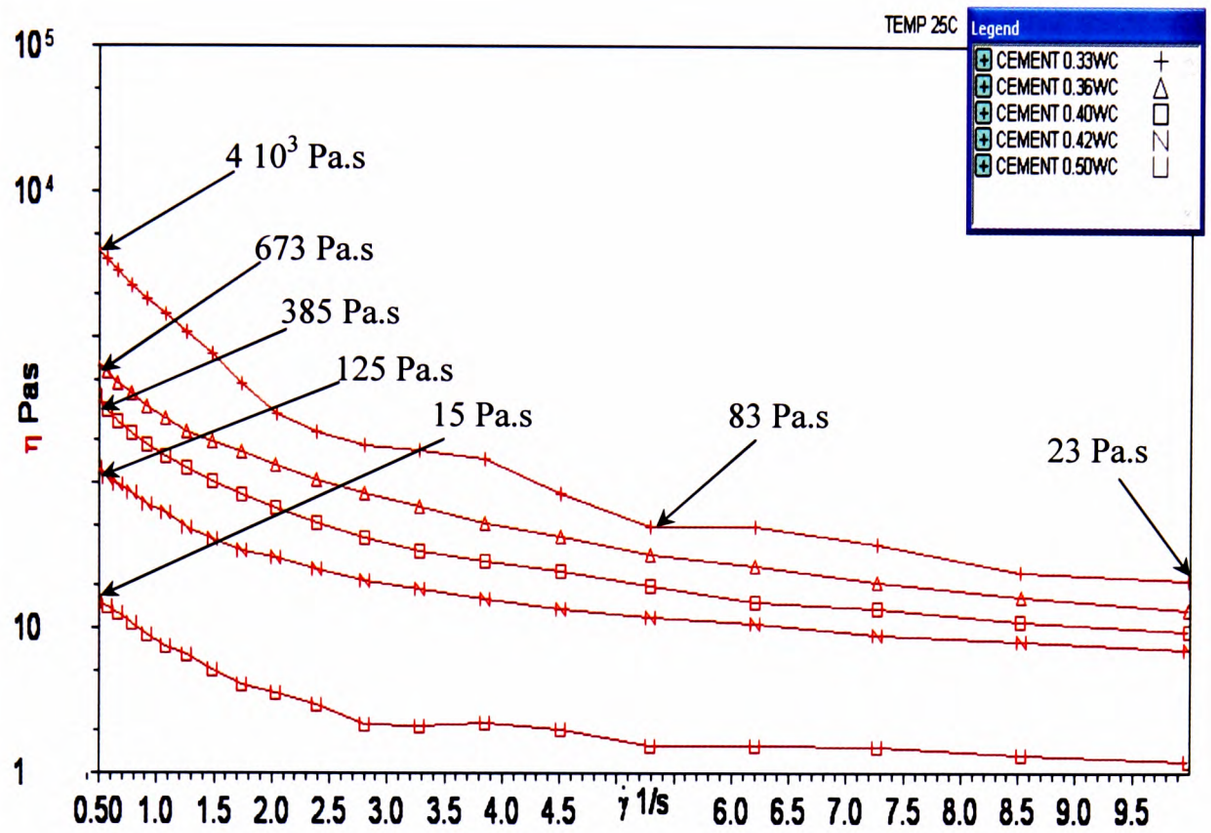

Figure 7.12: Viscosity of various cement pastes at shear rates of 0.5–10s^{-1}, at 25°C.

The corresponding time scale to the shear-rate shown in Figure 7.12 is represented in Figure 7.13.

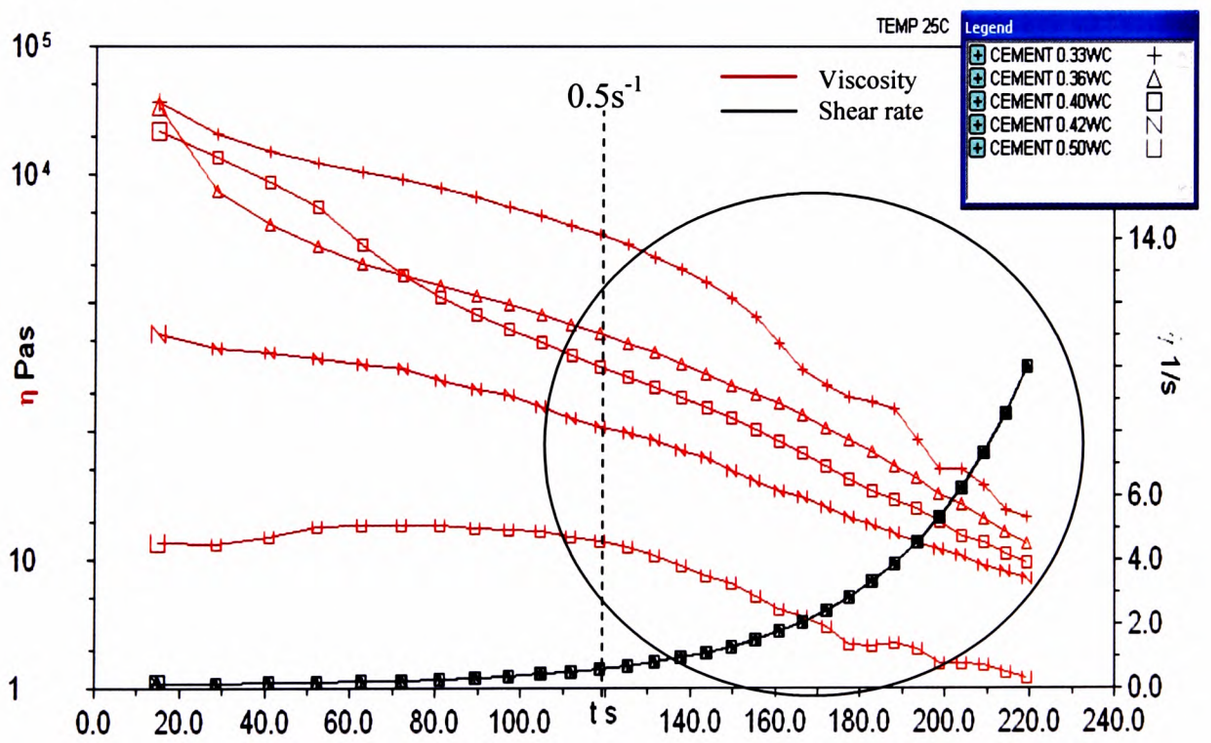

Figure 7.13: Viscosity of various cement pastes during the first 220seconds of curing.

In this set of experiments, tensile-strength compressive tests were also conducted using a Hounsfield tensile testing machine. Although the viscosity value at very low shear rates cannot provide a representative one-to-one result to the tensile strength of the concrete, it is obvious that the rheology tests on the cement pastes can be used as a guide for estimating the strength of the cured concrete. The tensile test results of 10-days-old cured concrete are shown in Table 7.2. Having information from Figure 7.12 and Table 7.2 at hand would allow one to easily estimate the tensile strength from its viscosity without having to wait 10 days for the cement paste to be fully cured. This would be a great benefit to the large scale civil engineering industry.

Water-to-cement ratio of sample	Tensile strength (MPa)
0.33	3.42
0.36	2.85
0.40	2.63
0.42	2.38
0.50	2.14

Table 7.2: Tensile-strength compressive test results for concrete samples after 10 days of curing.

The rheometer test results of cement paste samples with the inclusion of sand particles are not presented here as visual observation during the tests and the related test results indicated the presence of a 'wall slip effect', in which the samples experienced regular on-off contact with the surface of the parallel plate of the rheometer. The presence of 'wall slip' will effectively invalidate the test results as the test results generally contain irregular data points.

7.4.3. Comparative analysis of ultrasound and rheometer viscosity tests at early curing state (Stage1) of cement pastes

Although there is no standard formula to correlate the attenuation of cement paste directly with viscosity, the viscosity of cement paste at various water-to-cement ratios

determined using a rheometer seems to have a strong correlation to ultrasound velocity, as shown in Figures 7.14. In addition to that, the viscosity also shows an inverse relationship to ultrasound attenuation (see Figure 7.14). The challenge here was to find a formula that could predict the viscosity regardless of the variations in the cement paste's content. Realistically, cement pastes may contain different amount of sand/aggregate content, particle size distribution of the sand/aggregate or admixtures such as accelerators, retarders and air entrainers. The only formula available to correlate ultrasound parameters with viscosity of fluids is the formula provided by Stokes (1845) – see Equation 3.18 in Chapter 3. However, this formula is proven to be unsuitable to describe the viscosity of cement pastes (see Table 7.3) as this formula was originally used to describe the viscosity of gases. Furthermore, cement paste is a semi-solid non-Newtonian material. Hence, there is a significant different between the calculated viscosity values (Stokes's model) and the measured viscosity values (Bohlin Rheometer).

Looking at the viscosity of the samples at $10s^{-1}$ shear rate in Figure 7.12, the viscosity of the 0.33 w/c sample is 23Pa.s which is comparable to the viscosity of the 0.3w/c sample in Figure 5.5 at 220seconds (~15Pa.s).

Comparing the ultrasound velocity results in Figure 7.15 to the Stage1 ultrasound velocity results in Figure 5.5 and 7.2, it is obvious that the velocities at 220seconds are comparable (100–150m/s). The ultrasound velocity of the sample will continuously increase while the cement paste is curing. The ultrasound velocity of a fully cured (Stage2) cement paste could reach up to 3000m/s. A coupling gel or wetting the sample with water would be needed in order to measure the ultrasound velocity at Stage2 and Stage3. Rheometer's viscosity tests were not conducted for Stage2 and Stage3 cement paste samples because the cured cement can damage the motor of the rheometer. The viscosities shown in Figure 5.5 were measured using Brookfield viscometer at 10rpm (equivalent to $10s^{-1}$ of Bohlin rheometer).

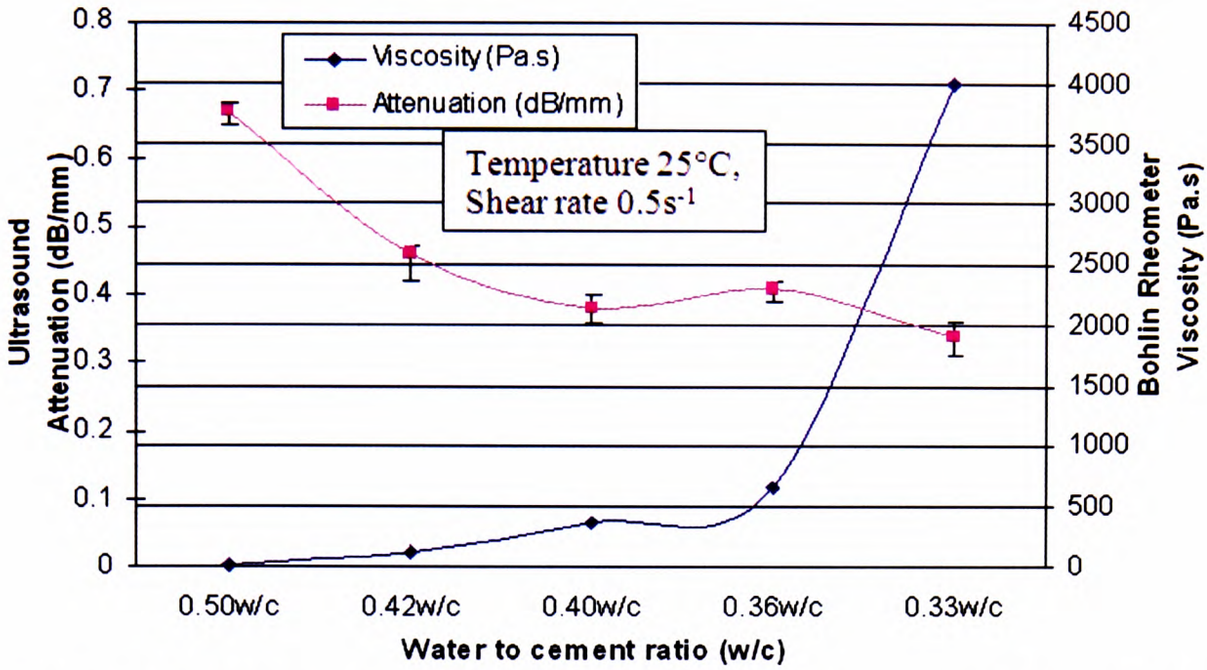

Figure 7.14: Viscosity and attenuation of various cement pastes at 220 seconds of curing.

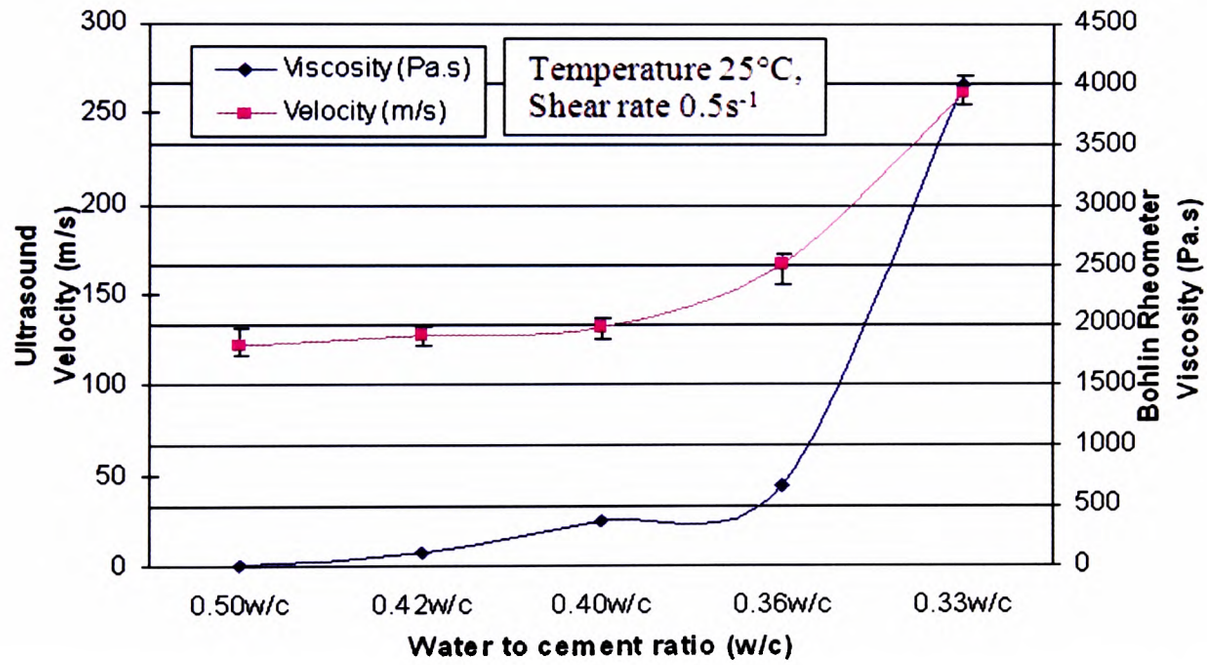

Figure 7.15: Viscosity and velocity of various cement pastes at 220 seconds of curing.

The phenomena of very low ultrasound velocity shown in Figure 7.15 is due to the fact that the data were those of the curing state up to first 220seconds of Stage1, such as shown in Figure 7.2. At this state (Stage1), the low velocity may be attributed to the fact that air bubbles are forming. As the curing progress to Stage2, air bubbles are

collapsing, therefore increasing the ultrasound velocity (also see Figure 3.39). Under this bubble formation effect, it is possible that some materials will give lower ultrasound velocity than that of for air. This phenomena has been pointed out by Povey (1998), see Figure 7.4, in which there is no ongoing chemical reaction in the suspension (water with a dispersion of 10μm bubbles). The ultrasound velocity of the suspension at the lowest frequency was 80m/s.

Water-to-cement ratio of sample	Velocity (m/s)	Attenuation (dB/mm)	Density (kg/m^3)	Bohlin Rheometer Measured Viscosity (Pa.s) @0.5 s^{-1}	Stokes's model Calculated Viscosity (Pa.s)
0.33w/c	262	0.34	1987	4000	2.69E-05
0.36w/c	167	0.41	1806	673	1.88E-05
0.40w/c	133	0.38	1643	385	1.26E-05
0.42w/c	128	0.46	1534	125	1.37E-05
0.50w/c	122	0.67	1418	15	1.76E-05

Table 7.3: Measured and calculated viscosity of cement pastes at 220 seconds of curing, at 500kHz.

The measured viscosity shown in Table 7.2 was obtained using a Bohlin Gemini rheometer at a shear rate of $0.5s^{-1}$, whilst the calculated viscosity is based on the ultrasound measurements through the formula provided by Stokes (1845) – see Chapter 3 Equation 3.28.

7.5. Conclusions

The author's findings presented in this chapter agree with the work of Aggelis and Philippidis (2004) on cement pastes. The study shows that the viscosity of the cement pastes measured using a rheometer may have a correlation with the ultrasound measurements. Because shear rates are not equivalent to ultrasound frequencies, it is difficult to cross-check the viscosity of the (non-Newtonian) cement pastes, especially as the viscosity non-Newtonian materials are known to vary with shear rate.

CHAPTER 8

DEVELOPMENT OF STOKES' THEORETICAL MODEL FOR NON-NEWTONIAN MATERIALS

8.1. Introduction

This chapter presents other approaches that can be used to describe the viscosity of non-Newtonian materials using the ultrasound technique. The validation using Newtonian fluids and dimensional analysis presented next were necessary. This is because the preliminary tests using Stokes' model on cement pastes described in Section 7.4.3 have proven that Stokes' model is not applicable for non-Newtonian material. The validation using Newtonian fluids provided a basic 'look-up table' for the viscosity, whilst the dimensional analysis part provided a possibility for finding other theoretical models suitable for describing the viscosity of non-Newtonian materials.

8.2. Validation of Stokes' model for Newtonian fluids

Recalling the Stokes's model for measuring the viscosity of Newtonian fluids from Equation 3.18:

$$\alpha = \frac{8\pi^2\eta}{3\lambda^2\rho_0 a}.$$

Rewriting this equation to provide a viscosity value based on ultrasound attenuation, velocity and frequency ($f = a/\lambda$) gives:

$$\eta = \frac{3\rho_0 a^3 \alpha}{8\pi^2 f^2}. \qquad (8.1)$$

It should be remembered that this model was developed based on the experiments in Kundt's tube for attenuation of sound in various gases. The model therefore needs to be checked against materials of known viscosity to validate the equation for use with non-gaseous fluids. In the first part of the validation, sugar solutions, which are natural Newtonian fluids, were used. In the second part, viscosity standard fluids, which are also Newtonian in character and covering wider range of viscosity values, were used.

8.2.1. Validation of Stokes' model using sugar solutions

A range of sugar solutions with different viscosities was prepared by dissolving a known amount of sugar granules into distilled water. A sugar solution with a higher amount of sugar content was found to result in higher viscosity, as shown in Figure 8.1. In this part of the experiment, a commercial white refined cane sugar (Silver Spoon™) was dissolved in distilled water to obtain 12 sample solutions with concentration ranging from 10% to 120% with incremental steps of 10%. 5 samples were made for each concentration.

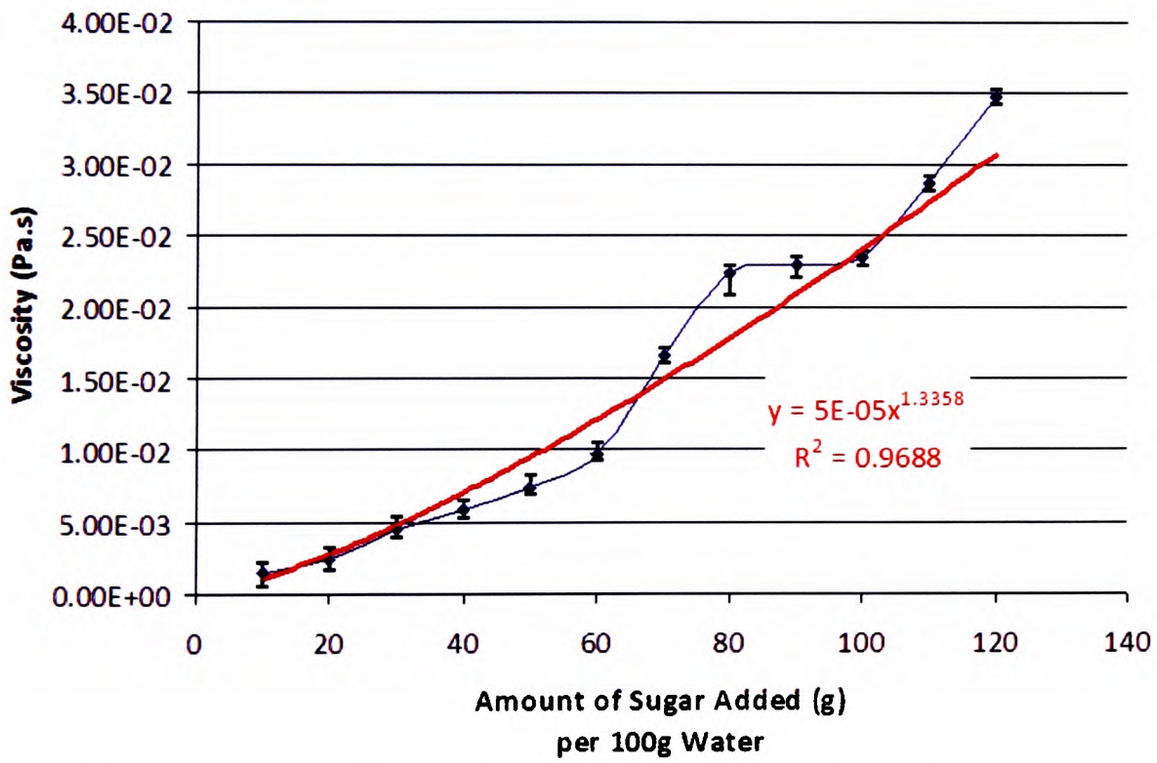

Figure 8.1: Viscosity of sugar solutions as a function of dissolved sugar.

The viscosity of sugar solutions shown in Figure 8.1 was obtained from Bohlin Gemini 150 rheometer readings. The test settings used were single shear at 50Pa shear stress (see Table 8.1). Since sugar solution is a Newtonian liquid, the viscosity is independent of the shear stress applied. However, if extremely high shear stress were to be applied, the sample could ooze out from the rheometer's plate and this would invalidate the test.

Parameters	Temperature	Pre-Shear	Shear Type	Number of Samples	Measuring Geometry	Gap Width
Settings	Temperature Controlled. Isothermal		Single Shear, Controlled Stress		Parallel Plate (Smooth)	
Values	25°C	Off	50Pa	10	Ø20mm	500μm

Table 8.1: Test settings for measuring viscosity of sugar solutions.

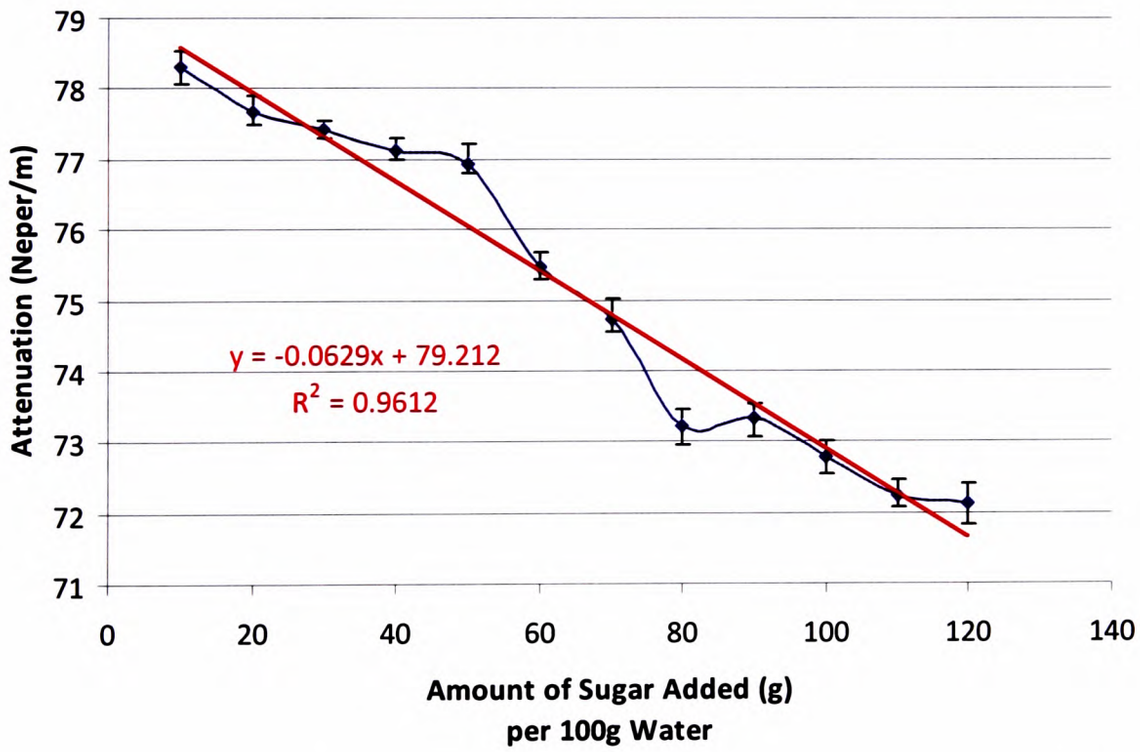

Figure 8.2: Correlation graph of through-transmission ultrasonic attenuation and dissolved sugar.

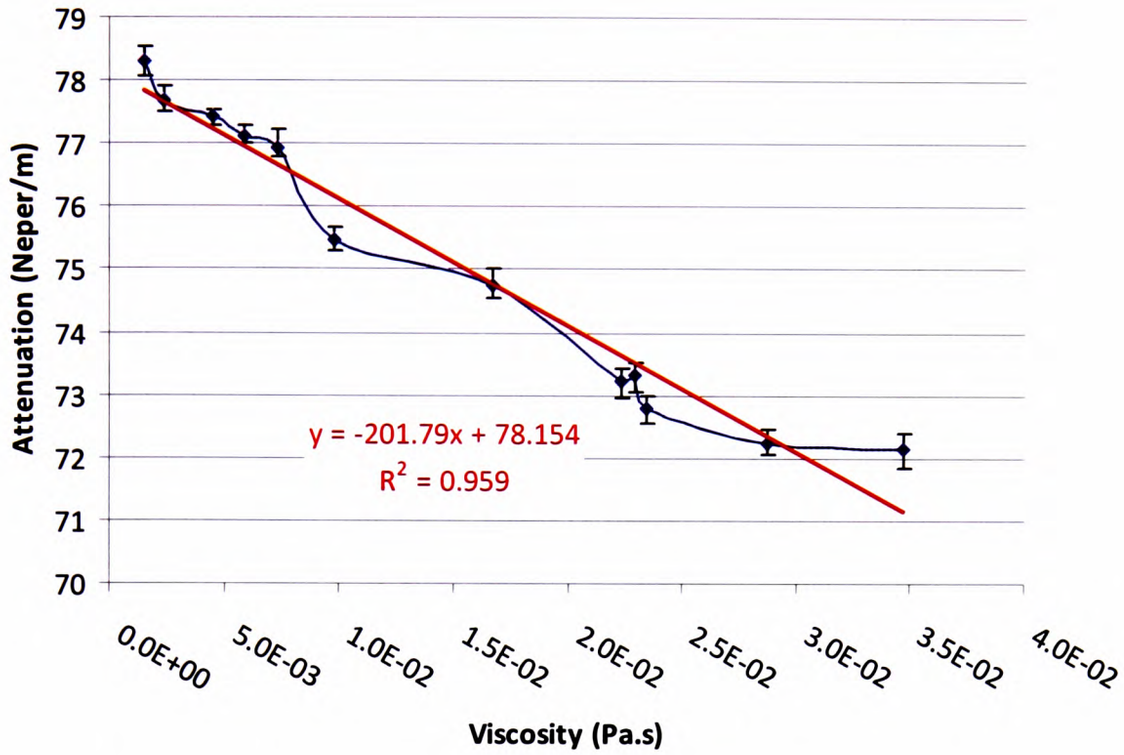

Figure 8.3: Correlation graph of through-transmission ultrasonic attenuation and viscosity of prepared aqueous sugar solutions measured using a rheometer.

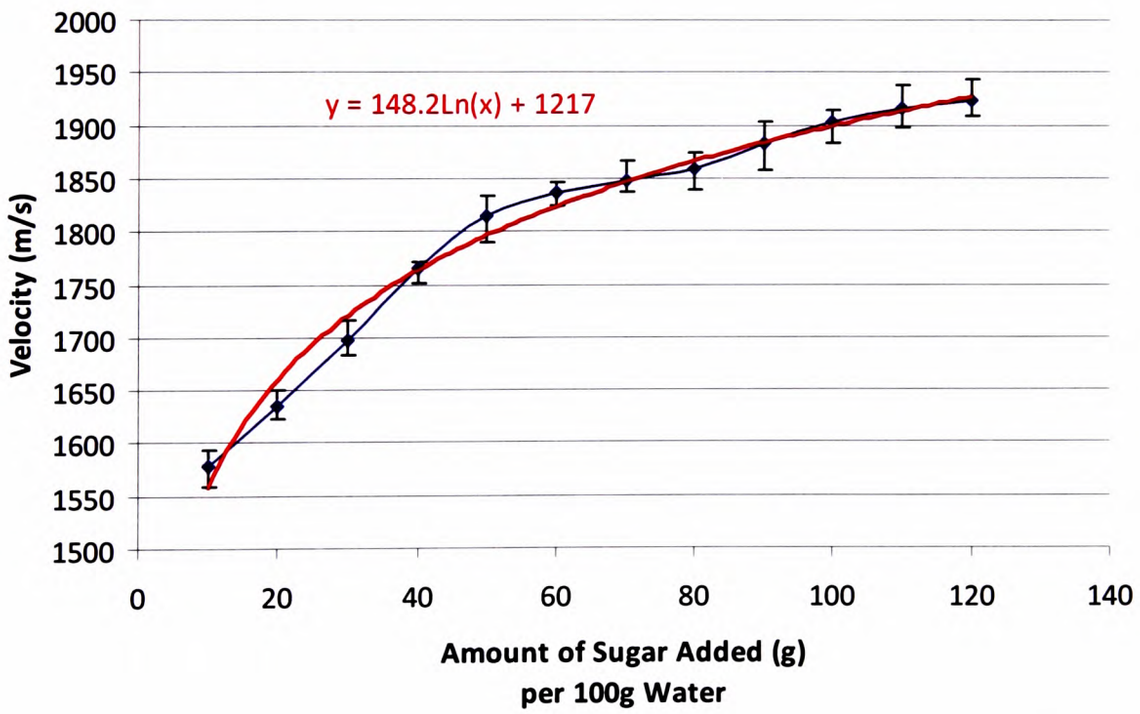

Figure 8.4: Correlation graph of through-transmission ultrasonic velocity and dissolved sugar.

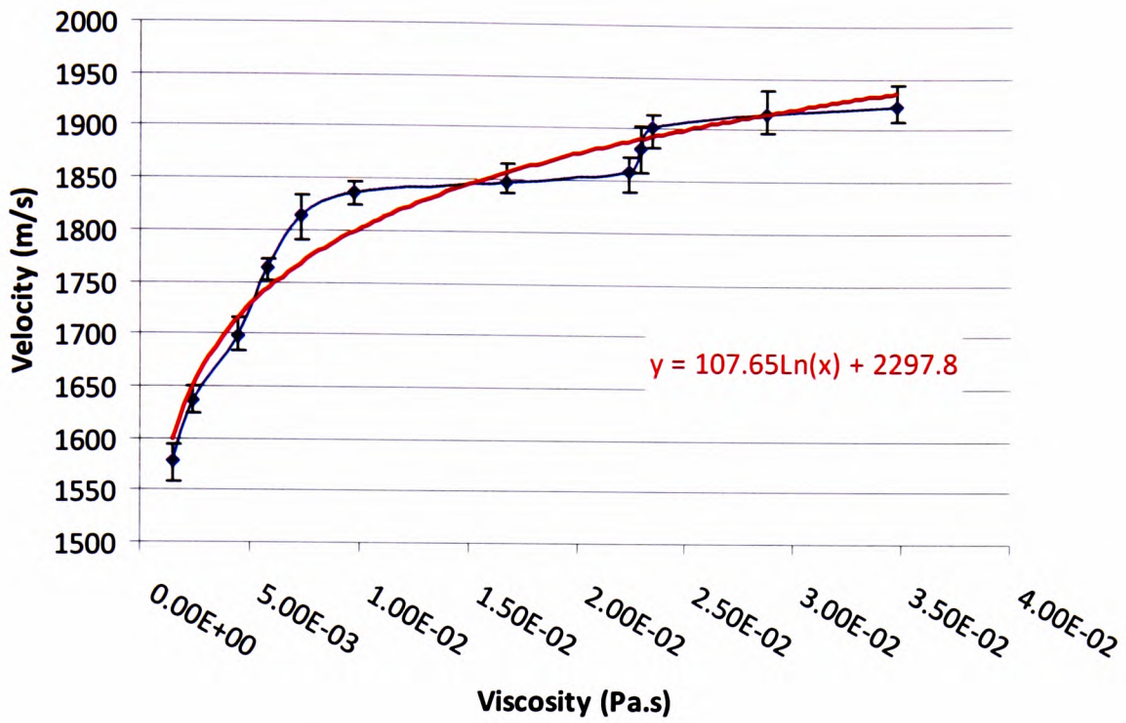

Figure 8.5: Correlation graph of through-transmission ultrasonic velocity and viscosity of prepared aqueous sugar solutions.

Sugar amount (g)	Velocity (m/s)	Average Deviation (+/-) (m/s)	Attenuation (Neper/m)	Average Deviation (+/-) (Neper/m)	Density (kg/m^3)	Measured Viscosity (Pa. s) Bohlin	Calculated Viscosity (Pa. s) Stokes
10	1578.95	17.5	78.31	0.23	1100	1.51E-03	8.05E+03
20	1636.36	13	77.68	0.21	1200	2.42E-03	9.70E+03
30	1698.11	16.5	77.43	0.13	1300	4.52E-03	1.17E+04
40	1764.71	10.5	77.12	0.15	1400	5.85E-03	1.41E+04
50	1814.52	21.5	76.93	0.21	1500	7.37E-03	1.64E+04
60	1836.73	11	75.49	0.20	1600	9.78E-03	1.78E+04
70	1848.05	14.5	74.75	0.23	1700	1.67E-02	1.90E+04
80	1859.50	17.5	73.23	0.24	1800	2.24E-02	2.01E+04
90	1882.85	22.5	73.34	0.24	1900	2.29E-02	2.21E+04
100	1902.75	16	72.79	0.23	2000	2.35E-02	2.38E+04
110	1914.89	20	72.25	0.21	2100	2.87E-02	2.53E+04
120	1923.08	17.5	72.14	0.29	2200	3.47E-02	2.68E+04

Table 8.2: Measured and calculated viscosity of sugar solutions at 40kHz.

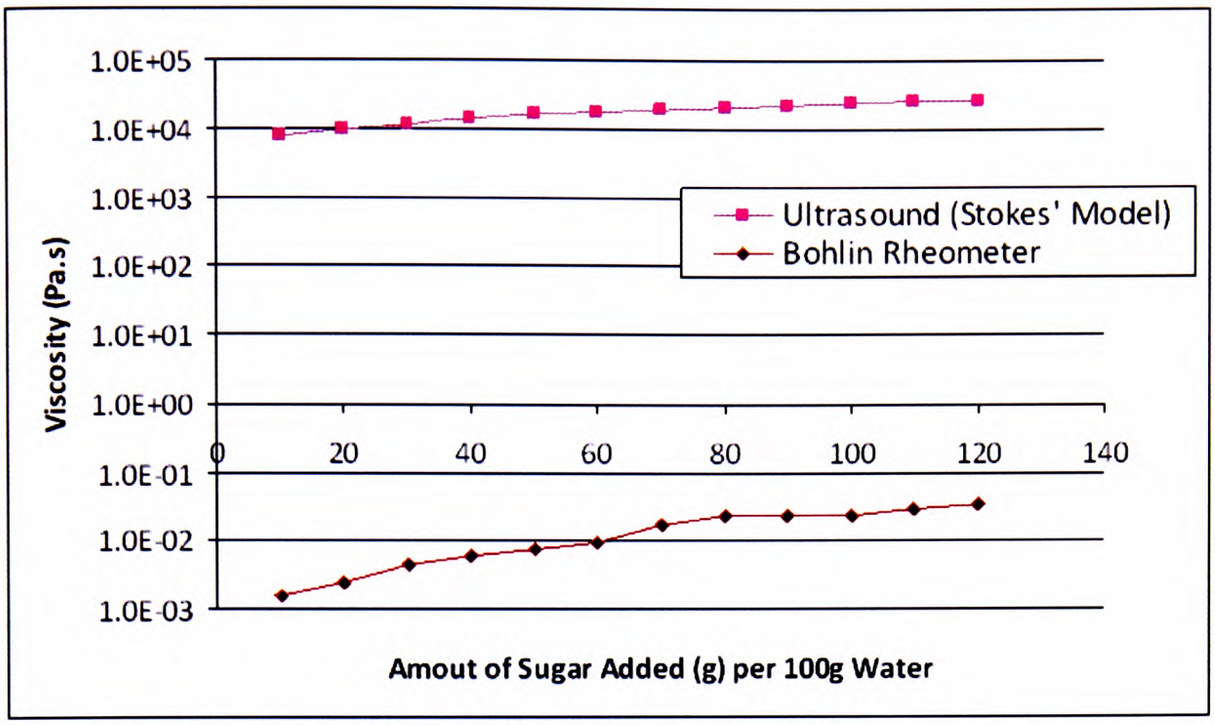

Figure 8.6: Viscosity of prepared aqueous sugar solutions using rheometer and ultrasound technique.

The results from Figure 8.3 show that sugar solutions have almost linear correlation with ultrasound attenuation with respect to increasing viscosity. The reduction in ultrasound attenuation with respect to the higher-viscosity sugar solutions is as expected. Previous studies conducted by Biwa *et al* (2003) showed that the increase of the volume fraction of carbon fibres in epoxy composites would cause a reduction in longitudinal through-transmission ultrasound attenuation at any given frequency. Biwa et al (2003) stipulated that the composite attenuation was given by the sum of the matrix attenuation and the scattering loss.

Similarly, the logarithmic velocity growth (see Figures 8.5) with respect to increasing viscosity is also as expected. The trend observed in the ultrasonic velocity was also similar to the work reported by Kuo (2008), Biwa *et al* (2003) and Létang *et al* (2001).

Results from Figure 8.6 and Table 8.2 indicate that the viscosity measured using ultrasound techniques (using Stokes' model) were much higher compared with the Bohlin rheometer results.

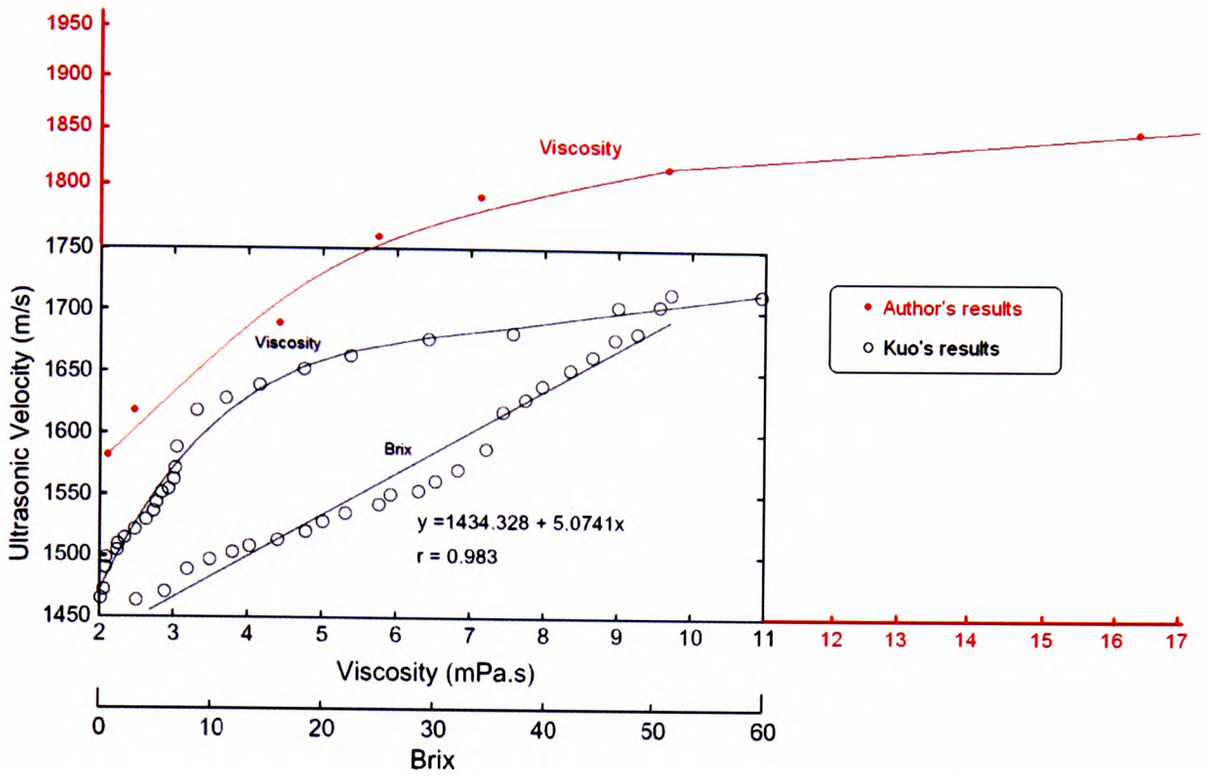

Figure 8.7: Comparison of author's results and Kuo's results on ultrasound velocity and viscosity of sugar solutions.

In comparison with the work reported by Kuo (2008) – see Figures 8.5 and 8.7 and Table 8.2 – the author's results are by no means identical, but a similar trend of increasing ultrasound velocity with the increase of viscosity or higher sugar content is apparent. The discrepancy in the viscosity values may be due to Kuo measuring the viscosity at 30°C. Unfortunately, Kuo did not carry out any attenuation measurement of the sugar solutions, and so no comparison can be made with the attenuation results. The author found that ultrasound attenuation has a linear relationship with the viscosity of dissolved sugar (see Figures 8.2 and 8.3). The difficulty in obtaining reliable ultrasound attenuation readings during a test was exacerbated by the fact that it is difficult to prepare sugar solutions with a very large range of viscosity values. This is because the dissolvability of the sugar particles reduces significantly as the mass of the sugar introduced gets closer to the mass of the water. Regardless of this, the maximum deviation of the ultrasound readings at every individual sample was only 1.4%.

During the tests, the ultrasonic velocity was found to have a logarithmic relationship (see Figures 8.4 and 8.5) with the increasing viscosity of the sugar solutions. Since the sugar solutions have relatively low viscosity, the viscosity curve only covers a narrow range of viscosity. One solution to this limitation was to extrapolate the curve to extend the range to higher viscosities. It would, however, be very difficult to justify the use of this extrapolated curve as a calibration curve to determine the viscosity of highly viscous material. Furthermore, a material with high ultrasonic velocity does not necessarily reflect that it has high viscosity. For example, lead has a longitudinal ultrasonic velocity of 2160m/s and a viscosity of 2.61×10^{-3}Pa.s at the melting point of 327.3°C (Iida et al, 1975). Empirical studies of ultrasonic velocity have found that most of the materials with longitudinal ultrasonic velocity of above 2000m/s are solids (see Appendix B).

In contrast with the work reported by Gülseren (2007) in Figure 5.11 and Wang (2004) in Figure 5.13, the temperature of the sugar solution (sucrose) may affect the ultrasound velocity of the material, particularly at low temperatures.

8.2.2. Validation of Stokes' model using viscosity standard fluids

The viscosity standards used in this experiment were obtained from Brookfield Engineering in the United States. The viscosity standards consist of several types of natural fluid of confirmed viscosity value, usually through the falling-sphere method or U-tube viscometer. Viscosity standards higher than 200Pa.s were not available for the test since Newtonian standard fluids of a few thousands or millions of Pa.s are very rare.

Sample Code	Material	Viscosity (mPa.s)	Density (kg/m^3)	Bulk modulus (Pa)
B0	Water	0.89	998.2	2.06E+09
B31	Mineral Oil	29.08	887.2	1.78E+09
B210	Mineral Oil	202.3	884.0	1.79E+09
B1000	Mineral Oil	1050	940.4	1.92E+09
B2000	Polyalphaolefin Oil	1990	930.8	1.92E+09
B20000	Polybutene	21350	948.0	2.11E+09
B100000	Polybutene	101760	979.5	1.18E+09
B200000	Polybutene	200400	900.6	1.95E+09

Table 8.3: Properties of viscosity standards used to benchmark ultrasonic viscosity. (Note: 200400mPa.s is equal to 50 × viscosity of typical honey.) Source: Brookfield Engineering.

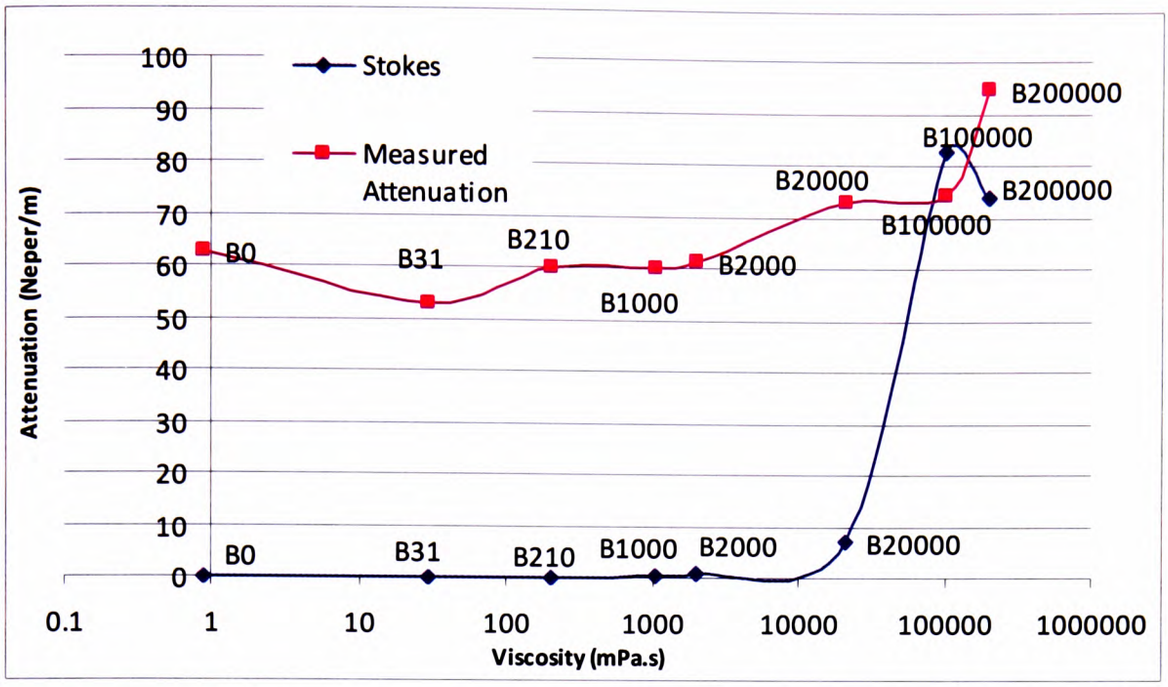

Figure 8.8: Ultrasonic attenuation of various viscosity standards based on Stokes' model and direct attenuation measurement.

Sample Code	Material	Density (kg/m^3)	Viscosity (mPa.s)	Stokes' model Attenuation (Neper/m)	Velocity (m/s)	Measured Attenuation (Neper/m)
B0	Water	998.2	0.89	3.17E-04	1436.26	62.59613
B31	Mineral Oil	887.2	29.08	1.22E-02	1415.67	52.78508
B210	Mineral Oil	884.0	202.3	8.36E-02	1423.23	59.93819
B1000	Mineral Oil	940.4	1050	4.04E-01	1428.19	60.21
B2000	Polyalphaolefin oil	930.8	1990	7.63E-01	1434.46	61.38315
B20000	Polybutene	948.0	21350	7.15E+00	1491.42	72.91003
B100000	Polybutene	979.5	101760	8.25E+01	1098.45	74.27634
B200000	Polybutene	900.6	200400	7.37E+01	1470.58	94.8822

Table 8.4: Ultrasound attenuation of viscosity standards based on Stokes' model and direct measurement.

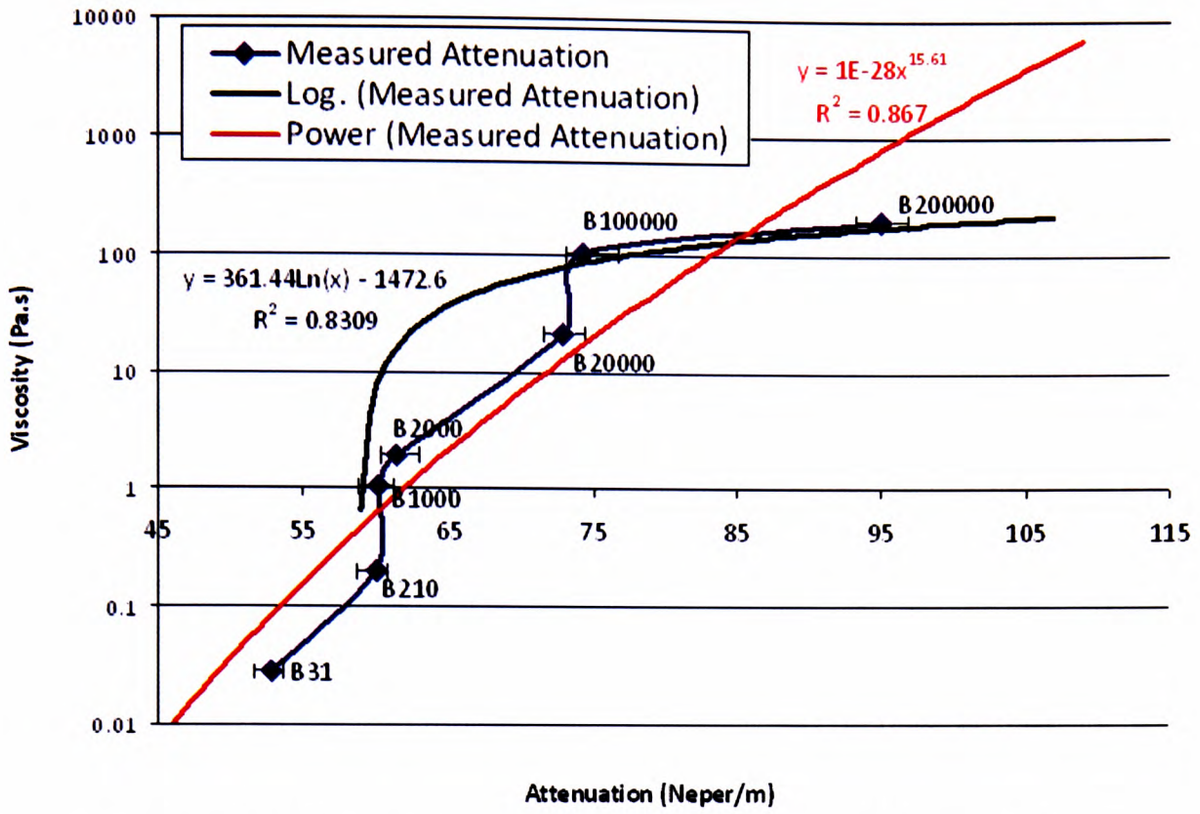

Figure 8.9: Viscosity calibration curve for ultrasound attenuation.

Figures 8.8 and 8.9 show that, experimentally, viscosity is an exponential function with respect to the attenuation of materials. As a result of the very wide viscosity range covered, the result in Figure 8.8 seems to give a false impression that the attenuation of fluids at low viscosity is linear and only becomes exponential at high viscosity. However, it should be noted that the theoretical attenuation value (see Table 8.4) of the corresponding viscosity based on the formula proposed by Stokes has quite a significant offset to the measured attenuation. As shown in Table 8.3, similar materials such as mineral oils and polybutenes may not have similar viscosity due to their structural differences in chemical formula, density and bulk modulus. Comparing polybutenes and mineral oils of approximately similar density (B31 vs B200000, or B1000 vs B20000) from Table 8.3, we can see that the viscosity of the polybutenes is significantly higher than those of the mineral oil. Remembering that both mineral oils and polybutenes (C_nH_{2n}) are hydrocarbon fluids, the huge difference in the viscosity could be due to the fact that longer chains and a compact branched polybutene structure leads to higher bulk modulus value and molecular weight, resulting in higher attenuation and viscosity.

As shown in Figure 8.10, there was no trend found with the ultrasound velocity of the viscosity standard fluids with respect to higher viscosity values.

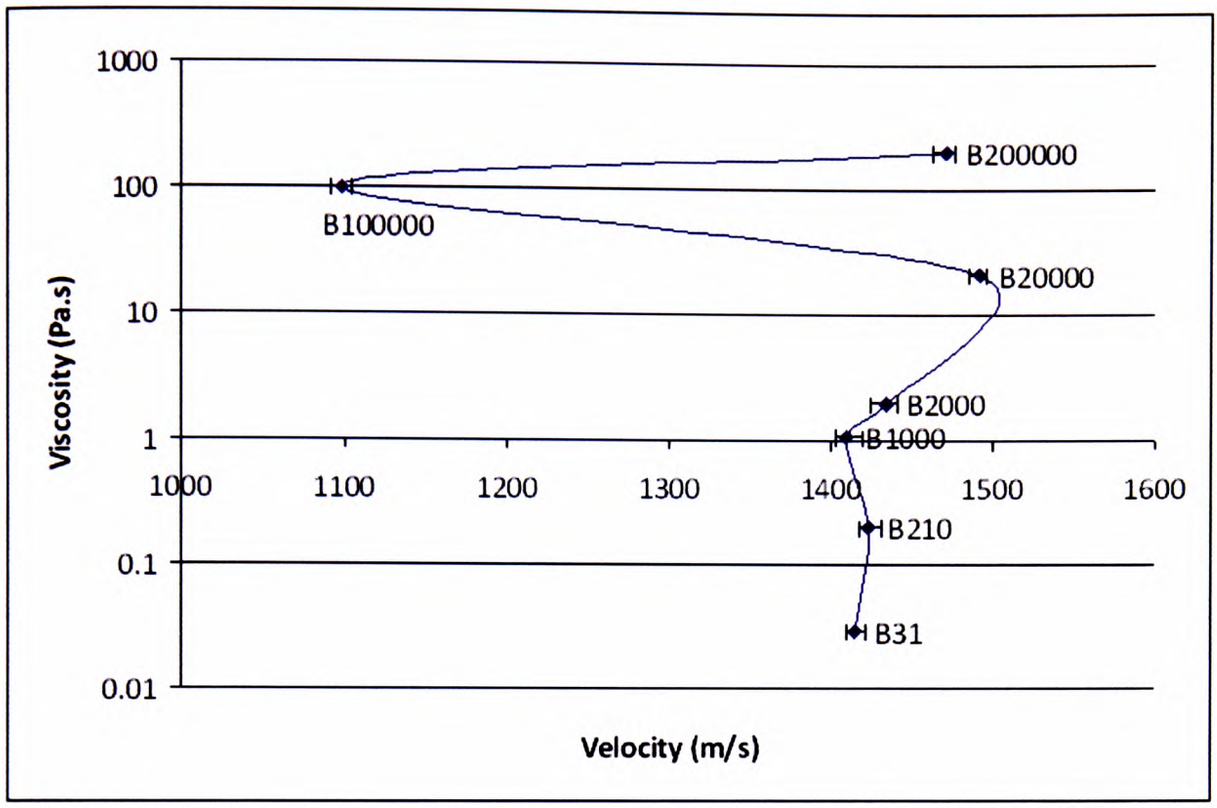

Figure 8.10: Ultrasound velocity of viscosity standards.

Since both validation techniques (i.e. using sugar solutions and viscosity standard fluids) based on Newtonian liquids cannot provide a good correlation to fit Stokes' theorem, Stokes' theorem needs to be re-evaluated for high-viscosity fluids. Equation 3.18 was derived based on the assumption that the viscosity was a small quantity and hence its square in Equation 3.16 may be neglected. It is possible to derive Stokes' theorem for high viscosity fluids from Equation 3.16 of Chapter 3 without neglecting the square of the viscosity (η) term. Recalling Equation 3.16:

$$\beta^2 - \alpha^2 = \frac{n^2 a^2}{a^4 + \frac{16\eta^2 n^2}{9\rho_0^2}}, \qquad 2\alpha\beta = \frac{\frac{4\eta n^3}{3\rho_0}}{a^4 + \frac{16\eta^2 n^2}{9\rho_0^2}}$$

Solving these equations would give a normal quadratic equation:

$$64\alpha^4\eta^2 - 12n\rho_0\eta + \frac{36\alpha^2 a^2 \rho_0^2(\alpha^2 a^2 + n^2)}{n^2} = 0 \qquad (8.2)$$

This would give two possible viscosity values due to fact that Equation 8.2 is a quadratic equation, with η as the variable. An attempt to use the equation to predict the viscosity of sugar solutions or viscosity standard fluids, based on ultrasound attenuation, velocity and density, would return very high viscosity values. These values do not reflect the viscosity of the materials as recorded by rheometer. Hence, it is required to use a dimensional analysis technique to search for a new equation that might describe the viscosity of the materials based on the ultrasound measurements.

8.3. Dimensional analysis

Dimensional analysis is a technique used to form reasonable hypotheses by analysing the combination and permutation of each variable that affects a certain phenomenon. The developed theories can usually be proven experimentally to check the plausibility of derived equations. One of the techniques for dimensional analysis was devised by Buckingham (1914). The technique is commonly referred to as the 'Buckingham pi theorem'.

The intention to use Buckingham pi theorem here was to investigate the possibility of other correlations of ultrasound with viscosity, all possible related variables (density, length between sensors, velocity, viscosity, bulk modulus, frequency and temperature) must be considered. These variables with their dimensions are listed in Table 8.5.

Variables	Symbol	Dimensions
Length between sensors	L	[L]
Density	ρ	$[ML^{-3}]$
Velocity	V	$[LT^{-1}]$
Viscosity	η	$[ML^{-1}T^{-1}]$
Bulk modulus	K	$[ML^{-1}T^{-2}]$
Frequency	f	$[T^{-1}]$
Temperature	θ	[θ]

Table 8.5: Dimensionless variables related to viscosity.

According to the Buckingham pi theorem, the number of possible dimensionless formulae is equal to the number of variables minus the number of repeating

dimensions. In addition, a variable can only be used if it has a repeating dimension in other variables. Since, in the case under consideration, temperature has a non-repeating dimension in the other variables, we have six variables (density, sample thickness, velocity, viscosity, bulk modulus and frequency) and three repeating dimensions (M, L and T), which results in 6-3=3 dimensionless formulae:

$$\Pi_1 = f^a \eta^b \rho^c V = [T^{-1}]^a [ML^{-1}T^{-1}]^b [ML^{-3}]^c [LT^{-1}] \tag{8.3}$$

$$\Pi_2 = f^d \eta^e \rho^f L = [T^{-1}]^d [ML^{-1}T^{-1}]^e [ML^{-3}]^f [L] \tag{8.4}$$

$$\Pi_3 = f^g \eta^h \rho^i K = [T^{-1}]^g [ML^{-1}T^{-1}]^h [ML^{-3}]^i [ML^{-1}T^{-2}] \tag{8.5}$$

Solving the Π formulae individually would give

$-a-b-1=0$; $b+c=0$; and $-b-3c+1=0$, and hence $a= -½$; $b= -½$; $c= ½$.

$-d-f=0$; $e+f=0$; $-e-3f+1=0$, and hence $d= ½$; $e= -½$; $f= ½$.

$-g-h-2=0$; $-h-3i-1=0$; $h+i+1=0$, and hence $g= -1$; $h= -1$; $i= 0$.

Therefore:

$$\Pi_1 = f^{½} \eta^{-½} \rho^{½} V = V\sqrt{\frac{\rho}{\eta \cdot f}} \tag{8.6}$$

$$\Pi_2 = f^{½} \eta^{-½} \rho^{½} L = L\sqrt{\frac{\rho \cdot f}{\eta}} \tag{8.7}$$

$$\Pi_3 = f^1 \eta^{-1} \rho^0 K = \frac{K}{\eta \cdot f} \tag{8.8}$$

It should be noted that Π_1, Π_2 and Π_3 are dimensionless

With $\Pi_1 = \Pi_2$, we have:

$$V\sqrt{\frac{\rho}{\eta \cdot f}} = L\sqrt{\frac{\rho \cdot f}{\eta}}. \tag{8.9}$$

Since attenuation is usually expressed in per-metre units, with

$\alpha = \frac{1}{L}$, then (8.10)

$$\alpha_{12} = \frac{f}{V}. \tag{8.11}$$

Equation 8.11 describes the correlation of the ultrasound attenuation of various materials at any frequency. However, this equation does not indicate any correlation with viscosity or other physical properties of materials.

With $\Pi_2 = \Pi_3$, we have:

$$L\sqrt{\frac{\rho \cdot f}{\eta}} = \frac{K}{\eta \cdot f}, \tag{8.12}$$

$$\alpha_{23} = \sqrt{\frac{\eta \cdot \rho \cdot f^3}{K^2}}. \tag{8.13}$$

And, since $V = \sqrt{\frac{K}{\rho}}$. (8.14)

$$\alpha_{23} = \sqrt{\frac{\eta \cdot f^3}{V^4 \cdot \rho}} \tag{8.15}$$

Equation 8.15 has the complete set of variables correlating ultrasound with viscosity and material properties at any frequency.

With $\Pi_1 = \Pi_3$, we have:

$$V\sqrt{\frac{\rho}{\eta \cdot f}} = \frac{K}{\eta \cdot f} \tag{8.16}$$

$$\frac{\rho}{\eta \cdot f} = \frac{K^2}{\eta^2 \cdot f^2 \cdot V^2} \tag{8.17}$$

$$V^2 = \frac{K^2 \cdot}{\rho \cdot \eta \cdot f} \cdot \tag{8.18}$$

Equation 8.18 can be used to describe the correlation of ultrasound velocity with the viscosity of materials at any frequency. However, Equation 8.18 lacks the ultrasound attenuation variable.

Hence, only Equation 8.15 is suitable for measuring the viscosity of materials, as it contains all the necessary variables. Through experimental data from Table 8.4, the coefficient for α_{23} was found to be as follows:

$$\alpha_{23} = 52 + \sqrt{\frac{\eta \cdot f^3}{V^4 \cdot \rho}} \cdot \tag{8.19}$$

However, Equation 8.19 seems to be relatively similar to the formula in Stokes' model. It was deduced that if Stokes' formula is modified as follows, it would achieve similar correlation values to that of α_{23}.

$$\alpha = 55 + \pi^2 \frac{\eta \cdot f^2}{\rho V^3} \cdot \tag{8.20}$$

Equations 8.19 and 8.20 indicate that the viscosity of the material will be dependent upon the frequency of the ultrasound, i.e. the viscosity is not constant.

Both of these formulae (Equation 8.19 and 8.20) show a correlation value (an R^2 value) of 83% with respect to the trend line of measured attenuation, see Figure 8.11.

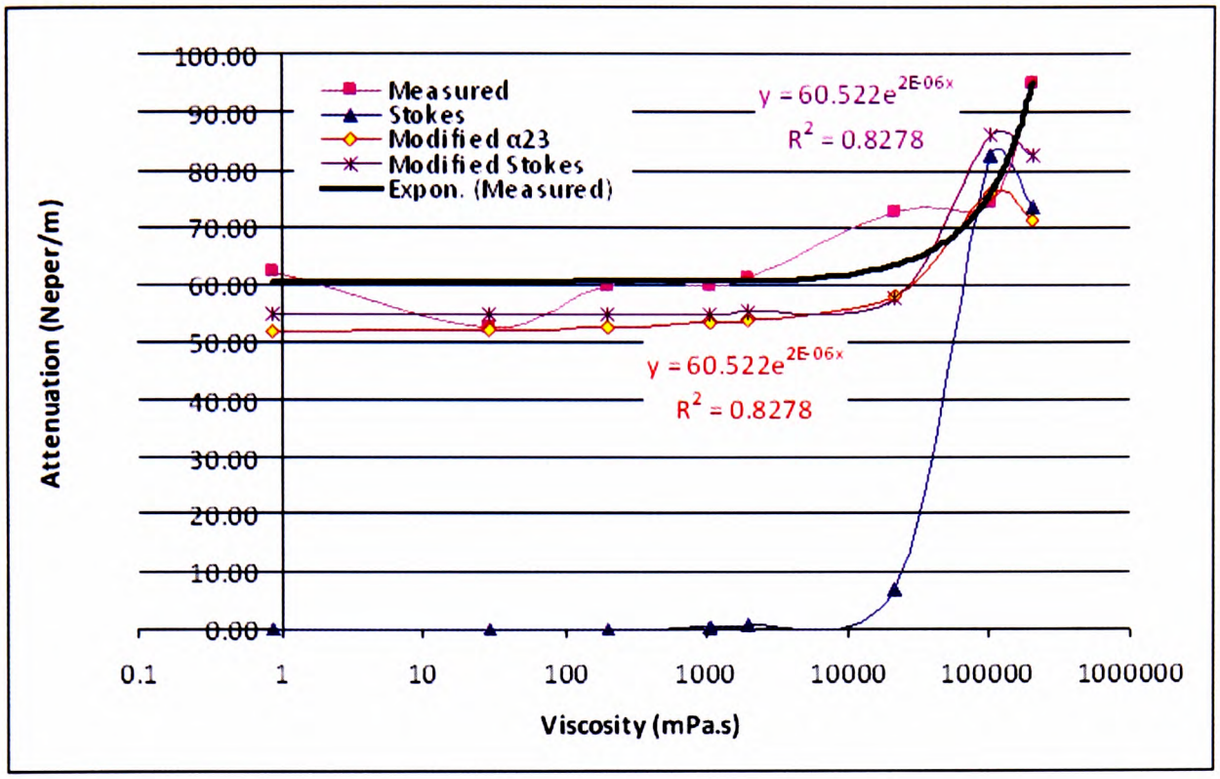

Figure 8.11: Curve fitting of various formulae to measured attenuation values of viscosity standards. (A trend line with continuous black solid line was used as R^2 value reference.) All formulae show R^2 correlation value close to 80%.

The challenges in using ultrasound techniques to predict the viscosity of the material under examination could be due to the fact that ultrasound is very sensitive to the material's physical structure (packing fraction) and chemical structure. Although there is a trend of ultrasound attenuation with an increase in viscosity, other variables (e.g. ultrasound velocity or density) that may affect the viscosity of the materials seem to have no trend with respect to an increase in viscosity. The accuracy of ultrasound techniques for predicting the viscosity of material over a wide range of viscosity values is not very good. In order to achieve a greater accuracy, a calibration graph, such as that shown in Figure 8.3, of the same material at various viscosities must be used. However, without the calibration graph, the ultrasound techniques can still be used to determine how viscous a material is compared with another material by using Equation 8.19 or Equation 8.20.

Earlier ultrasound attenuation tests with sugar solutions have shown contradictory results to the tests with viscosity standard fluids. Ultrasound attenuation tends to

reduce with higher-viscosity sugar solutions, whereas an increase in ultrasound attenuation was observed with viscosity standards of higher viscosity.

8.4. Conclusions

The original Stokes' model was proven to give excessively high viscosity values for low-viscosity materials (see Table 8.2). In contrast to that, the model gives a very low viscosity readings for very high-viscosity material (see Table 8.4). A new model and corrected Stokes' model, based on ultrasound attenuation, were developed. The ultrasound attenuation may increase or decrease with respect to an increase in viscosity. The trend is material-specific; however, the equation developed can still predict the viscosity of the material regardless of the trend. Employing a correction factor approach may not be the right solution as it may not be applicable to all materials covering a very broad range of viscosity. A 'look-up table' of ultrasound measurements for a very specific material covering a narrower range of viscosity might be more appropriate. Generating a 'look-up table' for solder paste is a real challenge as there are no material with viscosity equivalent to those of the solder pastes which can be used as a reference for generating the 'look-up table'.

CHAPTER 9

ULTRASONIC VISCOSITY STUDY OF LEAD-FREE SOLDER PASTE MATERIALS AT VARIOUS STATES AND THEIR CORRELATION WITH PRINTING PERFORMANCE

9.1. Introduction

Previous studies (Green, 1973; Reddy and Suryanayana, 1981; McClements, 1988; Farrow *et al*, 1995; Létang *et al*, 2001; Llull *et al*, 2002; Povey, 2006; Álava *et al*, 2007; Kuo, 2008) have shown that measureable ultrasonic parameters can be correlated with the physical characteristics of a material through which an acoustic wave propagates. The viscosity of solder paste, which can be measured using ultrasound techniques, is one of the important material properties that can be used to predict the printing quality for the solder pastes. Ideally, the variation in viscosity within the batch and from batch to batch should be kept to minimum as this will directly affect the level of electronic assembly-related defects.

This chapter presents results of the study on the correlation of ultrasound parameters with the viscosity of lead-free solder pastes in four different conditions:

- fresh solder paste samples;
- expired solder paste samples;
- low-temperature solder paste samples; and
- solder paste samples with different amounts of flux content (% by volume).

The theoretical model described by Equation 8.20 in the previous chapter is used to validate the ultrasonic viscosity results against the viscosity measurements from a

Bohlin rheometer and against the viscosity data of the solder paste provided by the solder paste supplier.

9.2. Experimental materials and equipment used in this study

9.2.1. Solder pastes

The solder pastes used in this study were formulated with two different types of flux systems, and each was used to formulate a type-3 and a type-4 solder paste (see Table 9.1). Six 500g samples of each of the four paste types shown in Table 9.1 were used in the study, which resulted in a total of 24 samples (6 bottles of each pastes type). The six samples were labelled A to F for reference purposes.

Flux Type	LF1	LF1	LF2	LF2
IPC Equivalent PSD	Type 3	Type 4	Type 3	Type 4
Particle Size, µm	20-45 (Δ25)	20-38 (Δ18)	20-45 (Δ25)	20-38 (Δ18)
Metal Content, % weight	88.5	88.5	88.5	88.5
Brookfield Viscosity @ 5rpm, Pa.s	526	530	765	780
Particle distribution *d*(0.9)	105.15 µm	79.23 µm	105.15 µm	79.23 µm
Particle distribution *d*(0.5)	32.18 µm	28.08 µm	32.18 µm	28.08 µm

Table 9.1: Summary of solder paste properties used in the test, as provided by the solder paste supplier.

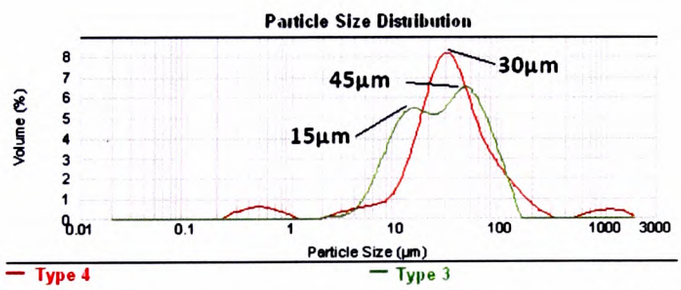

Figure 9.1: Type 3 and Type 4 particle size distribution tests for LF1 and LF2 solder pastes.

9.2.2. Ultrasound viscosity test equipment

The equipment set-up used in this study has been described earlier in Chapter 6, namely the ultrasonic rig design C with the Panametrics ultrasonic transducers (see Section 6.4).

9.2.3. Bohlin Gemini rheometer

The Bohlin Gemini rheometer has been described earlier in Section 4.5 (see Figures 4.22–25).

9.2.4. Stencil printing machine

The DEK 260 printer was used in this study (see Figure 9.2). As the DEK 260 is not equipped with an automatic board-alignment system, the PCB pattern needs to be manually adjusted to fit the stencil pattern using the board alignment knobs provided. The DEK 260 can only take a stencil of 585mm × 585mm. The PCB is secured to the table by using the magnetic pins provided or vacuum suction pads. Control of the printing parameters is performed via a touch-screen control panel. The maximum printing stroke (squeegee travel distance) for this printer is 450mm. The printing speed can be set in the range 10–250mm/s in both forward and reverse directions, with 1mm/sec increments. The print gap between the stencil and the PCB can be adjusted from 0 to 5mm with 0.1mm increments. The printing pressure can also be adjusted from 0 to 10kgf/m^2. For this study, the following settings were used: 450mm printing stroke; 250mm/s printing speed; 0mm printing gap and 5kgf/m^2 printing pressure. These printing settings are the standard industry setting used for maximum production rate. Hence, the requirements for using the maximum printing speed of the printing machine. The 0mm printing gap was selected because large SMT components were rarely used these days. Increasing printing gap can produce thicker print deposits which are required in order to hold large-size-heavy SMT components. Finally, a printing pressure of 10kgf/m^2 is rarely used as it can produce so much friction with

the stencil, often leading to no printing motion. A very high printing pressure can also cause an early wear of the stencil because of the high friction force between the squeegee and the stencil.

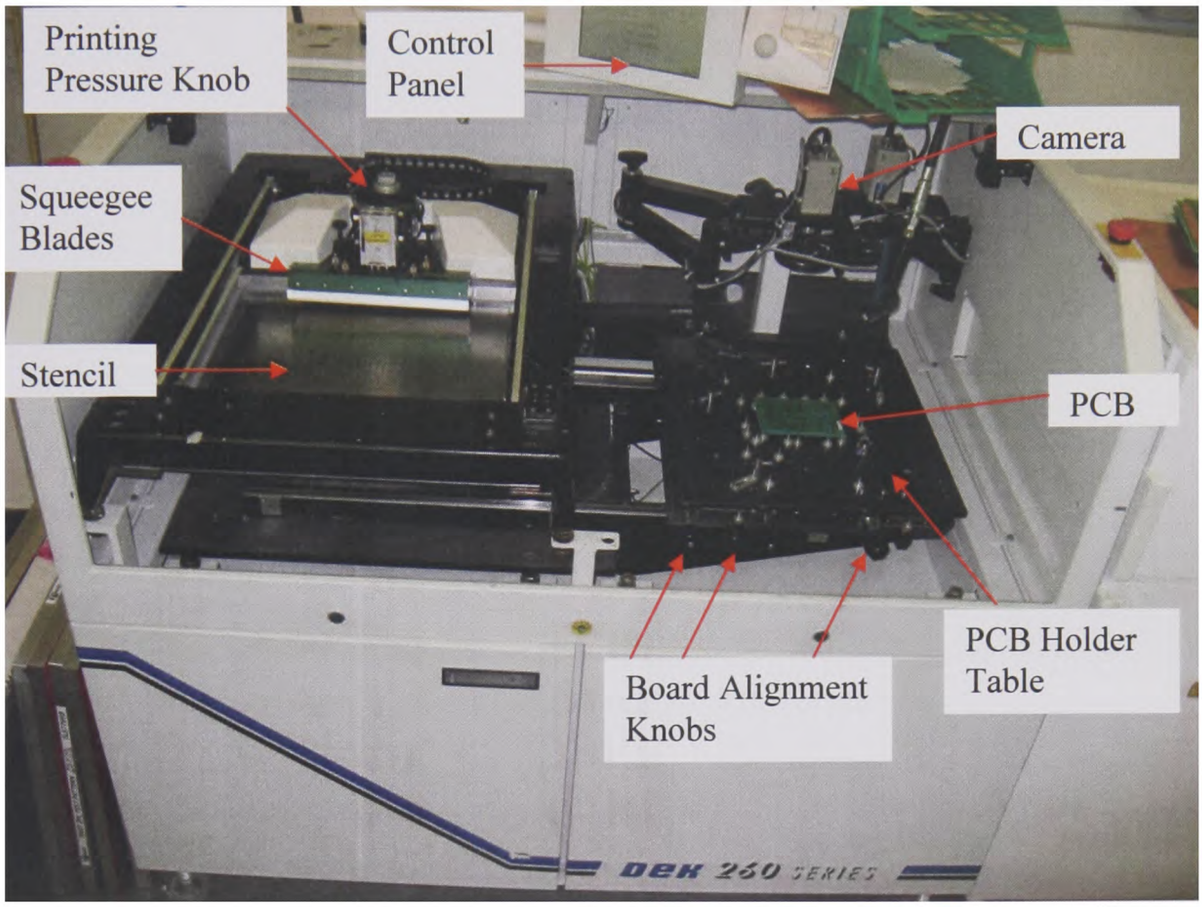

Figure 9.2: DEK stencil printing machine.

9.2.5. Bench Marker II stencil

A Bench Marker II laser-cut stainless-steel stencil of 0.127mm (5thou) thickness was used in this study – see Figure 9.3. This stencil pattern was composed of several combinations of IPC test standards, as indicated in Figure 9.4. The target area of study for this experiment was the IPC slump as defined by IPC TM 650-2.4.35 (see Appendix P3). The IPC slump test is a test designed for studying the possibility of bridging of solder paste deposits after printing.

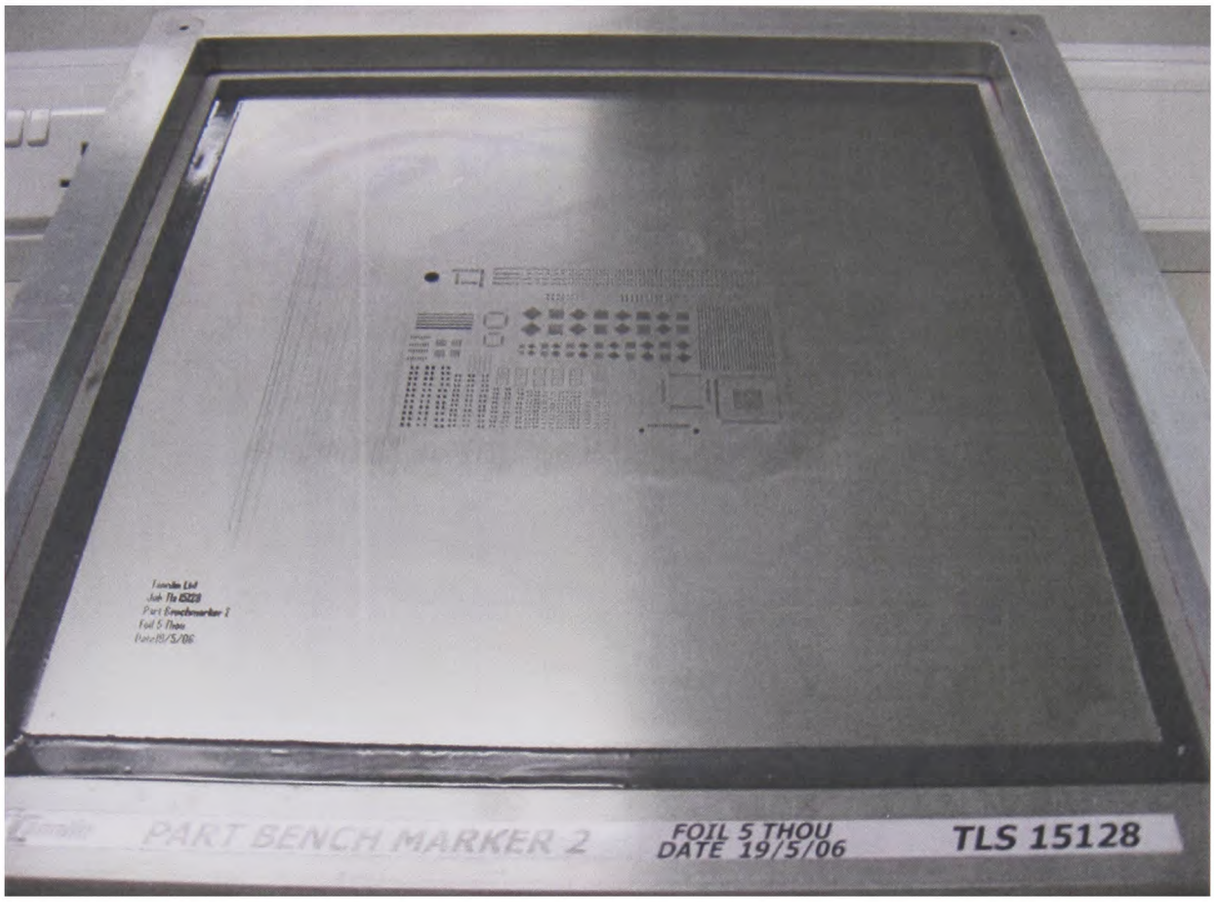

Figure 9.3: Bench Marker II laser-cut stencil.

9.2.6. Bench Marker II PCB test board

The Bench Marker II PCB boards were used for the printing trials of the solder pastes. The board has been specifically designed to test solder paste print deposit consistency after both printing and reflow soldering. The board has a specific target area for each test, as shown in Figure 9.4. For example, the patterns used for a solder-paste printing performance test were defined by the IPC slump test standard (IPC TM 650-2.4.35). The printing test results shown later in this chapter will be based on this IPC slump test area.

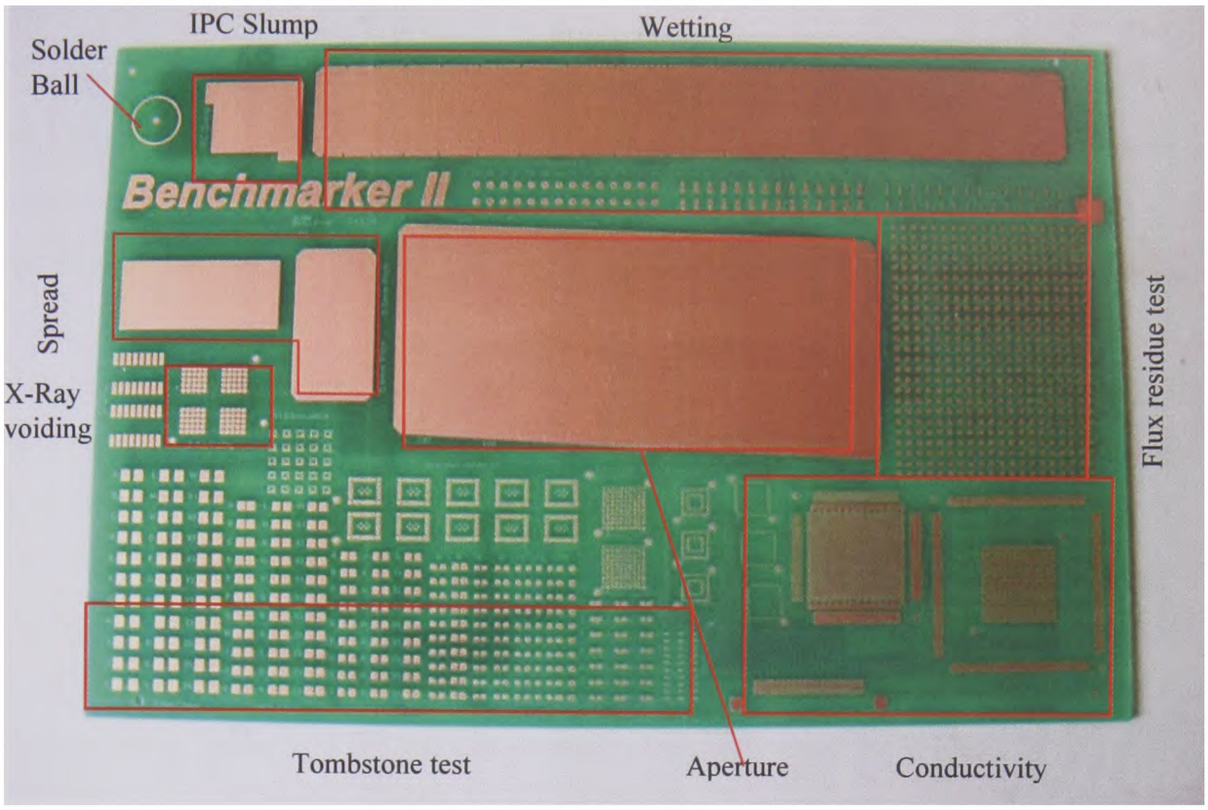

Figure 9.4: Bench Marker II test board.

9.3. Results and discussions

This section presents results of the study on the correlation of ultrasound parameters with the viscosity of lead-free solder pastes in the four different conditions described in Section 9.1, namely:

- fresh solder paste samples;
- expired solder paste samples;
- low-temperature solder paste samples and
- solder paste samples with different amounts of flux content (% by volume).

The printing results study of the fresh solder paste samples will be presented immediately after the fresh solder paste samples experiment to provide the reader with the idea of how ultrasound viscosity may be used to predict the printing quality of solder pastes.

In each condition mentioned above, the rheometer viscosity test results were also provided to allow comparative study of the results.

The solder pastes described in Section 9.2.1 were used for both ultrasound and rheometer viscosity tests. To avoid destroying the samples, the test using ultrasound was conducted first, and then a small amount of sample was removed for testing via the Bohlin rheometer.

The viscosity tests using the rheometer were undertaken with a controlled shear-rate setting – a controlled stress setting was not suitable for solder pastes materials under low stress as solder pastes materials usually have very high viscosity. This limitation is partly due to the high viscosity of the solder paste and partly due to the limitation of the Bohlin rheometer itself. It would be easier for the rheometer to cause a certain total displacement and measure how much force has been used to cause such a displacement through the feedback sensor, compared with the attempt to control and provide just enough force to shear the material to a certain displacement. Very high-viscosity materials tend to restore their viscosity quickly (through structural rearrangement), especially under low stress, causing the rheometer to have difficulty in measuring the amount of total displacement (showing positive total displacement when force is applied and negative total displacement once the force is removed).

The range of shear rate used was $0.1–50s^{-1}$ using a parallel-plate (Ø=20mm) geometric set-up. This range of shear rate was found to give access to values low enough for the planned experiments, but it also covered high shear rates. Higher shear rates were not used as the solder paste sample can easily ooze out from the plate at high shear rate, causing micro gaps between the plates. The micro gaps can result in stick–slip motion, leading to the 'wall slip' that is widely believed to cause unreliable viscosity readings.

The experiments were conducted at a constant temperature of 18°C (±0.1°C), controlled via the rheometer's integrated Peltier plate temperature-control unit. Because of the non-repeatability issue of the results, an average of five test runs for every sample was used so as to reduce variability. The cause of the variability in the rheometer test results was thought to be associated with the non-homogenous nature of the paste structure, itself due to the use of a bimodal particle size distribution in the

solder paste formulation. The rheometer used for the study was calibrated using standard Newtonian fluids (up to 200Pa.s). As standard Newtonian fluids beyond 200Pa.s were not available, the rheometer was not calibrated beyond this point.

9.3.1. Viscosity measurements of new solder pastes

a) Ultrasound measurements

In this part of study, the ultrasound viscosity of fresh solder pastes will be determined by fitting the ultrasound raw data to the theoretical model developed in Chapter 8 (see Equation 8.20). The raw data was extracted from the ADC unit using the program specified in Appendix A. An example of a screen shot from the program is shown in Figure 9.5.

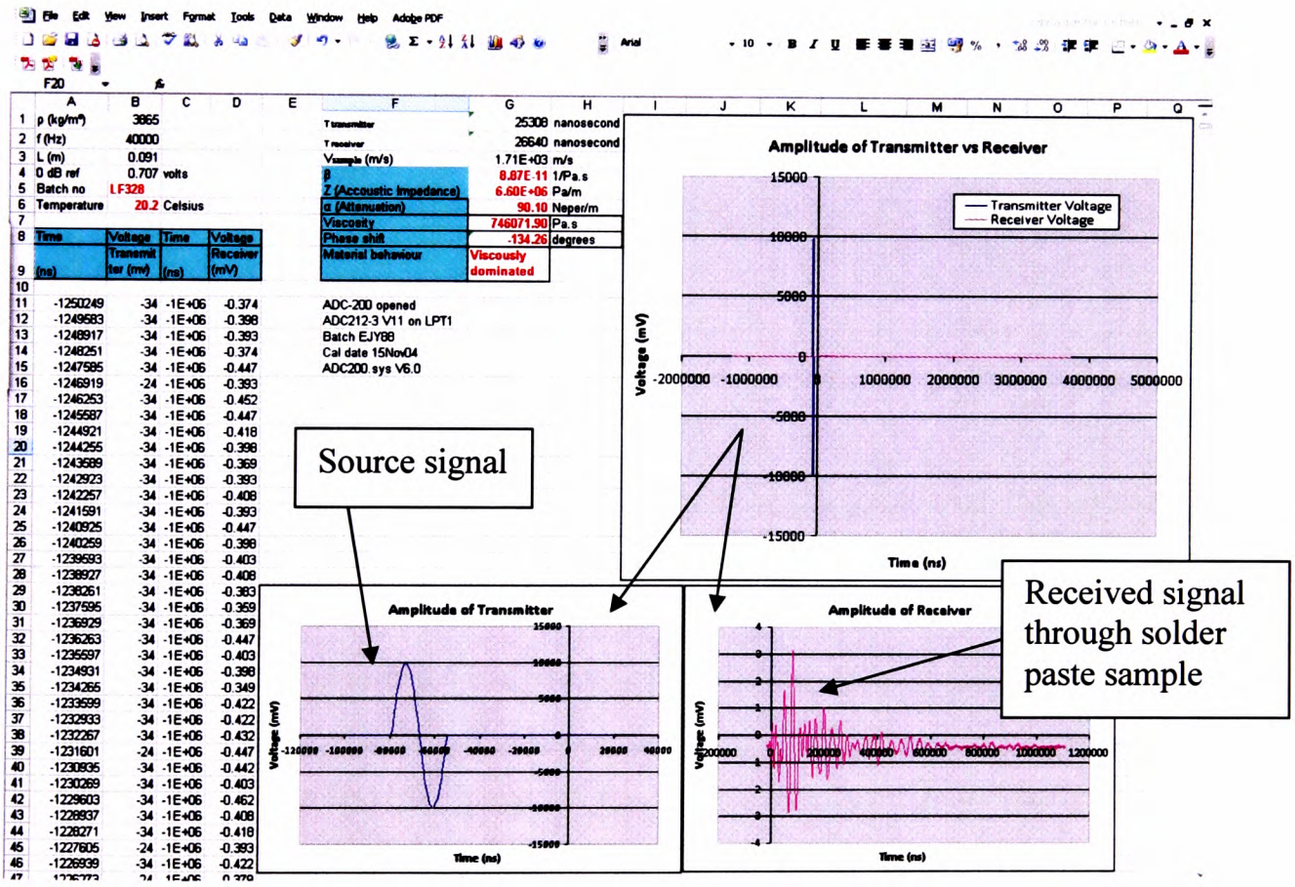

Figure 9.5: Screen shot from the ultrasound viscosity measurement program.

As was noted previously from Equation 8.20, the measured viscosity of any material can be shown to be a function of the measurement frequency. Thus, a number of trial

tests were carried out at different frequencies to determine the optimal frequency for solder paste materials – see Figure 9.6. The results showed that, for the paste and flux materials, a 40kHz frequency is best suited for the test because the attenuation is at its inflection point, namely where it started to increase (for solder pastes) or decrease (for flux). Also, at this point the signal is stronger as the attenuation is relatively low.The ease of the wave to penetrate the flux at higher frequency is reflected by the reduction in the attenuation.

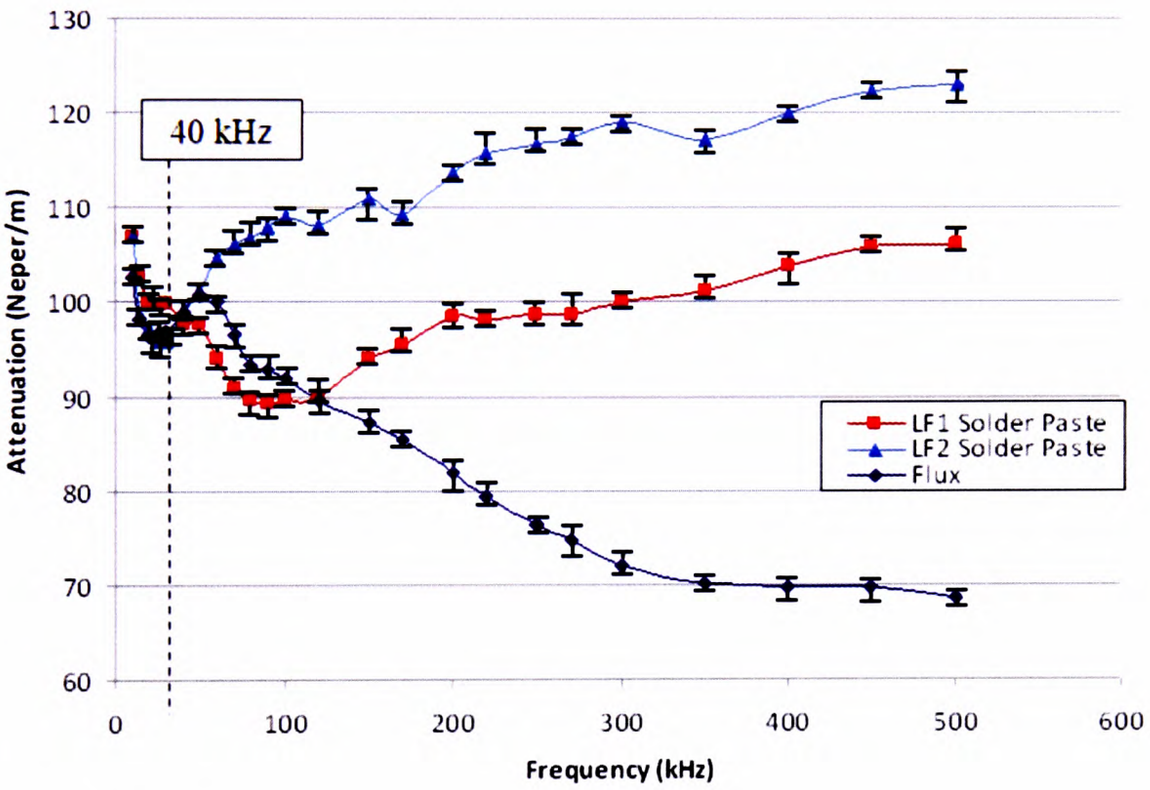

Figure 9.6: Ultrasound attenuation response from solder paste and flux at various frequencies.

Another reason that supports the use of a relatively low ultrasound frequency is shown in Figure 9.7. The test results indicate that there is a cut-off ultrasound signal at very high frequency (170kHz) for some solder pastes, beyond which the ultrasound velocity of the solder paste is relatively constant. Hence, a relatively low frequency (<170kHz) was chosen for testing solder paste materials.

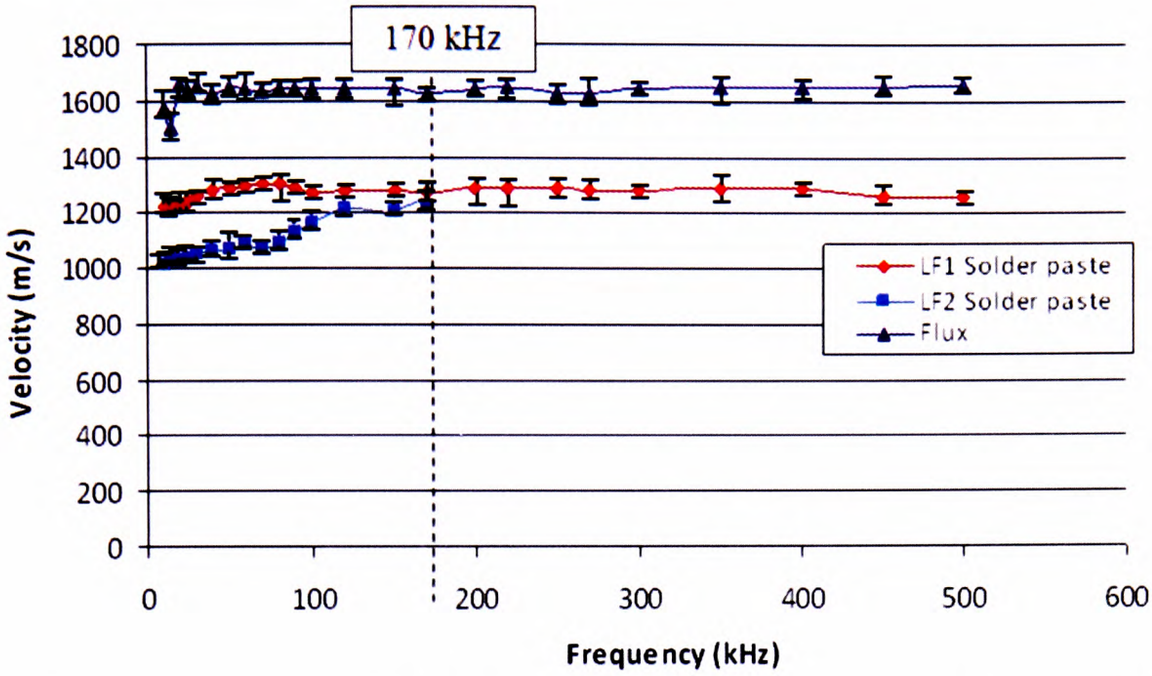

Figure 9.7: Ultrasound velocity response from solder paste and flux at various frequencies.

After the suitable ultrasound frequency for testing solder paste materials had been established, the remaining solder paste samples were tested at the same frequency (40kHz). The viscosity of the solder paste samples can be found by substituting the density, ultrasound attenuation and ultrasound velocity values into Equation 8.20. The ultrasound viscosity test results are shown in Figure 9.8.

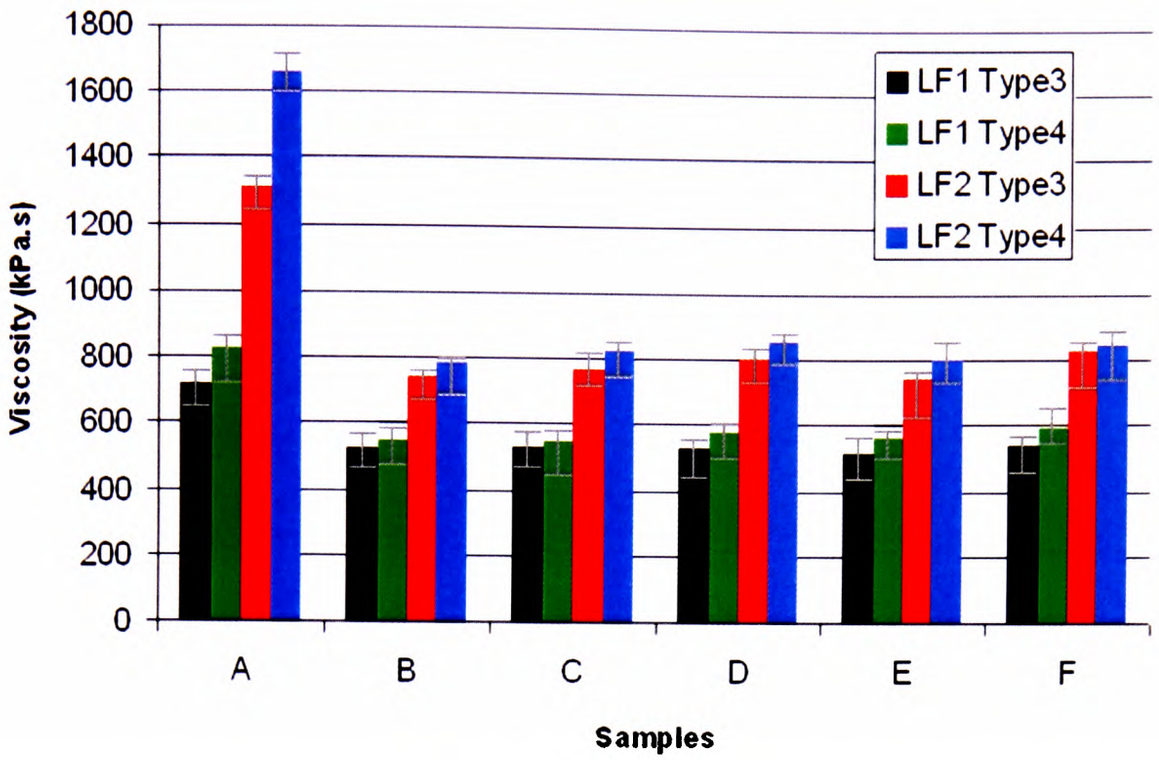

Figure 9.8: Average ultrasound viscosity of different batches of lead-free solder pastes at 40 kHz.

Sample A from each batch of the solder pastes has been intentionally exposed to 100°C for 30 minutes prior to the test, to replicate spoilt solder paste characteristics. This was done because the pastes will take six months to one year to show significant natural deterioration in a sealed container. Other collections of expired or spoiled pastes were not used as they were not from the same production batch. The results in Figure 9.8 suggest that the spoiled pastes tend to have higher viscosity. The increase of viscosity in these solder pastes could be due to the evaporation of the solvent, increasing the solder paste's solid-to-flux volume fraction. Empirical studies conducted by the author (see Figures 9.13 and 9.23) indicate that in order to produce good-quality print deposits the viscosity of the solder pastes must not be less than 100Pa.s or exceed 1200Pa.s (at a shear rate of $6s^{-1}$ using a rheometer) to avoid such defects shown in Figure 9.19.

The viscosities of the solder pastes from the same batch (e.g. LF1 Type 3 samples B–F) were found to show little difference, indicating that the solder paste supplier has very good control of the production line. Small variations in solder paste viscosity are

usually observed from batch to batch as a result of the effect of using multimodal particle size distribution (PSD) in paste formulations. This problem is very common in the powder-related industry (Carson *et al* 1986). In a worse-case scenario, a batch of solder paste may contain a significantly higher proportion of big particle sizes from the PSD range in the first few bottles of solder paste samples, median particle sizes from the PSD range in the middle of the batch of the solder paste samples, and a significantly higher proportion of small particle sizes from the PSD range in the last few bottles of solder paste samples. If this were to happen, the viscosity of the solder pastes from the same batch would vary significantly.

Comparing the ultrasound viscosity results with the viscosity values provided by the solder paste manufacturer (see Table 9.1), the ultrasound viscosity of the solder pastes were found to be 1000 times greater than those supplied by the solder paste manufacturer. Such a difference in viscosity values were not as expected, as Equation 8.20 has been deduced analytically and undergone refinement of coefficient correction by fitting the equation to viscosity-standard fluids. The difference could be accounted for if higher-viscosity standard fluids (>200Pa.s) were available to be used for the coefficient correction of Equation 8.20.

The difference can be corrected by downscaling the ultrasound viscosity graph 1000 times to match those supplied by the solder paste manufacturer: if the ultrasound test results of LF1 and LF2 solder pastes were downscaled 1000 times, it is clear that the results are very close to the viscosity values provided by the solder paste manufacturer. This means that Equation 8.20 would be specifically suitable for measuring the viscosity of solder paste materials if it includes a downscaling factor of 1000 times, but it would invalidate Equation 8.20 for measuring lower-viscosity materials.

Rheometer viscosity measurements were conducted (see next section) to complete the comparative work of how the ultrasound viscosity measurements compare with the other techniques available, i.e. the viscosity values provided by solder paste supplier (using Brookfield viscometer @ 5rpm) and rheometer measurements.

b) Rheometer measurements

As mentioned previously, the rheometer measurements were conducted after the ultrasound measurements to avoid destroying the samples. Sample A from each batch of the solder pastes, it should be remembered, has been intentionally exposed to 100°C for 30 minutes prior to the test to replicate a spoiled paste condition.

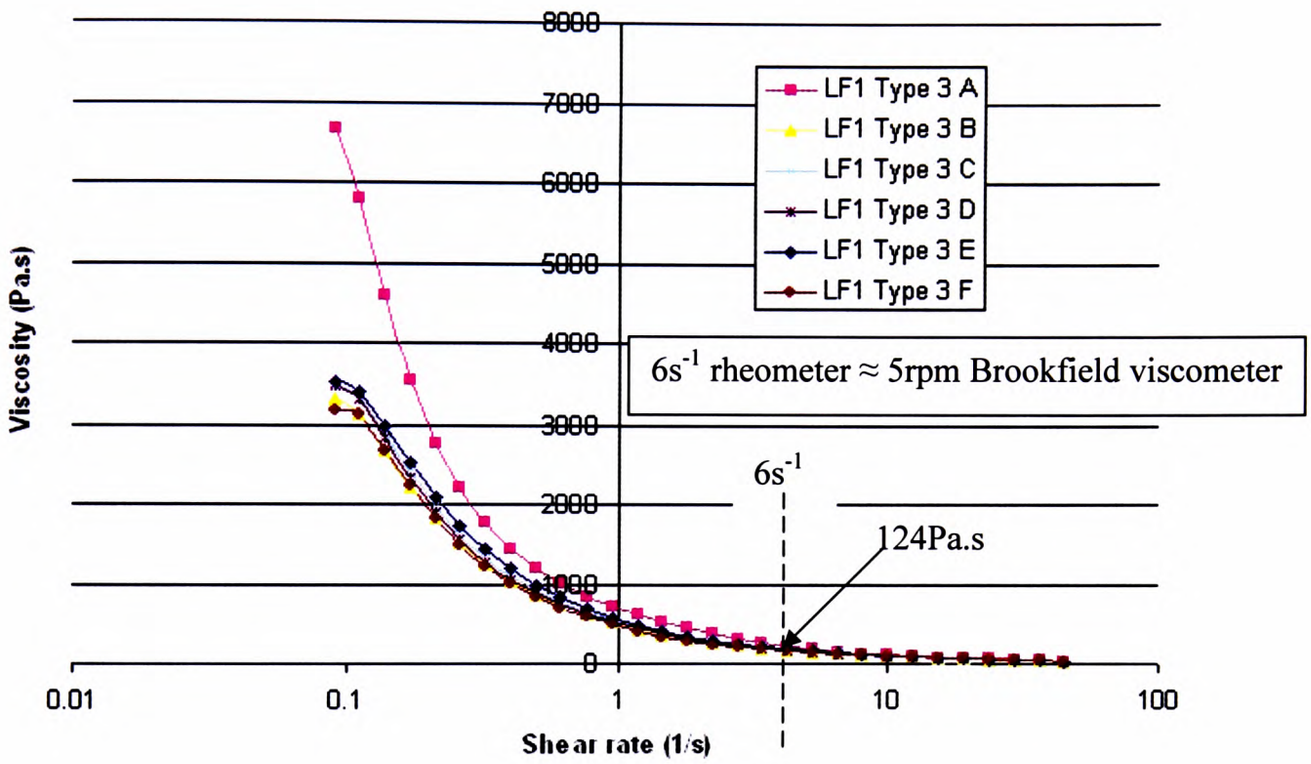

Figure 9.9: Viscosity of LF1 Type 3 solder paste batch using Bohlin rheometer.

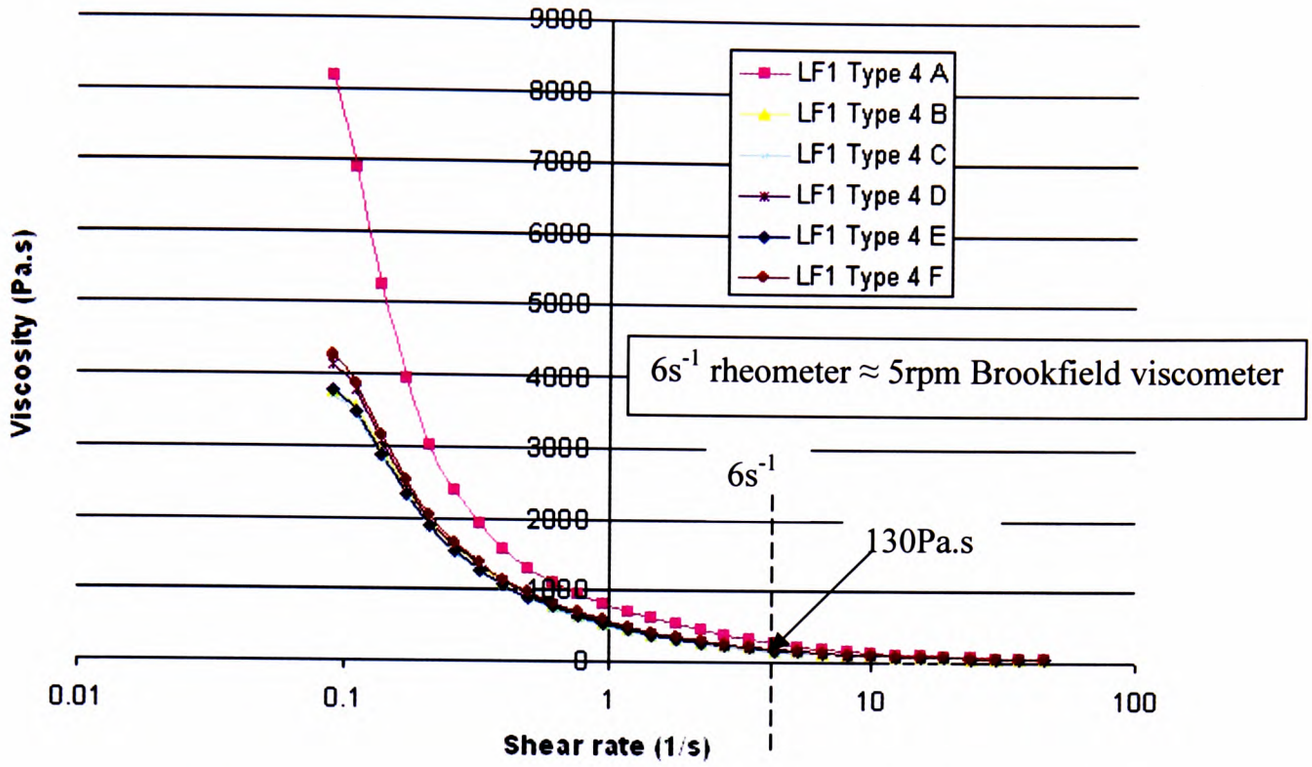

Figure 9.10: Viscosity of LF1 Type 4 solder paste batch using Bohlin rheometer.

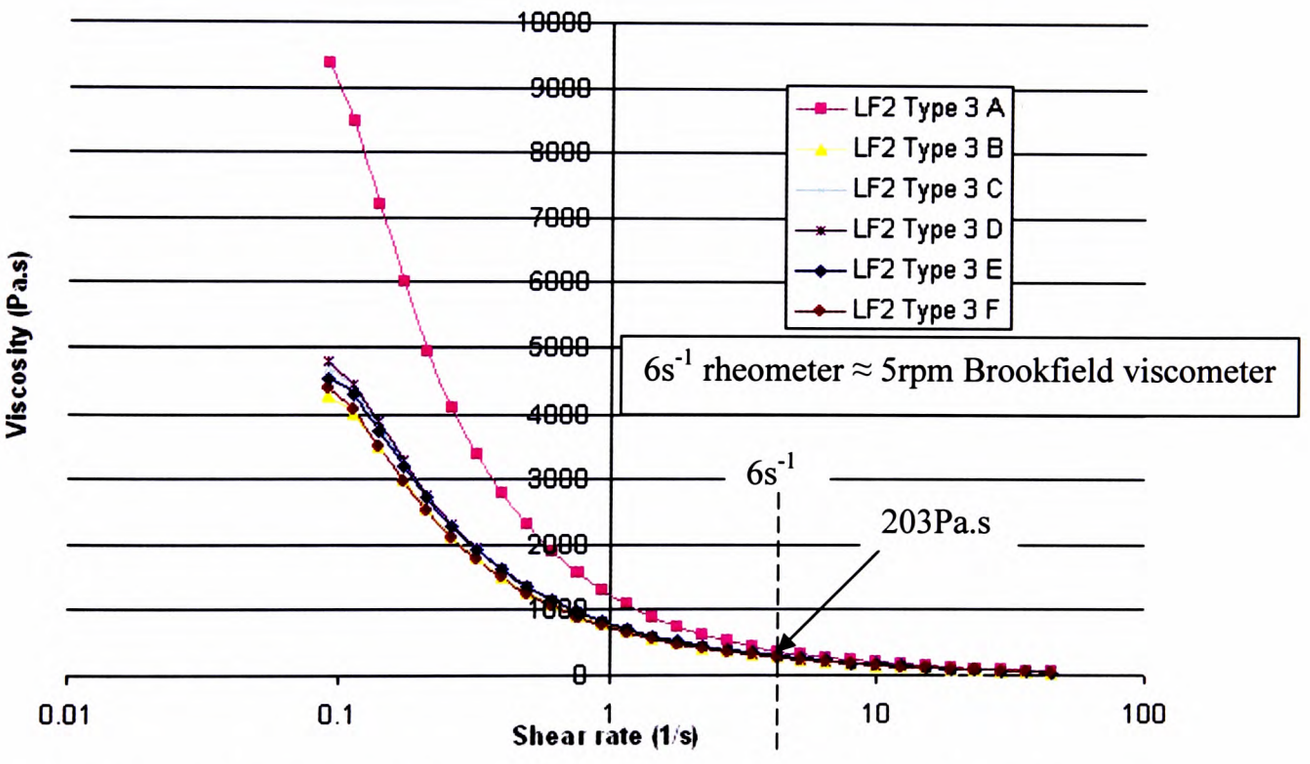

Figure 9.11: Viscosity of LF2 Type 3 solder paste batch using Bohlin rheometer.

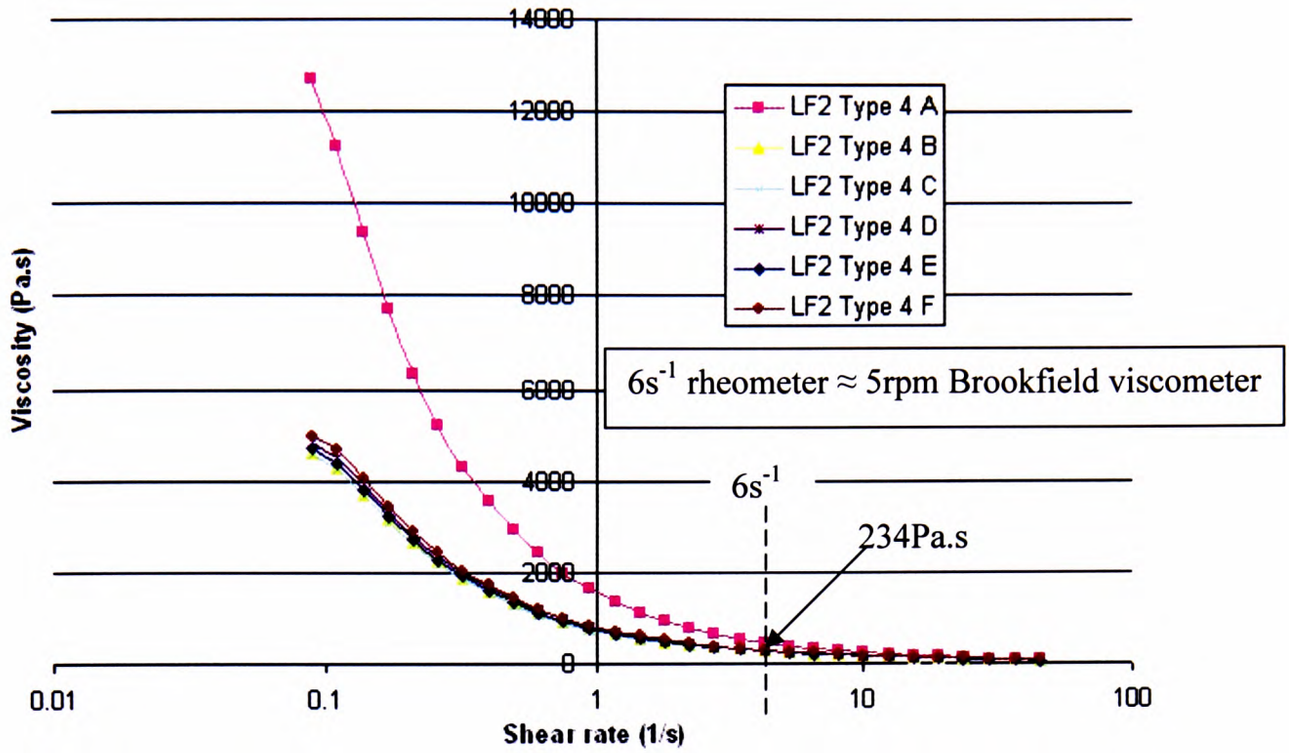

Figure 9.12: Viscosity of LF2 Type 4 solder paste batch using Bohlin rheometer.

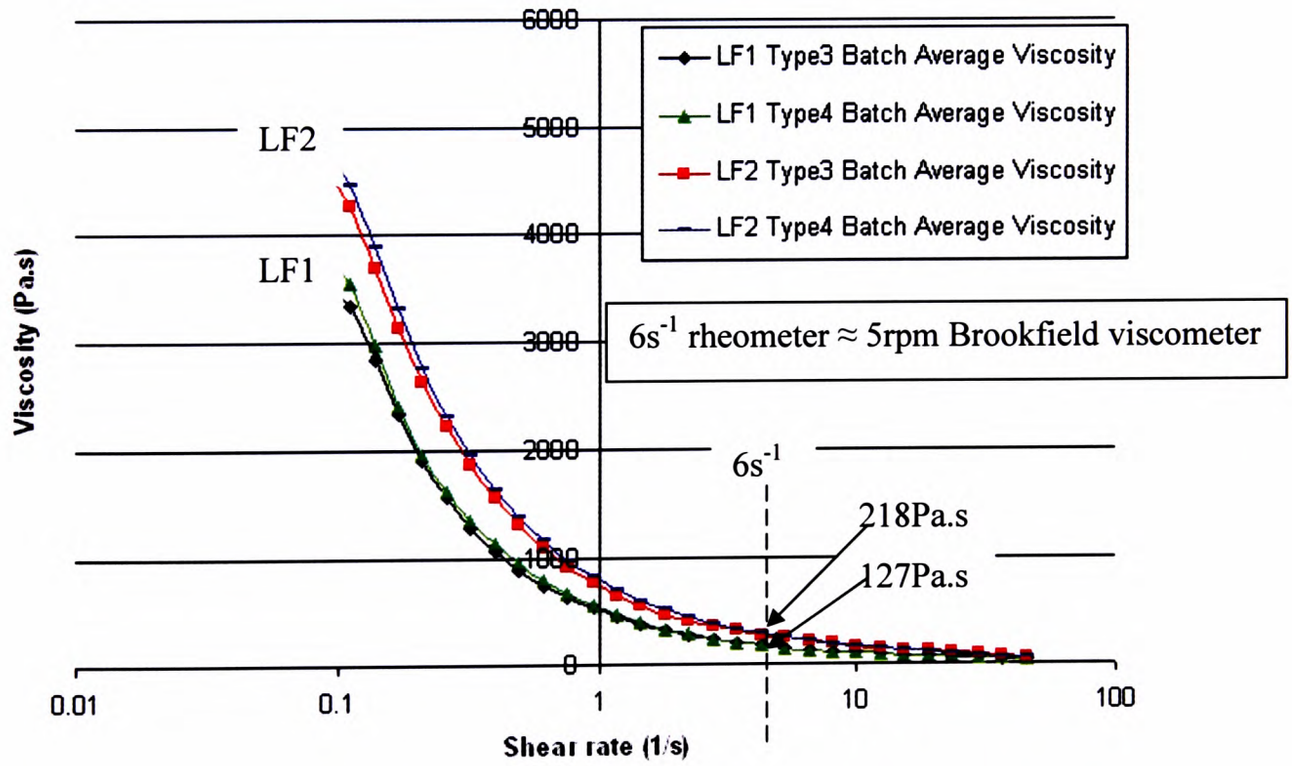

Figure 9.13: Average viscosity of different batches of lead-free solder pastes at various shear rates using Bohlin rheometer.

The rheometer test results shown in Figures 9.9–9.13 indicate that the rheometer can easily pick up the viscosity changes in the spoiled pastes represented by Sample A from four different batches of solder paste. The test results also confirm that there are variations of viscosity among the solder pastes from the same batch. One problem of using the rheometer is that it tends to give non-reproducible results, even from the very same sample. Hence it was necessary to average the results from five test runs for every sample in order to reduce variability.

The rheometer results at the shear rate of $6s^{-1}$ did not compare very well with the viscosity results provided by the solder paste manufacturer. The shear rate of a Brookfield viscometer at 5rpm is equivalent to the shear rate of $6s^{-1}$ of the rheometer fitted with Ø=20mm parallel-plate geometry. The average viscosity of LF1 (127Pa.s) and LF2 (218pa.s) solder pastes at $6s^{-1}$ were respectively 75% and 71% off the viscosity values provided by the solder paste manufacturer shown in Table 9.1. However, if compared to the viscosity values at the shear rate of $1s^{-1}$ (see Figures 9.9–9.12), the values for both LF1 and LF2 pastes were accurate to within 90% of the values shown in Table 9.1.

Comparing the rheometer results at $6s^{-1}$ to the ultrasound viscosity results obtained, it is clear that the ultrasound results need to be downscaled 4330 times to match those of the rheometer, accurate to within 95%. To match the rheometer results at $1s^{-1}$ with the same accuracy, the ultrasound viscosity results would need to be downscaled 1000 times.

To give an idea of how the viscosity values of these pastes may reflect the printing quality of the pastes, a stencil printing test was carried out and is explained in the following section.

9.3.2. Correlation of viscosity values with printing results

In this part of study, printing test results of the solder pastes used in Section 9.3.1 will be shown to illustrate how the ultrasound viscosity results (Figure 9.8) or the rheometer viscosity results (Figures 9.9–9.13) can be used to predict the printing

quality of the solder paste. Essentially, this section will provide the reader with the knowledge of the desired viscosity values range in order to achieve good printing characteristics. If a rheometer or the ultrasound viscosity measurement machine is available, this knowledge would come useful in an assembly plant for making critical decisions on whether a certain paste should be used or not when the viscosity of the paste is known.

a) Observation area

The target area of the study for the stencil printing of solder pastes is shown in Figures 9.14 and 9.15. This particular pattern is designed for studying solder paste slump properties according to the IPC TM 650-2.4.35 test standard. Solder paste slump behaviour is of great interest because slumping behaviour can be used to predict whether a particular solder paste can be used for a fine-pitch stencil printing.

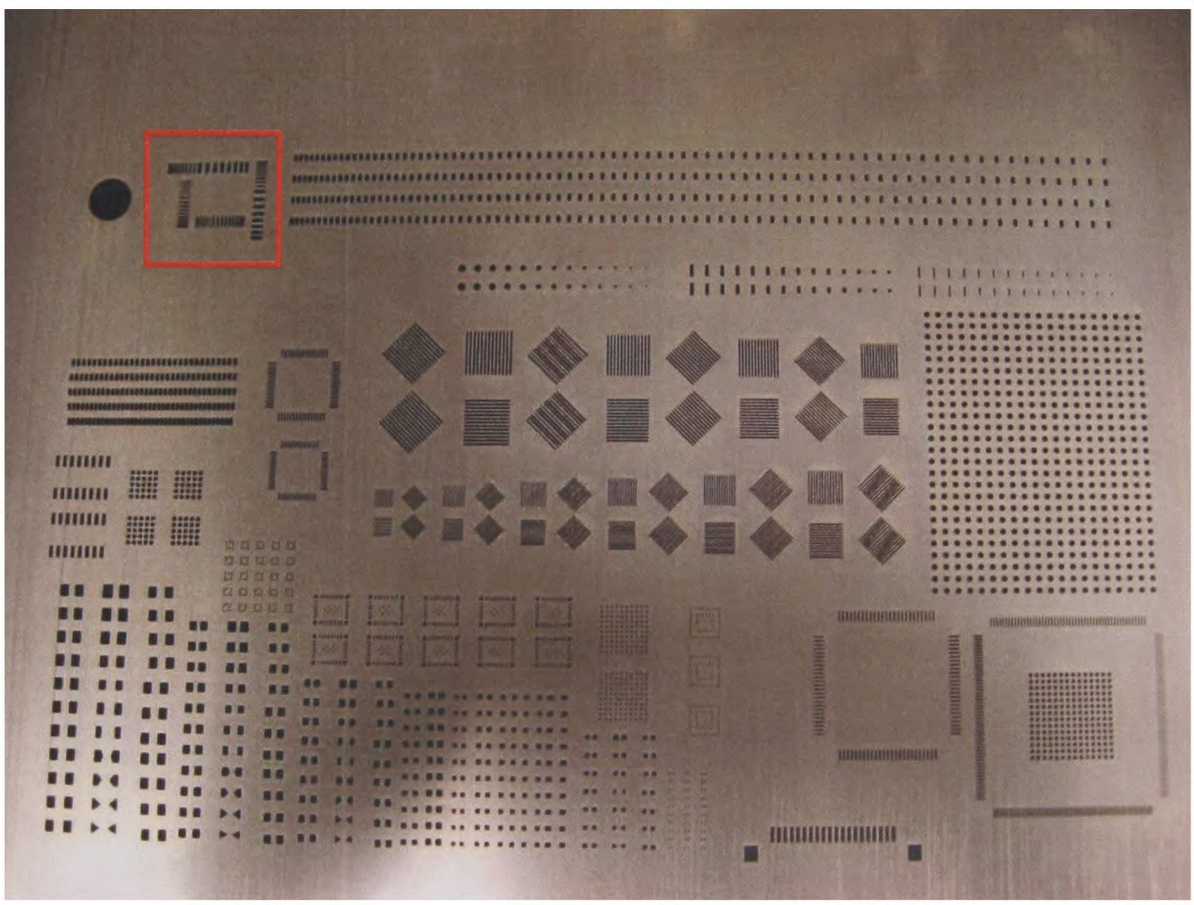

Figure 9.14: Close-up view of the apertures on the stencil used for solder paste printing. The red square indicates the observation area of study.

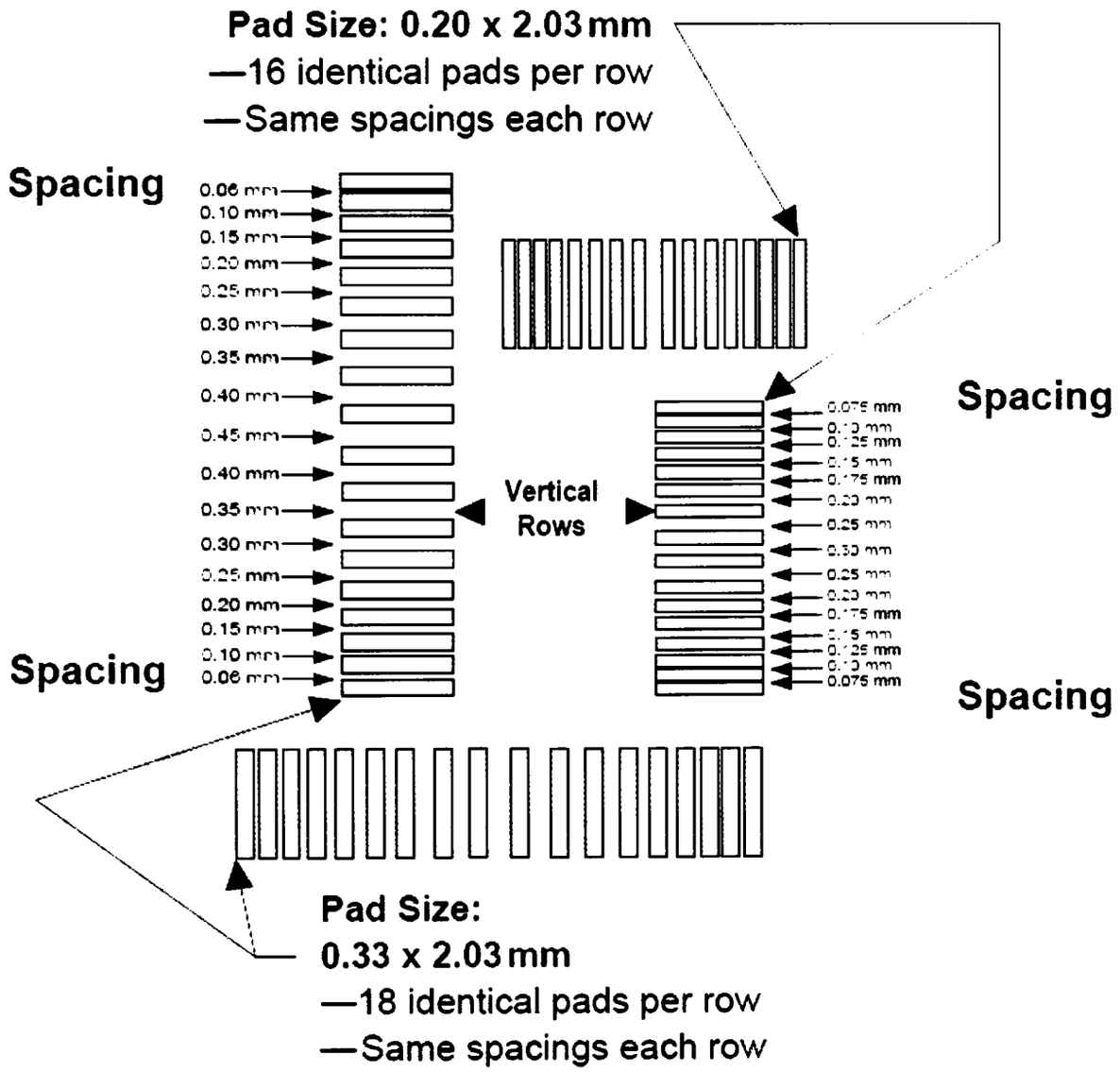

Figure 9.15: Engineering drawing of IPC TM 650-2.4.35 slump test pattern.

b) Printing results

The stencil printing process was carried out by dispensing the solder paste on the surface of the stencil, as shown in Figure 9.16. The inspection of the printing results was performed using a Leica S6D stereo-zoom microscope fitted with JVC KY-F55 CCD colour camera system, as shown in Figure 9.17. The microscope can provide a magnification from 6.3× to 40×; higher magnification can be achieved by attaching an optional objective lens. The resulting digital images were captured using the frame grabber module and saved to a computer for further analysis.

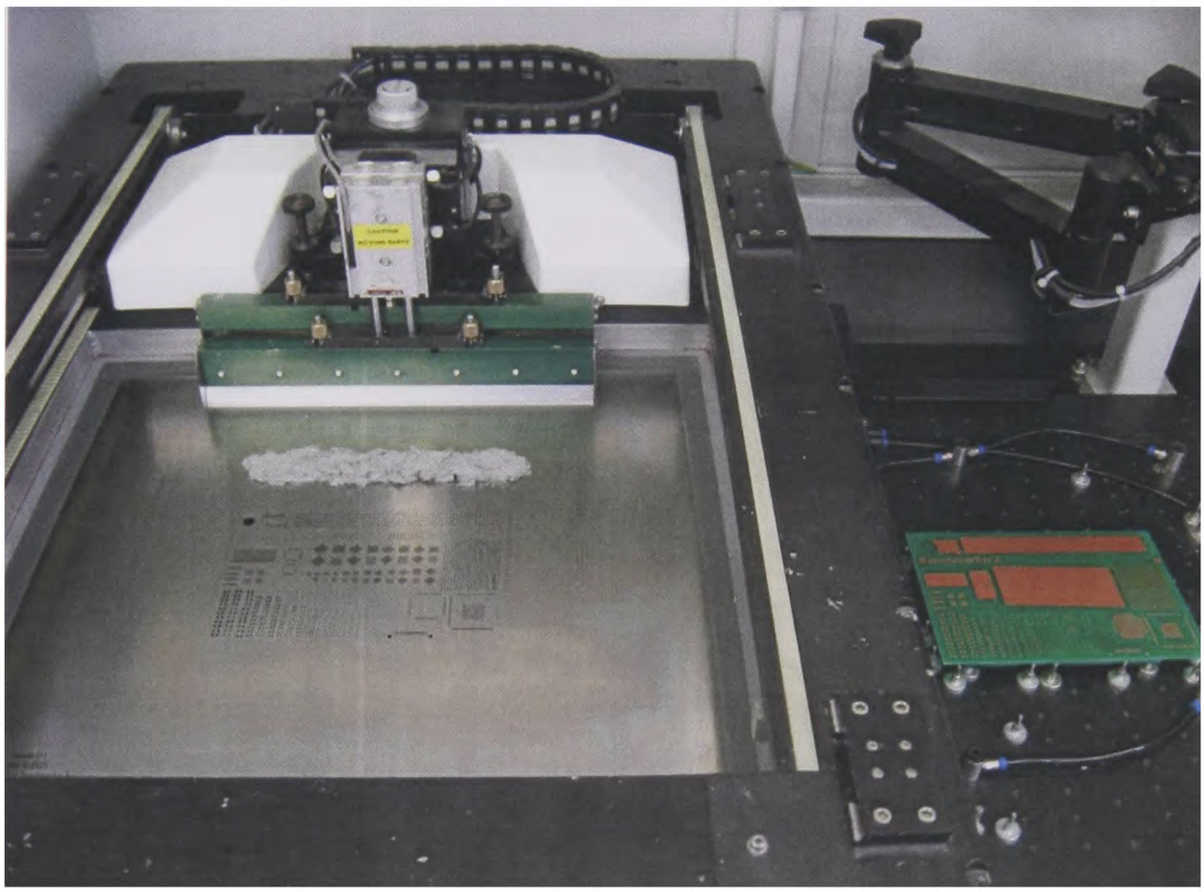

Figure 9.16: DEK stencil printing machine fitted with Bench Marker II stencil and Bench Marker II PCB.

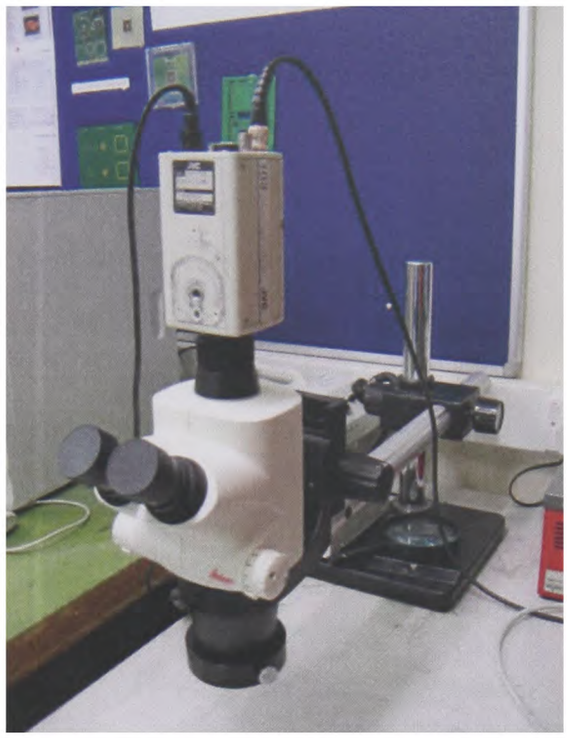

Figure 9.17: Leica S6D stereo-zoom microscope with JVC KY-F55 CCD colour camera system.

A close-up view of the typical print deposit obtained from LF1 and LF2 solder paste is shown in Figure 9.18. The print results shown in Figure 9.19 indicate that all the print deposits seemed to produce good print apart from those for LF2 Type 3 and LF2 Type 4 from sample A. The results also confirm that all of the solder paste samples is suitable for printing at a spacing of greater than 0.2mm. Linking these results to Figure 9.8 suggests that the skipping of the print deposits exhibited by LF2 Type 3 and LF2 Type 4 pastes may be due to the excessively high viscosity arising from evaporation of the highly volatile chemicals in the flux.

Empirical tests using a Brookfield viscometer conducted by the solder paste manufacturer indicate that, in order to achieve good print deposits, the solder paste viscosity must be in the range of 400Pa.s to 600Pa.s at 5rpm shear rate – see Appendix O. However, the range was found to be in the region of 100Pa.s to 400Pa.s at $6s^{-1}$ shear rate for the Bohlin rheometer (see Figures 9.9–9.13). For the ultrasound technique, this range was found to be in the region of 400kPa.s to 800kPa.s at a 40kHz frequency (see Figure 9.8).

The minimum print gaps achieved with LF1 and LF2 solder pastes were satisfactory – see Table 9.2. Results from Table 9.2 suggest that LF2 paste is more suitable for finer-pitch printing as most of the print deposits have a low minimum spacing gap. In order to achieve very good print deposits for fine-pitch printing, the viscosity of the solder paste must be significantly high, but not excessively high as this can lead to skipping, as indicated by LF2 Types 3 and 4 results for sample A (shown in Figure 9.19). The presence of bridging or slump indicates that the viscosity of the paste is too low (Anderson *et al*, 1995; Baluch and Evans, 1995; Costello, 1997). Formulating the viscosity of solder paste for fine-pitch printing is a very difficult task as viscosity needs to be kept low enough so that the paste can flow through the narrow apertures of the stencil but at the same time the viscosity needs to be as high as possible so as to prevent bridging by maintaining the shape of the paste deposits after being dispensed (Bao *et al*, 1996; Billotte *et al*, 2006). Examples of typical printing results resulting from excessively low viscosity are shown in Figure 9.20, while those for excessively high viscosity are shown in Figure 9.21.

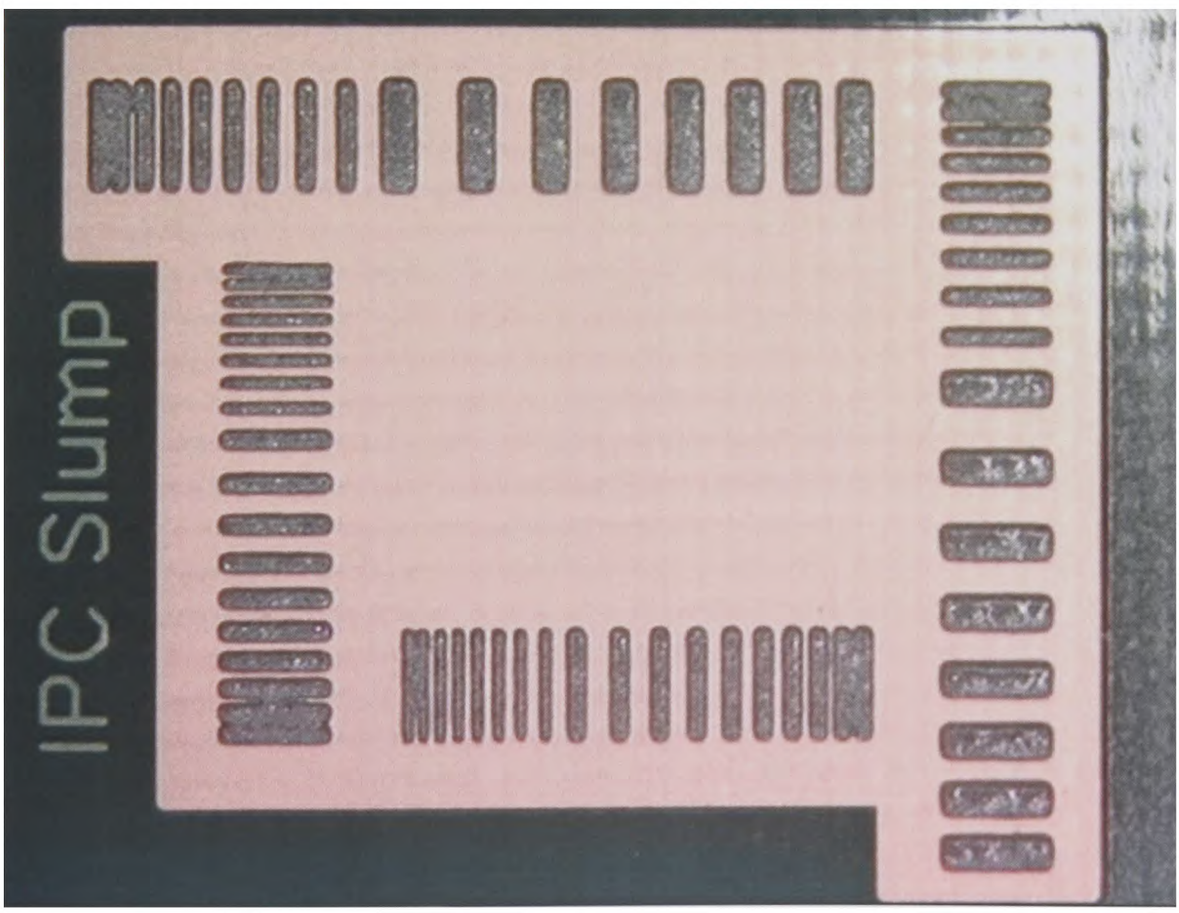

Figure 9.18: Close-up view example of the print result.

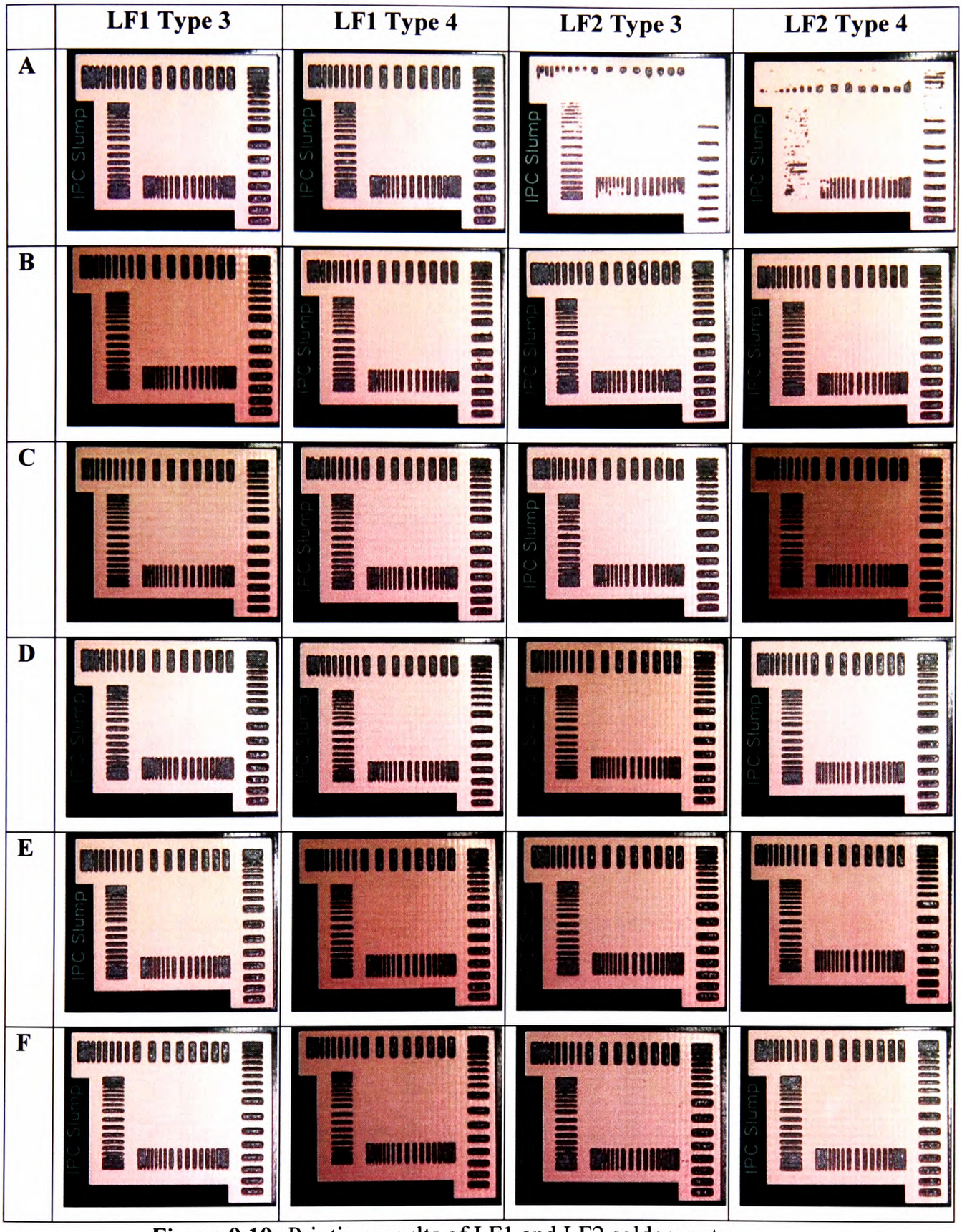

Figure 9.19: Printing results of LF1 and LF2 solder pastes.

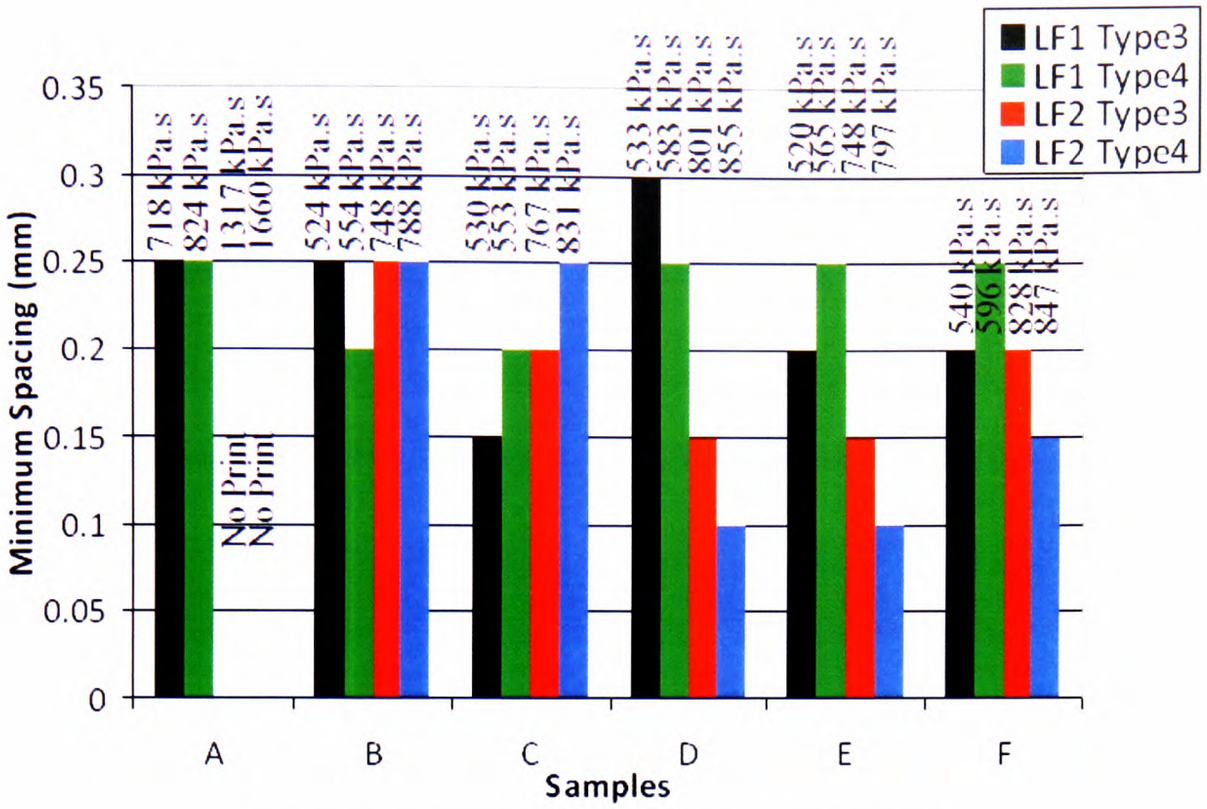

	Minimum Spacing Gap (mm)			
Sample	**LF1 Type3**	**LF1 Type4**	**LF2 Type3**	**LF2 Type4**
A	0.25	0.25	No print	No print
B	0.25	0.20	0.25	0.25
C	0.15	0.20	0.20	0.25
D	0.30	0.25	0.15	0.10
E	0.20	0.25	0.15	0.10
F	0.20	0.25	0.20	0.15

Table 9.2: Minimum spacing gap obtained from printing results of LF1 and LF2 solder pastes. Lower minimum spacing indicates ability to print at finer pitch

The results shown in Table 9.2 indicate that sample D and E of LF2 Type 4 solder paste achieved the best printing result as it appears capable for printing up to the 0.10mm pitch without causing any bridging defect. No minimum spacing gaps were obtained for sample A of LF2 Type 3 and LF2 Type 4 as the skipping of print deposits were observed during the test (see Figure 9.19). Note that all LF1 samples with viscosity of about 500kPa.s can print very well, especially for a minimum spacing gap greater than 0.15mm. Higher-viscosity samples of LF1 (sample A), i.e. greater than 800kPa.s, did not improve (lower) the minimum spacing gap. In fact, it seems that if the viscosity of LF1 (sample A) was even higher, it could lead to no print occurring, like the LF2 samples. In order to achieve a lower minimum spacing gap, a higher viscosity is required, but excessively high viscosity can result to no print at all.

From this print study it can be concluded that if a solder paste were to be formulated with a viscosity of 500–900kPa.s at 40kHz, it is very likely that the solder paste can print very well for a 0.2mm minimum spacing gap. However, if the solder paste has a viscosity beyond 900 kPa.s at 40kHz, then very likely no print at all can result. The opposite of this can also happen, in which the solder paste viscosity is significantly less than 500 kPa.s at 40kHz and then the solder paste would flow too easily after being dispensed, resulting in bridging or slumping as shown in Figure 9.20.

In order to achieve better fine-pitch print deposits (i.e. a lower minimum spacing gap), the solder paste must be made from solder particles of smaller particle size, preferably Type 5 (15–25μm) or Type 6 (5–15μm) and flux of high viscosity (Hill and Ng 2002). The combination of higher PSD type and high-viscosity flux would allow the solder paste to flow through small apertures (Mannan 1994a, 1994b, 1995) much more easily whilst maintaining its shape after being deposited onto the PCB pads (He *et al* 2003).

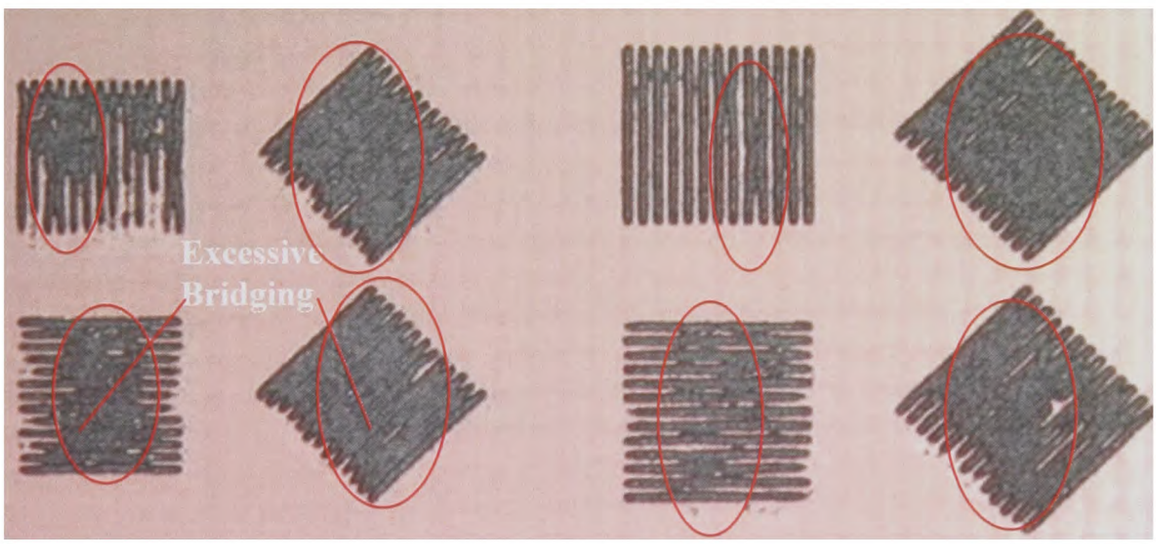

Figure 9.20: Typical printing results due to excessively low viscosity solder paste.

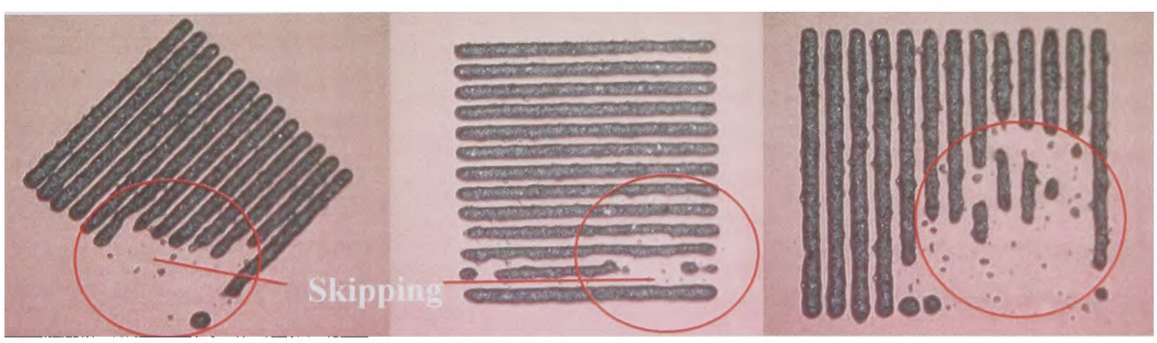

Figure 9.21: Typical printing results due to excessively high viscosity solder paste.

9.3.3. Viscosity measurements for expired solder pastes and flux mediums

a) Ultrasound measurements

In this part of the study, four batches of expired solder paste (namely DOE1 to DOE4) and three different fluxes (namely Flux A1 to Flux A3) were tested for their viscosity using the ultrasound technique. The results are presented in Figure 9.22. Generally, the solder pastes tend to have higher viscosity than the fluxes. This is because the presence of the solder alloy particles introduces friction between the particles themselves and between particles-flux. The test results shown in Table 9.3 indicate that some of the pastes were indeed no longer good for printing as their viscosity was far beyond the recommended viscosity range (less than 500Pa.s or beyond 700Pa.s) specified by the solder paste supplier (see Table 9.1). The variation in the viscosity among the samples from the same batch might be due to the non-homogenous nature of the paste structure owing to the use of bimodal particle-size distribution in the solder paste formulation. The test results also show that not all fluxes have low viscosity or similar viscosity; this is because the flux may contain different compositions and constituents of additives, as explained earlier in Section 2.2.

If the ultrasound results in Figure 9.22 are scaled down by a factor of 1000, then the results would match 70% of those values from the rheometer measurements shown in Figure 9.23.

	Viscosity (Pa.s)						
Material	Solder Paste				Flux		
Sample No.	DOE1	DOE2	DOE3	DOE4	FluxA1	FluxA2	FluxA3
1	258209.1	503905.6	320116.5	526576.8	33795.5	39547.4	150895.3
2	207137.4	413870.8	363790.9	766038.4	32529.9	39391.8	163148.5
3	234801.5	503187.0	352952.5	741427.0	34900.1	43385.2	163229.4
4	220724.0	357861.6	251024.2	757746.1	41240.1	39295.7	144294.7
5	241498.8	441443.7	301341.7	530414.8	36310.0	40975.6	145684.0
6	230093.9	410789.0	341094.6	665760.3	34382.2	40215.9	149624.9
7	236318.8	489047.9	305129.3	525299.8	40727.8	48849.6	163148.5
8	262781.7	411095.2	296873.1	635982.4	36023.8	48102.6	163229.4
9	188388.9	443640.0	304120.0	863343.7	35321.5	41226.1	145684.0
10	164326.7	503905.6	305396.1	694195.4	35847.2	42640.8	150895.3
Average	**224428.1**	**447874.6**	**314183.9**	**670678.5**	**36107.8**	**42363.1**	**153983.4**

Table 9.3: Ultrasound viscosity results of solder pastes and fluxes.

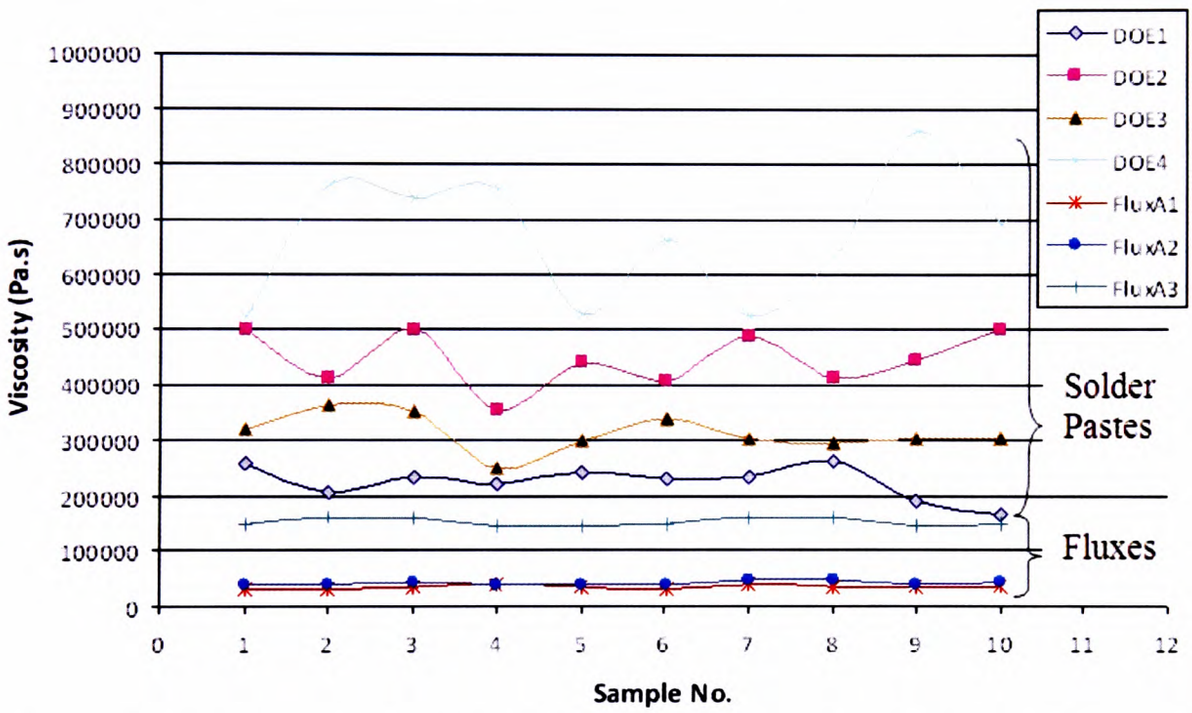

Figure 9.22: Ultrasound viscosity of different batches of expired lead-free solder pastes and fluxes at 40kHz.

b) Rheometer measurements

Comparing the rheometer results shown in Figure 9.23 at any shear rate to the ultrasound results shown in Figure 9.22, it is clear that the ultrasound viscosity and the rheometer viscosity show similar trend: Solder pastes generally have significantly higher viscosity than fluxes.

The rheometer test results shown in Figure 9.23 show that the expired solder pastes tend to have significantly higher viscosities compared with those of the fluxes and those of new pastes (see also Figure 9.13 at shear rate of $0.1s^{-1}$). It is also shown that some fluxes have significantly higher viscosity compared with solder paste.

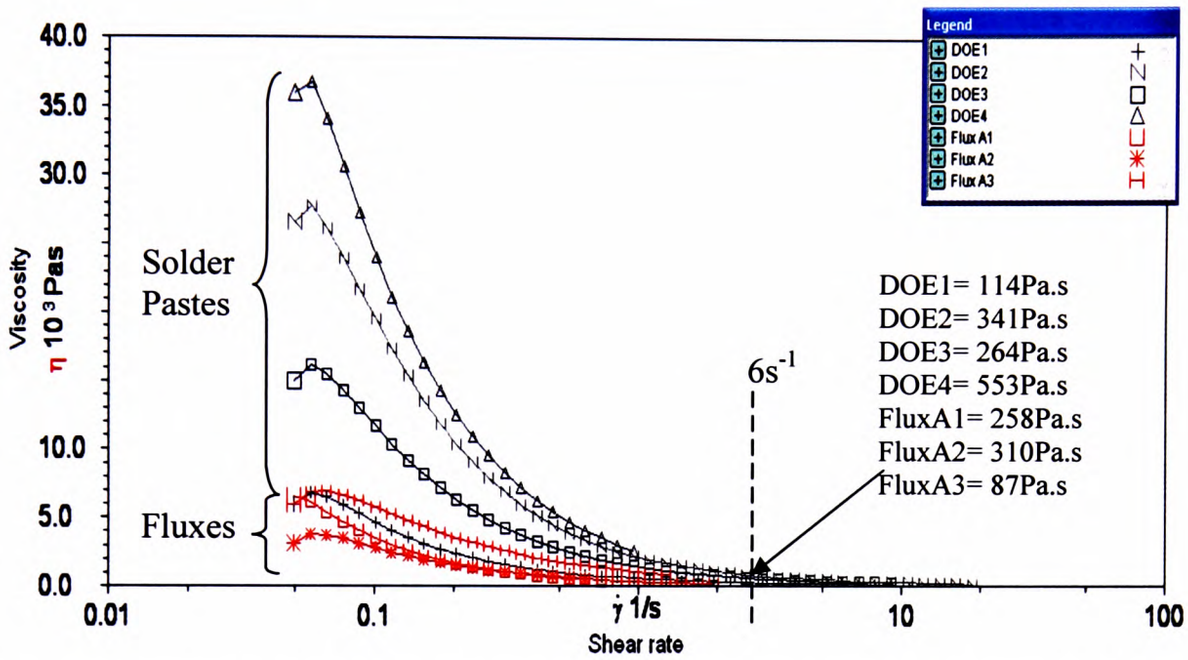

Figure 9.23: Average viscosity of different batches of expired lead-free solder pastes and fluxes at various shear rates using Bohlin rheometer.

9.3.4. Viscosity measurements for solder pastes at low temperatures

a) Ultrasound measurements

This part of the study was conducted to explore whether or not the ultrasound technique can be used to measure the viscosity of solder paste at low temperatures. Spare samples of LF1 solder paste Types 3 and 4 that were part of the same production batch of the samples used as described in Section 9.3.1 were tested by freezing the samples to -45°C. The first data point that was able to be recorded was at -35°C, owing to warming during the time required to remove the solder paste from the freezer and set it up in the ultrasound rig.

The data points were recorded for every 4°C change in temperature. The temperature was measured using a Digitron T228 digital thermometer attached to a K-type thermocouple probe. Each ultrasound data point shown in Figures 9.24–9.26 was an average of three readings.

The results in Figure 9.24 show that Type 3 solder paste has higher ultrasound attenuation than Type 4 solder paste. This result is as expected, because the median particle size for Type 3 solder paste is bigger (30μm) compared with the 18μm for Type 4. The bigger median particle size of Type 3 solder paste results in a lower packing fraction, which allows more air bubbles to be trapped in the solder paste. This conclusion is supported by the fact that Type 3 solder paste has a lower density compared with Type 4, even though both Type 3 and Type 4 solder paste have the same metal loading (88.5% by weight). The presence of air bubbles has been known to cause elevated levels of ultrasound attenuation, as demonstrated by Punurai *et al* (2006) who showed that, at any given frequency, an increase in the air bubbles' volume fraction will increase the ultrasound attenuation. Furthermore, the higher attenuation of Type 3 solder paste may also be due to the effect of ultrasound wave diffraction as described earlier in Chapter 3 (see Figure 3.14), where the bigger particle size of Type 3 solder paste is causing a higher amount of ultrasound wave diffraction.

The ultrasound velocity results given in Figure 9.25 show that the ultrasound velocity of both pastes was relatively constant. The change in temperature had little effect on the ultrasound velocity of the solder paste samples. The slight drop in the ultrasound velocity between -10°C and +10°C may be due to the melting of the ice – ice crystals were observed on the surface of the frozen solder paste at -30°C.

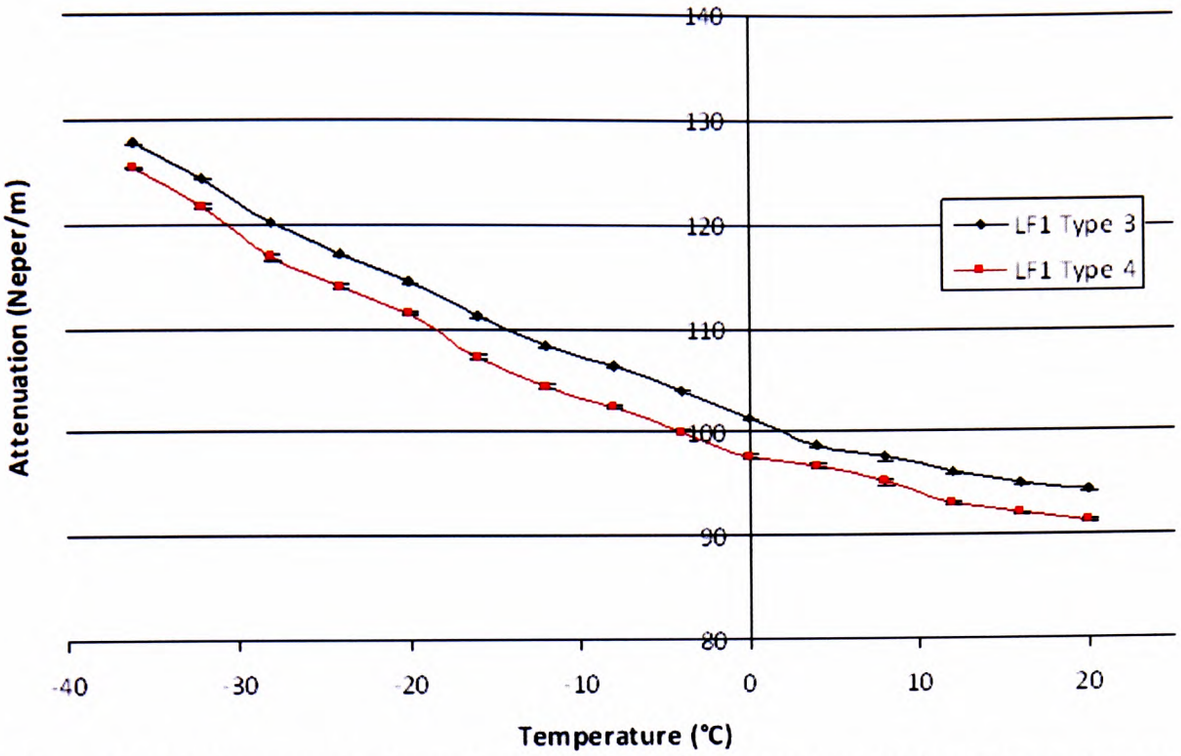

Figure 9.24: Ultrasound attenuation of LF1 solder pastes at various temperatures at 40kHz.

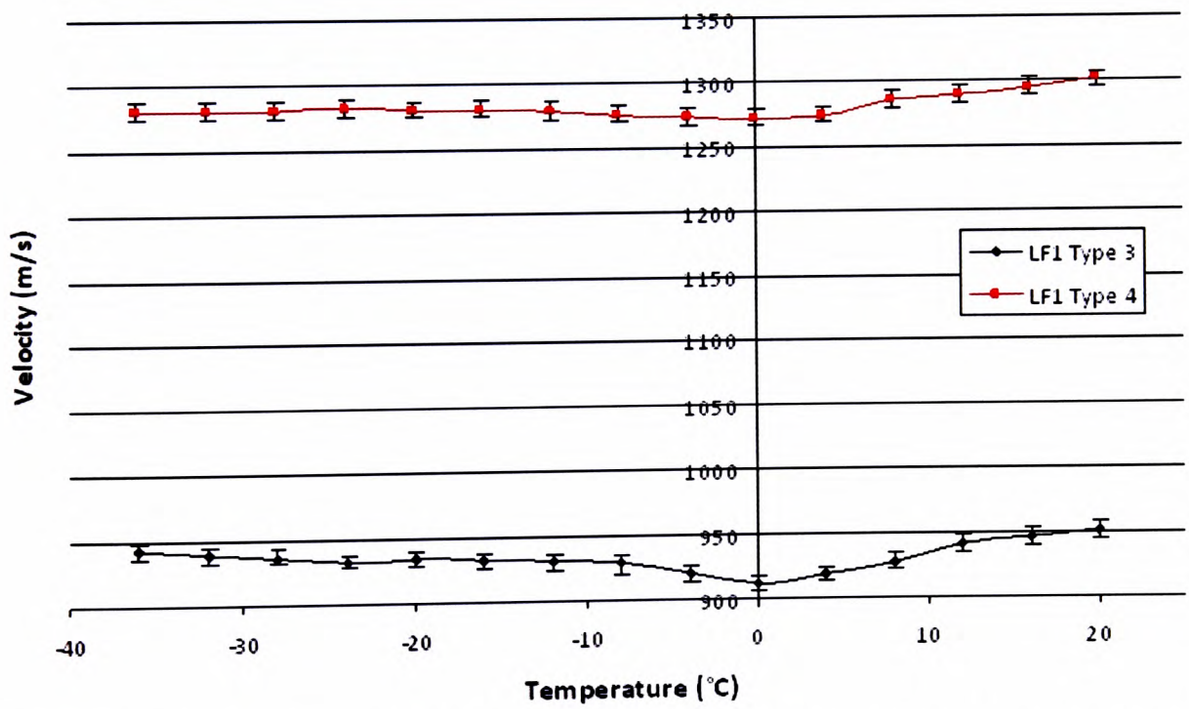

Figure 9.25: Ultrasound velocity of LF1 solder pastes at various temperatures at 40kHz.

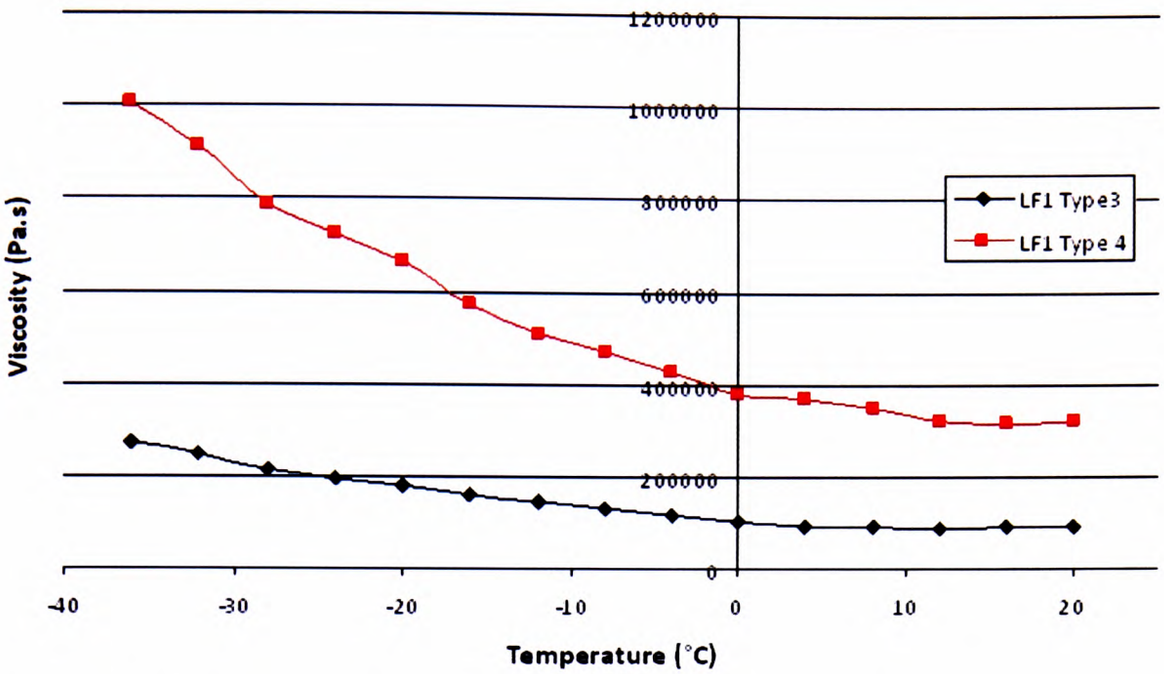

Figure 9.26: Ultrasound viscosity of LF1 solder pastes at various temperatures at 40kHz.

The reason why an increase in temperature would reduce the viscosity of a material may be related to the CTE (coefficient of thermal expansion) of the material. When a material expands due to heat, the chemical bonds also expand and hence the bonds get longer and become weaker (Samsonov *et al*, 1971; Moiseenko, 1980). This means the material is easier to shear and results in lower viscosity.

b) Rheometer measurements

The rheometer viscosity results shown in Figures 9.27 and 9.28 show that LF1 Type 4 solder paste has a higher viscosity compared with that for LF1 Type 3. These results are as expected and are in agreement with the viscosity values provided by the solder paste manufacturer; the results are also similar to those shown in Figure 9.26. The rheometer results also confirm that the changes in viscosity at high temperatures (28°C to 30°C) are significantly lower compared with those at lower temperatures (16°C to 18°C). The results have a trend similar to those for ultrasound and those reported by Mindel (1991).

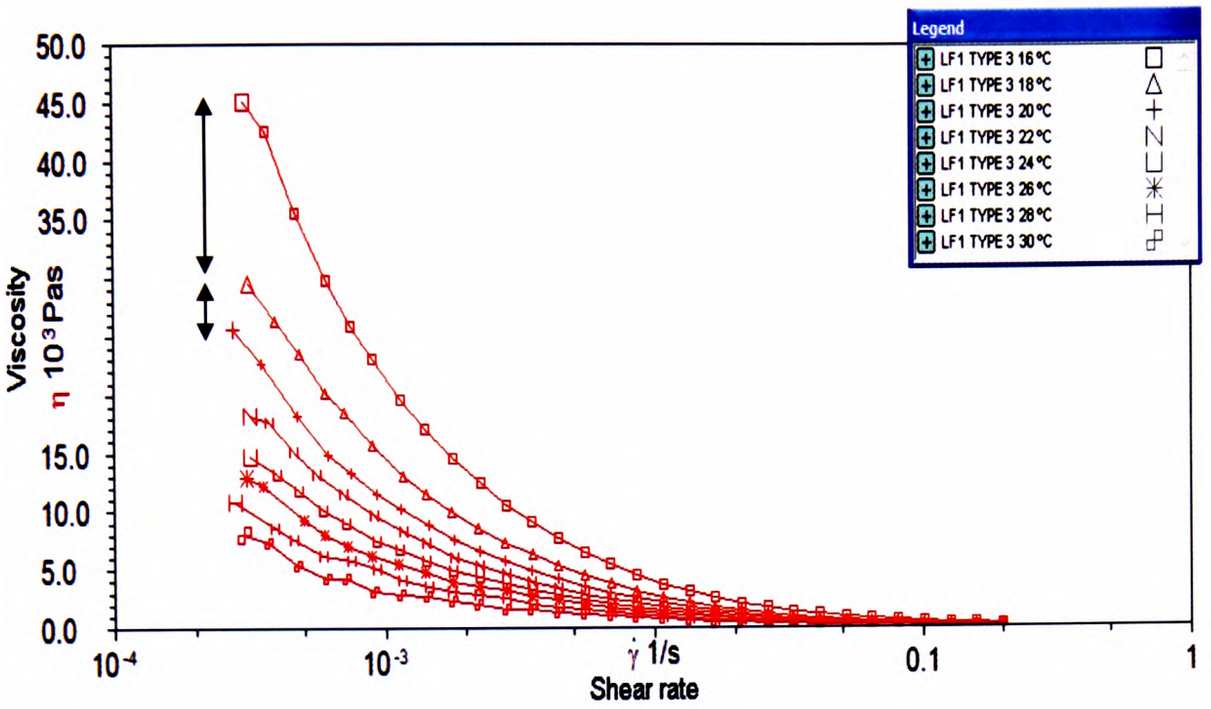

Figure 9.27: Average viscosity of LF1 Type 3 lead-free solder pastes at various temperatures and shear rates using Bohlin rheometer.

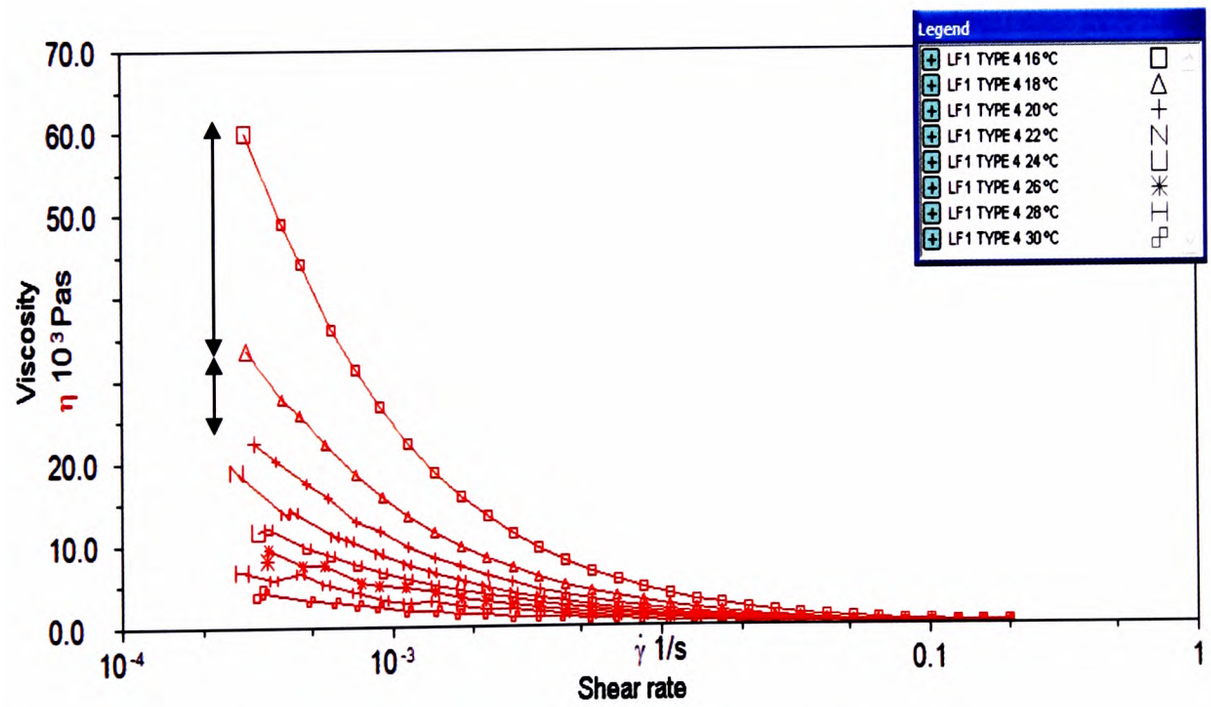

Figure 9.28: Average viscosity of LF1 Type 4 lead-free solder pastes at various temperatures and shear rates using Bohlin rheometer.

The study of solder paste viscosity at lower temperatures using a rheometer was not conducted as it is difficult to bring the temperature of the water-cooled Peltier plate system to any temperature significantly less than room temperature and this may render the results invalid because of a sample's extended period of exposure to room conditions and constant shear from the plate. (Increasing the temperature beyond room temperature and then bringing it back to room temperature is, however, much easier.) Freezing the sample to -45°C using a freezer cabinet was also considered, but sample removal from the bottle is not possible at such a temperature.

It is important to note that the significant change in viscosity due to the temperature is better observed at very low shear rate ($<0.001 s^{-1}$). Higher viscosity is observed at low temperature due to the thermal shrinkage. At low temperature, the solder paste may reduce in volume, bringing the solder particles closer together. This increases the chances that they rub against one another when the solder paste is being sheared. For the very brief moment when the particles rub, the intermolecular forces come into action and the resultant is greater resistance to flow. Hence, higher viscosity is observed at low temperature.

9.3.5. Viscosity measurements for solder pastes with different volumes of flux

a) Ultrasound measurements

In this part of the study, the solder pastes used previously to study the effect of temperature on ultrasound viscosity were once more used. The purpose was to study how the changes in packing fraction (due to flux addition) affect the ultrasound viscosity measurement. The test was conducted by diluting the solder pastes by the addition of incremental amounts of flux to the solder paste samples.

This experiment may be useful to solder paste manufacturers as it may help them to formulate their solder paste by allowing them to add the correct amount of flux to reach the desired viscosity of solder paste during the mixing process. Alternatively, it

can be used to provide the correct amount of solder particles to be added to increase the viscosity of the paste.

As shown in Figure 9.29 and Figure 9.30, the addition of flux to the solder paste resulted in different responses relating to ultrasound attenuation and ultrasound velocity. Both Type 3 and Type 4 pastes show an increase in ultrasound attenuation and a decrease in ultrasound velocity. The increase in ultrasound attenuation with increasing flux content could be due to the increasing amount of air bubbles trapped by the flux (see Figure 9.32). The ultrasound viscosity result shown in Figure 9.31 was obtained using Equation 8.20 – but the viscosity values shown in Figure 9.31 need to be downscaled by 1000 times to match the viscosity obtained using a rheometer.

One significant finding from this experiment was that once the added flux became more than 25% of the total volume of the solder paste, the viscosity of the solder paste would not reduce significantly further. It was observed that initially the solder paste is very sticky and would not drip when it was scooped; but once 10g (25%) of flux was added, the solder paste started to drip. This highlights how the strength of the intermolecular forces of the solder particles affects the viscosity of the solder paste. At low flux volume, most of the solder particles are always in contact with one another since the packing fraction is high, allowing the intermolecular forces to come into action – stronger intermolecular forces lead to higher viscosity. However, at high flux volume, most of the particles are spaced apart (low packing fraction) and only come into contact with one another occasionally when the solder paste is being sheared. This very brief instance of occasional contact is the reason that the solder paste sample with a high volume of flux is able to maintain its viscosity at 82kPa.s (see Figure 9.31).

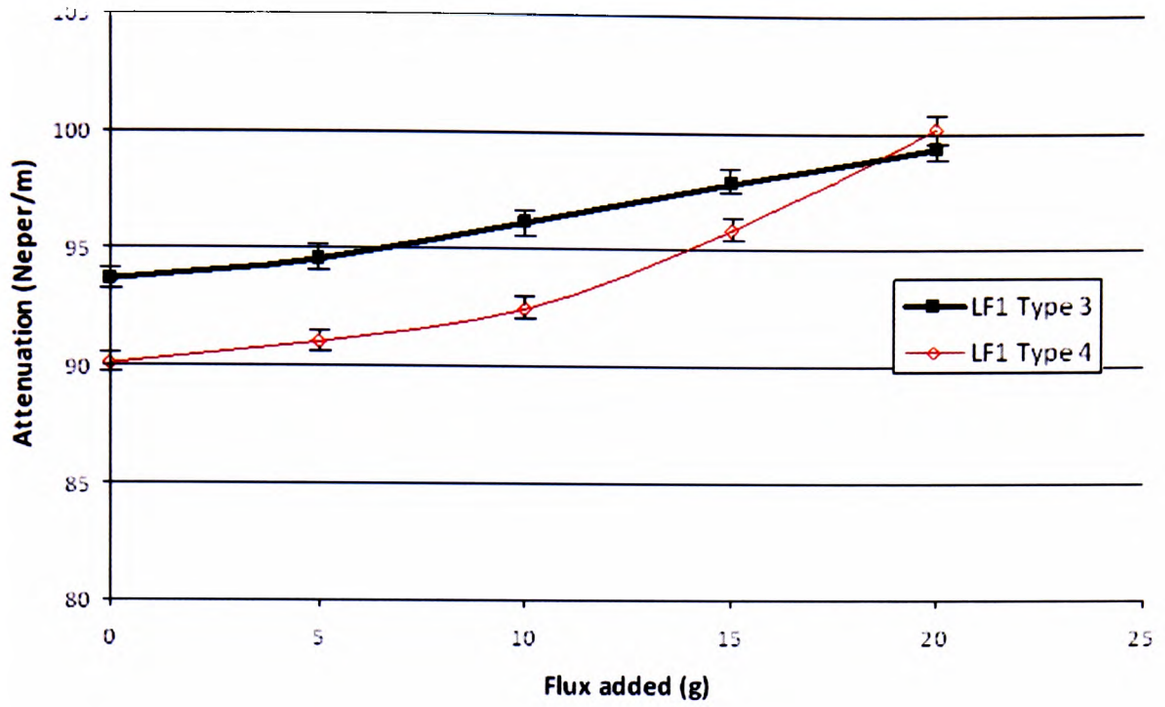

Figure 9.29: Effect of flux content on ultrasound attenuation on LF1 Type 3 and Type 4 lead-free solder pastes at 40kHz.

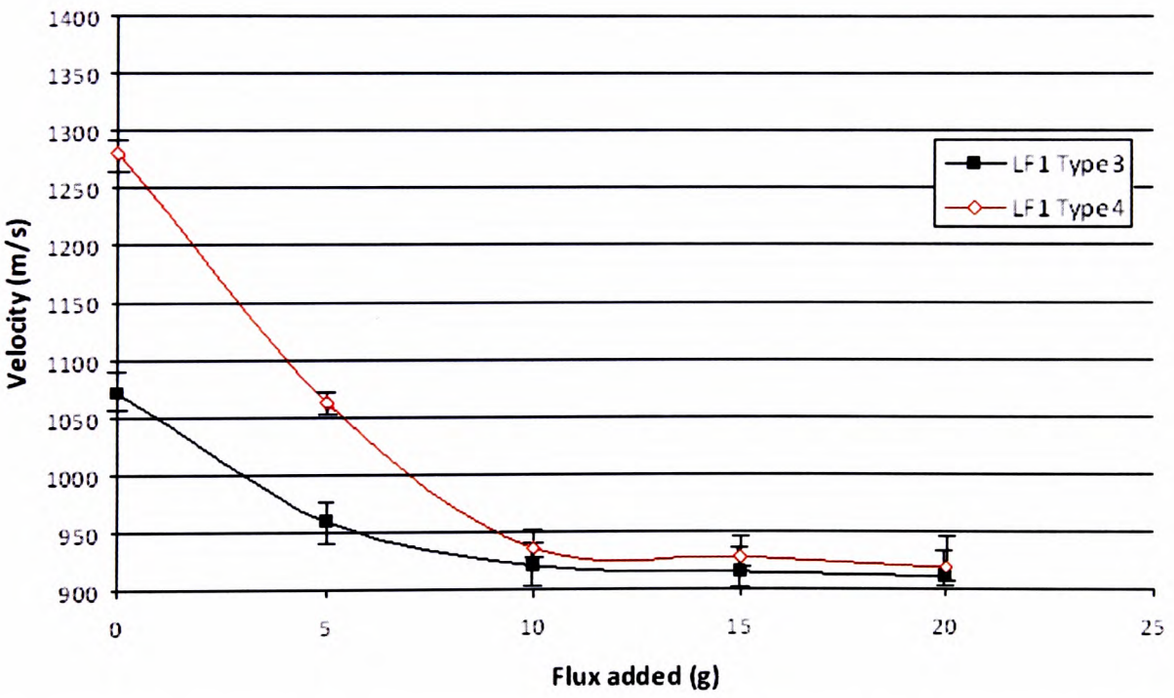

Figure 9.30: Effect of flux content on ultrasound velocity on LF1 Type 3 and Type 4 lead-free solder pastes at 40kHz.

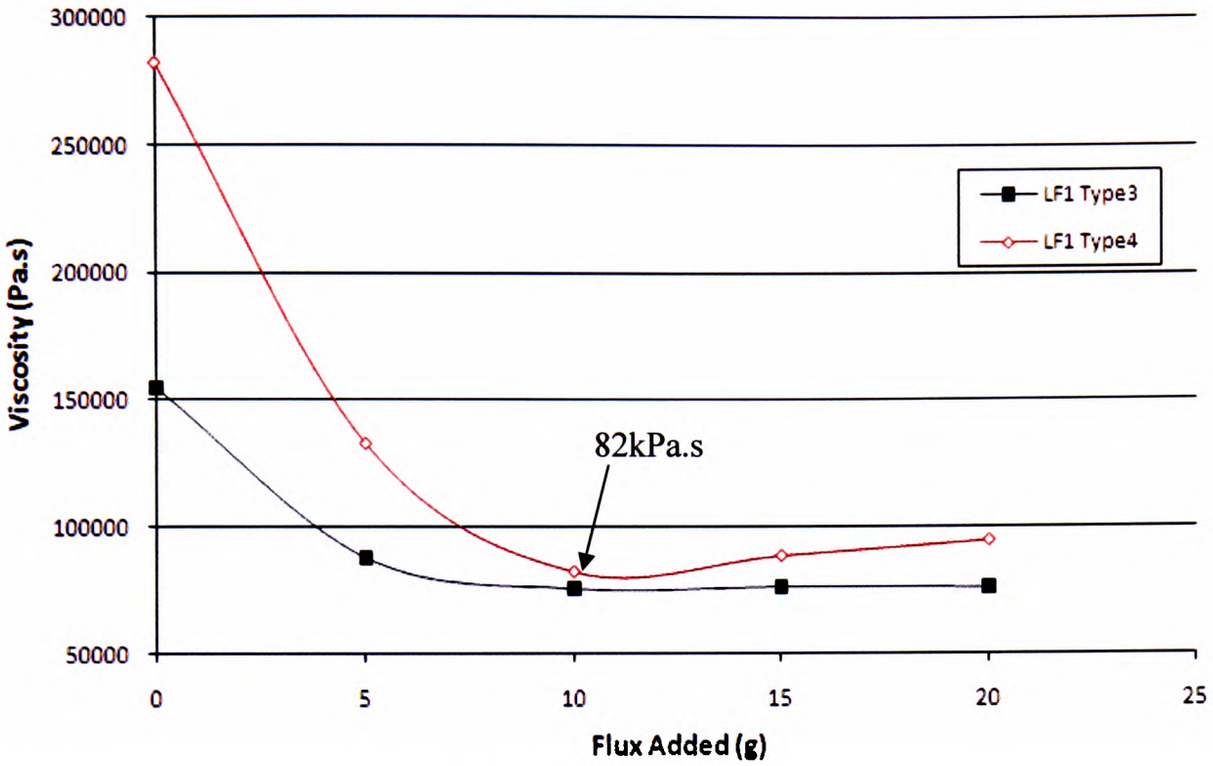

Figure 9.31: Effect of flux content on ultrasound viscosity on LF1 Type 3 and Type 4 lead-free solder pastes at 40kHz.

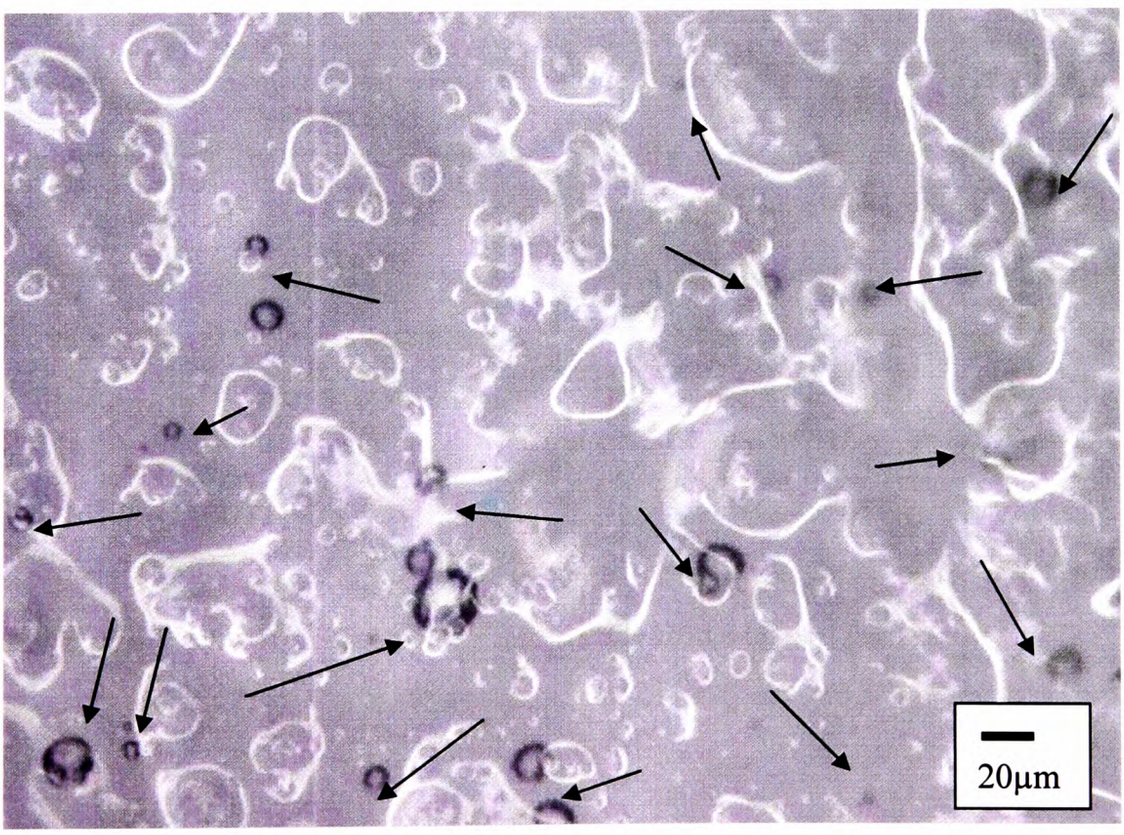

Figure 9.32: Air bubbles trapped in flux medium.

b) Rheometer measurements

The rheometer results for solder pastes with different flux content, shown in Figures 9.33–9.35, agree with the results shown in Figure 9.31. The results indicate that the initial addition of flux significantly reduces the viscosity of the solder pastes, by 15kPa.s. Subsequent addition of a similar amount of flux continued to reduce the viscosity of the solder pastes but not as significantly as the initial addition. This is considered to be because the intermolecular forces of the pastes with high flux volume are weaker because most of the particles are separated (low packing fraction) and only come into contact with one another when the solder paste is being sheared.

The probability of the solder particles coming into contact with one another while it is being sheared dictates in practice the viscosity of the solder paste. When a material is being sheared, the molecular bonds stretch and break. Continuous shearing reduces the viscosity of the material because more and more bonds are being broken. As a result of the intermolecular forces, most of the high-viscosity material would require a relatively high shear rate to break the bonds, thereby drastically reducing the viscosity.

It is shown in Figures 9.33 and 9.34 that, initially, LF1 Type 3 solder paste is more elastic than the LF1 Type 4 paste. This is indicated by the flat-plateau curve before flux was added. After the flux has been added, it can be seen that the solder paste is becoming more and more plastic, as indicated by the slope on the curve when the solder paste is being sheared within a shear-rate range of $0.001s^{-1}$ to $0.01\ s^{-1}$.

Elasticity at low shear rates normally represents stability, so that the solder paste maintains its shape after being dispensed. Moreover, plasticity at high shear rates represents how easily the paste flows into the apertures during the printing stroke. The combination of both of these properties in a solder paste reflects the paste being a paste of desirable characteristics.

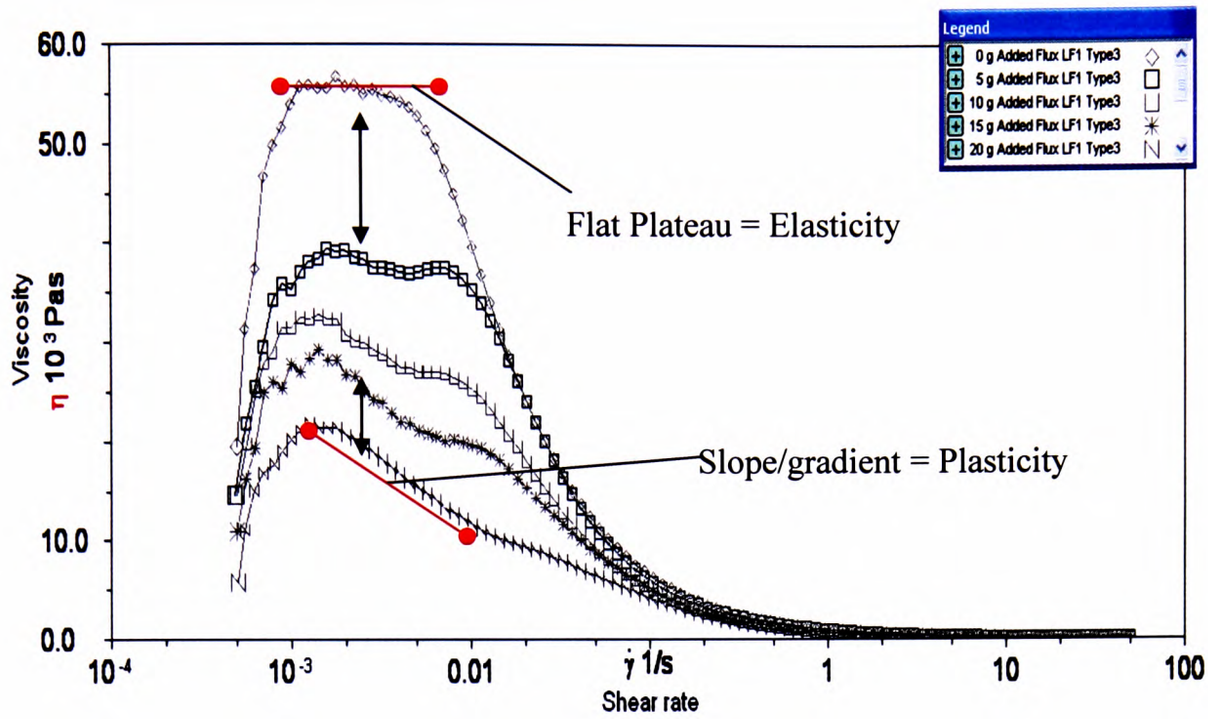

Figure 9.33: Average viscosity of LF1 Type 3 lead-free solder pastes with different amounts of added flux using Bohlin rheometer.

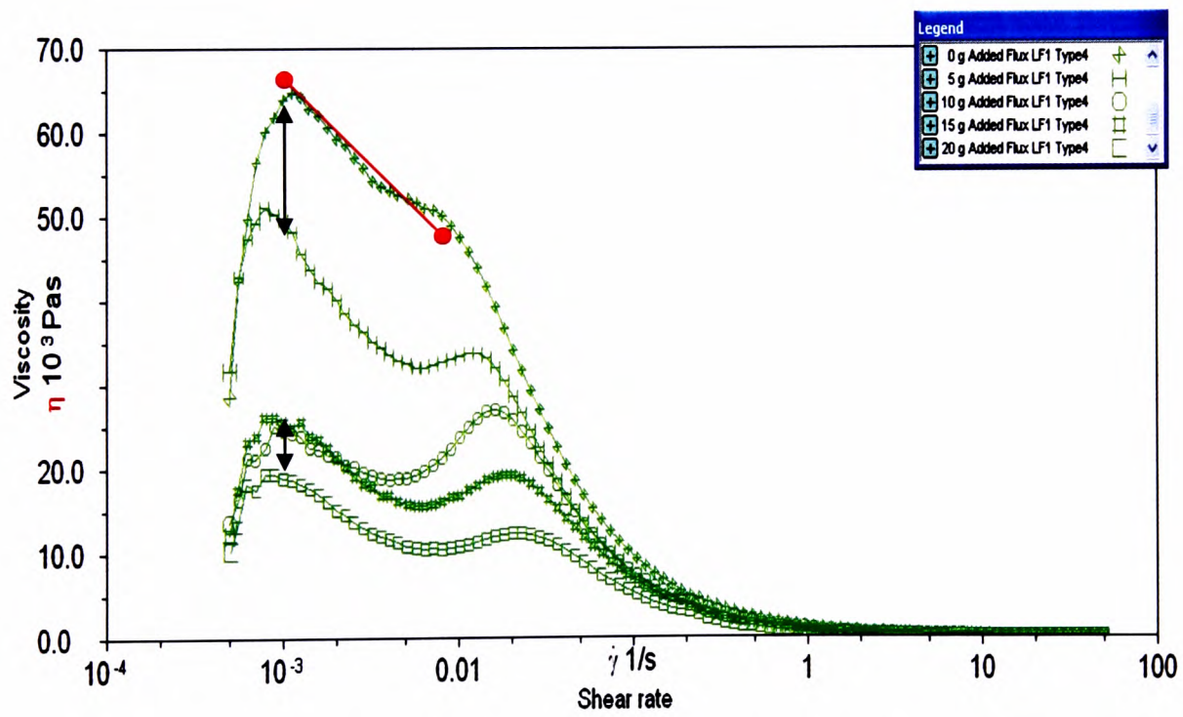

Figure 9.34: Average viscosity of LF1 Type 4 lead-free solder pastes with different amounts of added flux using Bohlin rheometer.

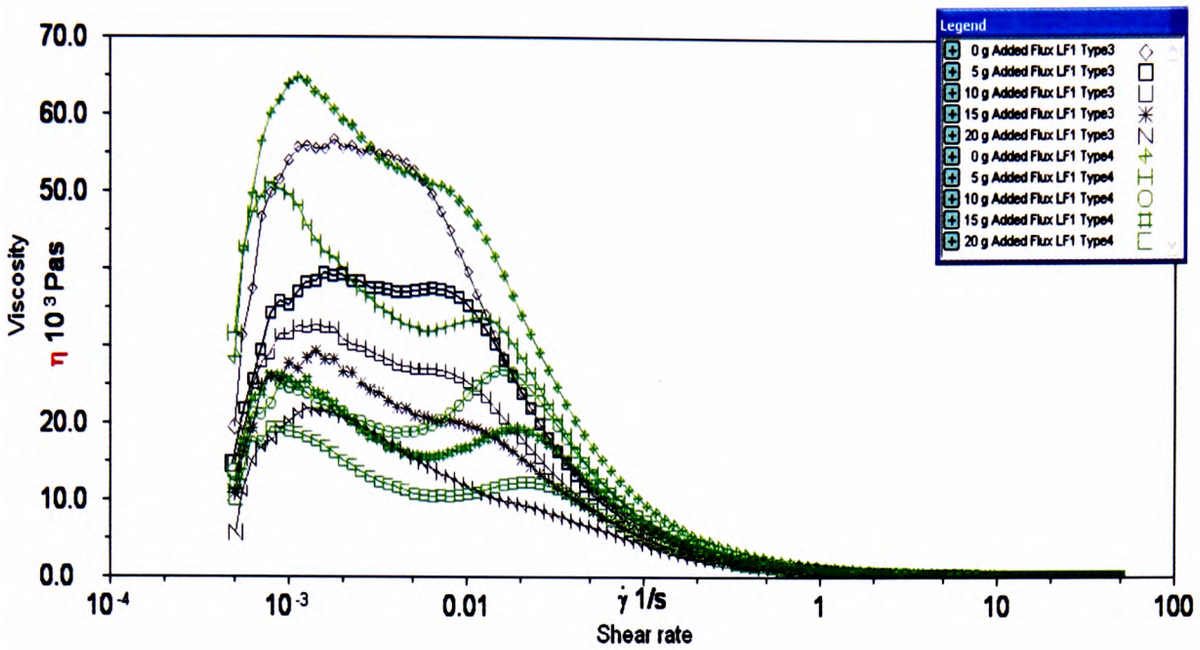

Figure 9.35: Average viscosity of LF1 Type 3 and Type 4 lead-free solder pastes with different amounts of added flux using Bohlin rheometer.

9.4. Conclusions

The viscosity of solder paste is governed by the intermolecular forces between the solder particles and the flux. The strength of these intermolecular forces depends on the probability of these particles rubbing up against one another while the paste is being sheared. The ultrasound viscosity results obtained are comparable to the rheometer viscosity results or to the viscosity provided by the solder paste manufacturer if the results are downscaled. The downscaling factor is dependent upon the shear rate of the measured viscosity i.e. 1000 times to match the rheometer's viscosity at $1s^{-1}$ and 4330 times for $6s^{-1}$. The ultrasound technique produced consistent results and was also proven to work at low temperatures. Based on the foregoing, it can be concluded that the ultrasound technique is a viable alternative to using a rheometer.

The ultrasound technique may be used to help solder paste manufacturers to add the correct amount of flux or solder particles to their paste in order to reach a desired viscosity.

CHAPTER 10

CONCLUSIONS AND SUGGESTIONS FOR FUTURE WORK

10.1. Introduction

The work reported in this thesis is concerned with the use of ultrasound techniques to provide a quick and simple solution for the analysis of solder paste quality, which is normally characterised through the measurement of viscosity.

The motivation for this study came about because of a repeatability issue with conventional rheological measurement technique using a viscometer or rheometer (see Section 1.4). Apart from the equipment settings, this repeatability issue is assumed to be associated with the sample collection and preparation, in which the process can irreversibly alter the structure and flow behaviour of the sample. Additionally, the conventional technique is a very time-consuming and daunting task, and it requires trained personnel to operate and interpret the test results. The non-destructive and non-intrusive features of ultrasound techniques make such techniques very attractive because the quality-control sampling of each and every bottle of solder paste during manufacture could be performed, rather than the currently implemented random sampling system of selecting two bottles of solder paste from each production batch.

10.2. Conclusions of this thesis

This thesis has demonstrated the utilisation of ultrasound techniques to provide a rheological measurement for solder paste. This was achieved by studying the technique theoretically (see Chapters 3–5) and experimentally (see Chapters 6–9) through critical analysis of the application of the techniques in various materials, such

as cement, polymers, slurry food products, beverages, cosmetic pastes and cream drug products.

The novelty of this work lies in the fact that it is able to measure the viscosity of materials when they are in a static condition (non-flowing system), unlike other techniques that require to make the material in a flowing condition in order to measure its viscosity. The idea was developed from the use of ultrasound as a flow meter, in which the flowing material inside a pipe at a certain flow rate should also possess a certain viscosity at a certain ultrasound attenuation or ultrasound velocity. The author's approach was to use the ultrasound wave to cause the material to vibrate, and then to measure the signal that passed through the sample in a static condition and compare the ultrasound measurements (attenuation and velocity) against the ultrasound measurements of Newtonian materials of known viscosity values. Material with higher viscosity usually has higher packing fraction, hence stronger intermolecular forces and higher viscosity (see Section 9.35). The ultrasound technique developed by the author was found to be more reproducible than the measurement performed using a rheometer because the ultrasound is capable of measuring the viscosity of materials at rest non-destructively. Hence, does not require a fresh load of sample to repeat the test. As non-Newtonian materials' viscosity are sensitive to the applied shear (see Figure 1.7), it is difficult to obtain the true viscosity value (viscosity at rest condition) of the material using a rheometer. If the ultrasound viscosity measurement were solely based on the ultrasound attenuation measurement only, deviation in reproducibility measurements could be kept to as low as 2% (±0.5Neper/m). Regarding the issue of the downscaling factor reported in the thesis, the downscaling factor can be easily integrated into the software to eliminate the discrepancy between the ultrasound measurements and rheometer measurements. The downscaling issue arose because Newtonian fluids up to such a viscosity of the solder paste were not available. The technique developed by the author has been proven to be feasible to be built as a commercial easy-to-use and reliable technique for measuring solder paste viscosity.

Although there was an example of indirect use of ultrasound to obtain the viscosity of Newtonian liquids, such as orange juice and sugar solution, getting the technique to

work with solder paste materials is viewed as a challenge. This is because solder pastes have extremely high viscosity, contain metal particles and are non-Newtonian in nature. There are no known natural Newtonian materials with viscosity as high as that of solder paste.

It was realised that, apart from the measurement of the viscosity of materials, ultrasound techniques may be used to directly identify batch-to-batch variation (Jaafar 1996 and Álava et al 2007) through the measurement of ultrasound attenuation. This is because variations in materials (packing fraction and chemical structure) cause different levels of ultrasound attenuation according to the amount of ultrasound wave being scattered (see Chapter 3). Although developed for investigating solder paste, the ultrasound viscosity measurement described in this thesis, and its ability to detect batch-to-batch variation, may be applicable for other materials too, such as those encountered in the paint, food and pharmaceutical industries. The use of this ultrasound technique in such industries could improve quality control and consistency of the product during manufacturing processes.

It has been demonstrated using the ultrasound technique described in this thesis that in order to achieve good printing results with solder paste, its viscosity must be in the region of 500kPa.s to 900kPa.s at the test frequency of 40kHz (see Figures 9.8 and Table 9.2). Direct ultrasound attenuation measurements may also be used as a quick go/no-go tool for predicting printing quality. The author did not use the 'look-up table' approach for predicting viscosity as the range of the Newtonian viscosity standard up to the viscosity those of the solder pastes were not available. The 'look-up table' approach might be more reliable than using a formula with a correction factor. This is because a look-up table may be tailor made for a very specific material, directly correlating the viscosity of the material against the corresponding ultrasound attenuation and velocity.

This thesis also studies the effect of temperature towards the ultrasound measurements of solder paste and flux. The results in terms of viscosity indicate an increase in viscosity as the temperature is lowered. The ultrasound viscosity measurement may be correct in its own right owing to its non-destructive and non-intrusive feature, which

cannot be simulated through rheometer measurement. This claim is supported by the fact that test results of the same samples using ultrasound and rheometer show a similar trend in viscosity measurement.

10.3. Recommendation for future work

The author would like to recommend an improvement for the algorithm to capture time of arrival of the first pulse of an ultrasound wave. The author has attempted to write an algorithm to detect time of arrival of the signal at the root of the first peak. The algorithm was designed to locate the first peak point and identify it as the first pulse. However, the algorithm cannot be successfully implemented as the first peak is not always the maximum point, often the maximum point is at the second or third peak. In this case, setting an upper threshold value would prematurely end the recording of the data, truncating the attenuation data after the triggered point. It will be a real challenge to write an algorithm that can detect time of arrival at the root of the first peak (see Figure 10.1) without having it mistakenly record the noise and without therefore assuming the noise to be the first time of arrival of the true signal. As a result, the algorithm used in this project was written to capture the first highest maximum or minimum (ie the so-called maximus point), not the first peak.

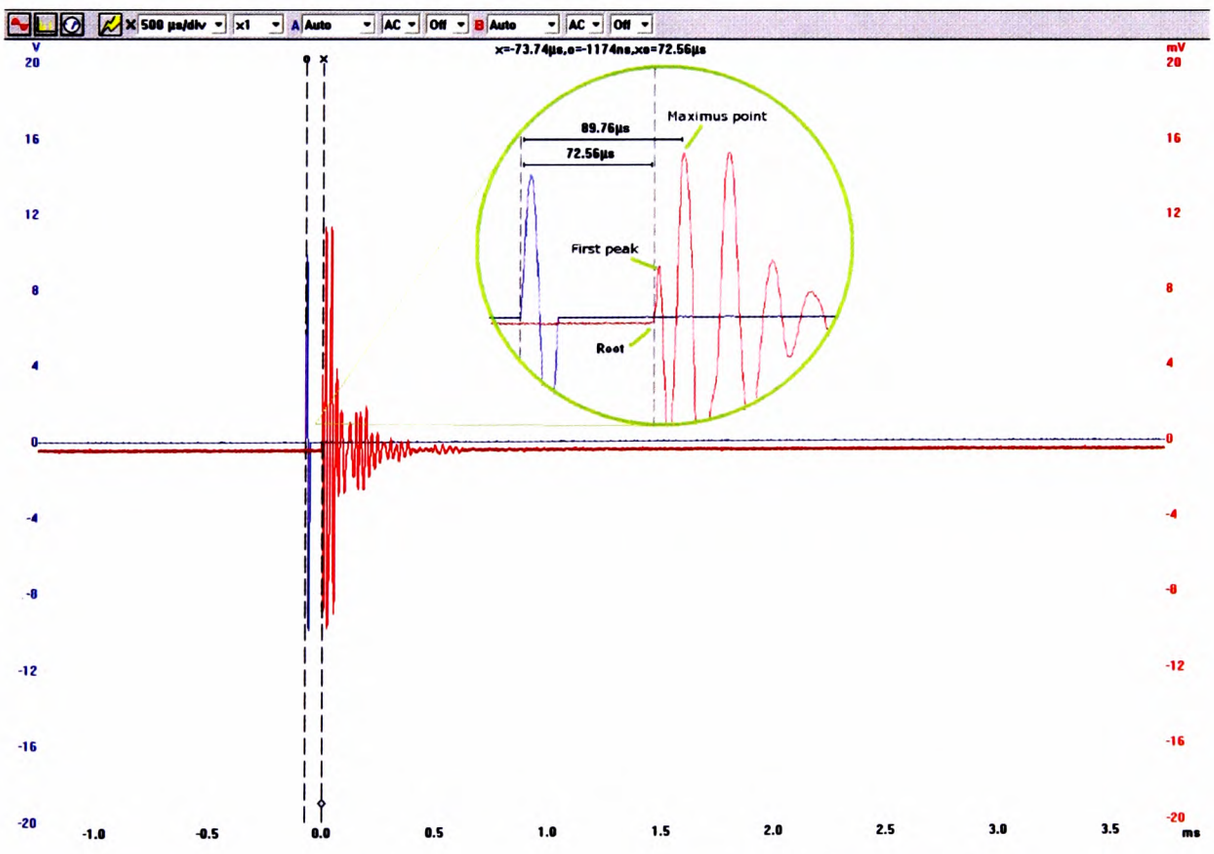

Figure 10.1: Illustration of capturing time of arrival at root of first peak.

The provision of an algorithm that can capture time of arrival at first peak should reduce the deviation in the measurements of ultrasound velocity, possibly to 1% of the average value. With this kind of algorithm, it might be possible to conduct relatively accurate measurements based on velocity. If this is achieved, it will also improve the accuracy of the ultrasound viscosity.

In addition to that, since the use of ultrasonic for solder paste material is new, there are some areas that are open to be explored further. Possible areas to be explored are set out next:

a) Predicting ultrasound viscosity from a 'look-up table'

If Newtonian standard fluids with the same range of viscosity to that of the material to be investigated are available, a complete 'look-up table' based on the ultrasound attenuation and velocity may be produced. This 'look-up table' may be used to provide direct ultrasound viscosity measurement.

There is an alternative to producing this 'look-up table' without the Newtonian viscosity standard fluids. This 'look-up table' can be produced, if it were possible to produce/alter the material to be investigated so that it consists of a series/range of the same material with different viscosity. By recording these viscosity values along with the ultrasound attenuation and velocity, one can produce a contiguous 'look-up table'. Because temperature has an effect on the viscosity, the table may be useful for a specific temperature only. To provide a comprehensive usefulness, several tables might be needed, possibly one for every decade of temperature i.e. 5°C, 15°C, and 25°C.

b) Investigation using shear wave transducer

Shear wave transducers were not used in the experiment as there have been many reports documenting that shear waves cannot easily travel in a liquid. This fact is also highlighted in the acoustic properties of materials provided in Appendix B. It is

shown that there is no recorded value for the shear wave velocity of liquid materials such as water, motor oil, glycerine and polystyrene. From a search of the literature, it has been found that when a shear wave transducer is used, the wave only survives on a very thin layer of the surface of the liquid being tested. This means that an ultrasonic shear wave would not travel the full breadth of the material being tested. It is for this reason that no shear wave transducers were procured for the experiment. However, since solder paste is a semi-solid material there is a possibility that shear waves might be able to travel the whole breadth/thickness of a sample under test.

c) Investigation of solder paste using ultrasound frequency spectra.

During the experiments for this thesis, the author observed a unique frequency spectrum for every material tested. The samples tend to emit backscatter signal (multi frequency) different to the original frequency signal sent from the signal generator. But for identical materials, the frequency peaks are similar. This indicates that the ultrasound technique may be used like XRF (x-ray fluorescence) or XRD (x-ray diffraction) for identifying the chemical composition of unknown materials – see Figures 10.2–10.5.

This area was not investigated any further as the focus of the work of this PhD thesis was aimed at using ultrasound to provide a more reliable and easier viscosity measurement technique than the rheometer.

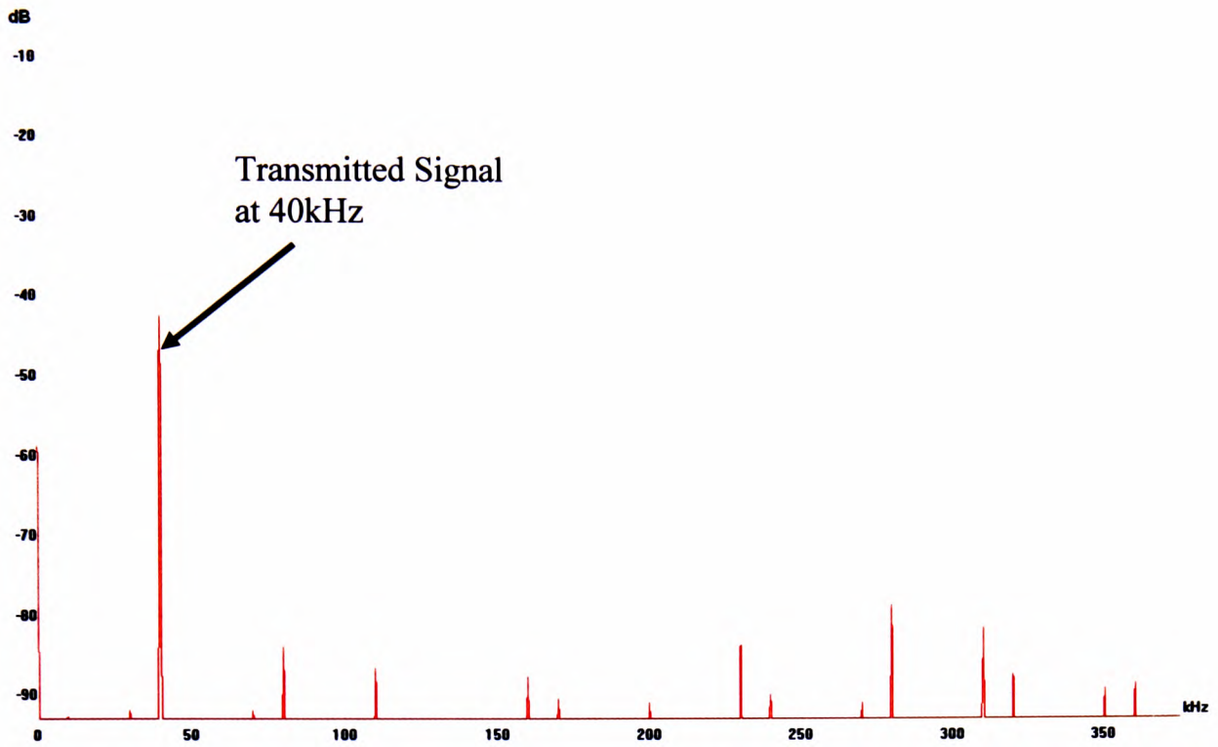

Figure 10.2: Illustration of frequency spectra of water.

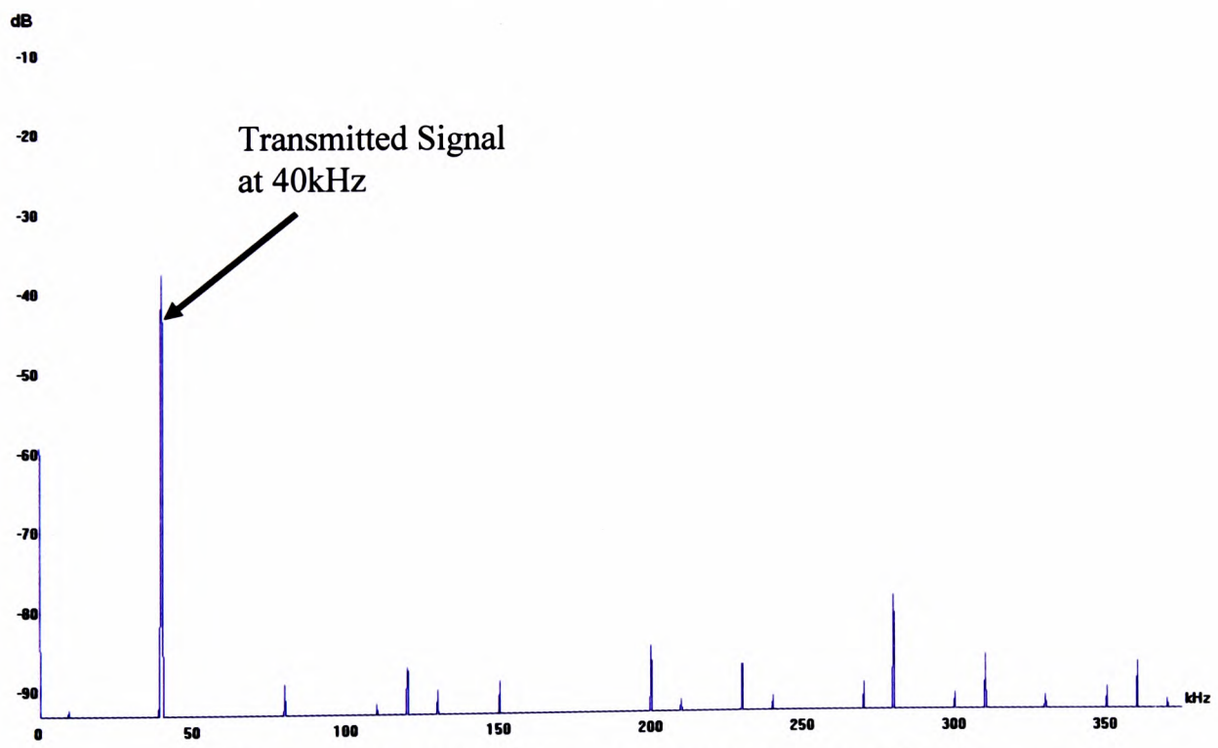

Figure 10.3: Illustration of frequency spectra of milk.

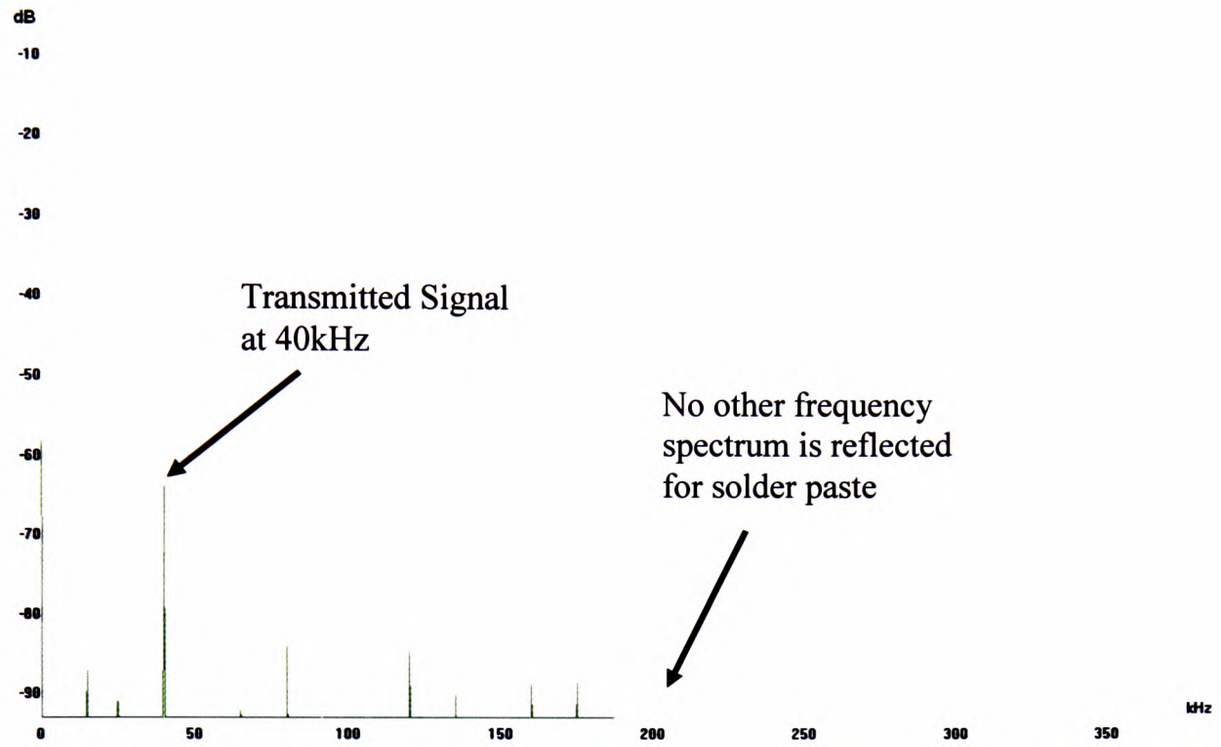

Figure 10.4: Illustration of frequency spectra of solder paste.

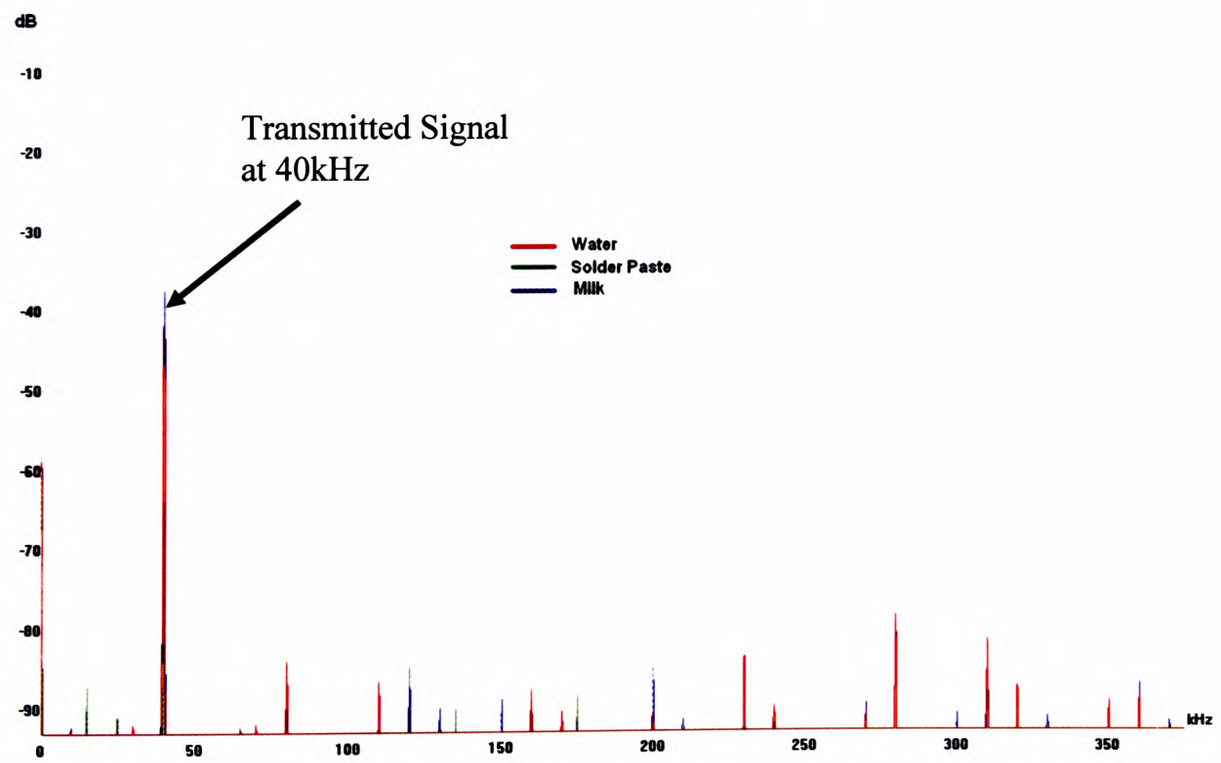

Figure 10.5: Illustration of combined frequency spectra of water, solder paste and milk.

d) Integrated close-loop feedback to solder paste manufacturing line.

Since it is possible to use ultrasound to predict the viscosity or the variation of the solder paste in a static condition, the ultrasound technique can be integrated into the solder paste manufacturing line to provide a closed-loop feedback to maintain a consistent solder paste quality. The feedback can be used to adjust the amount of a particular size of solder particle or flux to be added to the solder paste.

e) Detail study of ultrasonic response of particle size, particle distribution and packing fraction of solder paste materials.

Although the author did conduct experiments using solder pastes of different particle distribution (see Section 9.3.1) and flux (see Section 9.3.5) this range of samples only consist of two different types of particle distribution. Findings from the case studies in Chapter 5 indicate that particle size, particle distribution and packing fraction of solder pastes may significantly affect the ultrasonic response of the material. The author did not investigate in detail the effect of particle size, particle distribution and packing fraction of the solder paste as the author has no access to producing solder powders and flux formulations. Formulating the solder paste to specific particle size, particle distribution or packing fraction in order to study the ultrasonic response can be easily done, but the paste may be non-printable if the paste were formulated without the knowledge of the flux. Altering the particle size, particle distribution or packing fraction would require re-formulation of the flux in order to get a non-spatter printable solder paste (Lee, 2002).

In terms of rheological measurement using a Brookfield viscometer or a rheometer, the author would also like to suggest that solder paste manufacturers should use dual shear rate to quantify the viscosity of the solder paste. This dual shear rate should incorporate one low shear and one high shear rate for measuring the viscosity of some solder paste. This is necessary as a high shear rate represents the viscosity of the paste when the solder paste is flowing through the apertures, while a low shear rate represents the viscosity of the paste when it has been deposited onto the PCB, which

relates to the tendency of slumping. The author recommends the use of dual shear rate of

$0.1s^{-1}/10s^{-1}$ for rheometer use and 1rpm/10rpm for Brookfield and Malcom viscometers when measuring the viscosity of solder pastes.

References

Aggelis, D.G., and Philippidis, T.P., 2004.Ultrasonic wave dispersion and attenuation in fresh mortar. *NDT&E International*, 37, p. 617–631.

Álava, J.M., Sahi, S.S., García-Álvarez, J., Turó, A., Chávez, J.A., García, M.J. and Salazar, J., 2007. Use of ultrasound for the determination of flour quality, *Ultrasonics*, 46, p. 270–276.

Alig, I., and Lellinger, D., 2000. Ultrasonic methods for characterizing polymeric material. *Chemical Innovation*, 30(2), p. 12–18.

Alig, I., Steeman, P.A.M., Lellinger, D., Dias, A.A., and Wienke, D., 2005. Polymerization and network formation of UV-curable materials monitored by hyphenated real-time ultrasound reflectometry and near-infrared spectroscopy (RT-US/NIRS). *Progress in organic coatings*, 55(2), p. 88–96.

Allegra, J.R. and Hawley, S.A., 1972. Attenuation of sound in suspensions and emulsions: theory and experiments. *J. Acoust. Soc. Amer.*, 51(5), p. 1545.

Altberg, W., 1907. Short acoustic waves with the spark discharge of condensators. *Annalen der Physik*, 23 (7), p. 267–276.

Anderson, R., Gadala-Maria, F., and Kolli, V.G., 1995. Solder paste rheology and fine pitch slump. *J. Surface Mount Tech.*, 8(3), p. 12–18.

Anugonda, P., Wiehn, J.S., and Turner, J.A., 2001. Diffusion of ultrasound in concrete. *Ultrasonics*, 39, p. 429–435.

ASTM D4683. *ASTM D4683 - 04 Standard Test Method for Measuring Viscosity at High Shear Rate and High Temperature by Tapered Bearing Simulator.* http://www.astm.org/Standards/D4683.htm. Last accessed 14 Apr 2010.

Auld, B.A., 1973. *Acoustic fields and waves in solids*, Vol. 1. A Wiley-Interscience Publication, United States. Chapter 6, p. 163–190.

Baluch, D., and Evans, D., 1995. Rheological simulation of solder paste slump. *Cookson Tech. Centre Insight Journal*, 1(2), p. 4–6.

Ballentine, L.E., 1998. *Quantum Mechanics: A modern development.* World Scientific. p. 421–462.

Bao, X., Lee, N.C., Raj, R.B., Rangan, K.P., and Maria, A., 1996. Engineering solder paste performance via controlled stress rheology analysis. *SMI Proceedings,* San Diego, p.717–729.

Barnes, H.A., 2000. *A handbook of elementary rheology*. Institute of Non-Newtonian Fluid Mechanics, University of Wales.

Barnes, H.A., Hutton, J.F., and Walters, K., 1989. An introduction to rheology, *Elsevier*, Amsterdam, p. 122.

Batchelor, G.K., 1974. Ann. Rev. Fluid Mech. 6, p. 227.

Batchelor, G.K., 1977. The effect of Brownian motion on the bulk stress in a suspension of spherical particles. *J. Fluid. Mech.*, 83, p. 97–117.

Belkić, D., 2003. *Principles of Quantum Scattering Theory*. CRC Press, UK. p. 74–95.

Berrimann, J.R.S., 2004. The application of air-coupled ultrasonic systems and signal ultrasonic systems and signal processing to the interrogation of concrete. *PhD Thesis. Warwick University*, UK.

Betatek Inc., 2008. Available from www.betatekinc.com

Biot, M.A., 1956a. Theory of propagations of elastic waves in a fluid-saturated porous solid: I. Low-frequency range. *J. Acoust. Soc. Amer.*, 28(2), p. 168–178.

Biot, M.A., 1956b. Theory of propagations of elastic waves in a fluid-saturated porous solid: II. Higher-frequency range. *J. Acoust. Soc. Amer.*, 28(2), p. 179–191.

Biot, M.A., and Willis, D.G., 1957. The elastic coefficients of the theory of consolidation. *J. Appl. Mech.*, 24(4), p. 594–601.

Billotte, C., Carreau, P.J., and Heuzey, M.C., 2006. Rheological characterisation of a solder paste for surface mount applications. *Rheologica Acta*, 45, p. 374–386.

Bingham, E.C., 1922. *Fluidity and Plasticity,* Mcgraw-Hill Book Co. Inc., New York.

Biquard, P., and Ahier, C., 1943. *Cahiers Phys.*, 15, p. 21.

Biwa, S., Watanabe, Y., and Ohno, N., 2003. Analysis of wave attenuation in unidirectional viscoelastic composites by a differential scheme. *Composites Sci. Tech.*, 63, p. 237–247.

Boschiero, L., 2005. Post-Galilean thought and experiment in Seventeenth-century Italy: The life and work of Vincenzio Viviani, *History of Science*, 43, p. 77-100.

Bouhadjera, A., and Bouzrira, C., 2005. High-frequency ultrasonic testing of young cement-based materials using the 'prism technique'. *NDT&E Int.*, 38, p. 135–142.

Boyle, R., 1660. *New Experiments Physico-Mechanicall, Touching the Spring of the Air and its Effects*. Oxford University Press.

Brookfield Engineering, 2008. Available from www.brookfieldengineering.com

Brown, E.C, 1998. Ultrasonic monitoring of polymer melt extrusion. *PhD Thesis. Bradford University*, UK.

Brown, P.A., 1988. Ultrasonic studies of colloidal systems containing macro molecules. *PhD Thesis. Salford University*, Manchester, UK.

Buckingham, Edgar, 1914. On physically similar systems: Illustrations of the use of dimensional analysis. *Phys. Rev.*, 4, p. 345.

Burr, D., 1997. Solder paste inspection: process control for defect reduction. *International Proceedings of Test Conference*, 1–6November 1997, Washington D.C., U.S., p. 1036.

Cady, W.G., 1920. *Piezo-electric Resonator*. United States Patent 1450246, 28 January 1920.

Carey, F.A., and Sundberg, R.J., 2007. *Advanced organic chemistry Part A: Structure and mechanisms 5th ed.*. Springerlink, p. 8–18.

Carson, J.W., Royal, T.A., and Goodwill, D.J., 1986. Understanding and eliminating particle segregation problems. *Bulk Solids Handling*, 6, p. 139–144.

Chaix, J.F., Garnier,V., and Corneloup, G., 2006. Ultrasonic wave propagation in heterogeneous solid media: Theoretical analysis and experimental validation. *Ultrasonics*, 44, p. 200–210.

Challis, R.E., 1990. Digital signal processing applied to ultrasonic absorption measurements. *Ultrasonics*, 28(1), p. 5–15.

Challis, R.E., Tebbutt, J.S., and Holmes, A.K., 1998a. Equivalence between three scattering formulations for ultrasonic wave propagation in particulate mixtures. *J. Phys. D: Appl. Phys.*, 31, p. 3481–3497.

Challis, R.E., Wilkinson, G.P., and Freemantle, R.J., 1998b. Errors and uncertainties in the ultrasonic pulse-echo reflectometry method for measuring acoustic impedance. *Meas. Sci. Tech*, 9, p. 692–700.

Challis, R.E., Povey, M.J.W., Mather, M.L., and Holmes, A.K., 2005. Ultrasound techniques for characterizing colloidal dispersions. *Rep. Prog. Phys.*, 68, p. 1541–1637.

Chanamai, R., Herrmann, R., and McClements, D.J., 1998. The influence of flocculation on the ultrasonic properties of emulsions: experiment. *J. Phys. D: Appl. Phys*, 31, p. 2956–2963.

Chapman, J.R., 2001. Ultrasonic wave interactions with magnetic colloids. *PhD Thesis. Nottingham University*, UK.

Choi, D., 2002. Ultrasound propagation in various gases. *PhD Thesis. Warwick University*, UK.

Cohen-Tenoudji, F., Ahlberg, L.A., Tittmann, and B.R., Pardee, W.J., 1988. *High temperature ultrasonic viscometer*. United States Patent 4779452, 09 June 1986.

Colladon and Sturm. Telegraphing by Sound through Water. 1872. *New York Times*, 24 November.

Costello, B., 1997. The use of creep tests after preshear to predict the sagging and slumping properties of Multicore solders. *Multicore Report*.

Cross, M.M., 1965. Rheology of Non-Newtonian fluids: A new flow equation for pseudo-plastic systems. *J. Colloid Interface Sci.*, 20, p. 417–437.

Currie, M., Elyassi, A., Freeman, G., Warwick, M., and Wilding, I., 2001. *Lead-free solder paste.* United States Patent 6592020, 17 Oct 2001.

Damaj, W.T., 1990. Ultrasonic inspection of concrete structures to detect the condition of embedded steel components. *PhD Thesis. UMIST*, Manchester, UK.

Daniels, R., 2002. Ultrasonic velocity measurements of the shelf-life of topical formulations. www.*scf-online.com*, Issue 28. Last accessed 14 Apr 2010.

Döring, J., Stark, W., and Splitt, G., 1998. On-line process monitoring of Thermosets by Ultrasonic Methods. *Proceedings 7th European Conference on Non-Destructive Testing (ECNDT), 26–29May 1998, Copenhagen.* Available at www.ndt.net/article/ecndt98/material/159/159.htm. Last accessed 14 Apr 2010.

Dogan, N., 2003. Investigation of an in-line, non-destructive ultrasonic method to study flow and rheology of complex fluids. *PhD Thesis. University of California*, Davis, US.

Duff, A.W., 1898. The Attenuation of Sound and the Constant of Radiation of Air. Phys. Rev., 6(3), p. 129–139.

Dukhin, A.S. and Goetz, P.J., 2002. *Ultrasound for characterizing colloids*: Elsevier, p.101–117.

Duckhouse, H.L., 2006. The effect of sonication at different frequencies on microbial disinfection using hypochlorite. *PhD Thesis. University of Coventry*, UK.

Durairaj, R., 2006. Rheological characterisation of solder pastes and isotropic conductive adhesives (ICAS) for microsystems assembly technology. *PhD Thesis. University of Greenwich,* London, UK.

Dwyer, C., 2004. Ultrasonic analysis of selected meat and dairy colloids. *PhD Thesis. University College*, Dublin, Ireland.

Einstein, A., 1906. A New Determination of Molecular Dimensions. *Ann. Physik*, 19, p. 289–306.

Einstein, A., 1911. Correction to My Paper: "A New Determination of Molecular Dimensions". *Ann. Physik*, 34, p. 591–592.

Electronic Industry Alliance (EIA), http://www.eia.org

Epstein, P.S., 1941. On the absorption of sound by suspensions and emulsions. In contribution to applied mechanic, Theodore von Karman Anniversary volume, *CIT Pasadena*, p. 162–188.

Epstein, P.S., and Carhart, R.R., 1953. The absorption of sound in suspensions and emulsions: I. Water fog in air. *J. Acoust. Soc. Amer.*, 25(3), p. 553–565.

Euler L. 1757a. Principes géneraux du mouvement des fluides. *Mém. Acad. Sci. Berlin* 11(1755), p. 274–315. Reprinted in *Leonhardi Euleri Opera Omnia* Series 2, XII, p. 54–91. Available online from www.eulerarchive.org. Last accessed 14 Apr 2010.

Euler L. 1757b. Continuation des recherches sur la théorie du mouvement des fluides. *Mém. Acad. Sci. Berlin* 11(1755), p. 316–361. Reprinted in *Leonhardi Euleri Opera Omnia* Series 2, XII, p. 92–132. Available online from www.eulerarchive.org. Last accessed 14 Apr 2010.

Euler L. 1761. Principia motus fluidorum. *Novi Commentarii Acad. Sci. Petropolitanae* 6 (1756/7), p. 271–311. Reprinted in *Leonhardi Euleri Opera Omnia* Series 2, XII, p. 133–168. Available online from www.eulerarchive.org. Last accessed 14 Apr 2010.

Euler, L., 1765. *Theoria motus corporum solidorum seu rigidorum. "Theory of the motions of rigid bodies"* Available online from www.eulerarchive.org. Last accessed 14 Apr 2010.

Diepstraten, G., 2004. Introducing the 5 steps to successful lead-free soldering. *Dataweek Electronics and Communications Tech.* 7 Apr 2004. Available from http://dataweek.co.za/news.aspx?pklNewsId=13933. Last accessed 14 April 2010.

European Parliament, 2003. Directive 2002/95/EC of the European Parliament and of the Council of 27 January 2003 on the restriction of the use of certain hazardous substances in electrical and electronic equipment. *Official Journal* L 037, 13/02/2003, p. 19–23.

Fairley, P., 1992. Ultrasonic studies of foods containing air. *PhD Thesis*. University of Leeds, Leeds, UK

Farone, W.A., Sacher, R.F., and Fleck, C., 2002. *Acoustic viscometer and method of determining kinematic viscosity and intrinsic viscosity by propagation of shear waves.* United States Patent 6439034, 30 Oct 2002.

Farrow, C.A., Anson, L.W., and Chivers, R.C., 1995. Multiple scattering of ultrasound in suspensions, *Acustica*, 81, p. 402–411.

Farris, R.J., 1968. Prediction of the viscosity of multimodal suspensions from unimodal viscosity data. *Trans. Soc. Rheology*, 12(2), p. 281–301.

Ferguson, J. and Kemblowski, Z., 1991. *Applied Fluid Rheology*, Elsevier Applied Science, London, p. 47–133.

Fengler, P., Stark, W., Döring, J., and McHugh, J., 2004. Coupling of hidden ultrasound sensors to a moulding tool. *NDT.net*, 9(3). Available from www.ndt.net/article/v09n03/stark/stark.htm. Last accessed 14 Apr 2010.

Firestone, F.A., 1942. *Flaw detecting device and measuring instrument.* United States Patent 2280226, 21 Apr 1942.

Fisher, E., Hinerman, J.B, and Dixon, D., 2000. SMT adhesive deposition: The line to success. *SMT Magazine*, 14 (12). Available from www.electroiq.com/index/display/smt-article-display/89352/articles/smt/volume-14/issue-12/features/smt-manufacturing/smt-adhesive-deposition-the-line-to-success.html. Last accessed 14 Apr 2010.

Fletcher, J. and Hill, A., 2008. Making the connection - particle size, size distribution and rheology. Available from www.chemeurope.com/articles/e/61207/. Last accessed 25 Apr 2008.

Freemantle, R.J., and Challis, R.E., 1998. Combined compression and shear wave ultrasonic measurements on curing adhesive. *Meas. Sci. Tech.*, 9, p. 1–12.

Fulwyler, M.J., and Hatcher, W.C., 1976. *Method for producing uniform particles.* United States Patent 4162282, 22 April 1976.

Green, R.E., 1973. *Ultrasonic investigation of mechanical properties*, Academic Press, New York.

Grosse, C.U., Weiler, B., Herb, A., Schmidt, G., and Höfler, K., 1999. Advances in ultrasonic testing of cementitious materials. *In: "Werkstoffe und Werkstoffprüfung im Bauwesen - Festschrift zum 60. Geburtstag von Prof. Reinhardt" (Ed. Chr. Grosse), Hamburg: Libri-BOD.* p. 106–116.

Grosse, C.U., Reinhardt, H.W., 2000. Ultrasound technique for quality control of cementitious materials. *International Committee for Non-destructive Testing ICNDT. Proceedings of the 15th World Conf. on NDT, Rome.* Available from www.ndt.net/article/wcndt00/papers/idn232/idn232.htm. Last accessed 14 Apr 2010.

Grosse, C.U., Lura, P., Weiss, J., and Jensen, O., 2007. *Advances in construction materials 2007: Detection and analysis of microcracks in high-performance cementitious materials*, Berlin Heidelberg: Springer, p. 607–614.

Guericke, Otto von, 1672. *Experimenta Nova (ut vocantur) Magdeburgica De Vacuo Spatio*, Amsterdam.

Gülseren, I., and Coupland, J.N., 2007. Ultrasonic velocity measurements in frozen model food solutions. *Journal of Food Engineering*, 79, p. 1071–1078.

Guo, Z., Jones, A. G., Hao, H., Patel, B., and Li, N., 2007. Effect of ultrasound on the heterogeneous nucleation of BaSO4 during reactive crystallization. *J. Appl. Phys.*, 101(5).

Harwood, R., 2000. Ultrasonic examination of bitumen filled cable boxes. *PhD Thesis. UMIST*, UK.

He, D., Ekere N.N., Salam, B., Rajkumar, D., and Jackson, G., 2003. Monte Carlo study of solder paste microstructure and ultra-fine-pitch stencil printing. *Journal of Materials Science: Materials in Electronics*, 14(8), p. 501–506.

He, D. and Ekere N.N., 2004. Effect of particle size ratio on the conducting percolation threshold of granular conductive-insulating composites. *J. Phys. D: Appl. Phys.*, 37, p. 1848–1852.

Hernández, M.G., Izquierdo, M.A.G., Ibánez, A., Anaya, J.J, and Ullate, L.G., 2000. Porosity estimation of concrete by ultrasonic NDE. *Ultrasonics*, 38, p. 531–533.

Hernández, M.G., Anaya, J.J, Izquierdo, M.A.G., and Ullate, L.G., 2002. Application of micromechanics to the characterisation of mortar by ultrasound. *Ultrasonics*, 40, p. 217–221.

Hernández, M.G., Anaya, J.J., Sanchez, T.and Segura, I., 2006a. Porosity estimation of aged mortar using a micromechanical model. *Ultrasonics*, 44, p. 1007–1011.

Hernández, M.G., Anaya, J.J, Ullate, L.G., Cegarra, M., and Sanchez, T., 2006b. Application of micromechanical model of three phases to estimating the porosity of mortar by ultrasound. *Cement and Concrete Research*, 36, p. 617–624.

Hill, P.J., and Ng, Ka M., 2002. Particle size distribution by design. *Chemical Engineering Science*, 57, p. 2125–2138.

Hillman, S.R., Mannan, S.H., Durairaj, R., Seman, A., Ekere, N.N., Dusek, M., and Hunt, C., 2005. Correlation between jamming and skipping during solder paste printing. *Soldering & Surface Mount Technology*, 17(4), p. 17–26.

Hinrichs, R.J., and Thuen, J., 1985. *Method for detecting resin viscosity with ultrasonic waves*. United States Patent 4559810, 24 Dec 1985.

Hooke, R., 1678. *Lectures of spring: Explaining the power of springing bodies. (De Potentia Restitutiva)*. Royal Society, London. p. 1–24.

Hunter, J.L. and Derdul, P.R., 1967. Acoustic absorption and dynamic viscosity in a long chain polymer. *J. Acoust. Soc. Amer.*, 42(5), p. 1041–1044.

Hwang, J.S., 1996. *Modern solder technology for competitive electronics manufacturing*. McGraw-Hill Professional, ed.7th, p. 288.

Iida, T., Morita, Z. and Takeuchi, S., J. 1975. Viscosity measurement of pure liquid metals by the capillary method. *Japan Inst. Metals*, 39(11), p. 1169–1175.

Ince, O., 1978. Ultrasonic measurement on certain liquids and biological materials. *PhD Thesis. Salford University*, Manchester, UK.

IPC J-STD-004, 2004. *Requirements for soldering fluxes*. Northbrook , IL: IPC.

IPC J-STD-005, 1996. *Requirement for soldering pastes*. Northbrook , IL:IPC.

IPC TM-650: 2.3.32, 1995. *Flux induced corrosion*. Northbrook , IL:IPC.

Isakovich, M.A., 1948. Propagation of sound in emulsions. *J.Exp.Theor., USSR*, 18, p. 907–912.

ITRI (International Tin Research Institute), 1988. *Soldering surface mount devices-Photographic guide*, ITRI Publication 700, p. 27.

Jaafar, R., 1996. Ultrasonic non-destructive evaluation of natural rubber latex suspensions. *PhD Thesis. Keele University*, UK

Jackson, G.J., Hendriksen, M.W., Kay, R.W., Desmulliez, M., Durairaj, R., and Ekere, N.N., 2005. Sub process challenges in ultra fine pitch stencil printing of type-6 and type-7 Pb-free solder pastes for flip chip assembly applications. *Soldering & Surface Mount Technology*, 17(1), p. 24–32.

Johnson, C.C., Kevra, J., 1989. *Solder paste technology: Principles and Applications*, Tab Books, Blue Ridge Summit, PA.

Kamada, T., Uchida, S., and Rokugo, K., 2005. Nondestructive Evaluation of Setting and Hardening of Cement Paste Based on Ultrasonic Propagation Characteristics. *Journal of Advanced Concrete Technology*, 3(3), p. 343–353.

Kirchoff, G., 1868. *Prog. Ann. Phys.*, 134, p. 177–193.

Kneser, H.O., 1938. Absorption and dispersion of sound in liquids. *Ann. d. Physik*, 32, p. 277–282.

Köselí, V., Zeybek, S., and Uludag, Y., 2006. Online Viscosity Measurement of Complex Solutions Using Ultrasound Doppler Velocimetry. *Turk. J. Chem*, 30, p. 297–305.

Krautkramer, J., 1959. *Arch. Eisenheutten W.*, 30, p. 693.

Kreiger, I.M., and Dougherty, I.J., 1959. A mechanism for non-Newtonian flow in suspensions of rigid spheres. *Trans. Soc. Rheol.*, 3, p. 137–152.

Kundt, A., 1866. Ueber eine neue Art Akusticher Staubfiguren und über die Anwendung derselben zur Bestimmung der Shallgeschwindigkeit in festen Körpern und Gasen. *Annalen der Physik* (Leipzig: J.C. Poggendorff), 127 (4), p. 497–523.

Kundt, A., 1868. Acoustic Experiments. *The London, Edinburgh and Dublin Philosophical Magazine and Journal of Science* (UK: Taylor & Francis), 35 (4), p.41–48.

Kuo. F.J., 2008. Evaluation of ultrasonic propagation to measure sugar content and viscosity of reconstituted orange juice. *Journal of Food Engineering*, 86, p. 84–90.

Lamb, H., 1945. *Hydrodynamics*, Dover, New York, 6th ed., p. 361–363.

Landau L. D., and Rumer, G., 1937. Absorption of sound in solids. *Phys. Z. Sowjetunion*, 11, p. 18–25.

Landau L. D., and E. M. Lifshitz, 1986. Theory of Elasticity. 3rd edition: Butterworth-Heinemann, p. 153–162.

Landis E.N., 1993. A quantitative acoustic emission investigation of microcracking in cement-based materials. *PhD Thesis. Northwestern University*, Evanston, IL. US.

Landis E.N., and Shah, S.P., 1995. Frequency-Dependent Stress Wave Attenuation in Cement-Based Materials. *Journal of Engineering Mechanics*, 121, p. 737–743.

Laplace, P.S. Marquis de., 1816. On the Velocity of Sound through Air and through Water. *Ann. Chim. Phys.*, 3, p. 238–241.

Lee, N.C., 2002. *Reflow Soldering Processes and Troubleshooting SMT, BGA, CSP and Flip Chip Technologies*, Newnes, U.S.A., p. 139–141.

Lehmann, L., 2005. Application of high-resolution ultrasonic spectroscopy for analysis of heat stability and heat transitions in milks and their model systems. *PhD Thesis. University College*, Dublin, Ireland.

Létang C., Piau, M., Verdier, C., and Lefebvre, L., 2001. Characterization of wheat-flour–water doughs: a new method using ultrasound. *Ultrasonics*, 39(2), p. 133–141.

Llull, P., Simal, S., Benedito, J., Roselló, C., 2002. Evaluation of textural properties of a meat-based product (sobrassada) using ultrasonic techniques. *Journal of Food Engineering*, 53, p. 279–285.

Lodge, A.S., 1951. On the use of convected coordinate systems in the mechanics of continuous media. *Proc. Camb. Phil. Soc.*, 47, p. 575–584.

Long, R., 2000. Improvement of ultrasonic apparatus for the routine inspection of concrete. *PhD Thesis. Imperial College*, UK.

Longin, P.Y., Verdier, C., and Piau, M., 1998. Dynamic shear rheology of high molecular weight polydimethylsiloxanes: comparison of rheometry and ultrasound. *J. Non-Newtonian Fluid Mech.*, 76, p. 213–232.

Macosko, C. W. and Mewis, J., 2004. *Suspension Rheology, In: Rheology – Principles, Measurements and Applications*, Wiley-VCH, Inc., U.S.A., p. 425–470.

Maiso, P.S. and Bauer, B., 1990. Statistical Process Control in Solder Paste Manufacture and Use. *IPC Technical Review*, p. 20–26.

Malcomtech International Inc, 2008. Available from www.malcomtech.com

Mallik, S., 2008. A study of the time-dependent rheological behaviour of lead-free solder pastes and flux mediums used for flip-chip assembly applications. *PhD Thesis. University of Greenwich,* London, UK.

Malvern Instrument, 2008. Available from www.malvern.co.uk/home/index.htm

Mannan, S.H., Ekere, N.N., Lo, E.K., and Ismail, I., 1993. Predicting scooping and skipping in solder paste printing for reflow soldering of SMT devices. *Soldering & Surface Mount Technology*, 5(3), p. 14–17.

Mannan, S.H., Ekere, N.N., Ismail, I., and Currie, M.A., 1994a. Computer simulation of solder paste flow Part I: Dense suspension theory. *J. Elec. Manufacturing,* 4, p. 141–147.

Mannan, S.H., Ekere, N.N., Ismail, I., and Currie, M.A., 1994b. Computer simulation of solder paste flow Part II: Flow out of a stencil aperture. *J. Elec. Manufacturing,* 4, p. 149–154.

Mannan, S.H., Ekere, N.N., Ismail, I., and Currie, M.A., 1995. Flow processes in solder paste during stencil printing for SMT assembly. *J. Mat. Sci.: Mat. Elec.*, 6, p. 34–42.

Mangin, C.H., 1991. Where quality is lost on SMT boards, Circuits Assembly, p. 63–64.

Marczak, W., 1997. Water as a standard in the measurements of speed of sound in liquids. *J. Acoust. Soc. Am.*, 102(5), p. 2776–2779.

Matsumoto, Y., Allen, J.S., Yoshizawa, S., Ikeda, T., and Kaneko, Y., 2005. Medical ultrasound with microbubbles. *Experimental Thermal and Fluid Science*, 29, p. 255–265.

Mazzeo, F. A., 2002. Importance of Oscillatory Time Sweeps in Rheology. Available at www.tainstruments.co.jp/application/pdf/Rheology_Library/Application_Briefs/-RH081a.pdf. Last accessed 21 April 2008.

McClements, D.J., 1988. The use of ultrasonics for characterising fats and emulsions. *PhD Thesis. University of Leeds*, Leeds, UK.

McIntyre, C.S., 1999. The development of air-coupled ultrasonic transducers. *PhD Thesis. Warwick University*, UK.

Michaeli. W., and Starke, C., 2005. Ultrasonic investigations of the thermoplastics injection moulding process. *Polymer Testing*, 24, p. 205–209.

Mindel, M.J., 1991. Solder paste rheology as a function of temperature. *SMI Proceedings*, p. 490–495.

Mizrach. A., 2004. Assessing plum fruit quality attributes with an ultrasonic method *Food Research International*, 37, p. 627–631.

Moiseenko, L.L., 1980. Coeficients of thermal expansion and characteristics temperatures of cubic dodecarborides. *Powder Metallurgy and Metal Ceramics*, 19(7), p. 515–517.

Morse, P.M. and Feshbach, H., 1953. Method of Theoretical Physics: McGraw Hill. p. 803–833.

Morse, P.M. and Ingard, K.U., 1986. Theoretical Acoustics: Princeton University Press, p. 407–415.

Neklepajew, N., 1911. Ann. Physik, 35, p. 175–181.

Nguty, T.A., and Ekere, N.N., 2000. Monitoring the effects of storage on the rheological properties of solder paste. *J. Mat. Sci.: Mat. Elec.*, 11, p. 433–437.

Öztürk, T., Kroggel , Grübl , O.P., and Popovics, J.S., 2006. Improved ultrasonic wave reflection technique to monitor the setting of cement-based materials. *NDT&E Int.*, 39, p. 258–263.

Ogilvy, J.A., 1987. Wave scattering from rough surfaces. *Rep. Prog. Phys.*, 50, p. 1553–1608.

Okuru, T., Kanai, M., Ogata, S., Takei, T., and Takakusagi, 1995. Optimisation of solder paste printability with laser inspection technique. In: IEEE/CPMT International Electronics Manufacturing Symposium, p. 157–161.

Oldroyd, J.G., 1950. On the formulation of rheological equations of state. *Proc. Roy. Soc. Lond. A*, 200, p. 523–541.

Olympus NDT, 2008. Available from www.olympusndt.com/en/

Ophardt, C.E., 2003. *Virtual Chembook.*
Available from www.elmhurst.edu/~chm/vchembook/index.html. Last accessed 14 Apr 2010.

Orj, Jr., R., 1982. *Methods of measuring fluid viscosity and flow* rate. United States Patent 4331025, 25 May 1982.

Ostwald, W., 1925. About the rate function of the viscosity of dispersed systems. *Kolloid Z*, 36, p. 99–117.

Ostwald, W., 1929. Ueber die rechnerische Darstellung des Strukturgebietes der Viskosität "Computational representation of the structural area of viscosity: Ostwald called it the de Waele-Ostwald equation", *Kolloid Zeitschrift*, 47 (2), p. 176–187.

Ouriev, B., Windhab, E.J., 2002. Rheological study of concentrated suspension in pressure-driven shear flow using a novel in-line ultrasound Doppler method. *Experiments in Fluids*, 32, p. 201–211.

Ouriev, B., Windhab, E.J., 2007. *Method for determining rheological parameters of a fluid.* United States Patent 7228728B2, 12 June 2007.

Pereira, M.C., 1982. Ultrasonic absorption and velocity measurement in aqueous solutions and gelling polysaccharides. *PhD Thesis. Salford University*, Manchester, UK.

Peterson, G.G., 1987. A practical guide for specifying printing equipment for electronic applications. *SMT-III-21, Proceedings of the SMART III Conference (IPC/EIA).*

Pinkerton, J.M.M., 1949. On the pulse method of measuring ultrasonic absorption in liquids. *Proc. Phys. Soc.*, B62, p. 286–299.

Poisson, S.D., 1808. Mémoire sur la théorie du Son "Memory on the theory of sound", *Journal de l'Ecole Polytechnique*, 7, p. 319–392.

Poisson, S.D., 1818. Mémoire sur la théorie des ondes "Memory on wave theory". *Mém. Acad. R. Sci. Inst. France*. 1816, 2nd Ser. 1, p. 70–186.

Poisson, S.D., 1833. *Traité de Mécanique "Applied Mechanics"*. 2nd ed. Paris: Bachelier.

Povey, M.J.W., 1998. Ultrasonics of food. *Contemporary Physics*, 39(16), p. 467–478.

Povey, M.J.W., 2006. Acoustic Methods for Particle Characterisation, *KONA*, 24, p. 126–133.

Prasad, R.P., 1997. *Surface mount technology principles and practice.* 2nd Ed. Boston/Dordrecht/London, Kluwer Academic Publishers.

Prosser W.H., and Green, R.E., 1990. Characterization of the Nonlinear Elastic Properties of Graphite/Epoxy Composites Using Ultrasound. *J Reinforced Plastics and Composites*, 9(2), p. 162–173.

Punurai, W., Jarzynski, J., Qu, J., Kurtis, K.E., and Jacobs, L.J., 2006. Characterization of entrained air voids in cement paste with scattered ultrasound. *NDT&E International*, 39, p. 514–524.

Rao, P.P., and Sutton, D.L., 1981. *Method and apparatus for non-destructive testing of cement.* United States Patent 4259868, 7 April 1981.

Rayleigh B. (J.W. Strutt), 1876. On waves. *Philos. Mag.,* 5(1), p.257–79. Also 1899. *Scientific Papers of John William Strutt, Baron Rayleigh,* 1, p.251–71. Cambridge, UK: Cambridge Univ. Press.

Rayleigh B. (J.W. Strutt), 1878. *The theory of sound,* Vol 2, 1st edn. London: Macmillan.

Rayleigh B. (J.W. Strutt), 1884. On the Circulation of Air Observed in Kundt's Tubes, and on Some Allied Acoustical Problems, *Philosophical Transactions of the Royal Society of London*, 175, p. 1–21.

Rayleigh B. (J.W. Strutt), 1892. On the influence of obstacles arranged in rectangular order upon the properties of a medium, *Philos. Mag.*, 34, p. 481–502.

Reddy, M.A. and Suryanayana, M., 1981. Ultrasonic absorption in aqueous solutions of starch and gelatine, *Acustica*, 48, p. 19–22.

Reinhardt, H.W., Grosse, C.W., Herb, A., Weiler, B., and Schmidt, G., 2003. *Method for examining a solidified and/or hardening material using ultrasound, receptacle and ultrasound sensor for carrying out the method.* United States Patent 6655213B1, 2 December 2003.

Renaut, P., and Dory, J., 1965. *Ultrasonic inspection apparatus using short electric pulses.* United States Patent 3166931, 26 Jan 1965.

Reusch, W., 2007. *Virtual textbook of organic chemistry.* Available from www.cem.msu.edu/~reusch/VirtualText/Spectrpy/spectro.htm. Last accessed 14 Apr 2010.

Rivlin, R.S., 1948. The hydrodynamics of non-Newtonian fluids. I. *Proc. Roy. Soc. Lond. A*, 193, p. 260–281.

Romoscanu, A.I., Sayir, M.B., Häusler, K., and Servais, C., 2003. High frequency probe for the measurement of the complex viscosity of liquids. *Measurement Science and Technology*, 14, p. 451–462.

Ross, K.A., Pyrak-Nolte, L.J., and Campanella, O.H., 2004. The use of ultrasound and shear oscillatory tests to characterize the effect of mixing time on the rheological properties of dough. *Food Research International*, 37, p. 567–577.

Round, R., 1996. Evaluation of reaction kinetics and material properties of cementitious ceramic materials using ultrasonic velocity and attenuation measurements. *PhD Thesis. Brunel University*, UK.

Samsonov, G.V., Grebenkina, V.G., and Klimenko, V.S., 1971. Coefficient of thermal-expansion of refractory compounds. *Powder Metallury and Metal Ceramics*, 10 (8), p. 643–647.

Scherrer, R., 2006. *Quantum Mechanics: An Accessible Introduction.* Addison-Wesley, UK, p. 284–290.

Schmachtenberg, E., Schulte zur Heide, J., and Töpker, J., 2005. Application of ultrasonics for the process control of Resin Transfer Moulding (RTM). *Polymer Testing*, 24, p. 330–338.

Sewell, J.T., 1910. On the extinction of sound in a viscous atmosphere by small obstacles of cylindrical and spherical form. *Phil. Trans. Roy. Soc.*, A210, p. 239–270.

Sheen, S., Lawrence, W.P., Chien, H., and Raptis, A.C.,1994. *Method for measuring liquid viscosity and ultrasonic viscometer.* United States Patent 5365778, 28 Jan 1994.

Shepard, D.D., and Smith, K.R., 1997. A Complete Ultrasonic Measurement System for in-process Cure Monitoring and Control of Composites. *NDTnet*, 2(11). Available from www.ndt.net/article/aero1197/shepard/shepard.htm. Last accessed 14 Apr 2010.

Sidkey, M.A., and Abd El Aal, N.S., 1986. Ultrasonic absorption in polyisoprene rubber. *Acustica*, 60, p. 264.

Singh, J.P., Balasubramaniam, K., Costley, R.D., Shah, V.V., and Winstead, C., 1997. *Insitu, real time viscosity measurement of molten materials with laser induced ultrasonics.* United States Patent 5686661, 11 Nov 1997.

Smith, G.D., 2000. Ultrasonic monitoring of filled polymer melts. *PhD Thesis. Bradford University*, UK.

Smyth, C., 2001. Analysis of dairy colloids with novel high-resolution ultrasonic spectrometry. *PhD Thesis. University College Dublin*, Ireland.

Stakukis, V.J., Morse, R.W., Dill, M., and Beyer, T.R., 1955. Attenuation of ultrasound in aqueous suspensions. *J. Acoust. Soc. Amer.*, 27, p. 539–546.

Stokes G.G., 1845. On the theories of the internal friction in fluids in motion, and of the equilibrium and motion of elastic solids. *Transaction of the Cambridge Philosophical Society*, 8(22), p. 287–342.

Stokes, G.G., 1847. On the theory of oscillatory waves. *Trans. Camb. Philos. Soc.* 8, p. 441–455.

Stokes, G.G., 1880–1905. *Mathematical and Physical Papers*. 5 Vols. Cambridge, UK: Cambridge Univ. Press

Tabidze, A.A., Koshkin, N.I., and Novoselov, V.I., 1981. Low-frequency ultrasonic viscometer for liquids. *Measurement Techniques*, 24(12), p. 1101–1104.

Tavakoli, M.B., and Evans, J.A., 1991. Dependence of the velocity and attenuation of ultrasound in bone on the mineral content. *Phys. Med. Biol.*, 36(11), p. 1529–1537.

Tebbutt, J.S., 1996. Ultrasonic absorption and phase velocity spectra in colloids: theory, simulation and measurement. *PhD Thesis. Keele University*, UK.

Tenya, Y., and Adams, T., 2000. Lead-free processing: Thermal effect on components. *SMT*, 14 (11). Also available from http://www.electroiq.com/index/display/smt-article-display/86476/articles/smt/volume-14/issue-11/features/components/lead-free-processing-thermal-effect-on-components.html. Last accessed 17 Nov 2008.

Tian, Y., Qingze, J., Huaiyu, D., Yangqiao, S., and Biqian, L., 2006. The formation of honeycomb structure in polyphenylene oxide films. *Polymer*, 47(11), p. 3866–3873.

Trusler, J.P.M., 1991. *Physical acoustics and metrology of fluids*. CRC Press, p. 22–55.

Ueshima, M., 2006. *Lead-free solder paste*. WIPO Patent WO/2006/126564A1, 24 May 2006.

Urick, R.J., 1948. The absorption of sound in suspension of irregular particles. *J. Acoust. Soc. Amer.*, 20, p. 283–289.

Verdier, C., Longin, P.Y., and Piau, M., 1998. Dynamic shear and compressional behaviour of polydimethylsiloxanes: Ultrasonic and low frequency characterisation. *Rheol Acta*, 37, p. 234–244.

Wang, L., McCarthy, K.L., and McCarthy, M.J., 2004. Effect of temperature gradient on ultrasonic Doppler velocimetry measurement during pipe flow, *Food Research International*, 37, p. 633–642.

Wang, L., 2005. In-line viscosity measurement based on ultrasonic Doppler velocimetry: Effect of temperature gradients. *PhD Thesis. University of California*, Davis, US.

Wicker, T., and Han, P., 2005. *Lead-free solder paste.* United States Patent 20060180245, 15 Feb 2005.

Yang, Y., and Sigmund, W.M., 2001. Effect of particle volume fraction on the gelation behaviour of the temperature induced forming (TIF) aqueous alumina suspensions. *J. Am. Ceram. Soc.*, 84(9), p. 2138–2140.

Ye, G., Lura, P., van Breugel, K., and Fraaij, A.L.A., 2004. Study on the development of the microstructure in cement-based materials by means of numerical simulation and ultrasonic pulse velocity measurement. *Cement & Concrete Composites*, 26(4), p. 491–497.

Ying, C.F., and Truell, J., 1956. Scattering of a plane longitudinal wave by a spherical obstacle in an isotropically elastic solid. *J. Appl. Phys.*, 27, p. 1086–1097.

Young T. 1807. *A Course of Lectures on Natural Philosophy and the Mechanical Arts*. 2 Vols. London: J Johnson. 1845. 6th edn; ed. P Kelland. London: Taylor & Walton, Volume I, p. 106-116 and Volume II, p. 46–47.

Young T. 1821. *Elementary Illustrations of the Celestial Mechanics of Laplace*, Book 1. London: Murray. p. 325-326. Also Peacock 1855, p. 141–158.

Zhou, Q., Dong, P., and Cheng, B., 2003. Progress in three-dimensionally ordered self assembly of colloidal SiO2 particles. *China Particuology*, 1(3), p. 124–130.

Publications

1. Mallik, S., Thieme, J., Bauer, R., Ekere, N.N., **Seman, A.**, Bhatti, R., and Durairaj, R., December 2009. Study of the rheological behaviours of Sn–Ag–Cu solder pastes and their correlation with printing performance. *11th Electronics Packaging Technology Conference (EPTC)*, Singapore.

2. Bernasko, P.K., S., Mallik, S., **Seman, A.**, Ekere, N.N., and Takyi, G., December 2009. Effect of reflow profile and thermal cycle ageing on the intermetallic formation and growth in lead-free soldering. *11th Electronics Packaging Technology Conference (EPTC)*, Singapore.

3. Durairaj, R., Ramesh, S., Mallik, S., **Seman, A.**, and Ekere, N.N., October 2009. Rheological characterisation and printing performance of Sn/Ag/Cu solder pastes. *Journal of Materials and Design*, 30(9), p. 3812–3818.

4. Durairaj, R., Mallik, S., **Seman, A.**, Marks, A.E., and Ekere, N.N., April 2009. Rheological characterisation of solder pastes and isotropic conductive adhesives used for flip-chip assembly. *Journal of Materials Processing Technology*, 209(8), p. 3923–3930.

5. **Seman, A.**, Ekere, N.N., Ashenden, S.J., Mallik, S., Marks, A.E., Durairaj, R., December 2008. In-situ Non-destructive Ultrasonic Rheology Technique for Monitoring Different Lead-free Solder Pastes for Surface Mount Applications, *10th Electronics Packaging Technology Conference (EPTC)*, Singapore. p. 1448–1454.

6. Durairaj, R., Mallik, S., **Seman, A.**, Marks, A.E., Ekere, N.N., December 2008. Investigation of Wall-Slip Effect on Paste Release Characteristic in Flip Chip Stencil Printing Process, *10th Electronics Packaging Technology Conference (EPTC)*, Singapore. p. 1328–1333.

7. Durairaj, R., Mallik, S., **Seman, A.**, Marks, A.E., Ekere, N.N., November 2008. Viscoelastic Properties of Solder Pastes and Isotropic Conductive Adhesives Used for Flip-chip Assembly, *33rd International Electronics Manufacturing Technology Conference (IEMT),* Penang, Malaysia.

8. **Seman, A.**, Ekere, N.N., Ashenden, S.J., Mallik, S., Marks, A.E., Durairaj, R., September 2008. Development of an In-situ, Non-destructive Ultrasonic Monitoring Technique for Solder Pastes, *Electronic Systemintegration Technology Conference (ESTC)*, Greenwich, London, UK, p. 209–214.

9. Marks, A.E., Mallik, S., Ekere, N.N., **Seman, A.**, September 2008. Effect of Temperature on Slumping Behaviour of Lead-Free Solder Paste and its

Rheological Simulation, *Electronic Systemintegration Technology Conference (ESTC)*, Greenwich, London, UK, p. 829–832.

10. Mallik, S., Ekere, N.N., Marks, A.E., **Seman, A.**, Durairaj, R., September 2008. Modelling of the Time Dependent Flow Behaviour of Lead Free Solder Pastes used for Flip-Chip Assembly Applications, *Electronic Systemintegration Technology Conference (ESTC)*, Greenwich, London, UK, p. 1219–1224.

11. **Seman, A.**, Ekere, N.N., Ashenden, S.J., July 2008. In-situ Non-destructive Ultrasonic Rheology Technique for Monitoring Solder Pastes Production, *School Research Enterprise Conference*, Greenwich University, Medway, UK.

12. Durairaj, R., **Seman, A.**, Ekere, N.N., September 2006. Development of Quality Control (QC) Tools for Solder Pastes used for Flip Chip Assembly Based on Oscillatory Tests, *Electronics Systemintegration Technology Conference,* Dresden, Germany, p.347–353.

13. Hillman, S.R., Mannan, S.H., R. Durairaj, **Seman, A.**, Ekere, N.N., Dusek, M., Hunt, C., 2005. Correlation between jamming and skipping during solder paste printing, *Soldering & Surface Mount Technology*, 17(4), p.17–26.

Appendix A
Ultrasonic Rheology Program

This rheology program is used for generating viscosity-related data in conjunction with the Picoscope analogue-to-digital converter. The program was produced using Microsoft Visual Basic software.

The program can be compiled and run independently as an '.exe' file or run as a macro for Microsoft Excel. When used as an Excel macro, the program can be adjusted for measuring other material's viscosity since the user is allowed to modify or input a new value for the density, ultrasound frequency and distance between transducers.

```
Declare Function adc200_open_unit Lib "ADC20032.DLL" (ByVal port As Integer)
As Integer
Declare Function adc200_set_unit Lib "ADC20032.DLL" (ByVal port As Integer) As
Integer
Declare Sub adc200_close_unit Lib "ADC20032.DLL" (ByVal port As Integer)

Declare Function adc200_get_driver_version Lib "ADC20032.DLL" () As Integer
Declare Function adc200_get_product Lib "ADC20032.DLL" () As Integer
Declare Function adc200_get_hw_version Lib "ADC20032.DLL" () As Integer
Declare Function adc200_has_relays Lib "ADC20032.DLL" () As Integer
Declare Function adc200_get_unit_info Lib "ADC20032.DLL" (ByVal str As String,
ByVal lth As Integer, ByVal line_no As Integer, ByVal port As Integer) As Integer

Declare Function adc200_set_frequency Lib "ADC20032.DLL" (ByVal Frequency
As Long) As Long
Declare Function adc200_set_range Lib "ADC20032.DLL" (ByVal channel As
Integer, ByVal gain As Integer) As Integer
Declare Sub adc200_set_dc Lib "ADC20032.DLL" (ByVal channel As Integer,
ByVal enable_dc As Integer)

Declare Function adc200_set_channels Lib "ADC20032.DLL" (ByVal mode As
Integer) As Integer
Declare Function adc200_set_oversample Lib "ADC20032.DLL" (ByVal factor As
Integer) As Integer
Declare Function adc200_set_trigger Lib "ADC20032.DLL" (ByVal enabled As
Integer, ByVal source As Integer, ByVal direction As Integer, ByVal delay_percent
As Integer, ByVal threshold As Integer) As Integer
Declare Function adc200_set_timebase Lib "ADC20032.DLL" (ns As Long, is_slow
As Integer, ByVal timebase As Integer) As Integer
```

```
Declare Function adc200_max_samples Lib "ADC20032.DLL" () As Long
Declare Function adc200_run Lib "ADC20032.DLL" (ByVal no_of_values As Long)
As Integer
Declare Function adc200_ready Lib "ADC20032.DLL" () As Integer
Declare Function adc200_get_values Lib "ADC20032.DLL" (buffer_a As Integer,
buffer_b As Integer, ByVal no_of_values As Long) As Integer
Declare Function adc200_get_overflow Lib "ADC20032.DLL" (channel As Integer)
As Integer


Declare Sub adc200_get_single Lib "ADC20032.DLL" (buffer As Integer)
Declare Function adc200_get_ets_time Lib "ADC20032.DLL" () As Long
Declare Function adc200_get_max_ets Lib "ADC20032.DLL" () As Integer
Declare Sub adc200_set_ets Lib "ADC20032.DLL" (interleave As Integer,
max_cycles As Integer, mode As Integer)


Dim buffer_a(101) As Integer
Dim buffer_b(101) As Integer
Dim ns As Long
Dim is_slow As Integer
Dim S As String * 255



Sub Fillcell()

   Range("A1").Select
   ActiveCell.FormulaR1C1 = "ρ (kg/m³)"
   ActiveWorkbook.Names.Add Name:="density", RefersToR1C1:="=Sheet1!R1C1"

   Range("A2").Select
   ActiveCell.FormulaR1C1 = "f (Hz)"
   ActiveWorkbook.Names.Add Name:="frequency",
RefersToR1C1:="=Sheet1!R2C1"

   Range("A3").Select
   ActiveCell.FormulaR1C1 = "L (m)"
   ActiveWorkbook.Names.Add Name:="distance",
RefersToR1C1:="=Sheet1!R3C1"

   Range("A4").Select
   ActiveCell.FormulaR1C1 = "Batch no"

   Range("A5").Select
   ActiveCell.FormulaR1C1 = "Temperature"

   Range("C5").Select
   ActiveCell.FormulaR1C1 = "Celcius"
```

```
Range("A8").Select
ActiveCell.FormulaR1C1 = "Time"

Range("A9").Select
ActiveCell.FormulaR1C1 = "(ns)"

Range("B8").Select
ActiveCell.FormulaR1C1 = "Voltage"

Range("B9").Select
ActiveCell.FormulaR1C1 = "Transmitter (mv)"

Range("C8").Select
ActiveCell.FormulaR1C1 = "Voltage"

Range("C9").Select
ActiveCell.FormulaR1C1 = "Receiver (mv)"

Range("E4").Select
ActiveCell.FormulaR1C1 = "λreceiver"

Range("G4").Select
ActiveCell.FormulaR1C1 = "nanosecond"

Range("E5").Select
ActiveCell.FormulaR1C1 = "Vsample (m/s)"

Range("G5").Select
ActiveCell.FormulaR1C1 = "(m/s)"

Range("E6").Select
ActiveCell.FormulaR1C1 = "β"

Range("E7").Select
ActiveCell.FormulaR1C1 = "Z (Accoustic Impedance)"

Range("G6").Select
ActiveCell.FormulaR1C1 = "1/Pa.s"

Range("G7").Select
ActiveCell.FormulaR1C1 = "Pa/m"

Range("E8").Select
ActiveCell.FormulaR1C1 = "Attenuation trans"


Range("E9").Select
ActiveCell.FormulaR1C1 = "Attenuation rec"
```

```
    Range("G8").Select
    ActiveCell.FormulaR1C1 = "Neper/m"

    Range("G9").Select
    ActiveCell.FormulaR1C1 = "Neper/m"

    Range("E10").Select
    ActiveCell.FormulaR1C1 = "α (Total attenuation)"

    Range("G10").Select
    ActiveCell.FormulaR1C1 = "Neper/m"

    Range("E11").Select
    ActiveCell.FormulaR1C1 = "Viscosity"

    Range("G11").Select
    ActiveCell.FormulaR1C1 = "Pa.s"

    Range("E12").Select
    ActiveCell.FormulaR1C1 = "Phase Shift, θ"

    Range("G12").Select
    ActiveCell.FormulaR1C1 = "Degrees"

    Range("E15").Select
    ActiveCell.FormulaR1C1 = "Complex Modulus"

    Range("E17").Select
    ActiveCell.FormulaR1C1 = "Storage Modulus"

    Range("E18").Select
    ActiveCell.FormulaR1C1 = "Loss Modulus"

    Range("E21").Select
    ActiveCell.FormulaR1C1 = "Loss tangent, δ"

    Range("G11").Select
    ActiveCell.FormulaR1C1 = "rad"

End Sub



Sub Checkcell()

   If Range("B1").Value = "" Then
      MsgBox "Please enter a value of the density for B1 cell"
   End If
```

```
    If Range("B2").Value = "" Then
        MsgBox "Please enter a value of the frequency for B2 cell"
    End If

    If Range("B3").Value = "" Then
        MsgBox "Please enter a value of the distance between the sensors for B3 cell"
    End If

    If Range("B5").Value = "" Then
        MsgBox "Please enter a name of the sample for B5 cell"
    End If

    If Range("B6").Value = "" Then
        MsgBox "Please enter a value of the temperature for B6 cell"
    End If

End Sub



Sub GetData()

  port = 1
  ok = adc200_open_unit(port)

  For i = 0 To 4
    j = adc200_get_unit_info(S, 255, i, port)
    Cells(1 + i, "K").Value = S
  Next i

  If ok Then
    Cells(1, "K").Value = "ADC-200 opened"

    ok = adc200_set_trigger(True, 0, 0, -15, 0)
    ok = adc200_set_channels(2)
    mv = adc200_set_range(0, 10)        ' Channel A range
    mv = adc200_set_range(1, 10)        ' Channel B range
    Call adc200_set_dc(0, True)

    ok = adc200_set_oversample(1)
    ok = adc200_set_timebase(ns, is_slow, 0)
    ok = adc200_run(101)
    While adc200_ready() = 0
    Wend


    Call adc200_get_values(buffer_a(0), buffer_b(0), 15016)
```

```
  For i = 0 To 15015
    Cells(i + 11, "A").Value = ns * i
    Cells(i + 11, "B").Value = (mv * buffer_a(i) ) / 2048
    Cells(i + 11, "C").Value = (mv * buffer_b(i) ) / 2048
  Next i
 Else
  Cells(1, "K").Value = "Unable to open ADC-200"
 End If

 Call adc200_close_unit(port)

End Sub



Sub Filldata()

ActiveCell.FormulaR1C1 = "
=2*ABS(INDEX(A11:A21,MATCH(MAX(C11:C21),C11:C21,0))-
INDEX(A11:A21,MATCH(MIN(C11:C21),C11:C21,0))) "
   Range("F4").Select

ActiveCell.FormulaR1C1 = "=distance/(F4*0.000000001)"
   Range("F5").Select

ActiveCell.FormulaR1C1 = "=density^-1*F5^-2"
   Range("F6").Select

ActiveCell.FormulaR1C1 = "= density*F5"
   Range("F7").Select

ActiveCell.FormulaR1C1 = "=LN(B115)*1000/90"
   Range("F8").Select

ActiveCell.FormulaR1C1 = "=LN(C115)*1000/90"
   Range("F9").Select

ActiveCell.FormulaR1C1 = "=ABS(F9-F8)"
   Range("F10").Select

ActiveCell.FormulaR1C1 = "=ABS(($F9-$F8)-55)*
density*$F$5^3/(9.87*frequency^2)"
   Range("F11").Select                          'Equation 8.20

ActiveCell.FormulaR1C1 =
"=90*((INDEX(A11:A7519,MATCH(MAX(B11:B7519),B11:B7519,0))-
INDEX(C11:C7519,MATCH(MAX(D11:D7519),D11:D7519,0)))/((F4)))/4"
   Range("F12").Select
```

```
ActiveCell.FormulaR1C1 = "=ABS(ABS(MIN(B11:B111)))/ABS(MIN(C11:C111))"
   Range("F15").Select

ActiveCell.FormulaR1C1 = "=ABS(F15*COS(F12*PI()/180))"
   Range("F17").Select

ActiveCell.FormulaR1C1 = "=ABS(F15*SIN(F12*PI()/180))"
   Range("F18").Select

ActiveCell.FormulaR1C1 = "=ATAN(F18/F17)"
   Range("F21").Select


End Sub



Sub Plotgraph()

Range("F12").Select

Charts.Add
   ActiveChart.ChartType = xlXYScatterSmoothNoMarkers
   ActiveChart.SetSourceData Source:=Sheets("Sheet1").Range("H23")
   ActiveChart.SeriesCollection.NewSeries
   ActiveChart.SeriesCollection.NewSeries
   ActiveChart.SeriesCollection(1).XValues = "=Sheet1!R11C1:R7519C1"
   ActiveChart.SeriesCollection(1).Values = "=Sheet1!R11C2:R7519C2"
   ActiveChart.SeriesCollection(1).Name = "=""Transmitter Voltage"""
   ActiveChart.SeriesCollection(2).XValues = "=Sheet1!R11C1:R15026C1"
   ActiveChart.SeriesCollection(2).Values = "=Sheet1!R11C3:R15026C3"
   ActiveChart.SeriesCollection(2).Name = "=""Receiver Voltage"""
   ActiveChart.Location Where:=xlLocationAsObject, Name:="Sheet1"
   With ActiveChart
      .HasTitle = True
      .ChartTitle.Characters.Text = "Amplitude of Transmitter VS Receiver"
      .Axes(xlCategory, xlPrimary).HasTitle = True
      .Axes(xlCategory, xlPrimary).AxisTitle.Characters.Text = "Time (ns)"
      .Axes(xlValue, xlPrimary).HasTitle = True
      .Axes(xlValue, xlPrimary).AxisTitle.Characters.Text = "Voltage (mV)"
   End With
   ActiveChart.HasLegend = True
   ActiveChart.Legend.Select
   Selection.Position = xlBottom
   ActiveWindow.Visible = False
   Range("F37").Select
```

```
Charts.Add
ActiveChart.ChartType = xlXYScatterSmoothNoMarkers
ActiveChart.SetSourceData Source:=Sheets("Sheet1").Range("F37")
ActiveChart.SeriesCollection.NewSeries
ActiveChart.SeriesCollection(1).XValues = "=Sheet1!R11C1:R7519C1"
ActiveChart.SeriesCollection(1).Values = "=Sheet1!R11C2:R7519C2"
ActiveChart.SeriesCollection(1).Name = "=""Transmitter Voltage"""
ActiveChart.Location Where:=xlLocationAsObject, Name:="Sheet1"
With ActiveChart
   .HasTitle = True
   .ChartTitle.Characters.Text = "Amplitude of Transmitter"
   .Axes(xlCategory, xlPrimary).HasTitle = True
   .Axes(xlCategory, xlPrimary).AxisTitle.Characters.Text = "Time (ns)"
   .Axes(xlValue, xlPrimary).HasTitle = True
   .Axes(xlValue, xlPrimary).AxisTitle.Characters.Text = "Voltage (mV)"
End With
ActiveChart.HasLegend = False
ActiveChart.SeriesCollection(1).Select
ActiveChart.Axes(xlCategory).Select
With ActiveChart.Axes(xlCategory)
   .MinimumScale = -120000
   .MaximumScale = 40000
   .MinorUnit = 20000
   .MajorUnitIsAuto = True
   .Crosses = xlAutomatic
   .ReversePlotOrder = False
   .ScaleType = xlLinear
   .DisplayUnit = xlNone
End With
Range("X57").Select



Charts.Add
ActiveChart.ChartType = xlXYScatterSmoothNoMarkers
ActiveChart.SetSourceData Source:=Sheets("Sheet1").Range("X57"), PlotBy:= _
   xlColumns
ActiveChart.SeriesCollection.NewSeries
ActiveChart.SeriesCollection(1).XValues = "=Sheet1!R3705C1:R7091C1"
ActiveChart.SeriesCollection(1).Values = "=Sheet1!R3705C3:R7091C3"
ActiveChart.Location Where:=xlLocationAsObject, Name:="Sheet1"
With ActiveChart
   .HasTitle = True
   .ChartTitle.Characters.Text = "Amplitude of Receiver"
   .Axes(xlCategory, xlPrimary).HasTitle = True
   .Axes(xlCategory, xlPrimary).AxisTitle.Characters.Text = "Time (ns)"
   .Axes(xlValue, xlPrimary).HasTitle = True
   .Axes(xlValue, xlPrimary).AxisTitle.Characters.Text = "Voltage (mV)"
End With
```

```
    ActiveChart.HasLegend = False
    ActiveChart.SeriesCollection(1).Select
    With Selection.Border
        .ColorIndex = 7
        .Weight = xlThin
        .LineStyle = xlContinuous
    End With
    With Selection
        .MarkerBackgroundColorIndex = xlNone
        .MarkerForegroundColorIndex = xlNone
        .MarkerStyle = xlNone
        .Smooth = True
        .MarkerSize = 3
        .Shadow = False
    End With

End Sub
```

Appendix B
Acoustic Properties of Materials

Material	Longitudinal Velocity		Shear Velocity		Acoustic Impedance
	(in/μs)*	(m/s)	(in/μs)*	(m/s)	(Kg/m²s x 10⁶)
Acrylic resin (Perspex®)	0.107	2,730	0.056	1,430	3.22
Aluminum	0.249	6,320	0.123	3,130	17.06
Beryllium	0.508	12,900	0.350	8,880	23.5
Brass, naval	0.174	4,430	0.083	2,120	37.30
Cadmium	0.109	2,780	0.059	1,500	24.02
Columbium	0.194	4,920	0.083	2,100	42.16
Copper	0.183	4,660	0.089	2,260	41.61
Glycerine	0.076	1,920	—	—	2.42
Gold	0.128	3,240	0.047	1,200	62.60
Inconel®	0.29	5,820	0.119	3,020	49.47
Iron	0.232	5,900	0.127	3,230	45.43
Iron, cast					
(slow)	0.138	3,500	0.087	2,200	25.00
(fast)	0.220	5,600	0.126	3,220	40.00
Lead	0.085	2,160	0.028	700	24.49
Manganese	0.183	4,660	0.093	2,350	34.44
Mercury	0.057	1,450	—	—	19.66
Molybdenum	0.246	6,250	0.132	3,350	63.75
Motor Oil (SAE 20 or 30)	0.069	1,740	—	—	1.51
Nickel, pure	0.222	5,630	0.117	2,960	49.99
Platinum	0.156	3,960	0.066	1,670	84.74
Polyamide, (nylon, Perlon®)					
(slow)	0.087	2,200	0.043	1,100	.40
(fast)	0.102	2,600	0.047	1,200	3.10
Polystyrene	0.092	2,340	—	—	2.47
Polyvinylchloride, PVC, hard	0.094	2,395	0.042	1,060	3.35
Silver	0.142	3,600	0.063	1,590	37.76
Steel, 1020	0.232	5,890	0.128	3,240	45.63
Steel, 4340	0.230	5,850	0.128	3,240	45.63
Steel, 302	0.223	5,660	0.123	3,120	45.45
austenitic stainless Steel, 347	0.226	5,740	0.122	3,090	45.40
austenitic stainless Tin	0.131	3,320	0.066	1,670	24.20
Titanium, TI 150A	0.240	6,100	0.123	3,120	27.69
Tungsten	0.204	5,180	0.113	2,870	99.72
Uranium	0.133	3,370	0.078	1,980	63.02
Water (20°C)	0.058	1,480	—	—	1.48
Zinc	0.164	4,170	0.095	2,410	29.61
Zirconium	0.183	4,650	0.089	2,250	30.13

* Conversion Factor: 1 m/s = 3.937×10^{-5} in/μS

Source: Nondestructive Testing Handbook 2nd Edition Volume 7
Ultrasonic Testing ASNT 1991 ed Paul McIntire

Appendix C
Data-Processing Flowchart of Experimental Rig C

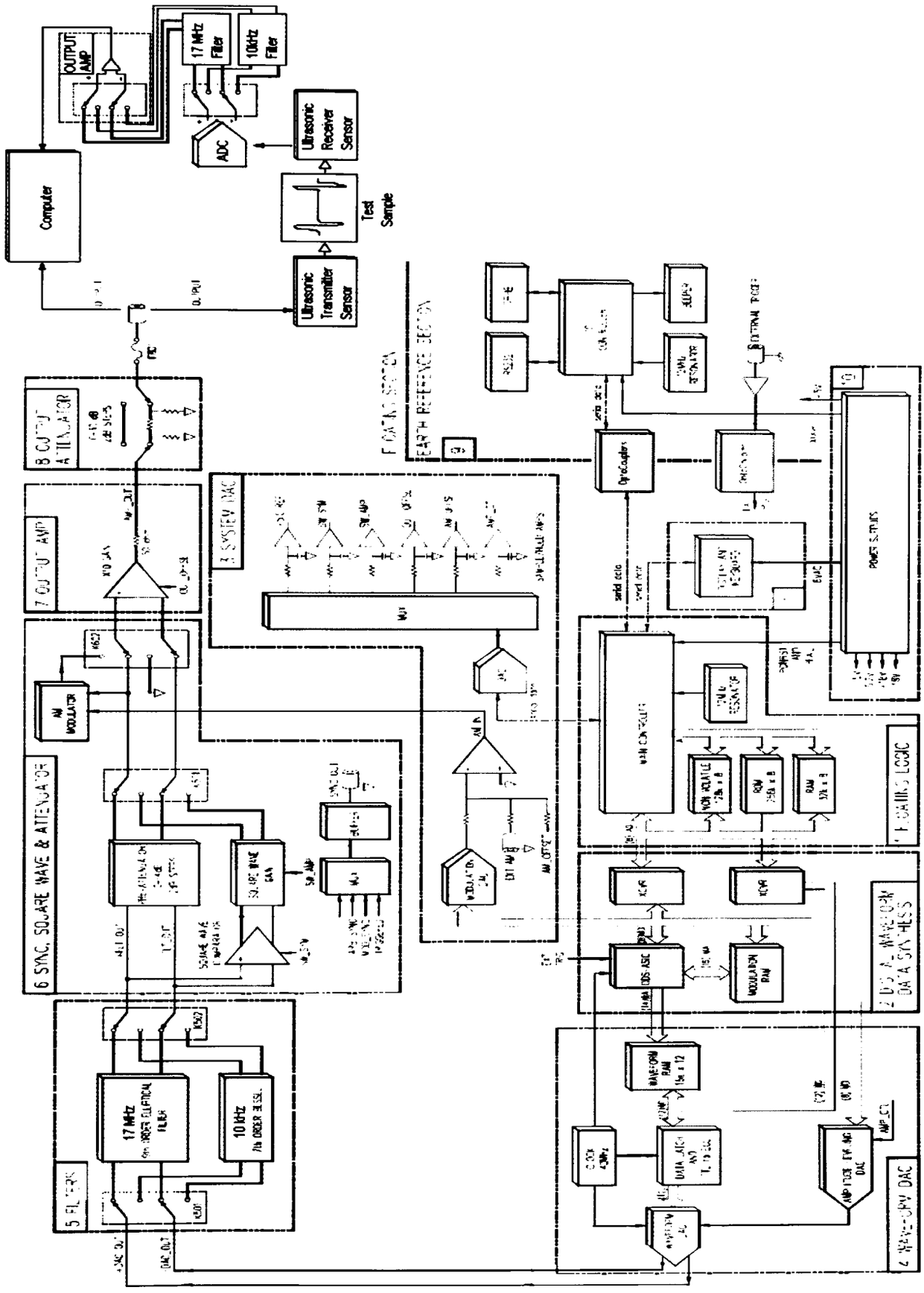

Appendix D
Viscosity of Gases

The following table gives the viscosity of some common gases as a function of temperature. Unless otherwise noted, the viscosity values refer to a pressure of 100 kPa (1 bar). The notation *P*=0 indicates the low pressure limiting value is given. The difference between the viscosity at 100 kPa and the limiting value is generally less than 1%. Viscosity is given in units of μPa s; note that 1 μPa s = 10 $^{-6}$ poise. Substances are listed in the modified Hill order (see Introduction).

		Viscosity in micropascal seconds (μPa s)						
		100 K	200 K	300 K	400 K	500 K	600 K	Ref.
	Air	7.1	13.3	18.6	23.1	27.1	30.8	1
Ar	Argon	8.0	15.9	22.9	28.8	34.2	39.0	2,8
BF_3	Boron trifluoride		12.3	17.1	21.7	26.1	30.2	13
ClH	Hydrogen chloride			14.6	19.7	24.3		13
F_6S	Sulfur hexafluoride (*P*=0)			15.3	19.8	23.9	27.7	10
H_2	Hydrogen (*P*=0)	4.2	5.8	9.0	10.9	12.7	14.4	4
D_2	Deuterium (*P*=0)	5.9	9.6	12.6	15.4	17.9	20.3	11
H_2O	Water			10.0	13.3	17.3	21.4	6
D_2O	Deuterium oxide			11.1	13.7	17.7	22.0	7
He	Helium (*P*=0)	9.7	15.3	20.0	24.4	28.4	32.3	8
Kr	Krypton (*P*=0)	8.8	17.1	25.6	33.1	39.8	45.9	8
NO	Nitric oxide		15.8	19.2	23.8	28.0	31.9	13
N_2	Nitrogen (*P*=0)		12.9	17.8	22.2	26.1	29.6	12
N_2O	Nitrous oxide		10.0	15.0	19.4	23.6	27.4	13
Ne	Neon (*P*=0)	14.4	24.3	32.1	38.9	45.0	50.8	8
O_2	Oxygen (*P*=0)	7.5	14.5	20.8	26.1	30.8	35.1	12
O_2S	Sulfur dioxide		8.6	12.8	17.5	21.7		13
Xe	Xenon (*P*=0)	8.3	15.4	23.2	30.7	37.5	44.0	8
CO	Carbon monoxide	6.7	12.9	17.8	22.1	25.8	29.1	13
CO_2	Carbon dioxide		10.0	15.0	19.7	24.0	28.0	9,10
$CHCl_3$	Chloroform			10.2	13.7	15.9	20.1	13
CH_4	Methane		7.7	11.2	14.8	17.9	19.4	10
CH_4O	Methanol				13.2	16.5	19.6	13
C_2H_2	Acetylene			10.4	13.5	16.5		13
C_2H_4	Ethylene		7.0	10.4	13.6	16.5	19.1	3
C_2H_6	Ethane		5.4	9.5	12.8	14.9	17.2	5
C_2H_6O	Ethanol				11.6	14.5	17.0	13
C_3H_8	Propane			8.3	10.9	13.4	15.8	5
C_4H_{10}	Butane			7.5	10.0	12.3	14.6	5
C_4H_{10}	Isobutane			7.6	10.0	12.3	14.5	5
$C_4H_{10}O$	Diethyl ether			7.6	10.1	12.4		13
C_5H_{12}	Pentane			6.7	9.2	11.4	13.4	13
C_6H_{14}	Hexane				8.6	10.8	12.8	13

REFERENCES

1. H. Kadoya, N. Matsunaga, and A. Nagashima. Viscosity and thermal conductivity of dry air in the gaseous phase. *J. Phys. Chem. Ref. Data*, 14, 947, 1985.
2. B. A. Younglove and H. J. M. Hanley. The viscosity and thermal conductivity coefficients of gaseous and liquid argon. *J. Phys. Chem. Ref. Data*, 15, 1323, 1986.
3. P. M. Holland, B. E. Eaton, and H. J. M. Hanley. A Correlation of the viscosity and thermal conductivity data of gaseous and liquid ethylene. *J. Phys. Chem. Ref. Data*, 12, 917, 1983.
4. M. J. Assael, S. Mixafendi, and W. A. Wakeham. The viscosity and thermal conductivity of normal hydrogen in the limit zero density. *J. Phys. Chem. Ref. Data*, 15, 1315, 1986.
5. B. A. Younglove and J. F. Ely. Thermophysical properties of fluids. II. Methane, ethane, propane, isobutane, and normal butane. *J. Phys. Chem. Ref. Data*, 16, 577, 1987.
6. J. V. Sengers and J. T. R. Watson, Improved international formulations for the viscosity and thermal conductivity of water substance, *J. Phys. Chem. Ref. Data*, 15, 1291, 1986.
7. N. Matsunaga and A. Nagashima, Transport properties of liquid and gaseous D_2O over a wide range of temperature and pressure, *J. Phys. Chem. Ref. Data*, 12, 933, 1983.
8. J. Kestin, et al., Equilibrium and transport properties of the noble gases and their mixtures at low density, *J. Phys. Chem. Ref. Data*, 13, 299, 1984.
9. V. Vesovic, et al., The transport properties of carbon dioxide, *J. Phys. Chem. Ref. Data*, 19, 1990.
10. R. D. Trengove and W. A. Wakeham, The viscosity of carbon dioxide, methane, and sulfur hexafluoride in the limit of zero density, *J. Phys. Chem. Ref. Data*, 16, 175, 1987.
11. M. J. Assael, S. Mixafendi, and W. A. Wakeham, The viscosity of normal deuterium in the limit of zero density, *J. Phys. Chem. Ref. Data*, 16, 189, 1987.
12. W. A. Cole and W. A. Wakeham, The viscosity of nitrogen, oxygen, and their binary mixtures in the limit of zero density, *J. Phys. Chem. Ref. Data*, 14, 209, 1985.
13. C. Y. Ho, Ed., *Properties of Inorganic and Organic Fluids, CINDAS Data Series on Material Properties*, Vol. V-1, Hemisphere Publishing Corp., New York, 1988.

© 2[illegible] CRC Press LLC

Appendix E
Viscosity of Liquids

The absolute viscosity of some common liquids at temperatures between −25 and 100°C is given in this table. Values were derived by fitting experimental data to suitable expressions for the temperature dependence. The substances are arranged by molecular formula in the modified Hill order (see Preface). All values are given in units of millipascal seconds (mPa s); this unit is identical to centipoise (cp).

Viscosity values correspond to a nominal pressure of 1 atmosphere. If a value is given at a temperature above the normal boiling point, the applicable pressure is understood to be the vapor pressure of the liquid at that temperature. A few values are given at a temperature slightly below the normal freezing point; these refer to the supercooled liquid.

The accuracy ranges from 1% in the best cases to 5 to 10% in the worst cases. Additional significant figures are included in the table to facilitate interpolation.

REFERENCES

1. Viswanath, D. S. and Natarajan, G., *Data Book on the Viscosity of Liquids*, Hemisphere Publishing Corp., New York, 1989.
2. Daubert, T. E., Danner, R. P., Sibul, H. M., and Stebbins, C. C., *Physical and Thermodynamic Properties of Pure Compounds: Data Compilation*, extant 1994 (core with 4 supplements), Taylor & Francis, Bristol, PA (also available as database).
3. Ho, C. Y., Ed., *CINDAS Data Series on Material Properties*, Vol. V-1, *Properties of Inorganic and Organic Fluids*, Hemisphere Publishing Corp., New York, 1988.
4. Stephan, K. and Lucas, K., *Viscosity of Dense Fluids*, Plenum Press, New York, 1979.
5. Vargaftik, N. B., *Tables of Thermophysical Properties of Liquids and Gases*, 2nd ed., John Wiley, New York, 1975.

Molecular formula	Name	Viscosity in mPa s					
		−25°C	0°C	25°C	50°C	75°C	100°C
	Compounds not containing carbon						
Br_2	Bromine		1.252	0.944	0.746		
Cl_3HSi	Trichlorosilane		0.415	0.326			
Cl_3P	Phosphorous trichloride	0.870	0.662	0.529	0.439		
Cl_4Si	Tetrachlorosilane			99.4	96.2		
H_2O	Water		1.793	0.890	0.547	0.378	0.282
H_4N_2	Hydrazine			0.876	0.628	0.480	0.384
Hg	Mercury			1.526	1.402	1.312	1.245
NO_2	Nitrogen dioxide		0.532	0.402			
	Compounds containing carbon						
CCl_3F	Trichlorofluoromethane	0.740	0.539	0.421			
CCl_4	Tetrachloromethane		1.321	0.908	0.656	0.494	
CS_2	Carbon disulfide		0.429	0.352			
$CHBr_3$	Tribromomethane			1.857	1.367	1.029	
$CHCl_3$	Trichloromethane	0.988	0.706	0.537	0.427		
CHN	Hydrogen cyanide		0.235	0.183			
CH_2Br_2	Dibromomethane	1.948	1.320	0.980	0.779	0.652	
CH_2Cl_2	Dichloromethane	0.727	0.533	0.413			
CH_2O_2	Formic acid			1.607	1.030	0.724	0.545
CH_3I	Iodomethane		0.594	0.469			
CH_3NO	Formamide		7.114	3.343	1.833		
CH_3NO_2	Nitromethane	1.311	0.875	0.630	0.481	0.383	0.317
CH_4O	Methanol	1.258	0.793	0.544			
CH_5N	Methylamine	0.319	0.231				
$C_2Cl_3F_3$	1,1,2-Trichlorotrifluoro-ethane	1.465	0.945	0.656	0.481		
C_2Cl_4	Tetrachloroethylene		1.114	0.844	0.663	0.535	0.442
C_2HCl_3	Trichloroethylene		0.703	0.545	0.444	0.376	
C_2HCl_5	Pentachloroethane		3.761	2.254	1.491	1.061	
$C_2HF_3O_2$	Trifluoroacetic acid			0.808	0.571		
$C_2H_2Cl_2$	*cis*-1,2-Dichloroethylene	0.786	0.575	0.445			
$C_2H_2Cl_2$	*trans*-1,2-Dichloroethylene	0.522	0.398	0.317	0.261		
$C_2H_2Cl_4$	1,1,1,2-Tetrachloroethane	3.660	2.200	1.437	1.006	0.741	0.570
$C_2H_3ClF_2$	1-Chloro-1,1-difluoro-ethane	0.477	0.376				

Appendix E
Viscosity of Liquids (*continued*)

Molecular formula	Name	Viscosity in mPa s					
		−25°C	0°C	25°C	50°C	75°C	100°C
C_2H_3ClO	Acetyl chloride			0.368	0.294		
$C_2H_3Cl_3$	1,1,1-Trichloroethane	1.847	1.161	0.793	0.578	0.428	
C_2H_3N	Acetonitrile		0.400	0.369	0.284	0.234	
$C_2H_4Br_2$	1,2-Dibromoethane			1.595	1.116	0.837	0.661
$C_2H_4Cl_2$	1,1-Dichloroethane			0.464	0.362		
$C_2H_4Cl_2$	1,2-Dichloroethane		1.125	0.779	0.576	0.447	
$C_2H_4O_2$	Acetic acid			1.056	0.786	0.599	0.464
$C_2H_4O_2$	Methyl formate		0.424	0.325			
C_2H_5Br	Bromoethane	0.635	0.477	0.374			
C_2H_5Cl	Chloroethane	0.416	0.319				
C_2H_5I	Iodoethane		0.723	0.556	0.444	0.365	
C_2H_5NO	*N*-Methylformamide		2.549	1.678	1.155	0.824	0.606
$C_2H_5NO_2$	Nitroethane	1.354	0.940	0.688	0.526	0.415	0.337
C_2H_6O	Ethanol	3.262	1.786	1.074	0.694	0.476	
C_2H_6OS	Dimethyl sulfoxide			1.987	1.290		
$C_2H_6O_2$	Ethylene glycol			16.1	6.554	3.340	1.975
C_2H_6S	Dimethyl sulfide		0.356	0.284			
C_2H_6S	Ethanethiol		0.364	0.287			
C_2H_7N	Dimethylamine	0.300	0.232				
C_2H_7NO	Ethanolamine			21.1	8.560	3.935	1.998
C_3H_5Br	3-Bromopropene		0.620	0.471	0.373		
C_3H_5Cl	3-Chloropropene		0.408	0.314			
C_3H_5ClO	Epichlorohydrin	2.492	1.570	1.073	0.781	0.597	0.474
C_3H_5N	Propanenitrile			0.294	0.240	0.202	
C_3H_6O	Acetone	0.540	0.395	0.306	0.247		
C_3H_6O	Allyl alcohol			1.218	0.759	0.505	
C_3H_6O	Propanal			0.321	0.249		
$C_3H_6O_2$	Ethyl formate		0.506	0.380	0.300		
$C_3H_6O_2$	Methyl acetate		0.477	0.364	0.284		
$C_3H_6O_2$	Propanoic acid		1.499	1.030	0.749	0.569	0.449
C_3H_7Br	1-Bromopropane		0.645	0.489	0.387		
C_3H_7Br	2-Bromopropane		0.612	0.458	0.359		
C_3H_7Cl	1-Chloropropane		0.436	0.334			
C_3H_7Cl	2-Chloropropane		0.401	0.303			
C_3H_7I	1-Iodopropane		0.970	0.703	0.541	0.436	0.363
C_3H_7I	2-Iodopropane		0.883	0.653	0.506	0.407	
C_3H_7NO	*N,N*-Dimethylformamide		1.176	0.794	0.624		
$C_3H_7NO_2$	1-Nitropropane	1.851	1.160	0.798	0.589	0.460	0.374
C_3H_8O	1-Propanol	8.645	3.815	1.945	1.107	0.685	
C_3H_8O	2-Propanol		4.619	2.038	1.028	0.576	
$C_3H_8O_2$	1,2-Propylene glycol		248	40.4	11.3	4.770	2.750
$C_3H_8O_3$	Glycerol			934	152	39.8	14.8
C_3H_8S	1-Propanethiol		0.503	0.385			
C_3H_8S	2-Propanethiol		0.477	0.357	0.280		
C_3H_9N	Propylamine			0.376			
C_3H_9N	Isopropylamine		0.454	0.325			
C_4H_4O	Furan	0.661	0.475	0.361			
C_4H_5N	Pyrrole		2.085	1.225	0.828	0.612	
$C_4H_6O_3$	Acetic anhydride		1.241	0.843	0.614	0.472	0.377
C_4H_7N	Butanenitrile			0.553	0.418	0.330	0.268
C_4H_8O	2-Butanone	0.720	0.533	0.405	0.315	0.249	
C_4H_8O	Tetrahydrofuran	0.849	0.605	0.456	0.359		
$C_4H_8O_2$	1,4-Dioxane			1.177	0.787	0.569	
$C_4H_8O_2$	Ethyl acetate		0.578	0.423	0.325	0.259	
$C_4H_8O_2$	Methyl propionate		0.581	0.431	0.333	0.266	
$C_4H_8O_2$	Propyl formate		0.669	0.485	0.370	0.293	
$C_4H_8O_2$	Butanoic acid		2.215	1.426	0.982	0.714	0.542

Appendix E
Viscosity of Liquids (*continued*)

Molecular formula	Name	Viscosity in mPa s					
		–25°C	0°C	25°C	50°C	75°C	100°C
$C_4H_8O_2$	2-Methylpropanoic acid		1.857	1.226	0.863	0.639	0.492
$C_4H_8O_2S$	Sulfolane				6.280	3.818	2.559
C_4H_8S	Tetrahydrothiophene			0.973	0.912		
C_4H_9Br	1-Bromobutane		0.815	0.606	0.471	0.379	
C_4H_9Cl	1-Chlorobutane		0.556	0.422	0.329	0.261	
C_4H_9N	Pyrrolidine	1.914	1.071	0.704	0.512		
C_4H_9NO	*N*,*N*-Dimethylacetamide			1.927			
C_4H_9NO	Morpholine			2.021	1.247	0.850	0.627
$C_4H_{10}O$	1-Butanol	12.19	5.185	2.544	1.394	0.833	0.533
$C_4H_{10}O$	2-Butanol			3.096	1.332	0.698	0.419
$C_4H_{10}O$	2-Methyl-2-propanol			4.312	1.421	0.678	
$C_4H_{10}O$	Diethyl ether		0.283	0.224			
$C_4H_{10}O_3$	Diethylene glycol			30.200	11.130	4.917	2.505
$C_4H_{10}S$	Diethyl sulfide		0.558	0.422	0.331	0.267	
$C_4H_{11}N$	Butylamine		0.830	0.574	0.409	0.298	
$C_4H_{11}N$	Isobutylamine		0.770	0.571	0.367		
$C_4H_{11}N$	Diethylamine			0.319	0.239		
$C_4H_{11}NO_2$	Diethanolamine				109.5	28.7	9.100
$C_5H_4O_2$	Furfural		2.501	1.587	1.143	0.906	0.772
C_5H_5N	Pyridine		1.361	0.879	0.637	0.497	0.409
C_5H_{10}	1-Pentene	0.313	0.241	0.195			
C_5H_{10}	2-Methyl-2-butene		0.255	0.203			
C_5H_{10}	Cyclopentane		0.555	0.413	0.321		
$C_5H_{10}O$	Mesityl oxide	1.291	0.838	0.602	0.465	0.381	0.326
$C_5H_{10}O$	2-Pentanone		0.641	0.470	0.362	0.289	0.238
$C_5H_{10}O$	3-Pentanone		0.592	0.444	0.345	0.276	0.227
$C_5H_{10}O_2$	Butyl formate		0.937	0.644	0.472	0.362	0.289
$C_5H_{10}O_2$	Propyl acetate		0.768	0.544	0.406	0.316	0.255
$C_5H_{10}O_2$	Ethyl propanoate		0.691	0.501	0.380	0.299	0.242
$C_5H_{10}O_2$	Methyl butanoate		0.759	0.541	0.406	0.318	0.257
$C_5H_{10}O_2$	Methyl isobutanoate		0.672	0.488	0.373	0.296	
$C_5H_{11}N$	Piperidine			1.573	0.958	0.649	0.474
C_5H_{12}	Pentane	0.351	0.274	0.224			
C_5H_{12}	Isopentane	0.376	0.277	0.214			
$C_5H_{12}O$	1-Pentanol	25.4	8.512	3.619	1.820	1.035	0.646
$C_5H_{12}O$	2-Pentanol			3.470	1.447	0.761	0.465
$C_5H_{12}O$	3-Pentanol			4.149	1.473	0.727	0.436
$C_5H_{12}O$	2-Methyl-1-butanol			4.453	1.963	1.031	0.612
$C_5H_{12}O$	3-Methyl-1-butanol		8.627	3.692	1.842	1.031	0.631
$C_5H_{13}N$	Pentylamine		1.030	0.702	0.493	0.356	
C_6F_6	Hexafluorobenzene			2.789	1.730	1.151	
$C_6H_4Cl_2$	*o*-Dichlorobenzene		1.958	1.324	0.962	0.739	0.593
$C_6H_4Cl_2$	*m*-Dichlorobenzene		1.492	1.044	0.787	0.628	0.525
C_6H_5Br	Bromobenzene		1.560	1.074	0.798	0.627	0.512
C_6H_5Cl	Chlorobenzene	1.703	1.058	0.753	0.575	0.456	0.369
C_6H_5ClO	*o*-Chlorophenol			3.589	1.835	1.131	0.786
C_6H_5ClO	*m*-Chlorophenol				4.041		
C_6H_5F	Fluorobenzene		0.749	0.550	0.423	0.338	
C_6H_5I	Iodobenzene		2.354	1.554	1.117	0.854	0.683
$C_6H_5NO_2$	Nitrobenzene		3.036	1.863	1.262	0.918	0.704
C_6H_6	Benzene			0.604	0.436	0.335	
C_6H_6ClN	*o*-Chloroaniline			3.316	1.913	1.248	0.887
C_6H_6O	Phenol				3.437	1.784	1.099
C_6H_7N	Aniline			3.847	2.029	1.247	0.850
$C_6H_8N_2$	Phenylhydrazine			13.0	4.553	1.850	0.848
C_6H_{10}	Cyclohexene		0.882	0.625	0.467	0.364	
$C_6H_{10}O$	Cyclohexanone			2.017	1.321	0.919	0.671

Appendix E
Viscosity of Liquids (*continued*)

Molecular formula	Name	Viscosity in mPa s					
		−25°C	0°C	25°C	50°C	75°C	100°C
$C_6H_{11}N$	Hexanenitrile			0.912	0.650	0.488	0.382
C_6H_{12}	Cyclohexane			0.894	0.615	0.447	
C_6H_{12}	Methylcyclopentane	0.927	0.653	0.479	0.364		
C_6H_{12}	1-Hexene	0.441	0.326	0.252	0.202		
$C_6H_{12}O$	Cyclohexanol			57.5	12.3	4.274	1.982
$C_6H_{12}O$	2-Hexanone	1.300	0.840	0.583	0.429	0.329	0.262
$C_6H_{12}O$	4-Methyl-2-pentanone			0.545	0.406		
$C_6H_{12}O_2$	Butyl acetate		1.002	0.685	0.500	0.383	0.305
$C_6H_{12}O_2$	Isobutyl acetate			0.676	0.493	0.370	0.286
$C_6H_{12}O_2$	Ethyl butanoate			0.639	0.453		
$C_6H_{12}O_2$	Dincetone alcohol	28.7	6.621	2.798	1.829	1.648	
$C_6H_{12}O_3$	Paraldehyde			1.079	0.692	0.485	0.362
$C_6H_{13}N$	Cyclohexylamine			1.944	1.169	0.782	0.565
C_6H_{14}	Hexane		0.405	0.300	0.240		
C_6H_{14}	2-Methylpentane		0.372	0.286	0.226		
C_6H_{14}	3-Methylpentane		0.395	0.306			
$C_6H_{14}O$	Dipropyl ether		0.542	0.396	0.304	0.242	
$C_6H_{14}O$	1-Hexanol			4.578	2.271	1.270	0.781
$C_6H_{15}N$	Triethylamine		0.455	0.347	0.273	0.221	
$C_6H_{15}N$	Dipropylamine		0.751	0.517	0.377	0.288	0.228
$C_6H_{15}N$	Diisopropylamine			0.393	0.300	0.237	
$C_6H_{15}NO_3$	Triethanolamine			609	114	31.5	11.7
C_7H_5N	Benzonitrile			1.267	0.883	0.662	0.524
C_7H_7Cl	*o*-Chlorotoluene		1.390	0.964	0.710	0.547	0.437
C_7H_7Cl	*m*-Chlorotoluene		1.165	0.823	0.616	0.482	0.391
C_7H_7Cl	*p*-Chlorotoluene			0.837	0.621	0.483	0.390
C_7H_8	Toluene	1.165	0.778	0.560	0.424	0.333	0.270
C_7H_8O	*o*-Cresol				3.035	1.562	0.961
C_7H_8O	*m*-Cresol			12.9	4.417	2.093	1.207
C_7H_8O	Benzyl alcohol			5.474	2.760	1.618	1.055
C_7H_8O	Anisole			1.056	0.747	0.554	0.427
C_7H_9N	*N*-Methylaniline		4.120	2.042	1.222	0.825	0.606
C_7H_9N	*o*-Methyl aniline		10.3	3.823	1.936	1.198	0.839
C_7H_9N	*m*-Methyl aniline		8.180	3.306	1.679	1.014	0.699
C_7H_9N	Benzylamine			1.624	1.080	0.769	0.577
C_7H_{14}	Methylcyclohexane		0.991	0.679	0.501	0.390	0.316
C_7H_{14}	1-Heptene		0.441	0.340	0.273	0.226	
$C_7H_{14}O$	2-Heptanone			0.714	0.407	0.297	
$C_7H_{14}O_2$	Heptanoic acid			3.840	2.282	1.488	1.041
C_7H_{16}	Heptane	0.757	0.523	0.387	0.301	0.243	
C_7H_{16}	3-Methylhexane			0.350			
$C_7H_{16}O$	1-Heptanol			5.810	2.603	1.389	0.849
$C_7H_{16}O$	2-Heptanol			3.955	1.799	0.987	0.615
$C_7H_{16}O$	3-Heptanol				1.957	0.976	0.584
$C_7H_{16}O$	4-Heptanol			4.207	1.695	0.882	0.539
$C_7H_{17}N$	Heptylamine			1.314	0.865	0.600	0.434
C_8H_8	Styrene		1.050	0.695	0.507	0.390	0.310
C_8H_8O	Acetophenone			1.681			0.634
$C_8H_8O_2$	Methyl benzoate			1.857			
$C_8H_8O_3$	Methyl salicylate					1.102	0.815
C_8H_{10}	Ethylbenzene		0.872	0.631	0.482	0.380	0.304
C_8H_{10}	*o*-Xylene		1.084	0.760	0.561	0.432	0.345
C_8H_{10}	*m*-Xylene		0.795	0.581	0.445	0.353	0.289
C_8H_{10}	*p*-Xylene			0.603	0.457	0.359	0.290
$C_8H_{10}O$	Phenetole			1.197	0.817	0.594	0.453
$C_8H_{11}N$	*N,N*-Dimethylaniline		1.996	1.300	0.911	0.675	0.523
$C_8H_{11}N$	*N*-Ethylaniline		3.981	2.047	1.231	0.825	0.596

Appendix E
Viscosity of Liquids (*continued*)

Molecular formula	Name	Viscosity in mPa s					
		−25°C	0°C	25°C	50°C	75°C	100°C
C_8H_{16}	Ethylcyclohexane		1.139	0.784	0.579		
$C_8H_{16}O_2$	Octanoic acid			5.020	2.656	1.654	1.147
C_8H_{18}	Octane		0.700	0.508	0.385	0.302	0.243
$C_8H_{18}O$	1-Octanol			7.288	3.232	1.681	0.991
$C_8H_{18}O$	4-Methyl-3-heptanol		1.904	1.085	0.702	0.497	0.375
$C_8H_{18}O$	5-Methyl-3-heptanol		2.052	1.178	0.762	0.536	0.401
$C_8H_{18}O$	2-Ethyl-1-hexanol		20.7	6.271	2.631	1.360	0.810
$C_8H_{18}O$	Dibutyl ether	1.417	0.918	0.637	0.466	0.356	0.281
$C_8H_{19}N$	Dibutylamine		1.509	0.918	0.619	0.449	0.345
$C_8H_{19}N$	Diisobutylamine		1.115	0.723	0.511	0.384	0.303
C_9H_7N	Quinoline			3.337	1.892	1.201	0.833
C_9H_{10}	Indane		2.230	1.357	0.931	0.692	0.545
C_9H_{12}	Cumene		1.075	0.737	0.547		
$C_9H_{14}O$	Isophorone		4.201	2.329	1.415	0.923	0.638
$C_9H_{18}O$	5-Nonanone			1.199	0.834	0.619	0.484
$C_9H_{18}O_2$	Nonanoic acid			7.011	3.712	2.234	1.475
C_9H_{20}	Nonane		0.964	0.665	0.488	0.375	0.300
$C_9H_{20}O$	1-Nonanol			9.123	4.032		
$C_{10}H_{10}O_4$	Dimethyl phthalate		63.2	14.4	5.309	2.824	1.980
$C_{10}H_{14}$	Butylbenzene			0.950	0.683	0.515	
$C_{10}H_{18}$	*cis*-Decahydronaphthalene	12.8	5.645	3.042	1.875	1.271	0.924
$C_{10}H_{18}$	*trans*-Decahydronaphthalene	6.192	3.243	1.948	1.289	0.917	0.689
$C_{10}H_{20}O_2$	Decanoic acid				4.327	2.651	
$C_{10}H_{22}$	Decane	2.188	1.277	0.838	0.598	0.453	0.359
$C_{10}H_{22}O$	1-Decanol			10.9	4.590		
$C_{11}H_{24}$	Undecane		1.707	1.098	0.763	0.562	0.433
$C_{12}H_{10}O$	Diphenyl ether				2.130	1.407	1.023
$C_{12}H_{26}$	Dodecane		2.277	1.383	0.930	0.673	0.514
$C_{13}H_{12}$	Diphenylmethane					1.265	0.929
$C_{13}H_{28}$	Tridecane		2.909	1.724	1.129	0.796	0.594
$C_{14}H_{30}$	Tetradecane			2.128	1.376	0.953	0.697
$C_{16}H_{22}O_4$	Dibutyl phthalate	483	66.4	16.6	6.470	3.495	2.425
$C_{16}H_{34}$	Hexadecane			3.032	1.879	1.260	0.899
$C_{18}H_{38}$	Octadecane				2.487	1.609	1.132

Appendix F
Viscosity of Liquid Metals

This table gives the viscosity of several liquid metals as a function of temperature. Experimental data from some of the references was smoothed to produce the table. Viscosity is given in millipascal second (mPa s), which equals the c.g.s. unit centipoise (cP).

REFERENCES

1. Shpil'rain, E. E., Yakimovich, K. A., Fomin, V. A., Skovorodjko, S. N., and Mozgovoi, A. G., in *Handbook of Thermodynamic and Transport Properties of the Alkali Metals*, Ohse, R. H., Ed., Blackwell Scientific Publishers, Oxford, 1985. [Li, Na, K, Rb, Cs]
2. Rothwell, E., *J. Inst. Metals* 90, 389, 1961. [Al]
3. Culpin, M. F., *Proc. Phys. Soc.* 70, 1079, 1957. [Ca]
4. *Landolt-Börnstein, Numerical Data and Functional Relationships in Science and Technology, Sixth Edition*, II/5a, *Transport Phenomena I (Viscosity and Diffusion)*, Springer-Verlag, Heidelberg, 1961 [Co, Au, Mg, Ni, Ag]
5. Spells, K. E., *Proc. Phys. Soc.* 48, 299, 1936. [Ga]
6. Waisdorfer, H., Arpshofen, I., and Predel, B., *Z. Met.* 79, 503, 1988. [In]

	Viscosity in mPa s					
t/°C	Lithium	Sodium	Potassium	Rubidium	Cesium	Gallium
50				0.542	0.598	1.921
100		0.687	0.441	0.435	0.469	1.608
150		0.542	0.358	0.365	0.389	1.397
200	0.566	0.451	0.303	0.316	0.334	1.245
250	0.503	0.387	0.263	0.280	0.294	1.130
300	0.453	0.341	0.234	0.252	0.264	1.040
350	0.412	0.306	0.211	0.230	0.240	0.968
400	0.379	0.278	0.193	0.212	0.221	0.909
450	0.352	0.255	0.178	0.197	0.206	0.859
500	0.328	0.237	0.166	0.185	0.192	0.817
550	0.308	0.221	0.155	0.174	0.181	0.781
600	0.290	0.208	0.146	0.165	0.171	0.750
650	0.275	0.196	0.138	0.157	0.163	0.722
700	0.261	0.186	0.132	0.150	0.156	0.698
750	0.249	0.177	0.126	0.143	0.149	0.677
800	0.238	0.170	0.120	0.138	0.143	0.657
850	0.228	0.163	0.115	0.133	0.138	0.640
900	0.219	0.156	0.111	0.128	0.134	0.624
950	0.211	0.151	0.107	0.124	0.129	0.610
1000	0.204	0.146	0.104	0.120	0.125	0.597
1050	0.197	0.141	0.101	0.117	0.122	0.585
1100	0.191	0.137	0.098	0.114	0.119	0.574
1150	0.185	0.133	0.095	0.111	0.116	
1200	0.180	0.129	0.092	0.108	0.113	
1250	0.175	0.126	0.090	0.105	0.110	
1300	0.170	0.123	0.088	0.103	0.108	
1350	0.166	0.120	0.086	0.101	0.106	
1400	0.162	0.117	0.084	0.099	0.104	
1450	0.158	0.115	0.082	0.097	0.102	
1500	0.155	0.113	0.081	0.095	0.100	
1550	0.151	0.110	0.079	0.093	0.098	
1600	0.148	0.108	0.078	0.092	0.097	
1650	0.145	0.106	0.076	0.090	0.095	
1700	0.142	0.105	0.075		0.094	
1750	0.139	0.103	0.074		0.092	
1800	0.137	0.101			0.091	
1850	0.135	0.100			0.090	
1900	0.132	0.098			0.089	
1950	0.130	0.097			0.088	
2000	0.128	0.096			0.086	

Appendix F
Viscosity of Liquid Metals (*continued*)

	Viscosity in mPa s							
t/°C	Aluminum	Calcium	Cobalt	Gold	Indium	Magnesium	Nickel	Silver
250					1.35			
300					1.22			
350					1.12			
400					1.04			
450					0.98			
700	1.289					1.10		
750	1.209					0.96		
800	1.115					0.84		
850	1.028	1.107				0.74		
900		0.959				0.67		
1000								3.89
1050								3.56
1100				5.130				3.31
1150				4.874				3.06
1200				4.640				2.82
1250				4.429				2.61
1300				4.240				2.42
1350								2.28
1400								2.20
1450								2.19
1500			4.15				4.35	
1550			3.89				4.09	
1600			3.64				3.87	
1650			3.41				3.67	
1700			3.20				3.49	
1750			2.99				3.32	

Appendix G1
Experimental Rig A Assembly Drawing

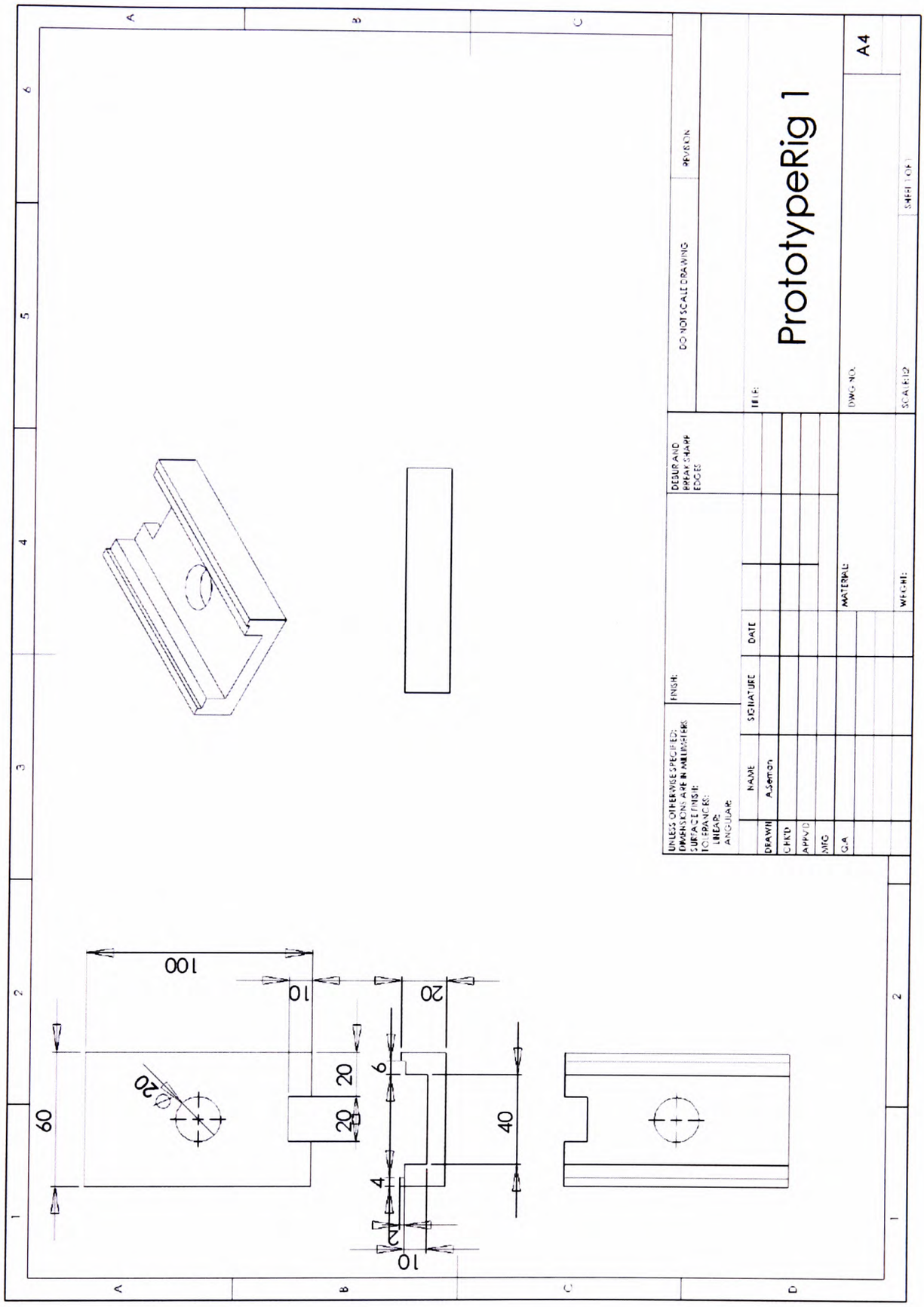

Appendix G2
Experimental Rig B Assembly Drawing

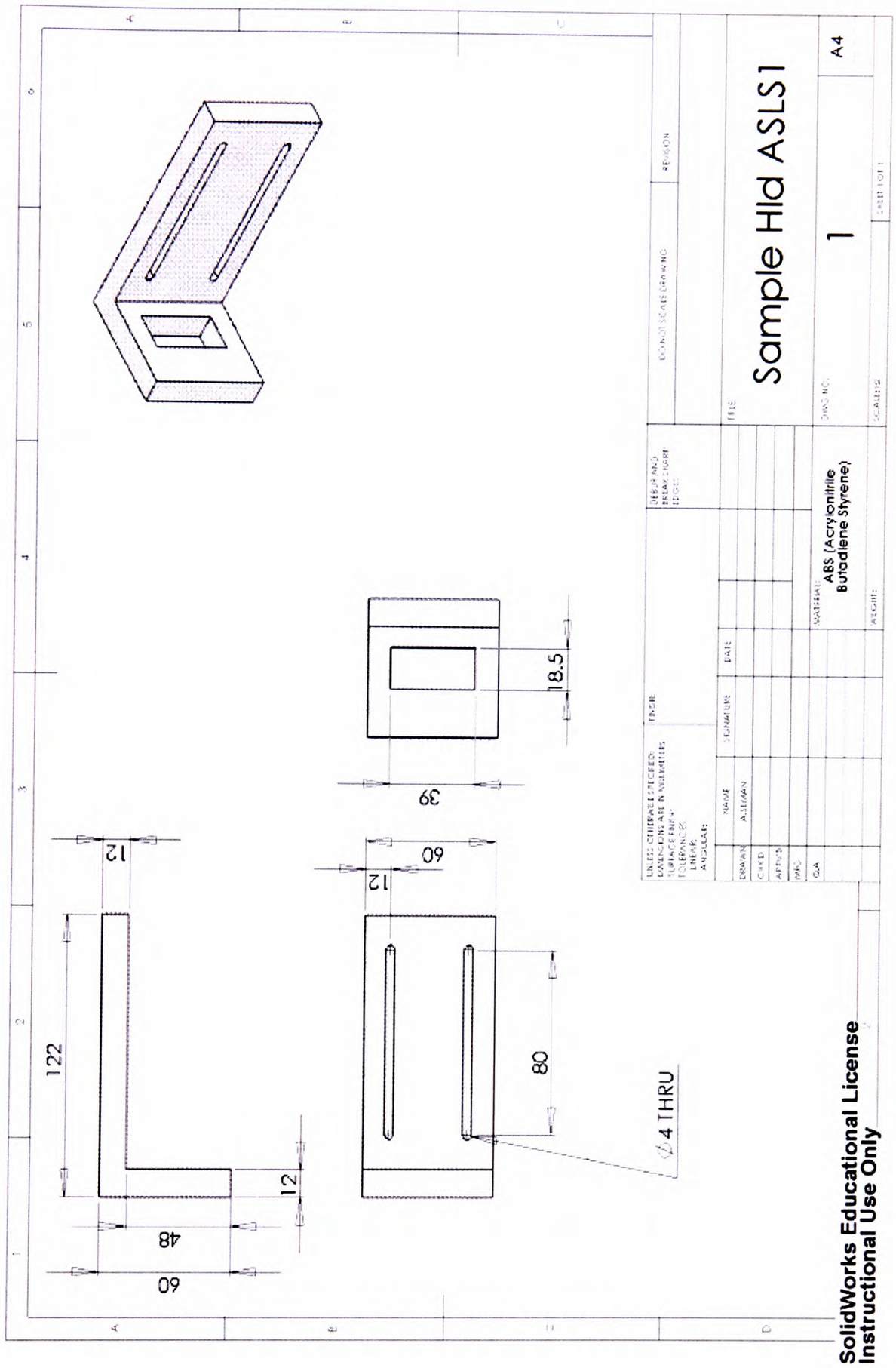

Appendix G3
Experimental Rig C Assembly Drawing

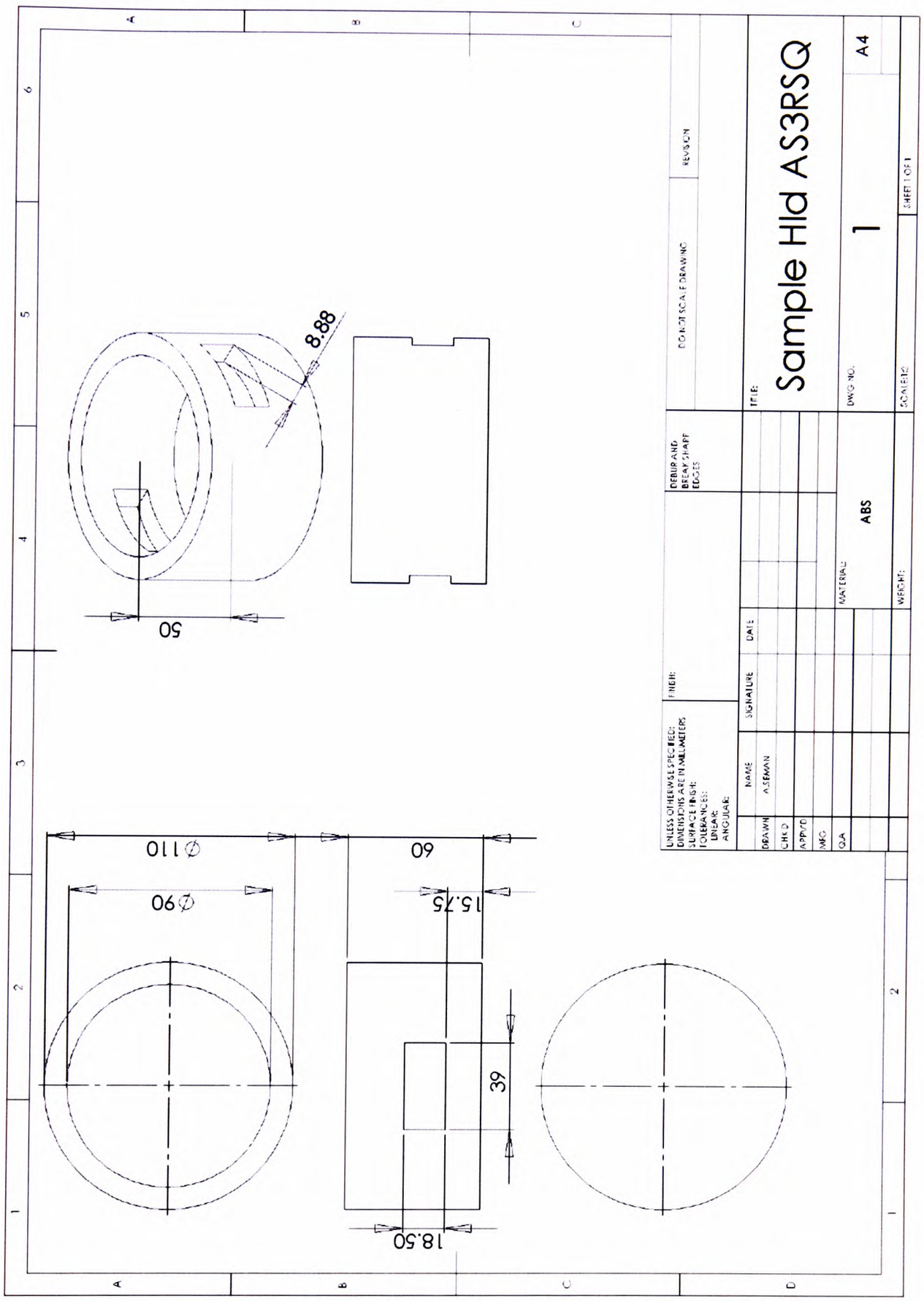

Appendix G4
Experimental Rig C Assembly Drawing

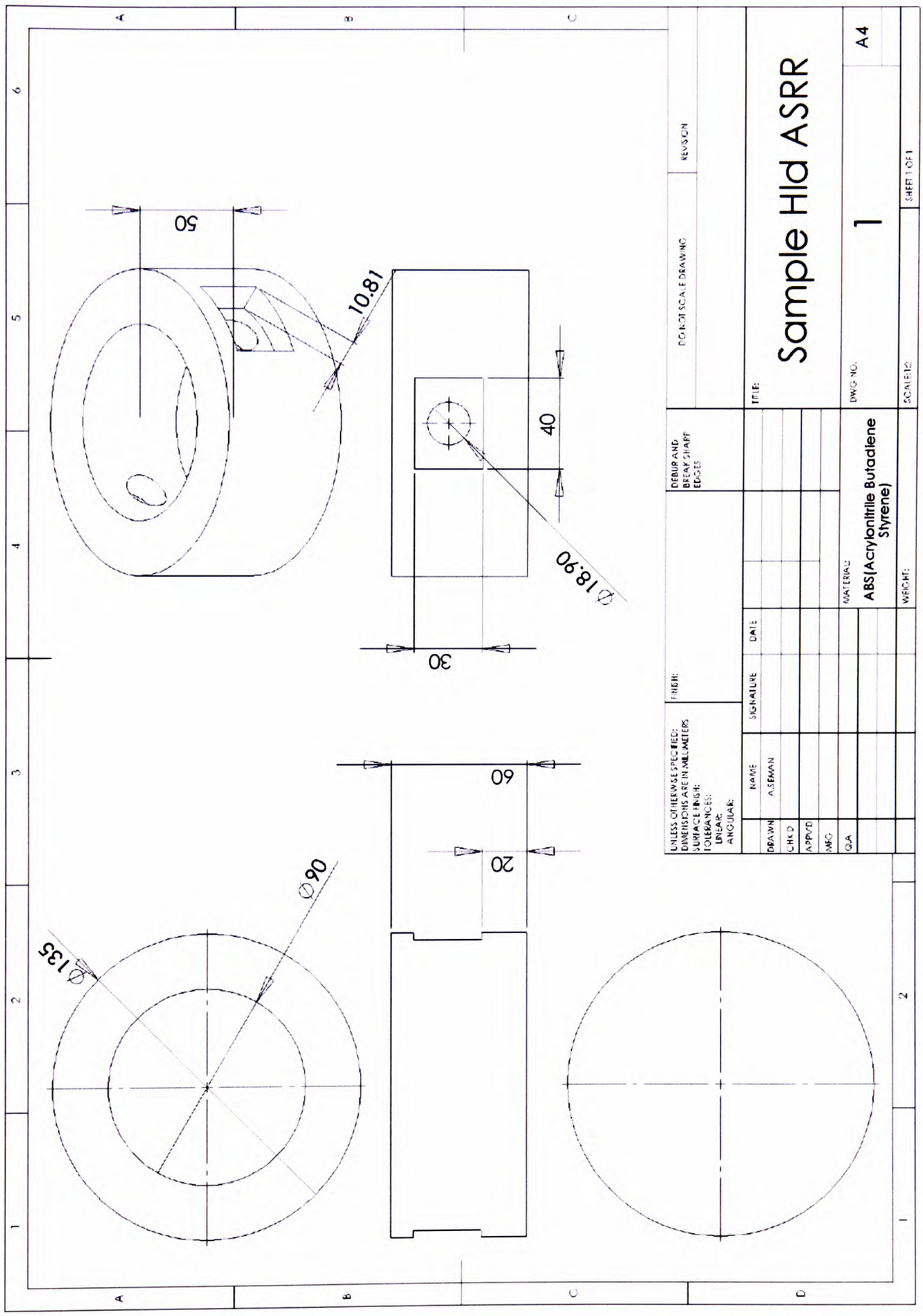

Appendix H1
20mm Sample Container (Engineering Drawing)

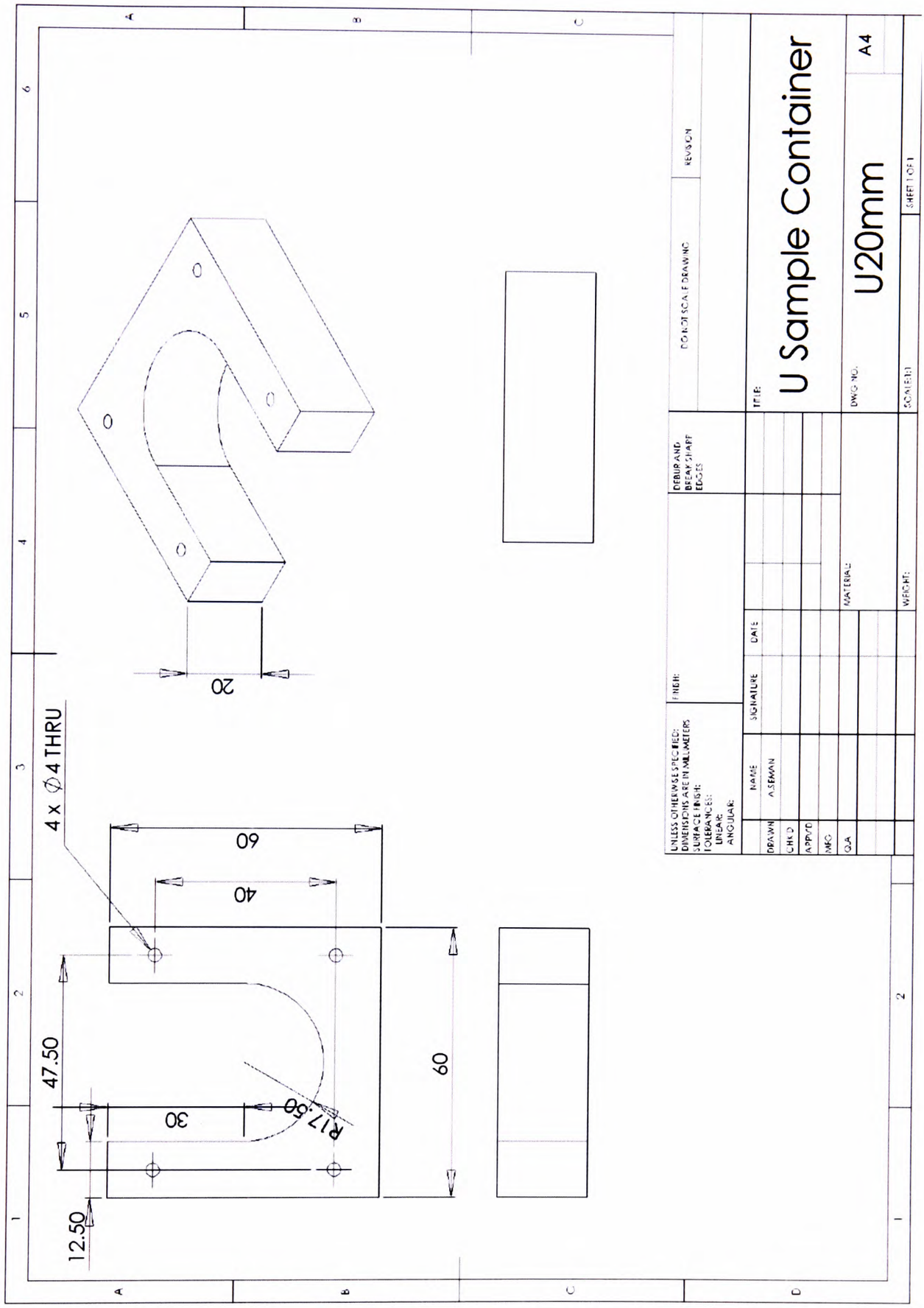

Appendix H2
30mm Sample Container (Engineering Drawing)

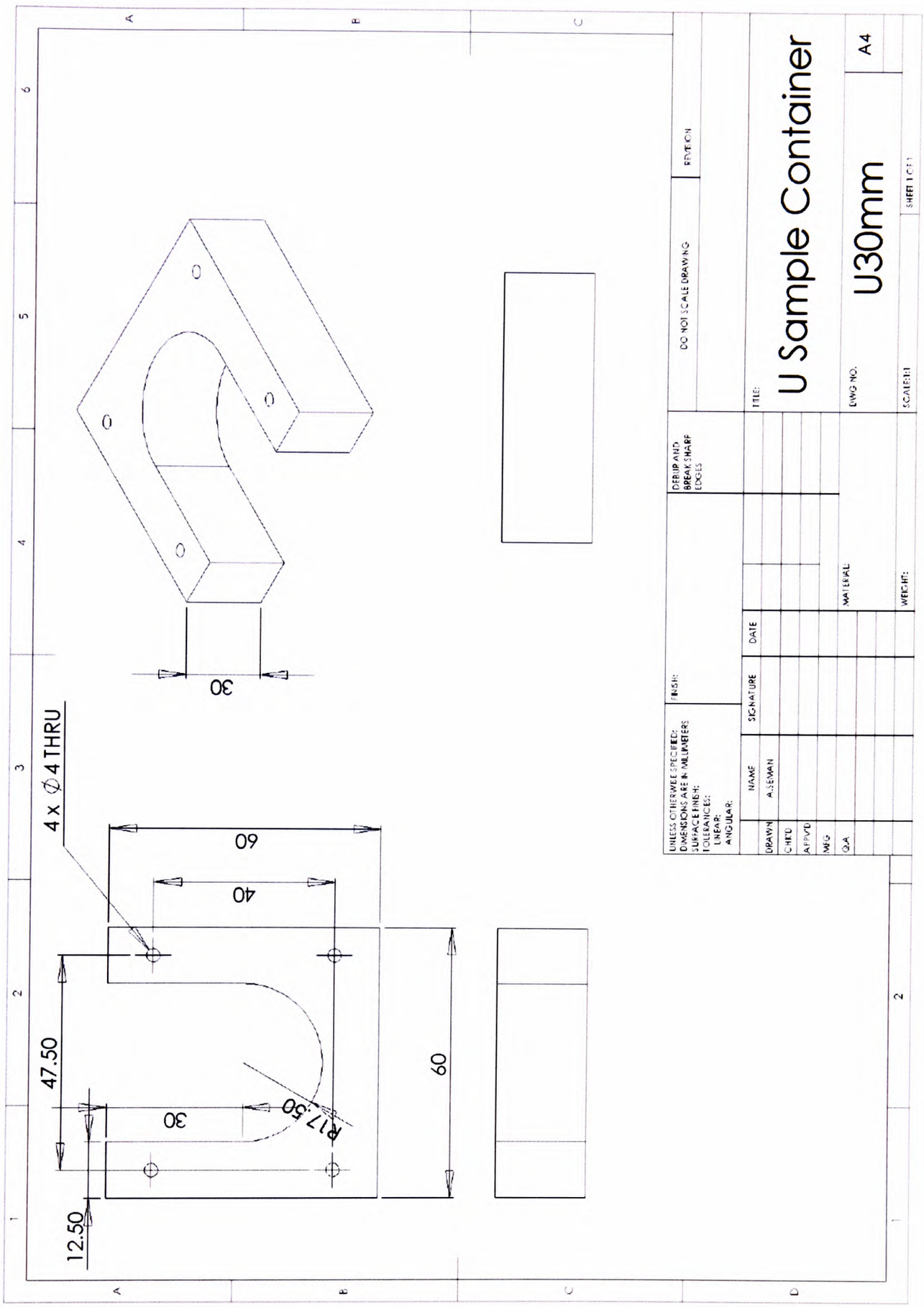

Appendix H3
40mm Sample Container (Engineering Drawing)

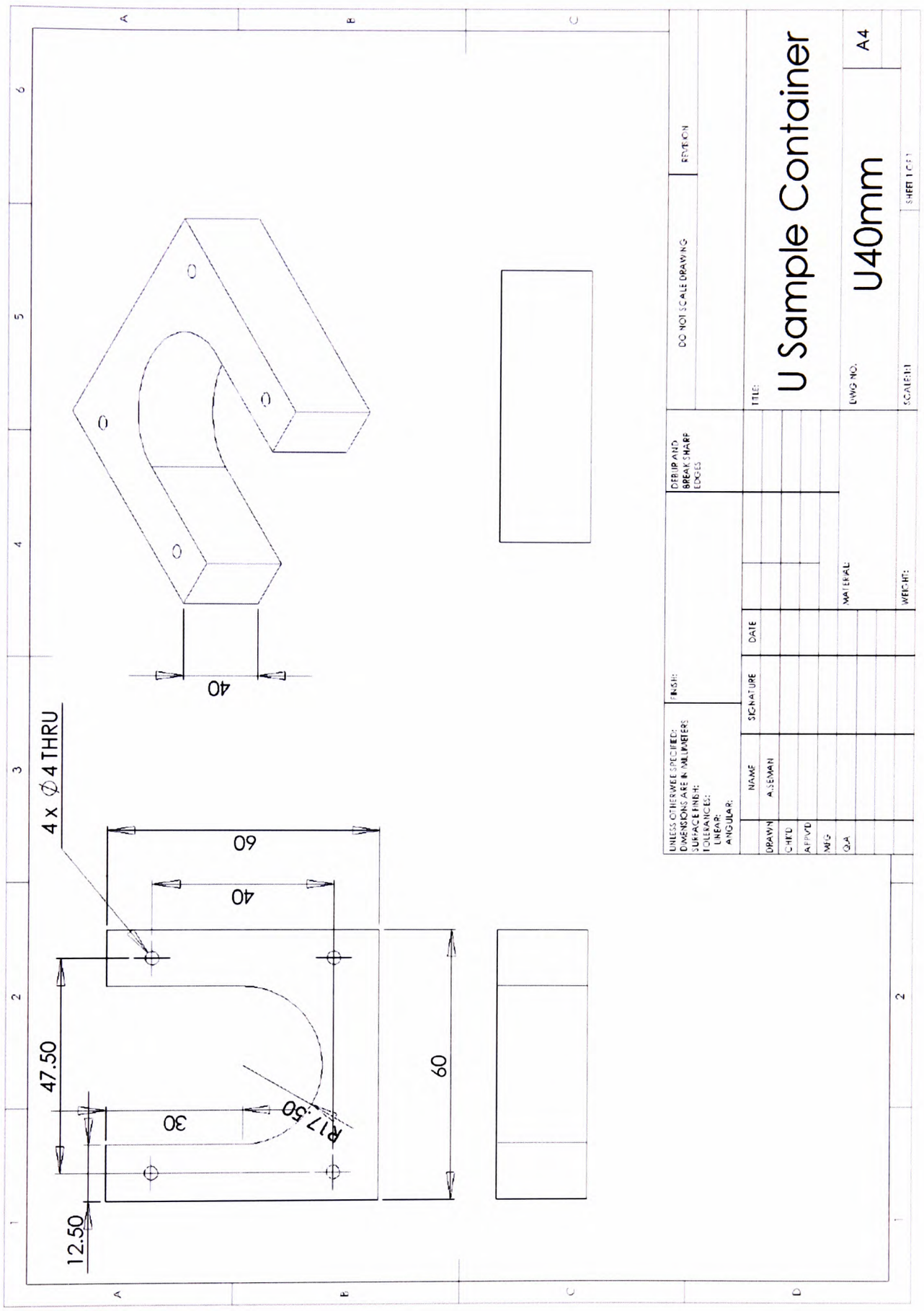

Appendix I1
Murata Ultrasonic Sensors – Specifications

Piezoelectric Ceramic Sensors (PIEZOTITE®)

muRata

Ultrasonic Sensors

Open Structure Type

■ Features

1. Compact and light weight.
2. High sensitivity and sound pressure.
3. Less power consumption.
4. High reliability.

■ Applications

Burglar alarms, Range finders, Automatic doors, Remote control.

MA40B8R/S

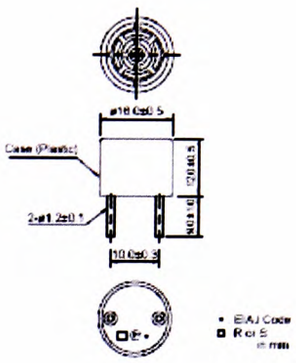

MA40S4R/S

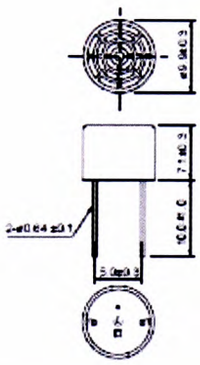

MA40S5

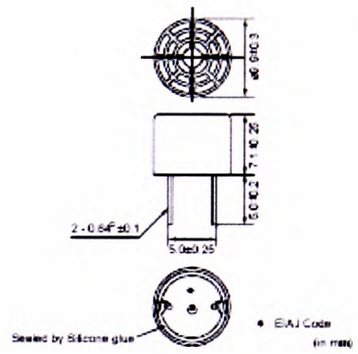

Part Number	Construction	Using Method	Nominal Freq. (kHz)	Overall Sensitivity (mVp-p)	Sensitivity (dB)	S.P.L. (dB)	Directivity (°)	Cap. (pF)	Operating Temp. Range (°C)	Detectable Range (m)	Resolution (mm)	Max. Input Voltage (Vp-p)
MA40B8R	Open struct.	Receiver	40	-	-63 typ. (0dB=1V/Pa)	-	50	2000	-30 to 85	0.2 to 6	9	-
MA40B8S	Open struct.	Transmitter	40	-	-	120 typ. (0dB=0.02mPa)	50	2000	-30 to 85	0.2 to 6	9	40 Continuous signal
MA40S4R	Open struct.	Receiver	40	-	-63 typ. (0dB=1V/Pa)	-	80	2550	-40 to 85	0.2 to 4	9	-
MA40S4S	Open struct.	Transmitter	40	-	-	120 typ. (0dB=0.02mPa)	80	2550	-40 to 85	0.2 to 4	9	20 Continuous signal
MA40S5	Open struct.	Dual Use	40	20 typ.	-	-	60 typ.	2550	-30 to 85	0.5 to 2	9	20 Pulse width 0.4ms Interval 100ms

Distance:30cm, Overall sensitivity:0dB=1(0Vp-p, Sensitivity:0dB=1Vrms/μbar, Sound pressure level:0dB=2x10⁻⁵μbar, 1μbar=0.1Pa
The sensor can be used in the operating temperature range.
Please refer to the individual specification for the temperature drift of Sensitivity/Sound pressure level or environmental characteristics in that temperature range.
Directivity, detectable range and resolution are typical values. They can be changed by application circuit and fixing method of the sensor.

Appendix I1
Murata Ultrasonic Sensors – Specifications (*continued*)

■ Directivity in Sensitivity

MA40B8R

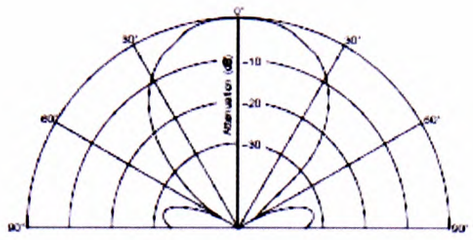

MA40S4R

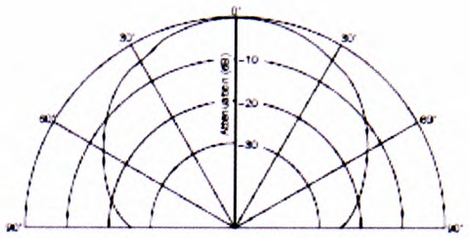

■ Directivity in S. P. L.

MA40B8S

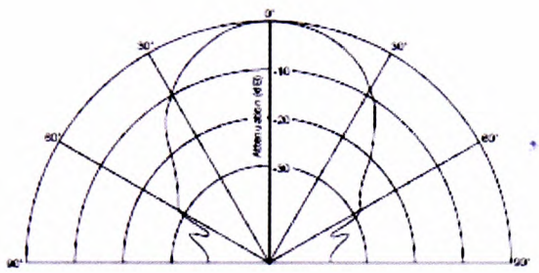

■ Directivity in S. P. L.

MA40S4S

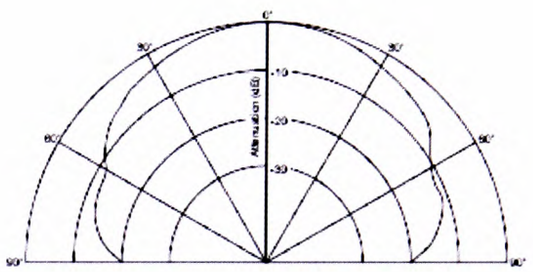

■ Directivity in Overall Sensitivity

MA40S5

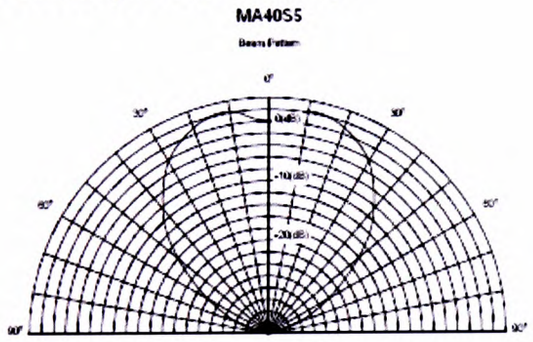

Appendix I1
Murata Ultrasonic Sensors – Specifications (*continued*)

■ S. P. L. -Freq. Characteristics

MA40B8R

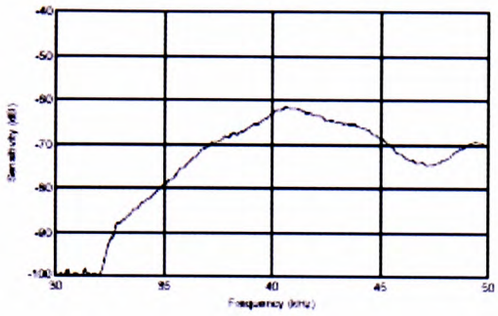

MA40S4R

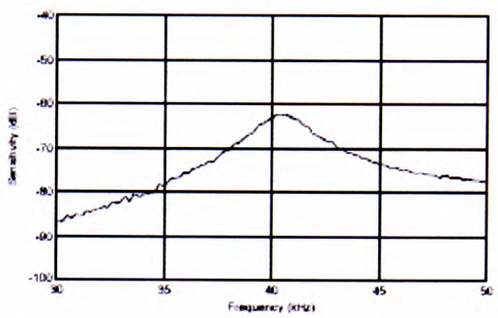

■ Sensitivity-Freq. Characteristics

MA40B8S

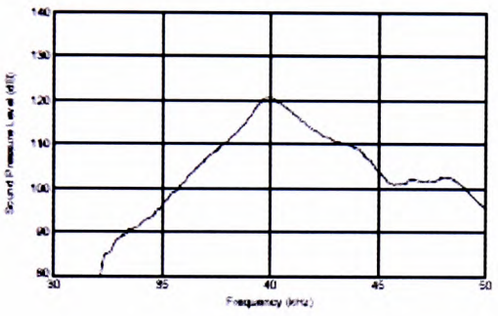

MA40S4S

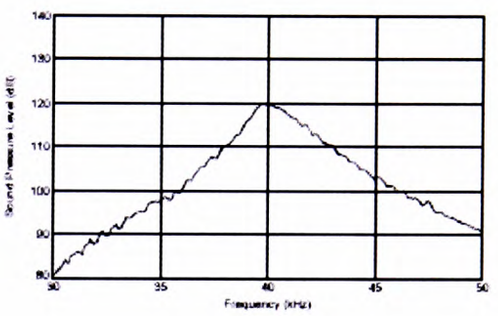

Appendix I1
Murata Ultrasonic Sensors – Specifications (*continued*)

Water Proof Type Symmetric Directivity

■ Features

1. Compact and light weight.
2. High sensitivity and sound pressure.
3. Less power consumption.
4. High reliability.

■ Applications

Back sonar of automobiles, Parking meters, Water level meters.

MA40E7R/S

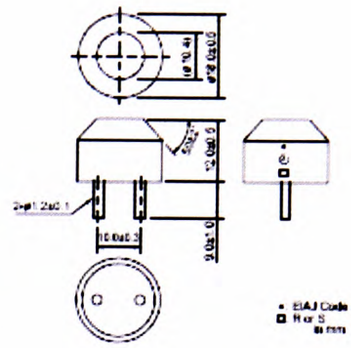

MA40E7S-1

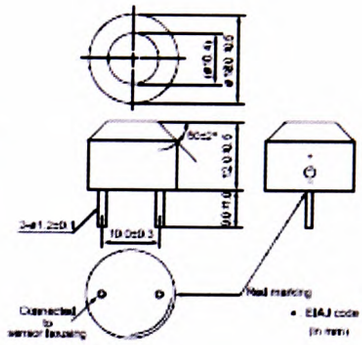

MA40E8-2

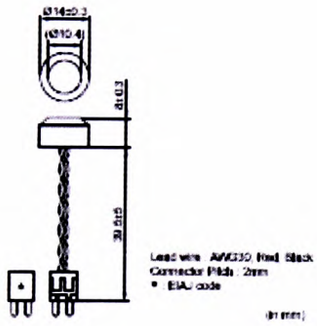

MA40MC10-1B

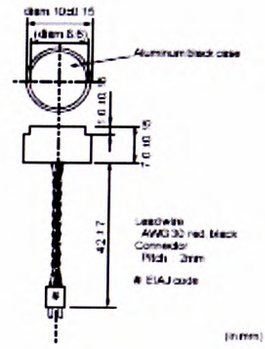

Part Number	Construction	Using Method	Nominal Freq. (kHz)	Overall Sensitivity	Sensitivity (dB)	S.P.L. (dB)	Directivity (°)	Cap. (pF)	Operating Temp. Range (°C)	Detectable Range (m)	Resolution (mm)	Max. Input Voltage (Vp-p)
MA40E7R	Water proof	Receiver	40	-	-74 min. (0dB=1V/Pa)	-	100	2200	-30 to 85	0.2 to 3	9	-
MA40E7S	Water proof	Transmitter	40	-	-	106 min. (0dB=0.02mPa)	100	2200	-30 to 85	0.2 to 3	9	100 Pulse width 0.4ms Interval 100ms
MA40E7S-1	Water proof	Dual Use	40	-	-72 min. (0dB=1V/Pa) : reference only	106 min. (0dB=0.02mPa)	75	2200	-30 to 85	0.2 to 3	9	100 Pulse width 0.4ms Interval 100ms
MA40E8-2	Water proof	Dual Use	40	-	-85 min. (0dB=1V/Pa)	106 min. (0dB=0.02mPa)	75	2800	-30 to 85	0.2 to 1.5	9	160 Pulse width 0.8ms Interval 60ms
MA40MC10-1B	Water proof	Dual Use	40	-	-86 min. (0dB=1V/Pa)	104 min. (0dB=0.02mPa)	100 typ.	2400	-30 to 85	0.2 to 1.5	9	160 Pulse width 0.8ms Interval 60ms

Distance:30cm, Overall sensitivity:0dB=1V/p-p, Sensitivity:0dB=1Vrms/μbar, Sound pressure level:0dB=2x10^{-5}μbar, 1μbar=0.1Pa

The sensor can be used in the operating temperature range.

Please refer to the individual specification for the temperature drift of Sensitivity/Sound pressure level or environmental characteristics in that temperature range.

Directivity, detectable range and resolution are typical values. They can be changed by application circuit and fixing method of the sensor.

Appendix I1
Murata Ultrasonic Sensors – Specifications (*continued*)

■ Directivity in Sensitivity

MA40E7R

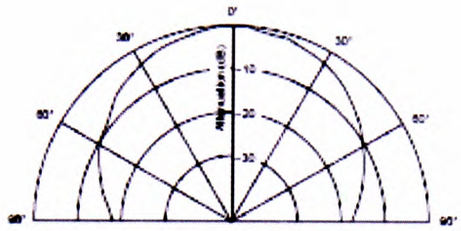

■ Directivity in S. P. L.

MA40E7S

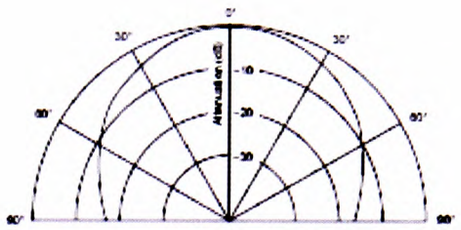

■ Directivity in Overall Sensitivity

MA40E7S-1

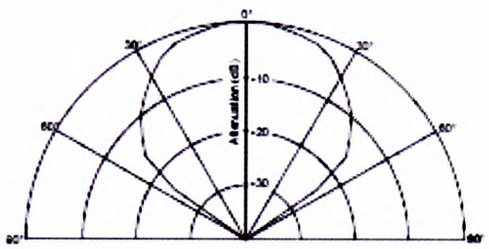

MA40E8-2

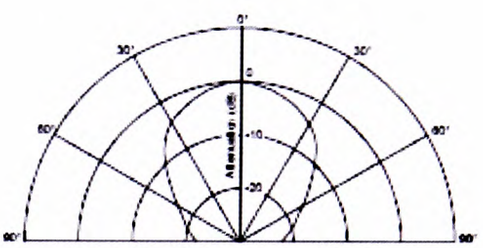

MA40MC10-1B

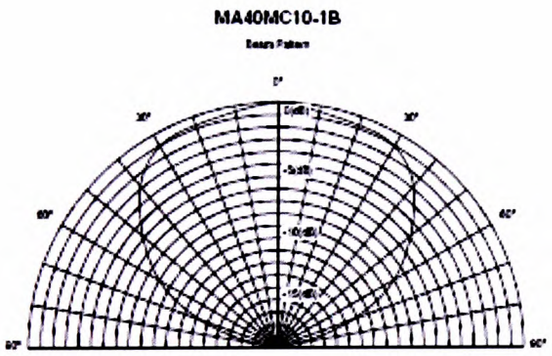

■ S. P. L. -Freq. Characteristics

MA40E7R

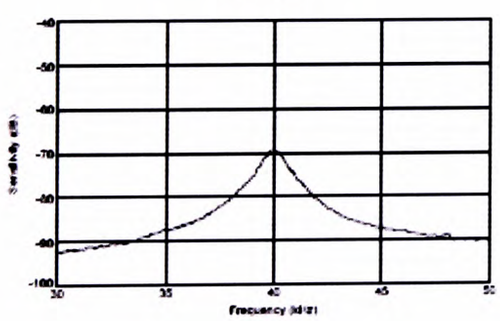

■ Sensitivity-Freq. Characteristics

MA40E7S

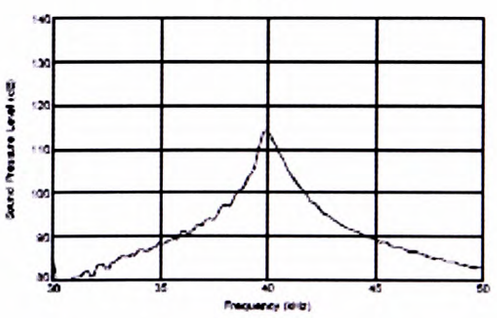

Appendix I1
Murata Ultrasonic Sensors – Specifications (*continued*)

High-frequency Type

■ Features

Using longitudinal vibration and matching with the air by acoustic matching layer, this type realized high sensitivity. Because of short wavelength, this type has sharp directivity and can be used high precise measurement.

■ Applications

Approach switch for FA, Distance meter, Water or liquid level meters.

MA80A1

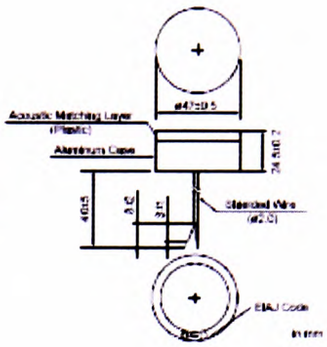

MA200A1

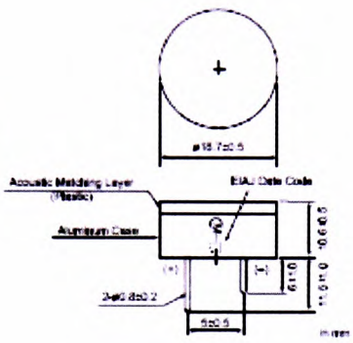

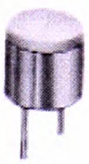

MA400A1

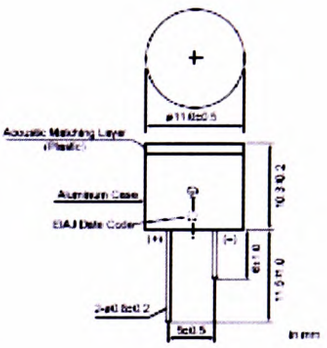

Part Number	Construction	Using Method	Nominal Freq. (kHz)	Overall Sensitivity (dB)	Sensitivity	S.P.L.	Directivity (°)	Cap.	Operating Temp. Range (°C)	Detectable Range (m)	Resolution (mm)	Max. Input Voltage (Vp-p)
MA80A1	High frequency type	Dual Use	75 +/-5	-47 min. 0dB=1Pa/pp (at 50cm)	-	-	7	-	-10 to 60	0.5 to 5	4	120 Pulse width 0.6ms Interval 50ms
MA200A1	High frequency type	Dual Use	200 +/-10	-54 min. 0dB=1Pa/pp (at 20cm)	-	-	7	-	-30 to 60	0.2 to 1	2	120 Pulse width 250µs Interval 20ms
MA400A1	High frequency type	Dual Use	400 +/-20	-74 min. 0dB=1Pa/pp (at 10cm)	-	-	7	-	-30 to 60	0.06 to 0.3	1	120 Pulse width 125µs Interval 10ms

The sensor can be used in the operating temperature range.
Please refer to the individual specification for the temperature drift of Sensitivity/Sound pressure level or environmental characteristics in that temperature range.
Directivity, detectable range and resolution are typical values. They can be changed by application circuit and fixing method of the sensor.

■ Directivity in Overall Sensitivity

MA_A1 Series

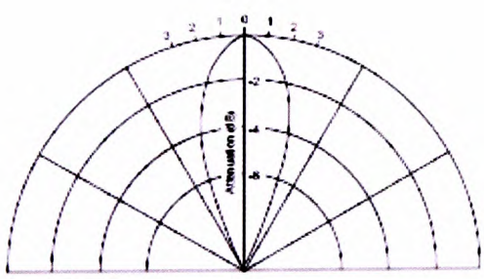

Appendix J
Schematic Diagram of In-house Customised Band-Pass Amplifier Filter Module

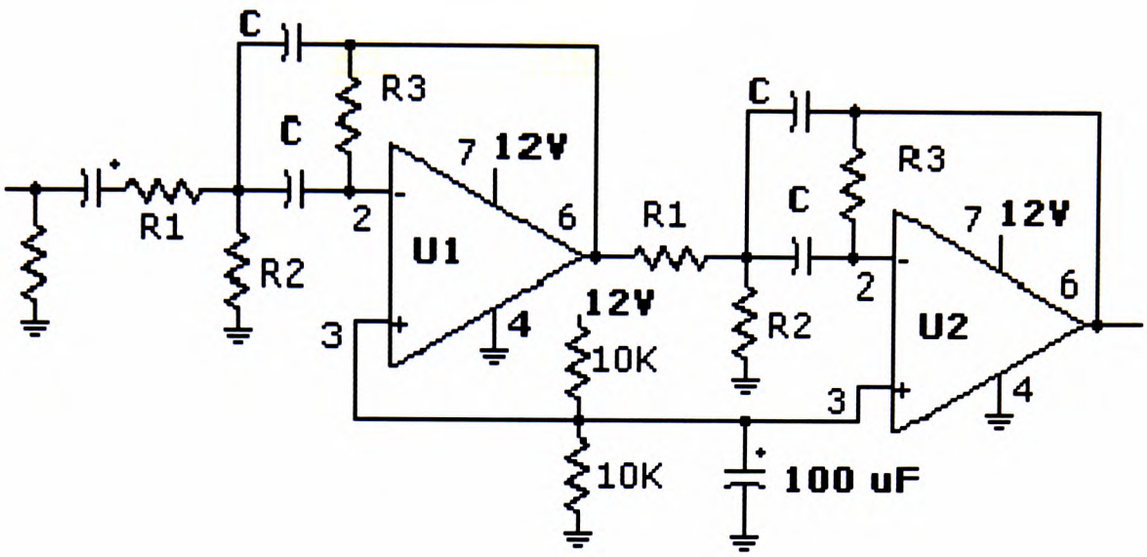

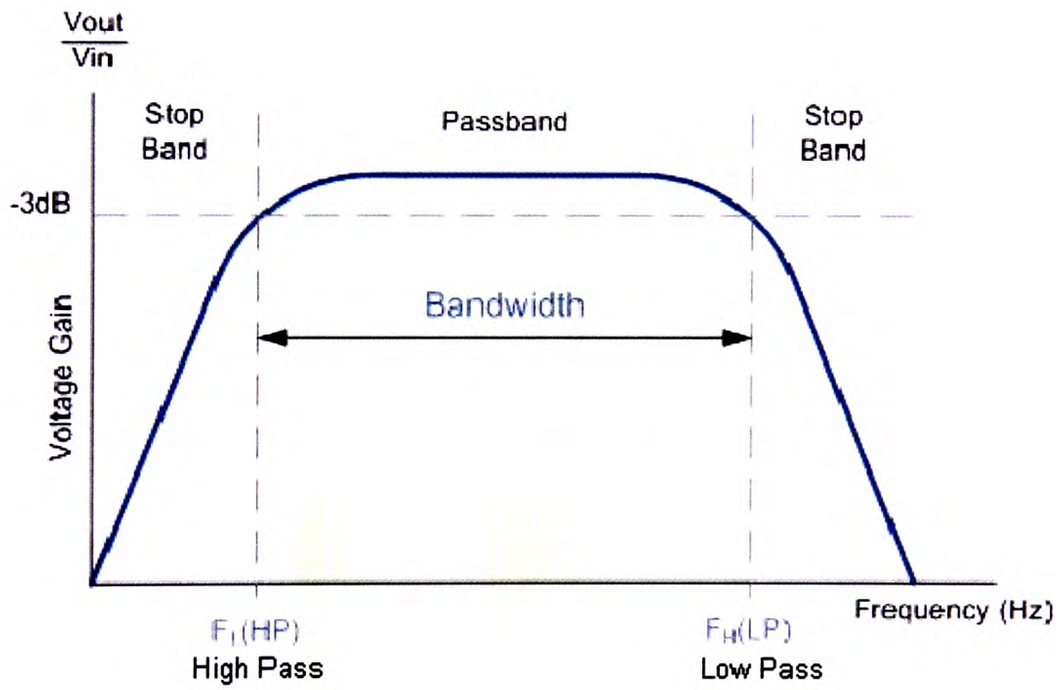

The amplifier filter module is powered by an external dual-rail power supply unit.

C represents the capacitors, while R1, R2 and R3 are resistors.

The values of R1, R2 and R3 can be calculated using the following formula:

$$R1 = \frac{Q}{H_0 \cdot W_0 \cdot C}$$

$$R2 = \frac{Q}{(2 \cdot Q^2 - H_0) \cdot W_0 \cdot C}$$

$$R3 = \frac{2 \cdot Q}{W_0 \cdot C},$$

where

$$Q = \frac{CentreFrequency}{Bandwidth}$$

The value of the capacitors should ideally be as large as possible, to avoid the use of very-large-value resistors. Thus, in this case for both the 40kHz and 200kHz modules, the capacitors used would be of 0.027μF. H_0 is the gain per stage, which is set at 3dB (3dB gain threshold is the most commonly used value in most amplifiers in order to prevent excessive loss of data).

The values of R1, R2 and R3 for the 40kHz module with a bandwidth of 20kHz are therefore 100Ω, 60Ω, and 590Ω respectively.

The values of C, R1, R2 and R3 for the 200kHz module with a bandwidth of 40kHz are therefore 0.027μF, 50Ω, 3Ω, and 295Ω respectively.

Appendix K
Picotech ADC-212/3 Analogue-to-Digital Converter – Specification

Channels	2 x BNC + 1 external trigger
Analog bandwidth	1.5 MHz
Sampling rate	3 MS/s
Sampling rate (dual channel)	3 MS/s
Resolution	12 bit
Buffer memory	32 kS
Dynamic range	80 dB
Scope timebases	2 µs/div to 50 s/div
Spectrum ranges	0 to 1.5 MHz
Trigger modes	Free run, Auto, Repeat & Single
Pre/ post trigger	±100 %
Voltage ranges	±10 mV to ±20 V in 11 ranges
Overload protection	±100 V
Input impedance	1 MΩ
Coupling	AC, DC
Accuracy	±1 %
Power supply	500 mA @ 12 V (mains adaptor supplied)
Output connector	D25 to PC parallel port (cable supplied)
Dimension	140 x 190 x 45 mm (5.51 x 7.48 x 1.77 in)

Appendix L
Brookfield Rotational Viscometer – Specification

DV-E Viscometer

our lowest cost digital viscometer

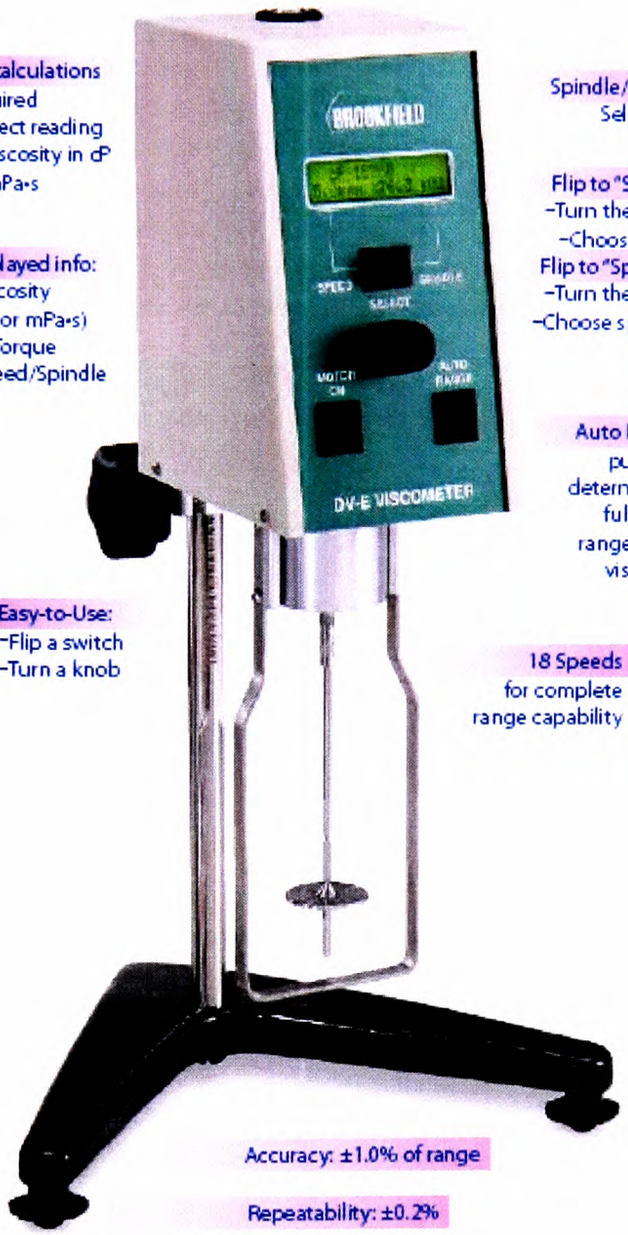

No calculations required
-Direct reading of viscosity in cP or mPa•s

Displayed info:
-Viscosity (cP or mPa•s)
-% Torque
-Speed/Spindle

Easy-to-Use:
-Flip a switch
-Turn a knob

Spindle/Speed Selection

Flip to "Speed"
-Turn the knob
-Choose RPM
Flip to "Spindle"
-Turn the knob
-Choose spindle

Auto Range push for determining full scale range (FSR) viscosity

18 Speeds for complete range capability

Accuracy: ±1.0% of range

Repeatability: ±0.2%

What's Included?

Instrument
6 spindles (RV/HA/HB) (p39)
or 4 spindles (LV) (p39)
Spindle Guard Leg*
Lab Stand (Model A) (p44)
Carrying Case
*Not applicable to HA or HB versions

Optional Accessories

Viscosity Standards (p46)
RV/HA/HB-1 Spindle (p39)
Quick Action Lab Stand (p44)
Temperature Bath (p27)
Small Sample Adapter (p32)
UL Adapter (p34)
Thermosel (p30)
Helipath Stand with T-bar Spindles (p36)
Spiral Adapter (p38)
DIN Adapter (p38)
Quick Connect/Extension Links (p44)
Vane Spindles (p37 & 42)

	VISCOSITY RANGE cP(mPa•s)		SPEEDS	
MODEL	Min.	Max.	RPM	Number of Increments
LVDV-E	1*	2M	.3-100	18
RVDV-E	100**	13M	.3-100	18
HADV-E	200**	26M	.3-100	18
HBDV-E	800**	104M	.3-100	18

*1 cP achieved with UL Adapter accessory. 15 cP on LV with standard spindles.
**Minimum viscosity is achieved with optional RV/HA/HB-1 spindle.
M = 1 million cP = Centipoise mPa•s = Millipascal-seconds

BROOKFIELD VISCOMETERS

T: 800.628.8139 or 508.946.6200 F: 508.946.6262 www.brookfieldengineering.com

Vane Spindles

for foods, cosmetics, sealants...

...for use with paste-like materials, gels and fluids where suspended solids migrate away from the measurement surface of standard spindles.

Minimal disruption of sample during spindle immersion

Keeps particles in suspension during testing cycle

Viscosity data includes complete flow curve analysis when software is used

Provides information on yield behavior at low rotational speeds

Follows industry recommendations on length/diameter ratios for vane spindles

3-piece spindle set for versatile range capability

Optional V-74 and V-75 spindles for even greater range capability and immersion into small size sample containers

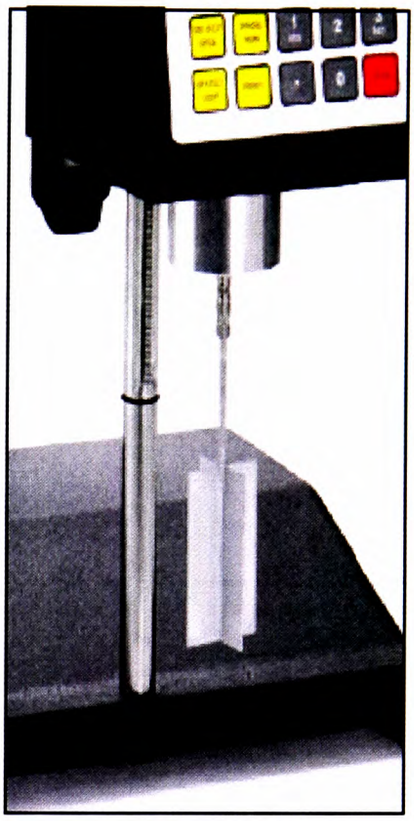

The instrument shown is a DV-III Ultra. These spindles also work well with other Brookfield Viscometers.

Vane Spindle Ranges

SPINDLE	TORQUE RANGE	SHEAR STRESS RANGE (Pa)	VISCOSITY RANGE cP(mPa•s)
V-71	NOT RECOMMENDED FOR USE ON LV TORQUE		
V-72	LV	.188-1.88	104.04-1.04K
V-73	LV	.938-9.38	502-5.02K
V-74	LV	9.38-93.8	5.09-50.9K
V-75	LV	3.75-37.5	1.996K-19.96K
V-71	RV	.5-5	262-2.62K
V-72	RV	2-20	1.11K-11.1K
V-73	RV	10-100	5.35K-53.5K
V-74	RV	100-1K	54.3K-543K
V-75	RV	40-400	21.3K-213K
V-71	HA	1-10	524-5.24K
V-72	HA	4-40	2.22K-22.2K
V-73	HA	20-200	10.7K-107K
V-74	HA	200-2K	108.6K-1.086M
V-75	HA	80-800	42.6K-426K
V-71	HB	4-40	2.096K-20.96K
V-72	HB	16-160	8.88K-88.8K
V-73	HB	80-800	42.8K-428K
V-74	HB	800-8K	434.4K-4.344M
V-75	HB	320-3.2K	170.4K-1.704M
V-71	5xHB	20-200	10.48K-104.8K
V-72	5xHB	80-800	44.4K-444K
V-73	5xHB	400-4000	214K-2.14M
V-74	5xHB	4K-40K	2.172M-21.72M
V-75	5xHB	1.6K-16K	852K-8.52M

Notes: 1. 1 Pa = 10 dyne/cm2 2. Viscosity Range is given at rotational speed of 10 RPM
3. 5xHB is the highest torque range available 4. Not for use with DV-E Viscometers
M = 1 million K = 1 thousand Pa = Pascal cP = Centipoise mPa•s = Millipascal•seconds

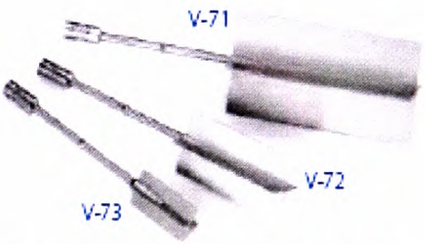

Brookfield Vane Spindle Set

Includes V-71, V-72, and V-73 vane spindles. See the individual specifications in the spindle section. (p42)

Optional V-74 and V-75 spindles are smaller in size than V-73.

Appendix L
Brookfield Rotational Viscometer – Specification (*continued*)

Spindles

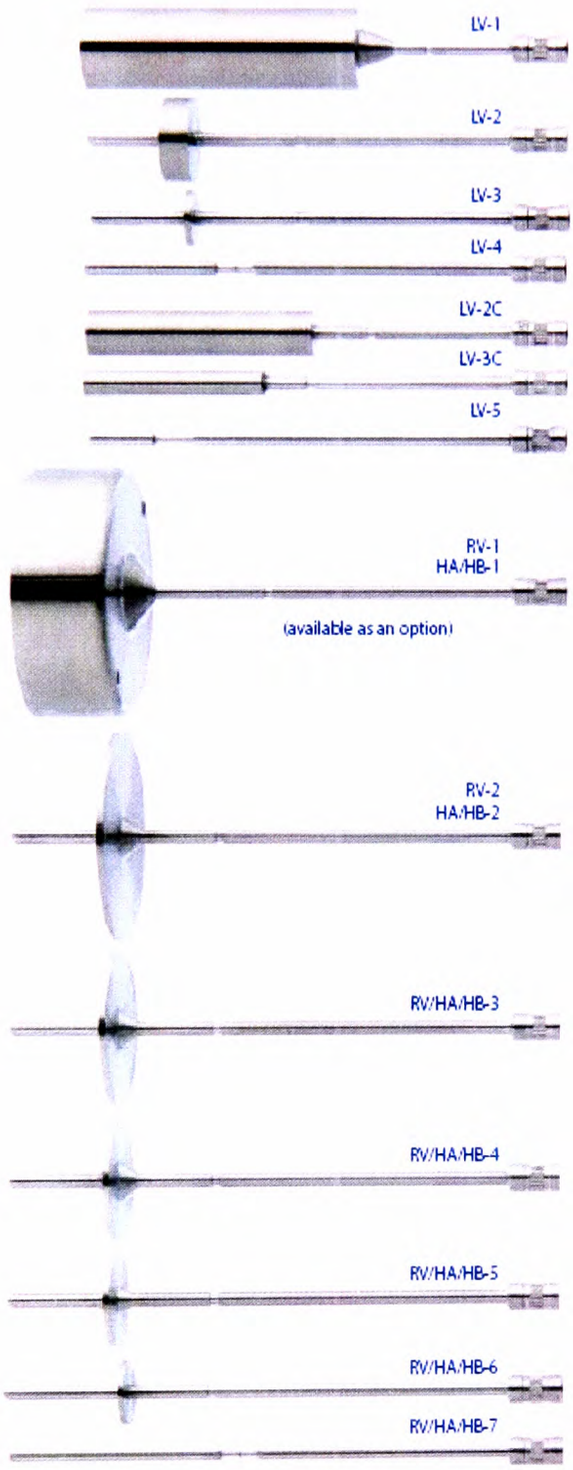

LV Spindles cP(mPa•s)

SPINDLE	RANGE*	
LV-1	15 - 20K	
LV-2	50 - 100K	
LV-3	200 - 400K	
LV-4	1K - 2M	
LV-5	2K - 4M	LV-5 is an optional spindle designed to increase measuring range.
LV-2C	50 - 100K	
LV-3C	200 - 400K	

* Based on Standard LV speeds .3 - 60 rpm M = 1 million K = 1 thousand
Note: LV-1 through LV-4 are supplied with LV instruments.
LV-2C & LV-3C are optional "cylindrical spindles" offering geometry for calculating shear rates.
LV and RV/HA/HB spindles are supplied in 302 stainless steel.
Optional 316 stainless or teflon coated spindles are available

RV/HA/HB Spindles cP(mPa•s)

SPINDLE	RANGE* RV SERIES	RANGE* HA SERIES	RANGE* HB SERIES
RV-1**	100 - 20K	200 - 40K	800 - 160K
HA/HB-1**	100 - 20K	200 - 40K	800 - 160K
RV-2	100 - 80K	200 - 160K	800 - 640K
HA/HB-2	100 - 80K	200 - 160K	800 - 640K
RV/HA/HB-3	100 - 200K	200 - 400K	800 - 1.6M
RV/HA/HB-4	200 - 400K	400 - 80K	1.6K - 3.2M
RV/HA/HB-5	400 - 800K	800 - 1.6M	3.2K - 6.4M
RV/HA/HB-6	1K - 2M	2K - 4M	8K - 16M
RV/HA/HB-7	4K - 8M	8K - 16M	32K - 64M

* Based on standard RV/HA/HB speeds .5-100 RPM. M = 1 million K = 1 thousand
Note: LV and RV/HA/HB spindles are supplied in 302 stainless steel.
Optional 316 stainless or teflon coated spindles are available
** This spindle available as an option

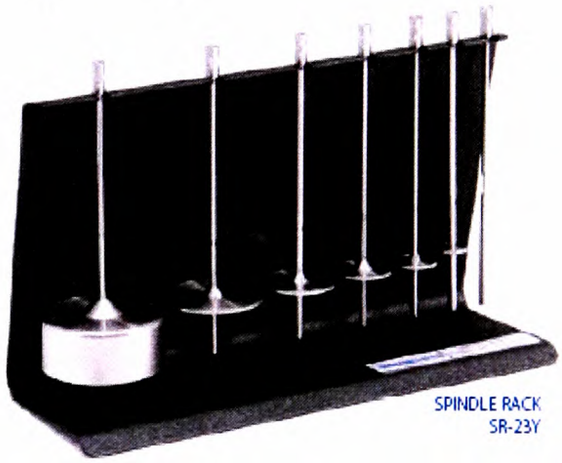

SPINDLE RACK
SR-23Y

RV/HA/HB Spindle Set includes spindles #2 - #7 and is supplied with standard Brookfield Viscometers and Rheometers.

Spindle #1 is available as an option.

Spindle Rack is also available as an option with both LV and RV/HA/HB spindle sets.

Appendix L
Brookfield Rotational Viscometer – Specification (*continued*)

Spindles

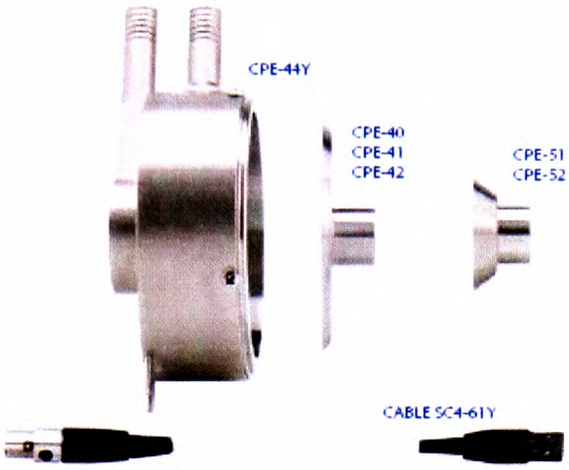

Wells/Brookfield Spindles & Cups

SPINDLE	SHEAR RATE	SAMPLE VOLUME	CONE ANGLE	CONE RADIUS
CPE-40	7.50N sec^{-1}	.5 mL	.8°	2.4cm
CPE-41	2.00N sec^{-1}	2.0 mL	3°	2.4cm
CPE-42	3.84N sec^{-1}	1.0 mL	1.5°	2.4cm
CPE-51	3.84N sec^{-1}	.5 mL	1.5°	1.2cm
CPE-52	2.00N sec^{-1}	.5 mL	3°	1.2cm
CUP				
CPE-44Y	Standard cup without temperature probe			
CPE-44PY	Standard cup with RTD temperature probe			
PCPE-3Y	Cup with 1 purge fitting			
PCPE-6Y	Cup with luer fitting and 1 purge fitting			
PCPE-4Y	Cup with luer fitting and 2 purge fittings			
PCPE-7Y	Cup with luer fitting and 4 purge fittings			

Note: 1. Wells-Brookfield cones and cups are calibrated at the factory.
Cones ordered after shipment require cups to be returned for calibration to new cone.
2. See page 12 for viscosity ranges

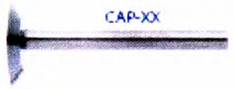

CAP Spindles

SPINDLE	SHEAR RATE	SAMPLE VOLUME	CONE ANGLE	CONE RADIUS
CAP-01	13.3N sec^{-1}	67 µL	0.45°	1.511cm
CAP-02	13.3N sec^{-1}	38 µL	0.45°	1.200cm
CAP-03	13.3N sec^{-1}	24 µL	0.45°	0.953cm
CAP-04	3.3N sec^{-1}	134 µL	1.8°	1.200cm
CAP-05	3.3N sec^{-1}	67 µL	1.8°	0.953cm
CAP-06	3.3N sec^{-1}	30 µL	1.8°	0.702cm
CAP-07	2.0N sec^{-1}	1700 µL	3.0°	2.399cm
CAP-08	2.0N sec^{-1}	400 µL	3.0°	1.511cm
CAP-09	2.0N sec^{-1}	100 µL	3.0°	0.953cm
CAP-10	5.0N sec^{-1}	170 µL	1.2°	1.511cm

Note: 1. Recommend ordering calibration fluids specific to cone for field calibration
2. See page 15 for viscosity ranges

UL Spindles & Chambers

SPINDLE	TYPE	SAMPLE VOLUME	SHEAR RATE
YULA-15(E)	Spindle - 304 stainless steel		1.224N
YULA-15(E)Z	Spindle - 316 stainless steel		1.224N
ULA-31(E)Y	Sample Chamber - 304 stainless steel	16mL	
ULA-35(E)YZ	Sample Chamber - 316 stainless steel	16mL	

Note: 1. See page 34 for viscosity ranges
2. (E) represents enhanced UL version (introduced Jan. 2006)

N = rpm

DIN Spindles

SPINDLE	SHEAR RATE	SAMPLE VOLUME
ULA-DIN-85	1.29N	17.0 mL
ULA-DIN-86	1.29N	6.5 mL
ULA-DIN-87	1.29N	2.0 mL
HT-DIN-81 for Thermocel	1.29N	7.0 mL
SC4-DIN-82 for SSA	1.29N	1.5 mL
SC4-DIN-83 for SSA	1.29N	1.5 mL
CHAMBER		
ULA-DIN-6Y	for use with ULA-DIN-86 and 87	
DAA-1	for use with ULA-DIN-85	

Appendix L
Brookfield Rotational Viscometer– Specification (*continued*)

Spindles

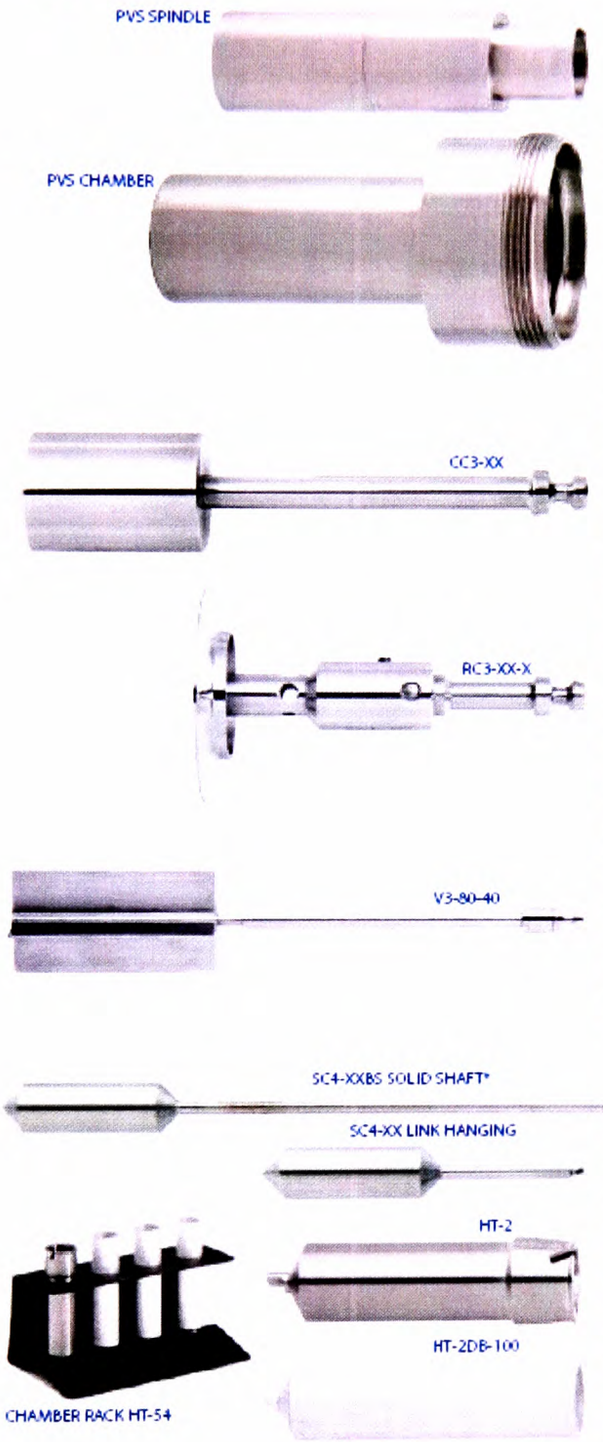

PVS Spindles and Chambers

BOB	SHEAR RATE	SAMPLE VOLUME
B1	1.7N	23 mL
B2	0.38N	53 mL
B5	0.85N	40 mL
CHAMBER		
PVS-30 (standard)	for use with B1, B2 or B5 spindle	
Triple Annulus	for use with PVS - TA5 B5 - D - HC	

R/S Spindle

RS Rheometers with serial numbers beginning with "302" and "303" use different spindles. Call for details.

SPINDLE COAXIAL	VISCOSITY RANGE (Pa•s)	SHEAR RATE	MAX. SHEAR STRESS	SAMPLE VOLUME
DG	0.002-19	4-4344 sec^{-1}	83 Pa	21mL
CC3-40	0.004-134	2-2148 sec^{-1}	287 Pa	45mL
CC3-25	0.026-883	1-1291 sec^{-1}	1140 Pa	17mL
CC3-14	0.151-5035	1-1291 sec^{-1}	6500 Pa	3mL
CC3-8	0.813-27111	1-1291 sec^{-1}	35000 Pa	0.5mL
CONE				
RC3-25-1	0.061-2037	6-6000 sec^{-1}	12223 Pa	0.08mL
RC3-25-2	0.122-4074	3-3000 sec^{-1}	12223 Pa	0.3mL
RC3-50-1	0.008-255	6-6000 sec^{-1}	1528 Pa	0.7mL
RC3-50-2	0.015-509	3-3000 sec^{-1}	1528 Pa	1.5mL
RC3-75-1*	0.002-75	6-6000 sec^{-1}	453 Pa	2.0mL
RC3-75-2*	0.005-151	3-3000 sec^{-1}	453 Pa	3.9mL
PLATE				
RP3-25	0.373-12450	1-1309 sec^{-1}	16297 Pa	0.5mL
RP3-50	0.023-779	3-2618 sec^{-1}	2040 Pa	2mL
RP3-75*	0.005-153	4-3927 sec^{-1}	600 Pa	4.5mL

VANE SPINDLE	VANE LENGTH (mm)	VANE DIAMETER (mm)	SHEAR STRESS
V3-80-40	80	40	6-200 Pa
V3-60-30	60	30	15-505 Pa
V3-40-20	40	20	51-1700 Pa
V3-30-15	30	15	120-4000 Pa
V3-20-10	20	10	408-13600 Pa
V3-10-5	10	5	3276-109200 Pa

*For use with water bath version only. 1 Pa•s = 1,000 cP
Notes: 1) Values based on minimum speed of 1 RPM and maximum speed of 1000 RPM
2) 75 mm plates cannot be used with Peltier Plate or electrically heated rheometers

Thermosel Spindles and Chambers

Link hanging configuration is standard

SPINDLE	SHEAR RATE	SAMPLE VOLUME
SC4-18	1.32N	8.0 mL
SC4-31	.34N	10.0 mL
SC4-34	.28N	9.5 mL
SC4-21	.93N	8.0 mL
SC4-27**	.34N	10.5 mL
SC4-28	.28N	11.5 mL
SC4-29	.25N	13.0 mL
HT-DIN-81	1.29N	7.0 mL

*SC4-XXBS = Solid Shaft. Not available for SC4-18 and SC4-21 spindles
**Also available as SC4-27D-100 = Disposable spindle, 100 units

CHAMBER	TYPE
HT-2	Sample Chamber - Reuseable, stainless steel
HT-2DB-100	Sample Chamber - Disposable, aluminum, 100 units

Appendix L
Brookfield Rotational Viscometer– Specification (*continued*)

Spindles

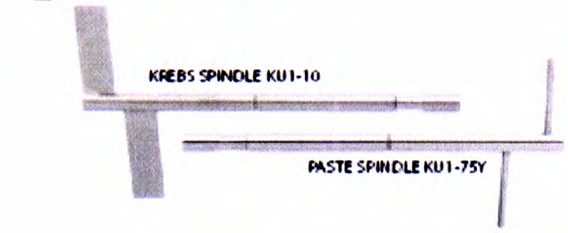

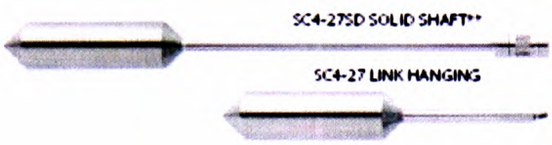

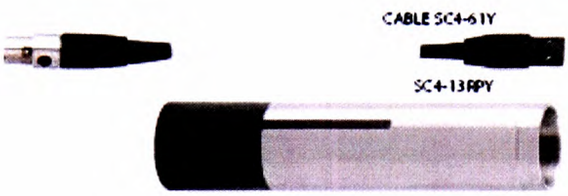

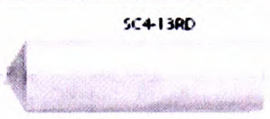

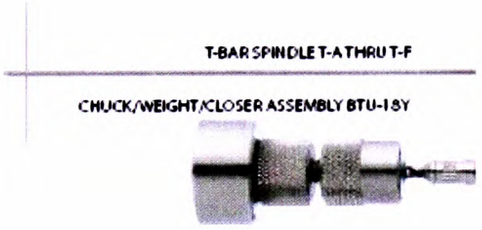

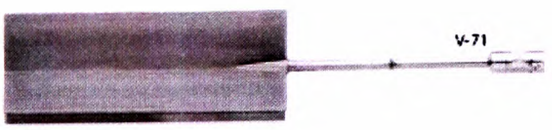

KU-2 Spindles

SPINDLE	TYPE
KU1-10	Standard Krebs Spindle
KU1-75Y	Optional Paste Spindle

Small Sample Spindles and Chambers

SPINDLE	SHEAR RATE	SAMPLE VOLUME
SC4-18	1.32N	6.7 mL
SC4-31	0.34N	9.0 mL
SC4-34	0.28N	9.4 mL
SC4-16	0.29N	4.2 mL
SC4-25	0.22N	16.1 mL
SC4-21	0.93N	7.1 mL
SC4-27	0.34N	10.4 mL
SC4-15	0.48N	3.8 mL
SC4-28	0.28N	11.0 mL
SC4-29	0.25N	13.5 mL
SC4-14	0.40N	2.1 mL
SC4-DIN-82	1.29N	1.5 mL
SC4-DIN-83	1.29N	1.5 mL

CHAMBER	TYPE
SC4-13R	Sample Chamber w/o temperature probe
SC4-13RPY	Sample Chamber w/RTD temperature probe & cable
SC4-8R	Sample Chamber w/o temperature probe
SC4-8RPY	Sample Chamber w/RTD temperature probe & cable
SC4-7R	Sample Chamber w/o temperature probe
SC4-7RPY	Sample Chamber w/RTD temperature probe & cable
SC4-6R	Sample Chamber w/o temperature probe
SC4-6RPY	Sample Chamber w/RTD temperature probe & cable
SC4-13RD-100†	Sample Chamber - Disposable, aluminum, 100 units

Note: See page 33 for spindle/chamber ranges
**Solid shaft option available for spindles SC4-21 (Part No. SC4-21SD) and SC4-27 (Part No. SC4-27SD).
† Requires the use of special water jacket SC4-45YD

T-Bar Spindles cP(mPa•s)

SPINDLE	LV	RV	HA	HB
T-A	156 - 62.5K	2K - 400K	4K - 800K	16K - 3.2M
T-B	312 - 124.8K	4K - 800K	8K - 6M	24K - 6.4M
T-C	780 - 312K	10K - 2M	20K - 4M	80K - 16M
T-D	1.5K - 624K	20K - 4M	40K - 8M	160K - 32M
T-E	3.9K - 1.5M	50K - 10M	100K - 20M	400K - 80M
T-F	7.8K - 3.1M	100K - 20M	200K - 40M	800K - 160M

M = 1 million K = 1 thousand

Spiral Adapter Spindle

SPINDLE	CHAMBER
SA-70	SA-1Y

Note: See page 38 for ranges

Vane Spindles

SPINDLE	VANE LENGTH (in)	VANE DIAMETER (in)
V-71	2.708	1.354
V-72	1.706	.853
V-73	.998	.499
V-74	.463	.232
V-75	.632	.316

Appendix M
Malcom Rotational Viscometer – Specification

Control Panel

1. Viscosity Digital Display
2. Temp/Speed Digital Display
3. Temp/Speed LEDs
4. Temp/Speed Select Switch
5. Condition LEDs
6. Thermostat LEDs
7. Option LEDs
8. Viscosity Set Switch
9. Temperature Set Switch
10. Speed Set Switch
11. Mix/Start Switch
12. Thermostat Select Switch and LED
13. Alarm Switch and LED
14. Adjust Switch and LED
15. Sensor Up/Down Switch
16. Time Switch
17. Print Switch

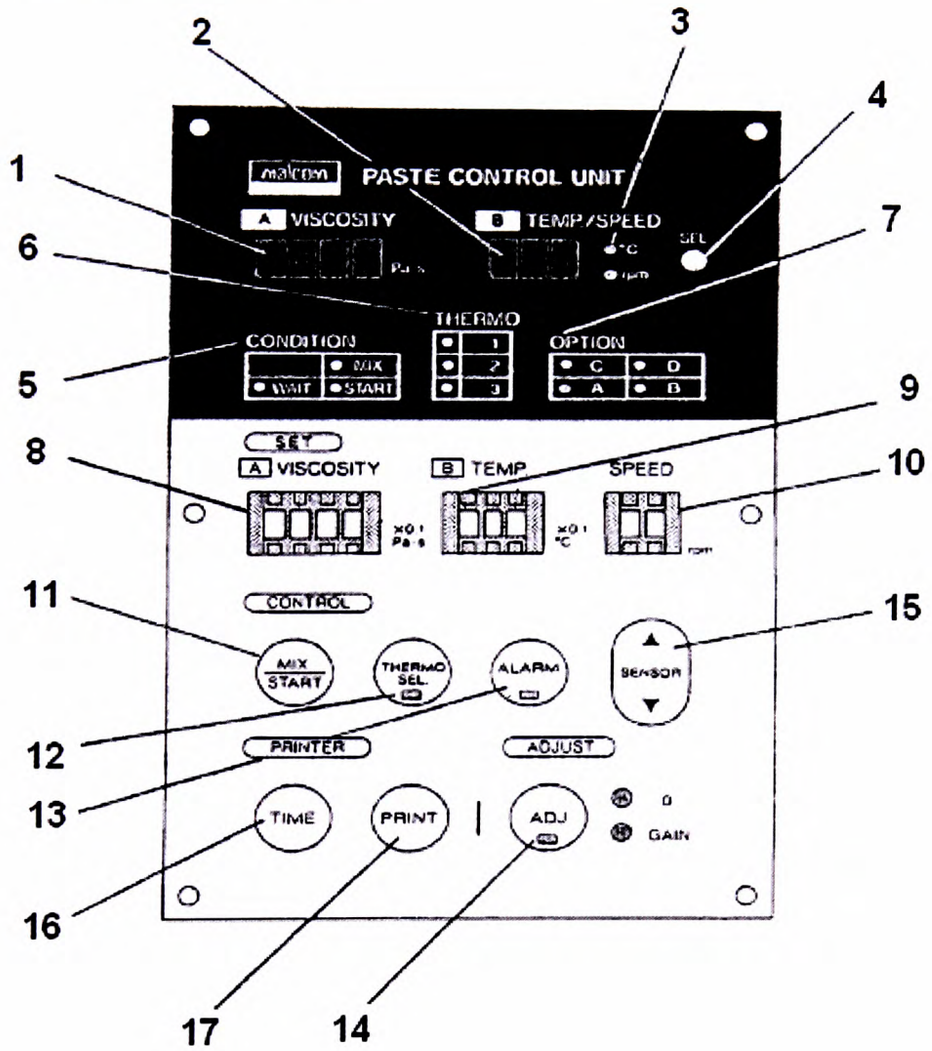

Appendix M
Malcom Rotational Viscometer – Specification (*continued*)

Front View

18. Control Panel
19. Sensor
20. Printer
21. Thermostat
22. Door

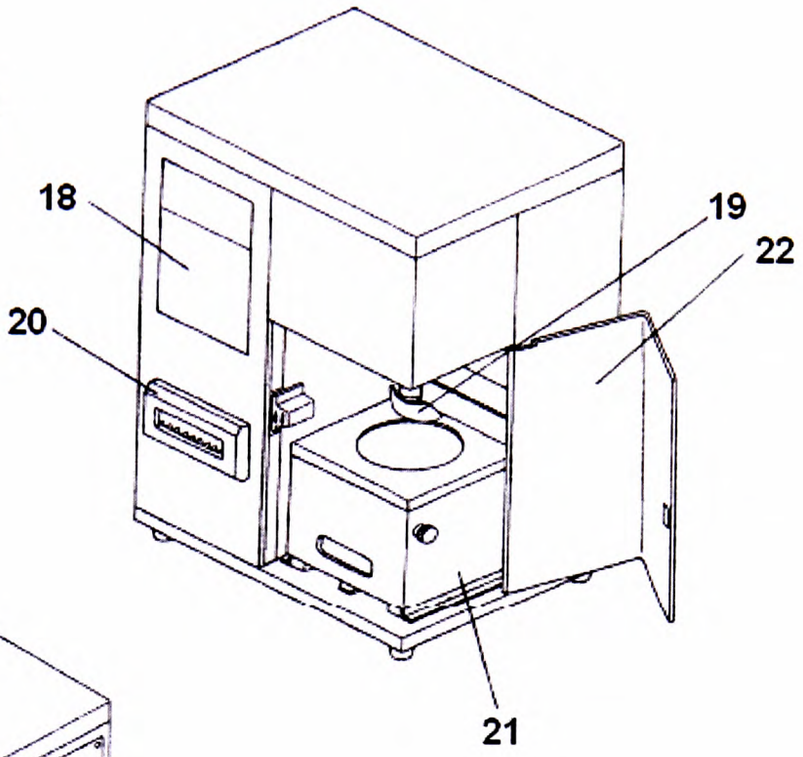

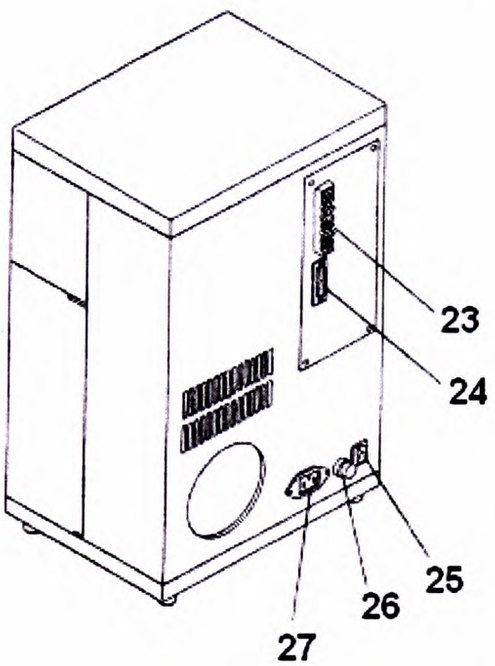

Rear View

23. Terminal Block
24. RS-232C Connector
25. Power Switch
26. Fuse Holder
27. Power Cord Receptacle

Appendix M
Malcom Rotational Viscometer – Specification (*continued*)

Model Number	PCU-201	PCU-203	PCU-205
Sample Size	100cc, 300cc containers (500g, 1500g solder paste)		
Sensor	Malcom Spiral Pump Type		
Measurement Range	5 Pa·s – 1000 Pa·s		
Speed Range	1 – 50 RPM		
Shear Rate	0.6 – 30 seconds^{-1} (0.6 x speed)		
Measurement Accuracy	±5% of indicated value		
Speed Accuracy	±2% of set point (encoder controlled)		
Repeatability	±1.0%		
Temp. Control Range	15 – 30°C (±5°C of room temperature)		
Alarm Audio Output	Beep when viscosity set point is reached		
Alarm Output Terminals	Switch rated 2.5A 120VAC		
Recorder Output	Viscosity: 1mV/Pa·s, Temperature: 10mV/°C		
Printer Displays	Temp, Visc, S. Rate, RPM, Date, Time	Same as PCU-201, plus JIS standard	
Interface	RS232C	Interface	

Sensor/ Cylinder Type Selection
Depending on the cylinder which you use, turn to the correct type of measurement range of viscosity.

Ex. Cylinder Type "A", 10 – 1000 (x10^3 mPa·s)
Cylinder Type "B", 20 – 1999 (x10 mPa·s)
Cylinder Type "C", 20 –1999 (x 1 mPa·s)

Appendix M
Malcom Rotational Viscometer – Specification (*continued*)

Immerse the cylinders into the liquid as shown in "Fig. F". For the "A" Type, the cylinders should extend no further out of the liquid than the diagram indicates. The positioning of the "B" and "C" type cylinders is ideal. The lower lip of the exhaust port is at or just above the liquid surface.

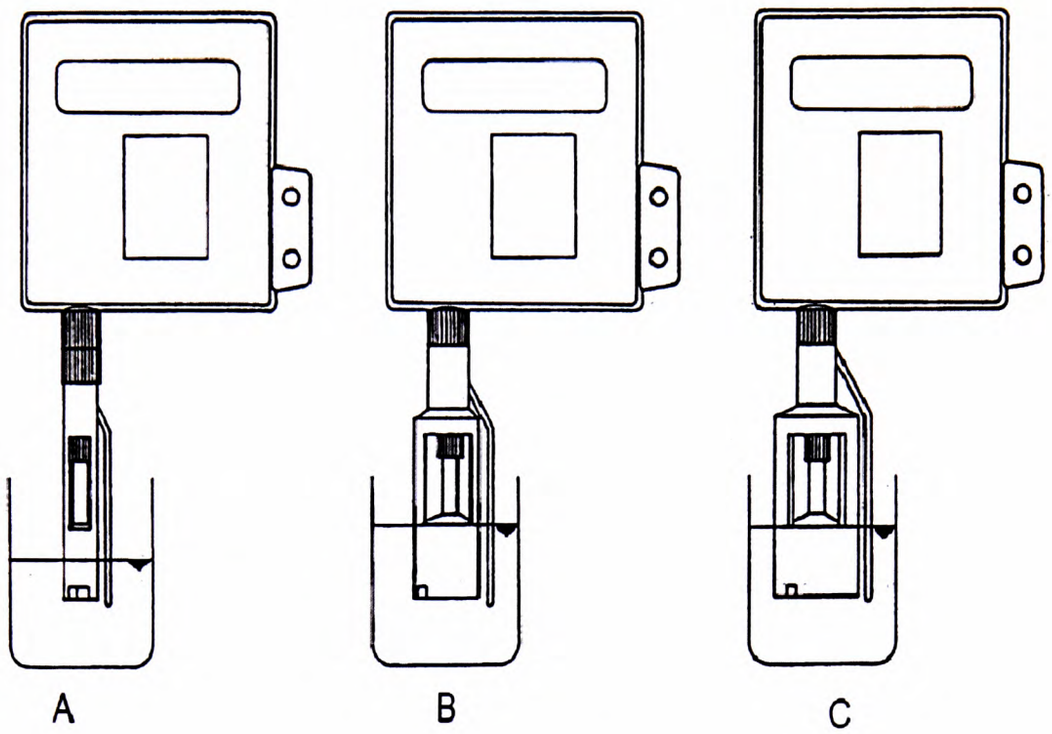

Figure F

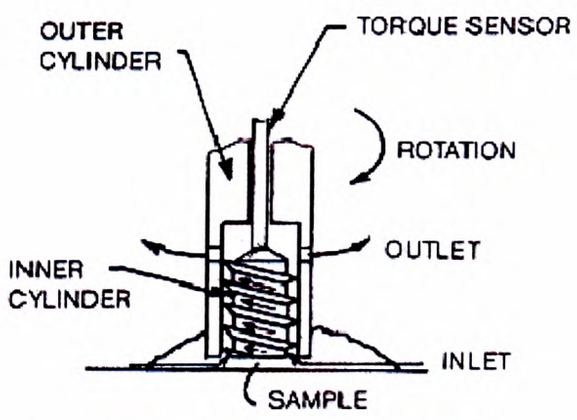

SPIRAL PUMP MEASURING HEAD

Appendix N
Bohlin Gemini Rheometer Data Sheet

Overview

Bohlin Gemini

Comprehensive rheological analysis

Torque range:	
Gemini 150	0.05µNm to 150mNm in controlled stress & rate viscometry 0.05µNm to 150mNm in controlled stress & strain oscillation
Gemini 200	0.05µNm to 200mNm in controlled stress & rate viscometry 0.05µNm to 200mNm in controlled stress & strain oscillation
Gemini HR^{nano}	10nNm to 200mNm in controlled stress & rate viscometry 3nNm to 200mNm in controlled stress & strain oscillation
Torque resolution:	Better than 1nNm
Position resolution:	50nrad
Frequency range:	1µHz to 150Hz
Controlled speed range (CR mode):	0.01mrad s^{-1} to 600rad s^{-1}
Measurable speed range (CS mode):	10nrad s^{-1} to 600rad s^{-1}
Normal force N1 measurement range:	0.001N to 20N (50N optional)
Step change in strain:	<10ms
Temperature range (dependent on control used):	-150°C to 550°C
Temperature controls	
Fluids Circulator:	-40°C to 250°C
ETO (Extended Temperature Option):	-15°C to 300°C
Melts Oven:	ambient to 450°C
Peltier Plate:	-30°C to 200°C
Peltier Cylinder:	-20°C to 180°C
Universal Peltier Option – Coaxial Cylinder or Cone/Plate Geometries	
ETC (Extended Temperature Cell):	ambient to 550°C
ETC with optional LTU (Low Temperature Unit):	-150°C to 550°C
Nominal operating voltage	110 or 220V
Size (with Peltier plate)	52cm (H) x 33cm (W) x 37cm (D)
Weight (with Peltier plate)	28kg
Optional equipment	
Measuring Systems	
Vacuum Disposable Plates:	Peltier Plate, Melts Oven or ETO
High Pressure (Sealed Cell):	40bar pressure, 30°C to 150°C
High Pressure/High Temperature Cell:	300bar pressure, ambient to 300°C
Optical UV Curing Cell	
Optical Analysis Cell	
Immobilisation Cell	
Electro-rheology Cell:	DC voltage up to c.10kV

Every Bohlin Gemini from Malvern is backed with the technical and sales support of Malvern Instruments, the only material characterization company with the resources and equipment to measure particle size and shape, zeta potential and molecular weight as well as the expertise to advise on how these parameters influence rheological properties.

Malvern Instruments Limited

Enigma Business Park • Grovewood Road • Malvern • Worcestershire • UK • WR14 1XZ

Tel: +44 (0)1684 892456 • **Fax:** +44 (0)1684 892789

Malvern Instruments Worldwide

Sales and service centres in over 50 countries for details visit www.malvern.co.uk/contact

Bohlin gemini

Malvern Instruments is part of Spectris plc, the Precision Instrumentation and Controls Company.

spectris

MALVERN

detailed specifications at www.malvern.co.uk

© 2005 MRK660-03

Appendix O
LF328 Solder Paste Data Sheet

Technical Data Sheet

LF328 Solder Paste

February 2006

LOW-VOIDING LEAD-FREE SOLDER PASTE

PRODUCT DESCRIPTION

Multicore™ LF328 solder paste is a halide-free, no clean, Pb-free solder paste, which has a broad process window, for printing, reflow and humidity resistance. LF328 solder paste has been formulated to give low voiding in BGA joints, a high tack force to resist component movement during high speed placement, long printer abandon times and excellent solderability over a wide range of reflow profiles in air and nitrogen and across a wide range of surface finishes including Ni/Au, Immersion Sn, Immersion Ag and OSP Copper.

FEATURES AND BENEFITS

- Excellent print process capability for 0.5mm and 0.4mm pitch CSP
- Long abandon time capability (>75minutes on 0.4mm CSP)
- Allows fast print speed with low print pressure
- Humidity resistance – excellent coalescence after 8 hours exposure to 27°C/80% RH.
- Colorless residues for easy post-reflow inspection
- Ultra-low voiding
- Halide free flux classification: ROL0 to ANSI/J-STD-004

TYPICAL PROPERTIES

Properties	LF328			
Alloys	96SC (95.5Sn 3.8Ag 0.7Cu, 217°C) 97SC (96.5Sn 3.0Ag 0.5Cu, 217°C)			
Powder Particle Size, µm	20-45		20-38	
Multicore Powder Size Coding	AGS		DAP	
IPC Equivalent	Type 3		Type 4	
Metal Loading (% weight)	88	88.5	88	88.5
Slump, J-STD-005, mm[4] RT (15 minutes) 0.33 x 2.03 mm pads 0.63 x 2.03 mm pads 150°C (15 minutes) 0.33 x 2.03 mm pads 0.63 x 2.03 mm pads	IPC A21 Pattern 0.06 0.33 0.20 0.33			
Viscosity measured at 25°C (Typical) Brookfield, cP[1] Malcom 10rpm, P[2] Thixotropic Index (Ti)[3]	440,000 880 0.55	526,000 953 0.56	490,000 920 0.54	530,000 1020 0.54
Tack[5] Initial tack force, gmm^{-2} Useful open time, hours	1.8 >24		2.4 >24	

[1] Measured at 25°C, TF spindle at 5rpm after 2 minutes
[2] Measured at 25°C, and a shear rate of 6s^{-1}
[3] TI = log (viscosity at 1.8s^{-1}/ Viscosity at18s^{-1})
[4] Slump data (AGS 88%only) are expressed as the minimum spacing between pads of the size shown that does not allow bridging
[5] Tack data are derived from comparative laboratory tests and do not necessarily relate directly to a particular user's conditions

Solder powder: Careful control of the atomisation process for production of solder powders for LF328 solder pastes ensures that the solder powder is produced to a quality level that exceeds IPC/J-STD006 & EN29453 requirements for sphericity, size distribution & impurities. Minimum order requirements may apply to certain alloys and powder particle sizes. For availability with other alloys and powder sizes, contact your local technical service helpdesk.

DIRECTIONS FOR USE

Printing: LF328 solder paste is available for stencil printing down to 0.4mm (0.016") pitch BGA devices, with type 4 (DAP) powder. Printing at speeds between 25mm/s (1.0"/s) & 150mm/s (6"/s) can be achieved using laser cut, electro-polished, or electroformed stencils and metal squeegees (preferably 60^0).

Excellent first prints have been achieved on 0.4mm (0.016") pitch CSP pads after printer down times of 75 minutes, without requiring a knead cycle.

Reflow:
Any of the available methods of heating to cause reflow may be used including IR, convection, hot belt, vapour phase and laser soldering. LF328 is not particularly sensitive to reflow profile type. There is no single reflow profile which is suitable for all processes & applications, but the following graph shows example profiles (in green) that have given good results in practice.

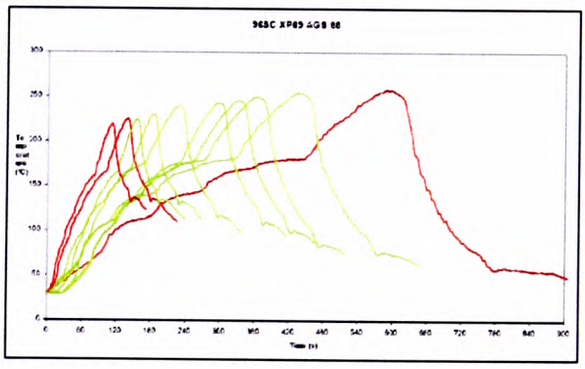

Cleaning: Multicore LF328 solder pastes are no-clean & are designed to be left on the PCB in many applications since they do not pose a hazard to long term reliability. However, should there be a specific requirement for residue removal, this may be achieved using conventional cleaning processes based on solvents such as Multicore MCF800, or suitable saponifying agents. For stencil cleaning and cleaning board misprints, Multicore SC-01 Solvent Cleaner is recommended.

NOT FOR PRODUCT SPECIFICATIONS
THE TECHNICAL INFORMATION CONTAINED HEREIN IS INTENDED FOR REFERENCE ONLY. PLEASE CONTACT HENKEL TECHNOLOGIES TECHNICAL SERVICE FOR ASSISTANCE AND RECOMMENDATIONS ON SPECIFICATIONS FOR THIS PRODUCT

Henkel Technologies

Appendix O
LF328 Solder Paste Data Sheet (continued)

RELIABILITY PROPERTIES

Solder paste medium: Multicore LF328 medium contains a stable resin system and slow evaporating solvents with minimal odour. The formulation meets the requirements of the Telcordia (formerly known as Bellcore) GR-78-CORE and ANSI/J-STD-004 for a type ROL0 classification.

Test	Specification	Results
Copper Plate Corrosion	ANSI/J-STD-004	Pass
Copper Mirror Corrosion	ANSI/J-STD-004	Pass
Chlorides & Bromides	ANSI/J-STD-004	Pass
Surface Insulation Resistance (without cleaning)	ANSI / J-STD-004 Telcordia GR-78-Core JIS-Z-3284	Pass Pass Pass
Flux Activity Classification (without cleaning)	ANSI/J-STD-004	ROL0

PACKAGING

Containers: Multicore LF328 solder paste is supplied in:

- 500g plastic jars with an air seal insert.
- 600g Semco cartridges

Other packaging types may be available on request: please contact your local technical service helpdesk for assistance.

Storage:

It is recommended to store LF328 at 0-10°C (NB cartridges should be stored tip down to prevent the formation of air pockets). The paste should be removed from cold storage a minimum of 4 hours prior to use. Do not use forced heating methods to bring solder paste up to temperature. Multicore LF328 solder paste has been formulated to minimize flux separation on storage but should this occur, gentle stirring for 15 seconds will return the product to its correct rheological performance.

To prevent contamination of unused product, do not return any material to its original container. For further specific shelf life information, contact your local Technical Service Centre.

Shelf Life:

Provided Multicore LF328 solder pastes are stored tightly sealed in the original container at 0-10°C, a minimum shelf life of 6 months can be expected. Air shipment is recommended to minimize the time that containers are exposed to higher temperatures.

DATA RANGES

The data contained herein may be reported as a typical value and/or range. Values are based on actual test data and are verified on a periodic basis.

GENERAL INFORMATION

For safe handling information on this product, consult the Material Safety Data Sheet, (MSDS).

Note

The data contained herein are furnished for information only and are believed to be reliable. We cannot assume responsibility for the results obtained by others over whose methods we have no control. It is the user's responsibility to determine suitability for the user's purpose of any production methods mentioned herein and to adopt such precautions as may be advisable for the protection of property and of persons against any hazards that may be involved in the handling and use thereof. In light of the foregoing, **Henkel Corporation specifically disclaims all warranties expressed or implied, including warranties of merchantability or fitness for a particular purpose, arising from sale or use of Henkel Corporation's products. Henkel Corporation specifically disclaims any liability for consequential or incidental damages of any kind, including lost profits.** The discussion herein of various processes or compositions is not to be interpreted as representation that they are free from domination of patents owned by others or as a license under any Henkel Corporation patents that may cover such processes or compositions. We recommend that each prospective user test his proposed application before repetitive use, using this data as a guide. This product may be covered by one or more United States or foreign patents or patent applications.

Americas
Henkel Corporation
15350 Barranca Parkway
Irvine, CA 92618 U.S.A.
949.789.2500

Europe
Henkel Loctite Adhesives Ltd
Kelsey House, Wood Lane End
Hemel Hempstead
Hertfordshire HP2 4RQ, United Kingdom
+44 (0) 1442 233 233

Asia
Henkel Loctite (China) Co. Ltd
No. 90 Zhujiang Road
Yantai Development Zone
Shandong, China 264006
+86 535 6399820

All trademarks, except where noted are the property of Henkel Corp.

Henkel Technologies

Appendix O
LF318 Solder Paste Data Sheet

Technical Data Sheet

LF318 Solder Paste

July 2005

PIN-TESTABLE LEAD-FREE SOLDER PASTE

PRODUCT DESCRIPTION

Multicore™ LF318 solder paste is a halide-free, no clean, pin testable Pb-free solder paste, which has excellent humidity resistance and a broad process window, both for reflow and printing. LF318 solder paste offers a high tack force to resist component movement during high speed placement, long printer abandon times and excellent solderability over a wide range of reflow profiles in air and nitrogen and across a wide range of surface finishes including Ni/Au, Immersion Sn, Immersion Ag and OSP Copper.

FEATURES AND BENEFITS

- Outstanding humidity resistance – gives excellent coalescence even after 72 hours exposure to 27°C/80% RH, thus reducing process variation due to environmental factors
- Colourless residues for easy post-reflow inspection
- Soft non-stick pin testable residues allow easy in-circuit testing
- Suitable for fine pitch, high speed printing up to 150mm/s (6"/s)
- Extended open time & tack-life leading to low wastage.
- Halide free flux classification: ROL0 to ANSI/J-STD-004

TYPICAL PROPERTIES

Based upon type 3 powder; other sizes also available

Properties	LF318
Alloys	96SC, 97SC
Powder Particle Size, µm	20-45
Multicore Powder Size Coding	AGS
Metal Loading (% weight)	88.5
Slump, J-STD-005, mm[4] RT (15 minutes)	IPC A21 Pattern
0.33 x 2.03 mm pads	0.06
0.63 x 2.03 mm pads	0.33
150°C (15 minutes)	
0.33 x 2.03 mm pads	0.25
0.63 x 2.03 mm pads	0.41
Viscosity measured at 25°C (Typical)	
Brookfield, cP[1]	765,000
Malcom 10rpm, P[2]	1961
Thixotropic Index (TI)[2]	0.54
Tack[5]	
Initial tack force, gmm^{-2}	2.0
Useful open time, hours	>24

[1] Measured at 25°C, TF spindle at 5rpm after 2 minutes
[2] Measured at 25°C, and a shear rate of 6s^{-1}
[3] TI = log (viscosity at 1.8s^{-1}/viscosity at 18s^{-1})
[4] Slump data are expressed as the minimum spacing between pads of the size shown that does not allow bridging
[5] Tack data are derived from comparative laboratory tests and do not necessarily relate directly to a particular user's conditions

Solder powder: Careful control of the atomisation process for production of solder powders for LF318 solder pastes ensures that the solder powder is produced to a quality level that exceeds IPC/J-STD006 & EN29453 requirements for sphericity, size distribution, impurities and oxide levels. Minimum order requirements may apply to certain alloys and powder particle sizes. For availability with other alloys and powder sizes, contact your local technical service helpdesk.

DIRECTIONS FOR USE

Printing: Multicore LF318 solder paste is available for stencil printing down to 0.4mm (0.016") pitch devices, with type 3 (AGS) powder. Printing at speeds between 25mm/s (1.0"/s) & 150mm/s (6"/s) can be achieved using laser cut, electro-polished, or electroformed stencils and metal squeegees (preferably 60°).

Acceptable first prints have been achieved at 0.4mm (0.016") pitch after printer down times of 4 hours without requiring a knead cycle.

Reflow:

Any of the available methods of heating to cause reflow may be used including IR, convection, hot belt, vapour phase and laser soldering. LF318 is not particularly sensitive to reflow profile type. There is no single reflow profile which is suitable for all processes & applications, but the following graph shows example profiles that have given good results in practice.

Example Reflow Profiles

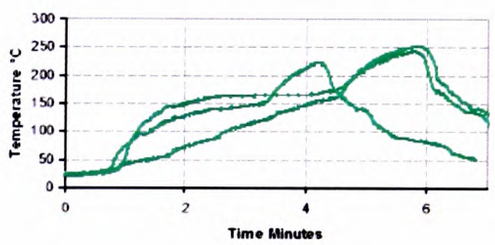

Cleaning: Multicore LF318 solder pastes are no-clean & are designed to be left on the PCB in many applications since they do not pose a hazard to long term reliability. However, should there be a specific requirement for residue removal, this may be achieved using conventional cleaning processes based on solvents such as Multicore MCF800, or suitable saponifying agents. For stencil cleaning and cleaning board misprints, Multicore SC-01 Solvent Cleaner is recommended.

NOT FOR PRODUCT SPECIFICATIONS
THE TECHNICAL INFORMATION CONTAINED HEREIN IS INTENDED FOR REFERENCE ONLY. PLEASE CONTACT HENKEL TECHNOLOGIES TECHNICAL SERVICE FOR ASSISTANCE AND RECOMMENDATIONS ON SPECIFICATIONS FOR THIS PRODUCT

Henkel Technologies

Appendix O
LF318 Solder Paste Data Sheet (continued)

RELIABILITY PROPERTIES

Solder paste medium: Multicore LF318 medium contains a stable resin system and slow evaporating solvents with minimal odour. The formulation meets the requirements of the Telcordia (formerly known as Bellcore) GR-78-CORE and ANSI/J-STD-004 for a type ROL0 classification.

Test	Specification	Results
Copper Plate Corrosion	ANSI/J-STD-004	Pass
Copper Mirror Corrosion	ANSI/J-STD-004	Pass
Chlorides & Bromides	ANSI/J-STD-004	Pass
Surface Insulation Resistance (without cleaning)	ANSI / J-STD-004 Telcordia GR-78-Core JIS-Z-3284	Pass Pass Pass
Flux Activity Classification (without cleaning)	ANSI/J-STD-004	ROL0

PACKAGING

Containers: Multicore LF318 solder paste is supplied in:

- 500g plastic jars with an air seal insert.
- 1kg, 600g or 500g Semco cartridges

Other packaging types may be available on request; please contact your local technical service helpdesk for assistance.

Storage:
It is recommended to store LF318 at 0-10°C (NB cartridges should be stored tip down to prevent the formation of air pockets). The paste should be removed from cold storage a minimum of 8 hours prior to use. Do not use forced heating methods to bring solder paste up to temperature. Multicore LF318 solder paste has been formulated to minimize flux separation on storage but should this occur, gentle stirring for 15 seconds will return the product to its correct rheological performance.

To prevent contamination of unused product, do not return any material to its original container. For further specific shelf life information, contact your local Technical Service Centre.

Shelf Life:
Provided Multicore LF318 solder pastes are stored tightly sealed in the original container at 0-10°C, a minimum shelf life of 6 months can be expected. Air shipment is recommended to minimize the time that containers are exposed to higher temperatures.

DATA RANGES

The data contained herein may be reported as a typical value and/or range. Values are based on actual test data and are verified on a periodic basis.

GENERAL INFORMATION

For safe handling information on this product, consult the Material Safety Data Sheet, (MSDS).

Note

The data contained herein are furnished for information only and are believed to be reliable. We cannot assume responsibility for the results obtained by others over whose methods we have no control. It is the user's responsibility to determine suitability for the user's purpose of any production methods mentioned herein and to adopt such precautions as may be advisable for the protection of property and of persons against any hazards that may be involved in the handling and use thereof. In light of the foregoing, **Henkel Corporation specifically disclaims all warranties expressed or implied, including warranties of merchantability or fitness for a particular purpose, arising from sale or use of Henkel Corporation's products. Henkel Corporation specifically disclaims any liability for consequential or incidental damages of any kind, including lost profits.** The discussion herein of various processes or compositions is not to be interpreted as representation that they are free from domination of patents owned by others or as a license under any Henkel Corporation patents that may cover such processes or compositions. We recommend that each prospective user test his proposed application before repetitive use, using this data as a guide. This product may be covered by one or more United States or foreign patents or patent applications.

Americas
Henkel Corporation
15350 Barranca Parkway
Irvine, CA 92618 U.S.A.
949.789.2500

Europe
Henkel Loctite Adhesives Ltd
Technologies House, Wood Lane End
Hemel Hempstead
Hertfordshire HP2 4RQ, United Kingdom
+44 (0) 1442 278 000

Asia
Henkel Loctite (China) Co. Ltd
No. 90 Zhujiang Road
Yantai Development Zone
Shandong, China 264006
+86 535 6399820

All trademarks, except where noted are the property of Henkel Corp.

Henkel Technologies

Appendix P1
Flux Induced Corrosion IPC-TM-650: 2.3.32

The Institute for Interconnecting and Packaging Electronic Circuits
2215 Sanders Road • Northbrook, IL 60062-6135

IPC-TM-650
TEST METHODS MANUAL

Number	
2.3.32	
Subject	
Flux Induced Corrosion (Copper Mirror Method)	
Date	Revision
1/95	**C**
Originating Task Group	
Flux Specifications Task Group (5-24a)	

1.0 Scope This test method is designed to determine the removal effect the flux has (if any) on the bright copper mirror film which has been vacuum deposited on clear glass.

2.0 Applicable Documents

ASTM E104 Maintaining Constant Relative Humidity by means of Aqueous Solutions

LLL-R-626 Rosin, Gum, Rosin Wood and Rosin Tall Oil

3.0 Test Specimen A minimum of 100 ml of liquid flux, a representative container of solder paste, reflowed solder-paste flux, extracted solder preform flux or extracted flux-cored wire.

4.0 Apparatus and Reagents

4.1 0.5L of control standard rosin flux, class A, type II, grade WW, of LLL-R-626.

4.2 0.5L of reagent grade (99% pure) 2-propanol.

4.3 A vacuum deposition system or the means to procure glass test panels having a copper mirror coating as described in paragraph 5 below.

4.4 0.5L of reagent grade 0.5% solution of ethylene diamine tetra acetic acid (EDTA).

4.5 0.5L of reagent grade ethanol or methanol.

4.6 100 ml medicine bottle with dropper.

4.7 Test cabinet capable of achieving 23 ± 2°C and 50 ± 5% relative humidity.

4.8 Glass slides

4.9 A relative humidity gauge having a ± 2% accuracy, or better, shall be used to continuously monitor the test environment. The gauge should be calibrated periodically.

5.0 Procedures

5.1 Preparation

5.1.1 Preparation of Control Standard Flux Dissolve 35 g of Federal Specification LLL-R-626 rosin into 100 ml of reagent grade 99% 2-propanol and stir thoroughly.

5.1.2 Preparation of Temperature/Humidity Chamber When acid or salt solutions, such as reported in ASTM E104, are used the environment shall be monitored for a minimum of 48 hours prior to exposing the copper mirror samples, to assure compliance with the 50% ± 5% relative humidity requirement.

5.1.3 Preparation of Copper Mirror Test Panels.

5.1.3.1 Apply by vacuum deposition, a film of copper metal on one surface of a flat sheet or clear, polished glass.

5.1.3.2 Apply a uniform thickness of approximately 50 nm and assure that the finished mirror permits 10 ± 5% transmission of normal incident light of nominal wave length of 500 nm. This may be determined using a suitable photoelectric spectrophotometer. Commercially available copper mirrors meeting the above specifications are acceptable. (See 6.2.)

5.1.3.3 Prevent oxidation of the copper mirror by storing in a closed container which has been flushed with nitrogen.

5.1.3.4 Immediately before testing, immerse the copper mirror in a 5 g/l solution of EDTA for copper oxide removal. Mirrors stored in a non-oxidizing environment, do not require cleaning with the EDTA solution prior to testing. The cleaning step must be used if test results are in dispute.

5.1.3.5 Rinse thoroughly in running water, immerse in clean ethanol or methanol and dry with clean, oil free air.

5.1.3.6 Carefully examine the mirror before testing. There must be no oxide.

5.2 Test

5.2.1 Place the copper mirror test panel on a flat surface, mirror side up, and protect from dust and dirt at all times.

5.2.2 Place one drop of test flux or extract to be tested (approximately 0.05 ml) on each copper mirror test panel. Do not allow the dropper to touch the test panel.

Material in this Test Methods Manual was voluntarily established by Technical Committees of the IPC. This material is advisory only and its use or adaptation is entirely voluntary. IPC disclaims all liability of any kind as to the use, application, or adaptation of this material. Users are also wholly responsible for protecting themselves against all claims or liabilities for patent infringement. Equipment referenced is for the convenience of the user and does not imply endorsement by the IPC.

Appendix P1
Flux Induced Corrosion IPC-TM-650: 2.3.32 (continued)

IPC-TM-650		
Number **2.3.32**	Subject **Flux Induced Corrosion (Copper Mirror Method)**	Date **1/95**
Revision **C**		

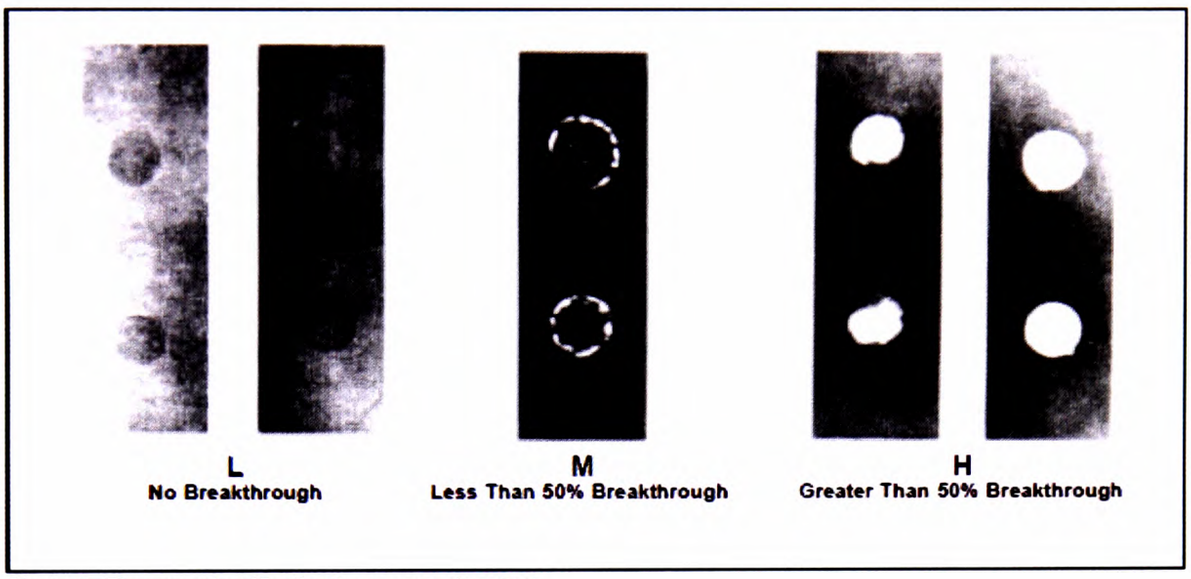

Figure 1 Flux type classification by copper mirror test

5.2.3 Solder-paste shall be applied directly to the mirror without scratching the copper mirror, with a volume approximating a 0.5 mm thickness and 8 mm diameter. (It has been determined that significant variations from this quantity have little effect for most materials.)

5.2.4 Immediately also place one drop of the control standard flux adjacent to the test flux. Do not allow drops to touch.

5.2.5 Place test panels in a horizontal position in the dust free cabinet at 23 ± 2°C and 50 ± 5% relative humidity for 24 ± 1/2 hours.

5.2.6 At the end of the 24 hour period, remove the test panels and remove the test flux and control standard fluxes by immersion in clean 2-propanol.

5.3 Evaluation

5.3.1 Carefully examine each test panel for possible copper removal or discoloration.

5.3.2 If there is any complete removal of the copper film as evidenced by the background showing through the glass, the test flux has failed the L category. Complete removal of the copper only around the perimeter of the drop denotes the flux as M. Complete removal of the copper places the flux in the H category. (See Figure 1).

5.3.3 If the control flux fails, repeat the entire test, using new copper mirror test panels.

5.3.4 Discoloration of the copper film due to a superficial reaction or only a partial reduction of the copper film thickness is not considered a failure.

5.3.5 A number of chemicals can cause failure of copper mirrors: free halides, stronger organic and inorganic acids and free amines.

6.0 Notes

6.1 Safety Observe all appropriate precautions on MSDS for chemicals involved in this test method.

6.2 Sources for prepared copper mirrors

6.2.1 Evaporated Metal Films, Inc., Ithaca, NY 14850.

6.2.2 Clausing PA Co., 8038 Monticello Ave., Skokie, IL, 708/207-3399

Appendix P2
Presence of Halides in Flux IPC-TM-650: 2.3.33

ASSOCIATION CONNECTING ELECTRONICS INDUSTRIES®

2215 Sanders Road
Northbrook, IL 60062-6135

IPC-TM-650
TEST METHODS MANUAL

Number	
2.3.33	
Subject: **Presence of Halides in Flux, Silver Chromate Method**	
Date: **06/04**	Revision: **D**
Originating Task Group: **Flux Specifications Task Group (5-24a)**	

1 Scope This qualitative test method is designed to determine the presence of chlorides and bromides in soldering flux by visual examination after placement on test paper.

2 Applicable Documents

IPC J-STD-004 Requirements for Soldering Fluxes

3 Test Specimen A minimum of 10 ml of liquid flux, a representative container of solder paste, reflowed solder paste flux, extracted solder preform flux or extracted cored wire flux. The reflow/extraction process should be carried out in accordance with J-STD-004.

4 Apparatus and Reagents

4.1 Six pieces of silver chromate test paper 51 mm x 51 mm.

4.2 250 ml of reagent grade 2-propanol.

4.3 Six glass microscope slides.

4.4 Spatula.

5 Procedures

5.1 Preparation

5.1.1 The silver chromate paper is extremely light sensitive and must be stored in a closed container away from light until used for testing.

5.1.2 To avoid contamination, the paper must be handled with forceps and must never be touched with bare hands.

5.2 Test for Liquid Flux or Flux Extract Solution

5.2.1 Place one drop of test flux or flux extract (approximately 0.05 ml) on each piece of silver chromate test paper. Allow the droplet to remain on each test paper for a minimum of 15 seconds.

5.2.2 After the 15 seconds, immediately immerse each test paper in clean 2 propanol to remove the residual organic materials.

5.2.3 Allow each test paper to dry and examine for color change.

5.3 Test for Paste Flux or Solder Paste Flux as Obtained from the Supplier

5.3.1 Clean six glass microscope slides with 2-propanol and air dry.

5.3.2 Moisten each piece of silver chromate reagent paper with deionized water.

5.3.3 Apply a wet paper to each glass slide and remove the excess water with blotting paper

5.3.4 Using a spatula, apply a thin coating of the paste flux or solder paste directly onto each moist reagent paper.

5.3.5 Allow the paste flux or solder paste to remain in contact with the paper for 15 seconds, then remove the flux with 2 propanol or other appropriate solvent without disturbing the paper.

5.3.6 Allow each test paper to dry and examine for color change.

5.4 Evaluation Carefully examine each test sheet for possible color change. A change to off-white or yellow-white indicates the presence of chlorides or bromides (see Figure 1).

5.4.1 Interferences A number of chemicals besides free halides may cause test failures. (Representative examples are, but are not limited to, amines, cyanides, and isocyanates.)

5.4.2 Certain acidic solutions may react with the reagent paper to produce a color change similar to that obtained with chlorides and bromides. When a color change is observed, it is advisable to check the acidity of the affected area by means of a pH indicating paper. If pH values of less than 3 are obtained, the presence of chlorides and bromides should be verified by other analytical means.

5.4.3 It is possible that the metal present in a solder paste sample may leave a white residue that is difficult to distinguish

Material in this Test Methods Manual was voluntarily established by Technical Committees of IPC. This material is advisory only and its use or adaptation is entirely voluntary. IPC disclaims all liability of any kind as to the use, application, or adaptation of this material. Users are also wholly responsible for protecting themselves against all claims or liabilities for patent infringement. Equipment referenced is for the convenience of the user and does not imply endorsement by IPC.

Appendix P2
Presence of Halides in Flux IPC-TM-650: 2.3.33 (continued)

IPC-TM-650		
Number **2.3.33**	Subject **Presence of Halides in Flux, Silver Chromate Method**	Date **06/04**
Revision **D**		

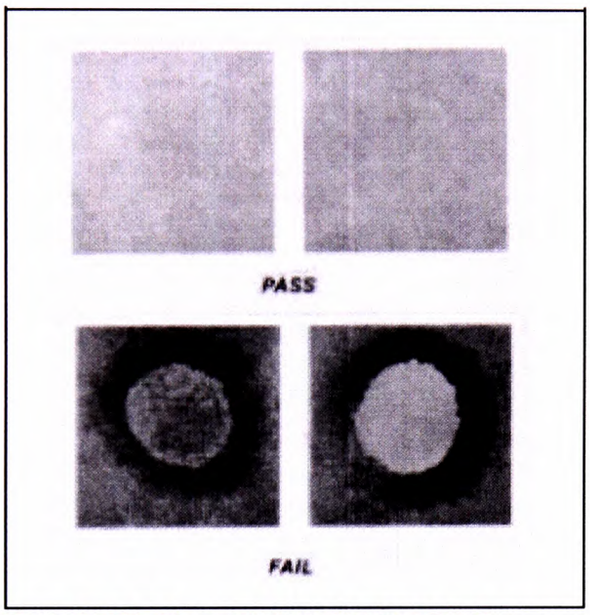

Figure 1 Chlorides and/or Bromides Test Results

from a true color change. A retest on the representative paste flux or flux extracted from the paste is advised.

6 Notes

6.1 Safety Observe all appropriate precautions on MSDS for chemicals involved in this test method.

Appendix P3
Solder Paste-Slump Test: IPC-TM-650: 2.4.35

The Institute for Interconnecting and Packaging Electronic Circuits
2215 Sanders Road • Northbrook, IL 60062-6135

IPC-TM-650
TEST METHODS MANUAL

Number **2.4.35**	
Subject **Solder Paste—Slump Test**	
Date **1/95**	Revision
Originating Task Group **Solder Paste Task Group (5-24b)**	

1.0 Scope This procedure determines vertical and horizontal slump for solder pastes.

2.0 Applicable Documents None

3.0 Test Specimen A standard specimen shall be prepared using a clean frosted glass microscope slide measuring 7.6 cm x 2.5 cm, minimum 1 mm thick. An equivalent alumina or glass epoxy substrate may be used.

4.0 Equipment/Apparatus

Stencils

IPC-A-21, IPC-A-20

Steel Squeegee (razor blade)

Oven

Microscope

5.0 Procedure

5.1 Preparation

5.1.1 Specimen preparation using appropriate stencil pattern IPC-A-21 or IPC-A-20. (Figures 1 & 2) Deposit solder paste patterns on 2 substrates for each stencil pattern. The printed pattern shall be uniform in thickness with no solder particles separated from the pads. The vendor and user should use the same printing method.

5.1.2 One test specimen shall be marked as specimen #1 and one specimen as #2 and processed in accordance with paragraphs 5.2.1 and 5.2.2.

5.2 Test

5.2.1 The specimens shall be stored for 10 to 20 minutes at 25 +/–5°C and 50% relative humidity +/–10% and specimen #1 examined for slump.

5.2.2 Specimen #2 from 5.2.1 shall be heated to 150 +/–10°C for 10 to 15 minutes, cooled to ambient and examined for slump.

5.3 Evaluation Enter data in Table 1 and/or Table 2 by entering spacings which have bridged with a suitable check mark.

Table 1

Stencil IPC-A-21 (0.2 mm Thick)					
Pad size 0.63 x 2.03 mm			Pad size 0.33 x 2.03 mm		
Spacing mm	Hor.	Vert.	Spacing mm	Hor.	Vert.
0.79			0.45		
0.71			0.40		
0.63			0.35		
0.56			0.30		
0.48			0.25		
0.41			0.20		
0.33			0.15		
			0.10		
			0.08		

Table 2

Stencil IPC-A-20 (0.1 mm Thick)					
Pad size 0.33 x 2.03 mm			Pad sie 0.2 x 2.03 mm		
Spacing mm	Hor.	Vert.	Spacing mm	Hor.	Vert.
0.45			0.30		
0.40			0.25		
0.35			0.20		
0.30			0.175		
0.25			0.15		
0.20			0.125		
0.15			0.10		
0.10			0.075		
0.08					

Material in the Test Methods Manual was voluntarily established by Technical Committees of the IPC. This material is advisory only and its use or adaptation is entirely voluntary. IPC disclaims all liability of any kind as to the use, application, or adaptation of this material. Users are also wholly responsible for protecting themselves against all claims or liabilities for patent infringement. Equipment referenced is for the convenience of the user and does not imply endorsement by the IPC.

Appendix P3
Solder Paste-Slump Test: IPC-TM-650: 2.4.35 (continued)

IPC-TM-650		
Number 2.4.35	Subject **Solder Paste—Slump Test**	Date 1/95
Revision		

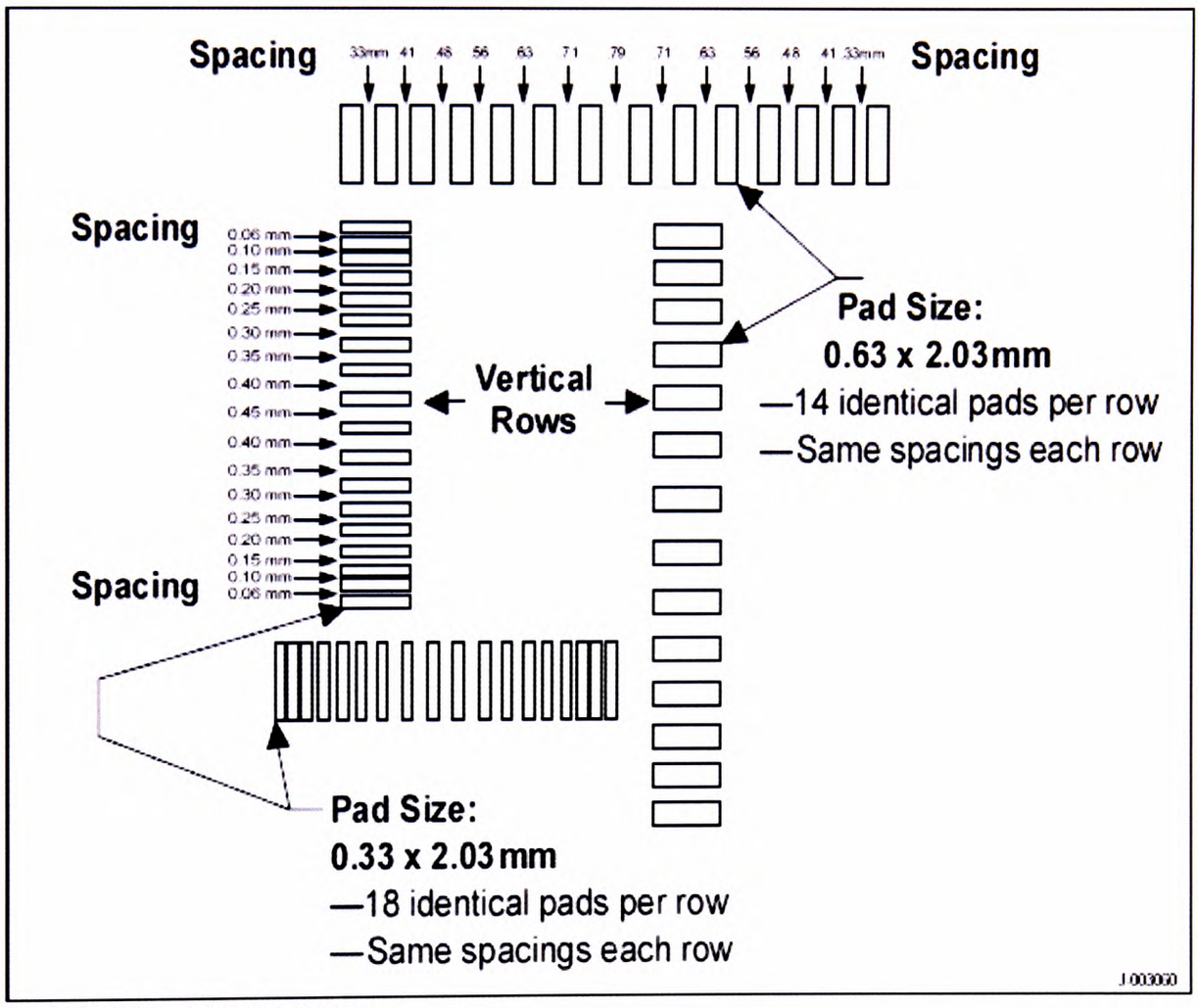

Figure 1 Slump test stencil, IPC-A-21

Appendix P3
Solder Paste-Slump Test: IPC-TM-650: 2.4.35 (continued)

IPC-TM-650		
Number 2.4.35	Subject **Solder Paste—Slump Test**	Date 1/95
Revision		

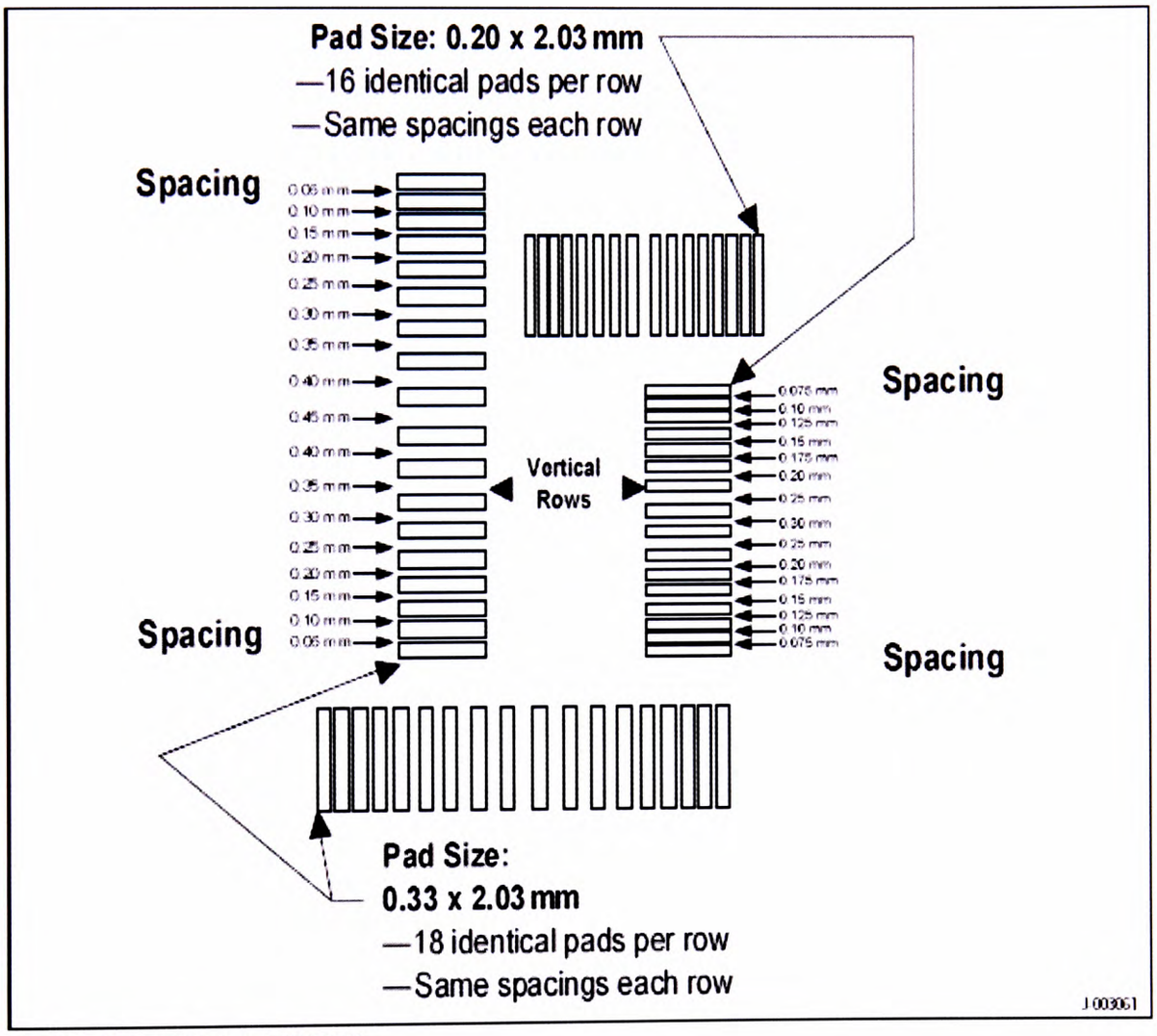

Figure 2 Slump test stencil, IPC-A-20